Systemic immune dynamics in cancer

Bakker, E.A.M.

Systemic Immune Dynamics in Cancer

Noor A.M. Bakker

Systemic Immune Dynamics in Cancer

Author: Noor A.M. Bakker
Cover & layout: Wendy Schoneveld || wenzid.nl
Lay-out and printing: ProefschriftMaken || proefschriftmaken.nl
ISBN:

The research described in this thesis was performed at the division of Tumor Biology & Immunology and the division of Molecular Oncology & Immunology at the Netherlands Cancer Institute – Antoni van Leeuwenhoek hospital (NKI-AvL).

The printing of this thesis was financially supported by the NKI-AvL and Oncology Graduate School of Amsterdam (OOA).

Systemic Immune Dynamics in Cancer

Proefschrift

ter verkrijging van
de graad van doctor aan de Universiteit Leiden,
op gezag van rector magnificus prof.dr.ir. H. Bijl,
volgens besluit van het college voor promoties
te verdedigen op vrijdag 9 januari 2026
klokke 13:00 uur

door

Eleonora Alida Maria Bakker

geboren te Heemstede
in 1988

Promotor
Prof. Dr. K.E. de Visser

Co-promotor
Dr. M. Kok, Netherlands Cancer Institute

Promotiecommissie
Prof. Dr. J.E.A. Portielje
Prof. Dr. M.H.M. Heemskerk
Prof. Dr. R. Arens
Prof. Dr. H. Jacobs, Netherlands Cancer Institute
Dr. R. van de Ven -van Balken, Amsterdam University Medical Center, location VUmc

Thesis outline

CHAPTER 1

Introduction and outline of this thesis

Cancer presents us with a tremendous challenge that is crucial to address. Approximately one in five people will develop cancer in a lifetime, causing death in around one in nine men and one in 12 women[1]. In the Netherlands, the cancer incidence is even higher, with one in two people expected to develop the disease during their lifetime[2]. Breast cancer is the second most common form of cancer in the world, and among women it is the cancer type with the highest global incidence[1,3]. Additionally, breast cancer is the leading cause of cancer-related death in women globally[1], underscoring the urgent need for novel therapeutic possibilities.

Histological subtypes of breast cancer

Breast cancer encompasses various histological subtypes (Figure 1), each with unique characteristics and clinical implications. The most prevalent subtype is Invasive Ductal Carcinoma (IDC), also known as "No Special Type"[4]. This histological subtype comprises about 70-80% of all breast cancer cases and is distinguished by the lack of specific features that would classify it into other special subtypes[5]. IDC begins in the milk ducts and invades surrounding breast tissue. It often presents as a palpable mass that can be detected during physical exams or imaging. While IDC lacks the unique histological traits of special subtypes, it can vary widely in its cellular appearance, tumor microenvironment and behavior, influencing its aggressiveness and response to treatment. The second most common histological subtype is Invasive Lobular Carcinoma (ILC), which makes up about 10-15% of breast cancers[4,6]. It begins in the milk-producing lobules and infiltrates nearby tissues, typically spreading in a single-file pattern that can make it more challenging to detect via physical examination or imaging. Other less common histological subtypes of breast cancer include, mucinous (colloid) carcinoma, tubular carcinoma, micropapillary carcinoma, metaplastic spindle cell carcinoma, lobular pleomorphic carcinoma, apocrine carcinoma, adenoid cystic carcinoma, which all exhibit distinct histological features and clinical behaviors[7].

Molecular subtypes of breast cancer

In addition to the histological features that influence clinical behavior, the molecular subtype of the tumor is the main determinant for treatment and prognosis in the clinic. Using immunohistochemistry breast cancer can be categorized into three distinct molecular tumor subtypes (Figure 1).

The first subtype comprises tumors that exhibit positivity for the estrogen receptor (ER) which make up approximately 70-80% of invasive breast cancer cases[5,8,9]. Globally, the cut-off for ER-positivity used in the clinic is ≥1% of cancer cells expressing ER. However, some

countries including the Netherlands are using a cut-off of ≥10% ER-positive cancer cells, justified by endocrine treatment outcomes and TIL profiles[10-12]. The progesterone receptor (PR) is expressed in more than 50% of ER-positive tumors and is very rare in patients with ER-negative breast cancer because PR expression is regulated by ER[13]. Therefore, physiological PR levels provide information about the functional ER pathway. Absence of PR expression is a biomarker for poor prognosis in ER positive tumors[14,15]. Tumors with ER/PR expression are commonly referred to as hormone receptor-positive (HR+) tumors and represent both Luminal A and Luminal B tumors (Figure 1). Where Luminal A tumors always express PR, this may be absent in Luminal B tumors. Additionally, Luminal B tumors have a higher grade than Luminal A tumors, characterized by reduced tumor cell differentiation and increased Ki67 staining, and it is therefore not surprising that patients with a Luminal A HR+ tumor have the best prognosis[16]. The five-year relative survival rate for patients with HR+ breast cancer is 100% for localized disease and 90.5% for patients with regional disease. Patients with HR+ tumors with distant metastasis have a five-year survival rate of 35.4% (table 1)[3]. Unlike many other tumor types, HR+ breast cancer often recurs beyond 5 years, making a 10-year survival analysis more informative. The 10-year overall survival rate for patients with HR+ breast cancer in the non-metastatic setting is 87.8%[17].

The second breast cancer subtype includes tumors that overexpress the human epidermal growth factor receptor 2 (HER2+) or exhibit gene amplification of HER2, accounting for approximately 15-20% of breast cancer cases[18]. HER2 is an oncogene that encodes a receptor tyrosine kinase, which promotes cell growth by activating signaling pathways like PI3K/AKT and MAPK, driving proliferation and survival; its overexpression amplifies these signals, leading to tumor development. Tumors that are both HR+ and HER2+ are also classified within the HER2+ subtype. Patients with HR+HER2+ breast cancer have five-year survival rate of 99.3% when disease was localized, 90.4% when disease had spread regionally and dropped to 45.8% once the disease had spread to distant sites. Patients with HR-HER2+ breast cancer have a slightly worse prognosis, with a five-year survival of 97.3% when disease was localized, 84.2% when disease had spread regionally and dropped to 39.7% once the disease had spread to distant sites (Table 1)[3]. Notably, patients with HR+HER2+ tumors exhibit higher long-term survival rates than those with HR+HER2- tumors in the metastatic setting. This was historically not the case and can be attributed to the beneficial effects of HER2 targeted therapies[19]. The 10-year overall survival rate for patients with HER2+ breast cancer in the non-metastatic setting is reported to be 76.1%[17].

Lastly, triple-negative breast cancer (TNBC), characterized by the absence of hormone receptor expression and HER2 overexpression or amplification, comprises about 15% of all breast cancer cases[20]. Patients with TNBC have the worst prognosis of all breast cancer patients, especially in the metastatic setting. Their five-year survival rate with localized disease is 92.0%, with regional disease 66.8% and with distant metastatic spread the five-

year survival rate for patients with TNBC is only 14.3%[3] (Table 1). The 10-year overall survival rate for patients with triple negative breast cancer in the non-metastatic setting is 77.8%[17].

While histopathological testing methods provide valuable information about breast cancer subtypes, they are not the sole determinants. Molecular profiling techniques, such as gene expression platforms like Oncotype DX and MammaPrint, also offer comprehensive subtype information by analyzing expression patterns of multiple genes[21,22]. These assays

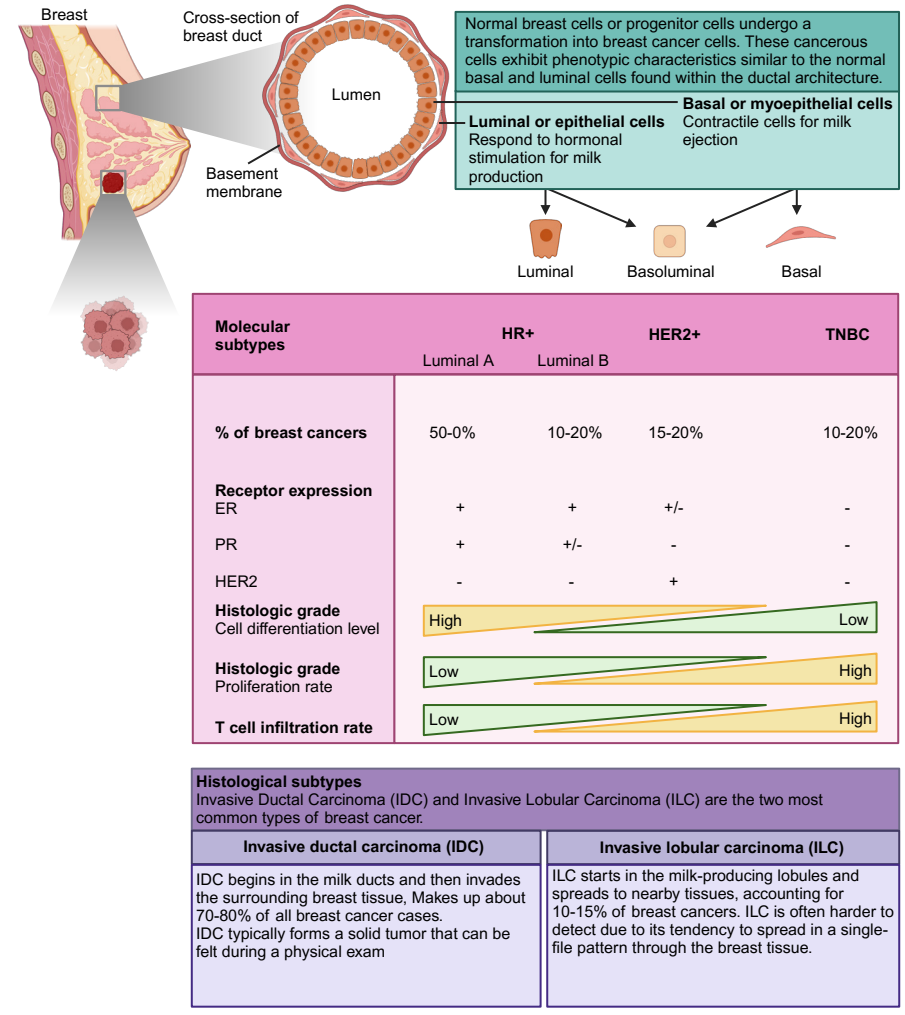

Figure 1: *Overview of breast anatomy and the molecular and histological subtypes of breast cancer. Created in BioRender.com.*

Table 1: *Five-year survival rate of female breast cancer patients by molecular subtype and stage at diagnosis. Based on 385841 women with HR+ breast cancer, 57990 women with HER2+ (HR+) breast cancer, 24028 women with HER2+ (HR-) breast cancer and 58438 women with TNBC. Five-year relative survival rates are calculated using monthly intervals and provided in combination with the upper and lower 95% confidence interval (CI). Data was obtained by the NIH National Cancer Institute SEER program, which was last updated in 2021[3].*

	Local (CI)	Regional (CI)	Distant (CI)
HR+	100 (-)	90.5 (90.2 – 90.8)	35.5 (34.5 – 36.4)
HER2+ (HR+)	99.3 (98.8 – 99.6)	90.4 (89.8 – 91.0)	45.8 (44.0 – 47.6)
HER2+ (HR-)	97.3 (96.6 – 97.8)	84.2 (83.2 – 85.2)	39.7 (37.4 – 42.0)
TNBC	92.0 (91.5 – 92.5)	66.8 (65.9 – 67.6)	14.3 (13.0 – 15.6)

primarily enhance the molecular classification of breast cancer and provide prognostic information. Specifically, the Prediction Analysis of Microarray 50 (PAM50) was designed to classify breast cancer subtypes, assigning tumors to intrinsic molecular subtypes—Luminal A, Luminal B, HER2-enriched, and Basal-like—based on the expression of 50 key genes[23,24]. This classification highlights breast cancer heterogeneity and underscores the need for personalized treatment strategies tailored to specific molecular subtypes[25]. Throughout this thesis, breast cancer subtypes are based on histopathological feature of the tumor. Despite advances in targeted treatments, breast cancer remains the leading cause of cancer-related mortality among women, emphasizing the ongoing need for innovative therapeutic approaches.

Breast cancer and the (systemic) immune landscape

The immune system is a highly complex assembly of cells that functions to protect the body against infections, eliminate damaged cells, and maintain overall homeostasis. The systemic immune composition refers to the diverse array of immune cells that circulate throughout the body and collectively contribute to the immune response. Understanding the systemic immune composition is particularly important in the context of diseases like cancer, where alterations can significantly impact disease progression and treatment efficacy. The immune system consists of two main branches: the innate immune system and the adaptive immune system, each with unique roles but deeply interconnected through various mechanisms of cross-talk.

The Immune System in Homeostasis

In a state of homeostasis, the immune system maintains a delicate balance, effectively protecting the host from pathogens while avoiding excessive or inappropriate responses that could cause tissue damage or autoimmune diseases. This equilibrium is achieved

through a tightly regulated interplay of immune cells, cytokines, and regulatory mechanisms. Regulatory T cells (Tregs), for example, play a crucial role in maintaining this balance by suppressing potentially harmful immune responses and preventing autoimmunity[26,27]. These cells act as a safeguard, ensuring that the immune system does not overreact to benign stimuli, which could lead to tissue damage. The production of anti-inflammatory cytokines, such as interleukin-10 (IL-10) and transforming growth factor-beta (TGF-β), helps to mitigate inflammatory responses and promote tissue repair[28-31]. Without a proper functioning immune system, one would either be confined to life in a bubble, or succumb from otherwise harmless pathogenic infection.

Innate and Adaptive Immunity

Innate immune cells, such as neutrophils, eosinophils, basophils, monocytes, macrophages, dendritic cells (DCs), and natural killer (NK) cells, provide the first line of defense against pathogens. They are characterized by their ability to respond rapidly and non-specifically to invading microorganisms. For example, neutrophils are the most abundant type of white blood cells, making up ~70-80% of the circulating white blood cells (WBCs). Neutrophils are among the first responders to sites of infection, where they engulf and destroy pathogens through phagocytosis. Regarding the role of neutrophils in cancer, preclinical studies have shown that neutrophils promote metastasis through various mechanisms[32-37]. Tumor-induced systemic inflammation often leads to elevated neutrophil counts in the blood, commonly represented in clinical settings by the Neutrophil-to-Lymphocyte Ratio (NLR). Clinical studies indicate that a high NLR is associated with poor prognosis and reduced therapy response across several cancer types, including breast cancer[38-43]. Eosinophils are under homeostatic conditions primarily involved in combating parasitic infections and modulating allergic inflammatory responses by releasing toxic granules and cytokines. In the context of immunotherapy against cancer, eosinophils can enhance the response to immune checkpoint inhibition, and correlate with clinical response[44,45]. Basophils play a key role in allergic reactions by releasing histamine and other mediators that increase vascular permeability and attract other immune cells to sites of inflammation. Monocytes can differentiate into macrophages and dendritic cells upon entering tissues, where they play critical roles in both pathogen elimination and the initiation of adaptive immune responses. Macrophages are highly versatile phagocytic cells that engulf pathogens, clear dead cells, and release cytokines to regulate immune responses. Macrophages play a dual role in cancer, either supporting tumor progression by promoting immunosuppression, angiogenesis, and metastasis or—when properly activated—combating the tumor through immune stimulation, phagocytosis of cancer cells, and direct cytotoxic activity. Tumor-associated macrophages (TAMs) are often skewed toward a pro-tumoral phenotype, making them a crucial target for cancer immunotherapy. Innate immune cells recognize pathogens

through pattern recognition receptors (PRRs), which detect pathogen-associated molecular patterns (PAMPs) and damage-associated molecular patterns (DAMPs), such as Toll-like receptors (TLRs) and NOD-like Receptors[46,47]. TLRs are membrane-bound receptors that recognize bacterial lipopolysaccharides (LPS), lipoproteins, flagellin, and unmethylated CpG DNA from bacteria and viruses[48]. NOD-like receptors are cytoplasmic receptors that detect intracellular PAMPs such as bacterial peptidoglycans[49,50]. In addition to PRRs, also chemokines like IL-8 and LTB-4, and components of the complement system, such as C3a and C5a, can attract and activate innate immune cells; particularly neutrophils[51-55].

The adaptive immune system is characterized by its specificity and memory, primarily mediated by T cells and B cells. T cells play a crucial role in the adaptive immune response, and they can be primarily categorized into two subsets: CD8+ T cells and CD4+ T cells. Each subset has distinct functions, mechanisms of action, and roles in immune regulation.

CD8+ T cells, also known as cytotoxic T lymphocytes (CTLs), are primarily responsible for directly killing infected or cancerous cells. They recognize antigens presented by Major Histocompatibility Complex (MHC) class I molecules, which are found on nearly all nucleated cells. Upon recognizing a foreign antigen, CD8+ T cells become activated and undergo clonal expansion, differentiating into effector cells capable of performing cytotoxic functions. The primary mechanism through which CD8+ T cells exert their cytotoxic effects involves the release of perforin and granzymes. Perforin forms pores in the target cell membrane, allowing granzymes, which are serine proteases, to enter and induce apoptosis (programmed cell death) in the infected or tumor cells. This process is vital for eliminating cells harboring intracellular pathogens, such as viruses, as well as malignant cells that present tumor-specific antigens[56]. In addition to their direct cytotoxic activity, CD8+ T cells can also produce a range of cytokines, such as interferon-gamma (IFN-γ), which enhances the immune response by activating macrophages and promoting inflammation. The effectiveness of CD8+ T cells in tumor surveillance has made them a significant target for cancer immunotherapy strategies, including immune checkpoint inhibitors and adoptive cell transfer therapies, such as CAR-T cell therapy[57-59].

CD4+ T cells, commonly referred to as helper T cells, are essential for orchestrating the adaptive immune response. They recognize antigens presented by MHC class II molecules, which are primarily expressed on professional antigen-presenting cells (APCs) such as dendritic cells, macrophages, and B cells. Upon activation, CD4+ T cells differentiate into various subtypes, each with specialized functions, including Th1, Th2, Th17 cells and Tregs. In short, Th1 cells primarily produce IFN-γ, promoting the activation of macrophages and enhancing the ability of CD8+ T cells to kill infected cells. They are crucial for combating intracellular pathogens, such as viruses and some bacteria[60]. Th2 cells are involved in promoting antibody production by B cells and are essential in orchestrating responses against extracellular pathogens like helminths. They secrete cytokines such as IL-4, IL-5, and

IL-13, which facilitate B cell activation and class switching to produce IgE antibodies[61,62]. Th17 cells are characterized by the production of IL-17 and are particularly important in defending against fungal and extracellular bacterial infections. Th17 cells play a role in promoting inflammation and recruiting neutrophils to sites of infection[63,64]. Tregs are a subset of CD4+ T cells that play a crucial role in maintaining immune tolerance and preventing autoimmune responses. They help suppress excessive immune activation and are characterized by the expression of the transcription factor FoxP3[27].

Both CD8+ and CD4+ T cells are integral components of the systemic immune composition, each playing distinct yet interconnected roles in immune surveillance, pathogen elimination, and the orchestration of adaptive immune responses. The balance between these CD4+ T cell subsets is vital for an effective immune response[65]. Dysregulation of this balance can lead to inadequate immune responses against pathogens or contribute to autoimmune diseases and cancer progression.

A component of the adaptive immune system that bridges innate and adaptive immunity are the B cells. B cells are activated by helper T cells and by directly encountering antigens. Activated B cells differentiate into memory B cells, and plasma cells that produce antibodies specific to the antigens[66]. These antibodies neutralize pathogens and mark them for destruction by other immune cells, thereby integrating the adaptive response with innate effector mechanisms such as phagocytosis[67,68]. In the context of cancer, B cells play a dual role, functioning as contributors to tumor immunity and as facilitators of tumor progression. They can produce antibodies that target tumor antigens, enhancing immune recognition and destruction of cancer cells. Additionally, B cells are key in the formation of tertiary lymphoid structures (TLS) in the TME, which are associated with immunotherapy response[69,70]. However, in some contexts, B cells may also promote systemic immunosuppression through the expansion of regulatory B cells, which are characterized by production of the anti-inflammatory cytokine IL-10[71,72]. Chemotherapy has lasting effects on B cells, leading to impaired memory B cell generation and maintenance, altered antibody production, and shifts in isotype distribution, which persist for months post-treatment[73,74].

DCs also serve as a crucial bridge between innate and adaptive immunity[75]. Upon encountering a pathogen, dendritic cells undergo maturation and migrate to lymphoid tissues, where they present processed antigens to naive T cells, along with necessary co-stimulatory signals and cytokines, initiating the adaptive immune response. This activation leads to the proliferation and differentiation of naïve T cells into effector cells, that secrete cytokines to further stimulate immune responses[76-79]. DCs can be classified into a three major subsets; plasmacytoid DC (pDCs), conventional DC type 1 (cDC1) and conventional DC type 2 (cDC2), each driving distinct immune responses. pDCs are known for their ability to produce significant amounts of type I interferons, particularly IFN-α, in response to viral infections[80]. In the cancer setting, pDCs can either support tumor elimination or facilitate

tumor evasion[81-84], underscoring the necessity of understanding the context in which pDCs operate. cDC1 cells are characterized by CD8α positivity and IL-12 production, promoting robust CD8+ T cell activation and Th1 differentiation, crucial for antiviral and antitumor immunity[79,80]. In contrast, cDC2 cells, typically CD8α-negative, enhance CD4+ T cell responses and are associated with Th2 polarization, playing a vital role in responses to extracellular pathogens and also in antitumor immune responses[79,80].

The last cell type that I will describe that bridges the innate and adaptive immune responses are natural killer (NK) cells. NK cells recognize stressed or abnormal cells through a balance of activating and inhibitory receptors. Activating receptors (e.g., NKG2D) detect stress ligands on target cells, while inhibitory receptors (e.g., KIRs) recognize normal MHC molecules, allowing NK cells to distinguish healthy cells from those that are infected or transformed[85,86]. Upon activation, NK cells release cytotoxic granules containing perforin and granzymes[86]. NK cells also express the low-affinity Fc receptor CD16, which enables them to detect antibody-coated target cells and to exert antibody-dependent cell cytotoxicity (ADCC)[85]. Additionally, NK cells secrete pro-inflammatory cytokines, such as interferon-gamma (IFN-γ), which enhance the immune response by activating macrophages and promoting T cell proliferation[86]. These combined functions make NK cells essential for early defense against infections and tumors, as well as for maintaining immune homeostasis.

Chronic Inflammation and Immunosuppression in Cancer

Inflammation is a double-edged sword in cancer. While inflammation can destroy tumor cells, it can also promote tumorigenesis and metastasis. Persistent inflammatory conditions create a microenvironment rich in cytokines, growth factors, and reactive oxygen species (ROS) that can lead to DNA damage, promoting mutations and cancer progression[87,88]. For example, chronic inflammation caused by conditions like inflammatory bowel disease can lead to continuous cellular turnover and mutation accumulation, fostering colorectal cancer development[89,90]. Immunosuppression is a significant hurdle in cancer immunotherapy[91-93]. Tumors can create an immunosuppressive microenvironment by recruiting Tregs, immunosuppressive neutrophils (often referred to as polymorphonuclear myeloid-derived suppressor cells (PMN-MDSCs)), monocytes (often referred to as M-MDSCs), and by producing immunosuppressive cytokines like TGF-β and IL-10[92,94-99]. These cells and mediators inhibit the function of effector T cells and NK cells, allowing the tumor to evade immune detection and destruction. Inflammatory cells, such as tumor associated macrophages (TAMs) and tumor associated neutrophils (TANs), often support tumor growth by producing factors that promote angiogenesis, tissue remodeling, and suppression of adaptive immunity[100-104]. TAMs and TANs can create a pro-tumor environment by releasing cytokines that inhibit the activation and function of cytotoxic T cells[101,105]. Additionally, in some tumors, immune checkpoint molecules such as PD-L1 are expressed by cancer cells and TAMs. PD-L1 can bind to PD-1 on T cells thereby leading to reduced activity of T cells.

Immunotherapies like the antibodies directed against PD-1/anti-PD-L1 inhibit this suppressive mechanism and reinvigorating the T-cell immune response against cancer.

In addition to immunosuppressive mechanisms within the TME described above, also systemic inflammation influences cancer progression and poses a challenge in the treatment of cancer. Cancer cells can secrete factors that influence hematopoiesis, prompting the bone marrow to release immune cells that favor tumor progression[106,107]. Tumors, for instance, often produce granulocyte-colony stimulating factor (G-CSF) and granulocyte–macrophage colony-stimulating factor (GM-CSF), which enhances the production and mobilization of myeloid cells[100,108]. This tumor-induced inflammation skews hematopoiesis towards increased myeloid cell mobilization, creating a supportive environment for metastasis. Such systemic changes aid in establishing a metastatic niche, comprising of supportive, non-malignant stromal cells, soluble factors, vascular networks, essential nutrients and metabolic components, along with the structural architecture of the extracellular matrix[109]. Moreover, pre-clinical studies have shown that neutrophils promote metastasis formation through various mechanisms, such as inducing systemic immune suppression, aiding circulating cancer cells, fostering (pre-)metastatic niche formation, facilitating cancer cell infiltration into distant tissues, and reactivating dormant cancer cells[32-37,87,110,111].

In addition to tumor-induced expansion of the systemic myeloid compartment, tumors can induce immunosuppressive states in immune cells such as neutrophils and monocytes through reprogramming and polarization processes[107]. In tumor-associated macrophages and monocytes, this cancer-specific reprogramming alters their transcriptional profiles, enabling them to support tumor growth rather than initiating an immune response[112]. Similarly, findings on polarization highlight how tumors direct immune cells toward pro-tumor phenotypes that favor immune evasion and tumor growth, reinforcing the tumor's survival strategy and contributing to an immunosuppressive macro-environment[100].

The immune system's ability to maintain homeostasis, its robust innate and adaptive responses, and the critical crosstalk between these systems are essential for effective cancer defense[71]. In fact, systemic immunity is essential for successful cancer immunotherapy[113]. However, chronic inflammation and systemic immunosuppression disrupt the balance between adaptive and innate immunity, contribute significantly to cancer progression and pose a challenge to treatment. Understanding these dynamics is crucial for developing strategies that enhance anti-tumor immunity while minimizing immune-related adverse effects. As we continue to unravel the complexities of the systemic immune landscape in cancer, we pave the way for innovative therapeutic approaches that harness the power of the immune system to combat cancer effectively.

Immunotherapy and Breast Cancer

Immunotherapy has become an important pillar in the treatment of various cancer types. The development of immune checkpoint inhibitors, particularly anti-CTLA-4 and anti-PD-1 therapies, marked a revolutionary shift in cancer treatment. In the 1990s, James Allison's research demonstrated that CTLA-4 (cytotoxic T-lymphocyte-associated protein 4) serves as an immune checkpoint that inhibits T-cell activation[114]. His subsequent work led to the development of anti-CTLA-4 antibodies, demonstrating improved survival for stage IV melanoma patients that were previously untreatable[115]. This led to the approval of ipilimumab for metastatic melanoma by the U.S. Food and Drug Administration (FDA) and the European Medicines Agency (EMA) in 2011, representing the first checkpoint inhibitor in clinical use. Around the same time, researchers, including Tasuku Honjo, were studying PD-1 (programmed cell death protein 1)[116], another inhibitory receptor on T cells. Blocking PD-1 with anti-PD-1 antibodies, such as nivolumab and pembrolizumab, showed remarkable clinical efficacy, particularly in cancers like melanoma, lung cancer, and renal cell carcinoma[117,118]. Pembrolizumab received FDA approval for melanoma in 2014 and EMA approval in 2015. These therapies unlocked the immune system's potential to attack tumors, initiating a new era of cancer immunotherapy. Allison and Honjo were awarded the 2018 Nobel Prize in Physiology or Medicine for their pioneering discoveries in immune checkpoint blockade.

After the introduction of immune checkpoint inhibitors like anti-CTLA-4 and anti-PD-1/PD-L1 antibodies, the application of immunotherapy in breast cancer has evolved significantly. Historically, breast cancer has been considered less immunogenic because of the limited mutational load and the typically lower levels of tumor-infiltrating lymphocytes (TILs) compared to other cancers such as melanoma, which resulted in a greater focus on traditional therapies[119,120]. However, we now know that breast cancer is heterogeneous in terms of TILs, and that the TME of breast tumors can be classified into three types: immune-desert ("cold") tumors, which lack lymphocytes; immune-excluded tumors, where lymphocytes are confined to the surrounding stroma; and immune-infiltrated ("hot") tumors, which are rich in TILs[121]. Recent advancements have revealed the potential of immunotherapy in breast cancer, particularly for specific subtypes and disease stages[122].

Triple-Negative Breast Cancer

Metastatic TNBC has emerged as a key area for immunotherapy research due to its aggressive nature and higher levels of immune infiltration compared to other subtypes. In the early days of immunotherapy for metastatic TNBC, the efficacy of PD-1 blockade was limited in the later lines of treatment for mTNBC[123-125], underscoring the need for novel approaches to enhance tumor microenvironment sensitivity to this therapy. Preclinical studies suggested that low-dose chemotherapy and irradiation could have beneficial

immunomodulatory effects. Irradiation has been shown to induce type I interferons via the stimulator of interferon genes (STING) pathway, thereby enhancing T cell priming[126,127]. Additionally, cyclophosphamide has been reported to deplete regulatory T cells, potentially restoring effector functions of both T cells and natural killer cells[128]. Cisplatin can upregulate major histocompatibility complex class I expression and directly stimulate T cell function[129,130], while doxorubicin has been associated with depletion of immunosuppressive myeloid cells, increased type I interferon levels, and induction of immunogenic cell death[131-133]. To investigate the immunomodulatory effects of irradiation and low-dose chemotherapy, the TONIC trial was designed[134]. In this trial, patients with metastatic TNBC were randomized into five different 2-week induction arms: 1) control arm without an induction treatment, 2) irradiation, 3) cyclophosphamide, 4) cisplatin, and 5) doxorubicin, with all five groups subsequently receiving nivolumab. Based on clinical and translational findings, both doxorubicin and cyclophosphamide induction prior to nivolumab treatment appear to create a more favorable tumor microenvironment, potentially increasing response rates to PD-1 blockade in metastatic TNBC. As a result, both induction treatments are currently being further studied in larger comparative cohorts of unselected patients with mTNBC.

The IMpassion130 trial (NCT02425891) was pivotal in demonstrating the efficacy of atezolizumab, an anti-PD-L1 antibody, combined with nab-paclitaxel for patients with metastatic PD-L1-positive TNBC[135]. This study showed a significant improvement in progression-free survival (PFS) and overall survival (OS), leading to the FDA and EMA approvals of atezolizumab for this indication. In addition, the KEYNOTE-355 trial (NCT02819518) explored the use of pembrolizumab, an anti-PD-1 antibody, in combination with chemotherapy for metastatic PD-L1-positive TNBC. Results from this trial indicated that pembrolizumab significantly improved PFS and OS, solidifying its role in treating this aggressive breast cancer subtype[136].

The potential of immunotherapy extends to early-stage TNBC as well. The KEYNOTE-522 trial (NCT03036488) evaluated pembrolizumab as neoadjuvant therapy combined with chemotherapy. This study demonstrated that adding pembrolizumab to standard-of-care chemotherapy significantly increased the rate of pathological complete response (pCR) and overall survival (OS) in high-risk early-stage TNBC[137], resulting in its recent approval for this treatment setting. Consequently, immunotherapy combined with chemotherapy has become the standard of care for stage II–III TNBC. However, it remains unknown which patients might benefit from immune checkpoint inhibitors alone, without chemotherapy, and what the potential advantages of combining immune checkpoint inhibitors (ICIs) could be in this patient population.

Hormone Receptor-Positive Breast Cancer

Hormone receptor-positive (HR+) breast cancer, has been less responsive to immunotherapy, primarily due to lower levels of immune infiltration. However, there is ongoing research to evaluate the efficacy of immune checkpoint inhibitors in combination with hormonal

therapies or other agents. Preliminary studies have explored the use of anti-PD-1/PD-L1 therapies in combination with endocrine therapy for advanced HR+ breast cancer, with mixed results[138,139]. However, two positive phase III studies have demonstrated preliminary evidence of the potential for combining immune checkpoint inhibitors with therapies such as chemotherapy and endocrine therapy for HR+ breast cancer[140,141]. Additionally, data from the I-SPY2 trial, which investigated pembrolizumab in combination with chemotherapy, showed promising outcomes in HR+ breast cancer[142]. These advancements highlight the importance of integrating immunotherapy strategies into HR+ treatment regimens while continuing research to refine patient selection and identify predictive biomarkers.

HER2-Positive Breast Cancer

For HER2-positive breast cancer, the incorporation of immunotherapy is also under investigation. Studies are exploring combinations of anti-HER2 therapies (like trastuzumab) with immune checkpoint inhibitors to evaluate whether this approach can enhance the immune response against HER2-expressing tumors, generating conflicting results[143-145]. Recent trials, such as those investigating the use of pembrolizumab in combination with trastuzumab and chemotherapy for advanced HER2-positive breast cancer are ongoing. The aim is to determine whether this combination can improve outcomes in a population that historically has benefitted from targeted therapies.

Challenges and Future Directions

While immunotherapy has made significant strides in TNBC, challenges remain in effectively treating other breast cancer subtypes, particularly HR+ and HER2-positive cancers. Ongoing clinical trials are focusing on combinations of immune checkpoint inhibitors with targeted therapies, chemotherapy, or radiation to overcome resistance and enhance therapeutic efficacy. Research is also focused on identifying predictive biomarkers, such as stromal TILs and immune gene signatures, to more effectively select patients likely to benefit from immunotherapy. Furthermore, efforts are directed at unraveling the mechanisms by which myeloid cells contribute to the immune response, aiming to understand their dual roles in promoting or suppressing immune activity within the tumor microenvironment.

Moreover, monitoring the systemic immune landscape in cancer patients could provide valuable insights into how immune suppression beyond the tumor microenvironment influences disease progression and response to therapy. Systemic immunosuppression may compromise the body's ability to mount an effective anti-tumor immune response. By assessing immune markers in peripheral blood, we could identify broader immune dysfunctions that contribute to tumor growth and resistance to treatments like immunotherapy. Understanding this relationship could guide new strategies to counteract immune suppression systemically, potentially improving therapeutic outcomes across cancer types.

Vulvar intraepithelial neoplasia (VIN)

While breast cancer develops as a result of mutations in the DNA, there are also virus induced cancers. Viruses can cause cancer by inserting their genetic material into host cells, which can disrupt normal cellular functions and lead to uncontrolled cell growth. Some viruses, like human papillomavirus (HPV) and Epstein-Barr virus (EBV), produce proteins that interfere with tumor-suppressor genes or activate oncogenes, driving the development of cancerous cells over time[146]. The most common transforming virus is HPV. HPV can cause several types of cancer, including cervical, uterus, head and neck, anal, penile, vaginal and vulvar cancers. Though not all cases of the carcinomas listed above are a result of an HPV infection, the vast majority are, and some of these cancer types remain the main cause of cancer-related death in women in certain areas of the world[1,3]. HPV causes cancer by producing two key oncoproteins, E6 and E7, which interfere with the cell's tumor-suppressor mechanisms. E6 binds to and degrades p53, a protein that regulates cell death, while E7 inactivates the retinoblastoma protein (pRb), disrupting cell cycle control and promoting unregulated cell division, leading to cancer development[146]. HPV-induced tumors might theoretically be more straightforward to be detected and eradicated by the immune system because they express viral epitopes. These epitopes can make tumors appear more foreign to the immune system, potentially enhancing the body's capacity to recognize and eliminate cancer cells. Despite this, spontaneous regression of tumors remains rare in clinical practice.

One of the cancer types that is often HPV-induced in vulvar cancer[147]. The pre-malignant stage of vulvar cancer is termed vulvar intraepithelial neoplasia (VIN). Though VIN lesions are not yet cancerous, they cause considerable discomfort to the women affected. Spontaneous regression of the condition is uncommon, occurring in only 1%–2% of women, while progression to vulvar cancer is observed in approximately 2%–8% of cases[148-151]. The current treatment options for VIN, which include surgical excision, laser therapy, and topical medications, often lead to mutilating or otherwise uncomfortable side effects. These treatments can severely impact a woman's sexual health and overall quality of life. Additionally, the responses to these treatments are frequently not durable, leading to high rates of recurrence.

Given these challenges, the development of novel immunotherapeutic approaches holds great promise. Immunotherapy could target the viral components of HPV-induced lesions, providing a more effective and less invasive treatment option and hopefully leading to more durable responses.

Scope of this Thesis

In this thesis, two parts can be distinguished. The first part consists of **chapters 2, 3, 4** and **5** and has a rather fundamental-translational character. In these chapters, the focus lies on

assessing the influence of breast cancer subtype and disease stage on the systemic immune landscape of breast cancer patients, and what the impact is of (triple negative) breast cancer on functional aspects of circulating immune cells, especially neutrophils. The aim of the studies described in the first part of this thesis was to unravel the influence of breast cancer subtypes and disease stages on the composition and function of the systemic immune system. We hypothesized that comprehensive immune profiling of breast cancer patients, compared to healthy donor reference profiles, would provide critical insights into systemic inflammatory states and immunosuppressive mechanisms.

The second part of this thesis, encompassing **chapters 6, 7,** and **8**, presents clinical trials in which I contributed as a member of the translational research team. The commonality of this part lies in investigating treatment effects, covering a range of approaches. These include examining treatment-induced changes in circulating immune cells in relation to specific clinical outcomes, as well as immunomonitoring of specific T cells that recognize antigens introduced by therapeutic vaccines. Regarding this second part of this thesis, it was my aim to monitor overall changes in the immune profiles of patients with breast cancer or VIN lesions during immunotherapy. This research explored varying response dynamics and immunosuppressive mechanisms, which may guide more effective immunotherapeutic interventions and lead to novel strategies to improve immunotherapy responses.

Chapter 2 provides a comprehensive method to assess the direct *ex vivo* motility and migration of freshly isolated human neutrophils, offering valuable insights into their behavior. Understanding neutrophil motility and migration is critical for comprehending immune responses and inflammatory processes, as it sheds light on their substantial contribution to cancer progression. Neutrophils possess a remarkable migratory capacity, enabling them to extravasate and infiltrate tissues but also tumors, where they carry out essential or detrimental effector functions, depending on the context. This ability contributes to their pivotal role in orchestrating tumor-induced systemic inflammation and their growing recognition as key players in both the initiation and progression of cancer.

The dysregulating properties of cancer reaches beyond the local tumor microenvironment, however, it remains largely unknown how the systemic immune landscape is modified during breast cancer progression and whether this is breast cancer subtype dependent. In **chapter 3**, I describe a comprehensive analysis of the systemic immune landscape in a large cohort of breast cancer patients, covering different tumor molecular subtypes and disease stages, alongside a control group of healthy donors. Employing multi-parameter flow cytometry, we assessed the abundance, phenotype, and activation status of various innate and adaptive immune cell populations across 420 peripheral blood samples. Because all blood samples were analyzed immediately after collection, we were able to include the often overlooked granulocyte populations, including neutrophils and eosinophils, in our analysis. Our data indicate that the immune landscape

is more markedly altered in metastatic breast cancer compared to non-metastatic cases, with the most significant changes observed in the triple-negative subtype.

In **chapter 4**, we comprehensively profiled the systemic immune landscape in patients with TNBC at distinct disease stages, to understand how cancer progression and treatment history shape the systemic immune landscape. We performed multi-parameter flow cytometry analysis to assess the global systemic immune landscape, including often overlooked granulocytes. We demonstrated that the systemic immune landscape of TNBC patients differs from that of healthy donors in a stage-dependent manner, with some—but not all—of these alterations attributable to prior chemotherapy treatment.

In **chapter 5**, I describe a research project in which we conducted single-cell RNA sequencing on fresh blood samples from patients with mTNBC and HDs, without any prior immune cell type enrichments. While this project did not reveal clear differences between HDs and mTNBC patients, the results were inconclusive due to the small sample size and the considerable heterogeneity observed. As such, we do not conclude that no differences exist between the two groups. Alongside detailing the methods and results, I also offer recommendations for future studies to help others avoid the challenges we encountered. These insights aim to improve experimental design and optimize the likelihood of generating more definitive results.

Chapter 6 describes the results of the adaptive phase II BELLINI trial, which explored the potential of short-term immune checkpoint inhibition (ICI) to induce immune activation in patients with non-metastatic TNBC. The aim was to explore the potential of treating non-metastatic TNBC patients with neoadjuvant ICI in the absence of chemotherapy. This window-of-opportunity trial describes three cohorts, each showing a response rate of 50-60%. In cohorts 1 and 2, the response was measured as a biological endpoint, while in cohort 3, pathological complete response (pCR) was used as the measure of response. Flow cytometry of fresh blood samples showed an increase in Ki-67+ cells within the PD-1+ conventional CD4+ T cell population in responders, with a similar trend observed for CD8+ T cells. The findings of the BELLINI-trial demonstrate that neoadjuvant immunotherapy, administered without chemotherapy, shows promising efficacy and warrants further investigation in patients with early-stage TNBC.

The translational research project described in **chapter 7** aims to identify factors associated with the response of mTNBC patients to PD-1 blockade (TONIC trial). Comprehensive immune profiling of fresh blood samples and paired tumor biopsies revealed that both systemic and intratumoral eosinophils increased in responders following PD-1 blockade, a pattern not observed in non-responders. *In vivo* experiments using spontaneous mouse models of primary and metastatic breast cancer further demonstrated the critical role of eosinophils in mediating the response to immune checkpoint blockade. These findings highlight that therapeutic engagement of eosinophils could enhance responses to immune checkpoint inhibitors in breast cancer.

Chapter 8 presents the results of a phase I/II clinical trial in which patients with usual vulvar intraepithelial neoplasia (uVIN) received a genetically optimized HPV-16 E6/E7 DNA tattoo vaccination. The primary endpoint of the trial was the induction of an immunological response. To assess this, I conducted ex vivo functional assays using patients' peripheral blood mononuclear cells to monitor systemic HPV-specific T cell responses before and after treatment. In addition to immune monitoring, the chapter also reports on the safety and clinical outcomes of the vaccination.

Finally, the results described in this thesis are summarized and discussed in **chapter 9**. In this chapter I highlight future perspectives of the work presented and focus on potential new research avenues.

References

1 Bray, F. *et al.* Global cancer statistics 2022: GLOBOCAN estimates of incidence and mortality worldwide for 36 cancers in 185 countries. *CA Cancer J Clin* **74**, 229-263 (2024). https://doi.org/10.3322/caac.21834

2 IKNL. *Nederlandse Kanker Registratie*, <https://nkr-cijfers.iknl.nl/viewer/incidentie-per-jaar> (2024).

3 Explorer, S. *An interactive website for SEER cancer statistics*, <https://seer.cancer.gov/statistics-network/explorer/> (2023).

4 Tan, P. H. *et al.* The 2019 World Health Organization classification of tumours of the breast. *Histopathology* **77**, 181-185 (2020). https://doi.org/10.1111/his.14091

5 Harbeck, N. *et al.* Breast cancer. *Nat Rev Dis Primers* **5**, 66 (2019). https://doi.org/10.1038/s41572-019-0111-2

6 Arpino, G., Bardou, V. J., Clark, G. M. & Elledge, R. M. Infiltrating lobular carcinoma of the breast: tumor characteristics and clinical outcome. *Breast Cancer Res* **6**, R149-156 (2004). https://doi.org/10.1186/bcr767

7 Dieci, M. V., Orvieto, E., Dominici, M., Conte, P. & Guarneri, V. Rare breast cancer subtypes: histological, molecular, and clinical peculiarities. *Oncologist* **19**, 805-813 (2014). https://doi.org/10.1634/theoncologist.2014-0108

8 Waks, A. G. & Winer, E. P. Breast Cancer Treatment: A Review. *JAMA* **321**, 288-300 (2019). https://doi.org/10.1001/jama.2018.19323

9 Zhang, M. H., Man, H. T., Zhao, X. D., Dong, N. & Ma, S. L. Estrogen receptor-positive breast cancer molecular signatures and therapeutic potentials (Review). *Biomed Rep* **2**, 41-52 (2014). https://doi.org/10.3892/br.2013.187

10 Allison, K. H. *et al.* Estrogen and Progesterone Receptor Testing in Breast Cancer: ASCO/CAP Guideline Update. *J Clin Oncol* **38**, 1346-1366 (2020). https://doi.org/10.1200/JCO.19.02309

11 Early Breast Cancer Trialists' Collaborative, G. *et al.* Relevance of breast cancer hormone receptors and other factors to the efficacy of adjuvant tamoxifen: patient-level meta-analysis of randomised trials. *Lancet* **378**, 771-784 (2011). https://doi.org/10.1016/S0140-6736(11)60993-8

12 Voorwerk, L. *et al.* Immune landscape of breast tumors with low and intermediate estrogen receptor expression. *NPJ Breast Cancer* **9**, 39 (2023). https://doi.org/10.1038/s41523-023-00543-0

13 Orrantia-Borunda, E., Anchondo-Nunez, P., Acuna-Aguilar, L. E., Gomez-Valles, F. O. & Ramirez-Valdespino, C. A. in *Breast Cancer* (ed H. N. Mayrovitz) (2022).

14 Nicolini, A., Ferrari, P. & Duffy, M. J. Prognostic and predictive biomarkers in breast cancer: Past, present and future. *Semin Cancer Biol* **52**, 56-73 (2018). https://doi.org/10.1016/j.semcancer.2017.08.010

15 Purdie, C. A. *et al.* Progesterone receptor expression is an independent prognostic variable in early breast cancer: a population-based study. *Br J Cancer* **110**, 565-572 (2014). https://doi.org/10.1038/bjc.2013.756

16 Cheang, M. C. *et al.* Ki67 index, HER2 status, and prognosis of patients with luminal B breast cancer. *J Natl Cancer Inst* **101**, 736-750 (2009). https://doi.org/10.1093/jnci/djp082

17 Intrieri, T., Manneschi, G. & Caldarella, A. 10-year survival in female breast cancer patients according to ER, PR and HER2 expression: a cancer registry population-based analysis. *J Cancer Res Clin Oncol* **149**, 4489-4496 (2023). https://doi.org/10.1007/s00432-022-04245-1

18 Loibl, S. & Gianni, L. HER2-positive breast cancer. *Lancet* **389**, 2415-2429 (2017). https://doi.org/10.1016/S0140-6736(16)32417-5

19 Howlader, N., Cronin, K. A., Kurian, A. W. & Andridge, R. Differences in Breast Cancer Survival by Molecular Subtypes in the United States. *Cancer Epidemiol Biomarkers Prev* **27**, 619-626 (2018). https://doi.org/10.1158/1055-9965.EPI-17-0627

20 Foulkes, W. D., Smith, I. E. & Reis-Filho, J. S. Triple-negative breast cancer. *N Engl J Med* **363**, 1938-1948 (2010). https://doi.org/10.1056/NEJMra1001389

21 Paik, S. *et al.* A multigene assay to predict recurrence of tamoxifen-treated, node-negative breast cancer. *N Engl J Med* **351**, 2817-2826 (2004). https://doi.org/10.1056/NEJMoa041588

22 van 't Veer, L. J. *et al.* Gene expression profiling predicts clinical outcome of breast cancer. *Nature* **415**, 530-536 (2002). https://doi.org/10.1038/415530a

23 Nielsen, T. O. *et al.* A comparison of PAM50 intrinsic subtyping with immunohistochemistry and clinical prognostic factors in tamoxifen-treated estrogen receptor-positive breast cancer. *Clin Cancer Res* **16**, 5222-5232 (2010). https://doi.org/10.1158/1078-0432.CCR-10-1282

24 Perou, C. M. *et al.* Molecular portraits of human breast tumours. *Nature* **406**, 747-752 (2000). https://doi.org/10.1038/35021093

25 Ohnstad, H. O. *et al.* Prognostic value of PAM50 and risk of recurrence score in patients with early-stage breast cancer with long-term follow-up. *Breast Cancer Res* **19**, 120 (2017). https://doi.org/10.1186/s13058-017-0911-9

26 Cheru, N., Hafler, D. A. & Sumida, T. S. Regulatory T cells in peripheral tissue tolerance and diseases. *Front Immunol* **14**, 1154575 (2023). https://doi.org/10.3389/fimmu.2023.1154575

27 Dominguez-Villar, M. & Hafler, D. A. Regulatory T cells in autoimmune disease. *Nat Immunol* **19**, 665-673 (2018). https://doi.org/10.1038/s41590-018-0120-4

28 Putra, A. *et al.* The Role of TNF-alpha induced MSCs on Suppressive Inflammation by Increasing TGF-beta and IL-10. *Open Access Maced J Med Sci* **6**, 1779-1783 (2018). https://doi.org/10.3889/oamjms.2018.404

29 Ip, W. K. E., Hoshi, N., Shouval, D. S., Snapper, S. & Medzhitov, R. Anti-inflammatory effect of IL-10 mediated by metabolic reprogramming of macrophages. *Science* **356**, 513-519 (2017). https://doi.org/10.1126/science.aal3535

30 Ouyang, W. & O'Garra, A. IL-10 Family Cytokines IL-10 and IL-22: from Basic Science to Clinical Translation. *Immunity* **50**, 871-891 (2019). https://doi.org/10.1016/j.immuni.2019.03.020

31 Wynn, T. A. & Vannella, K. M. Macrophages in Tissue Repair, Regeneration, and Fibrosis. *Immunity* **44**, 450-462 (2016). https://doi.org/10.1016/j.immuni.2016.02.015

32 Coffelt, S. B. *et al.* IL-17-producing gammadelta T cells and neutrophils conspire to promote breast cancer metastasis. *Nature* **522**, 345-348 (2015). https://doi.org/10.1038/nature14282

33 Jablonska, J., Lang, S., Sionov, R. V. & Granot, Z. The regulation of pre-metastatic niche formation by neutrophils. *Oncotarget* **8**, 112132-112144 (2017). https://doi.org/10.18632/oncotarget.22792

34 Kowanetz, M. *et al.* Granulocyte-colony stimulating factor promotes lung metastasis through mobilization of Ly6G+Ly6C+ granulocytes. *Proc Natl Acad Sci U S A* **107**, 21248-21255 (2010). https://doi.org/10.1073/pnas.1015855107

35 Sanz-Moreno, V. & Balkwill, F. R. Mets and NETs: The Awakening Force. *Immunity* **49**, 798-800 (2018). https://doi.org/10.1016/j.immuni.2018.11.009

36 Szczerba, B. M. *et al.* Neutrophils escort circulating tumour cells to enable cell cycle progression. *Nature* **566**, 553-557 (2019). https://doi.org/10.1038/s41586-019-0915-y

37 Yang, L. *et al.* DNA of neutrophil extracellular traps promotes cancer metastasis via CCDC25. *Nature* **583**, 133-138 (2020). https://doi.org/10.1038/s41586-020-2394-6

38 Ethier, J. L., Desautels, D., Templeton, A., Shah, P. S. & Amir, E. Prognostic role of neutrophil-to-lymphocyte ratio in breast cancer: a systematic review and meta-analysis. *Breast Cancer Res* **19**, 2 (2017). https://doi.org/10.1186/s13058-016-0794-1

39 Guo, W. *et al.* Prognostic value of neutrophil-to-lymphocyte ratio and platelet-to-lymphocyte ratio for breast cancer patients: An updated meta-analysis of 17079 individuals. *Cancer Med* **8**, 4135-4148 (2019). https://doi.org/10.1002/cam4.2281

40 Krenn-Pilko, S. *et al.* The elevated preoperative derived neutrophil-to-lymphocyte ratio predicts poor clinical outcome in breast cancer patients. *Tumour Biol* **37**, 361-368 (2016). https://doi.org/10.1007/s13277-015-3805-4

41 Liu, J. *et al.* Systemic immune-inflammation index, neutrophil-to-lymphocyte ratio, platelet-to-lymphocyte ratio can predict clinical outcomes in patients with metastatic non-small-cell lung cancer treated with nivolumab. *J Clin Lab Anal* **33**, e22964 (2019). https://doi.org/10.1002/jcla.22964

42 Shao, Y. *et al.* Prognostic value of pretreatment neutrophil-to-lymphocyte ratio in renal cell carcinoma: a systematic review and meta-analysis. *BMC Urol* **20**, 90 (2020). https://doi.org/10.1186/s12894-020-00665-8

43 Templeton, A. J. *et al.* Prognostic role of neutrophil-to-lymphocyte ratio in solid tumors: a systematic review and meta-analysis. *J Natl Cancer Inst* **106**, dju124 (2014). https://doi.org/10.1093/jnci/dju124

44 Blomberg, O. S. *et al.* IL-5-producing CD4(+) T cells and eosinophils cooperate to enhance response to immune checkpoint blockade in breast cancer. *Cancer Cell* **41**, 106-123 e110 (2023). https://doi.org/10.1016/j.ccell.2022.11.014

45 Simon, S. C. S. *et al.* Eosinophil accumulation predicts response to melanoma treatment with immune checkpoint inhibitors. *Oncoimmunology* **9**, 1727116 (2020). https://doi.org/10.1080/2162402X.2020.1727116

46 Li, D. & Wu, M. Pattern recognition receptors in health and diseases. *Signal Transduct Target Ther* **6**, 291 (2021). https://doi.org/10.1038/s41392-021-00687-0
47 Zindel, J. & Kubes, P. DAMPs, PAMPs, and LAMPs in Immunity and Sterile Inflammation. *Annu Rev Pathol* **15**, 493-518 (2020). https://doi.org/10.1146/annurev-pathmechdis-012419-032847
48 Takeda, K., Kaisho, T. & Akira, S. Toll-like receptors. *Annu Rev Immunol* **21**, 335-376 (2003). https://doi.org/10.1146/annurev.immunol.21.120601.141126
49 Zhong, Y., Kinio, A. & Saleh, M. Functions of NOD-Like Receptors in Human Diseases. *Front Immunol* **4**, 333 (2013). https://doi.org/10.3389/fimmu.2013.00333
50 Philpott, D. J. & Girardin, S. E. The role of Toll-like receptors and Nod proteins in bacterial infection. *Mol Immunol* **41**, 1099-1108 (2004). https://doi.org/10.1016/j.molimm.2004.06.012
51 de Oliveira, S., Rosowski, E. E. & Huttenlocher, A. Neutrophil migration in infection and wound repair: going forward in reverse. *Nat Rev Immunol* **16**, 378-391 (2016). https://doi.org/10.1038/nri.2016.49
52 Merle, N. S., Church, S. E., Fremeaux-Bacchi, V. & Roumenina, L. T. Complement System Part I - Molecular Mechanisms of Activation and Regulation. *Front Immunol* **6**, 262 (2015). https://doi.org/10.3389/fimmu.2015.00262
53 Merle, N. S., Noe, R., Halbwachs-Mecarelli, L., Fremeaux-Bacchi, V. & Roumenina, L. T. Complement System Part II: Role in Immunity. *Front Immunol* **6**, 257 (2015). https://doi.org/10.3389/fimmu.2015.00257
54 Schalper, K. A. *et al.* Elevated serum interleukin-8 is associated with enhanced intratumor neutrophils and reduced clinical benefit of immune-checkpoint inhibitors. *Nat Med* **26**, 688-692 (2020). https://doi.org/10.1038/s41591-020-0856-x
55 Yuen, K. C. *et al.* High systemic and tumor-associated IL-8 correlates with reduced clinical benefit of PD-L1 blockade. *Nat Med* **26**, 693-698 (2020). https://doi.org/10.1038/s41591-020-0860-1
56 He, T. *et al.* The role of CD8(+) T-cells in colorectal cancer immunotherapy. *Heliyon* **10**, e33144 (2024). https://doi.org/10.1016/j.heliyon.2024.e33144
57 Pardoll, D. M. The blockade of immune checkpoints in cancer immunotherapy. *Nat Rev Cancer* **12**, 252-264 (2012). https://doi.org/10.1038/nrc3239
58 Rosenberg, S. A. & Restifo, N. P. Adoptive cell transfer as personalized immunotherapy for human cancer. *Science* **348**, 62-68 (2015). https://doi.org/10.1126/science.aaa4967
59 Sterner, R. C. & Sterner, R. M. CAR-T cell therapy: current limitations and potential strategies. *Blood Cancer J* **11**, 69 (2021). https://doi.org/10.1038/s41408-021-00459-7
60 Zhu, J., Yamane, H. & Paul, W. E. Differentiation of effector CD4 T cell populations (*). *Annu Rev Immunol* **28**, 445-489 (2010). https://doi.org/10.1146/annurev-immunol-030409-101212
61 Walker, J. A. & McKenzie, A. N. J. T(H)2 cell development and function. *Nat Rev Immunol* **18**, 121-133 (2018). https://doi.org/10.1038/nri.2017.118
62 Romagnani, S. The role of lymphocytes in allergic disease. *J Allergy Clin Immunol* **105**, 399-408 (2000). https://doi.org/10.1067/mai.2000.104575
63 Dong, C. Defining the T(H)17 cell lineage. *Nat Rev Immunol* **21**, 618 (2021). https://doi.org/10.1038/s41577-021-00596-x
64 Yasuda, K., Takeuchi, Y. & Hirota, K. The pathogenicity of Th17 cells in autoimmune diseases. *Semin Immunopathol* **41**, 283-297 (2019). https://doi.org/10.1007/s00281-019-00733-8
65 Hirahara, K. & Nakayama, T. CD4+ T-cell subsets in inflammatory diseases: beyond the Th1/Th2 paradigm. *Int Immunol* **28**, 163-171 (2016). https://doi.org/10.1093/intimm/dxw006
66 Akkaya, M., Kwak, K. & Pierce, S. K. B cell memory: building two walls of protection against pathogens. *Nat Rev Immunol* **20**, 229-238 (2020). https://doi.org/10.1038/s41577-019-0244-2
67 Tay, M. Z., Wiehe, K. & Pollara, J. Antibody-Dependent Cellular Phagocytosis in Antiviral Immune Responses. *Front Immunol* **10**, 332 (2019). https://doi.org/10.3389/fimmu.2019.00332
68 Uribe-Querol, E. & Rosales, C. Phagocytosis: Our Current Understanding of a Universal Biological Process. *Front Immunol* **11**, 1066 (2020). https://doi.org/10.3389/fimmu.2020.01066
69 Fridman, W. H. *et al.* B cells and tertiary lymphoid structures as determinants of tumour immune contexture and clinical outcome. *Nat Rev Clin Oncol* **19**, 441-457 (2022). https://doi.org/10.1038/s41571-022-00619-z
70 Helmink, B. A. *et al.* B cells and tertiary lymphoid structures promote immunotherapy response. *Nature* **577**, 549-555 (2020). https://doi.org/10.1038/s41586-019-1922-8
71 Hiam-Galvez, K. J., Allen, B. M. & Spitzer, M. H. Systemic immunity in cancer. *Nat Rev Cancer* **21**, 345-359 (2021). https://doi.org/10.1038/s41568-021-00347-z
72 Yuen, G. J., Demissie, E. & Pillai, S. B lymphocytes and cancer: a love-hate relationship. *Trends Cancer* **2**, 747-757 (2016). https://doi.org/10.1016/j.trecan.2016.10.010
73 Sharma, A., Jasrotia, S. & Kumar, A. Effects of Chemotherapy on the Immune System: Implications for Cancer Treatment and Patient Outcomes. *Naunyn Schmiedebergs Arch Pharmacol* **397**, 2551-2566 (2024). https://doi.org/10.1007/s00210-023-02781-2
74 Verma, R. *et al.* Lymphocyte depletion and repopulation after chemotherapy for primary breast cancer. *Breast Cancer Res* **18**, 10 (2016). https://doi.org/10.1186/s13058-015-0669-x
75 Iwasaki, A. & Medzhitov, R. Control of adaptive immunity by the innate immune system. *Nat Immunol* **16**, 343-353 (2015). https://doi.org/10.1038/ni.3123
76 Cui, Q. *et al.* Immune signature and phagocytosis of circulating DC subsets in healthy adults during aging. *Int Immunopharmacol* **130**, 111715 (2024). https://doi.org/10.1016/j.intimp.2024.111715
77 Bourdely, P. *et al.* Transcriptional and Functional Analysis of CD1c(+) Human Dendritic Cells Identifies a CD163(+) Subset Priming CD8(+)CD103(+) T Cells. *Immunity* **53**, 335-352 e338 (2020). https://doi.org/10.1016/j.immuni.2020.06.002
78 Hilligan, K. L. & Ronchese, F. Antigen presentation by dendritic cells and their instruction of CD4+ T helper cell responses. *Cell Mol Immunol* **17**, 587-599 (2020). https://doi.org/10.1038/s41423-020-0465-0
79 Heras-Murillo, I., Adan-Barrientos, I., Galan, M., Wculek, S. K. & Sancho, D. Dendritic cells as orchestrators of anticancer immunity and immunotherapy. *Nat Rev Clin Oncol* **21**, 257-277 (2024). https://doi.org/10.1038/s41571-024-00859-1
80 Collin, M. & Bigley, V. Human dendritic cell subsets: an update. *Immunology* **154**, 3-20 (2018). https://doi.org/10.1111/imm.12888
81 Kiessler, M. *et al.* Tumor-infiltrating plasmacytoid dendritic cells are associated with survival in human colon cancer. *J Immunother Cancer* **9** (2021). https://doi.org/10.1136/jitc-2020-001813
82 Swiecki, M. & Colonna, M. The multifaceted biology of plasmacytoid dendritic cells. *Nat Rev Immunol* **15**, 471-485 (2015). https://doi.org/10.1038/nri3865
83 Wculek, S. K. *et al.* Dendritic cells in cancer immunology and immunotherapy. *Nat Rev Immunol* **20**, 7-24 (2020). https://doi.org/10.1038/s41577-019-0210-z
84 Zhou, B., Lawrence, T. & Liang, Y. The Role of Plasmacytoid Dendritic Cells in Cancers. *Front Immunol* **12**, 749190 (2021). https://doi.org/10.3389/fimmu.2021.749190
85 Vivier, E., Tomasello, E., Baratin, M., Walzer, T. & Ugolini, S. Functions of natural killer cells. *Nat Immunol* **9**, 503-510 (2008). https://doi.org/10.1038/ni1582
86 Wolf, N. K., Kissiov, D. U. & Raulet, D. H. Roles of natural killer cells in immunity to cancer, and applications to immunotherapy. *Nat Rev Immunol* **23**, 90-105 (2023). https://doi.org/10.1038/s41577-022-00732-1
87 McDowell, S. A. C. *et al.* Neutrophil oxidative stress mediates obesity-associated vascular dysfunction and metastatic transmigration. *Nat Cancer* **2**, 545-562 (2021). https://doi.org/10.1038/s43018-021-00194-9
88 Kennel, K. B. & Greten, F. R. Immune cell - produced ROS and their impact on tumor growth and metastasis. *Redox Biol* **42**, 101891 (2021). https://doi.org/10.1016/j.redox.2021.101891
89 Axelrad, J. E., Lichtiger, S. & Yajnik, V. Inflammatory bowel disease and cancer: The role of inflammation, immunosuppression, and cancer treatment. *World J Gastroenterol* **22**, 4794-4801 (2016). https://doi.org/10.3748/wjg.v22.i20.4794
90 Xie, J. & Itzkowitz, S. H. Cancer in inflammatory bowel disease. *World J Gastroenterol* **14**, 378-389 (2008). https://doi.org/10.3748/wjg.14.378
91 Gabrilovich, D. I., Ostrand-Rosenberg, S. & Bronte, V. Coordinated regulation of myeloid cells by tumours. *Nat Rev Immunol* **12**, 253-268 (2012). https://doi.org/10.1038/nri3175
92 Jaillon, S. *et al.* Neutrophil diversity and plasticity in tumour progression and therapy. *Nat Rev Cancer* **20**, 485-503 (2020). https://doi.org/10.1038/s41568-020-0281-y
93 Cane, S. *et al.* The Endless Saga of Monocyte Diversity. *Front Immunol* **10**, 1786 (2019). https://doi.org/10.3389/fimmu.2019.01786
94 Mengos, A. E., Gastineau, D. A. & Gustafson, M. P. The CD14(+)HLA-DR(lo/neg) Monocyte: An Immunosuppressive Phenotype That Restrains Responses to Cancer Immunotherapy. *Front Immunol* **10**, 1147 (2019). https://doi.org/10.3389/fimmu.2019.01147
95 Kiss, M., Caro, A. A., Raes, G. & Laoui, D. Systemic Reprogramming of Monocytes in Cancer. *Front Oncol* **10**, 1399 (2020). https://doi.org/10.3389/fonc.2020.01399

96 Togashi, Y., Shitara, K. & Nishikawa, H. Regulatory T cells in cancer immunosuppression - implications for anticancer therapy. *Nat Rev Clin Oncol* **16**, 356-371 (2019). https://doi.org/10.1038/s41571-019-0175-7

97 Hedrick, C. C. & Malanchi, I. Neutrophils in cancer: heterogeneous and multifaceted. *Nat Rev Immunol* **22**, 173-187 (2022). https://doi.org/10.1038/s41577-021-00571-6

98 Shaul, M. E. & Fridlender, Z. G. Tumour-associated neutrophils in patients with cancer. *Nat Rev Clin Oncol* **16**, 601-620 (2019). https://doi.org/10.1038/s41571-019-0222-4

99 Kos, K. *et al.* Tumor-educated T(regs) drive organ-specific metastasis in breast cancer by impairing NK cells in the lymph node niche. *Cell Rep* **38**, 110447 (2022). https://doi.org/10.1016/j.celrep.2022.110447

100 Ruffolo, L. I. *et al.* GM-CSF drives myelopoiesis, recruitment and polarisation of tumour-associated macrophages in cholangiocarcinoma and systemic blockade facilitates antitumour immunity. *Gut* **71**, 1386-1398 (2022). https://doi.org/10.1136/gutjnl-2021-324109

101 Noy, R. & Pollard, J. W. Tumor-associated macrophages: from mechanisms to therapy. *Immunity* **41**, 49-61 (2014). https://doi.org/10.1016/j.immuni.2014.06.010

102 Wu, L. & Zhang, X. H. Tumor-Associated Neutrophils and Macrophages-Heterogenous but Not Chaotic. *Front Immunol* **11**, 553967 (2020). https://doi.org/10.3389/fimmu.2020.553967

103 Coussens, L. M. & Werb, Z. Inflammation and cancer. *Nature* **420**, 860-867 (2002). https://doi.org/10.1038/nature01322

104 Pan, Y., Yu, Y., Wang, X. & Zhang, T. Tumor-Associated Macrophages in Tumor Immunity. *Front Immunol* **11**, 583084 (2020). https://doi.org/10.3389/fimmu.2020.583084

105 Gabrilovich, D. I. & Nagaraj, S. Myeloid-derived suppressor cells as regulators of the immune system. *Nat Rev Immunol* **9**, 162-174 (2009). https://doi.org/10.1038/nri2506

106 Heissig, B. *et al.* Recruitment of stem and progenitor cells from the bone marrow niche requires MMP-9 mediated release of kit-ligand. *Cell* **109**, 625-637 (2002). https://doi.org/10.1016/s0092-8674(02)00754-7

107 Garner, H. & de Visser, K. E. Immune crosstalk in cancer progression and metastatic spread: a complex conversation. *Nat Rev Immunol* **20**, 483-497 (2020). https://doi.org/10.1038/s41577-019-0271-z

108 Casbon, A. J. *et al.* Invasive breast cancer reprograms early myeloid differentiation in the bone marrow to generate immunosuppressive neutrophils. *Proc Natl Acad Sci U S A* **112**, E566-575 (2015). https://doi.org/10.1073/pnas.1424927112

109 Psaila, B. & Lyden, D. The metastatic niche: adapting the foreign soil. *Nat Rev Cancer* **9**, 285-293 (2009). https://doi.org/10.1038/nrc2621

110 Park, J. *et al.* Cancer cells induce metastasis-supporting neutrophil extracellular DNA traps. *Sci Transl Med* **8**, 361ra138 (2016). https://doi.org/10.1126/scitranslmed.aag1711

111 Zheng, C. *et al.* Neutrophils in triple-negative breast cancer: an underestimated player with increasingly recognized importance. *Breast Cancer Res* **25**, 88 (2023). https://doi.org/10.1186/s13058-023-01676-7

112 Cassetta, L. *et al.* Human Tumor-Associated Macrophage and Monocyte Transcriptional Landscapes Reveal Cancer-Specific Reprogramming, Biomarkers, and Therapeutic Targets. *Cancer Cell* **35**, 588-602 e510 (2019). https://doi.org/10.1016/j.ccell.2019.02.009

113 Spitzer, M. H. *et al.* Systemic Immunity Is Required for Effective Cancer Immunotherapy. *Cell* **168**, 487-502 e415 (2017). https://doi.org/10.1016/j.cell.2016.12.022

114 Leach, D. R., Krummel, M. F. & Allison, J. P. Enhancement of antitumor immunity by CTLA-4 blockade. *Science* **271**, 1734-1736 (1996). https://doi.org/10.1126/science.271.5256.1734

115 Hodi, F. S. *et al.* Improved survival with ipilimumab in patients with metastatic melanoma. *N Engl J Med* **363**, 711-723 (2010). https://doi.org/10.1056/NEJMoa1003466

116 Ishida, Y., Agata, Y., Shibahara, K. & Honjo, T. Induced expression of PD-1, a novel member of the immunoglobulin gene superfamily, upon programmed cell death. *EMBO J* **11**, 3887-3895 (1992). https://doi.org/10.1002/j.1460-2075.1992.tb05481.x

117 Brahmer, J. R. *et al.* Phase I study of single-agent anti-programmed death-1 (MDX-1106) in refractory solid tumors: safety, clinical activity, pharmacodynamics, and immunologic correlates. *J Clin Oncol* **28**, 3167-3175 (2010). https://doi.org/10.1200/JCO.2009.26.7609

118 Topalian, S. L. *et al.* Safety, activity, and immune correlates of anti-PD-1 antibody in cancer. *N Engl J Med* **366**, 2443-2454 (2012). https://doi.org/10.1056/NEJMoa1200690

119 Alexandrov, L. B. *et al.* Signatures of mutational processes in human cancer. *Nature* **500**, 415-421 (2013). https://doi.org/10.1038/nature12477

120 Schumacher, T. N. & Schreiber, R. D. Neoantigens in cancer immunotherapy. *Science* **348**, 69-74 (2015). https://doi.org/10.1126/science.aaa4971

121 El Bairi, K. *et al.* The tale of TILs in breast cancer: A report from The International Immuno-Oncology Biomarker Working Group. *NPJ Breast Cancer* **7**, 150 (2021). https://doi.org/10.1038/s41523-021-00346-1

122 Nederlof, I. *et al.* Neoadjuvant nivolumab or nivolumab plus ipilimumab in early-stage triple-negative breast cancer: a phase 2 adaptive trial. *Nat Med* (2024). https://doi.org/10.1038/s41591-024-03249-3

123 Adams, S. *et al.* Pembrolizumab monotherapy for previously treated metastatic triple-negative breast cancer: cohort A of the phase II KEYNOTE-086 study. *Ann Oncol* **30**, 397-404 (2019). https://doi.org/10.1093/annonc/mdy517

124 Nanda, R. *et al.* Pembrolizumab in Patients With Advanced Triple-Negative Breast Cancer: Phase Ib KEYNOTE-012 Study. *J Clin Oncol* **34**, 2460-2467 (2016). https://doi.org/10.1200/JCO.2015.64.8931

125 Schmid, P. *et al.* Atezolizumab and Nab-Paclitaxel in Advanced Triple-Negative Breast Cancer. *N Engl J Med* **379**, 2108-2121 (2018). https://doi.org/10.1056/NEJMoa1809615

126 Demaria, S. *et al.* Ionizing radiation inhibition of distant untreated tumors (abscopal effect) is immune mediated. *Int J Radiat Oncol Biol Phys* **58**, 862-870 (2004). https://doi.org/10.1016/j.ijrobp.2003.09.012

127 Vanpouille-Box, C. *et al.* DNA exonuclease Trex1 regulates radiotherapy-induced tumour immunogenicity. *Nat Commun* **8**, 15618 (2017). https://doi.org/10.1038/ncomms15618

128 Scurr, M. *et al.* Low-Dose Cyclophosphamide Induces Antitumor T-Cell Responses, which Associate with Survival in Metastatic Colorectal Cancer. *Clin Cancer Res* **23**, 6771-6780 (2017). https://doi.org/10.1158/1078-0432.CCR-17-0895

129 de Biasi, A. R., Villena-Vargas, J. & Adusumilli, P. S. Cisplatin-induced antitumor immunomodulation: a review of preclinical and clinical evidence. *Clin Cancer Res* **20**, 5384-5391 (2014). https://doi.org/10.1158/1078-0432.CCR-14-1298

130 Wan, S. *et al.* Chemotherapeutics and radiation stimulate MHC class I expression through elevated interferon-beta signaling in breast cancer cells. *PLoS One* **7**, e32542 (2012). https://doi.org/10.1371/journal.pone.0032542

131 Alizadeh, D. *et al.* Doxorubicin eliminates myeloid-derived suppressor cells and enhances the efficacy of adoptive T-cell transfer in breast cancer. *Cancer Res* **74**, 104-118 (2014). https://doi.org/10.1158/0008-5472.CAN-13-1545

132 Casares, N. *et al.* Caspase-dependent immunogenicity of doxorubicin-induced tumor cell death. *J Exp Med* **202**, 1691-1701 (2005). https://doi.org/10.1084/jem.20050915

133 Sistigu, A. *et al.* Cancer cell-autonomous contribution of type I interferon signaling to the efficacy of chemotherapy. *Nat Med* **20**, 1301-1309 (2014). https://doi.org/10.1038/nm.3708

134 Voorwerk, L. *et al.* Immune induction strategies in metastatic triple-negative breast cancer to enhance the sensitivity to PD-1 blockade: the TONIC trial. *Nat Med* **25**, 920-928 (2019). https://doi.org/10.1038/s41591-019-0432-4

135 Emens, L. A. *et al.* First-line atezolizumab plus nab-paclitaxel for unresectable, locally advanced, or metastatic triple-negative breast cancer: IMpassion130 final overall survival analysis. *Ann Oncol* **32**, 983-993 (2021). https://doi.org/10.1016/j.annonc.2021.05.355

136 Cortes, J. *et al.* Pembrolizumab plus Chemotherapy in Advanced Triple-Negative Breast Cancer. *N Engl J Med* **387**, 217-226 (2022). https://doi.org/10.1056/NEJMoa2202809

137 Schmid, P. *et al.* Overall Survival with Pembrolizumab in Early-Stage Triple-Negative Breast Cancer. *N Engl J Med* (2024). https://doi.org/10.1056/NEJMoa2409932

138 Debien, V. *et al.* Immunotherapy in breast cancer: an overview of current strategies and perspectives. *NPJ Breast Cancer* **9**, 7 (2023). https://doi.org/10.1038/s41523-023-00508-3

139 Goldberg, J. *et al.* The Immunology of Hormone Receptor Positive Breast Cancer. *Front Immunol* **12**, 674192 (2021). https://doi.org/10.3389/fimmu.2021.674192

140 Cardoso, F. *et al.* LBA21 KEYNOTE-756: Phase III study of neoadjuvant pembrolizumab (pembro) or placebo (pbo) + chemotherapy (chemo), followed by adjuvant pembro or pbo + endocrine therapy (ET) for early-stage high-risk ER+/HER2– breast cancer. *Annals of Oncology* **34**, S1260-S1261 (2023). https://doi.org/10.1016/j.annonc.2023.10.011

141 Loi, S. *et al.* LBA20 A randomized, double-blind trial of nivolumab (NIVO) vs placebo (PBO) with neoadjuvant chemotherapy (NACT) followed by adjuvant endocrine therapy (ET) ± NIVO in patients (pts) with high-risk, ER+ HER2− primary breast cancer (BC). *Annals of Oncology* **34**, S1259-S1260 (2023). https://doi.org/10.1016/j.annonc.2023.10.010

142 Nanda, R. *et al.* Effect of Pembrolizumab Plus Neoadjuvant Chemotherapy on Pathologic Complete Response in Women With Early-Stage Breast Cancer: An Analysis of the Ongoing Phase 2 Adaptively Randomized I-SPY2 Trial. *JAMA Oncol* **6**, 676-684 (2020). https://doi.org/10.1001/jamaoncol.2019.6650
143 Agostinetto, E., Curigliano, G. & Piccart, M. Emerging treatments in HER2-positive advanced breast cancer: Keep raising the bar. *Cell Rep Med* **5**, 101575 (2024). https://doi.org/10.1016/j.xcrm.2024.101575
144 Loi, S. *et al.* Pembrolizumab plus trastuzumab in trastuzumab-resistant, advanced, HER2-positive breast cancer (PANACEA): a single-arm, multicentre, phase 1b-2 trial. *Lancet Oncol* **20**, 371-382 (2019). https://doi.org/10.1016/S1470-2045(18)30812-X
145 Michelon, I. *et al.* Trastuzumab deruxtecan in human epidermal growth factor receptor 2-positive breast cancer brain metastases: a systematic review and meta-analysis. *ESMO Open* **9**, 102233 (2024). https://doi.org/10.1016/j.esmoop.2024.102233
146 Moore, P. S. & Chang, Y. Why do viruses cause cancer? Highlights of the first century of human tumour virology. *Nat Rev Cancer* **10**, 878-889 (2010). https://doi.org/10.1038/nrc2961
147 Li, Z. *et al.* Prevalence of human papillomavirus DNA and p16(INK4a) positivity in vulvar cancer and vulvar intraepithelial neoplasia: a systematic review and meta-analysis. *Lancet Oncol* **24**, 403-414 (2023). https://doi.org/10.1016/S1470-2045(23)00066-9
148 Jones, R. W., Rowan, D. M. & Stewart, A. W. Vulvar intraepithelial neoplasia: aspects of the natural history and outcome in 405 women. *Obstet Gynecol* **106**, 1319-1326 (2005). https://doi.org/10.1097/01.AOG.0000187301.76283.7f
149 McNally, O. M., Mulvany, N. J., Pagano, R., Quinn, M. A. & Rome, R. M. VIN 3: a clinicopathologic review. *Int J Gynecol Cancer* **12**, 490-495 (2002). https://doi.org/10.1046/j.1525-1438.2002.01140.x
150 Satmary, W., Holschneider, C. H., Brunette, L. L. & Natarajan, S. Vulvar intraepithelial neoplasia: Risk factors for recurrence. *Gynecol Oncol* **148**, 126-131 (2018). https://doi.org/10.1016/j.ygyno.2017.10.029
151 van Seters, M., van Beurden, M. & de Craen, A. J. Is the assumed natural history of vulvar intraepithelial neoplasia III based on enough evidence? A systematic review of 3322 published patients. *Gynecol Oncol* **97**, 645-651 (2005). https://doi.org/10.1016/j.ygyno.2005.02.012

CHAPTER 2

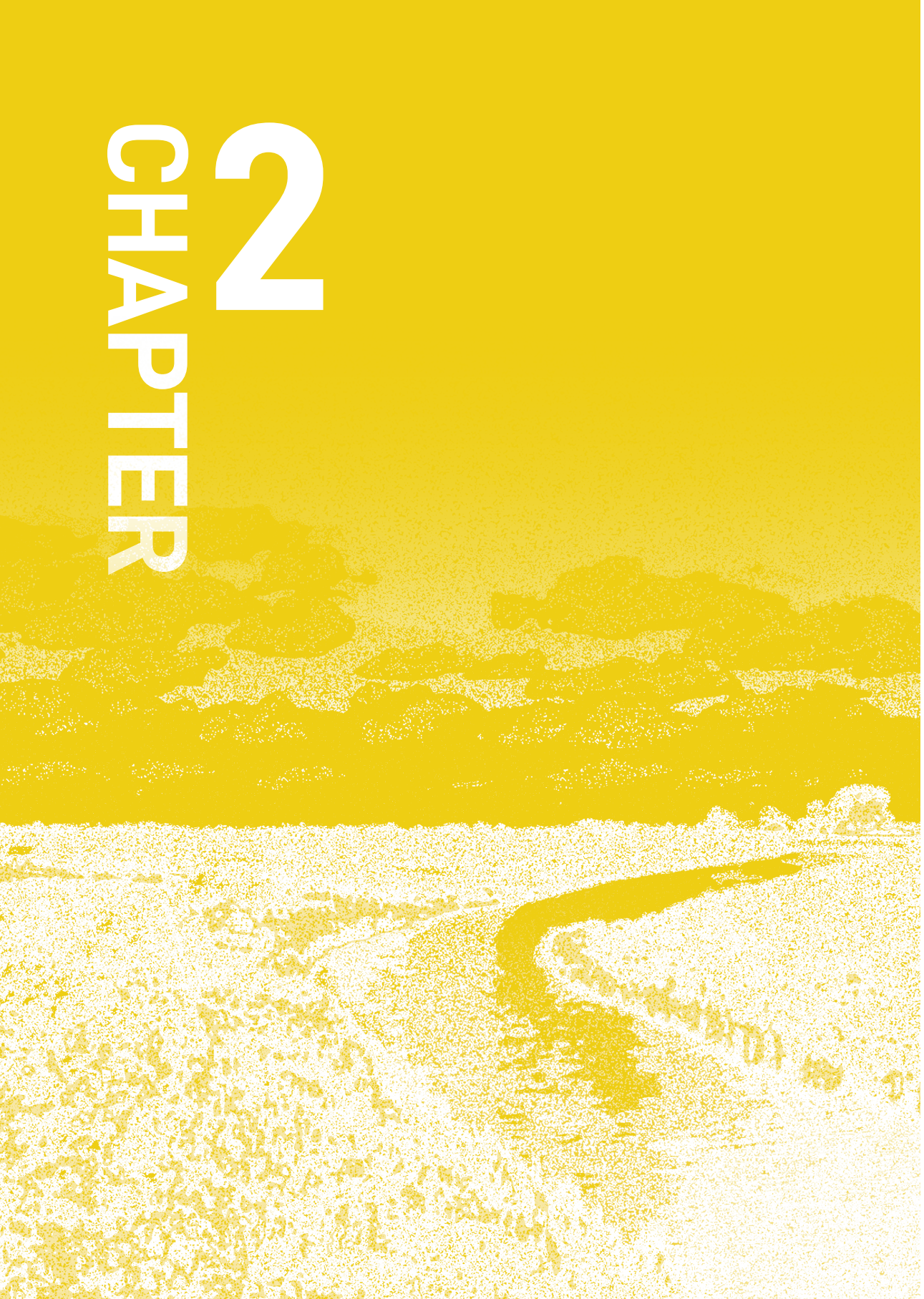

Ex vivo assessment of Human Neutrophil Motility and Migration

Noor A.M. Bakker[a, b, c], Claudia Burrello[a, c] and Karin E. de Visser[a, b, c *]

Methods Cell Biology: Immuno-oncology and Immunotherapy, 2025:191:115-133.
Epub 2024 Nov 19. DOI: 10.1016/bs.mcb.2024.10.008

a) Division of Tumor Biology and Immunology, The Netherlands Cancer Institute, Amsterdam, The Netherlands
b) Department of Immunology, Leiden University Medical Center, Leiden, The Netherlands
c) Oncode Institute, Utrecht, The Netherlands

* Corresponding author. E-mail address: k.d.visser@nki.nl

Abstract

Neutrophils are pivotal in orchestrating tumor-induced systemic inflammation and are increasingly recognized for their critical involvement in both the initiation and progression of cancer. A fundamental facet of neutrophil biology is their migratory capacity, which enables them to extravasate and infiltrate tumors other tissues, where they carry out essential effector functions. Unraveling the intricate mechanisms of neutrophil motility and migration is crucial for comprehending immune responses and inflammatory processes, shedding light on their substantial contribution to cancer progression. Here, we provide a comprehensive protocol to assess direct *ex vivo* motility and migration of freshly isolated human neutrophils, offering valuable insights into their behavior.

Introduction

Neutrophils are the most abundant white blood cell type in human circulation, comprising 40-70% of all white blood cells. They play a key role in the innate immune response, especially as first line of defense against infections. Recently, neutrophils have been intensively studied in the context of cancer immunology due to growing evidence of their involvement in various aspects of cancer onset and progression (1). Crosstalk between cancer cells and immune cells can lead to systemic accumulation and activation of neutrophils, resulting in a chronic inflammatory state (2-5). Tumor-induced systemic inflammation is clinically scored as the Neutrophil-to-Lymphocyte Ratio (NLR), indicative of the relative abundance of neutrophils versus lymphocytes in the peripheral circulation. Clinical investigations revealed a correlation between a high NLR and unfavorable disease outcomes as well as suboptimal therapy responses across various cancer types (6-9). Furthermore, preclinical research has shown that neutrophils contribute to the formation of metastases through various mechanisms. These include inducing systemic immune suppression, assisting circulating cancer cells and promoting the creation of the (pre-)metastatic environment (10-15). Additionally, pre-clinical investigations demonstrated that during the initial phases of tumor development, bone marrow neutrophils display a pronounced inherent capacity for spontaneous migration. This capability allows them to effectively navigate to distant organs, thereby promoting the infiltration of cancer cells into remote tissues and consequently facilitating the progression of tumor metastasis (16, 17). Collectively, these studies have revealed the pivotal role of neutrophils in metastasis formation, sparking a growing interest in studying these cells within the context of cancer (18).

Despite the growing recognition of the importance of neutrophils in cancer, they have often been overlooked in scientific investigations. While neutrophils constitute the most abundant white blood cell in human blood, their representation is notably absent in archival specimens such as frozen peripheral blood mononuclear cells (PBMCs). This absence can

be attributed to the inherent vulnerability of neutrophils; they do not withstand a freeze-thaw cycle, leading to their virtual elimination in preserved specimens. Additionally, their short lifespan, typically lasting from a few hours to a few days, poses a significant challenge for researchers, making them difficult to work with. Hence, possessing the necessary technical knowledge about human neutrophil isolation and *ex vivo* handling is crucial for the successful execution of functional experiments.

This methodology chapter provides detailed protocols to study the *ex vivo* motility and migration of human neutrophils. Motility refers to the ability of cells to move actively and undirected and is indispensable for neutrophils to execute their effector functions, such as patrolling the bloodstream and tissues, actively seeking out and destroying pathogens. Migration is a critical property that allows neutrophils to exit the bloodstream and actively navigate into tissues or sites of infection (or tumor, in the case of cancer), attracted by a gradient of chemical stimuli called chemoattractants. Important chemoattractants for neutrophils include interleukin-8 (IL-8, CXCL8), leukotriene B4 (LTB4), growth-regulated oncogene-1 (GRO-1, GROα, CXCL1), complement component C5a, N-Formylmethionyl-leucyl-phenylalanine (fMLF or fMLP) and stromal cell-derived factor-1 (SDF-1, CXCL12)(19, 20). In the migration assay described in this protocol, IL-8 and LTB-4 are used as chemoattractants because they are well characterized and commonly used moderately potent chemoattractants that exhibit minimal interference with adhesive properties and activation status of the neutrophils.

Understanding the intricacies of neutrophil motility and migration in different organs and disease contexts is essential for unraveling the dynamics of immune responses and inflammatory processes. *Ex vivo* motility and migration assays can be helpful tools to compare neutrophil functionality in homeostasis and disease or across different tissue sites. Furthermore, these assays can serve as a platform for fundamental research aimed at investigating mechanisms of neutrophil migration, and offer the potential to explore strategies targeting neutrophil migration. By comprehending the complexities of neutrophil motility and migration across various organs and disease scenarios, researchers can unravel the dynamics of immune responses and inflammatory processes, thereby illuminating the crucial role neutrophils play in cancer progression.

Materials

Common disposables

- Pipet tips
- 15 mL Falcon® Tubes (Thermo Fischer Scientific) (see Note 1)
- 50 mL Falcon® Tubes (Thermo Fischer Scientific) (see Note 1)
- Falcon® 24-well Clear Flat Bottom TC-treated Multiwell Cell Culture Plate, with Lid,

Individually Wrapped, Sterile (Corning) (see Note 1)
- 96-transwell plates with 3.0 µm pore polycarbonate permeable membranes (Sigma Aldrich) (see Note 1)
- Black 96-well flat bottom OptiPlates; low-binding surface (Perkin Elmer)
- Aluminum foil to keep stained cells in the dark

Cells and reagents
- Fresh human blood sample (2-4 mL), collected in EDTA tube (see Notes 2, 3 and 4)
- MACSxpress® Whole Blood Neutrophil Isolation Kit, human (Miltenyi)
- Medium: 20/80 mixed medium (20% Roswell Park Memorial Institute (RPMI)/ 80% AIM- V medium) (Gibco) (see Note 5), supplemented with 1% Human Serum (Sigma Aldrich)
- Red Blood Cell Lysis Buffer (dH2O, 8.02 g/L NH4Cl, 0.84 g/L NaHCCO3, 0.37g/L EDTA)
- Calcein acetoxymethyl, cell-permeant dye (Thermo Fischer Scientific)
- N-Formylmethionine-leucyl-phenylalanine (also known as fMLF or fMLP) (Sigma-Aldrich), make 10 µM stock
- HTAB buffer (1g/L Tween20, 2g/L CTAB, 2g/L BSA, 7.44 g/L EDTA)
- Recombinant Human IL-8 (Peprotech), make 10 µg/mL stock (= 100x)
- Recombinant LTB-4 (Sigma-Aldrich), make 1 µg/mL stock (=100x)

Equipment
- Pipets
- Magnet: MACSxpress Separator (Miltenyi)
- Cell counting equipment (manual/automated)
- Humidified cell culture incubator (37°C and 5% CO_2)
- Laboratory biosafety cabinet
- High-quality, inverted, wide field microscope system with motorized stage control (for time lapse), autofocus and temperature and CO_2 control for live cell imaging, (like the Zeiss Axio Observer Z1 Live) with standard filter cubes for GFP (Figure 1). The system needs to be equipped with a camera (like a sensitive Hamamatsu Orca Flash 4 monochrome camera for bright field, DIC, phase contrast and fluorescence imaging (LED or HXP light source) (see Note 1)
- Plate reader with excitation 485 and emission 520 such as PHERAstar FS (BMG labtech) (see Note 1)

Software
- PHERAstar FS plate reader software (BGM labtech)
- ZEN lite (Zeiss groep)
- TrackMate plugin Fiji (ImageJ)

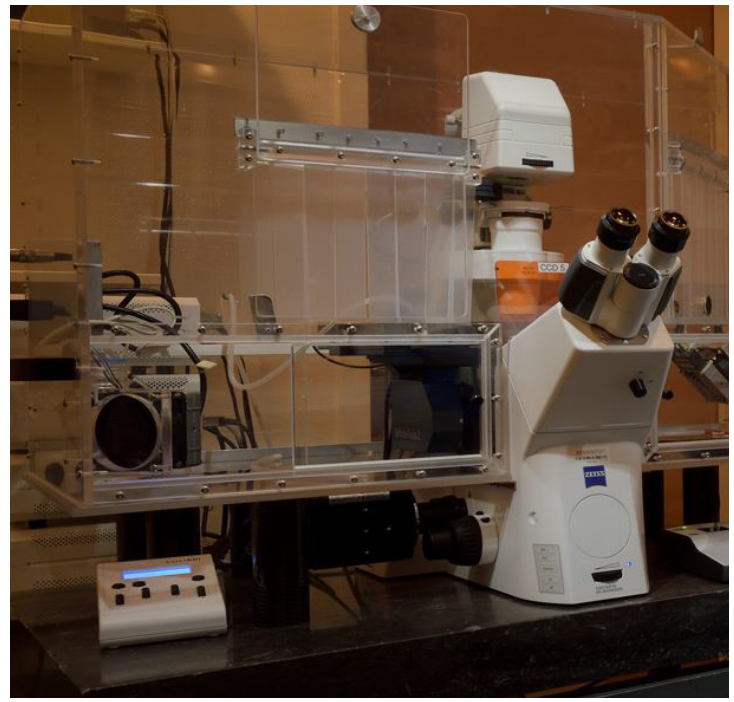

Figure 1: *Picture of the microscope, including the climate control chamber surrounding the microscope, maintaining the levels of CO_2 constantly at 5% and temperature at 37°C.*

Methods

Neutrophil isolation and staining

1. A ~5 mL peripheral blood sample is drawn and collected in an EDTA blood tube (see Notes 2-4). Keep the blood at RT and proceed to the next steps immediately.
2. Neutrophils are isolated according to the MACSxpress® Whole Blood Neutrophil Isolation Kit manual (see Note 6), which is a negative selection kit (see Note 7). In short:
   a. Beads are dissolved within 2 mL of Buffer A, which is included in the Kit (see Note 8).
   b. For each mL of whole blood that is used, 0.125 µL dissolved beads are mixed with 0.125 µL of Buffer B, which is included in the Kit (see Note 9).
   c. The appropriate amount of blood (for example 4 mL) is transferred to a 15 mL tube (see Note 10), after which the bead mix is added and incubated for 5 min. at RT. After 2-3 min., cell-bead suspension is mixed very gently by slowly pipetting up and down, without creating any bubbles.
   d. The 15 mL tube is placed in the magnet for 15 min.
   e. After 15 min., the fraction that does not stick to the magnet is harvested.

3. Cells are spun down for 5 min. at 250 *g*.
4. Red blood cells are lysed in 10 mL Red Blood Cell Lysis Buffer for 5 min. at RT.
5. 10 mL of medium is added and cells are spun down for 5 min. at 250 *g*.
6. Supernatant is discarded, the pellet is dissolved in 10 mL of mL of medium by gently pipetting up and down without creating any bubbles and cells are spun down again for 5 min., 250 *g*.
7. Cells are counted and diluted in medium to a final concentration of $4*10^6$/mL. It is strongly advised to perform a flow cytometry-based purity check on part of the isolated neutrophils (see Note 11).
8. The neutrophil suspension is transferred to a new 15 mL tube for staining (see Note 12).
9. Calcein is added to stain the neutrophils (final concentration: 1 µM).
10. Neutrophils are incubated for 30 min. at 37°C, and kept dark.
11. 10 mL of medium is added and cells are spun for 5 min. at 250*g*.
12. Supernatant is discarded, another 10 mL of medium is added and cells are spun at 5 min. at 250*g*.
13. Pellet is suspended in medium to a final concentration of $1*10^6$/mL.
14. Stained neutrophils can now be used for the motility (See 3.2) and migration assays (See 3.3).

Neutrophil motility assay

Plate preparation

1. 10.000 neutrophils are plated per well of a 24-well plate (10 µl of the stained neutrophil suspension in 1mL of medium per well) (see Note 13).
2. The remaining cells are kept at RT for use in the migration assay described in 3.3.
3. Neutrophils are allowed to settle in the plate for 30 min.
4. In the meantime, the microscope is prepared for the experiment (temperature is set at 37°C and CO_2 at 5%, the instrument is calibrated for a 24-well plate, correct focus and auto focus are established).

Data acquisition

1. Neutrophils are imaged using a 20x 0,4 objective and two channels:

a. Phase contrast, 30 ms exposure time.

b. Fluorescence contrast EGFP (Excitation wavelength 488, Emission wavelength 509), 50 ms exposure time.

2. To allow time lapse analysis, one frame every 2.5 min. is taken. Acquisition duration is typically between 30 min. and 4 hours, and can be chosen according to your experimental question (see Note 14).

Data analysis

1. After data acquisition, the pictures of one condition are digitally linked using the stitch function.
2. A fixed area of interest is chosen (see Note 15), a timespan is defined that is equal for all samples (typically 2-4 hours) and this homogenized data is exported.
3. For the quantification and visualization of neutrophil motility, TrackMate software is used (21, 22) (see Note 16).
4. To start, cells are segmented by overlaying each cell with a purple spot (see enlargement in Figure 2, Frame 1). It is important to choose a spot-size that fits your data (10-12 µm for neutrophils). This can be done by choosing 10-12 micron as 'Estimated object diameter'. Press 'Preview' to see whether the settings of choice correctly identify the cells in one sample frame. All cells will be automatically recognized in all frames.
5. Next, a check for software mistakes in cell fragmentation and a manual adjustment of the spot selection needs to be performed. In Figure 2, three consecutive frames are shown, illustrating the importance of this step. In some cases, multiple neutrophils are moving in close proximity to each other and they are recognized as one single cell by the software. Consequently, a spot can be lost during acquisition, resulting in fragmented tracks later on in the analysis. In this case, an extra spot should be added manually. On the other hand, the software sometimes considers a cell protrusion as a new cell and it incorrectly adds an extra spot. In this case, this extra spot must be removed manually (see Figure 2 Frame 3). If the software frequently misidentifies cell protrusions and adds inappropriate spots, it is recommended to increase the spot size to enhance accuracy.

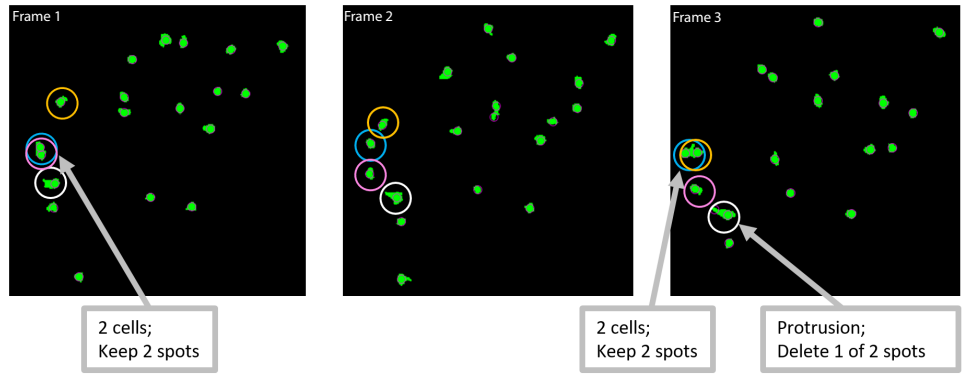

Figure 2: *Segmentation process of three consecutive frames of the same area in TrackMate. In green, the neutrophils are visible. The software annotates each cell with a purple circle that will eventually be tracked (see 2x enlargement in Frames 1 and 3). The four squares in yellow, blue, red and white are highlighting the same individual cells overtime for illustration purposes.*

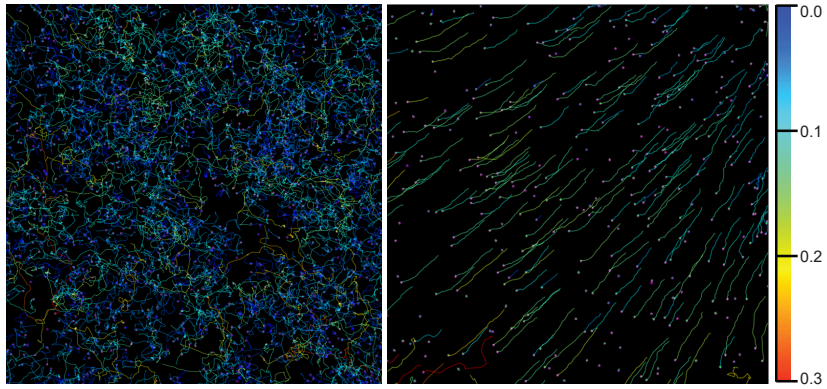

Figure 3: *Tracking live cell motility of human neutrophils for three hours: a good (left) and a bad (right) example (10x magnification plus 2x digital zoom). Tracks are colored for mean track velocity (micron/sec) and values are indicated by the bar on the right.*

6. Once all cells are correctly segmented throughout all frames, the next step is to connect the spots to study the tracks. Choose 'Simple LAP tracker' in the dropdown menu and set appropriate parameters (see Note 17).
7. When pressing "Next", the software creates 'links' connecting two spots in consecutive frames and 'tracks' that are the sum of all the links.
8. Make sure to verify that the plugin connected the correct dots, and adjust manually if necessary. Figure 3 shows two examples of cell tracking results. On the left, cells are actively moving across the well's surface, creating intricate patterns in their tracks. The left picture is therefore a good example of what actively moving neutrophils look like. On the right is an illustrative example of tracking caused by cells drifting within the well, as all the cells are following the same direction at the same speed; this does not represent actual active cell movement (see Note 18). The picture on the right is therefore an example of what passive/artefact movements look like.
9. After the tracks have been manually curated frame by frame, the resulting track data can be exported in a .txt or .xlsx format for statistical analysis and graphing purposes.
10. To obtain information about the percentage of moving neutrophils, you can set a very low threshold (e.g. 10 µm) to identify all cells that (hardly) moved, and calculate this as a fraction of total measured tracks. Alternatively, you can divide the number of tracks over the number of spots.
11. Additional informative parameters to investigate are:
    a. Mean track velocity: velocity values are defined as the distance between two spots (the link length) divided by the time difference for a single link. Mean velocity, is the average of the link velocities over all the links of the track.

    b. Track length: total distance travelled; sum of all link lengths for each track.
    c. Track displacement: net distance from start point to end point.
    d. Track displacement in combination with track length provides information about to which degree the neutrophils move linearly through space.

In Figure 4, an example is presented of the final data analysis results, in which multiple experiments are combined: 11 donors from Group A to 13 donors in Group B (see Note 19).

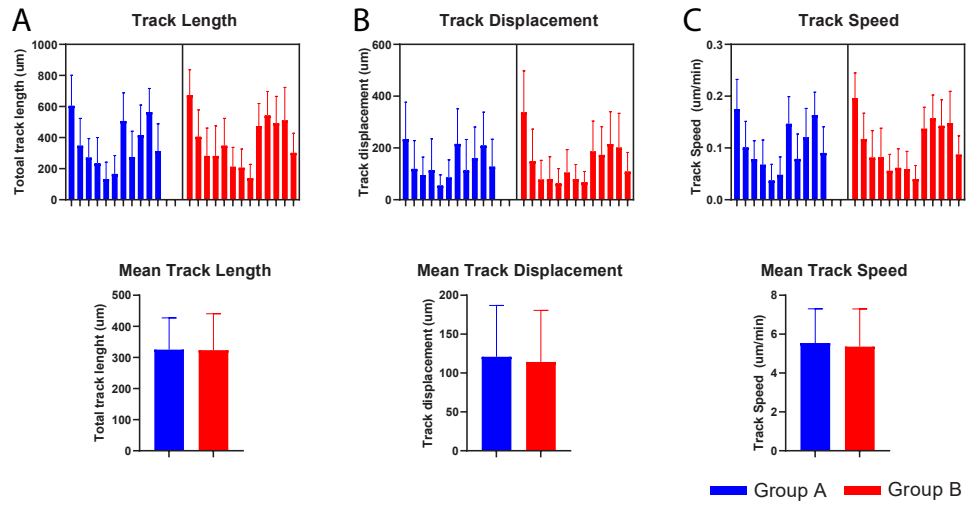

Figure 4: *Combined results of multiple experiments showing* ***(A)*** *Track Length,* ***(B)*** *Track Displacement and* ***(C)*** *Track Speed of individual donors (top row) and mean values per group (bottom row).*

Neutrophil migration assay

Plate preparation

1. After staining/washing the neutrophils as described in 3.1, allow them to rest for 30 min. in the dark at RT.
2. In the meantime, prepare the lower wells of a 96-well Transwell plate with a medium control and the chemoattractants (see Figure 5 for IL-8 and LTB-4 titrations).
3. Fill the bottom wells with 200 µL of the following conditions as described in Table 1 and illustrated in Figure 6 (the use of triplicates is recommended):
    a. Positive control: 100.000 cells (use 100 µL of cell suspension and add 100 µl of medium)
    b. Medium
    c. Medium +IL8 (final concentration of 0.1 µg/mL) (see Notes 20 and 21)
    d. Medium +LTB4 (final concentration of 0.01 µg/mL) (see Notes 20 and 21)

4. After the 30 min rest, the top wells are placed on the lower wells and 100 µL calcein stained neutrophils (100.000 cells) are added to the upper wells, according to the table 1.
5. The plate is incubated for 40 min. at 37°C.
6. After incubation, upper wells are removed and neutrophils are harvested from the lower wells by gently pipetting up and down without creating bubbles, and transferred to a V- 96-well plate (see Notes 22 and 23).
7. The V-bottom plate is spun down for 5 min. at 250 *g,* and supernatant is removed.
8. Cells are resuspended in 50 µL of medium + 1% HS and transferred to a black flat bottom plate.
9. 50 µL of HTAB buffer is added to all samples. Pipet up and down to lyse the cells.
10. Samples are kept dark until data acquisition, preferably on the same day.

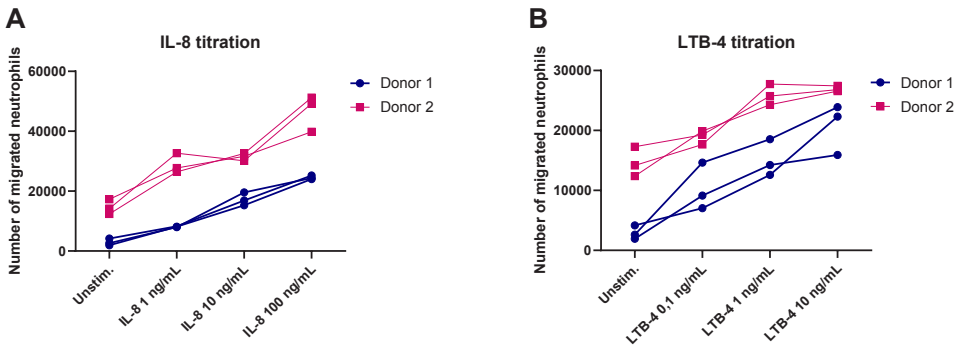

Figure 5: *Titration of chemoattractants (A) IL-8 and (B) LTB-4. Chemoattractant titrations were performed in medium supplemented with 1% human serum. Triplicates of two donors are shown here.*

Table 1: *Schematic overview of the experimental conditions of the neutrophil migration assay.*

	Bottom well	**Upper well**
Positive control	100,000 cells (100 µL) + 100 µL medium	Empty
Medium	Medium (200 µL)	100,000 cells (100 µL)
IL8	Medium + IL-8 (200 µL)	100,000 cells (100 µL)
LTB4	Medium + LTB4 (200 µL)	100,000 cells (100 µL)

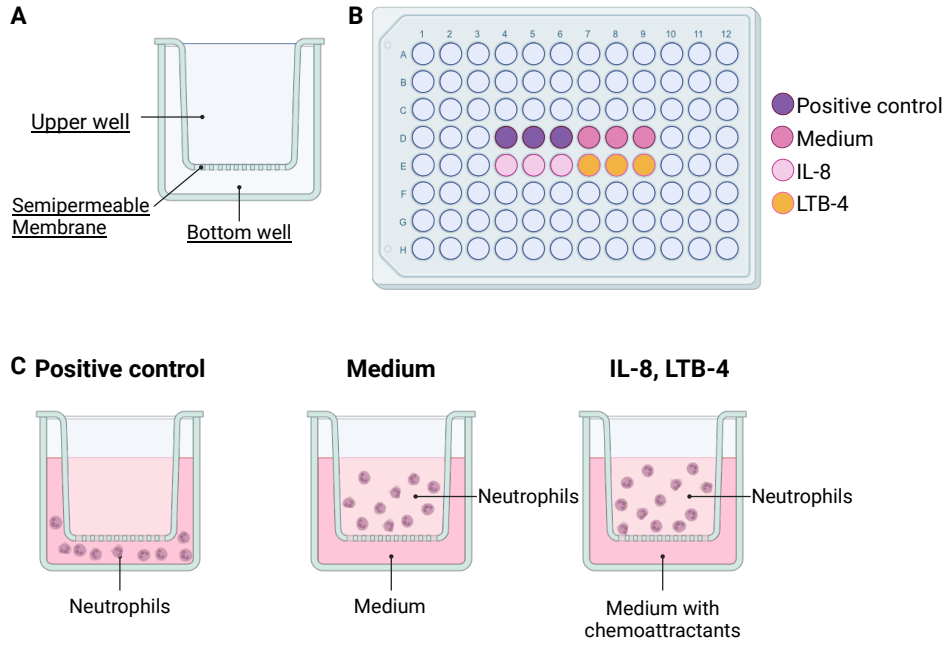

Figure 6*: Schematic overview of the experimental setup for the neutrophil migration assay, illustrating* ***(A)*** *the transwell components,* ***(B)*** *plate layout and* ***(C)*** *starting experimental conditions. Created with BioRender.com.*

Data acquisition and analysis

1. The plate reader is set up as follows: the focal height is determined and the gain is adjusted to prevent signal saturation in any of the wells.
2. 20 laser beam flashes per well are used.
3. The fluorescent signal is measured and quantified with the plate reader (excitation 485/ emission 520).
4. The average of the triplicates is used for each condition.
5. The positive control condition serves as reference (=100%) and migration rates of the other conditions are calculated relative to this signal.

Notes

1. Suppliers are given for reference, but equivalent products can be purchased from different providers or manufacturers.
2. Blood sampling is a reserved medical procedure, and may only be performed by certified

personnel. Subjects must be counseled and sign informed consent. Be sure to follow applicable regulations within your country and research institution.

3. Blood samples are considered primary human tissues and should be handled as biohazardous material under Biosafety Level 2: work in a Class II bio-safety cabinet while wearing appropriate protective PPE certified gloves and clothing.
4. Neutrophils follow the circadian rhythm in exiting the bone marrow. It is best to collect blood samples in the morning and to avoid large variation in time of blood draw. Since neutrophils do not survive a freeze-thaw procedure, the use of fresh blood samples is essential.
5. If no serum free T cell mixed medium is available, experiments can also be conducted with RPMI 1640 Medium without Phenol red (Gibco).
6. Depending on the number of magnets you have, you can process multiple samples at the same time.
7. To avoid neutrophil activation as much as possible, it is important to use a negative selection kit during neutrophil isolation.
8. Neutrophil isolation mix must be prepared freshly before each cell separation procedure, and reagents should be placed at RT before use for 15min.
9. Half the amount of Miltenyi Neutrophil Isolation beads was tested and was found to be equally effective.
10. When pipetting neutrophils, make sure to handle them very gently (e.g. avoid flicking the pellet after centrifugation and do not create bubbles).
11. For the purity check after neutrophil isolation, use forward scatter and side scatter to identify your single cells, life/dead staining in combination with a dump lineage channel containing markers like anti-CD3, anti-CD19 and anti-CD56, and antibodies against CD11b, CD66b and CD16 to identify neutrophils (see Figure 7).
12. The remaining cells can be used for other purposes, e.g. proteomics, secretomics, NET-formation assay.
13. Only the central wells of the 24 well plate are used and water is added to the wells that are not used to prevent evaporation of medium in the wells containing the neutrophils.
14. It is advisable to choose the acquisition duration generously. After acquisition, the user can choose the window of time of interest to export, for instance excluding the end if cells die.
15. To avoid (unintentional) bias in selecting the region of analysis, it is advised to work with fixed coordinates within the well.
16. TrackMate is a plugin within FIJI, with a user friendly interface. It follows a classical approach in which the cell segmentation step is distinct from the particle-linking steps. There is other tracking software available (like e.g. Spottracker), but TrackMate is most commonly used.

17. The parameters used in this experiment are: Linking max distance: 50,0 micron, Gap-closing max distance: 100,0 micron, Gap-closing max frame gap: 3. It is advisable to adjust these values to determine the parameters that best fit your data. In which the "Linking max distance" dictates the maximal distance between two spots. "Gap-closing max distance" dictates how far two spots can be apart, in case the spot was missed, and "Gap-closing max frame gap" describes the maximum allowed number of consecutive missed frames.

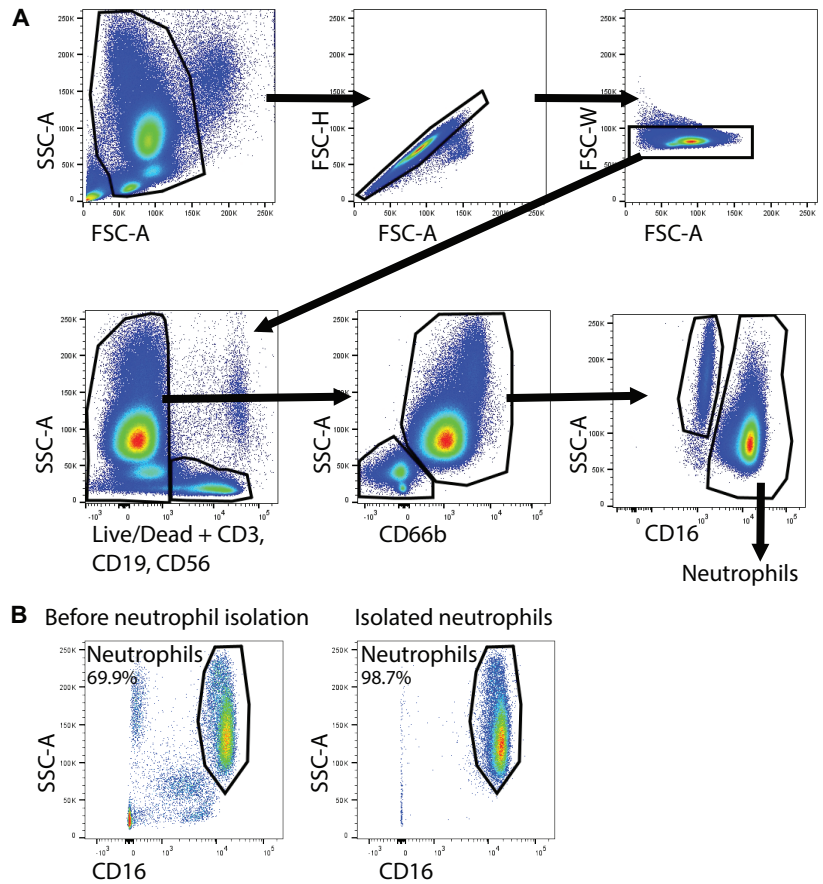

Figure 7: *Neutrophil isolation purity check based on flow cytometry.* ***A)*** *Representative flow cytometry dot plots illustrating strategy to gate on neutrophils (gating on singlets, live, lineage-, high side scatter, CD66b+ CD16+).* ***B)*** *Percentage of neutrophils from single live cells before and after neutrophil isolation.*

Typically two samples are taken along: a. before isolation sample; b. isolated neutrophils

18. To avoid cell drifting, lower the speed of the stage while moving to the next well to 50% with acceleration 30%.
19. In addition TrackMate plugin offers the opportunity to plot several other features of interest regarding the Spots, Links and Tracks.
20. IL-8 and LTB-4 concentrations were optimized and optimal conditions were chosen (Figure 8).
21. It is desirable to test multiple concentrations of the chemoattractants while setting up the experiments. In our lab, these were the optimal conditions with the biggest difference between the case and control group, but this might vary depending on the experiment and the lab. Additionally, researchers may opt to utilize alternative chemoattractants. In that case too, it is imperative to optimize the protocol accordingly.
22. V-bottom plates are preferred when spinning down only a small amount of cells because the pellet is more firm. Alternatively, a U-bottom plate can be used as well.
23. In some cases, the volume in the lower well might exceed the maximum of what can be plated in a V-bottom well (~220 µL). In this case, you need to separate the sample over two wells and combine them after the first spin. Wash wells to minimize cell loss.

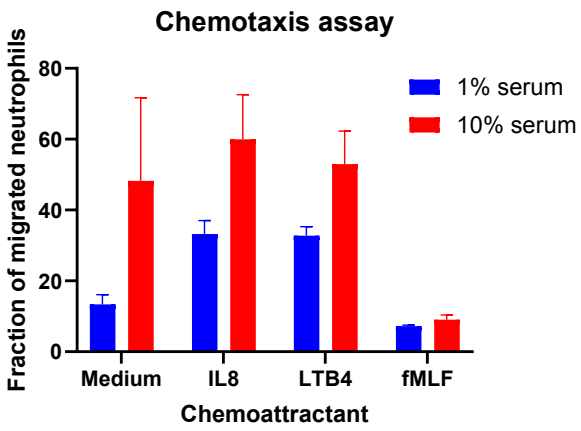

Figure 8: *Fraction of migrated neutrophils at different concentrations of human serum. For testing the best serum concentration, the chemoattractants were used in the following concentration: 100 ng/mL IL-8, 10 ng/mL LTB-4 and 100 nM fMLF.*

Concluding remarks

While descriptive analyses can provide correlative and static snapshots of cellular capabilities, functional assays give dynamic insights into cellular activity, and provide opportunities for mechanistic analyses of biological processes. Investigating the functional behavior of neutrophils takes on considerable importance within the context of tumor-induced systemic inflammation and tumor progression (16, 17). In this chapter we have described two distinct *ex vivo* assays tailored to quantify human neutrophil motility and migratory capacity. Taking into account the difficulties of working with unpredictable human samples, especially when dealing with cancer patients, our protocol offers a feasible and reproducible approach that allows a standardized sample analysis over extended periods of time. The motility and migration assays described in this chapter have a wide range of potential applications. These include, but are not limited to, comparing the migration capacity of neutrophils from healthy individuals with those from patients affected by a particular disease. Furthermore, these assays can function as a screening tool to evaluate the impact of specific drugs on neutrophil migration.

When a preference for more physiologically relevant conditions arises, the migration assay can be modified with the addition of a HUVEC (Human umbilical vein endothelial cells) monolayer in the transwell. This will better resemble the transmigration process across the blood vasculature. However, the execution of these assays poses significant logistical challenges, primarily due to the concomitant requirement for fresh blood samples and an already formed HUVEC cell monolayer in the transwell.

We advocate combining these functional assays with complementary techniques such as RNA sequencing and proteomics. This integrative approach not only enhances analytical depth but could also facilitate the elucidation of the underlying molecular mechanisms responsible for potential differences in migration between experimental and control groups.

When stimulating neutrophil migration and motility with chemoattractants, it is important to carefully consider the choice of the stimulus. IL-8 and LTB4 are acknowledged as “intermediary” signals, directing neutrophils from the bloodstream to the general vicinity of their target. These intermediary signals are disregarded once neutrophils perceive “end-target” signals in close proximity to their final destination (23). To draw a comparative analysis between “low-priority input” denoted by IL-8 and LTB4, and “high-priority input”, chemoattractants such as fMLF and C5a can be examined. However, previous studies have outlined that fMLF and complement C5a result in swift alterations in neutrophil morphology and adherence properties (24, 25), which can impact the outcomes of migration experiments. In our hands, fMLF persistently resulted in less migration than in the medium control condition (Figure 5), because the neutrophils adhere to the transwells. Therefore, when alternative chemoattractants like fMLF, C5a or others are intended to be used, additional refinement of this protocol is required.

Acknowledgements

Research in the de Visser laboratory is funded by the Dutch Cancer Society (KWF 14801, 13191), Oncode Institute, KWF/Oncode grant 14339, the Netherlands Organisation for Scientific Research (NWOVICI91819616) and Stichting La Vie est Belle. CB was supported by AIRC for Abroad fellowship (25299 year 2020) and EMBO fellowship (ALTF 1039-2020) and is currently supported by Marie Skłodowska-Curie Actions (IF 101025502 BreaKer). We acknowledge the supporting staff of the NKI Bioimaging facility.

Conflicts of interest

N.A.M.B. and C.B. have no conflicts of interest to declare. K.E.d.V. reports research funding from Roche/Genentech and is consultant for Macomics, outside the scope of this work.

References

1. Jaillon S, Ponzetta A, Di Mitri D, Santoni A, Bonecchi R, Mantovani A. Neutrophil diversity and plasticity in tumour progression and therapy. Nat Rev Cancer. 2020;20(9):485-503.
2. Blomberg OS, Spagnuolo L, de Visser KE. Immune regulation of metastasis: mechanistic insights and therapeutic opportunities. Dis Model Mech. 2018;11(10).
3. Garner H, de Visser KE. Immune crosstalk in cancer progression and metastatic spread: a complex conversation. Nat Rev Immunol. 2020;20(8):483-97.
4. McAllister SS, Weinberg RA. The tumour-induced systemic environment as a critical regulator of cancer progression and metastasis. Nat Cell Biol. 2014;16(8):717-27.
5. Duits DEM, de Visser KE. Impact of cancer cell-intrinsic features on neutrophil behavior. Semin Immunol. 2021;57:101546.
6. Silva TH, Schilithz AOC, Peres WAF, Murad LB. Neutrophil-lymphocyte ratio and nutritional status are clinically useful in predicting prognosis in colorectal cancer patients. Nutr Cancer. 2020;72(8):1345-54.
7. Liu J, Li S, Zhang S, Liu Y, Ma L, Zhu J, et al. Systemic immune-inflammation index, neutrophil-to-lymphocyte ratio, platelet-to-lymphocyte ratio can predict clinical outcomes in patients with metastatic non-small-cell lung cancer treated with nivolumab. J Clin Lab Anal. 2019;33(8):e22964.
8. Shao Y, Wu B, Jia W, Zhang Z, Chen Q, Wang D. Prognostic value of pretreatment neutrophil-to-lymphocyte ratio in renal cell carcinoma: a systematic review and meta-analysis. BMC Urol. 2020;20(1):90.
9. Shen M, Hu P, Donskov F, Wang G, Liu Q, Du J. Tumor-associated neutrophils as a new prognostic factor in cancer: a systematic review and meta-analysis. PLoS One. 2014;9(6):e98259.
10. Coffelt SB, Kersten K, Doornebal CW, Weiden J, Vrijland K, Hau CS, et al. IL-17-producing gammadelta T cells and neutrophils conspire to promote breast cancer metastasis. Nature. 2015;522(7556):345-8.
11. Kowanetz M, Wu X, Lee J, Tan M, Hagenbeek T, Qu X, et al. Granulocyte-colony stimulating factor promotes lung metastasis through mobilization of Ly6G+Ly6C+ granulocytes. Proc Natl Acad Sci U S A. 2010;107(50):21248-55.
12. Yang L, Liu Q, Zhang X, Liu X, Zhou B, Chen J, et al. DNA of neutrophil extracellular traps promotes cancer metastasis via CCDC25. Nature. 2020;583(7814):133-8.
13. Szczerba BM, Castro-Giner F, Vetter M, Krol I, Gkountela S, Landin J, et al. Neutrophils escort circulating tumour cells to enable cell cycle progression. Nature. 2019;566(7745):553-7.
14. McDowell SAC, Luo RBE, Arabzadeh A, Dore S, Bennett NC, Breton V, et al. Neutrophil oxidative stress mediates obesity-associated vascular dysfunction and metastatic transmigration. Nat Cancer. 2021;2(5):545-62.
15. Jablonska J, Lang S, Sionov RV, Granot Z. The regulation of pre-metastatic niche formation by neutrophils. Oncotarget. 2017;8(67):112132-44.
16. Patel S, Fu S, Mastio J, Dominguez GA, Purohit A, Kossenkov A, et al. Unique pattern of neutrophil migration and function during tumor progression. Nat Immunol. 2018;19(11):1236-47.
17. Fu S, Deng H, Bertolini I, Perego M, Chen ES, Sanseviero E, et al. Syntaphilin Regulates Neutrophil Migration in Cancer. Cancer Immunol Res. 2023;11(3):278-89.
18. Zheng C, Xu X, Wu M, Xue L, Zhu J, Xia H, et al. Neutrophils in triple-negative breast cancer: an underestimated player with increasingly recognized importance. Breast Cancer Res. 2023;25(1):88.
19. Metzemaekers M, Gouwy M, Proost P. Neutrophil chemoattractant receptors in health and disease: double-edged swords. Cell Mol Immunol. 2020;17(5):433-50.
20. Futosi K, Fodor S, Mocsai A. Neutrophil cell surface receptors and their intracellular signal transduction pathways. Int Immunopharmacol. 2013;17(3):638-50.
21. Ershov D, Phan MS, Pylvanainen JW, Rigaud SU, Le Blanc L, Charles-Orszag A, et al. TrackMate 7: integrating state-of-the-art segmentation algorithms into tracking pipelines. Nat Methods. 2022;19(7):829-32.
22. Tinevez JY, Perry N, Schindelin J, Hoopes GM, Reynolds GD, Laplantine E, et al. TrackMate: An open and extensible platform for single-particle tracking. Methods. 2017;115:80-90.
23. Lundgren SM, Rocha-Gregg BL, Akdogan E, Mysore MN, Hayes S, Collins SR. Signaling dynamics distinguish high- and low-priority neutrophil chemoattractant receptors. Sci Signal. 2023;16(805):eadd1845.
24. Denk S, Taylor RP, Wiegner R, Cook EM, Lindorfer MA, Pfeiffer K, et al. Complement C5a-Induced Changes in Neutrophil Morphology During Inflammation. Scand J Immunol. 2017;86(3):143-55.
25. Sengupta K, Aranda-Espinoza H, Smith L, Janmey P, Hammer D. Spreading of neutrophils: from activation to migration. Biophys J. 2006;91(12):4638-48.

CHAPTER 3

Comprehensive Analysis of the Systemic Immune Landscape Across Breast Cancer Subtypes and Disease Stages

Noor A.M. Bakker[1,2,4], Hannah Garner[1,2,#], Veerle C.M. Geurts[1,#], Elisa Champanhet[1], Chris Klaver[1], Maxime Duijst[1], Iris Nederlof[1], Robbert C.A.M. Gielen[1], Manon de Graaf[1], Rosie Voorthuis[5], Marte C. Liefaard[5], Esther H. Lips[5], Hendrika M. Oosterkamp[6], Marleen Kok[1,3,] and Karin E. de Visser[1,2,4]

Immuno-Oncology and Technology. 2025 July 23; 27. https://doi.org/10.1016/j.iotech.2025.101065

1 Division of Tumor Biology & Immunology, The Netherlands Cancer Institute, Amsterdam, The Netherlands
2 Oncode Institute, Utrecht, The Netherlands
3 Department of Medical Oncology, The Netherlands Cancer Institute, Amsterdam, The Netherlands
4 Department of Immunology, Leiden University Medical Centre, Leiden, The Netherlands
5 Division of Molecular Pathology, The Netherlands Cancer Institute, Amsterdam, The Netherlands
6 Department of Medical Oncology, Haaglanden Medical Center, The Hague, The Netherlands

# These authors contributed equally
Correspondence: m.kok@nki.nl (M.K.) and k.d.visser@nki.nl (K.E.d.V.)

Abstract

Breast cancer is a systemic disease, yet the impact of tumor molecular subtype and disease stage on the systemic immune landscape, remains poorly understood. In this study, we comprehensively analyzed the systemic immune landscape in a large cohort of breast cancer patients, encompassing all molecular subtypes and disease stages, alongside a control group of healthy donors. Using multi-parameter flow cytometry, we assessed the abundance, phenotype, and activation status of diverse innate and adaptive immune cell populations across peripheral blood samples from 355 breast cancer patients and 65 healthy donors. Analyzing all blood samples immediately after collection enabled analysis of often overlooked, but highly abundant granulocyte populations, including neutrophils and eosinophils. Our findings reveal that early-stage breast cancer patients exhibit increased cell counts of neutrophils, classical monocytes, and CD1c$^-$ DCs compared to healthy donors. In late-stage breast cancer patients, we observed elevated counts of neutrophils, classical monocytes, and non-classical monocytes compared to healthy donors. Additionally, reductions were observed in memory B cells, plasmablast-like cells, conventional CD4 T cells, and regulatory T cells. Notably, distinct molecular subtypes were associated with specific changes in the immune landscape, with the most significant changes observed in the triple-negative subtype. In conclusion, our data indicate that the systemic immune landscape undergoes more profound alterations in metastatic breast cancer than non-metastatic cases, with disease stage exerting a greater influence on systemic immune composition than tumor subtype.

Introduction

Breast cancer can be considered a systemic disease, but the influence of breast cancer on the systemic immune landscape, especially in relation to tumor molecular subtype and disease stage, is not well understood. Breast cancer accounts for nearly a quarter of all cancer diagnoses and necessitates complex treatment strategies, which frequently result in side effects that cause physical and emotional suffering for those who are affected and their loved ones[1]. Breast cancer is classified into three main subtypes, based on hormone receptor (HR) and human epidermal growth factor receptor 2 (HER2) expression: HR+ tumors (~70%), HER2+ tumors (15-20%), and triple-negative breast cancer (TNBC, ~15%)[2]. Each subtype exhibits distinct molecular signatures and clinical behaviors[3]. Despite advancements in treatment tailored to molecular subtypes and other clinical parameters, breast cancer continues to be the leading cause of cancer-related mortality among women worldwide[1], underscoring the urgent need for innovative therapeutic approaches.

Although immune checkpoint inhibitors (ICI) have transformed the treatment of various cancer types, their efficacy in breast cancer has been relatively modest. TNBC is considered the most immunogenic subtype of breast cancer, characterized by higher levels of tumor infiltrating lymphocytes (TILs), a higher tumor mutational burden, and increased expression of programmed death-ligand 1 (PD-L1) compared to the other breast cancer subtypes[4]. However, even in TNBC, only a minority of patients benefits from current immunotherapeutic strategies. This limited response to ICI can be partly attributed to the inherently low immunogenicity of many breast tumors. In addition, a significant contributing factor is tumor-associated immune suppression, which enables cancer cells to evade local immune responses[5-10]. Tumor-associated immune suppression often extends beyond the tumor microenvironment (TME)[11-13], leading to an impact on the systemic immune system of the host. This systemic effect can manifest as altered immune cell populations and functions throughout the body, weakening overall immune defense and contributing to disease progression. Most studies have highlighted the impact of breast tumor subtypes on the local immune microenvironment, but our understanding of the systemic immune landscape across different molecular subtypes and disease stages remains limited. While some studies have provided valuable insights into the impact of cancer on peripheral immune cells[14,15], several questions remain open for exploration. For instance, previous studies rely on PBMCs, excluding granulocytes and thereby omitting a significant portion of myeloid cells. The complex interplay between tumor stage, molecular subtypes, and systemic immune alterations remains poorly understood, yet is of critical importance for guiding the development of novel immunotherapeutic approaches tailored to individual patients.

Our goal is to study how tumor stage and molecular subtype impact the systemic immune landscape in patients with breast cancer. Therefore, we conducted a comprehensive characterization of the circulating immune landscape in a large cohort of breast cancer patients spanning different molecular subtypes and disease stages, alongside a matched healthy donor (HD) control group. Employing multi-parameter flow cytometry analysis, we assessed the abundance, phenotype, and activation status of various innate and adaptive immune cell populations from over 400 fresh peripheral blood samples. This enabled us to generate detailed quantitative and phenotypic data on circulating granulocyte subsets, dendritic cells (DCs), monocytes, T cells, B cells, and natural killer (NK) cells, shedding light on the intricate interplay between breast cancer and systemic immune profile. This dataset is unique because of its large, well-defined patient cohorts, the inclusion of age- and BMI-matched healthy controls, and the incorporation of neutrophils, eosinophils, and basophils on this large scale, enabling a comprehensive and integrative approach to analysis.

We show that changes in the systemic immune landscape are most pronounced in patients with late-stage breast cancer and characterized by a general increase in the myeloid lineage and a decrease in the lymphoid lineage, especially in the metastatic setting, indicating that disease stage is a critical factor influencing the immunological profile of breast cancer patients. Furthermore, specific molecular subtypes notably induce distinct alterations in

the immune landscape of breast cancer patients. Our findings suggest that the most significant differences in the systemic immune landscape between the three subtypes and HDs, are observed in the TNBC subtype. These data provide a valuable resource on the circulatory immune landscape of breast cancer patients compared to HDs, informing future pre-clinical and clinical research and paving the way for innovative, stage- and subtype-specific immunomodulatory treatment approaches.

Material and Methods

Human blood samples

Fresh blood samples from 53 healthy women (healthy donors, HD) were obtained after approval by the local medical ethical committee (NCT03819829). Additionally, fresh blood samples from 12 healthy women were obtained anonymously from the Dutch national blood transfusion service (Sanquin Blood supply, Amsterdam, The Netherlands). In our cohort of patients with breast cancer, blood samples were obtained from patients enrolled in either a clinical trial or biobank protocol, after approval by the local medical ethical committee and/or institutional review board of the Netherlands Cancer Institute. 185 patients were enrolled in a biobanking protocol of the Netherlands Cancer Institute (CFMPB450); 59 patients were included in the BELLINI trial[16] (NCT03815890); 91 patients were included in the Triple B trial[17] (NCT01898117); 10 patients were included in the MIMOSA trial[18] (NCT04307329). Where blood was obtained in the context of a clinical trial, only baseline blood samples were included in the analysis for this study. Basic clinical parameters were retrieved from the electronic patient records by qualified medical staff.

We included 121 patients with HR+ breast cancer (ER >10%, PR+/- and HER2 negative), of which 33 had stage I disease, 53 had stage II, 15 stage III and 20 patients had stage IV disease. Furthermore, we included 67 patients with HER2+ breast cancer (either score 3 for HER2 using immunohistochemistry (IHC) or positive at in situ hybridization [CISH or FISH]) in case of score 2 on IHC) were included, of which 16 had stage I disease, 17 stage II, 17 stage III and 17 patients had stage IV disease. Additionally, we included 167 patients with TNBC (histologically confirmed ER < 10% of positive tumor cells using IHC; HER2: either score 0 or 1 for HER2 at IHC with no amplification detected by in situ hybridization [CISH or FISH] in case of score 2 on IHC) of which 17 had stage I disease, 40 had stage II, 17 had stage III and 93 patients had stage IV disease (Figure 1a).

In this study, all patients with early-stage disease (stage I-III) were treatment naïve at the time of blood donation. In the late-stage disease (stage IV) setting, blood from patients with mTNBC was taken before any treatment for metastatic disease. Patients with HR+ tumors and HER2+ tumors did receive prior treatment for metastatic disease (Supplementary Table 1). For the treated patients from all subtypes, a washout period of at least 3 weeks was maintained between the last drug administration and the blood draw.

All study protocols were conducted in accordance with the ICH Harmonised Tripartite Guideline for Good Clinical Practice and the principles of the Declaration of Helsinki. All patients and HDs provided written informed consent before enrolment.

Flow cytometry

Blood samples were processed and analyzed within 24 hours after blood draw. All samples were processed uniformly, by the same team and within the same laboratory. Peripheral blood was collected in EDTA vacutainers (BD) and subjected to red blood cell lysis (lysis buffer: dH2O, NH4Cl, NaHCCO3, EDTA). Cells were resuspended in PBS containing 0.5% BSA and 2mM EDTA and counted using the NucleoCounter NC-200 automated cell counter (Chemometec). To obtain white blood cell (WBC) counts per mL of blood, the total amount of post lysis cells was divided by the volume (mL) of blood obtained from the patient (~10 mL).

For the labeling of surface antigens, cells underwent an initial incubation with human FcR Blocking Reagent (diluted 1:100 Miltenyi) for 15 minutes at 4°C, followed by a 30-minute incubation with fluorochrome-conjugated antibodies at 4°C, shielded from light. For intracellular staining, cells were fixed in Fixation/Permeabilization solution 1X (Foxp3/Transcription Factor Staining Buffer Set, eBioscience) at 4°C for 30 minutes, then stained with fluorochrome-conjugated antibodies in Permeabilization buffer 1X (eBioscience) for 30 minutes at room temperature. Viability was determined by staining with either 7AAD staining solution (diluted 1:10; eBioscience) or Zombie Red Fixable Viability Kit (diluted 1:800, BioLegend).

Data acquisition of all samples was performed on the same LSRII SORP flow cytometer (BD Biosciences) operated with Diva software. To make the performance of this machine as constant over time as possible, CS&T beads (BD) were used to optimize general performance and Sphero 8 peaks Rainbow Calibration particles (BD) were used to adjust PMT voltages if necessary. Additionally, single stained compensation controls are taken along for each experiment. Flow data analysis was conducted using FlowJo software (version 10). Flow cytometry antibody details are provided in Supplementary Table 2 and gating strategies are illustrated in Supplementary Figures 1a (Myeloid panel gating), 1b (B and NK cell panel gating), and 1c (T cell panel gating).

Data analysis and statistics

GraphPad Prism (version 10.1.2) software was used for statistical analysis and graphing of the flow cytometry data. Kruskal-Wallis test was applied when comparing multiple groups, followed by Dunn's test to obtain adjusted p-values corrected for the number of groups in the graph (not the number of immune cell populations). PCAs and heatmaps were generated using Qlucore software (version 3.8). Missing values were imputed by mean values from

the sample group. Correlation between neutrophil counts and time of blood draw was performed in R (version 4.3.2) using linear modeling function. Corrected p-values <0.05 were considered significant and are depicted in the graphs using asterixes: * p<0.05; ** p<0.01; *** p<0.001; **** p<0.0001.

Results

Breast cancer alters the systemic immune landscape

To gain insights into the impact of breast cancer on the circulatory immune compartment at early or late disease stages, we conducted high-dimensional flow cytometry on 420 fresh peripheral blood samples. We developed an analysis pipeline specifically tailored for fresh blood samples[19]. This pipeline employs a panel of 50 antibodies distributed across a myeloid panel, a B- and NK cell panel, and a T cell panel (Supplementary Figure 1a-c). This robust approach enables a comprehensive analysis of the systemic immune landscape, including granulocytes, which are typically lost in standard peripheral blood mononuclear cell (PBMC)-based analyses. We profiled samples of patients without distant metastases (stage I-III, referred to as early-stage, n=225) and patients with distant metastases (stage IV, referred to as late-stage, n=130) (Figure 1a). From the patients with early-stage breast cancer, 101 patients had HR+ disease, 50 patients had HER2+ disease and 74 patients had TNBC (Figure 1a). From the patients with late-stage breast cancer, 20 patients had HR+ disease, 17 patients had HER2+ disease and 93 patients had TNBC (Figure 1a). As a control group, we profiled age-, sex- and BMI-matched healthy donors (HDs, n=65) (Figure 1a). Age and BMI of breast cancer patients and HDs are visualized in Supplementary Figure 2 a, b. Given that neutrophil release from the bone marrow follows a circadian rhythm[20], we tested for correlations between neutrophil counts and time of blood draw using a linear model. No statistically significant correlations were found, except in the early-stage TNBC group, where a weak correlation was observed (r=0.0999, Supplementary Figure 2c). The very low rho-value (<10%) suggests minimal variance explained by blood draw time, so we chose not to adjust for it in our dataset.

To explore the flow cytometry data of the three antibody panels in an unbiased manner, we performed a principal component analysis (PCA). By taking the first three principal components into account, we could explain 77% of the variance in the data. When plotting these three principal components, we observed that the HDs cluster away from all breast cancer groups, and that the early-stage breast cancer groups clustered away from the late-stage breast cancer groups (Figure 1b). Moreover, disease stage seemed to have a dominant impact on the systemic immune landscape over tumor subtype (Figure 1c). Hierarchical clustering of 18 major immune populations analysed, confirmed our PCA analysis with HDs blood profile separating from breast cancer patient blood profiles (Figure 1d).

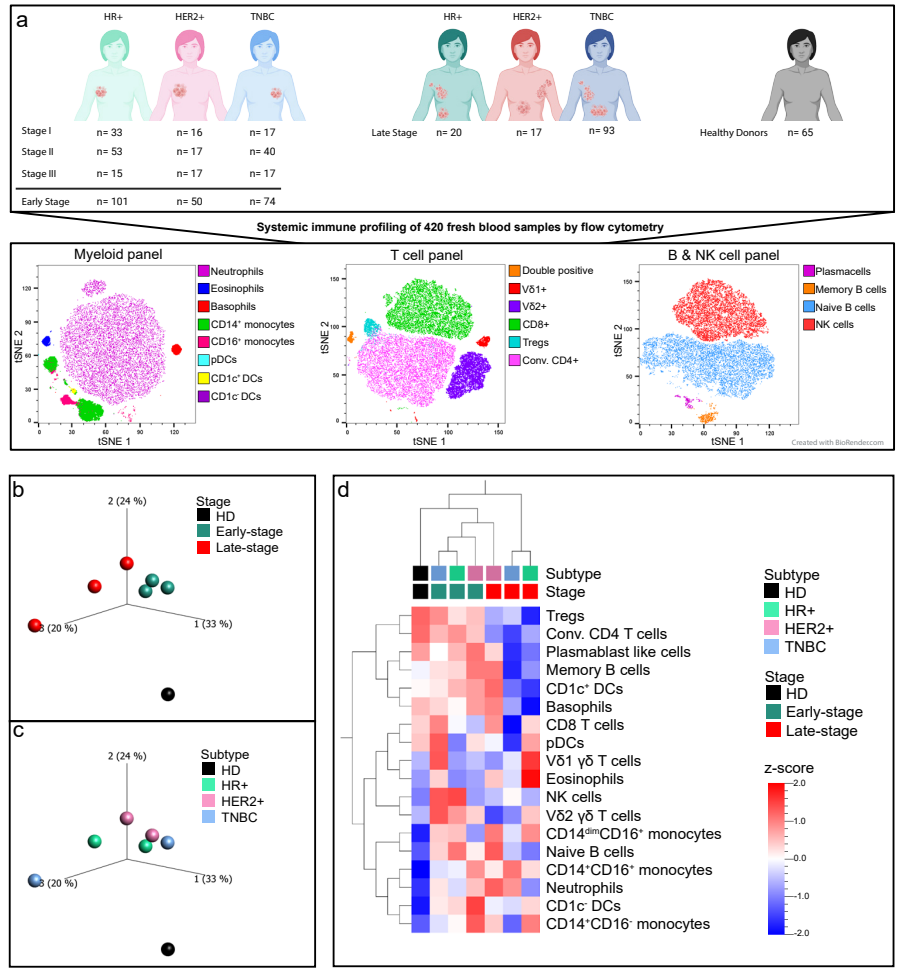

Figure 1. Breast cancer alters the systemic immune landscape. (a) *Graphical summary of included human blood samples and the systemic immune cell populations that were assessed immediately after blood collection using flow cytometry.* ***(b, c)*** *Principal component analysis was conducted on the Log_2-transformed median cell counts per mL of blood from major immune cell populations (see d), measured by flow cytometry in fresh blood samples. The results were colored by disease stage discriminating patients with early-stage breast cancer (n=225), late-stage breast cancer (n=130), and healthy donors (HD) (n=65)* ***(b)****, and by tumor subtype in discriminating between patients with a HR+ tumor (n=121), a HER2+ tumor (n=67) or a triple negative tumor (n=167), and healthy donors (n=65)* ***(c)****.* ***(d)*** *Heatmap based on the Log_2-transformed median cell counts per mL blood, visualizing the major immune cell populations, as assessed by flow cytometry in fresh blood samples from patients with early-stage breast cancer, late-stage breast cancer, across different breast cancer subtypes, and healthy donors. Hierarchical clustering was performed on the immune cell populations and on tumor subtype and disease stage. The color scale represents row Z-scores, ranging from -2 to 2.*

Breast cancer associated alterations to the systemic immune landscape are disease stage dependent

Next, we investigated which immune cell populations are driving the clustering patterns (Figure 1b, d) and how disease stage is impacting the circulating immune composition. We found both neutrophils and classical monocytes to be significantly increased in patients with early- and late-stage breast cancer compared to HDs (Figure 2a, b). Additionally, we observed a statistically significant increase in the number of circulating non-classical monocytes in patients with late-stage breast cancer compared to HDs (Figure 2b). Though no significant difference was observed between patients with early-stage and patients with late-stage breast cancer when all subtypes are grouped together in neutrophil and (non-) classical monocyte counts, we did observe an increasing trend, suggesting that neutrophil and (non-)classical monocyte numbers are being increasingly dysregulated as disease progresses (Figure 2a, b). Furthermore, we found CD1c$^+$ DCs to be reduced in the late-stage group compared to the early-stage group and an increase in CD1c$^-$ DCs in the early-stage group compared to the HDs (Figure 2c).

Within the circulating lymphoid compartment we found a decrease in memory B cells and plasmablast-like cells in patients with late-stage disease compared to HDs and patients with early-stage disease (Figure 2d). Similarly, we observed that the cell counts of CD8+ T cells, conventional CD4+ T cells, Tregs and Vδ2 γδ-T cells were reduced in patients with late-stage disease when compared to patients with early-stage disease (Figure 2e). Additionally, conventional CD4+ T cell and Treg counts were decreased in patients with late-stage disease when compared to HDs (Figure 2e). Together these data indicate that breast cancer impacts the systemic immune landscape in a disease stage dependent manner.

Systemic immune landscape of healthy donors and patients with early-stage breast cancer across different molecular subtypes

Our finding that disease stage is associated with multiple differences in the systemic immune landscape (Figure 2) raises the question of whether these alterations differ per breast cancer subtype. Therefore, we first sought to explore the influence of molecular subtype within the patients with early-stage disease and HDs. We observed that the increase in neutrophils, classical monocytes and CD1c$^-$ DCs is restricted to patients with early-stage HR+ tumors (Figure 3a-c). Conversely, the increase in non-classical monocytes was only found to be statistically significant in patients with early-stage TNBC compared to HDs (Figure 3b).

When evaluating the influence of molecular subtype in patients with early-stage breast on the circulating lymphoid compartment, we found that Vδ2 γδ-T cell counts were statistically significantly elevated in patients with TNBC compared to HDs (Figure 3e). Furthermore, we observed a reduced plasmablast-like cell count among patients with TNBC compared to patients with HR+ tumors (Figure 3d). Conversely, we found NK cell counts to

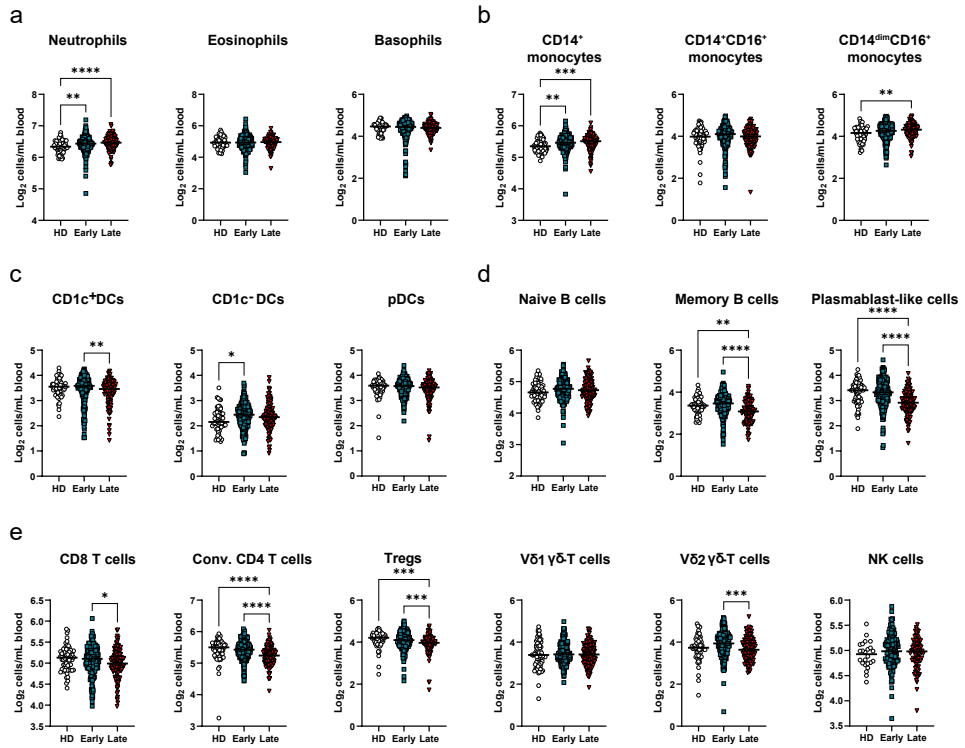

Figure 2. Breast cancer stage impacts the circulating immune composition. *Log$_2$-transformed cell counts per mL blood of major systemic immune cell populations measured by flow cytometry in patients with stage I-III breast cancer (Early) (n=225), stage IV breast cancer (Late) (n=130), and healthy donors (HD) (n=65), visualizing **(a)** granulocytes, **(b)** monocyte populations, **(c)** DC subsets, **(d)** B cell subpopulations and **(e)** different conventional and unconventional T cell subpopulations and NK cells. P-values for **(a-e)** were computed with the Kruskal-Wallis test followed by Dunn's multiple comparisons test.*

be increased in patients with TNBC compared to patients with HR+ tumors (Figure 3e). No other statistically significant differences between the molecular subtypes were observed, suggesting that disease stage had a stronger influence on the systemic immune landscape (Figure 2) than the molecular subtype in patients with early-stage breast cancer (Figure 3).

Systemic immune landscape of healthy donors and patients with late-stage breast cancer across different molecular subtypes

Next, we investigated which differences in the systemic immune landscape of advanced breast cancer patients were associated with a certain molecular subtype. To achieve this, we took the immune profiles of patients with late-stage breast cancer and compared the

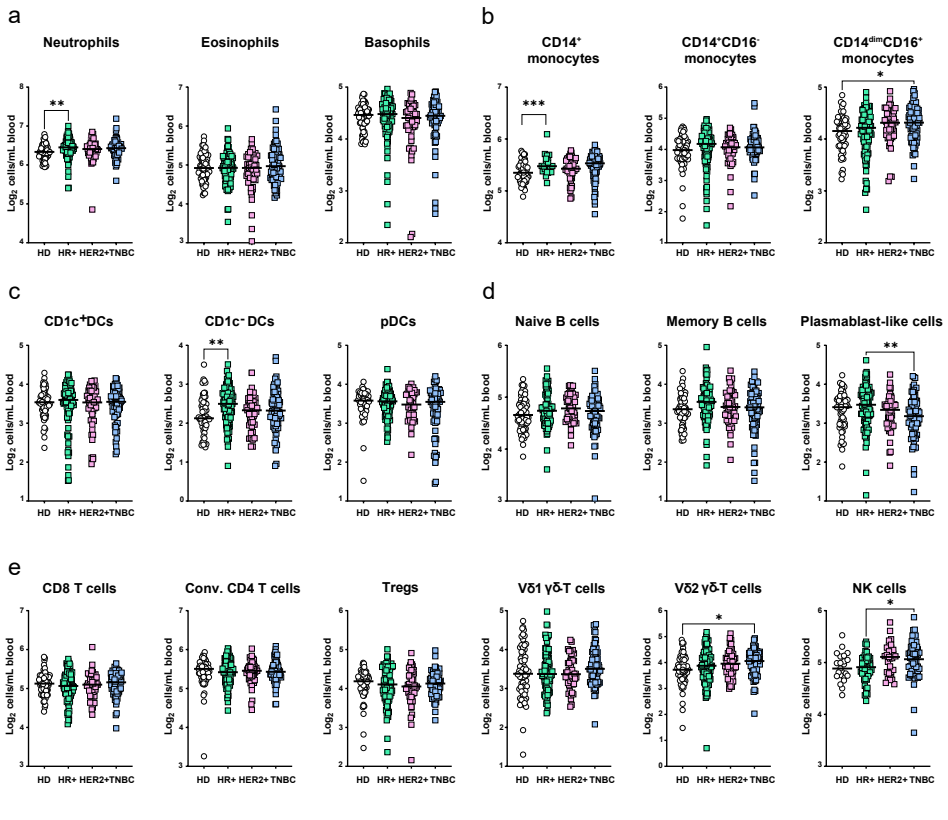

Figure 3. Systemic immune landscape of patients with early-stage breast cancer across different molecular subtypes. *Log_2-transformed cell counts per mL blood of major systemic immune cell populations measured by flow cytometry in patients with early-stage breast cancer with a HR+ tumor (n=101), a HER2+ tumor (n=50) or a triple negative tumor (n=74), and healthy donors (n=65), visualizing **(a)** granulocytes, **(b)** monocyte populations, **(c)** DC subsets, **(d)** B cell subpopulations and **(e)** different conventional and unconventional T cell subpopulations and NK cells. Adjusted p-values for **(a-e)** were computed with the Kruskal-Wallis test followed by Dunn's multiple comparisons test.*

three molecular subtypes to each other and to the immune profiles of HDs. When subdividing late-stage patients based on the molecular subtype of their tumor, we observed an imbalance in the n-number of patients per group (Figure 1a). However, our results confirm that the systemic increase in neutrophils observed in patients with late-stage disease compared to HDs (Figure 2) is present in both patients with HR+ breast cancer and those with TNBC, while this was not observed for HER2+ stage 4 disease (Figure 4a). The systemic increase in classical monocytes in late-stage patients compared to HDs (Figure 2) was predominantly driven by patients with TNBC (Figure 4b). In contrast, the observed increase

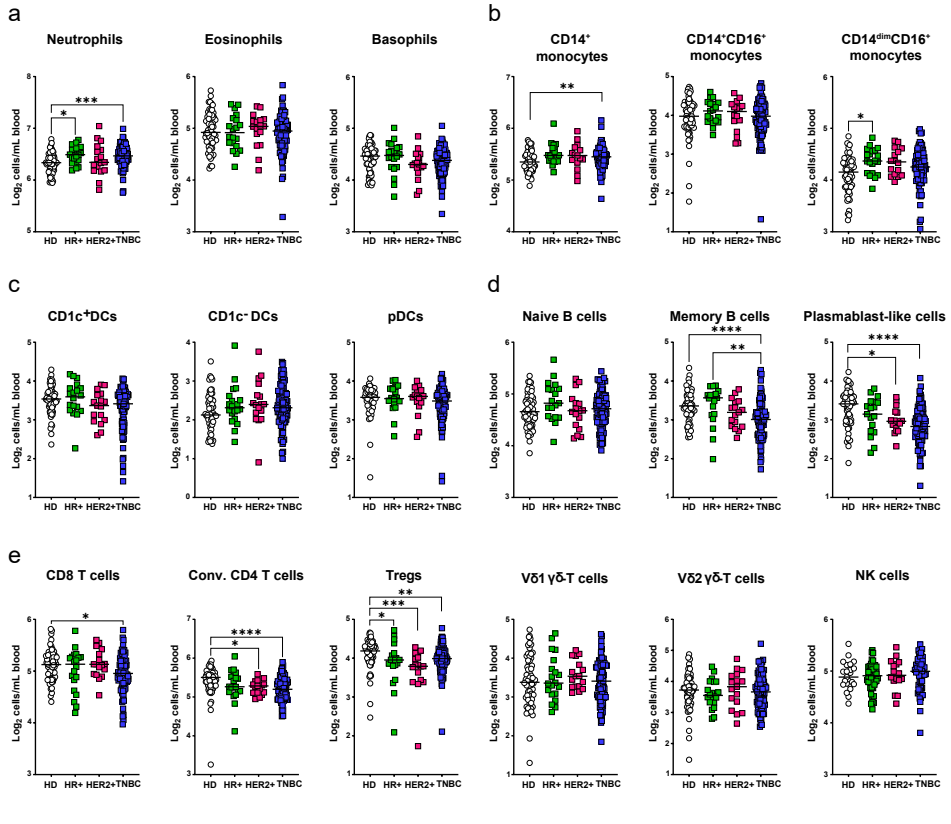

Figure 4. Systemic immune landscape of patients with late-stage breast cancer across different molecular subtypes. *Log_2-transformed cell counts per mL blood of major systemic immune cell populations measured by flow cytometry in patients with late-stage breast cancer with a HR+ tumor (n=20), a HER2+ tumor (n=17) or a triple negative tumor (n=93), and healthy donors (n=65), visualizing **(a)** granulocytes, **(b)** monocyte populations, **(c)** DC subsets, **(d)** B cell subpopulations and **(e)** different conventional and unconventional T cell subpopulations and NK cells. Adjusted p-values for **(a-e)** were computed with the Kruskal-Wallis test followed by Dunn's multiple comparisons test.*

in non-classical monocyte counts in patients with late-stage breast cancer compared to HDs (Figure 2) was found to be attributed to patients with a HR+ tumor (Figure 4b). These data indicate that the alterations detected in the circulating immune compartment exhibit varying degrees of penetration across the three molecular subtypes. Among the myeloid cell populations, eosinophils, basophils, $CD14^+CD16^+$ monocytes and the DC subsets remained unaffected in abundance across the different breast cancer subtypes (Figure 4a-c).

Within the lymphoid compartment, plasmablast-like cells were profoundly reduced in patients with mTNBC and HER2+ tumors compared to HDs (Figure 4d). Similarly, circulating

memory B cells were also found to be reduced in patients with mTNBC tumors. These data suggest that late-stage TNBC tumors, and to a lesser extent late-stage HER2+ tumors have a profound effect on the B cell compartment. When comparing the T cell subset abundances across molecular subtypes and HDs, we observed that patients with late-stage TNBC had reduced counts of CD8 T cells, conventional CD4 T cells and Tregs, patients with HER2+ tumors had reduced counts of conventional CD4 T cells and Tregs, and patients with HR+ tumors had reduced counts of Tregs (Figure 4e). These data indicate that circulating T cell abundances are most affected in patients with TNBC. Beyond the intrinsic effects of this tumor subtype on the systemic immune environment, this observation may also be attributable to a treatment history in the (neo)adjuvant setting with chemotherapeutic agents by a substantial proportion of late-stage TNBC patients. The observation that CD8 T cell counts are reduced in patients with TNBC compared to HDs was previously masked by other molecular subtypes, that did not show this decrease compared to HDs (Figure 4e). Apart from memory B cells (Figure 4d), no significant differences between the molecular subtypes were observed, suggesting once more that disease stage (Figure 2) has a stronger influence on circulating immune composition than the molecular subtype (Figure 4).

Breast cancer influences T cell phenotype and cytokine production in a tumor subtype- and disease stage-specific manner.

Given the observed decrease in total counts of CD8+, conventional CD4+, and regulatory T cells in patients with metastatic disease compared to those with non-metastatic disease — and for conventional CD4+ and regulatory T cells also compared to HDs— (Figure 2), we sought to investigate the phenotype and differentiation state of circulating T lymphocytes by flow cytometry (Supplementary Figure 1c) in relation to tumor subtype and disease stage. We observed a lower fraction of PD-1^{+} CD8+ T cells and PD-1^{+} conventional CD4+ T cells in patients with TNBC compared to HDs (Figure 5a), suggestive of altered systemic T cell activation. Furthermore, in patients with early-stage breast cancer, we observed a lower proportion of CTLA-4 expressing conventional CD4+ T cells in TNBC patients compared to patients with HR+ breast cancer (Figure 5a). When testing for differences in T cell phenotype in late-stage patients across molecular subtypes and HDs, we observed that patients with advanced HER2+ breast cancer had a lower frequency of CLTA-4+ and PD-1+ CD8+ T cells compared to HDs (Figure 5b), which was not yet observed in early disease stage (Figure 5a). Additionally, we found the frequency of PD-1+ conventional CD4 T cells to be reduced in patients with HER2+ advanced breast cancer compared to TNBC and HDs (Figure 5b).

Flow cytometry-based analysis of the T cell differentiation state (naïve T cells being CCR7+CD45RA+, central memory T cells (CM) being CCR7+CD45RA-, effector memory T cells (EM) being CCR7-CD45RA- and effector T cells (T eff) being CCR7-CD45RA+) (Supplementary Figure 1c), revealed a notable degree of heterogeneity in the T cell differentiation state,

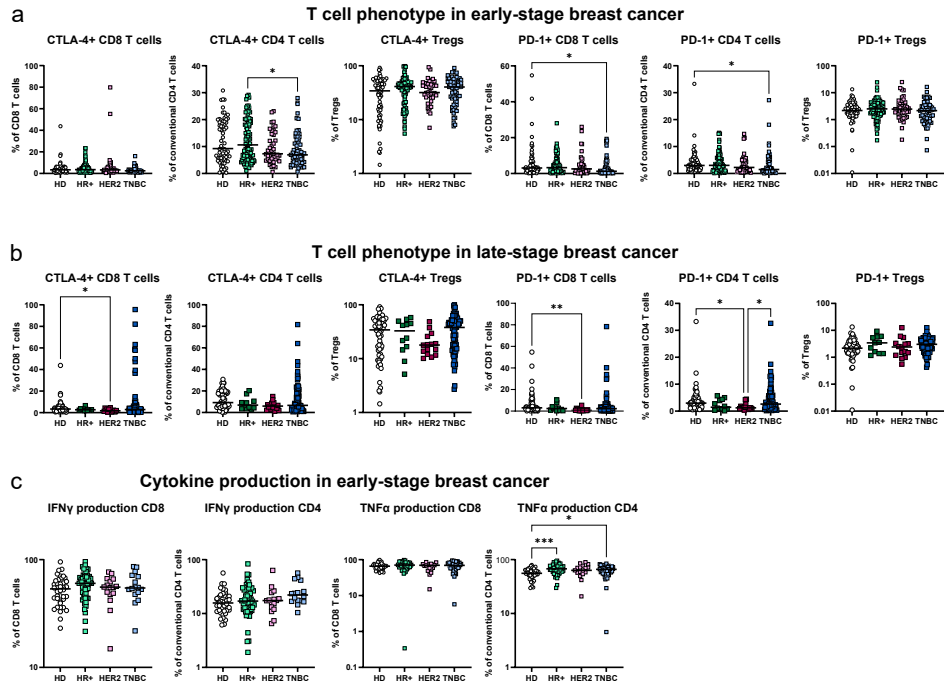

Figure 5. T cell phenotype and cytokine production in patients with early- and late-stage breast cancer across different molecular subtypes. (a) *Phenotypic characterization of circulating T cells at early disease stage, visualizing CTLA-4+ and PD-1+ CD8 T cells, conventional CD4 and regulatory T cells. Frequencies were determined using flow cytometry on fresh blood samples of patients with a HR+ tumor (n=20), a HER2+ tumor (n=17) or a triple negative tumor (n=93), and healthy donors (n=65).* ***(b)*** *CTLA-4 and PD-1 expression of CD8 T cells, conventional CD4 T cells and regulatory T cells. Frequencies of CTLA-4 and PD-1 positivity were determined using flow cytometry on fresh blood samples of patients with a HR+ tumor (n=20), a HER2+ tumor (n=17) or a triple negative tumor (n=93), and healthy donors (n=65).* ***(c)*** *Ex vivo production of cytokines IFNγ and TNFα by CD8 and conventional CD4 T cells. Stimulated fresh blood samples of patients with early-stage disease with a HR+ tumor (n=54), a HER2+ tumor (n=16) or a triple negative tumor (n=16) and healthy donors (n=41). Adjusted p-values for* ***(a-c)*** *were computed by effectuating the Kruskal-Wallis test followed by Dunn's multiple comparisons test.*

which appeared largely unaffected by the subtype of breast cancer at early-stage (Supplementary Figure 3a) or late-stage (Supplementary Figure 3b). Next, we investigated whether the capacity of T cells to produce cytokines IFNγ and TNFα following *ex vivo* stimulation with PMA-ionomycin for three hours, was altered in a breast cancer subtype dependent manner (Supplementary Figure 1c). Due to sample processing limitations, we confined this part of our analysis to patients with early-stage disease. The ability to produce IFNγ by CD8+ and conventional CD4+ T cells upon stimulation was not affected by the

presence of a tumor of any subtype (HR+, HER2+ and TNBC) (Figure 5c), suggesting that T cells from patients with early-stage breast cancer retained similar potential to produce this cytokine *ex vivo*. However, when analyzing T cells' ability to produce TNFα upon stimulation, we observed that CD4 T cells of breast cancer patients produced more of this cytokine compared to HDs. This increase in TNFα was statistically significant in patients with HR+ and TNBC subtypes, and showed a trend toward significance in HER2+ patients (Figure 5c). No differences were observed in cytokine production between the molecular breast cancer subtypes. Together these data indicate that T cell phenotype and functionality is modestly altered across the molecular subtypes in early and late stages of disease compared to HDs.

Discussion

In recent years, it has become increasingly clear that solid tumors impact the immune system in ways that extend far beyond the tumor microenvironment[12,13]. However, the influence of tumors on the systemic immune landscape, particularly in relation to (breast) cancer subtype and disease stage, remains poorly understood. This study aimed to investigate the changes in the circulating immune landscape across different disease stages and molecular subtypes of breast cancer. We utilized multi-parameter flow cytometry to comprehensively assess the abundance, phenotype, and activation states of both lymphoid and myeloid immune populations from freshly collected peripheral blood samples. Pre-clinical evidence indicates a critical role for neutrophils in disease progression[21-23]; however, these fragile and short-lived cells are often overlooked due to their inability to be stored. By analyzing fresh blood samples, we successfully captured the full complexity of the immune landscape, including all granulocyte populations.

Our data indicate that the systemic immune landscape in patients with breast cancer differs significantly from that of HDs, with more pronounced immune cell abnormalities in late-stage compared to early-stage disease. In metastatic breast cancer, we observed a general trend of the innate immune compartment expansion and adaptive immune compartment reduction relative to HDs. These findings highlight disease stage as a critical determinant of the circulating immunological profile in breast cancer, consistent with the expectation that more advanced, disseminated disease exerts a greater impact on the immune system. Moreover, we established that certain changes in the systemic immune landscape of breast cancer patients within early- and late-stage disease associated with a particular molecular subtype. For example, circulating CD8 T cells are specifically decreased in patients with mTNBC compared to HDs, but this was not observed in patients with late-stage HR+ or HER2+ breast cancer. Similarly, the systemic increase in neutrophils observed in late-stage breast cancer is seen only in HR+ and triple-negative subtypes, while neutrophil levels in late-stage HER2+ breast cancer closely resemble those observed in HDs. Notably,

the most profound immune dysregulation was observed in patients with TNBC, highlighting the subtype-specific nature of immune cell perturbations in breast cancer. Furthermore, we observed that disease stage seems a more dominant factor than molecular subtype in shaping the circulating immune landscape in patients with breast cancer.

The precise mechanisms by which breast tumors of different molecular subtypes differentially impact the systemic immune landscape are yet to be fully elucidated. Each breast cancer subtype is characterized by unique genetic mutations, copy number variations, and gene expression profiles, which can directly or indirectly lead to distinct patterns of cytokine and chemokine release[24-26]. These variations in cytokine and chemokine profiles may contribute to subtype-specific immune alterations. Additionally, epigenetic reprogramming of cancer cells—such as changes in DNA methylation and histone modifications—can further influence immune cell function and gene expression, leading to systemic immune changes. We hypothesize that these factors are crucial for understanding the differential immune responses observed among the various breast cancer subtypes.

Apart from tumor molecular subtype and disease stage, other factors could influence the systemic immune profile. It is important to acknowledge that the patients included in this study closely reflect those encountered in clinical practice, meaning that a proportion of patients with metastatic disease had received prior treatment for their primary tumor. It has previously been shown that treatment with chemotherapeutics impacts the circulating immune compartment for longer than the three-week washout period that was used in this study[27,28]. We would therefore like to emphasize that the observed differences regarding patients with late-stage disease are not necessarily purely tumor driven, but can be a result of multiple combined factors, including treatment history, tumor grade or histological subtype. In addition to treatment history, the genetic make-up of the tumors may have a strong additive effect on the systemic immune landscape[29-31], as described above. Though some driver mutations (e.g. mutations in *TP53* or *PIK3CA)* are more prevalent within a specific breast cancer subtype, they are not exclusively found in just one subtype[24,32,33]. If specific mutations influence the immune profile in blood and are present across different subtypes and stages, these tumor mutations may mask potential differences driven by disease subtype and stage. Since we do not have data on tumor mutations, further research is needed to investigate the relation between tumor-genotype/immuno-phenotype.

Finally, we would like to discuss the potential clinical significance of our findings. Clinical research has demonstrated that an elevated neutrophil-to-lymphocyte ratio (NLR) as well as an reduced lymphocyte-to-monocyte ratio (LMR) is associated with worse disease prognosis and diminished therapeutic response across various cancer types, including breast cancer[34-40]. Since we did not observe a concordant increase in lymphocyte counts with the increased numbers of classical monocytes and neutrophils, our findings suggests that patients with breast cancer exhibit a skewed immune profile, characterized by an increased

dominance of myeloid over lymphoid cells. This myeloid-skewed systemic immune landscape may leave patients less equipped to mount an effective immune response, potentially leading to poorer clinical outcomes than they would have experienced with a more balanced immune profile. Restoring the NLR and LMR to ratio's similar to those observed in HDs may represent a promising therapeutic strategy, potentially enhancing the efficacy of immunotherapy when administered either right after or in combination with it. Turning to the clinical implications of lymphoid perturbations, tumor-infiltrating B cells and plasma cells have shown considerable predictive and prognostic value in various cancers, particularly in the context of both conventional therapies and immune checkpoint inhibitors[41,42]. Others have shown in a small set of matched tumor-blood samples, that the decrease in memory B cells in the blood contrasts with an increase in class-switched memory B cells within the tumor[43]. Whether the observed systemic reduction in memory B cells and plasmablast-like cells is associated with an aberrant TME and altered patient outcomes remains to be determined and warrants further investigation. CD4 T cells, particularly T helper cells, are essential for orchestrating a robust immune response, as they facilitate the activation and differentiation of various immune cells, including cytotoxic T cells and B cells, which are crucial for effective tumor clearance[16,44,45].

Overall, our data show that patients with late-stage disease have more of the cell types that associate with poor clinical outcome like neutrophils and monocytes[37,39,40,46-48], and less of favorable immune cell types like cytotoxic T cells and T helper cells[49-51]. Given that the systemic immune profile of breast cancer patients appears to become increasingly dysregulated as the disease progresses, it is important to consider initiating immune modulatory strategies before metastatic spread occurs. Indeed, across cancer types, increased response rates are observed with neoadjuvant immune checkpoint blockade, when compared to immune checkpoint blockade administered in the more advanced disease setting[52-54], suggesting that earlier intervention may harness a more functional immune system to achieve better therapeutic outcomes. Lastly, we propose that developing therapeutic strategies aimed at normalizing the systemic immune landscape may hold potential to enhance treatment efficacy and improve overall outcomes for patients.

Supplementary Figures

A

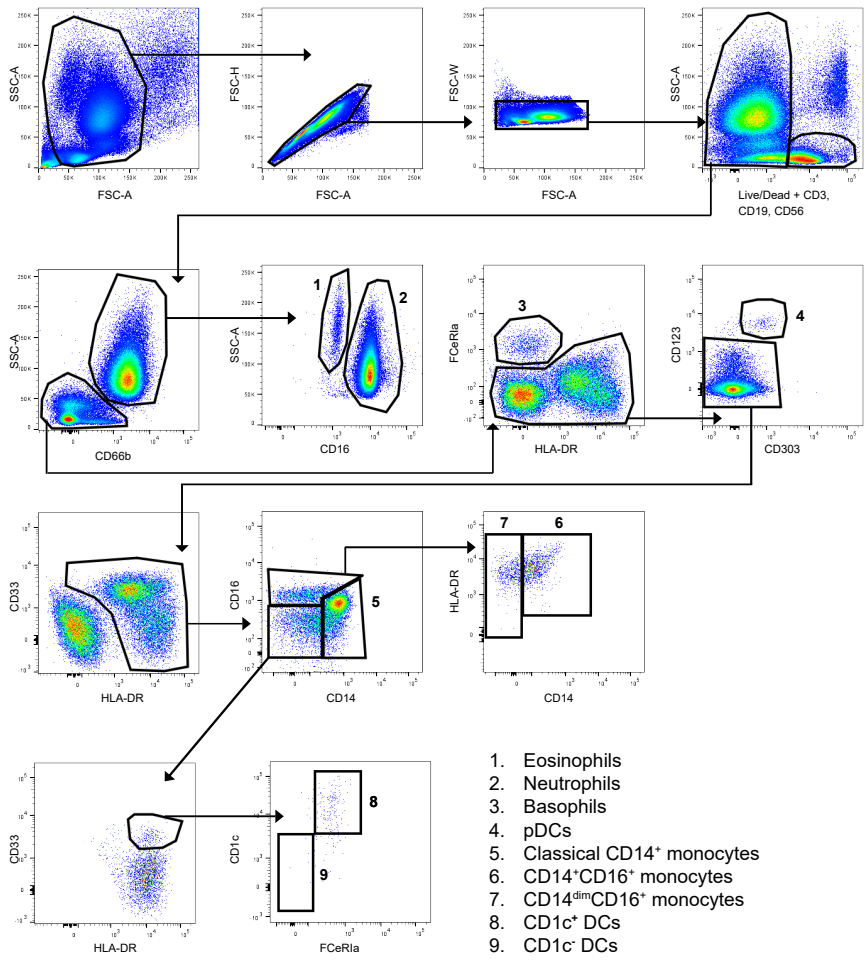

B

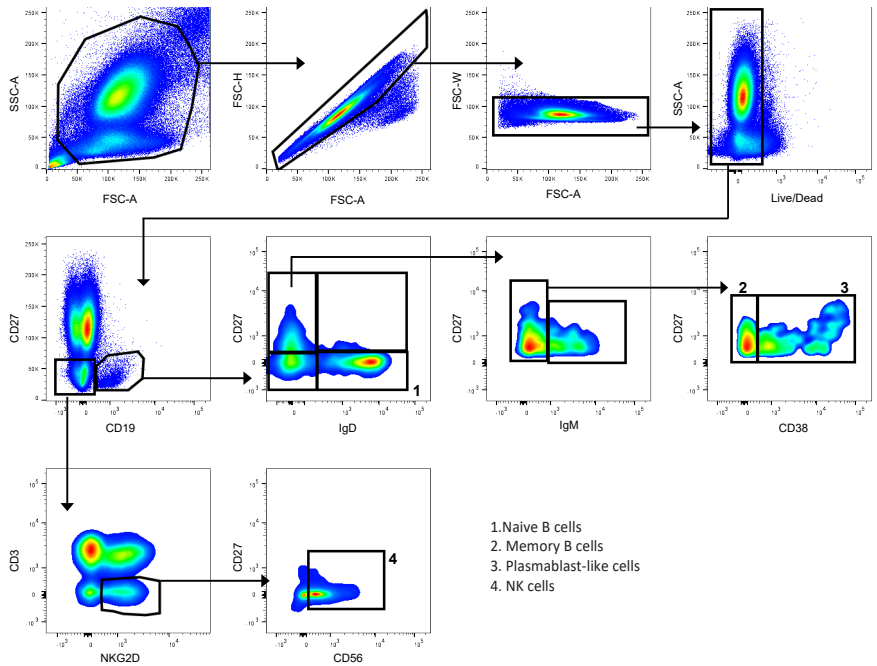

C

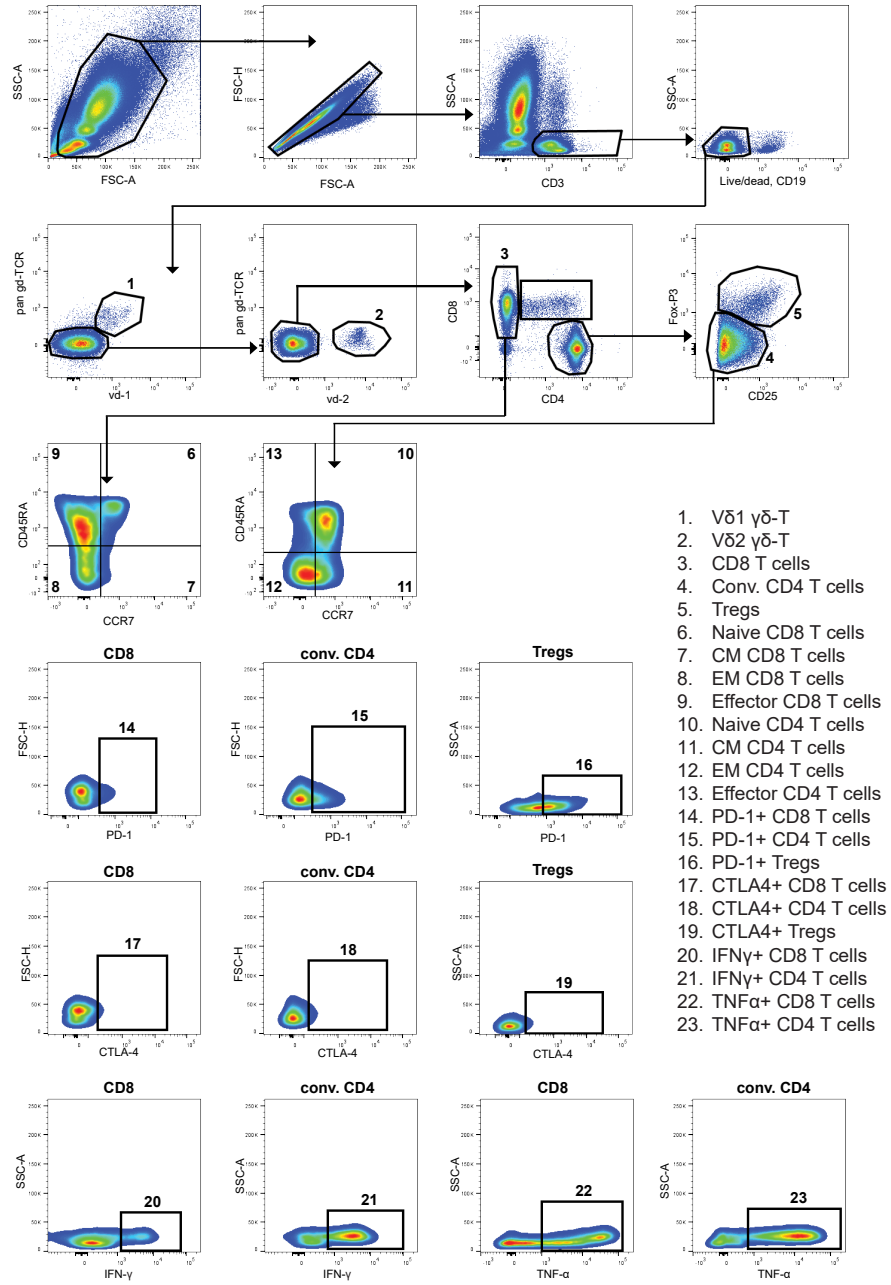

Supplementary Figure 1. Gating strategies for flow cytometry analysis of peripheral blood immune populations. (a) *Myeloid panel gating strategy identifying eosinophils (lineage$^-$, high side scatter, CD66b$^+$ CD16$^-$), neutrophils (lineage$^-$, high side scatter, CD66b$^+$ CD16+), basophils (lineage$^-$, FcεRIα$^+$, HLA-DR$^-$), plasmacytoid DCs (pDCs) (lineage$^-$, HLA-DR$^+$, CD303$^+$, CD123$^+$), Classical monocytes (lineage$^-$, HLA-DR$^+$, CD33$^+$, CD14$^+$, CD16$^-$), Transitional monocytes (lineage$^-$, HLA-DR$^+$, CD33$^+$, CD14$^+$, CD16$^+$), Non-classical monocytes (lineage$^-$, HLA-DR$^+$, CD33$^+$, CD14^{dim}, CD16$^+$), CD1c$^+$ DCs (lineage$^-$, HLA-DR$^+$, CD33$^+$, CD14$^-$, CD16$^-$, CD1c$^+$, FcεRIα$^+$) and CD1c$^-$ DCs (lineage$^-$, HLA-DR$^+$, CD33$^+$, CD14$^-$, CD16$^-$, CD1c$^-$, FcεRIα$^-$). **(b)** Gating strategy to identify B cell subsets identifying naive B cells (CD19$^+$, CD27$^-$, IgD$^+$), switched memory B cells (CD19$^+$, CD27$^+$, IgD$^-$, IgM$^-$, CD38$^-$), and plasmablasts-like cells (CD19$^+$, CD27$^+$, IgD$^-$, IgM$^-$, CD38$^+$). Gating strategy to identify NK cells (CD19$^-$, CD3$^-$, NKG2D$^+$, CD56$^+$). **(c)** T cell panel gating strategy identifying Vδ1 γδ T cells (CD3$^+$, Vδ1$^+$, pan γδ TCR$^+$), Vδ2 γδ T cells (CD3$^+$, Vδ2$^+$), CD8 T cells (CD3$^+$, Vδ1$^-$, pan γδ TCR$^-$, Vδ2$^-$, CD8$^+$, CD4$^-$), conventional CD4 T cells (CD3$^+$, Vδ1$^-$, pan γδ TCR$^-$, Vδ2$^-$, CD8$^-$, CD4$^+$, FoxP3$^-$), Tregs (CD3$^+$, Vδ1$^-$, pan γδ TCR$^-$, Vδ2$^-$, CD8$^-$, CD4$^+$, FoxP3$^+$, CD25^{hi}). Differentiation states were obtained as follows for both the conventional CD4 T cells and CD8 T cells: naïve T cells (CD45RA$^+$, CCR7$^+$), central memory (CM) T cells (CD45RA$^-$, CCR7$^+$), effector memory (EM) T cells (CD45RA$^-$, CCR7$^-$), effector T cells (CD45RA$^+$, CCR7$^-$). Additional phenotypic markers were gated according to the population names. Cytokine production was measured after PMA-ionomycin stimulation. Gating strategy identifying IFNγ$^+$ CD8 T cells (CD3$^+$, Vδ1$^-$, pan γδ TCR$^-$, Vδ2$^-$, CD8$^+$, CD4$^-$, IFNγ$^+$), TNFα$^+$ CD8 T cells (CD3$^+$, Vδ1$^-$, pan γδ TCR$^-$, Vδ2$^-$, CD8$^+$, CD4$^-$, TNFα$^+$), IFNγ$^+$ conventional CD4 T cells (CD3$^+$, Vδ1$^-$, pan γδ TCR$^-$, Vδ2$^-$, CD8$^-$, CD4$^+$, FoxP3$^-$, IFNγ$^+$), TNFα$^+$ conventional CD4 T cells (CD3$^+$, Vδ1$^-$, pan γδ TCR$^-$, Vδ2$^-$, CD8$^-$, CD4$^+$, FoxP3$^-$, TNFα$^+$).*

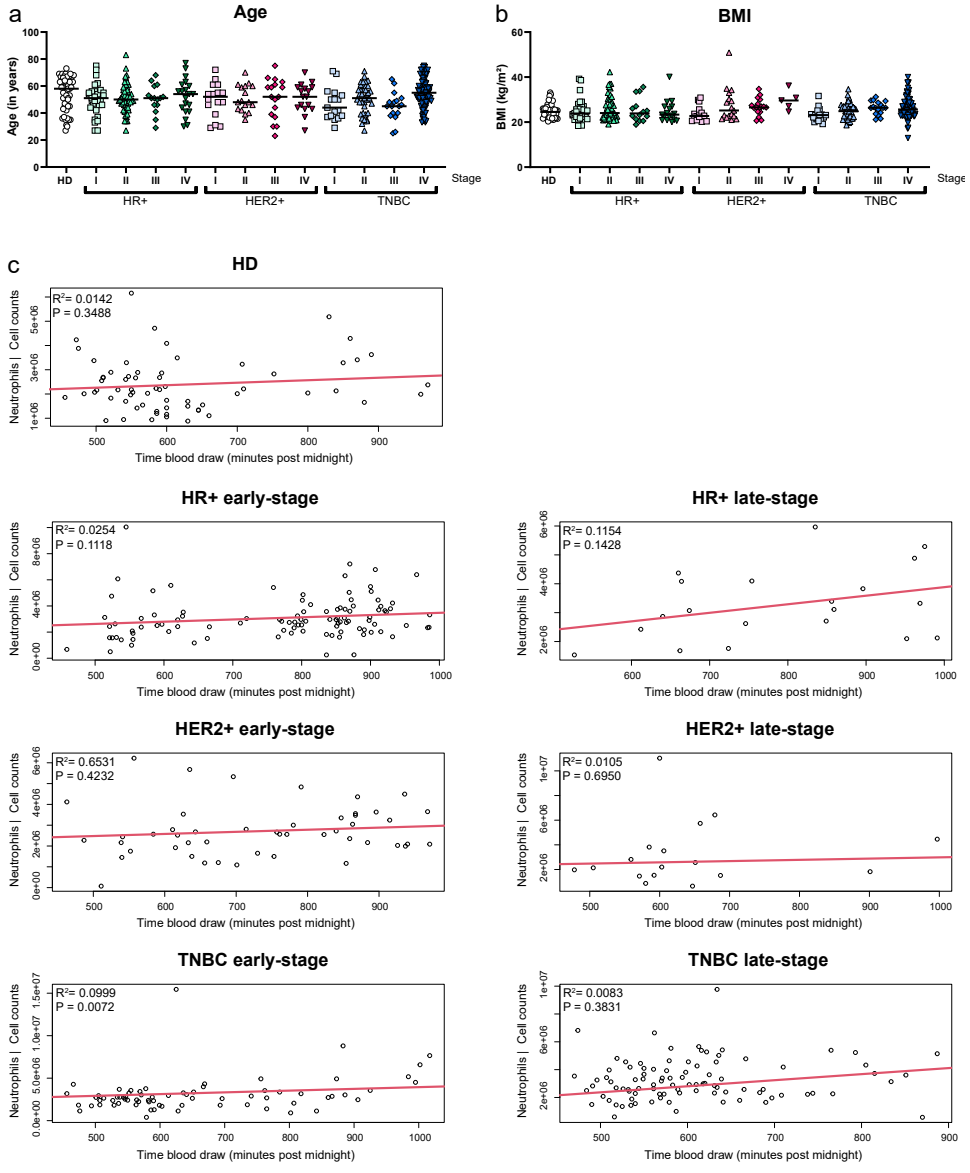

Supplementary Figure 2. Clinical parameters and time of blood draw of patients with early- and late-stage breast cancer across different molecular subtypes. (a) *Age distribution and* ***(b)*** *Body Mass Index (kg/length in m²) distribution in patients with breast cancer separated by disease stage and tumor subtype, and in healthy donors. Adjusted p-values for* ***(a)*** *and* ***(b)*** *were computed with the Kruskal-Wallis test followed by Dunn's multiple comparisons test.* ***(c)*** *Correlation analysis between neutrophil cell counts per mL blood and the time of day the blood was taken. R^2 and P values are provided in the top-left corner of each graph.*

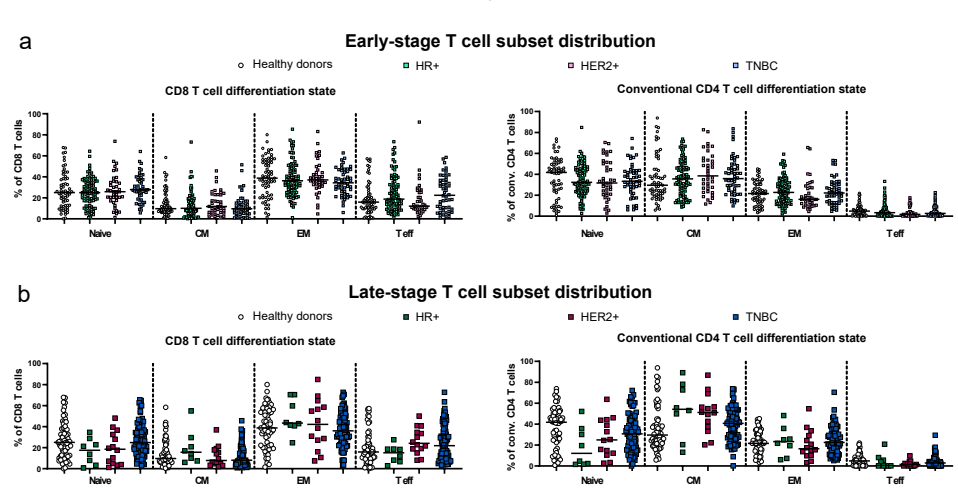

Supplementary Figure 3. T cell differentiation state in patients with early- and late-stage breast cancer across different molecular subtypes. *T cell differentiation state based on surface marker expression of CD45RA and CCR7 as determined by flow cytometry (see Supplementary Figure 1c), comparing proportions within conventional CD4+ and CD8+ T cells for* ***(a)*** *early-stage breast cancer patients with HR+ tumors (n=101), HER2+ tumors (n=50), triple negative tumors (n=74) and healthy donors (n=65) and* ***(b)*** *late-stage breast cancer patients with HR+ tumors (n=20), HER2+ tumors (n=17), triple negative tumors (n=93) and healthy donors (n=65). CM = central memory, EM = effector memory and T eff = effector T cells. Adjusted p-values for were computed with the Kruskal-Wallis test followed by Dunn's multiple comparisons test.*

Supplementary Tables

Supplementary Table 1: *Treatment history at the time of blood donation for patients with late-stage disease. Chemotherapy for mHER2+ BC: taxane, for 1 pt platinum agent. Dual anti-HER2: trastuzumab and pertuzumab. T-DM1 is Trastuzumab-Emtansine.*

	Treatment for metastatic disease
Late-stage HR+ *n=20*	n = 11 (55%) treatment-naïve for M1-diseaes n = 7 (35%) aromatase inhibitor n = 1 (5%) anti-hormonal therapy (e.g. tamoxifen) n = 1 (5%) oestrogen receptor antagonist (e.g. fulvestrant)
Late-stage HER2+ *n=17*	n = 6 (30%) chemo-naïve for M1-disease n = 11 (70%) chemotherapy + dual anti-HER2 blockade n = 7 (41%) T-DM1 as second line n = 4 (24%) chemo + trastuzumab as third line n = 1 (6%) Tyrosine kinase inhibitor
Late-stage TNBC *n=93*	Treatment-naïve for M1-disease

Supplementary Table 2: *List of antibodies used for flow cytometry.*

Human flow cytometry antibodies

Antigen	Fluorochrome	Clone	Dilution	Company	Catalogue number
CD3	PE Cy5	UCHT1	1:200	BD Bioscience	555334
CD4	BV421	RPA-T4	1:100	BD Bioscience	562424
CD8	BUV805	SK1	1:200	BD Bioscience	612754
Pan γδ TCR	PE	11F2	1:100	BD Bioscience	555717
vδ1	FITC	TS8.2	1:100	Thermofisher	TCR2730
vδ2	BUV395	B6	1:100	BD Bioscience	748582
FoxP3	PE Cy5.5	FJK-16s	1:50	Thermofisher	35-5773-82
CCR7	APC R700	150503	1:50	BD Bioscience	565868
CD45RA	BUV737	HI100	1:400	BD Bioscience	612846
CD25	AF647	BC96	1:100	BioLegend	302618
PD-1	APC Cy7	EH12.2H7	1:100	BioLegend	329922
CTLA-4	PE CF594	BNI3	1:200	BD Bioscience	562742
IL-17	PerCP Cy5.5	N49-653	1:50	BD Bioscience	560799
IFNγ	BV785	4S.B3	1:200	BioLegend	502542
TNFα	PE Cy7	Mab11	1:400	BioLegend	502930
CD27	BV786	L128	1:100	BD Bioscience	563327
TIGIT	PerCP Cy5.5	A151536	1:100	BioLegend	372718
Ki-67	PE Cy7	B56	1:50	BD Bioscience	561283
CTLA-4	PE CF594	PE/Dazzle594	1:200	BioLegend	369616
CD19	PE Cy5	HIB19	1:200	BD Bioscience	555414
CD3	BUV496	UCHT1	1:100	BD Bioscience	612940
CD56	PE Cy5	B159	1:100	BD Bioscience	555517
CD161	PE Cy5	DX12	1:100	BD Bioscience	551138
HLA-DR	BUV661	G46-6	1:100	BD Bioscience	612980
CD14	BUV737	M5E2	1:100	BD Bioscience	612763
CD16	BUV496	3G8	1:100	BD Bioscience	612944
CD16	AF700	3G8	1:200	BioLegend	302026
CD11b	BV421	ICRF44	1:200	BioLegend	301324
CD11c	BV785	3.9	1:100	BioLegend	301644
cKIT/CD117	PE Cy5.5	104D2	1:400	Thermofisher	CD11718
CD1c	PE Cy7	L161	1:100	BioLegend	331516
CD141	BV711	1A4	1:100	BD Bioscience	563155
CD123	PE	6H6	1:200	BioLegend	396604
CD66b	PerCP-Cy5.5	G10F5	1:200	BD Bioscience	562254
CD66b	AF647	G10F5	1:200	BD Bioscience	561645
CD33	PerCP Cy5.5	WM53	1:100	BioLegend	303414
CD303	APC vio770	REA693	1:100	Miltenyi Biotech	130-114-178
CD41a	BUV395	HIP8	1:400	BD Bioscience	740295
FcεRIα	PE Dazzle 594	AER-37(CRA-1)	1:200	BioLegend	334634
CD34	FITC	581	1:100	BD Bioscience	555821
CD19	BUV395	SJ25C1	1:50	BD Bioscience	563549
IgD	APC	IA6-2	1:100	BD Bioscience	561303
CD20	BUV805	2H7	1:200	BD Bioscience	612905
CD27	PE	M-T271	1:200	BD Bioscience	555441
CD10	AF700	HI10a	1:200	BD Bioscience	563509
CD24	BB515	ML5	1:200	BD Bioscience	564521
IgM	APC Cy7	MHM-88	1:100	BioLegend	314520
CD38	BUV737	HIT2	1:400	BD Bioscience	741837
CD5	PE Dazzle 594	L17F12	1:400	BioLegend	364012
CD1d	BV786	42.1	1:200	BD Bioscience	743608
CD138	BV711	MI15	1:200	BioLegend	563184

Conflicts of interest

N.A.M.B, H.G., V.G., E.C., C.K., M.D., I.N., R.C.A.M.G., M.d.G., R.V., M.C.L., E.L. have no conflicts of interest to declare. H.M.O reports funding to the institute from Roche in order to perform the Triple B study and an advisory board fee from Novartis, Pfizer, Gilead, AstraZeneca and Daiichi Sankyo outside the submitted work. M.K. reports funding to the institute from BMS, Roche/ Genentech, AZ, and an advisory role/speakers fee for Alderaan, BMS, Domain Therapeutics, Gilead, Roche, MSD, and Daiichi Sankyo, outside the submitted work. K.E.d.V. reports research funding from Roche/ Genentech and is consultant for Macomics, outside the scope of this work.

Authors contribution

N.A.M.B. analyzed and interpreted data and wrote the manuscript with K.E.d.V.. H.G. designed flow cytometry panels, which N.A.M.B. modified. N.A.M.B., H.G., E.C., C.K. and M.D. processed the fresh blood samples and applied compensation and gating strategy to the flow cytometry data. N.A.M.B., V.G., I.N., R.J.G., M.d.G., R.V., M.C.L., E.L., H.M.O. and M.K. wrote a biobank protocol, asked patients for informed consent to participate in this study and/or were coordinating/supervising clinical trials of which the baseline samples were used. K.E.d.V. and M.K. conceived the project, gave critical input throughout the analysis and supervised the study. All authors edited and approved the manuscript.

Acknowledgements

We thank patients and healthy donors for generously donating blood for the benefit of science. We thank Oncode Institute and the Dutch Cancer Society (10653ALPE) for funding the immunophenotyping of the TNBC patients and HDs. Research in the De Visser laboratory is funded by Oncode Institute, the Dutch Cancer Society (KWF14801; KWF13191), KWF/Oncode grant 14339, the Netherlands Organisation for Scientific Research (NWOVICI91819616). A Sister's Hope foundation contributed to the immunophenotyping of the TNBC patients. Research in the Kok group is funded by the Netherlands Organisation for Scientific Research (NWO-VIDI 09150172010043) and Victoria's Secret Global Fund for Women's Cancers Rising Innovator Research Grant, in Partnership with Pelotonia & AACR. Biobank initiative was partly supported by the Dutch Cancer Society (KWF11105). This research was further supported by an institutional grant to the NKI of the Dutch Cancer Society and the Dutch Ministry of Health, Welfare and Sport. The funders played no role in study design, data collection, analysis and interpretation of data, or the writing of this manuscript. We thank the Dutch Breast Cancer Research Group (BOOG) for providing the samples from patients of the TRIPLE-B study. We acknowledge the supporting staff of the clinical trials of the Departments of Medical Oncology and the Triallab. We thank the NKI-AVL Core Facility Molecular Pathology & Biobanking (CFMPB) for providing NKI-AVL Biobank material, the NKI Biostatistics Centre and the NKI Flow Cytometry Facility for their support. Finally, we would like to thank everyone in the De Visser and Kok labs for inspiring discussions.

References

1 WHO. *International Agency for Research on Cancer*, <https://gco.iarc.fr/today/en/dataviz/pie?mode=cancer&key=total&types=0&sort_by=value1&sexes=2&cancers=20&group_populations=1> (2024).

2 Waks, A. G. & Winer, E. P. Breast Cancer Treatment: A Review. *JAMA* **321**, 288-300 (2019). https://doi.org/10.1001/jama.2018.19323

3 Orrantia-Borunda, E., Anchondo-Nunez, P., Acuna-Aguilar, L. E., Gomez-Valles, F. O. & Ramirez-Valdespino, C. A. in *Breast Cancer* (ed H. N. Mayrovitz) (2022).

4 Geurts, V. & Kok, M. Immunotherapy for Metastatic Triple Negative Breast Cancer: Current Paradigm and Future Approaches. *Curr Treat Options Oncol* **24**, 628-643 (2023). https://doi.org/10.1007/s11864-023-01069-0

5 Galliverti, G. *et al.* Myeloid Cells Orchestrate Systemic Immunosuppression, Impairing the Efficacy of Immunotherapy against HPV(+) Cancers. *Cancer Immunol Res* **8**, 131-145 (2020). https://doi.org/10.1158/2326-6066.CIR-19-0315

6 Kalathil, S. G. & Thanavala, Y. High immunosuppressive burden in cancer patients: a major hurdle for cancer immunotherapy. *Cancer Immunol Immunother* **65**, 813-819 (2016). https://doi.org/10.1007/s00262-016-1810-0

7 Zhu, Y. *et al.* CSF1/CSF1R blockade reprograms tumor-infiltrating macrophages and improves response to T-cell checkpoint immunotherapy in pancreatic cancer models. *Cancer Res* **74**, 5057-5069 (2014). https://doi.org/10.1158/0008-5472.CAN-13-3723

8 Collins, N. B. *et al.* PI3K activation allows immune evasion by promoting an inhibitory myeloid tumor microenvironment. *J Immunother Cancer* **10** (2022). https://doi.org/10.1136/jitc-2021-003402

9 Kciuk, M. *et al.* Recent Advances in Molecular Mechanisms of Cancer Immunotherapy. *Cancers (Basel)* **15** (2023). https://doi.org/10.3390/cancers15102721

10 Kim, S. K. & Cho, S. W. The Evasion Mechanisms of Cancer Immunity and Drug Intervention in the Tumor Microenvironment. *Front Pharmacol* **13**, 868695 (2022). https://doi.org/10.3389/fphar.2022.868695

11 Blomberg, O. S., Spagnuolo, L. & de Visser, K. E. Immune regulation of metastasis: mechanistic insights and therapeutic opportunities. *Dis Model Mech* **11** (2018). https://doi.org/10.1242/dmm.036236

12 Garner, H. & de Visser, K. E. Immune crosstalk in cancer progression and metastatic spread: a complex conversation. *Nat Rev Immunol* **20**, 483-497 (2020). https://doi.org/10.1038/s41577-019-0271-z

13 Hiam-Galvez, K. J., Allen, B. M. & Spitzer, M. H. Systemic immunity in cancer. *Nat Rev Cancer* **21**, 345-359 (2021). https://doi.org/10.1038/s41568-021-00347-z

14 Chauhan, S. K. *et al.* Peripheral immune cells in metastatic breast cancer patients display a systemic immunosuppressed signature consistent with chronic inflammation. *NPJ Breast Cancer* **10**, 30 (2024). https://doi.org/10.1038/s41523-024-00638-2

15 Dyikanov, D. *et al.* Comprehensive peripheral blood immunoprofiling reveals five immunotypes with immunotherapy response characteristics in patients with cancer. *Cancer Cell* **42**, 759-779 e712 (2024). https://doi.org/10.1016/j.ccell.2024.04.008

16 Nederlof, I. *et al.* Neoadjuvant nivolumab or nivolumab plus ipilimumab in early-stage triple-negative breast cancer: a phase 2 adaptive trial. *Nat Med* **30**, 3223-3235 (2024). https://doi.org/10.1038/s41591-024-03249-3

17 van Rossum, A. G. J. *et al.* Carboplatin-Cyclophosphamide or Paclitaxel without or with Bevacizumab as First-Line Treatment for Metastatic Triple-Negative Breast Cancer (BOOG 2013-01). *Breast Care (Basel)* **16**, 598-606 (2021). https://doi.org/10.1159/000512200

18 Geurts, V. C. M. *et al.* Unleashing NK- and CD8 T cells by combining monalizumab and trastuzumab for metastatic HER2-positive breast cancer: Results of the MIMOSA trial. *Breast* **70**, 76-81 (2023). https://doi.org/10.1016/j.breast.2023.06.007

19 Blomberg, O. S. *et al.* IL-5-producing CD4(+) T cells and eosinophils cooperate to enhance response to immune checkpoint blockade in breast cancer. *Cancer Cell* **41**, 106-123 e110 (2023). https://doi.org/10.1016/j.ccell.2022.11.014

20 Adrover, J. M., Nicolas-Avila, J. A. & Hidalgo, A. Aging: A Temporal Dimension for Neutrophils. *Trends Immunol* **37**, 334-345 (2016). https://doi.org/10.1016/j.it.2016.03.005

21 Szczerba, B. M. *et al.* Neutrophils escort circulating tumour cells to enable cell cycle progression. *Nature* **566**, 553-557 (2019). https://doi.org/10.1038/s41586-019-0915-y

22 Yang, L. *et al.* DNA of neutrophil extracellular traps promotes cancer metastasis via CCDC25. *Nature* **583**, 133-138 (2020). https://doi.org/10.1038/s41586-020-2394-6

23 Coffelt, S. B. *et al.* IL-17-producing gammadelta T cells and neutrophils conspire to promote breast cancer metastasis. *Nature* **522**, 345-348 (2015). https://doi.org/10.1038/nature14282

24 Cancer Genome Atlas, N. Comprehensive molecular portraits of human breast tumours. *Nature* **490**, 61-70 (2012). https://doi.org/10.1038/nature11412

25 Li, X. *et al.* Uncovering the Subtype-Specific Molecular Characteristics of Breast Cancer by Multiomics Analysis of Prognosis-Associated Genes, Driver Genes, Signaling Pathways, and Immune Activity. *Front Cell Dev Biol* **9**, 689028 (2021). https://doi.org/10.3389/fcell.2021.689028

26 Wellenstein, M. D. *et al.* Loss of p53 triggers WNT-dependent systemic inflammation to drive breast cancer metastasis. *Nature* **572**, 538-542 (2019). https://doi.org/10.1038/s41586-019-1450-6

27 Verma, R. *et al.* Lymphocyte depletion and repopulation after chemotherapy for primary breast cancer. *Breast Cancer Res* **18**, 10 (2016). https://doi.org/10.1186/s13058-015-0669-x

28 Bakker, N. A. M. *et al.* Triple-negative breast cancer modifies the systemic immune landscape and alters neutrophil functionality. *NPJ Breast Cancer* **11**, 5 (2025). https://doi.org/10.1038/s41523-025-00721-2

29 Charoentong, P. *et al.* Pan-cancer Immunogenomic Analyses Reveal Genotype-Immunophenotype Relationships and Predictors of Response to Checkpoint Blockade. *Cell Rep* **18**, 248-262 (2017). https://doi.org/10.1016/j.celrep.2016.12.019

30 Wang, Y., Feng, W. & Liu, P. Genotype-immunophenotype analysis reveals the immunogenomic subtype and prognosis of multiple myeloma. *Carcinogenesis* **41**, 1746-1754 (2020). https://doi.org/10.1093/carcin/bgaa037

31 van Weverwijk, A. & de Visser, K. E. Mechanisms driving the immunoregulatory function of cancer cells. *Nat Rev Cancer* **23**, 193-215 (2023). https://doi.org/10.1038/s41568-022-00544-4

32 Martinez-Saez, O. *et al.* Frequency and spectrum of PIK3CA somatic mutations in breast cancer. *Breast Cancer Res* **22**, 45 (2020). https://doi.org/10.1186/s13058-020-01284-9

33 Silwal-Pandit, L. *et al.* TP53 mutation spectrum in breast cancer is subtype specific and has distinct prognostic relevance. *Clin Cancer Res* **20**, 3569-3580 (2014). https://doi.org/10.1158/1078-0432.CCR-13-2943

34 Templeton, A. J. *et al.* Prognostic role of neutrophil-to-lymphocyte ratio in solid tumors: a systematic review and meta-analysis. *J Natl Cancer Inst* **106**, dju124 (2014). https://doi.org/10.1093/jnci/dju124

35 Shao, Y. *et al.* Prognostic value of pretreatment neutrophil-to-lymphocyte ratio in renal cell carcinoma: a systematic review and meta-analysis. *BMC Urol* **20**, 90 (2020). https://doi.org/10.1186/s12894-020-00665-8

36 Liu, J. *et al.* Systemic immune-inflammation index, neutrophil-to-lymphocyte ratio, platelet-to-lymphocyte ratio can predict clinical outcomes in patients with metastatic non-small-cell lung cancer treated with nivolumab. *J Clin Lab Anal* **33**, e22964 (2019). https://doi.org/10.1002/jcla.22964

37 Guo, W. *et al.* Prognostic value of neutrophil-to-lymphocyte ratio and platelet-to-lymphocyte ratio for breast cancer patients: An updated meta-analysis of 17079 individuals. *Cancer Med* **8**, 4135-4148 (2019). https://doi.org/10.1002/cam4.2281

38 Chen, Y. *et al.* Association of Lymphocyte-to-Monocyte Ratio With Survival in Advanced Gastric Cancer Patients Treated With Immune Checkpoint Inhibitor. *Front Oncol* **11**, 589022 (2021). https://doi.org/10.3389/fonc.2021.589022

39 Ma, Y., Zhang, J. & Chen, X. Lymphocyte-to-Monocyte Ratio is Associated with the Poor Prognosis of Breast Cancer Patients Receiving Neoadjuvant Chemotherapy. *Cancer Manag Res* **13**, 1571-1580 (2021). https://doi.org/10.2147/CMAR.S292048

40 Zhang, Z. *et al.* Prognostic Evaluation of Metastasis-Related Lymphocyte/Monocyte Ratio in Stage I-II Breast Cancer Receiving Chemotherapy. *Front Oncol* **11**, 782383 (2021). https://doi.org/10.3389/fonc.2021.782383

41 Laumont, C. M. & Nelson, B. H. B cells in the tumor microenvironment: Multi-faceted organizers, regulators, and effectors of anti-tumor immunity. *Cancer Cell* **41**, 466-489 (2023). https://doi.org/10.1016/j.ccell.2023.02.017

42 Laumont, C. M., Banville, A. C., Gilardi, M., Hollern, D. P. & Nelson, B. H. Tumour-infiltrating B cells: immunological mechanisms, clinical impact and therapeutic opportunities. *Nat Rev Cancer* **22**, 414-430 (2022).

https://doi.org/10.1038/s41568-022-00466-1
43 Harris, R. J. *et al.* Tumor-Infiltrating B Lymphocyte Profiling Identifies IgG-Biased, Clonally Expanded Prognostic Phenotypes in Triple-Negative Breast Cancer. *Cancer Res* **81**, 4290-4304 (2021). https://doi.org/10.1158/0008-5472.CAN-20-3773
44 Tay, R. E., Richardson, E. K. & Toh, H. C. Revisiting the role of CD4(+) T cells in cancer immunotherapy-new insights into old paradigms. *Cancer Gene Ther* **28**, 5-17 (2021). https://doi.org/10.1038/s41417-020-0183-x
45 Ahrends, T. *et al.* CD4(+) T cell help creates memory CD8(+) T cells with innate and help-independent recall capacities. *Nat Commun* **10**, 5531 (2019). https://doi.org/10.1038/s41467-019-13438-1
46 Ethier, J. L., Desautels, D., Templeton, A., Shah, P. S. & Amir, E. Prognostic role of neutrophil-to-lymphocyte ratio in breast cancer: a systematic review and meta-analysis. *Breast Cancer Res* **19**, 2 (2017). https://doi.org/10.1186/s13058-016-0794-1
47 Kiss, M., Caro, A. A., Raes, G. & Laoui, D. Systemic Reprogramming of Monocytes in Cancer. *Front Oncol* **10**, 1399 (2020). https://doi.org/10.3389/fonc.2020.01399
48 Krenn-Pilko, S. *et al.* The elevated preoperative derived neutrophil-to-lymphocyte ratio predicts poor clinical outcome in breast cancer patients. *Tumour Biol* **37**, 361-368 (2016). https://doi.org/10.1007/s13277-015-3805-4
49 Kagamu, H. *et al.* CD4(+) T-cell Immunity in the Peripheral Blood Correlates with Response to Anti-PD-1 Therapy. *Cancer Immunol Res* **8**, 334-344 (2020). https://doi.org/10.1158/2326-6066.CIR-19-0574
50 Liu, J. *et al.* Circulating memory PD-1(+)CD8(+) T cells and PD-1(+)CD8(+)T/PD-1(+)CD4(+)T cell ratio predict response and outcome to immunotherapy in advanced gastric cancer patients. *Cancer Cell Int* **23**, 274 (2023). https://doi.org/10.1186/s12935-023-03137-9
51 Manjarrez-Orduno, N. *et al.* Circulating T Cell Subpopulations Correlate With Immune Responses at the Tumor Site and Clinical Response to PD1 Inhibition in Non-Small Cell Lung Cancer. *Front Immunol* **9**, 1613 (2018). https://doi.org/10.3389/fimmu.2018.01613
52 Blank, C. U. *et al.* Neoadjuvant versus adjuvant ipilimumab plus nivolumab in macroscopic stage III melanoma. *Nat Med* **24**, 1655-1661 (2018). https://doi.org/10.1038/s41591-018-0198-0
53 Robert, C. A decade of immune-checkpoint inhibitors in cancer therapy. *Nat Commun* **11**, 3801 (2020). https://doi.org/10.1038/s41467-020-17670-y
54 Vansteenkiste, J. *et al.* Current status of immune checkpoint inhibition in early-stage NSCLC. *Ann Oncol* **30**, 1244-1253 (2019). https://doi.org/10.1093/annonc/mdz175

CHAPTER 4

Triple-Negative Breast Cancer Modifies the Systemic Immune Landscape and Alters Neutrophil Functionality

Noor A.M. Bakker[1,2,5], Hannah Garner[1,2,#], Ewald van Dyk[1,2,3,#], Elisa Champanhet[1], Chris Klaver[1], Maxime Duijst[1], Leonie Voorwerk[1,10], Iris Nederlof[1], Rosie Voorthuis[6], Marte C. Liefaard[6], Marja Nieuwland[7], Iris de Rink[7], Onno B. Bleijerveld[8], Hendrika M. Oosterkamp[9], Lodewyk F.A. Wessels[2,3], Marleen Kok[1,4,*] and Karin E. de Visser[1,2,5,*]

NPJ Breast Cancer. 2025 jan 23; 11(5). DOI: 10.1038/s41523-025-00721-2

[1] Division of Tumor Biology & Immunology, The Netherlands Cancer Institute, Amsterdam, The Netherlands
[2] Oncode Institute, Utrecht, The Netherlands
[3] Division of Molecular Carcinogenesis, The Netherlands Cancer Institute, Amsterdam, The Netherlands
[4] Department of Medical Oncology, The Netherlands Cancer Institute, Amsterdam, The Netherlands
[5] Department of Immunology, Leiden University Medical Centre, Leiden, The Netherlands
[6] Division of Molecular Pathology, The Netherlands Cancer Institute, Amsterdam, The Netherlands
[7] Genomics Core Facility, The Netherlands Cancer Institute, Amsterdam, The Netherlands
[8] Proteomics Facility, The Netherlands Cancer Institute, Amsterdam, The Netherlands
[9] Department of Medical Oncology, Haaglanden Medical Center, The Hague, The Netherlands
[10] Current address: Department of Internal Medicine, Groene Hart hospital, Gouda, The Netherlands

# These authors contributed equally
* These authors contributed equally

Correspondence: k.d.visser@nki.nl (K.E.d.V.), m.kok@nki.nl (M.K.)

Abstract

Cancer disrupts intratumoral innate-adaptive immune crosstalk, but how the systemic immune landscape evolves during breast cancer progression remains unclear. We profiled circulating immune cells in stage I-III and stage IV triple-negative breast cancer (TNBC) patients and healthy donors (HDs). Metastatic TNBC (mTNBC) patients had reduced T cells, dendritic cells, and differentiated B cells compared to non-metastatic TNBC patients and HDs, partly linked to prior chemotherapy. Vδ1 γδ T cells from mTNBC patients produced more IL17 than those from HDs. Chemotherapy-naïve mTNBC patients showed increased classical monocytes and neutrophils. Transcriptional, proteomic and functional analyses revealed that neutrophils in mTNBC exhibited enhanced migratory capacity, elevated granule proteins, and higher ROS production. Some immune changes, such as reduced non-switched B cells and heightened neutrophil migration, were evident in earlier TNBC stages. This study comprehensively maps systemic immunity in TNBC, guiding future research on patient stratification and immunomodulation strategies.

Introduction

Over the past decade, immunotherapy has revolutionized cancer treatment by targeting the immune system. While much research has focused on local immune responses within the tumor microenvironment (TME), effective antitumor immunity requires ongoing coordination with the peripheral immune system. There is a growing recognition that solid tumors profound effects on the immune system, significantly altering the overall immune landscape beyond the TME[1-4]. Thus, a comprehensive understanding of cancer immunology must encompass the phenotypic and functional analysis of immune cell lineages in the peripheral immune system. Soluble mediators produced by cancer cells and other cells in the TME can induce the systemic expansion and polarization of myeloid cells, leading to chronic, systemic inflammation[4-10]. Depending on the context, this tumor-induced inflammation can either initiate or support tumor growth[11] and impact the therapeutic efficacy of systemic treatments[12].

Tumor-induced systemic inflammation can be characterized by increased neutrophil counts in blood, often represented in the clinic by the Neutrophil-to-Lymphocyte Ratio (NLR). Clinical studies have shown that a high NLR correlates with unfavorable disease outcome and poor therapy response across many cancer types, including breast cancer[13-18]. Pre-clinical studies have demonstrated that neutrophils support metastasis formation through diverse mechanisms, including inducing systemic immune suppression, supporting circulating cancer cells, fostering the establishment of the (pre-)metastatic niche, facilitating cancer cell infiltration into distant tissues, and awakening dormant cancer cells[19-27]. In addition to neutrophils, tumor progression has been reported to elicit systemic expansion of monocytes

and their reprogramming into an immunosuppressive phenotype[4,28-31]. Furthermore, it has been shown in mouse models and patients with breast and pancreatic cancer that dendritic cell (DC) differentiation is reduced in the bone marrow, leading to a reduction of the systemic cDC1 pool[32]. This could negatively affect anti-tumor immunity since DCs are the most effective antigen presenting cells and crucial for T cell activation. Tumor progression is also often associated with systemic lymphocyte perturbations, characterized by increased regulatory T cell (Treg) frequencies[33-35], and reduced CD8+ and conventional CD4+ T cells in blood of cancer patients[36,37]. Collectively, these data show that cancer influences circulating immune cell populations, which may impact disease progression and (immuno)therapy response. The majority of studies examine relative frequencies and rely on PBMC samples that lack granulocytes and therefore do not represent the entirety of the circulating immune system. How absolute cell counts and abundances relative to all immune cells change during disease progression, and how different stages of cancer affect their functionality is largely unclear. Although immune checkpoint blockade (ICB) has created a revolution in oncology, the majority of patients still do not benefit from ICB, including most of the advanced breast cancer patients. Better understanding of the systemic immune landscape is of critical importance to improve immunomodulatory treatments of cancer patients.

In this study, we set out to extensively profile the systemic immune landscape, including granulocytes, of patients with stage I-III TNBC, patients with mTNBC and a healthy donor (HD) control group (Figure 1a). We performed high-dimensional flow cytometry on fresh peripheral blood samples to assess the quantity and quality of circulating immune cell subpopulations. Our data revealed that patients with mTNBC – and to a lesser extent patients with stage I-III TNBC – have a markedly different systemic immune landscape compared to HDs. We found T cells, DC subsets and B cell differentiation to be decreased in blood of patients with mTNBC. In contrast, classical monocytes and neutrophils were increased. A substantial proportion of the included mTNBC patients received prior chemotherapy for their primary tumor, which allowed us to explore the changes in the systemic immune landscape that are associated with chemotherapy. Our findings suggest that the systemic reduction in T cell- and DC subsets in patients with mTNBC could be associated with recent chemotherapy. Conversely, the increase of classical monocytes and neutrophils was purely disease-related. Transcriptomic, proteomic and functional analysis revealed that neutrophils from patients with TNBC have increased migratory capacity, contained more granule proteins and produce more reactive oxygen species (ROS) than neutrophils from HDs, indicating that neutrophils are not only more abundant in the circulation of mTNBC patients, but also have distinct phenotypic and functional characteristics.

Overall, this study provides the first comprehensive characterization of the systemic immune landscape, including granulocytes, in a large cohort of patients with TNBC compared

to HDs. Our data highlight the substantial impact of TNBC and its disease stage on the systemic immune composition and function. This extensive analysis, which includes an independent validation cohort, offers novel insights into the immune profiles specific to patients with TNBC, thereby distinguishing between patients with and without prior chemotherapy treatment. Our data serve as a valuable resource for the field, guiding future preclinical and clinical research and paving the way for immunomodulatory treatment strategies.

Results

Metastatic TNBC reshapes the systemic immune landscape

To gain insights into how TNBC influences the systemic immune landscape during disease progression, we performed high-dimensional flow cytometry on fresh peripheral blood samples (Supplementary Figure 1a-d). We established a dedicated pipeline for the analysis of fresh blood samples[38], enabling a comprehensive interrogation of the full complexity of the systemic immune landscape, including granulocytes - cell types that are typically lost when working with peripheral blood mononuclear cell (PBMC) samples. We profiled patients with TNBC without distant metastases (stage I-III TNBC (n=44)) and stage IV patients with distant metastases (mTNBC (n=92)). As a control group we profiled healthy donors (HDs (n=65)) that were age-matched to mTNBC patients and sex- and BMI-matched to all TNBC patients (Supplementary Figure 2a, Supplementary Table 1). A separate cohort of patients with mTNBC (n=69) was used to validate our main findings (Figure 1a). Given that leukocyte numbers in the blood are circadian[39,40], we sought to withdraw blood in the morning. There was no statistically significant difference in time of blood draw between HD and patients with TNBC (Supplementary Figure 2a).

No differences in total white blood cell (WBC) counts were found between patients with stage I-III TNBC, patients with mTNBC and HDs (Figure 1b). Most significant differences were observed between HDs and patients with mTNBC, and between patients with non-metastatic versus metastatic disease (Figure 1b), indicating that the systemic immune system may become more dysregulated as disease progresses. We observed increased neutrophils in patients with mTNBC compared to HDs both in absolute cell counts (Figure 1b, c) and as relative frequency among WBCs (Supplementary Figure 3). We additionally observed an elevated NLR in patients with mTNBC compared to patients with stage I-III TNBC and HD (Supplementary Figure 2c), which is consistent with literature describing elevated NLR in patients with various types of stage IV cancer[18]. Although not statistically significant, we observed a trend towards increased neutrophils in patients with stage I-III TNBC compared to HDs, suggesting that neutrophils increase as disease progresses (Figure 1b, Supplementary Figure 3). Additionally, we found $CD14^{+}$ monocytes to be significantly increased in patients

with mTNBC compared to both HDs and patients with stage I-III TNBC (Figure 1b, c, Supplementary Figure 3). It was previously reported that breast cancer and pancreatic cancer alter the balance of monocytes and neutrophils compared to antigen presenting cDC1s in bone marrow and blood[32]. In line with this, we found that the frequencies and cell counts of $CD141^{hi}$ DCs (cDC1s) and $CD1c^{+}$ DCs (cDC2s) were decreased in patients with mTNBC compared to HDs (Figure 1b, c and Supplementary Figure 3).

cDCs are critical for cytotoxic T-cell activation, and $CD141^{hi}$ DCs are important for cross-presentation[41-43]. Others have shown in pre-clinical mouse models and patients with pancreatic cancer, that reduced numbers of (pre-)cDCs in blood and the TME are correlated with poor clinical outcome[32,44]. Hence these reduced numbers we found in patients with mTNBC could potentially have negative implications for inducing an adequate immune response.

Within the circulating lymphoid compartment we found that the total counts and frequencies of CD8+ T cells, conventional CD4+ T cells and Tregs were reduced in patients with mTNBC compared to stage I-III TNBC patients and HDs (Figure 1b, c, Supplementary Figure 3). Conversely, γδ-T cell subsets Vδ1 and Vδ2 T cells were unchanged in patients with mTNBC compared to HDs. Interestingly, Vδ2 T cells were increased in stage I-III TNBC patients (Supplementary Figure 2b) compared to HDs, but this difference was lost in the metastatic setting. No significant differences were found in cell counts and frequencies of CD1c negative DCs, plasmacytoid DCs (pDCs), natural killer (NK) cells, total B cells and eosinophils between any of the groups (Supplementary Figure 2). Overall, the frequency plots revealed similar trends (Supplementary Figure 3). Using an independent validation cohort of patients with mTNBC (n=69) we were able to validate all perturbations to the systemic immune landscape between mTNBC and HDs (Supplementary Figure 4a). Altogether, our data demonstrate multiple differentially regulated main immune cell populations in patients with mTNBC compared to HDs and patients with stage I-III TNBC.

IL-17 production by Vδ1 γδ T cells is increased in patients with mTNBC

Because total cell counts of CD8+, conventional CD4+ and regulatory T cells were decreased in patients with mTNBC (Figure 1), we wanted to investigate the composition and activation status of the circulating T lymphocyte pool in relation to disease stage. Analysis of the T cell differentiation state (Supplementary Figure 1c) revealed no differences between patients with stage I-III TNBC, patients with mTNBC and HDs (Figure 2a). Next, we profiled T cell phenotype and functional state by assessing the expression of the proliferation marker Ki67, PD-1 and CTLA-4, and *ex vivo* cytokine production of CD8+ and CD4+ T cells. Across different patients and HDs, there was notable heterogeneity in the peripheral CD8+ and conventional CD4+ T cell phenotype, which appeared largely unaffected by the presence of TNBC (Figure 2b). Additionally, the ability to produce IFNγ and TNFα by CD8+ and conventional

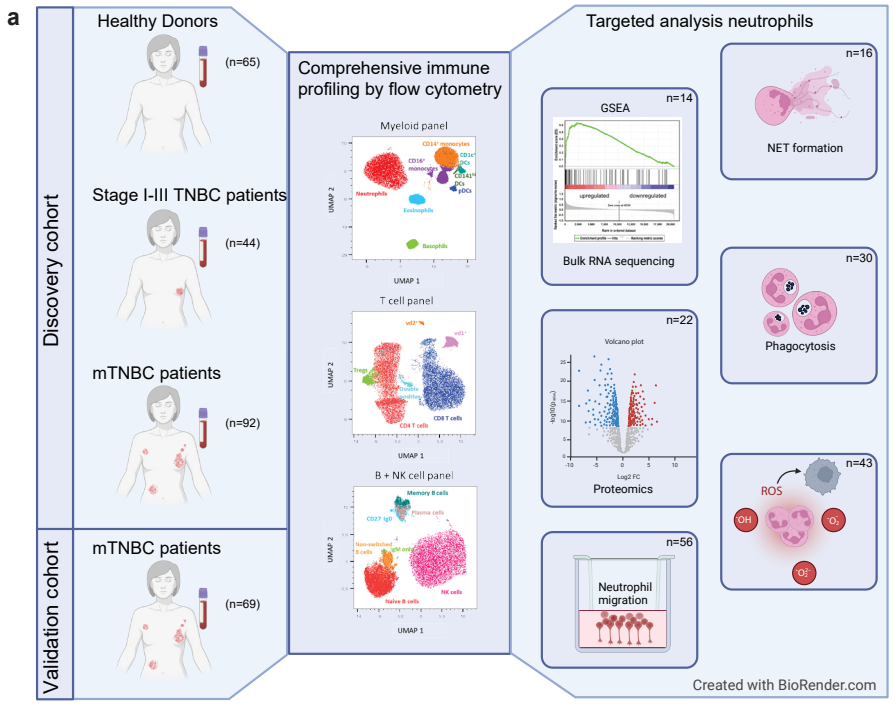

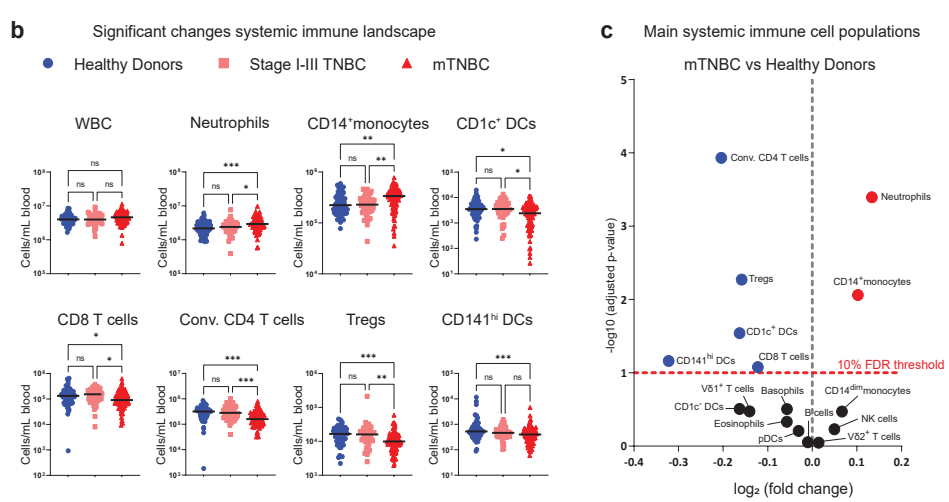

Figure 1. Comprehensive immune profiling of the systemic immune landscape in healthy donors, patients with stage I-III and metastatic triple-negative breast cancer. (a) *Graphical summary of included human blood samples and schematic overview of conducted experiments.* ***(b)*** *Overview of circulating immune cell populations that were significantly dysregulated in patients with triple-negative breast cancer (TNBC). Depicted are cell counts per mL blood as assessed by flow cytometry for healthy donors (HDs; n=65), stage I-III (Stage I-III TNBC; n=44) and metastatic TNBC patients (mTNBC; n=92). The y-axis is on a log scale. P-values were computed with the Kruskal-Wallis test followed by Dunn's multiple comparisons correction across groups.* ***(c)*** *Volcano plot summarizing major immune cell populations in blood accessed by flow cytometry comparing HDs to mTNBC patients. The x-axis represents log2 fold changes (red is more abundant in patients with mTNBC, blue is less abundant in patients with mTNBC) and the y-axis represents adjusted p-values on a negative log10 scale. P-values are corrected using the Benjamini-Hochberg procedure across immune cell types.*

CD4+ T cells upon stimulation with PMA-ionomycin for three hours was unaffected by TNBC (Figure 2c), suggesting that T cells from patients retained similar potential to produce those cytokines *ex vivo*. Next, we wanted to investigate whether we could retrieve certain aspects of the γδ T cell-IL17-neutrophil axis, that was previously described to drive systemic expansion of neutrophils and metastasis formation in distant organs in mice[19]. Here, we indeed confirm that circulating T cells from patients with mTNBC produced more IL17, with Vδ1-, but not Vδ2, γδ T cells showing a particularly pronounced increase in IL17 production upon *ex vivo* stimulation (Figure 2c). Moreover, this intriguing finding could be confirmed in the validation cohort consisting of patients with mTNBC (Supplementary Figure 4b).

Based on literature[45-47], we classified circulating Tregs into three subsets based on CD45RA and FoxP3 intensity, with Treg I expressing high levels of CD45RA and intermediate levels of FoxP3 (also referred to as "naïve Tregs"), Treg II expressing low levels of CD45RA and high levels of FoxP3 (also referred to as "activated Tregs") and Treg III expressing low levels of CD45RA and intermediate levels of FoxP3 (also referred to as "activated non-Treg") (Supplementary Figure 1c). We did not observe differences in Treg subset distribution in relation to TNBC status (Figure 2d). However, patients with mTNBC had a higher frequency of PD-1 positive circulating Tregs relative to HDs and patients with stage I-III TNBC (Figure 2d). In addition, Tregs in patients with stage I-III TNBC expressed more CTLA-4 compared to HDs (Figure 2d).

In summary, we revealed equal capability of T cells from patients with (m)TNBC and HDs to produce IFNγ and TNFα when stimulated *ex vivo*. Notably, we found that IL17 was significantly more produced by Vδ1 γδ T cells from patients with mTNBC.

Reduced circulating differentiated B cell subsets in patients with mTNBC

The roles of B cells in tumor development remain largely controversial[48-50]. To understand how metastatic disease affects the circulating B cell compartment we investigated B cell subsets in more detail by flow cytometry. Naive B cells, identified by IgD expression and lack of CD27 expression[51], make up the largest proportion of circulating B cells and their cell counts remained consistent between patients with stage I-III TNBC, mTNBC, and HDs (Figure 3a). However, when evaluating the subset distribution within the B cell compartment, we found that the proportion of naive B cells compared to differentiated B cell subsets was

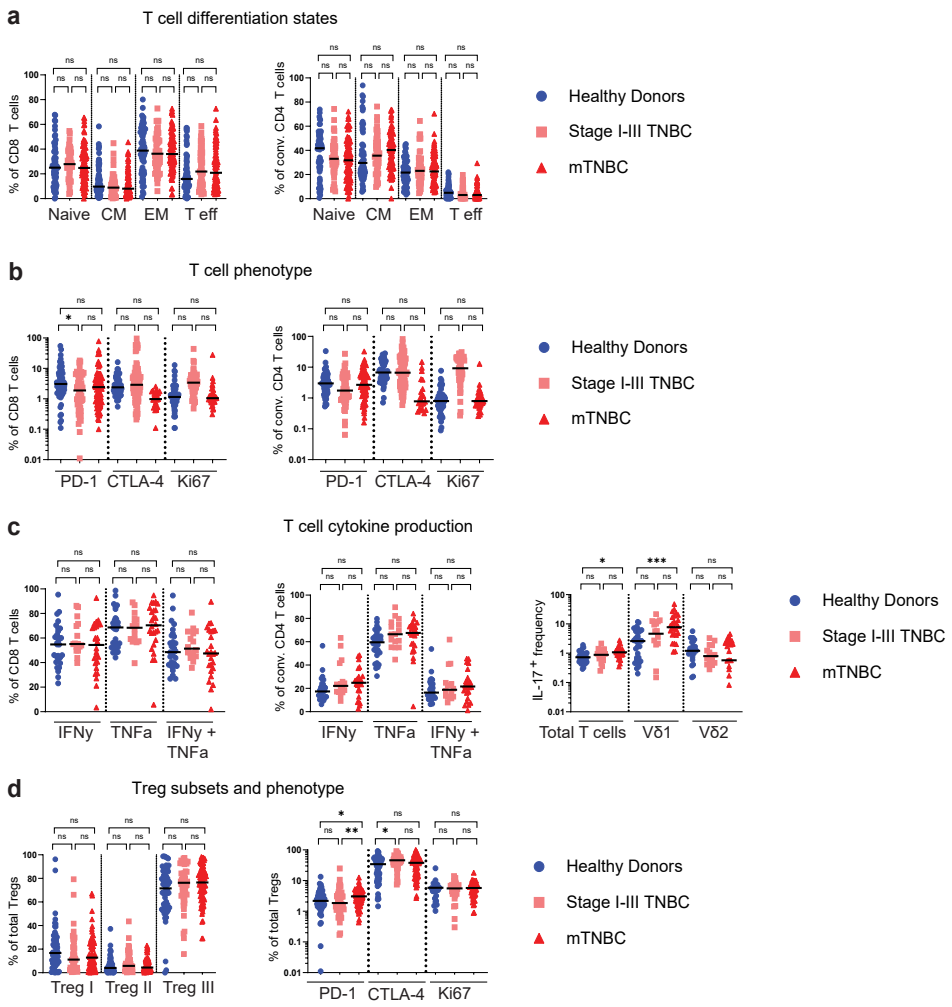

Figure 2. Characterization of circulating T cell subsets. (a) *T cell differentiation state based on surface marker expression of CD45RA and CCR7 (see Supplementary Fig. 1c) , comparing proportions within conventional CD4+ and CD8+ T cells for HD (n=65), stage I-III TNBC (n=44) and mTNBC (n=92). CM = central memory, EM = effector memory and T eff = effector T cells.* ***(b)*** *T cell phenotype comparing fractions within CD8+ and conventional CD4+ T cells for HD (n=23), stage I-III TNBC (n=32) and mTNBC (n=52).* ***(c)*** *IFNγ and TNFα production by CD8+ and conventional CD4+ T cells, and IL17 expression on Total T cells and γδ T cells subsets Vδ1 and Vδ2. Determined by flow cytometry for HDs (n=29), stage I-III TNBC patients (n=16) and mTNBC patients (n=26).* ***(d)*** *Regulatory T cell subsets and phenotype comparing HD (n=23), stage I-III TNBC (n=32) and mTNBC (n=52). P-values for* ***a-d*** *are computed with the Kruskal-Wallis test followed by Dunn's multiple comparisons test.*

elevated in patients with metastatic disease (Supplementary Figure 5a). Furthermore, we observed reduced cell counts and frequencies of non-class switched memory B cells, IgM-only switched memory B cells, switched memory B cells and CD38^{+} plasmablast-like cells in patients with mTNBC compared to HDs (Figure 3a, b and Supplementary Figure 5a). Patients with stage I-III TNBC were found to have a similar B cell subset distribution to HDs, except for non-switched B cells, which were reduced in patients with any stage of TNBC compared to HDs (Figure 3a). Analysis of the B cell compartment in an independent cohort of 69 patients with mTNBC confirmed reduced differentiated B cell subsets in patients with mTNBC compared to HDs (Supplementary Figure 5b), emphasizing the validity of our findings. In summary, our investigation revealed a reduced presence of differentiated B cell subsets—both in absolute numbers and as a proportion within the total B cell population—in the blood of individuals with mTNBC compared to HDs. We observed some of these changes already in patients with stage I-III disease, with even stronger effects noted in those with metastatic disease.

Prior chemotherapy is associated with transient changes in the systemic immune landscape

Beyond tumor characteristics, the immune contexture of cancer can be significantly influenced by patient characteristics and treatment history, like prior chemotherapy. Chemotherapy not only targets cancer cells but also rapidly dividing normal cells, such as the hematopoietic stem- and progenitor cells in the bone marrow responsible for immune cell production. Understanding the effects of chemotherapy on the immune system is a complex task, as the impact varies significantly depending on the tumor (sub)type[11] and the type and dosing schedule of chemotherapeutic agents. However, the impact of chemotherapy on the systemic immune landscape after discontinuation of the treatment remains unclear.

To explore the impact of chemotherapy that was previously administered to treat the primary tumor (Supplementary Table 2), we stratified mTNBC patients (Figures 1-3) based on their treatment history. Patients were divided in three groups: chemotherapy-naïve (mTNBC^{chemo_naïve}, n=29); last dose of (neo-)adjuvant chemotherapy more than one year ago (mTNBC$^{>1yr_chemo_free}$, n=38) and last dose of (neo-)adjuvant chemotherapy between 3 weeks and 1 year ago (mTNBC^{recent_chemo} , n=16). This stratification revealed that mTNBC^{chemo_naïve} patients exhibited elevated total leukocyte counts compared to HDs; a phenomenon that was not observed in patients who had previously received chemotherapy (Figure 4a), implying that this increase was disease-driven and mitigated by prior chemotherapy. Similarly, we found that neutrophil and CD14^{+} monocyte counts were significantly increased in mTNBC^{chemo_naïve} patients when compared to HDs (Figure 4a-b), demonstrating that the systemic increase in neutrophil and classical monocyte counts was mTNBC induced, and not chemotherapy-related. In contrast, although our initial analysis revealed reduced CD8+

T cells, conventional CD4+ T cells, Tregs, CD1c+ DCs, and CD141^{hi} DCs in patients with mTNBC (Figure 1b), stratification based on prior chemotherapy treatment revealed that these differences were predominantly driven by patients who had previously been treated with chemotherapy (Figure 4a-b). Prior chemotherapy was not associated with T cell differentiation state, phenotype, and Treg subset distribution (Supplementary Figure 6b-d). Comparing B cell subsets between mTNBC^{chemo_naive} patients to HDs revealed a significant reduction in non-switched B cells and plasmablast-like cells (Figure 4e, f), but not IgM only - and memory B cells, suggesting that the reduced differentiated B cell subsets we identified (Figure 3) were partly cancer-driven and partly impacted by prior chemotherapy.

To study the effects of recent chemotherapy on the systemic immune system, we compared mTNBC^{chemo_naïve} to mTNBC^{recent_chemo}. We observed increased cell counts for conventional CD4+ T cells and basophils in the mTNBC^{chemo_naïve} group compared to the mTNBC^{recent_chemo} group (Figure 4a-c), indicating that chemotherapy continues to have a profound effect on the systemic immune landscape after a washout period of at least three

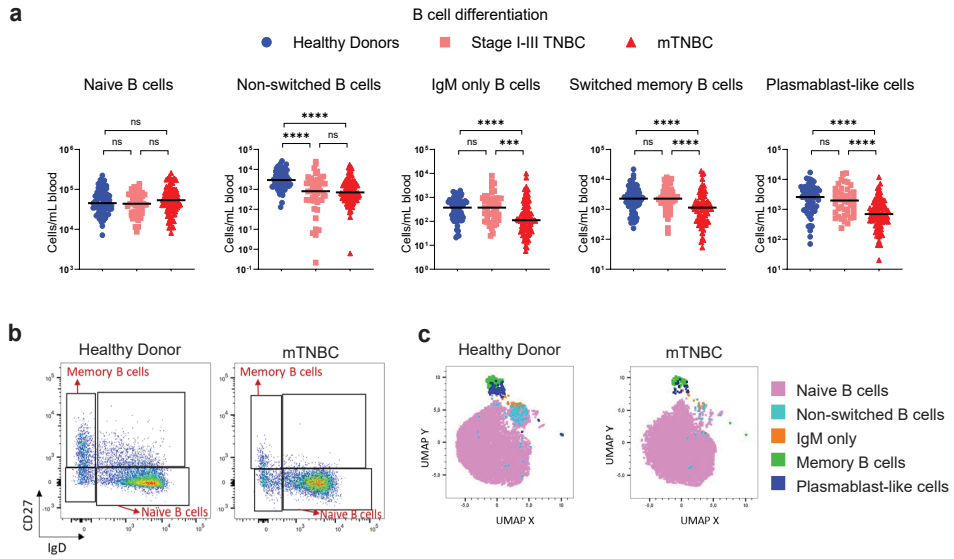

Figure 3. Reduced differentiated B cell subsets in blood of patients with metastatic triple-negative breast cancer compared to healthy donors. (a) *Absolute counts per ml blood for B-cell subsets identified using flow cytometry, split according to HD (n=65), stage I-III TNBC (n=44) and mTNBC (n=92). The y-axis is on a log scale. P-values are computed with the Kruskal-Wallis test followed by Dunn's multiple comparisons test to obtain adjusted p-values.* ***(b)*** *Representative dot plots of naïve and differentiated B cells in HD and mTNBC.* ***(c)*** *UMAP plot demonstrating the B cell subset distribution of a representative HD and a patient with mTNBC that were analyzed by flow cytometry on the same day.*

weeks (to one year). Furthermore, we found reduced numbers of IgM only – and switched memory B cells in the mTNBC^{recent_chemo} group, suggesting that previous chemotherapy treatment and TNBC both contributed to the dysregulated B cell pool in blood of patients with TNBC (Figure 4e, g). The apparent reduction of Tregs, plasmablast-like cells, and memory B cells in mTNBC^{recent_chemo} compared to mTNBC^{chemo_naïve} (Figure 4c, g) was not statistically significant when examining individual cell types (Figure 4a, e) despite matching raw p-values, due to the necessity of applying different multiple testing corrections.

In order to study the long-term effects of chemotherapy on the systemic immune landscape, we compared mTNBC^{chemo_naïve} to mTNBC$^{>1yr_chemo_free}$ and did not find any of the main immune cell populations to remain perturbed (Figure 4a, d). Additionally, we demonstrated that B cell differentiation in the mTNBC$^{>1yr_chemo_free}$ group resembled levels found in the mTNBC^{chemo_naive} group (Figure 4e, h). In conclusion, our data indicate that within this cohort, prior chemotherapy did not have significant long-term effects on the relative and absolute abundances of circulating immune cell populations.

We observed an overall declining trend in cell counts from mTNBC^{chemo_naïve}, to mTNBC$^{>1yr_chemo_free}$, to mTNBC^{recent_chemo} for most cell types or subsets (Figure 4a, e). Consistently, we did not find any of the immune cell populations to be significantly more abundant in patients with mTNBC that received chemotherapy (regardless of the wash out period) compared to the mTNBC^{chemo_naïve} group (Figure 4c, d), aligning with the idea that chemotherapy has an overall depleting effect on proliferating progenitors. Collectively, our data imply that prior chemotherapy influences the composition of the systemic immune landscape by reducing cell counts of basophils, conventional CD4+ T cells, IgM only B cells and non-switched memory B cells. Importantly, these changes are not detectable in the group that received the last dose of chemotherapy more than one year ago, suggesting that chemotherapy-induced changes are not persistent in patients with mTNBC. In contrast, systemic increases in neutrophils and monocytes are disease driven.

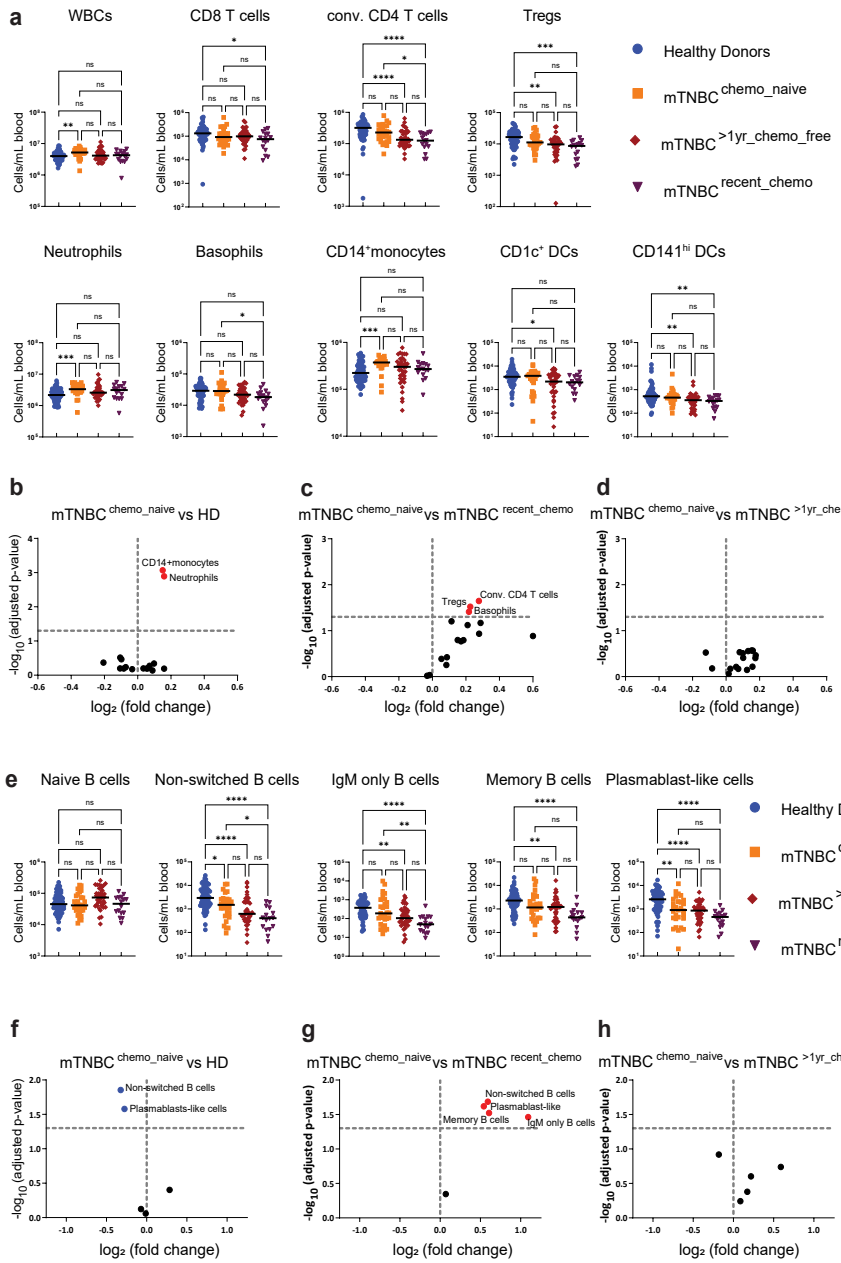

Figure 4. The impact of prior chemotherapy on major immune cell type abundances in blood of patients with metastatic triple-negative breast cancer. (a) *Absolute counts per ml blood of WBC and main circulating immune cells in patients with mTNBC that were split according to treatment history: chemotherapy-naive (mTNBC^{chemo_naive}, n=29), received chemotherapy more than one year ago (mTNBC$^{>1yr_chemo_free}$, n=38) or received chemotherapy between 3 and 52 weeks ago mTNBC^{recent_chemo}, n=16), and HDs (n=65). The y-axis is on a log scale.* ***(b-d)*** *Volcano plots summarizing differences in main systemic immune cell counts between* ***(b)*** *HDs and patients with mTNBC that were chemotherapy-naïve,* ***(c)*** *patients with mTNBC that were chemotherapy-naïve and patients with mTNBC that received chemotherapy within the last year, and* ***(d)*** *patients with mTNBC that were chemotherapy-naïve and patients with mTNBC that received chemotherapy more than one year ago.* ***(e)*** *Absolute counts per ml blood of differentiated B cell subsets. Patients were split as described in panel* ***(a)****.* ***(f-h)*** *Volcano plots summarizing differences in counts of differentiated B cell subset between* ***(f)*** *HDs and patients with mTNBC that were chemotherapy-naïve,* ***(g)*** *patients with mTNBC that were chemotherapy-naïve and patients with mTNBC that received chemotherapy within the last year, and* ***(h)*** *patients with mTNBC that were chemotherapy-naïve and patients with mTNBC that received chemotherapy more than one year ago. For* ***a*** *and* ***e****, p-values were computed with the Kruskal-Wallis test followed by Dunn's multiple comparisons correction across groups. For (****b-d) and (f-h****), p-values are corrected using the Benjamini-Hochberg procedure across immune cell populations.*

Neutrophils from patients with TNBC have enhanced migratory capacity

Our comprehensive immune profiling analysis demonstrated that neutrophils are the most increased cell population in circulation of chemotherapy-naive patients with mTNBC (Figure 4a, b). Previous research demonstrated that tumor-induced neutrophils promote mammary tumor progression and metastatic spread in preclinical mouse models[10,19,25,52,53] and that TNBC patients with increased NLR have a worse clinical prognosis[54]. We therefore hypothesized that neutrophils in the blood of patients with mTNBC are phenotypically and functionally different from neutrophils in HDs. To test this hypothesis, we interrogated the transcriptome profile of freshly isolated circulating neutrophils from seven patients with mTNBC and seven HDs by bulk RNA-sequencing. We identified 90 up-regulated and 37 down-regulated genes between neutrophils from patients with mTNBC and HDs (adjusted p-value < 0.05) (Figure 5a-b). *In silico* pathway analysis indicated that, among the various differential pathways, multiple pathways related to neutrophil migration were significantly enriched in neutrophils from patients with mTNBC compared to those from HDs (Figure 5c). Gene Set Enrichment Analysis (GSEA) similarly indicated that neutrophils from patients with mTNBC were enriched for genes involved in migration (Figure 5d-e). One of the most upregulated genes was *CD177* (Figure 5b), encoding a glycosyl-phosphatidylinositol (GPI)-linked cell surface glycoprotein. CD177 is expressed by activated neutrophils, is upregulated in inflammatory settings and modulates neutrophil migration[55,56]. Since CD177 is an important driver of the migration signature, we sought to confirm whether the increased CD177 transcription in neutrophils from patients with mTNBC corresponds to differences in protein levels at the cell surface. Using flow cytometry analysis, we verified in an independent set of patients with mTNBC a significantly higher number of CD177 positive neutrophils compared to HDs; this difference was not observed for CD177 negative neutrophils (Figure 5f).

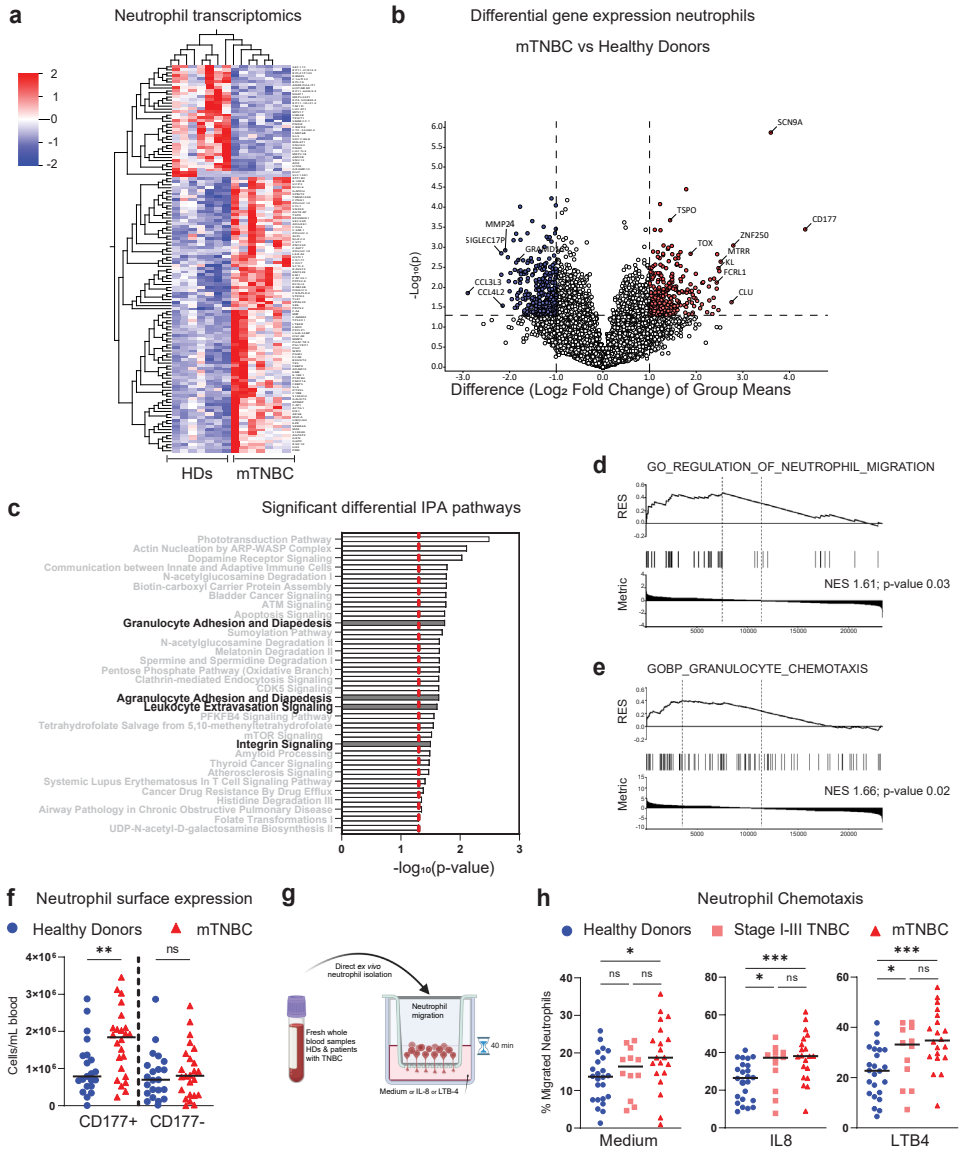

Figure 5. Neutrophils derived from individuals with triple-negative breast cancer exhibit heightened migratory capabilities. (a) *Bulk RNA-sequencing data of purified blood neutrophils from patients with HDs (n=7) and mTNBC (n=7). Heatmap visualizing the differentially expressed genes between HDs and patients mTNBC. Colors indicate the row Z-score ranging from 2 to -2.* ***(b)*** *Volcano-plot showing fold changes for genes described in* ***a****.* ***(c)*** *All statistically significant pathways that came out of the Ingenuity Pathway Analysis on differentially expressed genes between neutrophils from HDs and patients with mTNBC.* ***(d-e)*** *Gene Set Enrichment Analysis performed on same neutrophil bulk RNA-sequencing dataset, with* ***(d)*** *GO gene set "regulation of neutrophil migration" and* ***(e)*** *GO gene set "granulocyte chemotaxis".* ***(f)*** *Surface marker expression of CD177 determined by flow cytometry on neutrophils from HDs (n=21) and patients with mTNBC (n=25). P-values are computed with an ANOVA followed by Šídák's multiple comparisons test.* ***(g-h)*** *Neutrophil migration rates determined in direct ex vivo chemotaxis assays using IL-8 and LTB-4 as chemo-attractants. Neutrophils were processed immediately after blood draw from HDs (n=24), stage I-III TNBC patients (n=12) and mTNBC patients (n=20). P-values are computed with the Mann-Whitney U-test.*

To functionally validate the predicted enhanced migratory capacity of neutrophils from patients with mTNBC, we performed transwell migration assays. The results confirmed increased migratory capacity of circulating neutrophils from an independent set of mTNBC patients compared to those from HDs, even in the absence of chemo-attractants. This effect was further heightened in the presence of chemo-attractants (Figure 5g-h). Importantly, neutrophils from stage I-III TNBC patients already exhibited increased migration towards chemo-attractants compared to neutrophils from HDs, indicating that this altered neutrophil behavior is instigated during early or locally advanced disease stage and maintained during disease progression. To conclude, our findings demonstrate that circulating neutrophils from patients with TNBC have greater migratory capacity compared to neutrophils from HDs.

Neutrophils from patients with mTNBC contain more granule proteins and produce more ROS

To further investigate the effects of mTNBC on the functional state of circulating neutrophils, we performed a full proteomic analysis comparing neutrophils from patients with mTNBC and neutrophils from HDs. We identified a total of 111 differentially regulated proteins (adjusted p <0.05): 42 upregulated and 69 downregulated proteins in neutrophils from patients with mTNBC compared to HDs (Figure 6a). Reactome analysis identified various up- and down-regulated pathways, including a significant increase in proteins involved in neutrophil degranulation in neutrophils from patients with mTNBC (Figure 6b). This pathway consists of 450 proteins that are important for neutrophil vesicle exocytosis, as well as proteins present in those vesicles. In addition, we found that neutrophil granule proteins were significantly enriched in neutrophils from patients with mTNBC (Fisher's exact test, p=0.021) (Figure 6c-d).

We next assessed several additional important effector functions of neutrophils, and how they are influenced by TNBC, including Neutrophil Extracellular Trap (NETs) formation, phagocytosis and ROS production. We found no differences in *ex vivo* NET-formation, either spontaneously or after PMA stimulation (Figure 6e) or phagocytic ability in neutrophils from patients with mTNBC compared to HDs (Figure 6f). In contrast, we found that neutrophils from patients with mTNBC produce significantly more ROS than HD neutrophils (Figure 6g).

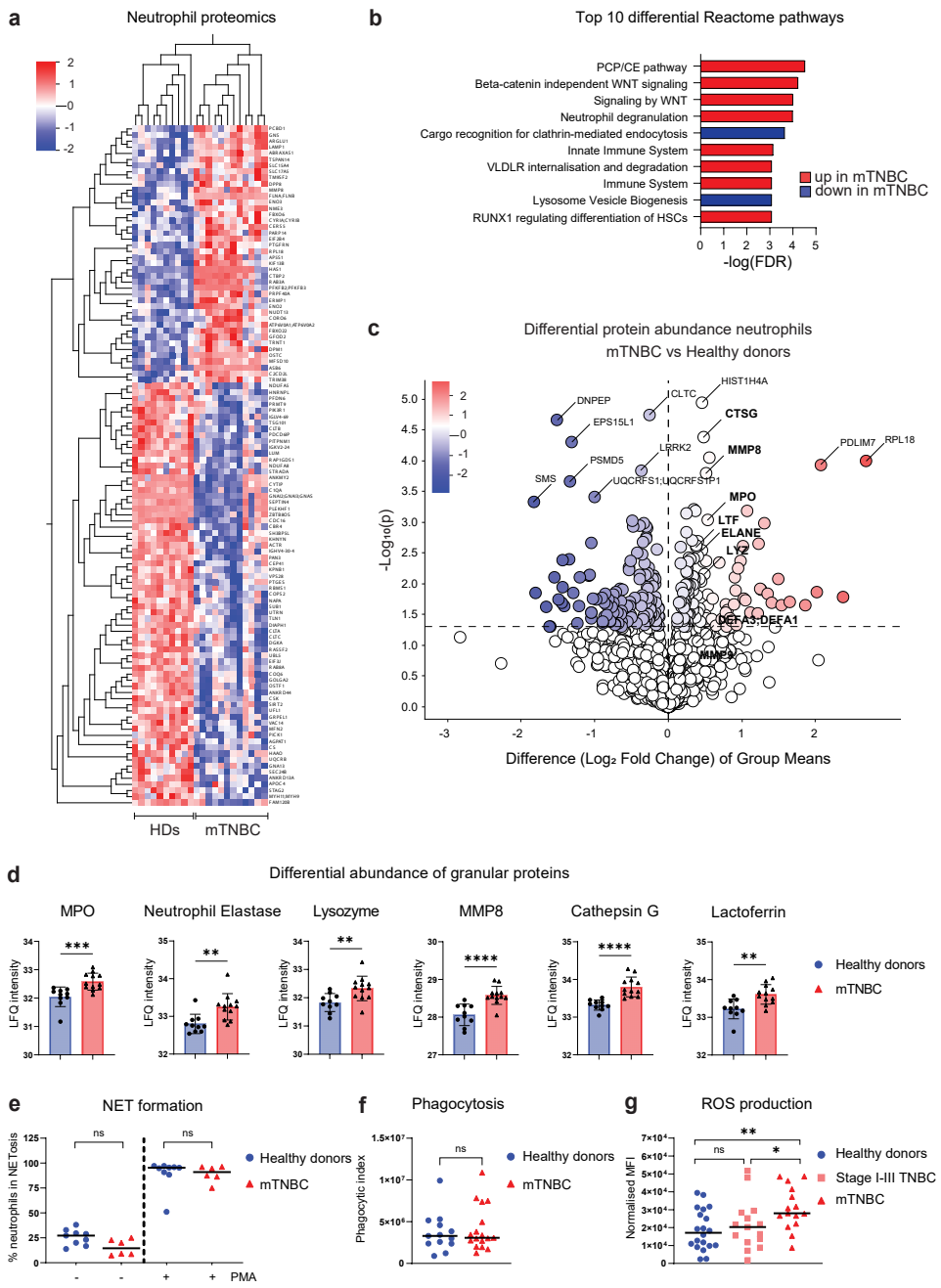

Figure 6. Altered proteome and more ROS production by circulating neutrophils from patients with metastatic triple-negative breast cancer compared to healthy donors. (a) *Heatmap visualizing differentially abundant proteins between freshly isolated blood neutrophils from HDs (n=10) and mTNBC patients (n=12). Colors indicate the row Z-score ranging from 2 to -2.* ***(b)*** *Top 10 Reactome pathways representing the functional domains of the differentially abundant proteins between neutrophils from HDs and patients with mTNBC.* ***(c)*** *Volcano plot showing log fold changes of differentially abundant proteins (p <0,05) and highlighting all granule proteins of the dataset in bold. Additionally, proteins with the highest fold change and lowest p-value are labeled (not in bold).* ***(d)*** *Quantification of the significantly differentially abundant granule proteins from the proteomics dataset between HDs and patients with mTNBC. P-values are computed with the Mann-Whitney U-test.* ***(e)*** *Proportion of blood neutrophils from patients with mTNBC and HDs undergoing ex vivo NETosis with and without PMA stimulation.* ***(f)*** *Phagocytic index representing opsonizing rate of E.coli BioParticles by freshly isolated blood neutrophils from patients with mTNBC and HDs.* ***(g)*** *Reactive Oxygen Species (ROS) production by neutrophils isolated from fresh blood samples of HDs (n=20), patients with stage I-III TNBC (n=15) and patients with mTNBC (n=15). P-values are computed with the Mann-Whitney U-test.*

Furthermore, there was a modest trend toward increased ROS production by neutrophils from stage I-III TNBC patients compared with HDs, which could indicate a gradual change in the functional phenotype of neutrophils as the disease progresses. According to existing data[57], increased levels of ROS from neutrophils could potentially exert an immunosuppressive influence. Although the patient numbers were insufficient to statistically test the effect of prior chemotherapy treatment on *ex vivo* migration- and ROS production capacity of neutrophils, we observed no clear separation of the patients based on chemotherapy treatment history (Supplementary Figure 7a, b).

In summary, these results show that neutrophils from patients with mTNBC contain more granule proteins and produce more ROS compared to neutrophils from HDs, indicating that patient neutrophils are not only more abundant and transcriptionally distinct but are also functionally altered by TNBC.

Discussion

The impact of solid tumors on the overall systemic immune landscape during cancer progression is not fully understood. This study aimed to investigate the changes in the systemic immune landscape at different TNBC stages. Additionally, we explored how prior chemotherapy treatment could be associated with changes in the systemic immune landscape in the metastatic setting. We applied multi-parameter flow cytometry to comprehensively assess abundance, phenotype and activation states of both lymphoid and myeloid immune populations from fresh peripheral blood samples. Pre-clinical evidence strongly implicates a critical role for neutrophils in disease progression[13-16,58-62]. However, these fragile cells are often overlooked due to the fact they cannot be stored. By analyzing fresh blood samples, we were able to capture the full complexity of the immune landscape, including all granulocytes, and we were able to perform in-depth functional neutrophil analyses.

Our data established that disease stage had a major impact on the systemic immune composition and function in patients with TNBC. We demonstrated that patients with mTNBC manifested lower levels of circulating T cells, DC subsets, and differentiated B cells. In contrast, classical monocyte and neutrophil counts and frequencies were higher in mTNBC patients compared to HDs. When subjecting circulating neutrophils to more qualitative analysis, we revealed that neutrophils from patients with mTNBC had heightened transcription of genes associated with neutrophil trafficking, showed an increased *ex vivo* migratory capacity, presented elevated levels of granule proteins, and had increased ROS production. While no apparent changes in cell counts or frequencies were observed in patients with stage I-III TNBC, alterations in neutrophil functionality, and in particular in migratory capacity, did emerge in the non-metastatic disease setting.

In more detail, within the circulating lymphocyte compartment we observed that Tregs in patients with stage I-III TNBC expressed more CTLA-4 compared to HDs, something that was not observed in patients with mTNBC. This raises the question whether Tregs in stage I-III TNBC patients have a more immunosuppressive phenotype than at the metastatic stage, and may contribute to systemic immunosuppression. Additionally, we observed a reduction in CD8+ T cells, conventional CD4+ T cells and Tregs in patients with mTNBC compared to HDs, which seemed predominantly associated with prior chemotherapy. Others have previously discussed lymphocyte repopulation dynamics after chemotherapy, noting that NK T cells and CD8+ T cells return to pre-chemotherapy levels within a year. However, B cells remain significantly lower after 9 months and memory CD4+ T cells exhibit an abnormal bias toward inflammatory effectors that persists for years, albeit in cohorts of breast cancer patients with mixed or unknown molecular subtypes[63,64]. To the best of our knowledge, we are the first to explore the effects of chemotherapy on the systemic immune landscape in its full complexity more than one year after the last chemotherapy administration. Notably, we observed no differences in CD8+ T cell and Treg counts between chemotherapy-naïve mTNBC patients and those who received chemotherapy recently. However, the combined effect of having mTNBC and recent chemotherapy significantly reduced CD8+ T cell and Treg counts compared to HDs. These cumulative impacts on the overall immune status of patients may carry substantial clinical consequences, including diminished vaccine responses, heightened infection risks[65], and are likely to influence the efficacy of cancer immunotherapy, given the pivotal role of CD8 T cells in anticancer immunity[66]. When investigating the functional consequences of TNBC on T cells, we uncovered that Vδ1 γδ-T cells from patients with mTNBC produced more IL-17 compared to those from HDs, which seemed independent from chemotherapy treatment history, along with increased circulating neutrophils. These findings are in line with our published preclinical work showing that IL-17-producing γδ-T cells are increased in mammary tumor bearing mice, and that they drive systemic expansion and polarization of neutrophils towards a CD8 T cell-suppressive

phenotype, promoting metastatic spread[19]. Additionally, it has previously been described that HER2- ER+/- breast cancer patients had an increased frequency of Th2/ Th17 cells, based on the surface marker expression of CXCR3, CCR4, and CCR6[67]. We suggest that exploring the clinical application of targeting the IL-17 pathway may be of interest. Furthermore, we found that patients with stage I-III TNBC had a lower frequency of PD-1 positive circulating CD8 T cells compared to HDs, while PD-1 expression on Tregs is increased in patients with mTNBC compared to patients with stage I-III TNBC and HDs. These findings suggest differential regulation of PD-1 expression across immune cell subsets in TNBC. Correlation analysis showed no association between tumor TIL scores and the systemic immune profiles of patients with either non-metastatic or metastatic TNBC (data not shown).

Furthermore, patients with mTNBC were found to have an increased frequency of naïve B cells compared to HDs, accompanied by a reduction in differentiated B cell subsets such as memory B cells and plasmablast-like cells. It has previously been reported that elevated frequency of circulating plasmablasts in patients of various cancer types (melanoma, lung and renal) correlates with improved patient outcomes[68,69]. Moreover, high baseline IgG titers in blood of melanoma patients showed a positive correlation with response to immune checkpoint blockade[70,71]. Our findings of reduced numbers of differentiated B cells suggests a previously unappreciated impact of chemotherapy and disease stage on the circulating B cell compartment that may have consequences for patients' humoral immune responses. Further research is needed to understand whether differentiated B cell subsets are decreased in tumors as disease progresses, since tumor infiltrated B cells can also have a profound influence on the clinical outcome of TNBC[72].

Within the myeloid compartment we observed increased levels of classical $CD14^+$ monocytes in patients with mTNBC compared to HDs, reinforcing the notion that cancer induces systemic inflammation. Others previously described that human breast cancer changes classical/non-classical monocyte ratios and alters transcriptional profiles of monocytes[28,73]. Furthermore, a high lymphocyte-to-monocyte ratio and high monocyte frequencies in peripheral blood correlate with poor clinical outcome in cancer patients[74-77]. Our findings underscore that the dysregulation of classical monocytes represents a progressive disruption of the immune system closely associated with disease progression in TNBC. Importantly, this monocyte dysregulation is a tumor-driven phenomenon. Interestingly, non-classical monocytes, previously associated with enhanced control of metastasizing cells in murine models[78-80], remain unaffected by these systemic changes.

In our study, we observed a statistically significant increase in circulating neutrophil levels among chemotherapy-naïve patients with mTNBC compared to HDs, which constituted the most pronounced difference in quantity between the two groups. Combining complementary technologies including RNA-sequencing, proteomics and functional assays, revealed that neutrophils from patients with mTNBC show enhanced migratory capacity.

This is in line with published work describing increased neutrophil migration in patients with other cancer types (non-small cell lung cancer and head-and-neck cancer), albeit in small cohorts with mixed disease stages[81,82]. In this study, we show that neutrophils have increased migratory capacity in TNBC in a disease stage dependent manner. Cell migration is an important feature of neutrophil biology and – in the context of cancer – is a critical component of their ability to prepare the (pre-)metastatic niche and contribute to disease progression[52,83-86].

Moreover, we found that mTNBC neutrophils produce significantly more ROS than HD neutrophils. ROS produced by neutrophils can exert immunosuppressive effects on T and NK cells, induce DNA damage and enhance tumor metastasis by disrupting endothelial cell junctions, facilitating extravasation. However, in specific tumor contexts, neutrophils may counteract invasion, partly by inducing cancer cell death through elevated ROS levels[57,87]. Given this context-dependent nature of the effects of ROS, further research is needed on the implications of increased ROS production in patients with TNBC. There is a critical need to normalize the systemic effects of cancer on the immune system, and our data provide valuable insights into the functional changes that are induced by TNBC, which might lay a foundation for future (pre-)clinical studies. For instance, the altered biology of neutrophils suggests that their migration could represent a novel angle for future therapeutic strategies.

Additionally, proteomic analysis identified alterations in neutrophil degranulation pathways and revealed increased abundances of granule proteins like MPO, Neutrophil Elastase and Lysozyme in neutrophils from patients with mTNBC compared to HDs. Secretion of granules filled with toxic proteins is a key pillar in neutrophils' effector function and their ability to control invading pathogens. Granules are divided into four subgroups depending on their protein content and synthesis during granulopoiesis[88,89]. Our data did not reveal a specific pattern in the type of granule proteins. Specifically, no cancer associated enrichment was observed for primary/azurophil, secondary/specific or tertiary/gelatinase granule proteins. Although the vast majority of (pre-)clinical studies found that tumor associated neutrophils correlate with poor clinical outcome, neutrophils have also been described to play an anti-tumorigenic role in the TME by direct killing of tumor cells or by interacting with other immune cells[86,89-92]. Our data hint at the preservation of cytotoxic potential in neutrophils from patients with mTNBC, perhaps suggesting that they still have the potency to be mobilized against the tumor. Further investigations are warranted to substantiate the implications of the increase in granule proteins for patients. Since our study reveals increased levels of systemic neutrophils in the metastatic TNBC setting and a progressive alteration of several functional aspects of neutrophils such as increased ROS production and enhanced migration capacity with disease advancement, it is tempting to speculate that these progressive changes contribute to the accumulating clinical data showing immunotherapy exhibits greater efficacy in non-metastatic (breast) cancer compared to

late stage disease[93,94]. Encouragingly, FDA (but not EMA) approval for immunotherapy as (neo-)adjuvant therapy has been extended not only to highly immunogenic cancers such as melanoma and non-small cell lung cancer but also to TNBC, offering new avenues for improved treatment strategies.

While elevated NLR is associated with disease progression in various cancers[13-18], and we observe a significant increase in systemic neutrophils in patients with mTNBC compared to HDs (Figure 1b, c), it exhibits significant variability, even among healthy individuals, making blood neutrophil abundance an unreliable standalone biomarker for early metastasis or recurrence. However, based on our findings, it is intriguing to speculate that the neutrophil transcriptome or proteome may harbor prognostic signatures with potentially greater specificity and reliability. Further validation studies in larger patient cohorts are needed to explore this hypothesis.

In our cohort, patients with mTNBC who had undergone chemotherapy had received varying types and numbers of chemotherapy lines; a limitation of our study is the insufficient statistical power to analyze patients' pre-treatments based on specific chemotherapy types or the number of treatment lines administered. Additionally, since this is a retrospective analysis, and the patient cohort was originally not designed to study the impact of chemotherapy on the immune system, we cannot formally rule out a confounding factor arising from potential variations in tumor or patient characteristics between the chemotherapy-naïve and chemotherapy-exposed groups. Nonetheless, given the substantial size of our cohort, and access to historic treatment information, it offers us a unique opportunity to explore the association between prior chemotherapy and the systemic immune landscape. Strengths of our study include the comprehensive approach we took using fresh blood samples, the validation cohort further substantiating our findings and the assessment of neutrophil functionality in addition to quantitative approaches.

Our data revealed that TNBC profoundly impacts the systemic immune landscape. Furthermore, our data indicate that prior chemotherapy treatment could be associated with systemic immune alterations. When patients with mTNBC had not received chemotherapy for over a year, the levels of immune cells in their blood resemble those of patients with mTNBC who had never undergone chemotherapy. Investigating prospective longitudinal chemotherapy effects on TCR/BCR-repertoire, assessing the functionality of other immune cell types besides neutrophils, and exploring potential epigenetic rewiring are important to fully understand the impact of standard of care chemotherapy in breast cancer patients. In the future, dissecting the role of different types of chemotherapy may shed new light on which types and combinations of chemotherapeutic drugs are less impactful for the effector immune system, resulting in a more favorable immune profile.

Methods

Patients and Healthy Donors

TNBC patient blood samples were obtained from patients enrolled in either a clinical trial or biobank protocol, after approval by the local medical ethical committee and/or institutional review board of the Netherlands Cancer Institute. All patients provided informed consent for the current study. 14 Patients were enrolled in a biobanking protocol of the Netherlands Cancer Institute (CFMPB450); 31 patients were included in the BELLINI trial (stage I-III TNBC, NCT03815890); 91 patients were included in the Triple B trial[95] (discovery cohort mTNBC, all before first line of palliative treatment, NCT01898117); 69 patients were included in the TONIC trial[38,96] (validation cohort mTNBC, with no to max three lines of prior treatment, NCT02499367). For samples obtained in the context of a clinical trial, only baseline blood samples were included in the analysis for this paper and the current analyses were not part of the main study plan of the clinical trial. Stage I-III TNBC patients did not receive chemotherapy in the past. From the 92 mTNBC patients in our discovery cohort, 29 patients (32%) did not receive prior chemotherapy treatment, for 9 patients it was unknown or the date of the last chemotherapy administration was unknown, and 54 patients (59%) received prior chemotherapy for their primary tumor. Of the pre-treated patients, 38 patients received their last dose of chemotherapy more than one year ago, with a median wash out period of 2.3 years (range 395-4423 days), and 16 patients received their last dose of chemotherapy less than one year ago, with a median wash out period of 223 days (range 21-365 days). Both chemotherapy-experienced and chemotherapy-naïve patients had a full range of tumor sizes from T1-T4 at the time of diagnosis, although a part of the chemotherapy-naïve patients (76%) presented with metastatic disease at the time of diagnosis, which was not the case for chemotherapy-experienced patients. Of note, NK cell markers were added later to the panels, so n-numbers for NK cell analysis are as follows: HD n=23, stage I-III n=29 and mTNBC n= 25. All study protocols were conducted in accordance with the ICH Harmonised Tripartite Guideline for Good Clinical Practice and the principles of the Declaration of Helsinki.

Fresh blood samples from 53 healthy women (healthy donors, HD) were obtained after approval by the local medical ethical committee (NCT03819829). Additionally, fresh blood samples from 12 healthy women were obtained anonymously from the Dutch national blood transfusion service (Sanquin Blood supply, Amsterdam, The Netherlands). All patients and healthy donors provided written informed consent before enrolment. Basic clinical characteristics of these cohorts are described in Supplementary Table 1. HDs were age matched to mTNBC patients (Supplementary Figure 2a). Blood samples were drawn primarily in the morning (88% was taken before noon) and blood draw times were comparable for HDs, stage I-III TNBC patients and mTNBC patients (Supplementary Figure 2a).

Flow cytometry

Blood samples were processed and analyzed within 24 hours after blood draw. All samples were processed in the same way, by the same team and in the same lab. Peripheral blood was collected in EDTA vacutainers (BD) and subjected to red blood cell lysis (lysis buffer: dH2O, NH4Cl, NaHCCO3, EDTA). Cells were resuspended in PBS containing 0.5% BSA and 2mM EDTA and counted using the NucleoCounter NC-200 (Chemometec) automated cell counter. To obtain absolute leukocyte counts per mL of human blood, the total amount of post lysis cells was divided by the volume (mL) of blood obtained from the patient (~10 mL). For surface antigen staining, cells were first incubated with human FcR Blocking Reagent (1:100 Miltenyi) for 15 min at 4°C and then incubated with fluorochrome-conjugated antibodies for 30 min at 4°C, in the dark. For intracellular antigen staining, cells were fixed with Fixation/Permeabilization solution 1X (Foxp3/Transcription Factor Staining Buffer Set, eBioscience) for 30 min at 4°C and stained with fluorochrome-conjugated antibodies in Permeabilization buffer 1X (eBioscience) for 30 min at room temperature. Viability was assessed by staining with either 7AAD staining solution (1:10; eBioscience), Zombie Red Fixable Viability Kit (1:800, BioLegend) or Propidium Iodide (Thermo Fisher Scientific). For the analysis of cytokine production, cells were stimulated with PMA (0.25ng/mL) and Ionomycin (1 nM) in the presence of GolgiPlug for 3 hours at 37°C, 5% CO2. After stimulation, cells were prepared according to the intracellular staining protocol described above. Data acquisition was performed on an LSRII SORP flow cytometer (BD Biosciences) using Diva software. To standardize the performance of this machine over time as good as possible, CS&T beads (BD) were used to optimize general performance and Sphero 8 peaks Rainbow Calibration particles (BD) were used to adjust PMT voltages if necessary. Additionally, single stained compensation controls were taken along for each experiment. Data analysis was performed using FlowJo software version 10.6.2. Flow cytometry antibodies can be found in Supplementary Table 3. Gating strategies are displayed in Supplementary Figures 1a (Myeloid panel gating), 1b (B and NK cell panel gating) and 1c, d (T cell panel gating). The Neutrophils to Lymphocyte ratio (NLR) was calculated by dividing neutrophil counts by lymphocyte counts.

Neutrophil Isolation from fresh blood samples

For bulk RNA-sequencing, neutrophils were FACS isolated on a FACSAria Fusion sorter (BD Biosciences) from fresh peripheral blood samples from 7 patients with metastatic TNBC and 7 age- and BMI-matched HDs (see Flow Cytometry paragraph above for staining procedures). Cells were sorted directly into RLT buffer (Qiagen) supplemented with 1% beta-mercaptoethanol and snap frozen using dry ice and ethanol. For functional assays, neutrophils were isolated from fresh whole blood samples using the human MACSxpress Whole Blood Neutrophil Isolation Kit (Miltenyi Biotec B.V.). Residual red blood cells were lysed using red blood cell lysis buffer (dH2O, NH4Cl, NaHCCO3, EDTA), resulting in a neutrophil suspension with typically >98% purity.

Bulk RNA-sequencing

We included 7 patients with mTNBC (of which 1 (14%) was chemotherapy naïve, 1 (14%) was chemo-free for more than 1 year, and 5 (72%) received recent chemotherapy) and 7 HDs, without any pre-selection. RNA was isolated from sorted neutrophil samples using the RNeasy Micro Kit (Qiagen), including an on column DNase digestion (Qiagen), according to the manufacturer's instructions. Quality and quantity of the total RNA was assessed on the 2100 Bioanalyzer instrument following manufacturer's instructions "Agilent RNA 6000 Pico" (Agilent Technologies). In general RNA yields of 5-20 ng total RNA and RNA integrity numbers (RIN) above 8 were obtained. RNA library preparation was performed according to a published protocol by Picelli *et. al.*[97] with modifications. In short, 2-7 ng of total RNA for each sample was prepared in a volume of 4 ul. Oligo dT primer hybridization was performed by the addition of Oligo dT mix (0.7ul H2O, 0.1 ul RNAse inhibitor (40U/ul), 0.1 ul dNTP mix (100mM) and 0.1 ul Oligo-dT30VN primer (100uM)). Reverse transcription was performed as described but the MgCl2 concentration was adjusted to 10 mM. Template switching and 10 (1-4 ng RNA input) or 11 (5-8ng RNA input) cycles pre-amplification of full length cDNAs with template switching oligo's was performed using ISPCR primer at a final concentration of 0.08 uM. The amplified full length cDNA was used for NGS library construction by Tagmentation for Illumina sequencing, using the Illumina Nextera XT DNA sample preparation kit (Illumina). RNA sequencing libraries were quantified and normalized based library QC data generated on the Bioanalyzer system according to manufacturer's protocols (Agilent Technologies). A multiplex sequencing pool of all uniquely indexed RNA libraries was composed by equimolar pooling before sequencing on the HiSeq 2500 Illumina sequencing platform. HiSeq 2500 single-end sequencing was performed using 65 cycles for Read 1, 8 cycles for Read i7, using HiSeq SR Cluster Kit v4 cBot (GD-401-4001, Illumina) and HiSeq SBS Kit V4 50 cycle kit (FC-401-4002, Illumina). Almost 95% of the sequenced reads were passing filter and approximately 93% of the reads have quality values above Q30. This resulted in, on average, 16 M passing filter reads per sample. All reads passing filter have been used for further analysis. Reads were aligned with Hisat (version 2.1.0), allowing for exon-exon junctions, against the ensembl human build 38. After mapping, on average, 95% of the reads have been mapped to the reference genome. Read counts were generated using Itreecount (https://github.com/NKI-GCF/itreecount), a perl script which gives similar output compared to the HTSeq-count python package. As a reference, ensembl gtf version 87 was used to count the reads. All samples were merged into one dataset. Genes that have zero expression across all samples were removed from the dataset. Data analysis was performed using the DESeq2 package in RStudio under R version 4.1.0 for differential gene expression analysis and Qlucore software (Qlucore Omics Explorer 3.8, Lund, Sweden) for GSEA and visualization purposes. GSEA was performed using the and the "GOBP_GRANULOCYTE_CHEMOTAXIS" geneset and the "GO_REGULATION_OF_NEUTROPHIL_MIGRATION"[98].

Proteomics

Isolated neutrophils from fresh blood samples were washed 3x with PBS and $1*10^6$ cells were frozen and stored at -80°C until the dataset was complete. We included 12 patients with mTNBC (of which 5 (42%) were chemotherapy naïve, 3 (25%) were chemo-free for more than 1 year, and 4 (33%) received recent chemotherapy) and 10 HDs, without applying any pre-selection criteria. The proteomic samples were independent from the RNA-sequencing samples. Frozen neutrophil cell pellets from HDs and patients with mTNBC were heated for 10 min. at 95°C in 1x S-Trap lysis buffer (5% SDS in 50mM TEAB pH 8.5), followed by sonication. Lysate protein concentrations were determined with a BCA Protein Assay Kit (Thermo Fisher Scientific), proteins were reduced with DTT and alkylated with iodoacetamide and 50µg protein amounts were digested o/n with trypsin (Sigma-Aldrich; enzyme/substrate ratio 1:10) on S-Trap Micro spin columns according to the manufacturer's instructions (ProtiFi, NY, USA). Peptides were eluted, vacuum dried and stored at -80°C until LC-MS/MS analysis. LC-MS/MS was performed by nanoLC-MS/MS on an Orbitrap Exploris 480 mass spectrometer (Thermo Fischer Scientific) connected to a Proxeon nLC1200 system. Peptides were directly loaded onto the analytical column (ReproSil-Pur 120 C18-AQ, 2.4 µm, 75 µm × 500 mm, packed in-house) and eluted in a 210-minutes gradient containing a linear increase from 6% to 23% solvent B (solvent A was 0.1% formic acid/water and solvent B was 0.1% formic acid/80% acetonitrile). The Exploris 480 was run in data-dependent acquisition (DDA) mode, with 2 sec. cycle time. Survey scans of peptide precursors from m/z = 375–1500 were acquired in the Orbitrap at 60K resolution with AGC target and maximum injection time mode set to "Standard" and "Auto", respectively. Tandem MS was performed by quadrupole isolation at 1.2 Th. followed by HCD fragmentation with normalized collision energy of 30 and Orbitrap MS2 fragment detection at 15K resolution, AGC target and maximum injection time mode set the same as described for MS1. Only precursors with charge state 2-6 were sampled for MS2. Monoisotopic precursor selection was turned on; the dynamic exclusion duration was set to 32.5s with a 10 ppm tolerance around the selected precursor.

Neutrophil proteome data were analyzed with label-free quantification using MaxQuant (version 2.0.1.0)[99,100] using standard settings. Fragment spectra were searched against the Swissprot human database (version 2021_04; 20,395 entries). Trypsin/P was specified as protease specificity allowing a maximum of 2 miscleavages; oxidation (M) and acetyl (protein N-terminus) were selected as variable modifications and carbamidomethylation (C) was selected as fixed modification; for identification, "match between runs" was applied. Protein group abundances were extracted from the MaxQuant proteinGroups.txt file, imported into Perseus (1.6.15.0)[101] and Log2-transformed. Values were filtered for presence in at least 50% of all samples in either the donor or patient group. Missing values were replaced by an imputation-based normal distribution using a width of 0.3 and a downshift of 1.8. Proteins with T-test $p<0.05$ were considered differential; further data analysis and interpretation was performed using Qlucore software and the Reactome pathway database[102,103].

Chemotaxis Assay

Purified neutrophils (as described in "Neutrophil Isolation from fresh blood samples") were stained for 30 min. at 37°C with the cell permeant dye Calcein acetoxymethyl (Thermo Fisher Scientific) at a final concentration of 1 µM. After washing the cells with 20/80 mixed medium (20% Roswell Park Memorial Institute (RPMI)/ 80% AIM- V medium) without serum, cells were rested for 30 min. at RT. For the trans-migration assay, 96-transwell plates were used with 3.0 µm pore polycarbonate permeable membranes (Sigma Aldrich). Top wells contained $0.1*10^6$ neutrophils and bottom wells contained 200 µL 20/80 mixed medium as a control, or 200 µL 20/80 mixed medium supplemented with a final concentration of either 100 ng Recombinant Human IL-8 (Peprotech) or 10 ng LTB-4 (Sigma-Aldrich). Additionally, $0.1*10^6$ neutrophils were plated in the lower well (top wells left empty) to calculate the quantity of migrated neutrophils relative to maximum migration. All conditions and controls were performed in triplicate. Plates were incubated for 40 min. at 37°C, after which the migrated neutrophils were harvested, transferred to low-binding surface, black 96-well flat bottom OptiPlates (Perkin Elmer) and lysed using HTAB buffer (1 g/L Tween 20, 2 g/L CTAB, 2 g/L BSA and 7,44 g/L EDTA). As a read out, fluorescent Calcein was measured at excitation 485/ emission 520 on a PHERAstar FS (BMG labtech) microplate reader.

Phagocytosis Assay

After isolation (as described in "Neutrophil Isolation from fresh blood samples"), neutrophils were rested for 30 min. at RT in 20/80 mixed medium and transferred to 96-well plates at a concentration of $0.5*10^6$ cells/mL. Cells were incubated for 1 hour at 37°C with or without 50µL/mL pHrodo™ Red *E. coli* BioParticles™ Conjugate for Phagocytosis (Thermo Fisher Scientific). All conditions and controls were performed in duplicate, of which the average was taken during the analysis. Flow cytometry was used to quantify the percentage of phagocytic neutrophils and the MFI to quantify the quantity of phagocytosis. By multiplying those two numbers, the Phagocytosis Index was calculated for each person.

NET Formation

Isolated neutrophils (as described in "Neutrophil Isolation from fresh blood samples") were plated in DMEM medium (Thermo Fisher Scientific) at a density of 10.000 cells per well on a Poly-L-Lysine pre-coated 8-well Glass Bottom µ-Slide (Ibidi). Cells were allowed to adhere for 30 min at 37°C, 5% CO_2, before relevant wells were stimulated with 100 nM PMA. Both stimulated and unstimulated neutrophils were incubated for 4 hours at 37°C, 5% CO_2 after which cells were washed with PBS and fixed for 30 min. at RT with 2% methanol free formaldehyde (w/v) (Thermo Fischer Scientific). Slides were stained for NETs using Abcam antibodies against myeloperoxidase (MPO) (1:50, ab11729), Citrullinated H3 rabbit (1:200, ab 150083) and goat anti rabbit (1:500, ab5103). Subsequently, samples were mounted with ProLong™ Gold Antifade Mountant with DAPI (Thermo Fisher Scientific). Images were

acquired at 20x in a blindly predefined area of the slide, on an Axio Scan (Zeiss) equipped with a Hamamatsu Orca Flash 4.0 monochrome camera. NETosis was quantified in FIJI as the fraction of neutrophils that produced a NET in a randomly selected area of fixed size.

ROS Assay

Fresh WBC were plated at a concentration of $1*10^6$ cells per well of a 96 well round bottom plate in the Assay Buffer that is part of the Total Reactive Oxygen Species (ROS) assay kit (Thermo Fischer Scientific). ROS staining was added to the relevant wells and the plate was incubated for 1 hour at 37°C. As positive controls, a 100 ng/mL LPS stimulated condition and a hydrogen peroxide condition were taken along. As a negative control, cells without ROS staining were taken along, which were used to calculate the normalized MFI. After ROS staining, cells were stained for flow cytometry and data acquisition was performed on a LSRII flow cytometer using Diva software (BD Biosciences).

Statistical analyses

GraphPad Prism 9 software was used for statistical analysis and graphing of bar graphs of the flow cytometry and proteomics data. Kruskal-Wallis test was used when comparing more than two groups, followed by Dunn's test to obtain adjusted P-values. P-values that appear in the volcano plots are corrected using the Benjamini-Hochberg procedure across immune cell populations. For two group comparisons Mann-Whitney test was applied. When testing matched samples (e.g. before and after stimulation) p-values were computed with the Wilcoxon signed-rank test. Qlucore 3.8 software and DESeq2 in R v.4.1.0 were used for statistical analysis and graphing of the bulk RNA-sequencing data and proteomics data.
ns = not significant; * p<0.05; ** p<0.01; *** p<0.001; **** p<0.0001

Code availability

All analyses were conducted using publicly accessible open-source software tools, such as DESeq2, without the development of novel code; therefore, no custom scripts are available for sharing. The DESeq2 package was run in RStudio under R version 4.1.0 for differential gene expression analysis.

Data availability

Bulk RNA sequencing data from human neutrophils in this study is deposited in GEO under accession number GSE264108.

Proteomics data from neutrophils in this study have been deposited to the ProteomeXchange Consortium via the PRIDE partner repository[104] with identifier PXD051334.

Acknowledgements

We thank patients and healthy donors for generously donating blood for the benefit of science. We thank Oncode Institute and the Dutch Cancer Society (10653ALPE) for funding the immunophenotyping of the TNBC patients and HDs. Research in the De Visser laboratory is funded by the Dutch Cancer Society (KWF14801; KWF13191), KWF/Oncode grant 14339, and the Netherlands Organisation for Scientific Research (NWOVICI91819616). We thank the BMS-International Immuno-Oncology Network (BMS/II-ON) and the Dutch Cancer Society (NKI2015-7710) for funding the TONIC study. A Sister's Hope foundation contributed to the immunophenotyping of the TNBC patients. Research in the Kok group is funded by the Netherlands Organisation for Scientific Research (NWO-VIDI 09150172010043) and Victoria's Secret Global Fund for Women's Cancers Rising Innovator Research Grant, in Partnership with Pelotonia & AACR. Biobank initiative was partly supported by the Dutch Cancer Society (KWF11105). O.B.B acknowledges support of the X-omics Initiative ((Project 184.034.019), part of the NWO National Roadmap for Large-Scale Research Infrastructures. The funders played no role in study design, data collection, analysis and interpretation of data, or the writing of this manuscript. We acknowledge the supporting staff of the clinical trials of the Departments of Medical Oncology and the Triallab. We acknowledge the Genomics Core Facility for RNA-sequencing support. We thank the NKI Flow Cytometry Facility, the NKI BioImaging facility and the NKI Proteomics facility for their support. We want to thank Melissa van Gool and Prof. Marjolein van Egmond for kindly helping us with setting up the phagocytosis assay. Finally, we would like to thank everyone in the De Visser and Kok labs for inspiring discussions.

Authors contribution

N.A.M.B. analyzed and interpreted data and wrote the manuscript with H.G. and K.E.d.V.. H.G. set up the original flow cytometry panels. N.A.M.B. modified flow cytometry panels, set up and performed the functional assays, analyzed proteomic- and bulk RNA sequencing datasets. E.v.D. performed bioinformatics analysis under supervision of K.E.d.V. and L.F.A.W.. E.C., C.K. and M.D. processed the fresh blood samples and applied compensation and gating strategy to the flow cytometry data. L.V., I.N., R.V., M.L. and H.M.O. asked patients for informed consent to participate in this study and/or were coordinating/supervising clinical trials of which we used the baseline samples. M.N. and I.d.R. performed RNA sequencing and pre-processed the raw RNA sequencing data. O.B. generated the proteomics dataset and pre-processed the raw data. K.E.d.V. and M.K. conceived the project, gave critical input throughout the analysis and supervised the study. All authors edited and approved the manuscript.

Conflicts of interest

N.A.M.B., E.v.D, H.G., E.C., C.K., M.D., L.V., I.N., R.V., M.L., M.N., I.d.R. and O.B. have no conflicts of interest to declare. H.M.O reports funding to the institute from Roche in order to perform the Triple B study and an advisory board fee from Novartis, Pfizer, Gilead, AstraZeneca and Daiichi Sankyo outside the submitted work. L.F.A.W. reports funding to the institute from Genmab BV. M.K. reports funding to the institute from BMS, Roche/ Genentech, AZ, and an advisory role/speakers fee for Alderaan, BMS, Domain Therapeutics, Gilead, Roche, MSD, and Daiichi Sankyo, outside the submitted work. K.E.d.V. reports research funding from Roche/Genentech and is consultant for Macomics, outside the scope of this work.

Supplementary Material

Supplementary Tables

Supplementary Table 1: *basic characteristics of participating TNBC patients and healthy donors.*

	Healthy donors	Stage I-III TNBC		mTNBC Discovery cohort	mTNBC Validation cohort
Number of participants	65	Stage I	12	92	69
		Stage II	27		
		Stage III	5		
Distant metastasis	No	No		Yes	Yes
Median age, years (range)	58 (27-73)	50 (25-71)		55 (33-75)	51 (29-70)
Median BMI	24,5	25,1		25,5	25,4
Previous chemotherapy exposure	x	unknown		54 (59%)	68 (99%)

Supplementary Table 2: *List of antibodies used for flow cytometry.*

Human flow cytometry antibodies					
Antigen	**Fluorochrome**	**Clone**	**Dilution**	**Company**	**Catalogue number**
CD3	PE Cy5	UCHT1	1:200	BD Bioscience	555334
CD4	BV421	RPA-T4	1:100	BD Bioscience	562424
CD8	BUV805	SK1	1:200	BD Bioscience	612754
Pan γδ TCR	PE	11F2	1:100	BD Bioscience	555717
vδ1	FITC	TS8.2	1:100	Thermofisher	TCR2730
vδ2	BUV395	B6	1:100	BD Bioscience	748582
FoxP3	PE Cy5.5	FJK-16s	1:50	Thermofisher	35-5773-82
CCR7	APC R700	150503	1:50	BD Bioscience	565868
CD45RA	BUV737	HI100	1:400	BD Bioscience	612846
CD25	AF647	BC96	1:100	BioLegend	302618
PD-1	APC Cy7	EH12.2H7	1:100	BioLegend	329922
CTLA-4	PE CF594	BNI3	1:200	BD Bioscience	562742
IL-17	PerCP Cy5.5	N49-653	1:50	BD Bioscience	560799
IFNγ	BV785	4S.B3	1:200	BioLegend	502542
TNFα	PE Cy7	Mab11	1:400	BioLegend	502930
CD27	BV786	L128	1:100	BD Bioscience	563327
TIGIT	PerCP Cy5.5	A151536	1:100	BioLegend	372718
Ki-67	PE Cy7	B56	1:50	BD Bioscience	561283
CTLA-4	PE CF594	PE/Dazzle594	1:200	BioLegend	369616
CD19	PE Cy5	HIB19	1:200	BD Bioscience	555414
CD3ε	BUV496	UCHT1	1:100	BD Bioscience	612940

Human flow cytometry antibodies					
Antigen	**Fluorochrome**	**Clone**	**Dilution**	**Company**	**Catalogue number**
CD56	PE Cy5	B159	1:100	BD Bioscience	555517
CD161	PE Cy5	DX12	1:100	BD Bioscience	551138
HLA-DR	BUV661	G46-6	1:100	BD Bioscience	612980
CD14	BUV737	M5E2	1:100	BD Bioscience	612763
CD16	BUV496	3G8	1:100	BD Bioscience	612944
CD16	AF700	3G8	1:200	BioLegend	302026
CD11b	BV421	ICRF44	1:200	BioLegend	301324
CD11c	BV785	3.9	1:100	BioLegend	301644
cKIT/CD117	PE Cy5.5	104D2	1:400	Thermofisher	CD11718
CD1c	PE Cy7	L161	1:100	BioLegend	331516
CD141	BV711	1A4	1:100	BD Bioscience	563155
CD123	PE	6H6	1:200	BioLegend	396604
CD66b	PerCP-Cy5.5	G10F5	1:200	BD Bioscience	562254
CD66b	AF647	G10F5	1:200	BD Bioscience	561645
CD33	PerCP Cy5.5	WM53	1:100	BioLegend	303414
CD303	APC vio770	REA693	1:100	Miltenyi Biotech	130-114-178
CD41a	BUV395	HIP8	1:400	BD Bioscience	740295
FcεRIα	PE Dazzle 594	AER-37(CRA-1)	1:200	BioLegend	334634
CD34	FITC	581	1:100	BD Bioscience	555821
CD19	BUV395	SJ25C1	1:50	BD Bioscience	563549
IgD	APC	IA6-2	1:100	BD Bioscience	561303
CD20	BUV805	2H7	1:200	BD Bioscience	612905
CD27	PE	M-T271	1:200	BD Bioscience	555441
CD10	AF700	HI10a	1:200	BD Bioscience	563509
CD24	BB515	ML5	1:200	BD Bioscience	564521
IgM	APC Cy7	MHM-88	1:100	BioLegend	314520
CD38	BUV737	HIT2	1:400	BD Bioscience	741837
CD5	PE Dazzle 594	L17F12	1:400	BioLegend	364012
CD1d	BV786	42.1	1:200	BD Bioscience	743608
CD138	BV711	MI15	1:200	BioLegend	563184
CXCR4	PE	12G5	1:50	BioLegend	306506
CD3	PerCP Cy5.5	SK7	1:100	BioLegend	344808
CD19	PerCP Cy5.5	HIB19	1:100	BioLegend	302230
CD161	PerCP Cy5.5	HP-3610	1:100	BioLegend	339908
CD14	BV605	M5E2	1:100	BioLegend	301834
CD49d	BUV737	9F10	1:100	BD Bioscience	612850
CD62L	BUV805	DREG-56	1:100	BD Bioscience	742024
CD80	BUV395	L3074	1:100	BD Bioscience	565210
CD101	PE Cy7	BB27	1:100	BioLegend	331014
CD11b	BV785	ICRF44	1:100	BioLegend	301246
CD15	eFluor450	H198	1:100	Invitrogen	48-0159-42
CD86	BV711	IT2.2	1:100	BioLegend	305440
CD177	FITC	MEM-166	1:200	BioLegend	3115804
Siglec8	PE Dazzle 594	7C9	1:200	BioLegend	315804

a Myeloid panel

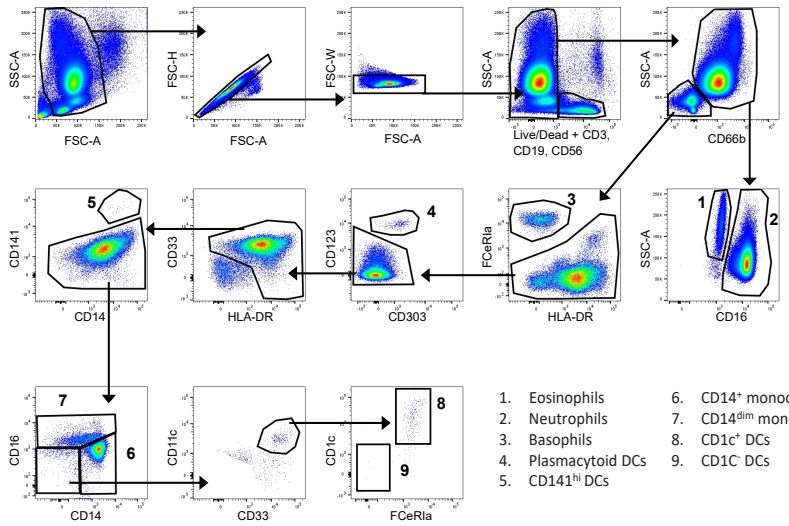

1. Eosinophils
2. Neutrophils
3. Basophils
4. Plasmacytoid DCs
5. CD141^{hi} DCs
6. CD14^{+} monocytes
7. CD14^{dim} monocytes
8. CD1c^{+} DCs
9. CD1C^{-} DCs

b B and NK cell panel

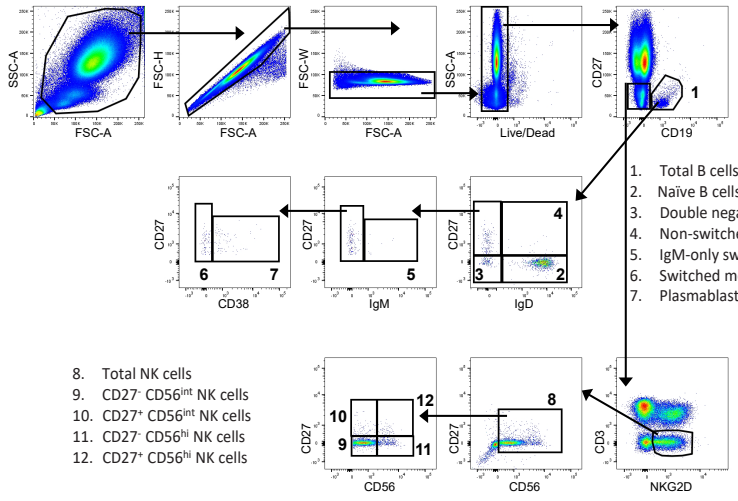

1. Total B cells
2. Naïve B cells
3. Double negative B cells
4. Non-switched B cells
5. IgM-only switched memory B cells
6. Switched memory B cells
7. Plasmablast-like cells
8. Total NK cells
9. CD27^{-} CD56^{int} NK cells
10. CD27^{+} CD56^{int} NK cells
11. CD27^{-} CD56^{hi} NK cells
12. CD27^{+} CD56^{hi} NK cells

c T cell panel

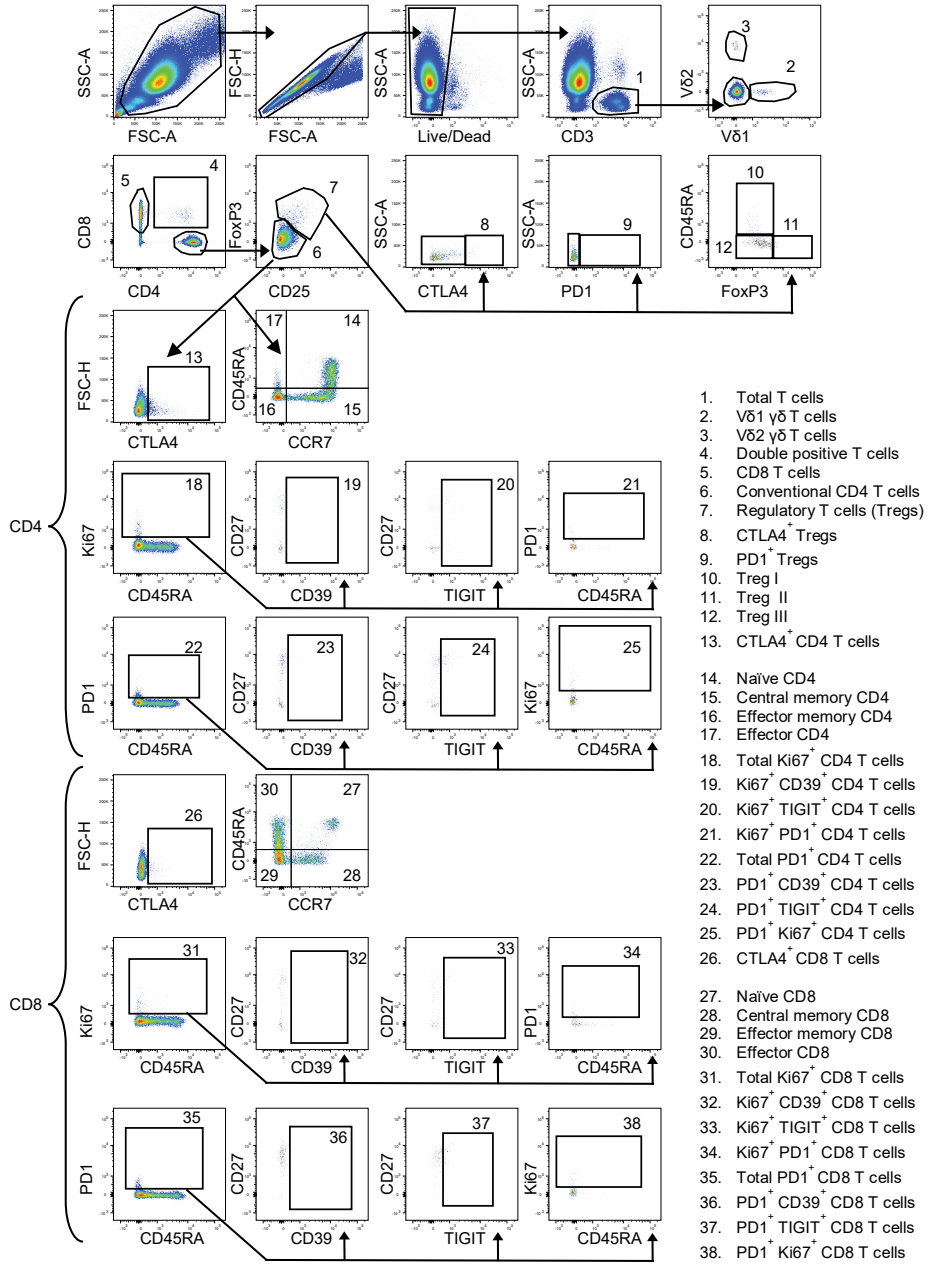

1. Total T cells
2. Vδ1 γδ T cells
3. Vδ2 γδ T cells
4. Double positive T cells
5. CD8 T cells
6. Conventional CD4 T cells
7. Regulatory T cells (Tregs)
8. CTLA4^{+} Tregs
9. PD1^{+} Tregs
10. Treg I
11. Treg II
12. Treg III
13. CTLA4^{+} CD4 T cells
14. Naïve CD4
15. Central memory CD4
16. Effector memory CD4
17. Effector CD4
18. Total Ki67^{+} CD4 T cells
19. Ki67^{+} CD39^{+} CD4 T cells
20. Ki67^{+} TIGIT^{+} CD4 T cells
21. Ki67^{+} PD1^{+} CD4 T cells
22. Total PD1^{+} CD4 T cells
23. PD1^{+} CD39^{+} CD4 T cells
24. PD1^{+} TIGIT^{+} CD4 T cells
25. PD1^{+} Ki67^{+} CD4 T cells
26. CTLA4^{+} CD8 T cells
27. Naïve CD8
28. Central memory CD8
29. Effector memory CD8
30. Effector CD8
31. Total Ki67^{+} CD8 T cells
32. Ki67^{+} CD39^{+} CD8 T cells
33. Ki67^{+} TIGIT^{+} CD8 T cells
34. Ki67^{+} PD1^{+} CD8 T cells
35. Total PD1^{+} CD8 T cells
36. PD1^{+} CD39^{+} CD8 T cells
37. PD1^{+} TIGIT^{+} CD8 T cells
38. PD1^{+} Ki67^{+} CD8 T cells

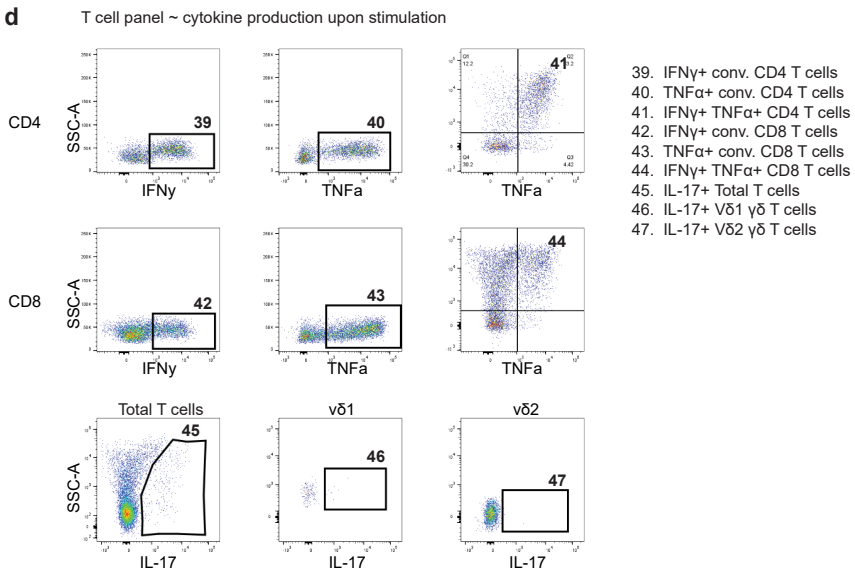

39. IFNγ+ conv. CD4 T cells
40. TNFα+ conv. CD4 T cells
41. IFNγ+ TNFα+ CD4 T cells
42. IFNγ+ conv. CD8 T cells
43. TNFα+ conv. CD8 T cells
44. IFNγ+ TNFα+ CD8 T cells
45. IL-17+ Total T cells
46. IL-17+ Vδ1 γδ T cells
47. IL-17+ Vδ2 γδ T cells

Supplementary Figure 1. *Gating strategies for flow cytometry analysis of peripheral blood immune populations.* ***(a)*** *Myeloid panel gating strategy identifying eosinophils (lineage-, high side scatter, CD66b+ CD16-), neutrophils (lineage-, high side scatter, CD66b+ CD16+), basophils (lineage-, FcεRIα+, HLA-DR-), plasmacytoid DCs (lineage-, HLA-DR+, CD303+, CD123+), CD141hi DCs (lineage-, HLA-DR+, CD33+, CD141+), CD14+ monocytes (lineage-, HLA-DR+, CD33+, CD14+, CD16-/+), CD14dim monocytes (lineage-, HLA-DR+, CD33+, CD14dim, CD16+), CD1c+ DCs (lineage-, HLA-DR+, CD33+, CD14-, CD16-, CD1c+, FcεRIα+) and CD1c- DCs (lineage-, HLA-DR+, CD33+, CD14-, CD16-, CD1c-, FcεRIα-).* ***(b)*** *Gating strategy to identify B cell subsets identifying naive B cells (CD19+, CD27-, IgD+), double negative B cells (CD19+, CD27-, IgD-), non-switched memory B cells (CD19+, CD27+, IgD+), IgM-only switched memory B cells (CD19+, CD27+, IgD-, IgM+), switched memory B cells (CD19+, CD27+, IgD-, IgM-, CD38-/+), and plasmablasts-like cells (CD19+, CD27+, IgD-, IgM-, CD38hi). Gating strategy to identify NK cells (CD19-, CD3-, NKG2D+, CD56+), CD27- CD56int NK cells (CD19-, CD3-, NKG2D+, CD56int, CD27-), CD27+ CD56int NK cells (CD19-, CD3-, NKG2D+, CD56int, CD27+), CD27- CD56hi NK cells (CD19-, CD3-, NKG2D+, CD56hi, CD27-) and CD27+ CD56hi NK cells (CD19-, CD3-, NKG2D+, CD56hi, CD27+).* ***(c)*** *T cell panel gating strategy identifying Vδ1 γδ T cells (CD3+, Vδ1+, pan γδ TCR+), Vδ2 γδ T cells (CD3+, Vδ2+), double positive T cells (CD3+, Vδ1-, pan γδ TCR-, Vδ2-, CD8+, CD4+), CD8 T cells (CD3+, Vδ1-, pan γδ TCR-, Vδ2-, CD8+, CD4-), conventional CD4 T cells (CD3+, Vδ1-, pan γδ TCR-, Vδ2-, CD8-, CD4+, FoxP3-), Tregs (CD3+, Vδ1-, pan γδ TCR-, Vδ2-, CD8-, CD4+, FoxP3+, CD25hi), Treg I (CD3+, Vδ1-, pan γδ TCR-, Vδ2-, CD8-, CD4+, CD25hi, FoxP3int, CD45RA+), Treg II (CD3+, Vδ1-, pan γδ TCR-, Vδ2-, CD8-, CD4+, CD25hi, FoxP3hi, CD45RA-) and Treg III (CD3+, Vδ1-, pan γδ TCR-, Vδ2-, CD8-, CD4+, CD25hi, FoxP3int, CD45RA-). Differentiation states were obtained as followed for both the conventional CD4 T cells and CD8 T cells: naïve T cells (CD45RA+, CCR7+), central memory T cells (CD45RA-, CCR7+), effector memory T cells (CD45RA-, CCR7-), effector T cells (CD45RA+, CCR7-). Additional phenotypic markers were gated according to the population names.* ***(d)*** *Cytokine production was measured after PMA-ionomycin stimulation. Gating strategy identifying IFNγ+ conventional CD4 T cells (CD3+, Vδ1-, pan γδ TCR-, Vδ2-, CD8-, CD4+, FoxP3-, IFNγ+), TNFα+ conventional CD4 T cells (CD3+, Vδ1-, pan γδ TCR-, Vδ2-, CD8-, CD4+, FoxP3-, TNFα+), IFNγ+ TNFα+ conventional CD4 T cells (CD3+, Vδ1-, pan γδ TCR-, Vδ2-, CD8-, CD4+, FoxP3-, IFNγ+, TNFα+), IFNγ+ CD8 T cells (CD3+, Vδ1-, pan γδ TCR-, Vδ2-, CD8+, CD4-, IFNγ+), TNFα+ CD8 T cells (CD3+, Vδ1-, pan γδ TCR-, Vδ2-, CD8+, CD4-, TNFα+), IFNγ+ TNFα+ CD8 T cells (CD3+, Vδ1-, pan γδ TCR-, Vδ2-, CD8+, CD4-, IFNγ+, TNFα+). IL17 production is assessed by the following gating strategy: IL17+ total T cells (CD3+, IL17+), IL17+ Vδ1 γδ T cells (CD3+, Vδ1+, IL17+) and IL17+ Vδ2 γδ T cells (CD3+, Vδ2+, IL17+).*

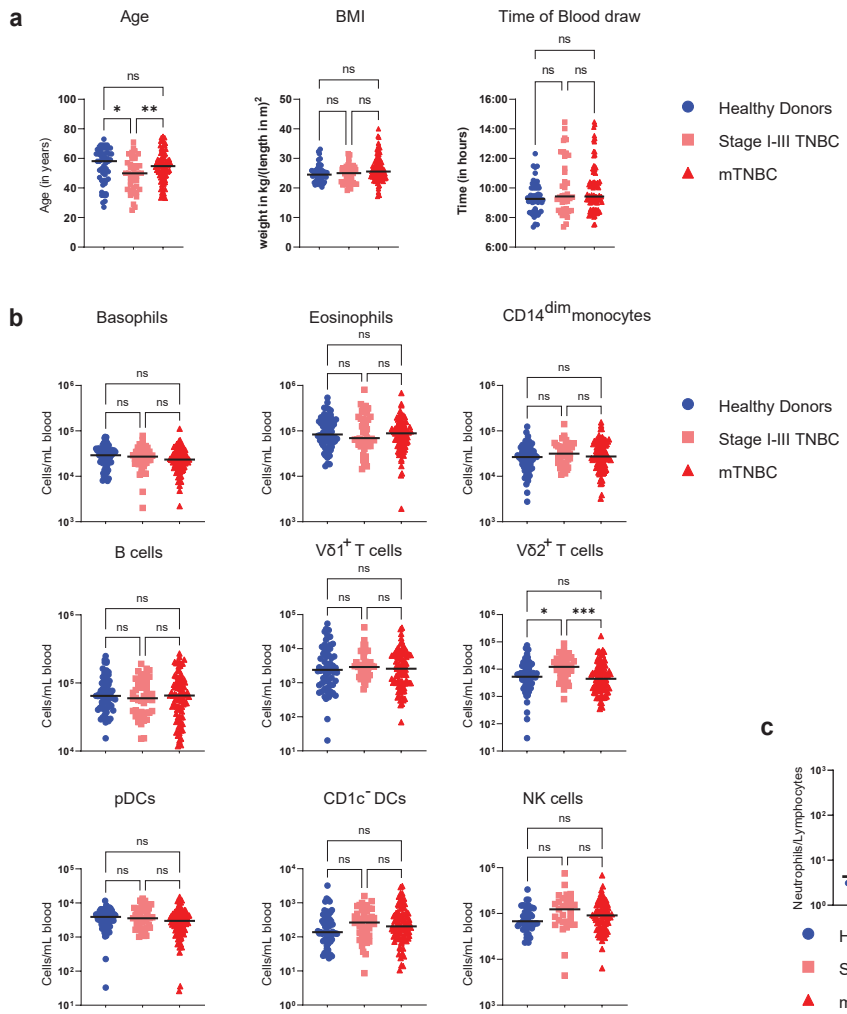

Supplementary Figure 2. *Patient characteristics, NLR and immune cell subsets that did not show statistically significant abundance differences.* ***(a)*** *Age- and BMI-distribution and the times at which the blood was taken from the healthy donors, patients with stage I-III TNBC and patients with mTNBC that participated in our discovery cohort.* ***(b)*** *Absolute counts of major circulating immune cell subsets that were not significantly dysregulated in patients with TNBC. Depicted are cell counts per mL blood (log scale) assessed by flow cytometry in healthy donors (HDs; n=65), stage I-III (Stage I-III TNBC; n=44) and metastatic TNBC patients (mTNBC; n=92). Circulating immune cell subsets that were significantly dysregulated are depicted in main Figure 1b.* ***(c)*** *Neutrophils to Lymphocyte ratio (NLR) calculated by dividing neutrophil counts by lymphocyte counts in HDs (n=65), patients with stage I-III TNBC (n=44) and patients with mTNBC (n=92). P-values are computed with the Kruskal-Wallis test followed by Dunn's multiple comparisons correction for number of groups.*

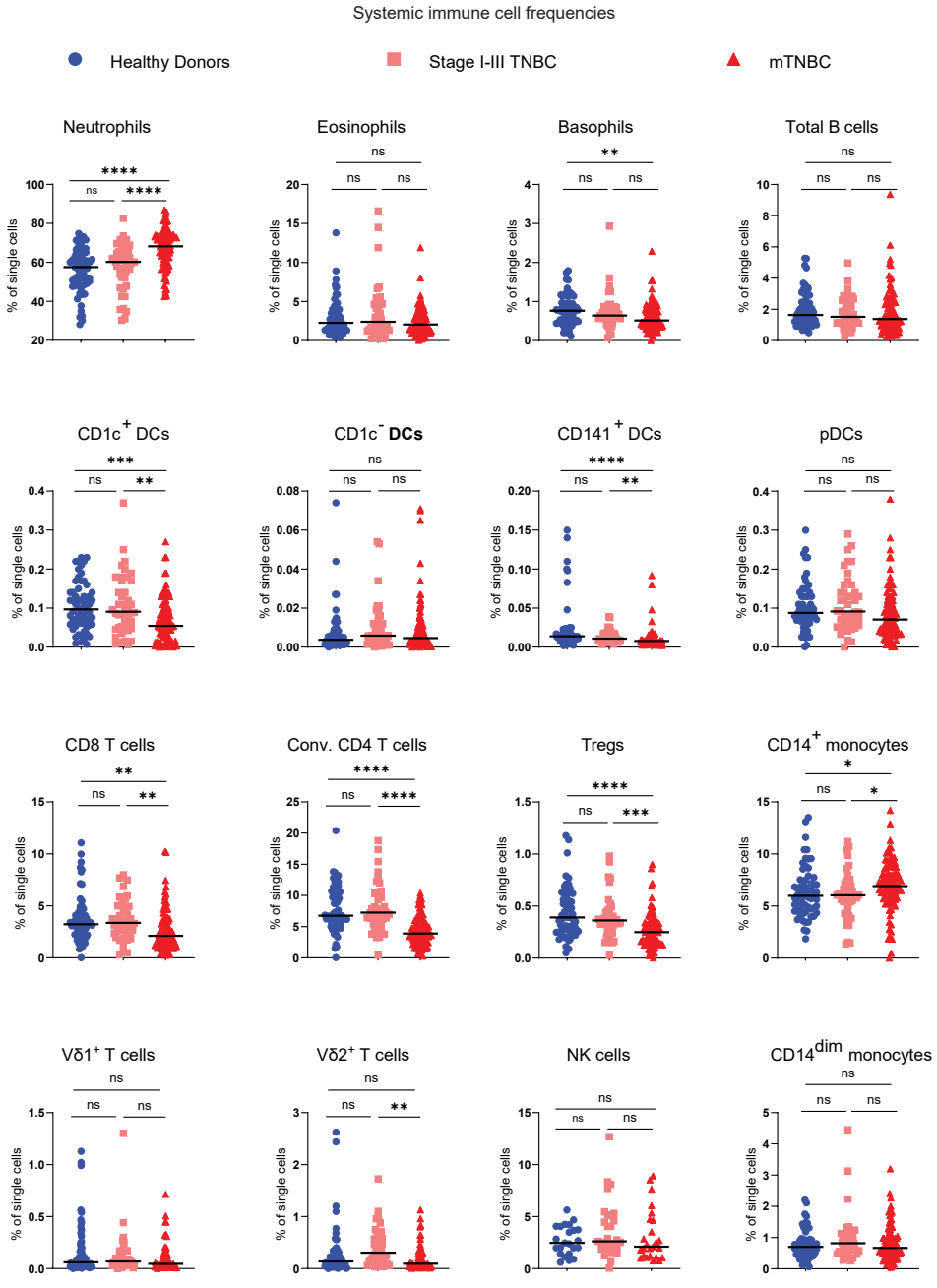

Supplementary Figure 3. *Frequencies of main systemic immune cell populations. Depicted are percentages of single cells, assessed by flow cytometry in fresh blood samples from healthy donors (HDs; n=65), stage I-III (Stage I-III TNBC; n=44) and metastatic TNBC patients (mTNBC; n=92). P-values are computed with the Kruskal-Wallis test followed by Dunn's multiple comparisons correction.*

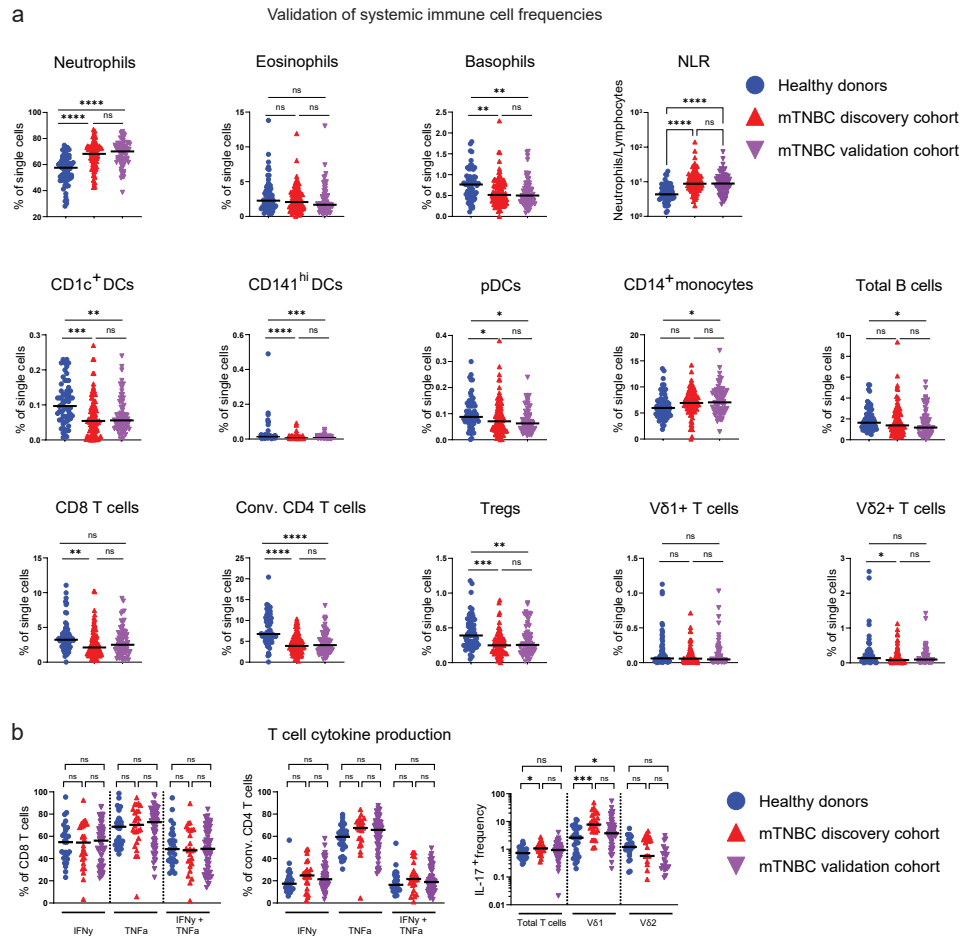

Supplementary Figure 4. *Tumor induced immune perturbations to the systemic immune landscape in patients with mTNBC could be confirmed in an independent validation cohort.* ***(a)*** *Validation of systemic immune cell frequencies and NLR in fresh blood samples of our discovery cohort: HDs (n=65) and patients with mTNBC (n=92), and our validation cohort comprising of a group of independent patients with mTNBC (n=69). Depicted are frequencies of single cell, assessed by flow cytometry.* ***(b)*** *Validation of IFNγ and TNFα production by CD8+ and conventional CD4+ T cells, and IL17 expression on Total T cells and γδ T cells subsets Vδ1 and Vδ2 upon ex vivo stimulation, determined by flow cytometry for HDs (n=29), mTNBC patients validation cohort (n=26) and mTNBC validation cohort (n=56). P-values are computed with the Kruskal-Wallis test followed by Dunn's multiple comparisons correction.*

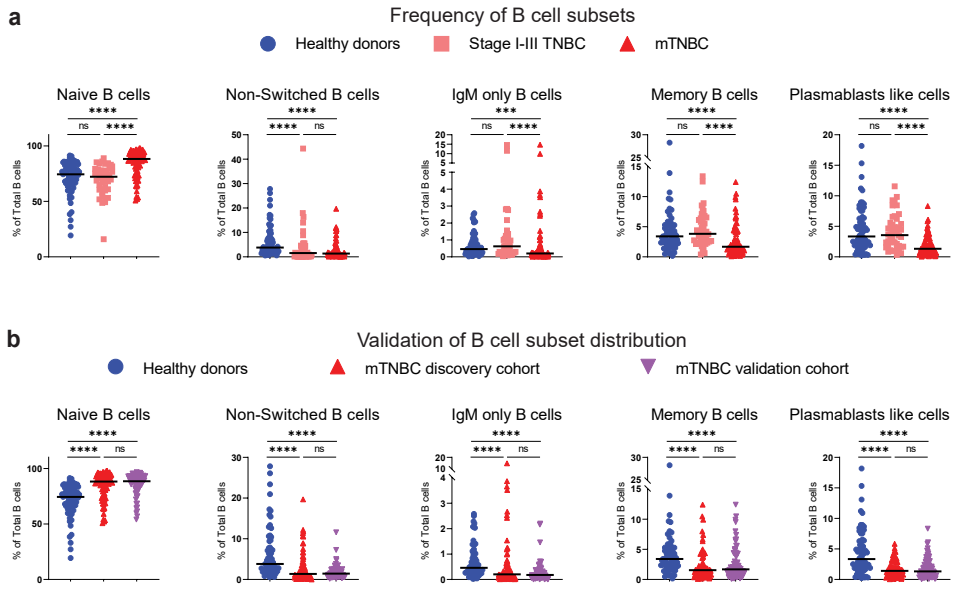

Supplementary Figure 5. *Frequencies of differentiated B cell subsets. B cell subpopulations as a relative proportion of total B cells, determined by flow cytometry.* ***(a)*** *Discovery cohorts representing healthy donors (HDs; n=65), stage I-III (Stage I-III TNBC; n=44) and metastatic TNBC patients (mTNBC; n=92).* ***(b)*** *Validation cohort (mTNBC; n=69) compared to the discovery cohorts representing HDs and patients with mTNBC described in a. P-values are computed with the Kruskal-Wallis test followed by Dunn's multiple comparisons correction.*

Supplementary Figure 6. *Prior chemotherapy treatment does not significantly impact T cell differentiation state and phenotype in patients with metastatic triple-negative breast cancer.* ***(a)*** *Prior chemotherapy effect on circulating immune cell populations that were not significantly dysregulated in patients with TNBC according to main Figures 1c and 4b-d.* ***(b)*** *Differentiation state of CD8+ T cells and conventional CD4+ T cells, based on surface marker expression of CD45RA and CCR7 determined by flow cytometry and grouped based on prior chemotherapy. HD (n=65), mTNBCchemo_naïve (n=29), mTNBC>1yr_chemo_free (n=38) and mTNBCrecent_chemo (n=16). CM = central memory, EM = effector memory and T eff = effector T cells.* ***(c)*** *T cell phenotype as determined by flow cytometry comparing fractions within CD8+, conventional CD4+, and regulatory T cells for HD (n=65), mTNBCchemo_naïve (n=29), mTNBC>1yr_chemo_free (n=38) and mTNBCrecent_chemo (n=16).* ***(d)*** *Regulatory T cell subset distribution based on relative expression of FoxP3 and CD45RA as determined by flow cytometry. All p-values are computed with the Kruskal-Wallis test followed by Dunn's multiple comparisons test.* ▶▶▶

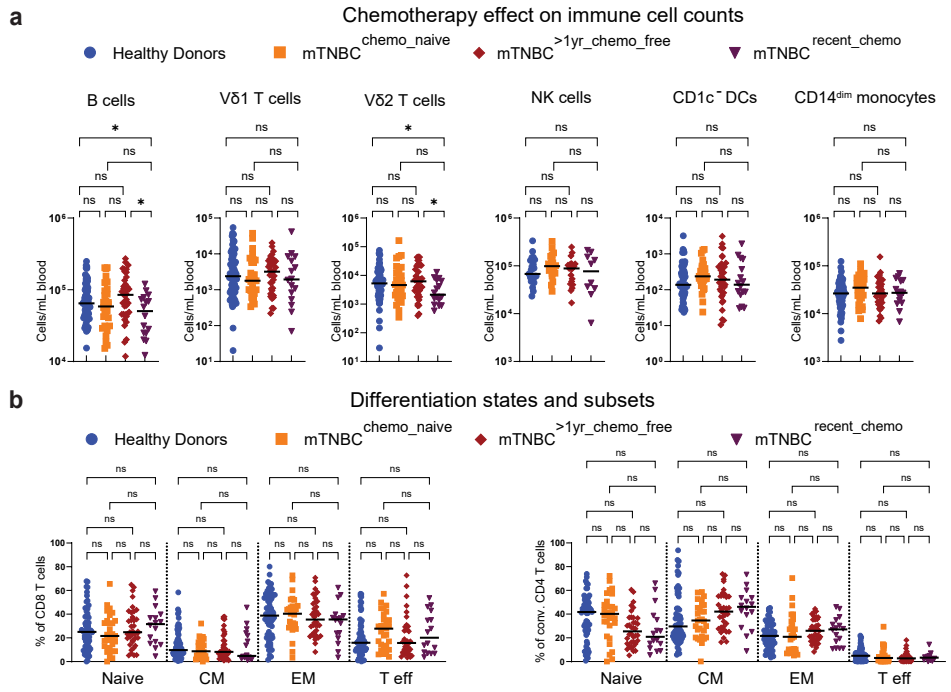

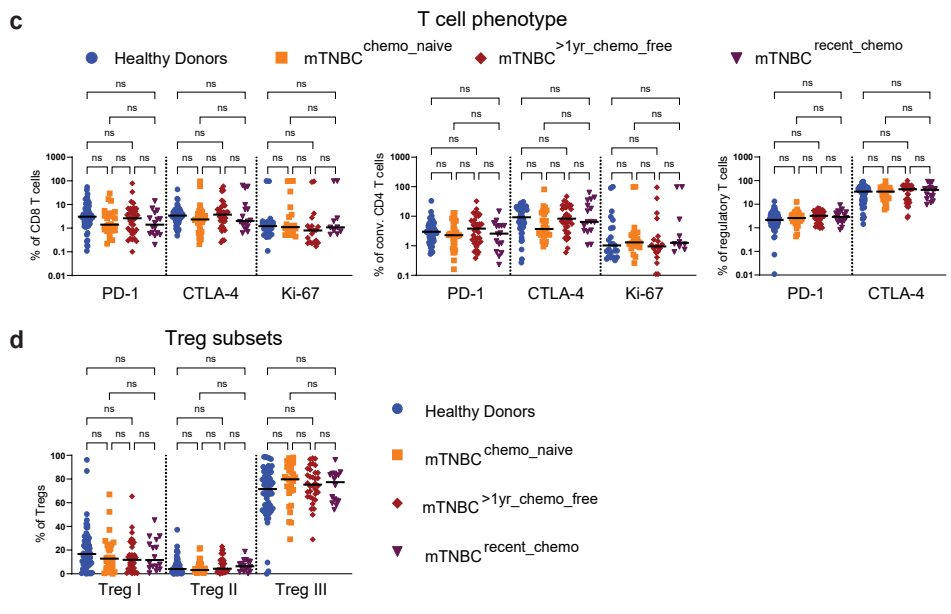

References

1 Blomberg, O. S., Spagnuolo, L. & de Visser, K. E. Immune regulation of metastasis: mechanistic insights and therapeutic opportunities. *Dis Model Mech* **11** (2018). https://doi.org/10.1242/dmm.036236

2 Garner, H. & de Visser, K. E. Immune crosstalk in cancer progression and metastatic spread: a complex conversation. *Nat Rev Immunol* **20**, 483-497 (2020). https://doi.org/10.1038/s41577-019-0271-z

3 Diakos, C. I., Charles, K. A., McMillan, D. C. & Clarke, S. J. Cancer-related inflammation and treatment effectiveness. *Lancet Oncol* **15**, e493-503 (2014). https://doi.org/10.1016/S1470-2045(14)70263-3

4 McAllister, S. S. & Weinberg, R. A. The tumour-induced systemic environment as a critical regulator of cancer progression and metastasis. *Nat Cell Biol* **16**, 717-727 (2014). https://doi.org/10.1038/ncb3015

5 Semerad, C. L., Liu, F., Gregory, A. D., Stumpf, K. & Link, D. C. G-CSF is an essential regulator of neutrophil trafficking from the bone marrow to the blood. *Immunity* **17**, 413-423 (2002). https://doi.org/10.1016/s1074-7613(02)00424-7

6 Kersten, K. *et al.* Mammary tumor-derived CCL2 enhances pro-metastatic systemic inflammation through upregulation of IL1beta in tumor-associated macrophages. *Oncoimmunology* **6**, e1334744 (2017). https://doi.org/10.1080/2162402X.2017.1334744

7 Hao, Q., Vadgama, J. V. & Wang, P. CCL2/CCR2 signaling in cancer pathogenesis. *Cell Commun Signal* **18**, 82 (2020). https://doi.org/10.1186/s12964-020-00589-8

8 Duits, D. E. M. & de Visser, K. E. Impact of cancer cell-intrinsic features on neutrophil behavior. *Semin Immunol* **57**, 101546 (2021). https://doi.org/10.1016/j.smim.2021.101546

9 Robinson, A. *et al.* Systemic Influences of Mammary Cancer on Monocytes in Mice. *Cancers (Basel)* **14** (2022). https://doi.org/10.3390/cancers14030833

10 Wellenstein, M. D. *et al.* Loss of p53 triggers WNT-dependent systemic inflammation to drive breast cancer metastasis. *Nature* **572**, 538-542 (2019). https://doi.org/10.1038/s41586-019-1450-6

11 Hiam-Galvez, K. J., Allen, B. M. & Spitzer, M. H. Systemic immunity in cancer. *Nat Rev Cancer* **21**, 345-359 (2021). https://doi.org/10.1038/s41568-021-00347-z

12 Dyikanov, D. *et al.* Comprehensive peripheral blood immunoprofiling reveals five immunotypes with immunotherapy response characteristics in patients with cancer. *Cancer Cell* **42**, 759-779 e712 (2024). https://doi.org/10.1016/j.ccell.2024.04.008

13 Guo, W. *et al.* Prognostic value of neutrophil-to-lymphocyte ratio and platelet-to-lymphocyte ratio for breast cancer patients: An updated meta-analysis of 17079 individuals. *Cancer Med* **8**, 4135-4148 (2019). https://doi.org/10.1002/cam4.2281

14 Liu, J. *et al.* Systemic immune-inflammation index, neutrophil-to-lymphocyte ratio, platelet-to-lymphocyte ratio can predict clinical outcomes in patients with metastatic non-small-cell lung cancer treated with nivolumab. *J Clin Lab Anal* **33**, e22964 (2019). https://doi.org/10.1002/jcla.22964

15 Shao, Y. *et al.* Prognostic value of pretreatment neutrophil-to-lymphocyte ratio in renal cell carcinoma: a systematic review and meta-analysis. *BMC Urol* **20**, 90 (2020). https://doi.org/10.1186/s12894-020-00665-8

16 Krenn-Pilko, S. *et al.* The elevated preoperative derived neutrophil-to-lymphocyte ratio predicts poor clinical outcome in breast cancer patients. *Tumour Biol* **37**, 361-368 (2016). https://doi.org/10.1007/s13277-015-3805-4

17 Ethier, J. L., Desautels, D., Templeton, A., Shah, P. S. & Amir, E. Prognostic role of neutrophil-to-lymphocyte ratio in breast cancer: a systematic review and meta-analysis. *Breast Cancer Res* **19**, 2 (2017). https://doi.org/10.1186/s13058-016-0794-1

18 Templeton, A. J. *et al.* Prognostic role of neutrophil-to-lymphocyte ratio in solid tumors: a systematic review and meta-analysis. *J Natl Cancer Inst* **106**, dju124 (2014). https://doi.org/10.1093/jnci/dju124

19 Coffelt, S. B. *et al.* IL-17-producing gammadelta T cells and neutrophils conspire to promote breast cancer metastasis. *Nature* **522**, 345-348 (2015). https://doi.org/10.1038/nature14282

20 Kowanetz, M. *et al.* Granulocyte-colony stimulating factor promotes lung metastasis through mobilization of Ly6G+Ly6C+ granulocytes. *Proc Natl Acad Sci U S A* **107**, 21248-21255 (2010). https://doi.org/10.1073/pnas.1015855107

21 Yang, L. *et al.* DNA of neutrophil extracellular traps promotes cancer metastasis via CCDC25. *Nature* **583**, 133-138 (2020). https://doi.org/10.1038/s41586-020-2394-6

22 Szczerba, B. M. *et al.* Neutrophils escort circulating tumour cells to enable cell cycle progression. *Nature* **566**, 553-557 (2019). https://doi.org/10.1038/s41586-019-0915-y

23 McDowell, S. A. C. *et al.* Neutrophil oxidative stress mediates obesity-associated vascular dysfunction and metastatic transmigration. *Nat Cancer* **2**, 545-562 (2021). https://doi.org/10.1038/s43018-021-00194-9

24 Jablonska, J., Lang, S., Sionov, R. V. & Granot, Z. The regulation of pre-metastatic niche formation by neutrophils. *Oncotarget* **8**, 112132-112144 (2017). https://doi.org/10.18632/oncotarget.22792

25 Park, J. *et al.* Cancer cells induce metastasis-supporting neutrophil extracellular DNA traps. *Sci Transl Med* **8**, 361ra138 (2016). https://doi.org/10.1126/scitranslmed.aag1711

26 Zheng, C. *et al.* Neutrophils in triple-negative breast cancer: an underestimated player with increasingly recognized importance. *Breast Cancer Res* **25**, 88 (2023). https://doi.org/10.1186/s13058-023-01676-7

27 Sanz-Moreno, V. & Balkwill, F. R. Mets and NETs: The Awakening Force. *Immunity* **49**, 798-800 (2018). https://doi.org/10.1016/j.immuni.2018.11.009

28 Cassetta, L. *et al.* Deciphering myeloid-derived suppressor cells: isolation and markers in humans, mice and non-human primates. *Cancer Immunol Immunother* **68**, 687-697 (2019). https://doi.org/10.1007/s00262-019-02302-2

29 Serbina, N. V. & Pamer, E. G. Monocyte emigration from bone marrow during bacterial infection requires signals mediated by chemokine receptor CCR2. *Nat Immunol* **7**, 311-317 (2006). https://doi.org/10.1038/ni1309

30 Kiss, M., Caro, A. A., Raes, G. & Laoui, D. Systemic Reprogramming of Monocytes in Cancer. *Front Oncol* **10**, 1399 (2020). https://doi.org/10.3389/fonc.2020.01399

31 Trovato, R. *et al.* Immunosuppression by monocytic myeloid-derived suppressor cells in patients with pancreatic ductal carcinoma is orchestrated by STAT3. *J Immunother Cancer* **7**, 255 (2019). https://doi.org/10.1186/s40425-019-0734-6

32 Meyer, M. A. *et al.* Breast and pancreatic cancer interrupt IRF8-dependent dendritic cell development to overcome immune surveillance. *Nat Commun* **9**, 1250 (2018). https://doi.org/10.1038/s41467-018-03600-6

33 Wolf, A. M. *et al.* Increase of regulatory T cells in the peripheral blood of cancer patients. *Clin Cancer Res* **9**, 606-612 (2003).

34 Foulds, G. A. *et al.* Immune-Phenotyping and Transcriptomic Profiling of Peripheral Blood Mononuclear Cells From Patients With Breast Cancer: Identification of a 3 Gene Signature Which Predicts Relapse of Triple Negative Breast Cancer. *Front Immunol* **9**, 2028 (2018). https://doi.org/10.3389/fimmu.2018.02028

35 Kos, K. & de Visser, K. E. The Multifaceted Role of Regulatory T Cells in Breast Cancer. *Annu Rev Cancer Biol* **5**, 291-310 (2021). https://doi.org/10.1146/annurev-cancerbio-042920-104912

36 Sabbioni, M. E. *et al.* Interaction of tamoxifen with concurrent cytotoxic adjuvant treatment affects lymphocytes and lymphocyte subsets counts in breast cancer patients. *Support Care Cancer* **7**, 149-153 (1999). https://doi.org/10.1007/s005200050245

37 Whitehead, R. H., Thatcher, J., Teasdale, C., Roberts, G. P. & Hughes, L. E. T and B lymphocytes in breast cancer stage relationship and abrogation of T-lymphocyte depression by enzyme treatment in vitro. *Lancet* **1**, 330-333 (1976). https://doi.org/10.1016/s0140-6736(76)90085-4

38 Blomberg, O. S. *et al.* IL-5-producing CD4(+) T cells and eosinophils cooperate to enhance response to immune checkpoint blockade in breast cancer. *Cancer Cell* **41**, 106-123 e110 (2023). https://doi.org/10.1016/j.ccell.2022.11.014

39 Pick, R., He, W., Chen, C. S. & Scheiermann, C. Time-of-Day-Dependent Trafficking and Function of Leukocyte Subsets. *Trends Immunol* **40**, 524-537 (2019). https://doi.org/10.1016/j.it.2019.03.010

40 Adrover, J. M. *et al.* A Neutrophil Timer Coordinates Immune Defense and Vascular Protection. *Immunity* **51**, 966-967 (2019). https://doi.org/10.1016/j.immuni.2019.11.001

41 Joffre, O. P., Segura, E., Savina, A. & Amigorena, S. Cross-presentation by dendritic cells. *Nat Rev Immunol* **12**, 557-569 (2012). https://doi.org/10.1038/nri3254

42 Mellman, I., Chen, D. S., Powles, T. & Turley, S. J. The cancer-immunity cycle: Indication, genotype, and immunotype. *Immunity* **56**, 2188-2205 (2023). https://doi.org/10.1016/j.immuni.2023.09.011

43 Pittet, M. J., Di Pilato, M., Garris, C. & Mempel, T. R. Dendritic cells as shepherds of T cell immunity in cancer. *Immunity* **56**, 2218-2230 (2023). https://doi.org/10.1016/j.immuni.2023.08.014

44 Salmon, H. *et al.* Expansion and Activation of CD103(+) Dendritic Cell Progenitors at the Tumor Site Enhances Tumor Responses to Therapeutic PD-L1 and BRAF Inhibition. *Immunity* **44**, 924-938 (2016). https://doi.org/10.1016/j.immuni.2016.03.012

45 Mohr, A., Malhotra, R., Mayer, G., Gorochov, G. & Miyara, M. Human FOXP3(+) T regulatory cell heterogeneity. *Clin Transl Immunology* **7**, e1005 (2018). https://doi.org/10.1002/cti2.1005

46 Mason, G. M. *et al.* Phenotypic Complexity of the Human Regulatory T Cell Compartment Revealed by Mass Cytometry. *J Immunol* **195**, 2030-2037 (2015). https://doi.org/10.4049/jimmunol.1500703

47 Wing, J. B., Tanaka, A. & Sakaguchi, S. Human FOXP3(+) Regulatory T Cell Heterogeneity and Function in Autoimmunity and Cancer. *Immunity* **50**, 302-316 (2019). https://doi.org/10.1016/j.immuni.2019.01.020

48 Bod, L. *et al.* B-cell-specific checkpoint molecules that regulate anti-tumour immunity. *Nature* **619**, 348-356 (2023). https://doi.org/10.1038/s41586-023-06231-0

49 de Visser, K. E., Korets, L. V. & Coussens, L. M. De novo carcinogenesis promoted by chronic inflammation is B lymphocyte dependent. *Cancer Cell* **7**, 411-423 (2005). https://doi.org/10.1016/j.ccr.2005.04.014

50 Tan, R., Nie, M. & Long, W. The role of B cells in cancer development. *Front Oncol* **12**, 958756 (2022). https://doi.org/10.3389/fonc.2022.958756

51 Akkaya, M., Kwak, K. & Pierce, S. K. B cell memory: building two walls of protection against pathogens. *Nat Rev Immunol* **20**, 229-238 (2020). https://doi.org/10.1038/s41577-019-0244-2

52 Wculek, S. K. & Malanchi, I. Neutrophils support lung colonization of metastasis-initiating breast cancer cells. *Nature* **528**, 413-417 (2015). https://doi.org/10.1038/nature16140

53 Hedrick, C. C. & Malanchi, I. Neutrophils in cancer: heterogeneous and multifaceted. *Nat Rev Immunol* **22**, 173-187 (2022). https://doi.org/10.1038/s41577-021-00571-6

54 Liu, Y., He, M., Wang, C., Zhang, X. & Cai, S. Prognostic value of neutrophil-to-lymphocyte ratio for patients with triple-negative breast cancer: A meta-analysis. *Medicine (Baltimore)* **101**, e29887 (2022). https://doi.org/10.1097/MD.0000000000029887

55 Bai, M. *et al.* CD177 modulates human neutrophil migration through activation-mediated integrin and chemoreceptor regulation. *Blood* **130**, 2092-2100 (2017). https://doi.org/10.1182/blood-2017-03-768507

56 Gohring, K. *et al.* Neutrophil CD177 (NB1 gp, HNA-2a) expression is increased in severe bacterial infections and polycythaemia vera. *Br J Haematol* **126**, 252-254 (2004). https://doi.org/10.1111/j.1365-2141.2004.05027.x

57 Kennel, K. B. & Greten, F. R. Immune cell - produced ROS and their impact on tumor growth and metastasis. *Redox Biol* **42**, 101891 (2021). https://doi.org/10.1016/j.redox.2021.101891

58 Silva, T. H., Schilithz, A. O. C., Peres, W. A. F. & Murad, L. B. Neutrophil-lymphocyte ratio and nutritional status are clinically useful in predicting prognosis in colorectal cancer patients. *Nutr Cancer* **72**, 1345-1354 (2020). https://doi.org/10.1080/01635581.2019.1679198

59 Wong, L. *et al.* Underlying liver disease and advanced stage liver cancer are associated with elevated neutrophil-lymphocyte ratio. *Clin Mol Hepatol* **25**, 305-316 (2019). https://doi.org/10.3350/cmh.2019.0004

60 Gentles, A. J. *et al.* The prognostic landscape of genes and infiltrating immune cells across human cancers. *Nat Med* **21**, 938-945 (2015). https://doi.org/10.1038/nm.3909

61 Shen, M. *et al.* Tumor-associated neutrophils as a new prognostic factor in cancer: a systematic review and meta-analysis. *PLoS One* **9**, e98259 (2014). https://doi.org/10.1371/journal.pone.0098259

62 Gago-Dominguez, M. *et al.* Neutrophil to lymphocyte ratio and breast cancer risk: analysis by subtype and potential interactions. *Sci Rep* **10**, 13203 (2020). https://doi.org/10.1038/s41598-020-70077-z

63 Verma, R. *et al.* Lymphocyte depletion and repopulation after chemotherapy for primary breast cancer. *Breast Cancer Res* **18**, 10 (2016). https://doi.org/10.1186/s13058-015-0669-x

64 Gustafson, C. E. *et al.* Immune cell repertoires in breast cancer patients after adjuvant chemotherapy. *JCI Insight* **5** (2020). https://doi.org/10.1172/jci.insight.134569

65 Velardi, E., Tsai, J. J. & van den Brink, M. R. M. T cell regeneration after immunological injury. *Nat Rev Immunol* **21**, 277-291 (2021). https://doi.org/10.1038/s41577-020-00457-z

66 Blank, C. U., Haanen, J. B., Ribas, A. & Schumacher, T. N. CANCER IMMUNOLOGY. The "cancer immunogram". *Science* **352**, 658-660 (2016). https://doi.org/10.1126/science.aaf2834

67 Chauhan, S. K. *et al.* Peripheral immune cells in metastatic breast cancer patients display a systemic immunosuppressed signature consistent with chronic inflammation. *NPJ Breast Cancer* **10**, 30 (2024). https://doi.org/10.1038/s41523-024-00638-2

68 DeFalco, J. *et al.* Non-progressing cancer patients have persistent B cell responses expressing shared antibody paratopes that target public tumor antigens. *Clin Immunol* **187**, 37-45 (2018). https://doi.org/10.1016/j.clim.2017.10.002

69 Griss, J. *et al.* B cells sustain inflammation and predict response to immune checkpoint blockade in human melanoma. *Nat Commun* **10**, 4186 (2019). https://doi.org/10.1038/s41467-019-12160-2

70 Fassler, M. *et al.* Antibodies as biomarker candidates for response and survival to checkpoint inhibitors in melanoma patients. *J Immunother Cancer* **7**, 50 (2019). https://doi.org/10.1186/s40425-019-0523-2

71 Diem, S. *et al.* Immunoglobulin G and Subclasses as Potential Biomarkers in Metastatic Melanoma Patients Starting Checkpoint Inhibitor Treatment. *J Immunother* **42**, 89-93 (2019). https://doi.org/10.1097/CJI.0000000000000255

72 Kuroda, H. *et al.* Prognostic value of tumor-infiltrating B lymphocytes and plasma cells in triple-negative breast cancer. *Breast Cancer* **28**, 904-914 (2021). https://doi.org/10.1007/s12282-021-01227-y

73 Cassetta, L. *et al.* Human Tumor-Associated Macrophage and Monocyte Transcriptional Landscapes Reveal Cancer-Specific Reprogramming, Biomarkers, and Therapeutic Targets. *Cancer Cell* **35**, 588-602 e510 (2019). https://doi.org/10.1016/j.ccell.2019.02.009

74 Sanford, D. E. *et al.* Inflammatory monocyte mobilization decreases patient survival in pancreatic cancer: a role for targeting the CCL2/CCR2 axis. *Clin Cancer Res* **19**, 3404-3415 (2013). https://doi.org/10.1158/1078-0432.CCR-13-0525

75 Chen, Y. *et al.* Association of Lymphocyte-to-Monocyte Ratio With Survival in Advanced Gastric Cancer Patients Treated With Immune Checkpoint Inhibitor. *Front Oncol* **11**, 589022 (2021). https://doi.org/10.3389/fonc.2021.589022

76 Zhang, Z. *et al.* Prognostic Evaluation of Metastasis-Related Lymphocyte/Monocyte Ratio in Stage I-II Breast Cancer Receiving Chemotherapy. *Front Oncol* **11**, 782383 (2021). https://doi.org/10.3389/fonc.2021.782383

77 Ma, Y., Zhang, J. & Chen, X. Lymphocyte-to-Monocyte Ratio is Associated with the Poor Prognosis of Breast Cancer Patients Receiving Neoadjuvant Chemotherapy. *Cancer Manag Res* **13**, 1571-1580 (2021). https://doi.org/10.2147/CMAR.S292048

78 Padgett, L. E. *et al.* Nonclassical monocytes potentiate anti-tumoral CD8(+) T cell responses in the lungs. *Front Immunol* **14**, 1101497 (2023). https://doi.org/10.3389/fimmu.2023.1101497

79 Olingy, C. E., Dinh, H. Q. & Hedrick, C. C. Monocyte heterogeneity and functions in cancer. *J Leukoc Biol* **106**, 309-322 (2019). https://doi.org/10.1002/JLB.4RI0818-311R

80 Hanna, R. N. *et al.* Patrolling monocytes control tumor metastasis to the lung. *Science* **350**, 985-990 (2015). https://doi.org/10.1126/science.aac9407

81 Patel, S. *et al.* Unique pattern of neutrophil migration and function during tumor progression. *Nat Immunol* **19**, 1236-1247 (2018). https://doi.org/10.1038/s41590-018-0229-5

82 Fu, S. *et al.* Syntaphilin Regulates Neutrophil Migration in Cancer. *Cancer Immunol Res* **11**, 278-289 (2023). https://doi.org/10.1158/2326-6066.CIR-22-0035

83 Lee, W. *et al.* Neutrophils facilitate ovarian cancer premetastatic niche formation in the omentum. *J Exp Med* **216**, 176-194 (2019). https://doi.org/10.1084/jem.20181170

84 Brostjan, C. & Oehler, R. The role of neutrophil death in chronic inflammation and cancer. *Cell Death Discov* **6**, 26 (2020). https://doi.org/10.1038/s41420-020-0255-6

85 Obeagu, E. I. & Obeagu, G. U. Exploring neutrophil functionality in breast cancer progression: A review. *Medicine (Baltimore)* **103**, e37654 (2024). https://doi.org/10.1097/MD.0000000000037654

86 Jaillon, S. *et al.* Neutrophil diversity and plasticity in tumour progression and therapy. *Nat Rev Cancer* **20**, 485-503 (2020). https://doi.org/10.1038/s41568-020-0281-y

87 Cheung, E. C. & Vousden, K. H. The role of ROS in tumour development and progression. *Nat Rev Cancer* **22**, 280-297 (2022). https://doi.org/10.1038/s41568-021-00435-0

88 Rorvig, S., Ostergaard, O., Heegaard, N. H. & Borregaard, N. Proteome profiling of human neutrophil granule subsets, secretory vesicles, and cell membrane: correlation with transcriptome profiling of neutrophil precursors. *J Leukoc Biol* **94**, 711-721 (2013). https://doi.org/10.1189/jlb.1212619

89 Coffelt, S. B., Wellenstein, M. D. & de Visser, K. E. Neutrophils in cancer: neutral no more. *Nat Rev Cancer* **16**, 431-446 (2016). https://doi.org/10.1038/nrc.2016.52

90 Eruslanov, E. B. *et al.* Tumor-associated neutrophils stimulate T cell responses in early-stage human lung cancer. *J Clin Invest* **124**, 5466-5480 (2014). https://doi.org/10.1172/JCI77053

91 Finisguerra, V. *et al.* MET is required for the recruitment of anti-tumoural neutrophils. *Nature* **522**, 349-353 (2015). https://doi.org/10.1038/nature14407

92 Shaul, M. E. & Fridlender, Z. G. Tumour-associated neutrophils in patients with cancer. *Nat Rev Clin Oncol* **16**, 601-620 (2019). https://doi.org/10.1038/s41571-019-0222-4

93 Wang, Y. *et al.* Comparison between immunotherapy efficacy in early non-small cell lung cancer and advanced non-small cell lung cancer: a systematic review. *BMC Med* **20**, 426 (2022). https://doi.org/10.1186/s12916-022-02580-1

94 Geurts, V. & Kok, M. Immunotherapy for Metastatic Triple Negative Breast Cancer: Current Paradigm and Future Approaches. *Curr Treat Options Oncol* **24**, 628-643 (2023). https://doi.org/10.1007/s11864-023-01069-0
95 van Rossum, A. G. J. *et al.* Carboplatin-Cyclophosphamide or Paclitaxel without or with Bevacizumab as First-Line Treatment for Metastatic Triple-Negative Breast Cancer (BOOG 2013-01). *Breast Care (Basel)* **16**, 598-606 (2021). https://doi.org/10.1159/000512200
96 Voorwerk, L. *et al.* Immune induction strategies in metastatic triple-negative breast cancer to enhance the sensitivity to PD-1 blockade: the TONIC trial. *Nat Med* **25**, 920-928 (2019). https://doi.org/10.1038/s41591-019-0432-4
97 Picelli, S. *et al.* Full-length RNA-seq from single cells using Smart-seq2. *Nat Protoc* **9**, 171-181 (2014). https://doi.org/10.1038/nprot.2014.006
98 Warren, J. S. Intrapulmonary interleukin 1 mediates acute immune complex alveolitis in the rat. *Biochem Biophys Res Commun* **175**, 604-610 (1991). https://doi.org/10.1016/0006-291x(91)91608-f
99 Demichev, V., Messner, C. B., Vernardis, S. I., Lilley, K. S. & Ralser, M. DIA-NN: neural networks and interference correction enable deep proteome coverage in high throughput. *Nat Methods* **17**, 41-44 (2020). https://doi.org/10.1038/s41592-019-0638-x
100 Tyanova, S., Temu, T. & Cox, J. The MaxQuant computational platform for mass spectrometry-based shotgun proteomics. *Nat Protoc* **11**, 2301-2319 (2016). https://doi.org/10.1038/nprot.2016.136
101 Tyanova, S. *et al.* The Perseus computational platform for comprehensive analysis of (prote)omics data. *Nat Methods* **13**, 731-740 (2016). https://doi.org/10.1038/nmeth.3901
102 Cox, J. *et al.* Accurate proteome-wide label-free quantification by delayed normalization and maximal peptide ratio extraction, termed MaxLFQ. *Mol Cell Proteomics* **13**, 2513-2526 (2014). https://doi.org/10.1074/mcp.M113.031591
103 Fabregat, A. *et al.* Reactome pathway analysis: a high-performance in-memory approach. *BMC Bioinformatics* **18**, 142 (2017). https://doi.org/10.1186/s12859-017-1559-2
104 Perez-Riverol, Y. *et al.* The PRIDE database resources in 2022: a hub for mass spectrometry-based proteomics evidences. *Nucleic Acids Res* **50**, D543-D552 (2022). https://doi.org/10.1093/nar/gkab1038

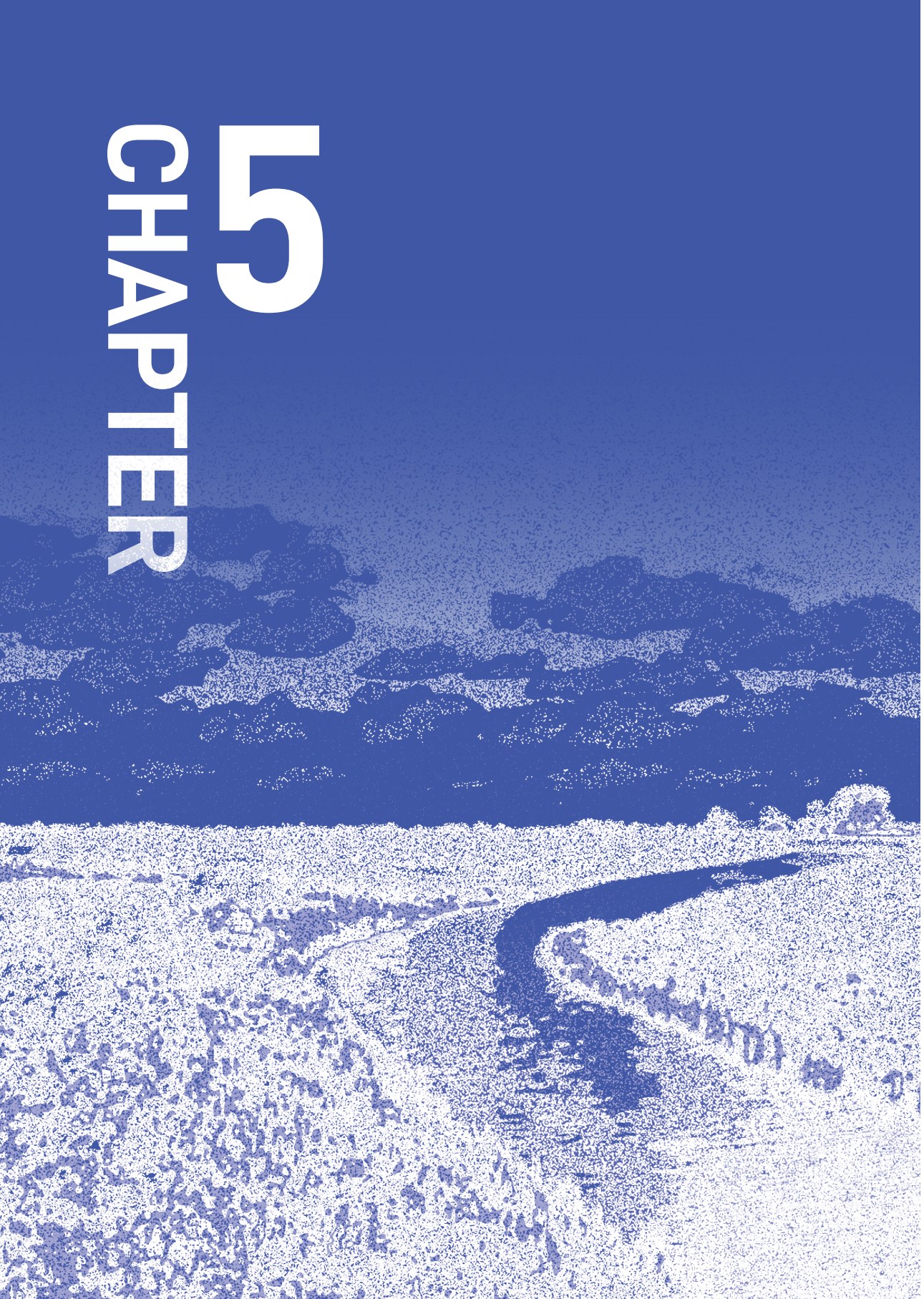

Single-cell RNA-sequencing of whole blood of patients with metastatic triple negative breast cancer and healthy donors: a chapter of inconclusive data

Noor A.M. Bakker[1,2,5], Ewald van Dyk[1,2,3], Lodewyk F.A. Wessels[2,3], Marleen Kok[1,4] and Karin E. de Visser[1,2,5]

Unpublished work

[1] Division of Tumor Biology & Immunology, The Netherlands Cancer Institute, Amsterdam, The Netherlands
[2] Oncode Institute, Utrecht, The Netherlands
[3] Division of Molecular Carcinogenesis, The Netherlands Cancer Institute, Amsterdam, The Netherlands
[4] Department of Medical Oncology, The Netherlands Cancer Institute, Amsterdam, The Netherlands
[5] Department of Immunology, Leiden University Medical Centre, Leiden, The Netherlands

Introduction

In science, publishing negative or inconclusive data is essential for advancing knowledge. These results, which may not support a hypothesis or expected outcome, provide valuable insights into what does not work, helping to prevent the unnecessary repetition of experiments. Additionally, they guide future research towards a more promising direction. When researchers share negative results, they contribute to a fuller understanding of a field, help refine theoretical frameworks, and promote transparency, which are all fundamental to scientific progress. However, sharing negative or inconclusive data is not common. Many researchers face significant barriers, including a preference within academic journals for positive, groundbreaking findings, which are seen as more publishable and impactful. Inconclusive data are often perceived as less exciting or premature and, therefore, less likely to gain visibility or career advancement. Additionally, researchers may be hesitant to publish negative results for fear of being perceived as unsuccessful or facing scrutiny from their peers. This reluctance creates a publication bias that skews the scientific literature, hindering cumulative knowledge and leading to inefficiencies in research. Encouraging the sharing of negative data would promote a more balanced and honest scientific discourse, ultimately fostering a more reliable and effective research ecosystem.

In this chapter, a research project centered on our scientific endeavors involving single-cell RNA-sequencing experiments is discussed. Due to the lack of discriminating results, which was primarily a result of insufficient statistical power due to low sample numbers and substantial inter-individual heterogeneity, we chose not to publish the “inconclusive data” in one of the few journals that accept such studies, such as the Journal of Articles in Support of the Null Hypothesis or the Journal of Negative Results in BioMedicine. Instead, I opted to include this work as a chapter of inconclusive data in my thesis. Including this work in my thesis not only documents and shares the findings from this project but also allows me to reflect on what I would have done differently in hindsight. I hope that this reflection will help guide the experimental design of scientists with similar goals, ensuring more efficient use of time and resources while increasing the likelihood of success. Additionally, by sharing this less successful aspect of my PhD journey, I aim to contribute to a more transparent and realistic understanding of the challenges a PhD can entail, which I hope will benefit future PhD students.

The aim of our study was to investigate transcriptional differences in the systemic immune landscape, encompassing both adaptive and myeloid immune cells, using single-cell RNA-sequencing of fresh whole blood samples from metastatic triple-negative breast cancer (mTNBC) patients and healthy donors (HDs). This approach allowed us to capture the full complexity of the immune system, enabling the analysis of not only cell-specific differences but also potential correlations and interactions among various immune cell types. Additionally, collecting whole blood samples without pre-processing or enriching for

certain cell types increased the likelihood of successfully capturing neutrophils, which are highly sensitive and prone to rapid cell death. Neutrophils, making up approximately 70% of circulating white blood cells, play a critical role in systemic inflammation and cancer[1-4]. Despite their abundance, distinct neutrophil subsets have yet to be clearly defined. By comparing the single-cell RNA profiles of neutrophils from mTNBC patients and HDs, we aimed to identify unique transcriptional states or neutrophil subsets that differ between the two groups. In addition to single-cell RNA-sequencing, we performed matched TCR- and BCR-sequencing to obtain insight into clonality and diversity of the circulating T cell and B cell repertoire. This comprehensive analysis was designed to offer deeper insights into the systemic immune dysregulation associated with mTNBC

Methods and Materials

Patients and Healthy Donors

Blood samples from patients with mTNBC were collected at baseline of the Triple B clinical trial[5], (NCT01898117). All patients with mTNBC were chemotherapy naïve for metastatic disease, and four out of five patients were chemotherapy-naïve for their primary tumor. The study protocol was conducted in accordance with the ICH Harmonised Tripartite Guideline for Good Clinical Practice and the principles of the Declaration of Helsinki. Baseline blood samples were used after approval by the institutional review board of the Netherlands Cancer Institute. Fresh blood samples from the healthy women (healthy donors, HD) were obtained after approval by the local medical ethical committee (NCT03819829). All patients and HDs provided written informed consent before enrolment. HDs were age matched to mTNBC patients. Blood samples were drawn in the morning and blood draw times were comparable for HDs and mTNBC patients.

Sample preparation

Peripheral blood was collected in EDTA vacutainers (BD) and processed immediately after blood draw. After erythrocyte lysis (lysis buffer: dH2O, NH4Cl, NaHCCO3, EDTA), cells were resuspended in Cell Staining Buffer (BioLegend). We included five patients with mTNBC and five HDs. For each run, blood cells from a patient with mTNBC were combined with blood cells from an age-, sex- and BMI-matched HD. For this purpose, cells were labeled for 30 min. at 4°C with a barcode using hashing antibodies against LNH-94 and 2M2 from BioLegend. We used TotalSeq-C0257 (394673) and TotalSeq-C0258 (394675) both in a 1:200 dilution. The barcoded single-cell suspensions of a patient and a HD were mixed in equal ratio, and further processed using 10X genomics Chromium Next GEM Single Cell 5’ Library and Gel Bead Kit v1.1 and Chromium Next GEM Chip G Single Cell Kit, following manufactures’ instructions (CG000208 Rev E, 10X Genomics). All libraries were quantified and normalized

based on library QC data generated on the Bioanalyzer system according to manufacturer's protocols (G2938-90321 and G2938-90024, Agilent Technologies). For each library type, based on the expected target cell counts, a balanced library pool of all samples was composed. Then all 4 library pools (Single Cell 5' Gene expression, TotalSeq-C Cell hashing and both types of V(D)J Enriched libraries) were quantified by qPCR, according to the KAPA Library Quantification Kit Illumina® Platforms protocol (KR0405, KAPA Biosystems). The Single Cell 5' Gene Expression and TotalSeq-C Cell hashing libraries were sequenced together on a NextSeq 550 Instrument (Illumina) using a NextSeq 500/550 High Output Kit v2.5 (cat. no. 20024906, Illumina). Paired end sequencing was performed using 28 cycles for Read 1, 8 cycles for Read i7 and 56 cycles for Read 2. For the Single Cell 5' Gene Expression sequencing this resulted in an average sequencing depth of 30.000 reads pairs/cell. The V(D)J Enriched libraries were sequenced together on a NextSeq 550 Instrument (Illumina) using a NextSeq 500/550 Mid Output Kit v2.5 (cat. no. 20024904, Illumina). Paired end sequencing was performed using 28 cycles for Read 1, 8 cycles for Read i7 and 130 cycles for Read 2.

Computational analysis single-cell RNA-sequencing data

Demultiplexing with cell hashing

Demultiplexing was performed using the HTODemux function provided by Seurat with default parameters[6,7]. Cells were split into four categories: one for each sample, a negative category for cells with insufficient hash and a doublet category where appreciable hashtags were observed for both samples.

Quality control

Cells with negative or doublet labels from hash demultiplexing were removed from the analysis. Using hashtag doublets as a positive control, we were unable to see a correlation between read counts and doublet status. Furthermore, computational methods such as Scrublet[8] were unable to confidently predict doublets. As a consequence, we were unable to remove doublets sharing the same hashtags.

We removed cells with less than 10 total read counts or a mitochondrial percentage above 20%. The low read count threshold was used to retain cell types such as neutrophils that naturally contain very few read counts. Cells with low read counts were filtered out indirectly after applying a posterior threshold of 80% using a multinomial cell type classifier (see "Automatic cell type classification").

Automatic cell type classification

We performed automatic cell type identification based on the blood derived cell type categories in the CIBERSORT LM22 dataset[9] using a multinomial model similar to that

proposed in[10]. We extended the CIBERSORT signature gene list with platelet specific genes PF4, ITGA2B, F13A1 and NCOA4 since they are frequently expressed in platelets and not in other cell types as specified in PanglaoDB. In total, we used a set S containing 548 signature genes to differentiate between cell types. For each cell, we compute the likelihood of observed read counts for each cell type: $P(x_b, \bar{x}|c) \propto p_b^{x_b} \prod_{i \in S} p_i^{x_i}$ where c represents the cell type under consideration, $\bar{x}$ represents the vector of read counts of genes in the signature list S with x_i representing the read counts of the i-th gene, x_b represents a single background read count (i.e. total number of reads not from genes in the signature list) and the parameters p (and p_b) that represent the expected proportion of reads in signature genes (and background). These model parameters are estimated from bulk sequencing datasets provided by CIBERSORT and the Human Primary Cell Atlas[11]. Posterior probabilities were derived from the likelihoods using Bayes' theorem. Average proportions of different cell types across our flow cytometry dataset were used as priors except for neutrophils and platelets, where the priors were both set to 30%. Neutrophil frequencies are typically high (>50%) in human blood, but due to their low read counts, many do not survive our original quality control, which justifies a lower prior.

Batch alignment

Batches were aligned using the fastMNN algorithm[12]. After alignment we modeled the remaining batch effect and sample type (mTNBC vs HD) simultaneously using the generalized linear modeling framework in MiloR (see differential abundance analysis section). Since all batches were processed in the same core facility, fastMNN resulted in superior performance compared to the diagonalized CCA method provided by Seurat.

Count normalization and dimensionality reduction

For the analysis that included all cell types, we retained the top 2000 highest varying genes based on the vst method in Seurat. Read counts were normalized by per-cell library size and log (+1) normalized. The top 50 principal components were extracted for further downstream analysis. For visualization in two dimensions, we performed UMAP manifold learning[13]. For the differential abundance analysis, cell types were separated based on the multinomial classifier described earlier. For each cell type, the top 2000 highest varying genes were recomputed as before, except for the neutrophils where we used the top 500 varying genes due to low overall read counts. For each cell type we extracted the top 10 principal components, except for the T cells. T cells exhibit higher heterogeneity than other cell types and we extracted the top 20 principal components.

Clustering

Unsupervised clustering was performed using a smart local moving algorithm based on

shared nearest neighbor (SNN) networks[14]. Optimization of parameters was collectively controlled with a resolution parameter in the Seurat package.

Differential Gene Expression Analysis

Analyzing single-cell RNA-sequencing data using mixed-effects models can be computationally prohibitive due to the large number of observations. To simplify the process, we aggregated unique molecular identifier (UMI) counts for each immune cell population within each sample, generating pseudobulk data. This approach allows for differential expression analysis using well-established methods originally developed for bulk RNA-sequencing. Prior to this conversion, we created subsets of the data corresponding to distinct immune cell populations, ensuring that DE analysis could be performed for each population separately. For immune cell populations that exhibit significant differences in gene expression between patients with mTNBC and HDs, we could further conduct gene set enrichment analysis and other pathway analyses to interpret the biological significance of the differentially expressed genes.

Differential abundance analysis

We detected groups of similar cell states and tested for differentially abundance when comparing triple-negative breast cancer samples and healthy donors using MiloR[15]. Traditionally, clusters of cells sharing similar states are identified prior to performing a differential abundance analysis. However, MiloR is independent of clustering and can potentially pick up differential regions in transition phases. Batch effects were modeled simultaneously as a nuisance parameter (see “Batch alignment”). The TCR and BCR diversity was calculated using Pielou’s evenness procedure.

Results

No differential gene expression and cell state abundances between mTNBC and HDs

To gain deeper insights into the cellular states of circulating cells in TNBC patients, we performed single-cell RNA-sequencing along with matched single-cell BCR- and single-cell TCR-sequencing on fresh blood samples from five mTNBC patients and five age-matched HDs (Figure 1a). The samples were processed in five batches, with each batch comprising white blood cells from a fresh blood sample of both a mTNBC patient and a HD. After hash tagging, the two samples in each batch were pooled, and all batches were sequenced in a single run.

We observed a large variation in RNA-content between different immune cell types; both in the number of genes detected in each cell (nFeature_RNA) as well as in the total number of RNA molecules detected within a cell (nCount_RNA) (Figure 1b). Cells in clusters

0, 1, 4 and 7 have low RNA content and are identified as neutrophil clusters, as anticipated (Figure 1b). Cluster 10 is also comprised of cells with a low RNA content and was identified as a platelet cluster.

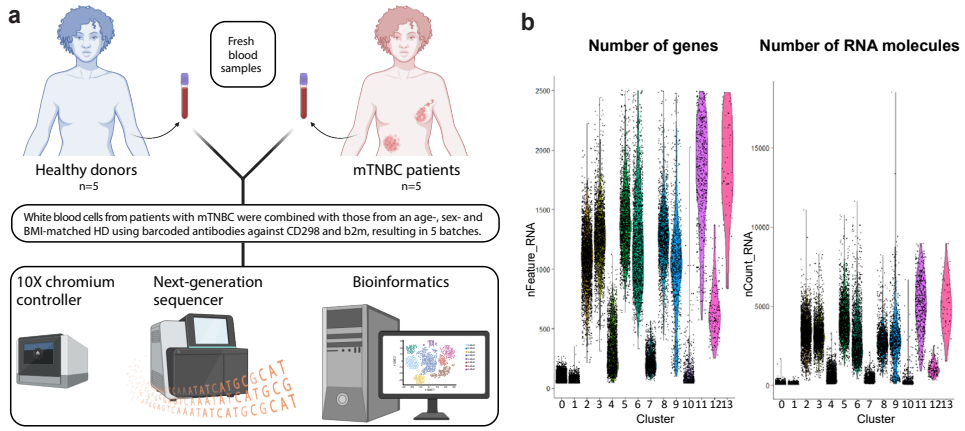

Figure 1: *Experimental setup* ***(a)*** *and quality control* ***(b)*** *of single-cell RNA-sequencing experiments. nFeature_RNA is the number of genes detected in each cell. nCount_RNA is the total number of RNA molecules detected within a cell. Neutrophils are divided over clusters 0, 1, 4 and 7.*

In all samples, we captured a great diversity of immune cell types, including the technically challenging neutrophil population (Figure 2a). For most immune cell populations, we found multiple subpopulations. Intriguingly, eight continuous neutrophil states were identified in our dataset, suggestive of neutrophil subset diversity (Figure 2a). This is in agreement with what has previously been described[10,16,17]. However, none of these states were unique to either HDs or mTNBC patients and no statistically significant enrichments or depletions in those cell states were found (Figure 2b).

After subsetting the major immune cell populations (Figure 2a) and generating pseudobulk data for each cell type, we conducted differential gene expression analysis comparing mTNBC patients and HDs. However, this analysis did not reveal a list of significantly differentially expressed genes between the two groups. As a result, subsequent analyses such as pathway enrichment and gene set enrichment analysis on differentially expressed genes could not be performed. We found that the variance between the two groups in gene expression at the level of the selected immune cell populations was similar to the variance within each group. This suggests that gene expression differences between mTNBC patients and HDs potentially requires an alternative analytical approach.

Such an alternative analytical approach is the application of the MiloR algorithm, which achieves greater power by reducing sparsity and noise, improving the detection of subtle abundance changes, and increasing sensitivity to shifts in cell population composition across groups or conditions. After extensive analysis of this single-cell transcriptomic dataset using the MiloR package, we did not find specific cell states or subsets that were enriched or depleted in mTNBC when compared to HDs (Figure 2b). Moreover, analyzing TCR clonality and clone sizes did not reveal statistically significant differences between patients with mTNBC and HDs (Figure 2c). Calculating TCR diversity measured by Pielou's evenness, revealed equal TCR diversity in HDs and mTNBC patients (Figure 2d). BCR clonality and clone sizes did not differ in a statistically significant manner between patients with mTNBC and HDs (Figure 2e). Calculating BCR diversity measured by Pielou's evenness, showed comparable BCR diversity in HDs and mTNBC patients (Figure 2f). Important to mention is the substantial degree of inter-individual and inter-batch heterogeneity that was observed (Figures 2c, e), making it increasingly challenging to identify breast cancer driven differences between the two groups. Combining transcriptional profiling with single-cell BCR or single-cell TCR sequencing did not yield any discriminatory information between HDs and mTNBC patients.

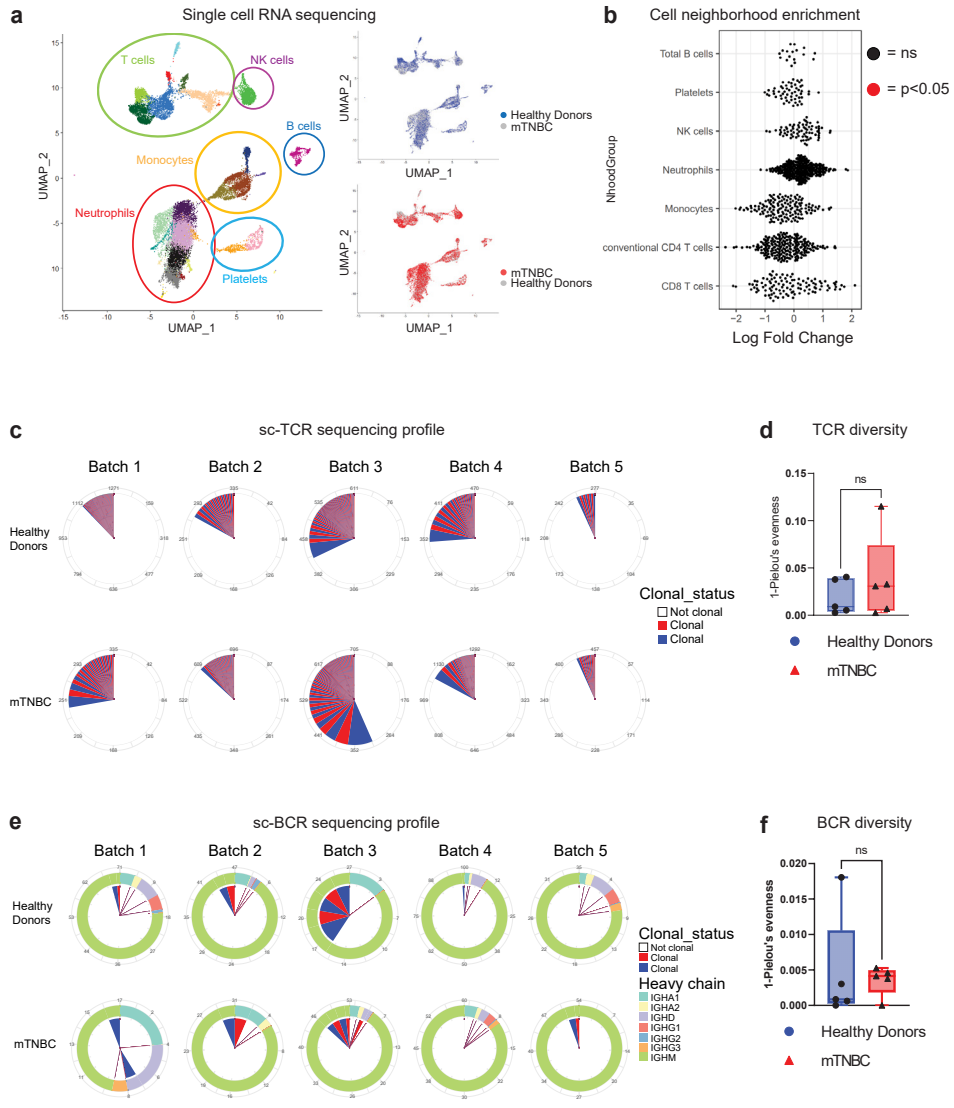

Figure 2. Single-cell RNA-sequencing and matched TCR- and BCR-sequencing on fresh whole blood samples. (a) *UMAP showing aggregated cells from HDs (n=5) and patients with mTNBC (n=5). On the left, unsupervised clustering was performed using shared nearest neighbor networks, resulting in multiple cellular states. On the right, UMAPs are colored according to sample type; blue are cells from HDs and red are cells from patients with mTNBC.* ***(b)*** *Differentially abundant cell counts grouped into Milo neighborhoods after correcting for batch effect. No significant neighborhoods were found.* ***(c)*** *TCR clonality derived from single-cell TCR sequencing for five HDs (top row) and five mTNBC patients (bottom row). Each vertical pair of pie charts corresponds to a batch of two samples that were processed together. Alternating red and blue pieces of the pie chart represent T cells that are clonal (>1 cell with identical TCR sequences).* ***(d)*** *T cell receptor repertoire diversity measure for HDs and patients with mTNBC. Diversity is defined as 1 – Pielou's evenness (i.e. 1 – normalized entropy). High values represent less diversity and therefore more clonality.* ***(e)*** *BCR clonality derived from single-cell BCR sequencing for five HDs (top row) and five mTNBC patients (bottom row). Each vertical pair of pie charts corresponds to a batch of two samples that were processed together. Alternating red and blue pieces of the pie chart represent B cells that are clonal (>1 cell with identical BCR sequences). The outer ring of the pie chart is colored according to the heavy chain.* ***(f)*** *B cell receptor repertoire diversity measure for HDs and patients with mTNBC. Diversity is defined as 1 – Pielou's evenness (i.e. 1 – normalized entropy). High values represent less diversity and therefore more clonality.* ▶▶▶

Discussion

To gain more insight in potential differences in the cellular states from various circulating immune cell populations between mTNBC patients and HDs, single-cell RNA-sequencing and matched single-cell TCR and single-cell BCR sequencing was performed on fresh leukocytes of five mTNBC patients and five HDs. Extensive analysis of this dataset did not yield any substantial differences between mTNBC and HD transcriptomes or the identification of differentially abundant cell states between the two groups. We believe the lack of discriminating results is mostly an issue of limited group sizes. Given the high degree of heterogeneity within the five HDs and five patients with mTNBC, identifying differences between the two groups became near impossible.

Interestingly, eight distinct neutrophil states were identified in our dataset, suggesting possible subset diversity; however, none of these states were exclusive to either healthy donors (HDs) or metastatic triple-negative breast cancer (mTNBC) patients, and no differences in their abundances were detected. We speculate that the lack of discriminating features of the neutrophils is – in addition to the low n-number of individuals – a result of the low read-depth within this cell type. Because we chose not to enrich for any specific cell type and neutrophils have very low RNA content, most reads in the dataset came from other immune cells. Since the number of genes coming from e.g. lymphocytes and monocytes (Figure 1b clusters 2, 3, 5, 6, 8, 9, 11-13) is so much larger compared to those coming from neutrophils (Figure 1b clusters 0, 1, 4 and 7), increasing the number of sequencing runs would mainly lead to more reads of genes that are already covered. It is expected that with increased read depth in the neutrophils and an increased sample size, there are transcriptional differences in neutrophils from HDs and mTNBC patients. Therefore, we hypothesize that subjecting purified neutrophils from well defined, untreated mTNBC patients to single-cell RNA-sequencing in comparison to purified neutrophils from HDs, may provide valuable information about which neutrophil states are associated with mTNBC. By combining this with barcoded antibodies to identify surface markers associated with a particular cell state, followed by live cell sorting, one could possibly even link certain over- or underrepresented neutrophil cell states to their functional properties. This would further advance our understanding about the role of neutrophils in cancer, and nearer the step towards modulation of myeloid cells in cancer patients.

Lastly, I would like to point out an unexpected advantage of the approach we took. To minimalize batch effects and reduce costs, we combined a patients sample with an age- and sex matched HD sample for each run by making use of barcoded antibodies against two antigens that are present on virtually all cells. During quality control, cells with low RNA yield are typically filtered out to exclude apoptotic or dying cells, which often show poor RNA quality. However, this process unintentionally removes neutrophils, as they naturally have low RNA content despite being viable. To avoid losing neutrophils during this filtering step,

we leveraged the use of cell barcode handles to identify intact cells. Within this pool of cells that were initially filtered out, neutrophils can be accurately identified and retained, preserving them in the analysis despite their low RNA levels. Additionally, the barcodes provided a straightforward handle to filter out doublets. Most published doublet-removal algorithms are based of RNA content, but when doublets are formed with low RNA content cells (like neutrophils or eosinophils), this will not be picked up. However, when a doublet is formed of cells coming from two donors, they can be filtered out because they carry two different barcodes. This still does not solve the doublet issue for situations in which a doublet is formed involving low RNA content cells from the same donor, but it certainly cleans up the dataset. To take this idea a step further, one could even consider dividing each sample over multiple wells, staining each well with a different barcode, increasing the effectiveness of this doublet removal approach even further, and potentially even allow for increasing the number of cells that can be loaded per experiment.

Overall, we conclude that in this limited cohort of five mTNBC patients and five HDs, no statistically significant discriminatory results were observed within the single-cell RNA-sequencing dataset. However, we acknowledge the potential for significant differences to emerge with an expanded sample size. By increasing the number of individuals and refining our pre-processing methods to separate immune cells based on RNA content—specifically targeting high- and low-RNA populations to ensure consistent read-depth across all immune cell types—we may uncover statistically significant differences in the single-cell RNA-sequencing profiles between mTNBC patients and HDs.

References

1 Carnevale, S. *et al.* Neutrophil diversity in inflammation and cancer. *Front Immunol* **14**, 1180810, doi:10.3389/fimmu.2023.1180810 (2023).

2 Coffelt, S. B., Wellenstein, M. D. & de Visser, K. E. Neutrophils in cancer: neutral no more. *Nat Rev Cancer* **16**, 431-446, doi:10.1038/nrc.2016.52 (2016).

3 Siwicki, M. & Pittet, M. J. Versatile neutrophil functions in cancer. *Semin Immunol* **57**, 101538, doi:10.1016/j.smim.2021.101538 (2021).

4 Wellenstein, M. D. *et al.* Loss of p53 triggers WNT-dependent systemic inflammation to drive breast cancer metastasis. *Nature* **572**, 538-542, doi:10.1038/s41586-019-1450-6 (2019).

5 van Rossum, A. G. J. *et al.* Carboplatin-Cyclophosphamide or Paclitaxel without or with Bevacizumab as First-Line Treatment for Metastatic Triple-Negative Breast Cancer (BOOG 2013-01). *Breast Care (Basel)* **16**, 598-606, doi:10.1159/000512200 (2021).

6 Hao, Y. *et al.* Integrated analysis of multimodal single-cell data. *Cell* **184**, 3573-3587 e3529, doi:10.1016/j.cell.2021.04.048 (2021).

7 Stoeckius, M. *et al.* Cell Hashing with barcoded antibodies enables multiplexing and doublet detection for single cell genomics. *Genome Biol* **19**, 224, doi:10.1186/s13059-018-1603-1 (2018).

8 Wolock, S. L., Lopez, R. & Klein, A. M. Scrublet: Computational Identification of Cell Doublets in Single-Cell Transcriptomic Data. *Cell Syst* **8**, 281-291 e289, doi:10.1016/j.cels.2018.11.005 (2019).

9 Chen, B., Khodadoust, M. S., Liu, C. L., Newman, A. M. & Alizadeh, A. A. Profiling Tumor Infiltrating Immune Cells with CIBERSORT. *Methods Mol Biol* **1711**, 243-259, doi:10.1007/978-1-4939-7493-1_12 (2018).

10 Zilionis, R. *et al.* Single-Cell Transcriptomics of Human and Mouse Lung Cancers Reveals Conserved Myeloid Populations across Individuals and Species. *Immunity* **50**, 1317-1334 e1310, doi:10.1016/j.immuni.2019.03.009 (2019).

11 Mabbott, N. A., Baillie, J. K., Brown, H., Freeman, T. C. & Hume, D. A. An expression atlas of human primary cells: inference of gene function from coexpression networks. *BMC Genomics* **14**, 632, doi:10.1186/1471-2164-14-632 (2013).

12 Haghverdi, L., Lun, A. T. L., Morgan, M. D. & Marioni, J. C. Batch effects in single-cell RNA-sequencing data are corrected by matching mutual nearest neighbors. *Nat Biotechnol* **36**, 421-427, doi:10.1038/nbt.4091 (2018).

13 Becht, E. *et al.* Dimensionality reduction for visualizing single-cell data using UMAP. *Nat Biotechnol*, doi:10.1038/nbt.4314 (2018).

14 Waltman, L. a. v. E., N. J. A smart local moving algorithm for large-scale modularity-based community detection. *The European Physical Journal* **471**, doi:doi:10.1140/epjb/e2013-40829-0 (2013).

15 Dann, E., Henderson, N. C., Teichmann, S. A., Morgan, M. D. & Marioni, J. C. Differential abundance testing on single-cell data using k-nearest neighbor graphs. *Nat Biotechnol* **40**, 245-253, doi:10.1038/s41587-021-01033-z (2022).

16 Xie, X. *et al.* Single-cell transcriptome profiling reveals neutrophil heterogeneity in homeostasis and infection. *Nat Immunol* **21**, 1119-1133, doi:10.1038/s41590-020-0736-z (2020).

17 Grieshaber-Bouyer, R. *et al.* The neutrotime transcriptional signature defines a single continuum of neutrophils across biological compartments. *Nat Commun* **12**, 2856, doi:10.1038/s41467-021-22973-9 (2021).

CHAPTER 6

Neoadjuvant nivolumab or nivolumab plus ipilimumab in early-stage triple negative breast cancer: a phase 2 adaptive trial

Iris Nederlof[1,*], Olga I. Isaeva[1,*], Manon de Graaf[1,#], Robbert C.A.M. Gielen[1,#], Noor A. M. Bakker[1,2,#], Adrianne L. Rolfes[1], Hannah Garner[1,2], Bram Boeckx[3,4], Joleen J.H. Traets[1], Ingrid A.M. Mandjes[5], Michiel de Maaker[6], Thomas van Brussel[3,4], Maksim Chelushkin[1], Elisa Champhanet[1], Marta Lopez-Yurda[5], Koen van de Vijver[7,8], José G. van den Berg[8], Ingrid Hofland[6], Natasja Kliouеva[9], Ritse M. Mann[10], Claudette E. Loo[10], Frederieke H. van Duijnhoven[11], Victoria Skinner[11], Sylvia Luykx[12], Emile Kerver[13], Ekaterina Kalashnikova[14], Marloes G. J. van Dongen[15], Gabe S. Sonke[15], Sabine C. Linn[15], Christian U. Blank[15,16], Karin E. de Visser[1,2,17], Roberto Salgado[18,19], Lodewyk F.A. Wessels[2,20], Caroline A. Drukker[11], Ton N. Schumacher[2,16,21], Hugo M. Horlings[8], Diether Lambrechts[3,4], Marleen Kok[1,15]

* and # These authors contributed equally
Corresponding author: Marleen Kok, m.kok@nki.nl

Nature Medicine. 2024 August 14; 30(3223–3235). DOI: 10.1038/s41591-024-03249-3

1 Division of Tumor Biology and Immunology, The Netherlands Cancer Institute, Amsterdam, the Netherlands
2 Oncode Institute, Utrecht, the Netherlands
3 Laboratory for Translational Genetics, Department of Human Genetics, KU Leuven, Leuven, Belgium
4 VIB Center for Cancer Biology, Leuven, Belgium
5 Biometrics Department, The Netherlands Cancer Institute, Amsterdam, the Netherlands
6 Core Facility Molecular Pathology & Biobanking, The Netherlands Cancer Institute, Amsterdam, the Netherlands
7 Department of Pathology, UZ Gent - Universitair Ziekenhuis Gent, Gent, Belgium
8 Department of Pathology, The Netherlands Cancer Institute, Amsterdam, the Netherlands
9 Department of Pathology, OLVG Hospital, Amsterdam, Netherlands
10 Department of Radiology, The Netherlands Cancer Institute, Amsterdam, the Netherlands
11 Department of Surgical Oncology, The Netherlands Cancer Institute, Amsterdam, the Netherlands
12 Medical Oncology department, Tergooi Hospital - locatie Hilversum, Hilversum, the Netherlands
13 Department of Oncology, OLVG Hospital, Amsterdam, Netherlands
14 Natera, Natera Inc., San Carlos, CA, United States of America
15 Department of Medical Oncology, The Netherlands Cancer Institute, Amsterdam, the Netherlands
16 Division of Molecular Oncology and Immunology, The Netherlands Cancer Institute, Amsterdam, the Netherlands
17 Department of Immunology, Leiden University Medical Center, Leiden, the Netherlands
18 Department of Pathology, ZAS hospitals, Antwerp, Belgium
19 Division of Research, Peter MacCallum Cancer Centre, Melbourne, Victoria, Australia
20 Division of Molecular Carcinogenesis, The Netherlands Cancer Institute, Amsterdam, the Netherlands
21 Department of Hematology, Leiden University Medical Center, Leiden, the Netherlands

Abstract

Immune checkpoint inhibition (ICI) with chemotherapy is now standard of care for stage II-III triple negative breast cancer (TNBC). However, it is largely unknown for which patients ICI without chemotherapy could be an option and what the benefit of combination ICI could be. The adaptive BELLINI trial explored whether short combination ICI induces immune activation (primary endpoint: two-fold increase in CD8+ T cells or IFNG), providing rationale for neoadjuvant ICI without chemotherapy. In window of opportunity cohorts A (4 weeks anti-PD1) and B (4 weeks anti-PD1 + anti-CTLA4), we observed immune activation in 53% (8/15) and 60% (9/15) of patients, respectively. High tumor-infiltrating lymphocytes (TILs) correlated with response. Single-cell RNA sequencing revealed that higher pretreatment tumor-reactive CD8+ T cells, follicular helper T cells and shorter distances between tumor and CD8+ T cells correlated with response. Higher levels of regulatory T cells post-treatment associated with non-response. Based on these data, we opened cohort C for patients with high TILs (≥50%) who received 6 weeks neoadjuvant anti-PD1 + anti-CTLA4 followed by surgery (primary endpoint: pathological complete response, pCR). 53% (8/15) of patients had major pathological response (< 10% viable tumor) at resection, with 33% (5/15) having pCR. All cohorts met Simon's two-stage threshold for expansion to stage II. We observed grade ≥3 adverse events for 17% of patients, and a high rate (57%) of immune-mediated endocrinopathies. In conclusion, neoadjuvant immunotherapy without chemotherapy demonstrates potential efficacy and warrants further investigation in patients with early TNBC. ClinicalTrials.gov Identifier: NCT03815890.

Introduction

The addition of programmed death (ligand) 1 blockade (anti-PD(L)1) to neoadjuvant chemotherapy has changed the treatment landscape for patients with early (stage II-III) triple negative breast cancer (TNBC)1. However, all trials evaluating the efficacy of anti-PD(L)1 in TNBC combined it with chemotherapy[1–4]. This chemotherapy backbone inevitably results in a high rate of adverse events, significantly affects quality of life and could diminish T cell activity[5,6].

So far, no biomarkers have been established to predict which patients with early stage TNBC will benefit from anti-PD1. Therapy is currently given for a total duration of one year, while data in other tumor types have shown that a pCR can be reached after only a few weeks of treatment with immune checkpoint inhibitors (ICI)[7–11]. Overtreatment prevention is an increasingly important consideration due to the high number of patients needed to treat to prevent one recurrence and increasing toxicity with more intense and longer treatments. Therefore, there is an urgent clinical need to optimize treatment schedules and improve patient selection for specific treatments[12].

While numerous studies have integrated anti-PD(L)1 therapy with chemotherapy in early stage TNBC[1–3,13], data on combination ICIs are limited. ICIs targeting CTLA4 have revolutionized treatment for non-small cell lung cancer (NSCLC)8 and melanoma[14–16]. Additionally, neoadjuvant trials across various tumor types have shown impressive major pathological response rates when combining anti-PD(L)1 with low-dose anti-CTLA4[7,8,10,17]. A trial in metastatic breast cancer revealed long-lasting responses after combining low-dose anti-CTLA4 with anti-PD1[18], which are infrequently observed with anti-PD(L)1 alone. These findings provide a rationale to test low-dose anti-CTLA4 in combination with anti-PD(L)1 in early TNBC.

Simultaneously with the advent of ICI, tumor-infiltrating lymphocytes (TILs) have emerged as a putative prognostic and predictive biomarker[19–22]. TNBC patients with high TIL levels have an excellent prognosis even without chemotherapy[19,23], suggesting that TILs reflect an endogenous antitumor T cell response. Moreover, in metastatic TNBC, high TIL levels are associated with response to ICI[24,25]. Collectively, these findings imply that TILs may serve as a tool for identifying TNBC patients who are more likely to benefit from ICI and have a favorable prognosis, paving the way for exploring chemotherapy de-escalation. The BELLINI trial is an adaptive platform trial exploring the effect of ICI without chemotherapy starting with window of opportunity cohorts with a biological endpoint followed by neoadjuvant cohorts with complete pathological response (pCR) endpoint. This adaptive platform trial consists of sequential, single-cohort, phase 2 studies, where new cohorts can be opened based on signals obtained in prior cohorts. The first two cohorts evaluated whether four weeks of nivolumab (anti-PD1, cohort A) or nivolumab and low-dose ipilimumab (anti-PD1 and anti-CTLA4, cohort B) can lead to immune activation (primary endpoint). This four-week therapy regimen was scheduled before the start of regular therapy, and therefore the effect of ICI could be assessed independently of chemotherapy. Promising results in cohorts A and B among patients with high TILs (≥50%) led to the initiation of cohort C. In cohort C, we used a neoadjuvant design with six weeks of nivolumab plus low-dose ipilimumab followed by surgery to assess the pCR rate[14,26].

This is the first trial combining anti-PD1 with anti-CTLA4 in early breast cancer, as well as the first trial exploring what pCR rate could be achieved with ICI-only approaches and using TIL levels as an entry criterion to enrich for inflamed tumors.

Methods

Patients

Patients in cohorts A and B were eligible for enrollment if they were at least 18 years of age and had stage I-III (clinical tumor stage T1c-3, nodal stage N0-3, according to the primary tumor regional lymph node staging criteria of the American Joint Committee on Cancer, 7th

edition) triple negative breast cancer with confirmation of estrogen receptor and HER2 negativity (ER < 10% and HER2 0, 1 or 2 in the absence of amplification as determined by in situ hybridization) on a biopsy from the primary tumor in the breast; newly diagnosed, previously untreated disease; a WHO performance status score[63] of 0 or 1 and adequate organ functions. The TILs percentage needed to be 5% or more. To ensure balanced enrollment based on TIL levels, each cohort included 5 patients with low (5-10%), 5 patients with intermediate (11-49%), and 5 patients with high (≥50%) TIL levels. Patients with concurrent ipsilateral, bilateral, or multifocal primary tumors were also eligible for enrollment. For cohort C, patients had to meet the same criteria, but the nodal stage had to be N0, tumor stage T1c-T2, and TILs had to be 50% or more. The intention for cohort C was to explore the potential feasibility of chemotherapy de-escalation in patients with high TILs. Since withholding adjuvant capecitabine for high-risk patients and/or escalating locoregional treatment for patients with more extensive disease was undesired, cohort C included only LN-negative patients.

Exclusion criteria included history of immunodeficiency, autoimmune disease or conditions requiring immunosuppression (>10 mg daily prednisone or equivalent); other immunosuppressive medications intake within 28 days of study drug administration; chronic or recurring infections; occult breast cancer; fertility preservation due to breast cancer diagnosis; active hepatitis B virus or hepatitis C virus infection; clinically significant cardiovascular disease; previous systemic anti-cancer treatment.

Trial design and treatments

The BELLINI trial (full title: Pre-operative Trial for Breast Cancer With Nivolumab in Combination With Novel IO; NCT03815890) is a single center, non-blinded, non-randomized, non-comparative phase II study designed to evaluate the feasibility and efficacy of checkpoint inhibition before regular neoadjuvant therapy or surgery in patients with primary breast cancer. Cohorts for prespecified breast cancer subgroups are opened in a sequential manner. Here we report the first three TNBC cohorts for patients who were treated with nivolumab (cohort A) or nivolumab + ipilimumab for four (cohort B) or six (cohort C) weeks. A: Nivolumab monotherapy, 240mg on D1 and D15. B: Nivolumab+ipilimumab 1 mg/kg on D1 and nivolumab 240mg on D15. C: Nivolumab+ ipilimumab 1 mg/kg on D1 and D21. Regular therapy, consisting of neoadjuvant chemotherapy or primary surgery, started on D29 and onwards. Given the poor prognosis of patients with low TIL levels and the hypothesis that these women will probably not be the super-responders to ICI, patients were only eligible with TILs≥5%. A threshold of 5% TILs was selected to exclude true immune-deserted tumors. Equal distribution of patients with different levels of tumor of infiltrating lymphocytes over the cohorts was ensured by inclusion of 5 patients with TILs-low (5-10%), 5 patients with TILs-intermediate (11-49%), and 5 patients with TILs-high (≥50%) scores per cohort.

After cohorts A (in the protocol defined as cohort 1B) and B (in the protocol defined as cohort 2B) the protocol was amended to open cohort C (in the protocol defined as cohort 3B). Cohort C had the same inclusion criteria as cohort A and B, except that only inclusion of patients with clinically node-negative disease and with TIL levels of 50% or higher was allowed. With the amendment to open cohort C, the window of opportunity design was changed into a true neoadjuvant design with all patients going to surgery after the immunotherapy. After completing the interim analysis of cohorts A and B an amendment was approved to use pathological complete response (pCR) as primary endpoint instead of immune activation for cohort C and subsequent cohorts (see details on Endpoints below).

Ethics statement

All patients provided written informed consent before enrollment. This investigator-initiated trial was designed by the Netherlands Cancer Institute (NKI).The trial was conducted in accordance with the protocol, Good Clinical Practice standards and the Declaration of Helsinki. The full protocol, amendments, and the informed consent form were approved by the medical ethical committee of the Netherlands Cancer Institute (NKI, Amsterdam).

Endpoints

Cohorts A and B:

The primary endpoint for cohorts A and B is immune activation following two cycles of neoadjuvant ICI, defined as a 2-fold increase in CD8+ T cells assessed via immunohistochemistry and/or an increase in *IFNG* gene expression. High-quality paired biopsies are necessary for the evaluability of this primary endpoint.

As a secondary endpoint for cohorts A and B, we evaluated the clinical response.

Clinical response was defined as:

Radiological signs of response: At least a 30% decrease on MRI (partial response (PR) according to RECIST 1.1, not confirmed). The target (or index) lesion is defined as the largest enhancing lesion. In case of multifocality or multicentricity the largest mass and/or non-mass enhancement was measured in the axial/sagittal or coronal plane and defined as target/index lesion. In these cases, the total area occupied by the tumor (including all masses and non-mass enhancement) was also measured. The total tumor area was used for the RECIST measurements.

AND/OR

Pathological signs of response: Pathological response could be studied in biopsies from 28 patients due to the window of opportunity design. Absence of viable tumor after four weeks of therapy in the post-treatment biopsy was classified as a clinical response. For patients proceeding to surgery this was defined as partial or complete pathological response, according to the European Society of Mastology (EUSOMA criteria).

Cohort C:

The primary endpoint for cohort C is pathological complete response (pCR), defined as no viable tumor remaining in the breast and lymph nodes (ypT0N0)[64]. Major pathologic response (MPR, secondary endpoint) is a frequently used surrogate endpoint for efficacy in neoadjuvant trials evaluating immune checkpoint blockade across cancer types[8,11,26]. MPR was defined as ≤10% of residual viable tumor in the surgical specimen[17,65,66] or no viable tumor in the breast but residual tumor cells in the lymph nodes.

All Cohorts (A, B, C):

Secondary endpoints included feasibility, safety, and radiological response. Feasibility was determined based on any treatment-related complications that led to a delay in chemotherapy or primary surgery beyond six weeks from the start of therapy. All patients were closely monitored for adverse events (AEs) for 100 days after the administration of the last study treatment, following the Common Terminology Criteria for Adverse Events (CTCAE) v.5[67]. In addition, we reported all immune-related adverse events in the first year of follow-up. Radiological response was assessed according to the RECIST 1.1 guidelines, but not confirmed.

Statistical analysis

For this exploratory, hypothesis-generating study, no formal sample size calculation was performed for efficacy because there was no data on the efficacy of neoadjuvant immunotherapy in breast cancer at the time of the design of this study. For cohorts A and B, the null hypothesis of a true immune activation in ≤30% of patients was tested against a one-sided alternative. For cohort C, design was identical with the exception of null hypothesis being pCR in ≤30% of patients tested against a one-sided alternative. For 80% power, at a one-sided significance level of 0.05, 15 patients were accrued per cohort to be evaluated in the first stage. If there were 5 or less responses among these 15 patients, the cohort was closed for futility. Otherwise, the cohort could be expanded with 31 additional patients, reaching a total of 46. We decided to publish after stage I, which was allowed by protocol, due to the observation that very early responses to ICI without chemotherapy are possible in TNBC, which warrants efforts to de-escalate therapy for a subset of patients, in contrast to the current therapy escalation for all TNBC patients. Median follow-up time was obtained using the reverse Kaplan-Meier method. Analyses were performed using R[68] v.4.2.1.

Pathology assessments and IHC analyses

All patients underwent baseline tumor staging, consisting of ultrasound of the breast, axilla and periclavicular region and MRI imaging of the breast. PET-CT imaging was performed in all participants to confirm the clinical stage. Pretreatment tumor histological biopsies (4

core biopsies, 14G needle) were taken for all patients, and post-treatment tissue was either obtained through a biopsy (3 core biopsies, 14G needle) for patients continuing neoadjuvant chemotherapy (n=28) and the surgical specimen was used for those undergoing surgery right after the ICI study treatment (n=3). Histopathological examination of biopsies and resection specimens was carried out by five experienced breast cancer pathologists (HMH, RS, KvdV, JvdB, NK). Resected tumors were examined in their entirety and regression of resected tumors was assessed by estimating the percentage of residual viable tumor of the macroscopically identifiable tumor bed, as identified on routine hematoxylin and eosin (H&E) staining. Formalin-fixed paraffin-embedded tissue sections were used for H&E stainings and for immunohistochemical analysis of CD8 (C8/144B, DAKO), PDL1 (22C3, DAKO) and PD1 (NAT105, Roche Diagnostics). The percentage of tumor cells and TILs was assessed by pathologists trained for TILs assessment on H&E-stained slides according to the international standard from the International Immuno-Oncology Biomarker Working Group[22] (see www.tilsinbreastcancer.org for all guidelines on TILs assessment in solid tumors). After a pathologist provided an initial TILs score, an 'expert TILs score' was generated as a consensus score from at least 2 out of 4 trained pathologists using slidescore.com for online scoring[69]. TILs scores for inclusion were scored on the diagnostic biopsy of the patient to allow for stratification of patients (low ≥5-10%, intermediate 11-49%, high ≥50%).

Immunohistochemistry

Immunohistochemistry of the FFPE tumor samples was performed on a BenchMark Ultra autostainer (Ventana Medical Systems). The double stain was performed on a Discovery Ultra autostainer. Briefly, paraffin sections were cut at 3 um, heated at 75°C for 28 minutes and deparaffinized in the instrument with EZ prep solution (Ventana Medical Systems). Heat-induced antigen retrieval was carried out using Cell Conditioning 1 (CC1, Ventana Medical Systems) for 48 minutes at 95°C (PDL1) or 64 minutes at 95°C. (PD1/CD8 double). PDL1 was detected using clone 22C3 (1/40 dilution, 1 hour at RT, Agilent/DAKO, Lot11654144). Bound antibody was detected using the OptiView DAB Detection Kit (Ventana Medical Systems). Slides were counterstained with Hematoxylin and Bluing Reagent (Ventana Medical Systems).

For the double staining PD1 (Yellow) followed by CD8 (Purple) the PD1 was detected in the first sequence using clone NAT5 (Ready-to-Use, 32 minutes at 370C, Roche Diagnostics, Lot11654144). The PD1-bound antibody was visualized using Anti-Mouse NP (Ventana Medical systems, Ready to Use dispenser, LotK09956) for 12 minutes at 37C followed by Anti-NP AP (Ventana Medical systems, Ready to Use dispenser, LotJ23971) for 12 minutes at 37C, followed by the Discovery Yellow detection kit (Ventana Medical Systems). In the second sequence of the double staining procedure, CD8 was detected using clone C8/144B (1/200 dilution, 32 minutes at 37C, Agilent, Lot41527763). CD8 was visualized using Anti-Mouse HQ (Ventana Medical systems, Ready to Use dispenser, LotK20711) for 12 minutes

at 370C followed by Anti-HQ HRP (Ventana Medical systems, Ready to Use dispenser, LotK22062) for 12 minutes at 37C, followed by the Discovery Purple Detection Kit (Ventana Medical Systems). Slides were counterstained with Hematoxylin and Bluing Reagent (Ventana Medical Systems). A PANNORAMIC® 1000 scanner from 3DHISTECH was used to scan the slides at a 40x magnification.

Distance analysis between tumor and CD8+ T cells

Spatial analysis was performed on the pretreatment biopsies of all included patients. The stained slides were scanned, and image analysis was performed with the HALO image analysis software from Indica Labs, v3.4.2986.185 (cohorts A and B) and v.3.6.4134 (cohort C). Within HALO, the multiplex IHC module was used to phenotype and quantify CD8-positive cells. Cell segmentation was performed by the detection of hematoxylin (detection weight = 1) and PD1 (detection weights 0.045 for cohorts A&B; 0.5 for cohort C) and CD8 for cohort C (detection weight = 0.5) staining, utilizing a nuclear segmentation aggressiveness of 0.045. Minimal intensity thresholds to consider a cell positive for a marker were set for hematoxylin (0), PD1 (0.25 for cohorts A&B, 0.1 for cohort C), and CD8 (0.1) separately. Biopsies were analyzed in total, while for resection specimens the analysis was restricted to representative tumor beds as annotated by a breast cancer pathologist. The quantified levels of CD8+ and PD1+CD8+ cells were corrected for the analyzed tissue area (cells /μm^2).

Artificial intelligence tumor classifiers (Object Phenotyper, HALO AI) were developed to discriminate between tumor and non-tumor cells in cohorts A&B and in cohort C. Individual cells were segmented (nuclei seg BF v.1.0.0), and the classifiers were trained by annotating single cells as tumor or non-tumor. The annotations were guided by marked tumor regions on H&E-stained slides by a trained BC pathologist. The classifiers were finalized with 20.000 iterations and a cross-entropy of 0.009 (cohort A&B) and >10.000 iterations and cross-entropy of 0.021 (cohort C).

Merging the results of the multiplex IHC and tumor classifier enabled the visualization of the spatial distribution of tumor and CD8+ cells (**ED Fig.1B-F**). Using the nearest neighborhood analysis, the average distance between the tumor and immune cells was quantified by taking the mean of the distances between every tumor cell and its nearest cell of the above-mentioned immune phenotypes in the pretreatment biopsies (**ED Fig.1F**). Distances from tumor cells to the nearest CD8+ T cells were taken as a measure of proximity of CD8+ T cells to the tumor.

DNA and RNA isolation

DNA and RNA were extracted from fresh-frozen, pre- and post-treatment tumor material using the AllPrep DNA/RNA Kit (QIAGEN) for frozen material, following the manufacturer's protocol, in a QIAcube (QIAGEN). Germline DNA was isolated from patient peripheral blood mononuclear cells using the DNeasy Blood & Tissue Kit (QIAGEN).

Bulk RNA sequencing

Total RNA Quality Control

Quality and quantity of the total RNA was assessed by the 2100 Bioanalyzer using a Nano chip (Agilent, Santa Clara, CA). Total RNA samples having RIN>8 were subjected to library generation.

TruSeq Stranded mRNA library generation

Strand-specific libraries were generated using the TruSeq Stranded mRNA sample preparation kit (Illumina Inc., San Diego, RS-122-2101/2) according to the manufacturer's instructions (Illumina, Document # 1000000040498 v00). Briefly, polyadenylated RNA from intact total RNA was purified using oligo-dT beads. Following purification, the RNA was fragmented, random primed and reverse transcribed using SuperScript II Reverse Transcriptase (Invitrogen, part # 18064-014) with the addition of Actinomycin D. Second strand synthesis was performed using Polymerase I and RNaseH with replacement of dTTP for dUTP. The generated cDNA fragments were 3' end adenylated and ligated to IDT xGen UDI(10bp)-UMI(9bp) paired-end sequencing adapters (Integrated DNA Technologies, Inc., Coralville) and subsequently amplified by 12 cycles of PCR. The libraries were analyzed on a 2100 Bioanalyzer using a 7500 chip (Agilent, Santa Clara, CA), diluted and pooled equimolar into a multiplex sequencing pool.

Sequencing

The libraries were sequenced with 54 paired-end reads on a NovaSeq6000 using a S1 Reagent Kit v1.5 (100cycles) (Illumina Inc., San Diego).

Data analysis

RNA sequencing data were aligned to GRCh38 with STAR[70] 2.7.1a, with the twopassMode='Basic'. FPKM were obtained with RSeQC[71] 4.0.0 FPKM_count.py and subsequently normalized to transcripts per million. Data quality was assessed with FastQC[72] 0.11.5, FastQ Screen[73] 0.14.0, the Picard CollectRnaSeqMetrics[74,75] and RSeQC[71] 4.0.0 read_distribution.py and read_duplication.py and were found to be suitable for the downstream analysis. TNBCtype[76] was used for the Lehmann subtype classification[77]. The Gseapy[78] 1.0.3 ssgsea tool with the sample_norm_method='rank' was used for gene set signature scoring. For the signature analysis, p-values were significant after FDR correction (Benjamini–Hochberg) at 10% significance level. Data were analyzed with Python[79] 3.10.5. Pandas[80,81] 2.0.0 and numpy[82] 1.22.4 were used for data handling. Matplotlib[74] 3.5.2, seaborn[83] 0.12.2 and statannotations[84] 0.5.0 were used for plotting.

Whole exome sequencing

For each sample the amount of double stranded DNA was quantified by using the Qubit® dsDNA HS Assay Kit (Invitrogen, cat no Q32851). A maximum amount of 2 µg of double stranded genomic DNA was fragmented by covaris AFA technology to obtain fragment sizes of 200-300 bp. Samples were purified using Agencourt AMPure XP Reagent (Beckman Coulter, cat no A63881) in a 2x reaction volume settings according to manufacturer's instructions. The fragmented DNA was quantified and qualified on a BioAnalyzer system using the DNA7500 assay kit (Agilent Technologies cat no. 5067- 1506). With a maximum input amount of 1 µg fragmented DNA, NGS library preparation for Illumina sequencing was performed using the KAPA HTP Prep Kit (KAPA Biosystems, KK8234) in combination with xGen UDI-UMI Adapters of IDT (Integrated DNA Technologies). During the library amplification step, 4 cycles of PCR were performed to obtain enough yield for the exome enrichment assay. All DNA libraries were quantified on a BioAnalyzer system using the DNA7500 assay kit. Exome enrichment was performed on library pools of 6 unique dual indexed libraries, 500 ng each, using the xGen™ Exome Hyb Panel v2 (IDT, cat no 10005152) and xGen™ Hybridization Capture Core Reagents according to manufacturer's protocol, with hybridization time adjusted to 16 hours and 10 cycles of PCR performed during post-capture PCR. All exome enriched library pools were quantified on a BioAnalyzer system using the DNA7500 assay kit, pooled equimolar to a final concentration of 10nM and subjected to paired-end 100 bp sequencing on an Illumina Novaseq 6000 instrument using a NovaSeq 6000 S4 Reagent Kit v1.5 (Illumina, 20028313), according to manufacturer's instructions.

Data analysis

Sequencing reads were aligned to the human reference GRCh38 (Ensemble, v. 105) using BWA[85] 0.7.17. Duplicated reads were marked using Picard[75] MarkDuplicates 2.25.0, after which quality scores were recalibrated using GATK4[86] BaseRecalibrator 4.2.2.0. Single-nucleotide variants (SNVs) and short insertions and deletions (indels), were called using GATK4[86] Mutect2 4.2.2.0 on the tumor samples matched with germline samples. Subsequently, variants were filtered by the PASS filter, and annotated using Ensembl Variant Effect Predictor 105. maftools[87] 2.10.5 package was used for the analysis. Tumor mutational burden (TMB) was calculated by summarizing the total number of non-synonymous somatic mutations with a minimal variant allele frequency of 20%. Data were analyzed with Python[79] 3.10.5 and R[88] 4.1.3. Pandas[80,81] 2.0.0 was used for data handling. maftools[87] 2.10.5, Matplotlib[74] 3.5.2, seaborn[83] 0.12.2, and statannotations[84] 0.5.0 were used for plotting.

Single cell RNA sequencing and TCR sequencing

Preparation of the single cell suspension

Following biopsy or obtaining resection specimens, samples were rapidly processed for single-cell RNA sequencing (scRNA-seq). Samples from cohort A were minced on ice and frozen in

10% DMSO FCS in the -80˚C degrees. Within 4 weeks after freezing, samples were defrosted in 37˚C degrees medium. Samples from cohort B were minced on ice and immediately processed for single cell sequencing (not frozen), which did not result in a batch effect.

Samples were transferred to a tube containing 1mL digestion medium containing collagenase P (2 mg/ml, ThermoFisher Scientific) and DNAse 1 (10 U/µL, Sigma) in RPMI (ThermoFisher Scientific). Samples were incubated for 20 min at 37˚C degrees and were pipetted up and down every 5 minutes for 30 seconds. Next, samples were filtered on a 40 micron nylon mesh (ThermoFisher Scientific) and directly after the same volume of ice cold PBS containing 0.04% BSA was added. Following centrifugation at 300 g and 4˚C degrees for 5 min, the supernatant was removed and discarded, and the cell pellet was resuspended in red cell blood lysis buffer for 5 minutes at room temperature and then centrifuged again at 300 g at 4 ˚C degrees for 5 min. The supernatant was removed and discarded and the pellet was resuspended in PBS containing 0.04% BSA. Next, 10 µl of this cell suspension was counted using an automated cell counter (ChemoMetec NucleoCounter NC-200) to determine the concentration of live cells. The entire procedure was usually completed within 1h and 15 minutes.

Single cell RNA-seq data acquisition and preprocessing

Libraries for scRNA-seq were generated using the Chromium Single Cell 5' library and Gel Bead & Multiplex Kit from 10x Genomics. We aimed to profile 10 000 cells per library if a sufficient number of cells was retained during dissociation. All libraries were sequenced on a HiSeq4000 or NovaSeq6000 until sufficient saturation was reached.

Data analysis

After quality control, raw sequencing reads were aligned to the human reference genome GRCh38 and processed to a matrix representing the UMI's per cell barcode per gene using CellRanger (10x Genomics, v2.0). The data were analyzed with scanpy[89] 1.9.3 and Seurat[90] v3. Cellbender[91] 0.3.0 was used for eliminating technical artifacts, and cells above the quality cutoff of 0.5 were filtered out. Cells with mitochondrial RNA content >0.25, the number of genes <200 or >6000 and <400 counts were filtered out. After normalization, regression for the number of UMIs, percentage mt-RNA, sample ID, cell cycle, hypoxia, interferon content and cell stress was performed on the 2000 most variable genes followed by a principal component analysis. Next a UMAP was generated and clustering was performed at resolution 0.2 using the 30 most informative components. Major cell types were identified based on canonical marker genes.

For the T cell subclustering, the T cells were selected from the full Seurat object and the analysis described above was repeated with 10 principal components based on the elbow plot and clusters were identified at a resolution of 0.6 and were annotated based on breast

cancer tissue-specific marker genes[92]. Cells expressing markers of other cell types (immunoglobulins, hemoglobin) were filtered out. PCA was calculated on highly variable genes with k=30. Clustering was performed with Phenograph[93] with k=30. Cluster identification was performed based on canonical marker genes. Signature scores were calculated with sc.tl.score_genes. Groups were compared with sc.tl.rank_genes_groups, with method='wilcoxon' and use_raw=True. EnrichR[94,95] was used for the pathway enrichment analysis. Activated Tregs were defined based on the level of *CD137* gene expression >0.5 in the Treg cell population. PD1+Ki67+CD4+ cells were defined based on the level of *MKI67* gene expression >0 in the Tfh cell population. Scirpy[96] 0.11.2 was used for the TCR analysis. Clonotypes were defined based on the amino acid structure. Clonality was calculated as (1 - normalized Shannon entropy). Data were analyzed with Python[79] 3.10.5. Pandas[80,81] 2.0.0 and numpy[82] 1.22.4 were used for data handling. Matplotlib[74] 3.5.2, seaborn[83] 0.12.2, sc-toolbox[97] 0.12.3 and statannotations[84] 0.5.0 were used for plotting.

ctDNA analysis

A proprietary bioinformatics tissue variant calling pipeline was used to select a set of 16 high-ranked, patient-specific, somatic, clonal single nucleotide variants (SNVs) from WES. The Signatera amplicon design pipeline was used to generate mPCR primer pairs for the given set of 16 variants. For cfDNA library preparation, up to 20 000 genome equivalents of cfDNA from each plasma sample were used. The cfDNA was end-repaired, A-tailed, and ligated with custom adapters, followed by amplification (20 cycles) and purified using Ampure XP beads (Agencourt/Beckman Coulter). A proprietary multiplex PCR (mPCR) methodology was used to run patient-specific assays. Sequencing was performed on these mPCR products on an Illumina HiSeq 2500 Rapid Run (50 cycles) using the Illumina Paired End v2 kit with an average read depth of >100000X per amplicon. All paired-end reads were merged using Pear 0.9.8 software and mapped to the hg19 reference genome with Novoalign version 2.3.4 (http://www.novocraft.com/). Plasma samples with at least 2 variants with a confidence score above a predefined algorithm threshold were defined as ctDNA-positive.

Flow cytometry of fresh blood

The flow cytometry was performed as previously described[98]. In short, fresh blood samples were processed and analyzed within 24 hours after blood draw. Peripheral blood was collected in EDTA vacutainers (BD) and subjected to red blood cell lysis (lysis buffer: dH2O, NH4Cl, NaHCCO3, EDTA). Cells were suspended in PBS containing 0.5% BSA and 2mM EDTA and counted using the NucleoCounter NC-200 (Chemometec) automated cell counter. To obtain absolute white blood cell (WBC) counts per mL of human blood, the total amount of post-lysis cells was divided by the volume (mL) of blood obtained from the patient. For surface antigen staining, cells were first incubated with human FcR Blocking Reagent (1:100

Miltenyi) for 15 min at 4°C and then incubated with fluorochrome-conjugated antibodies for 30 min at 4°C. For intracellular antigen staining, cells were fixed with Fixation/Permeabilization solution 1X (Foxp3/Transcription Factor Staining Buffer Set, eBioscience) for 30 min at 4°C and stained with fluorochrome-conjugated antibodies in Permeabilization buffer 1X (eBioscience) for 30 min at room temperature. Viability was assessed by staining with either 7AAD staining solution (1:10; eBioscience) or Zombie Red Fixable Viability Kit (1:800, BioLegend). Data acquisition was performed on an LSRII SORP flow cytometer (BD Biosciences) using Diva software and data analysis was performed using FlowJo 10.6.2. Gating strategy is displayed in **ED Fig.5A**.

Data availability

DNA and RNA-seq data are stored in the European Genome–Phenome Archive EGAS50000000567 (RNA-Seq) and EGAS50000000568 (WES)). Sequencing data and source data supporting the findings of this study will be made available from the corresponding author (m.kok@nki.nl) for academic use, within the limitations of the provided informed consent. Data will not be made available for commercial use. A first response to the request will be sent in <4 weeks. Data requests will be reviewed by the corresponding author and Institutional Review

Board of the NKI and after approval, applying researchers will have to sign a data transfer agreement with the NKI.

Code availability

No custom developed code was used for the analysis of the study data.

Results

Design and patient characteristics

The BELLINI trial (NCT03815890; Fig.1A,G, ED Fig.1A) is a pre-operative, window of opportunity (WOO), phase II, multiple-cohort non-randomized study in early (stage I-III) breast cancer utilizing an adaptive Simon's two-stage design[27]. Here, we report the initial results from the first two WOO cohorts exploring the immune-activating capacity of short-term neoadjuvant nivolumab ± ipilimumab (cohorts A and B, n=31) in patients with ≥5% TILs as well as the initial results of cohort C that was opened based on the results of cohorts A and B. The first patient was included on 19 September 2019 and the last patient on 24 January 2023.

Cohort A (n=15) received two cycles of nivolumab (240 mg) on days 1 and 15. Cohort B (n=15) received two cycles of nivolumab (240 mg) on days 1 and 15, plus one cycle of ipilimumab (1 mg/kg) on day 1. To exclude patients with a poor prognosis, less likely to

respond to ICI and not suitable for chemotherapy de-escalation, we enrolled patients with ≥5% TILs in cohorts A and B. Baseline characteristics were similar between cohorts A and B, except for a higher proportion of patients with positive lymph nodes in cohort B (Table 1).

The primary endpoint for cohorts A and B was immune activation, defined as at least a two-fold increase in CD8+ T cells (measured by immunohistochemistry (IHC), ED Fig. 1B-F) and/or increased interferon gamma (IFNG) gene expression. This endpoint was based on the observation that significant increases in intratumoral CD8+ T cells[25,28] and higher IFNG signature scores[17,29] in serially biopsied tumors are correlated with responses to anti-PD(L)1.

Clinical response (secondary endpoint) in cohorts A and B was defined as PR/CR on MRI (RECIST1.1) or no viable tumor in post-treatment biopsy for patients proceeding to neoadjuvant chemotherapy. For patients directly proceeding to surgery this was defined as partial or complete pathological response (EUSOMA). Other secondary endpoints included safety and translational analyses. MRI scans and biopsies were collected at baseline and after two ICI cycles.

Efficacy of short-term nivolumab and nivolumab+ipilimumab in early TNBC (window of opportunity)

Immune activation was achieved in 8 tumors (53.3%) in the nivolumab cohort (A) and 9 (60%) in the nivo-ipi cohort (B) (Fig.1B). Therefore, both cohorts met the Simon's two-stage27 threshold for expansion to stage II. After four weeks, patients proceeded to standard neoadjuvant chemotherapy followed by surgery (n=28) or surgery without neoadjuvant chemotherapy (n=3). Clinical response was observed in 12/31 patients (38.7%, 95% CI 23.7%-56.2%) with 7/31 patients (22.6%, 95% CI 11.4%-39.8%) having a partial response (PR) according to RECIST 1.130 (Fig.1C,D). 10/31 patients had no viable tumor in the biopsy and in the three patients who underwent surgery directly after ICI, two partial and one complete pathological response was seen. Despite these clear pathological responses, MRI showed modest downsizing, indicating MRI underestimates early ICI response (ED Fig. 1H), consistent with findings in early-stage melanoma31, colorectal and gastroesophageal cancers17,32. Strikingly, clinical response was only observed for patients with TILs ≥30% (Fig.1E) and a CPS PDL1 ≥20% (Fig.1F). Patients with lower pretreatment CD8+ T cell levels were more likely to achieve immune activation (ED Fig.1G), likely due to either less possibility for value doubling or to a very early immune response in highly inflamed tumors.

Short-term neoadjuvant nivolumab + ipilimumab can induce pathological responses in patients with high TILs

Both cohorts A and B met the predefined thresholds of the Simon's two-stage design[27], allowing expansion to stage II. However, given the promising clinical responses observed in cohorts A and B and the approval of neoadjuvant pembrolizumab plus chemotherapy[4],

Table 1. *Baseline patient characteristics*

Characteristic	A: Nivo *(n=16)*	B: Nivo-ipi 4 wks *(n=15)*	C: Nivo-ipi 6 wks *(n=15)*
Median age, years (IQR range)	48 (39.8-53.2)	50 (42.5-57.5)	51 (36.0-56.5))
WHO PS[a], *n (%)*			
0	16 (100)	14 (93.3)	15 (100)
1	0 (0.0)	1 (6.7)	(0.0)
Histological subtype, *n (%)*			
NST	16 (100)	13 (86.7)	14 (93.3)
Metaplastic	0 (0.0)	1 (6.7)	0 (0.0)
Lobular pleiomorphic	0 (0.0)	1 (6.7)	1 (6.7)
Tumor stage, *n (%)*			
T1	5 (31.3)	5 (33.3%)	2 (13.3)
T2	10 (62.5)	9 (60.0)	13 (86.7)
T3	1 (6.2)	1 (6.7)	0 (0.0)
Nodal status, *n (%)*			
N0	13 (81.3)	5 (33.3)	15(100)[d]
N1	2 (12.5)	9 (60.0)	0 (0.0)
N3	1 (6.3)	1 (6.7)	0 (0.0)
Tumor grade[b], *n (%)*			
2	1 (6.3)	4 (26.7)	0 (0.0)
3	15 (93.8)	11 (73.3)	15 (100)
Germline BRCA1/2 mutation, *n (%)*			
Yes	3 (18.8)	3 (20.0)	4 (26.7)
No	12 (75.0)	10 (66.7)	11 (0.0)
Unknown	1 (6.3)	2 (13.3)	0 (0.0)
TILs[c], *(%)*			
Median (IQR)	40.8 (6.2, 60.3)	37.5 (23.8, 61.4)	52.5 (45.3, 73.8)

[a]WHO performance status. [b]Tumor grade according to Bloom Richardson. [c]TILs were averaged between the diagnostic TILs score and the study pretreatment TILs score. sTILs were scored according to international guidelines[22] as a numerical variable. All samples were evaluated by at least two breast cancer pathologists and their score for each sample was averaged. [d]Cohort C only allowed inclusion of N0 patients. Abbreviations: NST, no special type; TILs, stromal tumor-infiltrating lymphocytes.

the study team decided not to proceed to stage II with the WOO design but to open cohort C with a true neoadjuvant design (n=15, Fig.1G). Since all patients with a clinical response in cohorts A and B had high TILs, cohort C was opened for patients with ≥50% TILs and allowed only patients with node-negative disease since for this patient population chemotherapy de-escalation could be an option in the future. The treatment schedule with combination ICI for cohort C was based on our data obtained in cohorts A and B as well as on the well-established effective and tolerable combination ICI schedule in melanoma[14,26].

Patients in cohort C underwent a 6-week treatment regimen of nivolumab and ipilimumab (administered on days 1 and 21), followed by surgery (Fig.1G). Five patients had a pCR, (33.3%, 95% CI 15.2%-58.3%, Fig.1H) with confirmed tumor-negative lymph nodes (ypT0N0). Less than 10% viable tumor remaining was seen in 3/15 patients (20%, 95% CI 4%-48%, Fig.1H), making major pathological response rate (MPR) 8/15=53% (95% CI 27%-

Figure 1

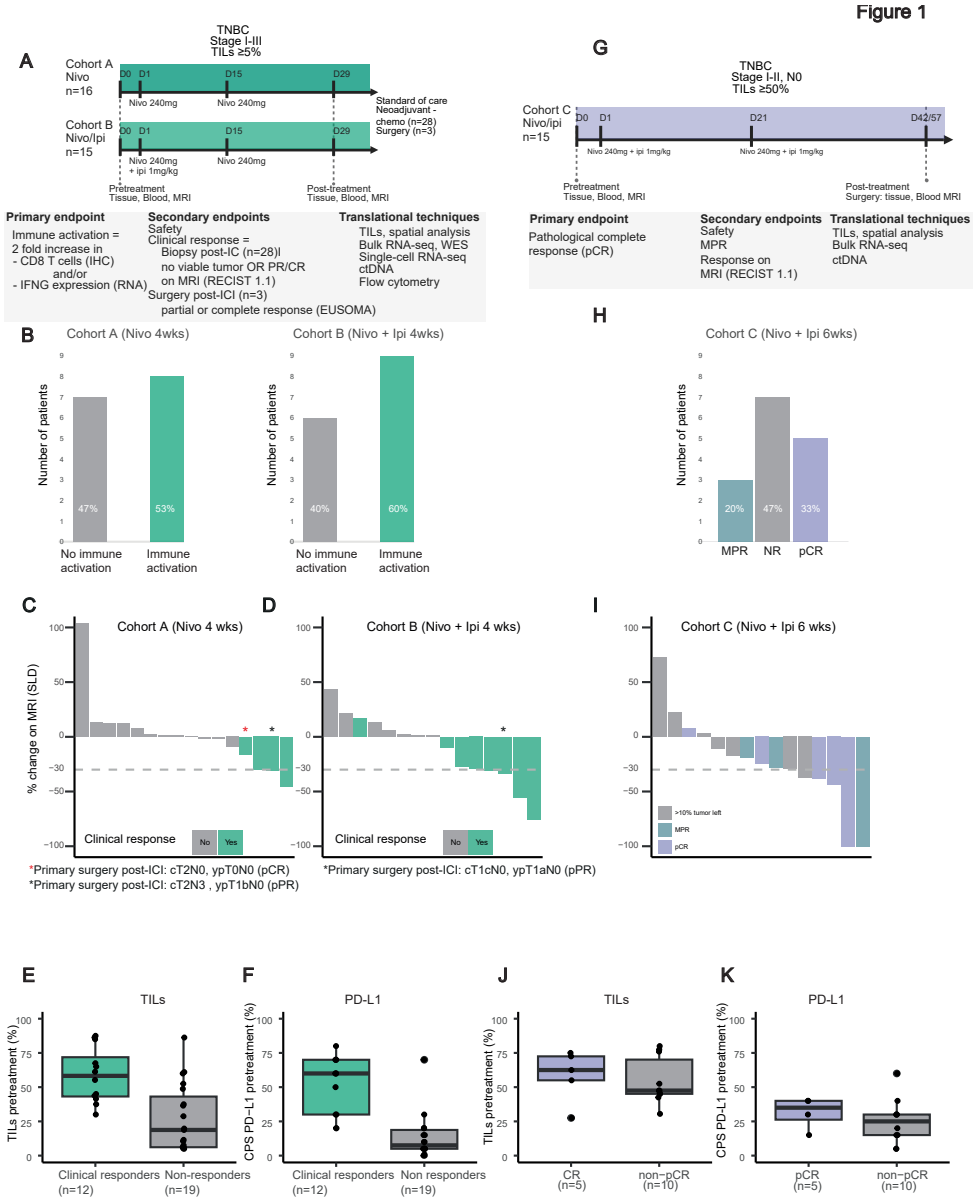

***Figure 1: BELLINI trial design, efficacy data and baseline biomarkers**. **A.** Trial design for cohorts A and B. Cohort A received 2 cycles of nivolumab (anti-PD1). Cohort B received 2 cycles of nivolumab (anti-PD1) and one cycle of ipilimumab (anti-CTLA4). Biopsies and blood were taken pretreatment and after 4 weeks of treatment after which patients proceeded to standard of care: neoadjuvant chemotherapy (n=28) or primary surgery (n=3). **B.** Numbers of patients reaching immune activation in cohorts A (n=15) and B (n=15). **C-D.** Changes in tumor size according to the MRI for cohort A (C) and cohort B (D). The gray dashed line at -30%: radiological PR. The green bars indicate clinical responses (radiological PR and/or pathological response). Asterisks (*) represent patients with resection after ICI only (n=3). pPR: pathological partial response according to EUSOMA. **E.** TILs in pretreatment biopsies of patients with and without clinical response in cohorts A and B. n=31 patients. **F.** Combined positive PDL1 score (CPS) in pretreatment biopsies of patients with and without clinical response in cohorts A and B. n=31 patients. **G.** BELLINI trial design for cohort C. Cohort C (n=15) received 2 cycles of nivolumab and ipilimumab on days 1 and 21. Biopsies and blood were taken pretreatment and after 6 weeks. Patients proceeded to primary surgery (n=15). **H.** pCR and MPR (<10% viable tumor left) rates in cohort C. **I.** Changes in tumor size according to the MRI in cohort C. The gray dashed line at -30%: radiological PR. Dark blue bars; pCR. **J.** TILs in pretreatment biopsies of patients according to pCR status in cohort C. n=15 patients. **K.** CPS in pretreatment biopsies for patients according to pCR status in cohort C. n=15 patients. Figures **A, G** were created with BioRender.com. In **E, J** levels of TILs calculated as average from TIL levels at diagnostic- and pretreatment study. In **E-F, J-K** boxplots display a minimum (Q0), a maximum (Q4), a median (Q2) and the interquartile range. P-values were derived using a two-sided Mann-Whitney test.*

79%). Notably, of the 5 patients with a pCR only one had a complete radiological response (Fig.1I). Because of high TILs, N0 status and pCR which are all very favorable prognostic features, all 5 patients with a pCR were offered the option of omitting adjuvant chemotherapy and all chose not to undergo adjuvant chemotherapy (shared decision). Patients without pCR were advised adjuvant chemotherapy.

Safety data and follow-up

Toxicity data are summarized in Table 2 (all events required steroids or persisted) and detailed in ED Table 1. Neither neoadjuvant nivolumab nor nivolumab-ipilimumab resulted in previously unreported toxicities. All patients were monitored for (immune-related; IR) toxicities until one year post ICI-therapy. Treatment-related adverse events (AEs) of any grade occurred in 41/46 patients (89%). A total of 8 (17%) patients developed grade ≥3 treatment-related AEs, of which 6 were treated in cohort C. Except for the endocrinopathies all adverse events resolved. Notably, 19/46 patients (41%) developed treatment-related hypothyroidism. All patients with hypothyroidism remain dependent on replacement therapy. Six patients (13%) developed adrenal insufficiency and require ongoing corticoid replacement therapy. One patient developed a diabetic ketoacidosis and remains insulin-dependent.

All patients proceeded with tumor resection or neoadjuvant chemotherapy as scheduled. 44 patients received both ICI doses, and two patients only received one dose due to suspected immunotoxicity.

With a median follow-up duration of 32.5 months in cohorts A and B (interquartile range 28.1-40.3 months), one patient in cohort A (cT2N0; intermediate TILs) developed a second primary tumor, and one patient in cohort B (cT2N1; intermediate TILs) died from metastatic TNBC despite receiving standard of care (neo)adjuvant chemotherapy. Median follow-up for cohort C was 17.6 months (interquartile range 18.8-22.1 months). One patient (no response to ICI) refused adjuvant chemotherapy and radiotherapy and developed recurrent TNBC (pT1cNx, 80% TILs).

Table 2. *Summary of adverse events*

	A: Nivolumab (N=16)		B: Nivo+Ipi 4 wks (N=15)		C: Nivo+Ipi 6 wks (N=15)	
	Number of patients (percent)					
Immune-mediated adverse events	Any grade	Grade ≥3	Any grade	Grade ≥3	Any grade	Grade ≥3
Hypothyroidism^	6 (38%)	0 (0%)	7 (47%)	0 (0%)	6 (40%)	0 (0%)
Adrenal insufficiency*	1 (6%)	0 (0%)	2 (13%)	1 (7%)	3 (20%)	1 (7%)
Diabetes Mellitus	0 (0%)	0 (0%)	1 (7%)	1 (7%)	0 (0%)	0 (0%)
Colitis	0 (0%)	0 (0%)	0 (0%)	0 (0%)	0 (0%)	1 (7%)
Hepatitis**	0 (0%)	0 (0%)	2 (13%)	0 (0%)	3 (20%)	3 (20%)
Polymyalgia rheumatica	0 (0%)	0 (0%)	0 (0%)	0 (0%)	1 (7%)	0 (0%)
Pneumonitis	0 (0%)	0 (0%)	0 (0%)	0 (0%)	2 (13%)	1 (7%)

This table sums all immune-mediated adverse events that required treatment with steroids or didn't resolve (endocrinopathies). A detailed list of all adverse events according to CTCAE criteria can be found in Table S1. * All patients were classified as having secondary adrenal insufficiencies and all patients remain dependent on corticosteroid replacement. ** We have included all patients requiring steroids and one patient with grade 3 IR hepatitis that did not receive steroid treatment ^ All patients are still dependent on hormone replacement therapy.

Pretreatment composition of the tumor microenvironment is associated with ICI response

Due to limited sample size, we compared clinical responders versus non-responders from both cohorts (A+B) combined and not for the cohorts separately. Clinical responders in cohorts A and B had significantly higher pretreatment TILs (p=0.0014, Fig.1E) and PDL1 scores (p=8.6e-05, Fig.1F) compared to non-responders. CD8+ T cell density was not significantly associated with clinical response (Fig.2A, ED Fig.1B-F). Spatial analysis showed that responders had significantly shorter distances from tumor cells to the nearest CD8+ T cells (p=0.00001, Fig.2B). Responders also exhibited a larger density of double-positive CD8+PD1+ cells (p=0.02, ED Fig.2A) and PD1+ cells (p=0.001, IHC, ED Fig.2B) pretreatment.

In cohort C, TILs were not different between responders and non-responders, probably due to the more homogeneous patient population with only patients with ≥50% TILs (Fig.1J). In line with this, patients with pCR had similar PDL1 scores , CD8+ T cell density (cells /µm2) and distances from tumor to nearest CD8+ T cells as patients without pCR (Fig.1K, Fig. 2D-E). We found no association between tumor mutational burden and clinical response (ED Fig.2C-D). There were no statistically significant differences between clinical responders and non-responders in TNBC subtypes33 (ED Fig. 2E).

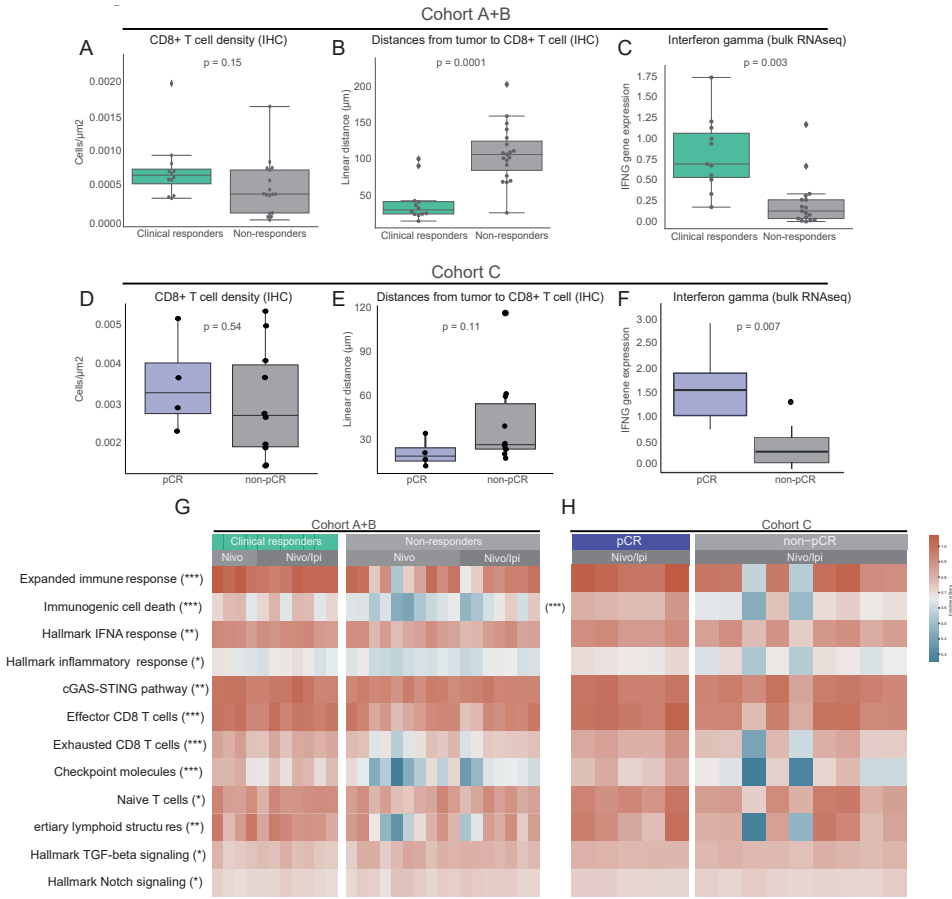

Figure 2: Pretreatment immune activation associated with clinical response. A. *CD8+ density (IHC) in pretreatment biopsies of patients with and without clinical response in cohorts A and B. n=31 patients.* ***B.*** *Median distances (µm) from tumor cells to the nearest CD8+ T cells in pretreatment biopsies of patients with and without clinical response in cohorts A and B. n=31 patients.* ***C.*** *IFNG gene expression scores in pretreatment biopsies of patients with and without clinical response in cohorts A and B. n=28 patients.* ***D.*** *CD8+ density (IHC) in pretreatment biopsies of patients with and without pCR in cohort C. n=14 patients.* ***E.*** *Median distances from tumor cells to the nearest CD8+ T cells in pretreatment biopsies of patients with and without pCR in cohort C. n=14 patients.* ***F.*** *IFNG gene expression scores in pretreatment biopsies of patients with and without pCR in cohort C. n=14 patients.* ***G-H.*** *Gene set enrichment expression scores in pretreatment biopsies of patients with and without clinical response in cohorts A and B (G, n=28 patients) or pCR (H, n=14 patients) in cohort C. Heatmaps include: Expanded immune signature57, Immunogenic cell death signature58, Hallmark IFNA response gene set, Hallmark inflammatory response gene set, cGAS-STING pathway gene set59, Effector CD8+ T cell gene set60, Exhausted T cell gene set60, Checkpoint molecules gene set60, Naive T cell gene set61, Tertiary lymphoid structures gene set62, Hallmark TGF-beta signaling gene set, Hallmark Notch signaling. Asterisks represent the p-value levels: "*": p≤0.05, "**": p≤0.01, "***": p≤0.001. Reported p-values were significant after Benjamini-Hochberg (FDR) correction at 10% significance level. In* ***A-F****, boxplots display a minimum (Q0), a maximum (Q4), a median (Q2) and the interquartile range. P-values were derived using a two-sided Mann-Whitney test.*

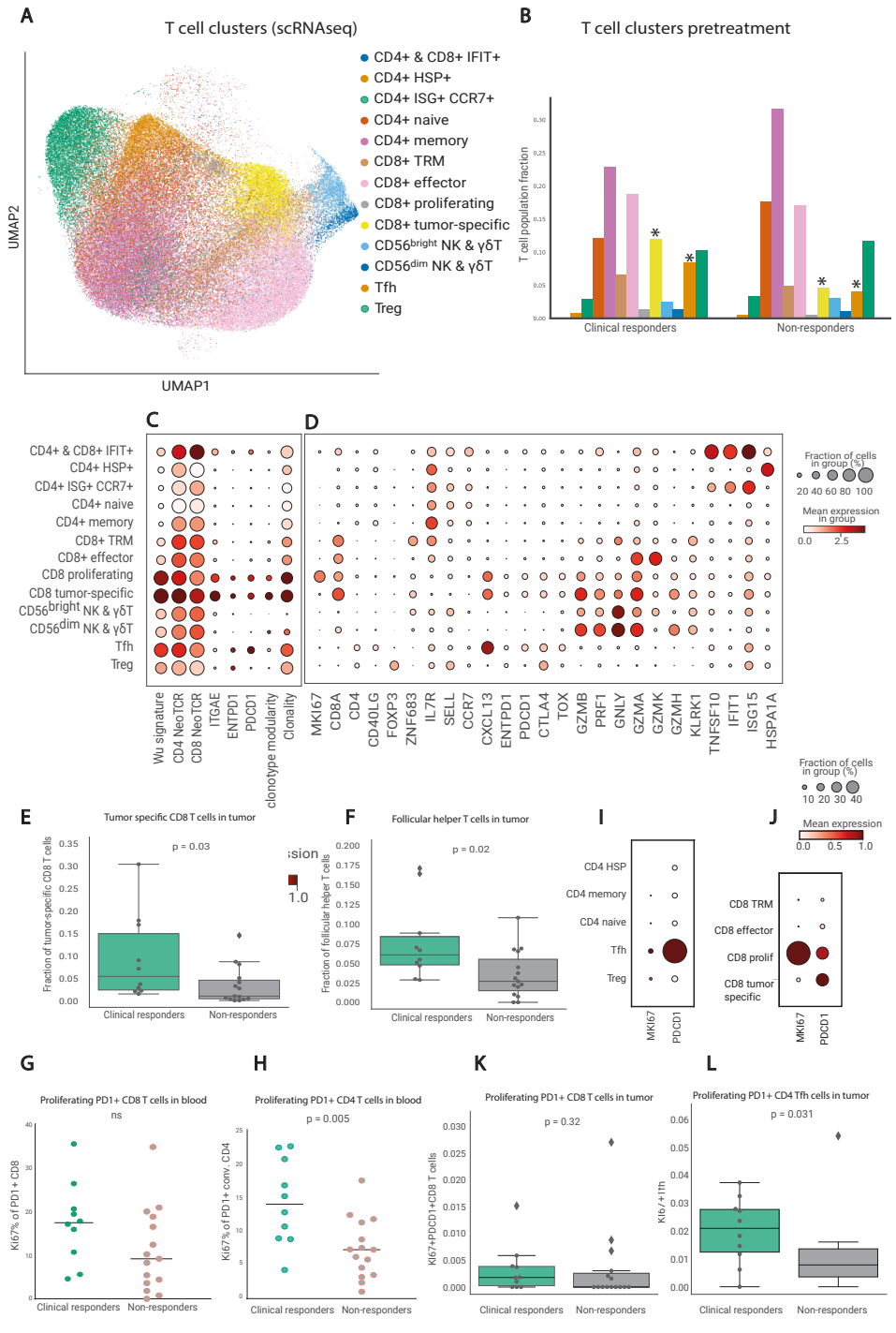

◀◀◀ Figure 3: Pretreatment T cell profiles of the tumor microenvironment and peripheral blood associated with clinical response in cohorts A and B. A. *UMAP representation of the T cell clusters in the single-cell RNA-Seq dataset (cohorts A and B). n=52 samples from 29 patients, 80 000 cells.* ***B.*** *Fractions of different T cell populations relative to all T cells in the pretreatment biopsies from clinical responders (left) and non-responders (right) in cohorts A and B.* ***C.*** *Dotplot illustrating markers of different T cell clusters based on single-cell RNA-Seq data (cohorts A and B).* ***D.*** *Dotplot illustrating differences in tumor reactivity markers in different T cell clusters based on single-cell RNA-Seq data (cohorts A and B). Wu_signature - CD8+ T cell tumor specificity signature34; CD4_NeoTCR - CD4+ T cell tumor specificity signature35; CD8_ NeoTCR - CD8+ T cell tumor specificity signature35.* ***E.*** *Tumor-specific CD8+ T cell fractions relative to all T cells in pretreatment biopsies of patients with and without clinical response (cohorts A and B). n = 25 patients.* ***F.*** *Tfh fractions relative to all T cells in pretreatment biopsies of patients with and without clinical response (cohorts A and B). n=25 patients.* ***G-H.*** *Ki-67 expression on (G) PD1+ CD8+ T cells and (H) conventional CD4+ T cells pretreatment in peripheral blood of patients with and without clinical response in cohorts A and B. n= 25 patients* ***I.*** *Dotplot for PDCD1 and MKi67 expression in CD4+ T cell clusters (tumoral, scRNA-Seq, cohorts A and B).* ***J.*** *Dotplot for PDCD1 and MKi67 expression in CD8+ T cell clusters (tumoral, scRNA-Seq, cohorts A and B).* ***K.*** *Fraction of Ki-67+ Tfh cells relative to all T cells in pretreatment biopsies of patients with and without clinical response (cohorts A and B). n=25 patients.* ***L.*** *Fraction of proliferating PD1+ CD8+ T cells relative to all T cells in pretreatment biopsies of patients with and without clinical response based on single-cell RNA-seq data (cohorts A and B). n=25 patients. In* ***E–F, K-L*** *boxplots display a minimum (Q0), a maximum (Q4), a median (Q2) and the interquartile range. P-values were derived using a two-sided Mann-Whitney test.*

Tumors of clinical responders harbor preexisting inflammatory profiles and tumor-specific CD8+ T cells

We conducted in-depth analyses between clinical responders and non-responders using bulk RNA-Seq (all cohorts) and single-cell RNA-Seq and TCR sequencing (cohorts A and B) pre- and post-treatment. Bulk RNA-Seq revealed higher pretreatment levels of IFNG gene expression (p=0.0003, Fig.2C) and inflammatory gene signatures in clinical responders (p<0.05 for all, FDR 10%, Fig.2G, ED Fig.3A-E). Clinical responders also exhibited higher gene signatures associated with immune infiltration (p<0.05 for all, FDR 10%, Fig.2G, ED Fig.3F-J). Conversely, clinical non-responders displayed upregulation of TGF-beta and Notch signaling (p<0.05 for both, FDR 10%, Fig.2D, ED Fig. 3L-M). Though TIL levels and distances from tumor cells to CD8+ T cells were not different in responders versus non-responders in cohort C that included TIL high patients only, patients with pCR had significantly higher pretreatment IFNG gene expression (Fig. 2F) and higher scores of gene signatures related to immune response and T cell infiltration (Fig. 2H), consistent with our previous observations of a more inflammatory profile of the tumor microenvironment in clinical responders in cohorts A and B.

After single-cell RNA-Seq data preprocessing, we obtained 80 000 high quality T cells from 52 samples (29 patients). Following unsupervised clustering of the T cells, we identified various subpopulations (Fig.3A-D, ED Fig.4A-T), including CD8+ effector T cells, CD8+ tissue resident memory (CD8+ TRM) T cells, proliferating CD8+ T cells, naive CD4+ T cells, follicular B helper T cells (Tfh), memory CD4+ T cells, regulatory T cells (Tregs), CD56bright and CD56dim NK cells. Intriguingly, we identified a cluster of CD8+ T cells with features of tumor-

specific T cells. This cluster was characterized by the highest clonality and highest expression of tumor recognition signatures derived using functional tumor recognition experiments34,35 (Fig.3C-D). This CD8+ tumor-specific cluster was marked by high expression of tumor-reactive markers (CD39, CD103, PDCD1), IFNG, effector molecules (GZMB, NKG7, PRF1, GNLY), chemokines (CCL5, CCL4, CXCL13, CCL3) and exhaustion markers (LAG3, HAVCR2, TIGIT, TOX, CTLA4, Fig.3C,D). Clinical responders exhibited higher fractions of pretreatment CD8+ tumor-specific T cells (Fig.3E). This is a first report of tumor-specific T cell population identified using single-cell RNA-Seq in clinical trial data showing an association with response. Clinical responders also had higher fractions of CD4+ Tfh cells (Fig.3F). Presence of tumor-specific CD8+ T cells and Tfh in pretreatment biopsies was correlated with tumor decrease on MRI, indicating a continuous association between the abundances of these cells pretreatment and the depth of the tumor response (ED Fig.4U, V). Patients with different TIL levels had similar T cell subtypes pretreatment (EDFig.4W).

Flow cytometry of blood samples (19 markers, ED Table 2, ED Fig.5A) revealed increased Ki-67-positive cells within the PD1+ conventional CD4+ T cell population in clinical responders (p=0.005, Fig.3G). A similar trend was observed for CD8+ T cells (Fig.3H). The increased proliferation of PD1+CD4+ T cells observed in the blood could also be traced back to the tumor, with responders having higher levels of Ki67+ Tfh which was the CD4+ T cell cluster with the highest PDCD1 gene expression in the tumor single-cell RNA-Seq data (Fig.3I, L). In line with the blood data, the levels of PD1+ proliferating CD8+ T cells were not significantly different between clinical responders and non-responders (Fig.3J-K), suggesting a specific role for proliferating CD4+ T cells systemically as well as in the TME.

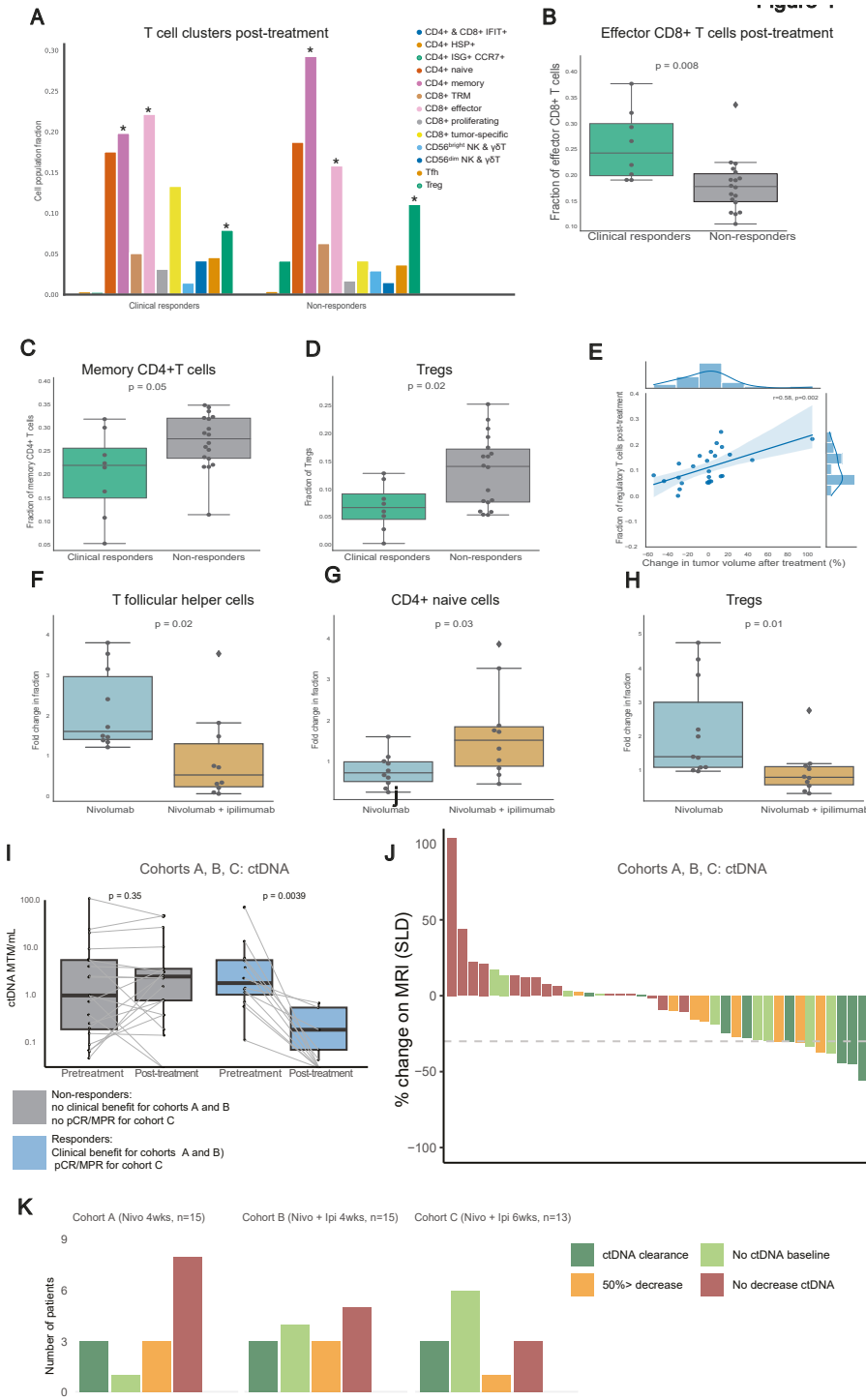

Figure 4: Effects of anti-PD1 ± anti-CTLA4 on the T cell profiles in the tumor microenvironment after treatment in cohorts A and B. ctDNA data for all cohorts. A. *Fractions of different T cell clusters relative to all T cells in post-treatment biopsies of patients who did (left) and did not (right) experience clinical response based on single-cell RNA-Seq data.* ***B.*** *Effector CD8+ T cell fractions relative to all T cells in post-treatment biopsies versus response (cohorts A, B). n=26 patients.* ***C.*** *Memory CD4+ T cell fractions relative to all T cells in post-treatment biopsies versus response (cohorts A and B). n=26 patients.* ***D.*** *Regulatory T cell fractions relative to all T cells in post-treatment biopsies versus response (cohorts A, B). n=26 patients.* ***E.*** *Fractions of regulatory T cells relative to all T cells in post-treatment biopsies of patients (cohorts A and B) in relation to the change in tumor volume after treatment assessed using MRI (RECIST 1.1). n=26 patients.* ***F-H.*** *Fold changes in fractions of T cell populations relative to all T cells in cohort A and cohort B. n=22 patients.* ***F.*** *Follicular B helper T cells.* ***G.*** *Naive CD4+ T cells.* ***H.*** *Regulatory T cells.* ***I.*** *Changes in circulating tumor DNA (ctDNA) levels of responding and non-responding patients upon treatment. Patients from all cohorts (A, B, C) were included.* ***J.*** *Waterfall plot of all patients (n=46, all cohorts) colored according to the fold change in ctDNA levels in blood upon treatment. The groups represent: ctDNA clearance; post-therapy decrease in ctDNA levels of 50% or more post therapy; no ctDNA at baseline; no decrease in ctDNA. The gray dashed line at -30%: radiological PR.* ***K.*** *Barplots summarizing the number of patients for each ctDNA response category in each cohort (A, B, C). ctDNA at baseline was available for 43/46 patients. In* ***B-D, F-I*** *boxplots display a minimum (Q0), a maximum (Q4), a median (Q2) and the interquartile range. P-values in* ***B-D, F-H*** *were derived using a two-sided Mann-Whitney test. P-values in I were derived using paired Wilcoxon test.*

Dynamics and post-treatment composition of the tumor microenvironment are distinct in clinical responders and non-responders

Single-cell RNA-Seq analysis revealed that though the clinical responders had higher proportions of tumor-specific CD8+ T cells pretreatment, post-treatment their tumors included higher levels of effector CD8+ T cells compared to non-responders (p=0.008, Fig.4A, B). This suggests that effector CD8+ T cells contribute to ICI-induced tumor regression and underscore the ongoing antitumor CD8+ T cell response even four weeks after treatment initiation.

Conversely, non-responders had elevated memory CD4+ T cells (p=0.05, Fig.4A, C) and Tregs (p=0.02, Fig.4A, D) post-treatment, potentially suggesting the involvement of Tregs in mediating resistance to ICI, consistent with prior studies[36]. Intriguingly, we observed an association between the fraction of Tregs after treatment and the lack of response or in some patients even increase in tumor volume on MRI (Fig.4E). This correlation was specifically mediated by activated (CD137+) Tregs, rather than non-activated Tregs (ED Fig.5B-C).

We also investigated whether the addition of anti-CTLA4 led to differential alterations in the TME compared to nivolumab monotherapy, though the study was not powered for cohort comparisons. Patients receiving nivolumab plus ipilimumab showed a reduced fold change in Tfh cells (p=0.02, Fig.4F), but an increased fold change in naive CD4+ T cells (p=0.03, Fig.4G). Additionally, the combination ICI resulted in a decreased fold change in Tregs (p=0.01, Fig.4H) compared to monotherapy, including both activated and non-activated Tregs (ED Fig.5D-E).

ctDNA dynamics during early response to ICI

To assess the impact of short-term ICI on circulating tumor DNA (ctDNA), we conducted ctDNA analysis pretreatment and after four weeks (cohorts A and B) or six weeks (cohort C) of ICI using a tumor-informed ctDNA assay (Signatera). Despite the early tumor stages included (mostly I-II), pretreatment ctDNA was detected in 32/43 (74%) patients. After treatment, 9 (21%) patients had complete ctDNA clearance, while additional seven patients had a reduction of ≥50% in ctDNA load (MTM/mL, Fig.4I-J). All clinical responders in cohorts A+B and pCR/MPR patients (n=8) in cohort C demonstrated at least a 50% drop in ctDNA or were negative for ctDNA at baseline (Fig.4I-K).

Discussion

In this study, we demonstrate that neoadjuvant nivolumab, with or without ipilimumab, is a feasible chemotherapy-free regimen for patients with early stage TNBC. We show that nivolumab ± ipilimumab induces immune activation in the majority of patients and can result in complete pathological responses and ctDNA clearance. Pre-existing inflammatory features such as higher TILs, shorter distances from CD8+ T cells to the tumor and higher baseline fractions of tumor-specific CD8+ T cells were associated with response. In contrast, higher fractions of Tregs post-treatment were associated with lack of response. While standard chemo-immunotherapy for TNBC with 4 chemotherapy agents plus anti-PD1 is a 5-month treatment regimen leading to a 63% pCR rate, our work suggests that with only six weeks of anti-PD1 plus low-dose anti-CTLA4 a 33% pCR rate may be obtained in TNBCs with high TILs. This suggests that for some patients a short-term immunotherapy-first approach may be an option if confirmed by future research in larger cohorts with more robust follow-up. However, a substantial group of patients still needs chemotherapy and/or longer treatment in order to obtain a pCR. Although we did not observe any unexpected toxicity, the rate of persisting endocrinopathies, in particular hypothyroidism, was high compared to reports in other tumor types or in breast cancer when anti-PD(L)1 is added to neoadjuvant chemotherapy. Although the 33% pCR rate would allow expansion of cohort C to stage II, with 40% grade 3-4 toxicity, 40% hypothyroidism and 20% adrenal gland insufficiencies, substantial toxicity is a serious concern, especially considering the relatively good prognosis of TNBC patients with high TILs.

To our knowledge, the BELLINI trial is the first to investigate the feasibility and potential efficacy of ICI without concurrent chemotherapy in early stage TNBC. Moreover, for the first time, the scoring of TILs is used as an inclusion criterion to select patients with a good prognosis for whom development of de-escalated treatment regimens is most promising. Larger clinical trials also using TILs according to this workflow when including patients have recently started (NCT05929768). In addition, ETNA trial (NCT06078384) will explore whether stage I TNBC patients with high TILs can forgo (neo)adjuvant chemotherapy or be treated with immunotherapy alone. The larger international OPTImaL patient preference study (NCT06476119) will also allow the option of no chemotherapy for this patient population. In addition, other studies use TILs as inclusion criteria for immunotherapy-first approaches: Pop-Durva (NCT05215106) and pan-cancer NEOASIS trial (NCT06279130). Further studies that are sufficiently powered to assess long-term outcomes are needed on the use of TILs or other immune-based biomarkers as entry criteria for immunotherapy or de-escalation studies, especially since patients with lower stage TNBC and high TILs can have an excellent outcome with local treatment alone[19,37].

Immune-related endocrine disorders were the most common adverse events observed. Specifically, 41% of the patients developed hypothyroidism, which, though usually easy to

manage, is a permanent condition, and 13% developed adrenal insufficiency, a serious long-term toxicity. Comparable neoadjuvant ICI-only studies with nivolumab + low-dose ipilimumab in head and neck squamous carcinoma, colorectal cancer, urothelial carcinoma and melanoma reported hypothyroidism in 4-8% of patients[9–11,14] and adrenal insufficiency in 0-8% of patients[9–11,14]. However, the recent largest phase III trial (stage III melanoma, n=423) reports substantial higher rates of endocrinopathies with 23.6% hypothyroidism and 9.9% adrenal gland insufficiency[26]. Importantly, for cancer types with poor prognosis such as stage III melanoma, high toxicity rates might be acceptable, while this is different for patient populations with more favorable outcomes. The higher rates of hypothyroidism and adrenal insufficiencies in BELLINI compared to these studies could stem from different patient demographics. Patients with TNBC are typically female and relatively young, potentially contributing to different systemic immunity and adverse event incidence[38]. In BELLINI, we reported all immune-mediated adverse events during the first year of follow-up, with 4/6 patients developing adrenal insufficiency >100 days since inclusion. Trials with shorter reporting periods may miss these late events, leading to underreported delayed toxicity, especially in centers not specialized in evaluating ICI regimens. When focusing on patients with similar demographics and disease, we still observe a higher rate of endocrine adverse events in BELLINI compared to neoadjuvant trials for TNBC evaluating ICI plus chemotherapy. The KEYNOTE-522 trial reported thyroid dysfunction in 22% of patients treated with anti-PD1 plus chemotherapy[1]. Adrenal insufficiency/hypophysitis was reported for 4.5% of patients in the KEYNOTE-522 study. A recent study with an oncolytic virus without chemotherapy found that 3/6 breast cancer patients developed hypothyroidism[39], which is more in line with our observations. The lower hypothyroidism rate in the KEYNOTE-522 compared to the oncolytic virus study[39] and BELLINI could suggest that chemotherapy results in partial blunting of the immune response. Lastly, the preselection of patients with higher TILs in BELLINI may have resulted in patients that are more likely to develop immune-related adverse events due to a different systemic immunity. We also cannot rule out the influence of chemotherapy given after ICI, where steroids are used as antiemetics. Our cohort sizes are too small to compare toxicities induced by 4-week nivolumab versus 4-week nivo-ipi versus 6-week nivo-ipi. However, in the latter group, we observed more non-endocrinopathies such as colitis, hepatitis, and pneumonitis, while endocrinopathies were already remarkably high with nivolumab monotherapy. This potentially signifies that neoadjuvant ICI without chemotherapy could result in a higher rate of hypothyroidism in breast cancer patients. Of note, it was demonstrated that immunotherapy-related thyroid dysfunction and other immune-related adverse events are associated with improved survival in multiple cancer types[40,41,42,43]. Nevertheless, upfront prediction of risk of immunotherapy-related toxicity for individual patients is a large unmet clinical need and the burden of adverse events should be evaluated in light of the prognosis of each patient[44].

The advantage of WOO studies like BELLINI is the opportunity to evaluate promising drugs and drug combinations in an efficient manner and to analyze pre- and post-treatment tumor material that can provide insights into the therapy effects. Our primary endpoint, immune activation defined as doubling of CD8+ T cells and/or IFNG expression, was reached in 17/30 patients (57%). Although both cohorts reached the >30% immune activation rate, allowing cohort expansion, we observed more doubling of CD8+ T cells in patients with low pretreatment levels of these features. This could be due to the biopsy timing with deep responses at 4 weeks in tumors with high endogenous CD8+ T cells and/or a 'saturation' of CD8+ T cells in patients with high pretreatment values. In contrast to CD8+ T cells, IFNG counts may double even with high pretreatment values, however, they could also be impacted by decreased antigen availability in case of tumor regression. This suggests that different biomarker approaches could apply to inflamed and non-inflamed tumors. Recent insights from the developments of personalized neoadjuvant immunotherapy in melanoma indicate that patients with high pre-existing IFNG levels or a significant increase in IFNG signature upon treatment were most likely to benefit45. The disadvantage of WOO designs with short scheduled treatments is the non-guaranteed benefit for participating patients. Also, information on established endpoints such as pCR rate is needed before a novel treatment approach will be tested in larger trials. For this reason, the adaptive BELLINI trial allowed opening of new cohorts with established endpoints to bring therapies to the next step. Although allowed by the protocol and statistical analysis plan, reporting only stage I data of a Simon's 2-stage design comes with the risk of false-positive findings. Similarly to the cohorts A and B, cohort C also reached the threshold of sufficient responders to expand into stage II. However, given the relatively high rate of endocrinopathies, which are chronic, cohort C was not expanded to stage II. In this view, testing novel anti-CTLA4-targeting antibodies, such as botensilimab46, intentionally designed to overcome the limitations of conventional ICI such as persisting endocrinopathies could be interesting for breast cancer patients.

When analyzing pretreatment tumor characteristics in high-TIL tumors only (cohort C), we found that the inflammatory phenotype and markers were still discriminative between responders and non-responders and remarkably similar to the clinical responders and non-responders in cohorts A+B. In cohort C, pathological complete responders had higher inflammatory gene expression profiles pretreatment, including signatures for IFNG response, checkpoint molecules, exhausted CD8+ T cells and immunogenic cell death. This suggests that, even in patients with high TILs, the profiling of baseline inflammatory status may facilitate early identification of (non)responders and should be considered in addition to TILs.

The recent publication of the tumor-specific T cell signatures[34,35] enabled us to identify and follow tumor-specific CD8+ T cells in a clinical trial setting. Importantly, using these signatures as a proxy for the tumor reactivity, we demonstrate for the first time that the presence of tumor-specific CD8+ T cells pretreatment is linked to ICI response.

Additionally, we observed decreased fractions of Tregs in clinical responders compared to non-responders after treatment, in line with prior reports on the role of Tregs in resistance to ICI47. In a resistant mouse tumor model, anti-PDL1 therapy led to Treg activation, and Tregs were shown to be activated in the single-cell data of NSCLC and basal cell carcinoma patients not responding to anti-PD(L)1 ICI[36]. In this recent study, ICI treatment induced higher expression of genes involved in Treg-mediated immune suppression (PDCD1, CTLA4, CD38) and cell cycle (MKI67) in Tregs from the tumors of non-responders[36]. Together, these findings demonstrate that Treg cells might play a critical role in resistance to ICI.

To date, data on combining anti-PD(L)1 with low-dose anti-CTLA4 was lacking in early-stage breast cancer. Due to the non-comparative design and the small sample size, our data on the potential additive effect of ipilimumab should be considered exploratory. At the single-cell level, the addition of ipilimumab resulted in lower fold change in Tregs in the TME upon treatment. We also observed a correlation between higher levels of activated Tregs post-treatment and the lack of response or in some cases even slight increase in tumor volume on MRI. This suggests that activated Tregs play a role in resistance to immune checkpoint blockade and that depleting activated Tregs could be a promising strategy for TNBC patients unresponsive to anti-PD1-based treatments. Of note, we cannot exclude that the lack of response or the increase of tumor volume observed by imaging was in part due to pseudoprogression. A growing body of literature analyzing anti-CTLA4 using in-vivo models indicates that anti-CTLA4 can deplete Tregs48. However, whether anti-CTLA4 can deplete Tregs in human tumors remains a matter of debate49. A recent study by van der Leun et al. in head and neck squamous cell carcinoma also demonstrated an increase in transitional CD8+ T cells and a decrease in CD137+ Tregs in responders after treatment with anti-PD1 and anti-CTLA4 therapy[50], indicating that this might be a consistent pattern across multiple tumor types.

After the results of the landmark trials in early stage TNBC that added PD1 blockade to standard neoadjuvant chemotherapy[1,3,51,52], our current data provide a rationale to further explore the following observations. First, we observed complete and near-complete pathological responses after only six weeks of treatment with ICI in patients with high TILs. This suggests that a subgroup of TNBC could be treated with chemo-free regimens if further research powered for long-term outcome analysis will confirm our results. More research is needed on the optimal selection strategy and treatment regimen, especially in view of the observed high endocrinopathy rate. It is tempting to speculate whether extending the six-week treatment period could result in higher pCR rates and thereby reach responses similar to outcomes obtained with chemo+IO. This can only be done if accompanied toxicity would not increase. However, it remains unknown whether pCR after immunotherapy has the same prognostic value as pCR after chemotherapy. Therefore, larger trials are needed to validate the pCR rate after short-term ICI alone and to determine if this results in excellent

survival rates, as seen in other cancers[53,54]. Moreover, pCR might not be the optimal endpoint since KEYNOTE-522 and GeparNUEVO have indicated that the benefit of PD1-blockade is not exclusively seen in patients with pCR[51,55]. Second, our exploratory clinical and translational data suggest that combination ICI is feasible and could potentially enhance the effects of PD1 blockade. However, the benefit-risk ratio of such combinations should always be carefully monitored. Third, establishing the feasibility of patient inclusion based on TIL opens the door for more immune biomarker-driven trials, which is particularly important in diseases like TNBC that include both inflamed and non-inflamed subtypes. The potential integration of additional inflammation analyses, for example, using IFNG gene expression on top of TILs as suggested by our data, may optimize patient selection, increase pCR rates for ICI-only approaches and could help treatment personalization in the future. Lastly, a substantial fraction of patients achieved ctDNA clearance after short-term ICI. Given the strong prognostic value of early ctDNA decrease, as shown by the I-SPY trial[56], future studies are needed to investigate the feasibility and reliability of TILs-informed patient inclusion and the potential of ctDNA-informed therapy adjustments.

Acknowledgements

We are grateful to the participants and their families for participating in the trial. We thank all supporting clinical trial staff, in particular nurse specialists and the Departments of Medical Oncology, Surgery, Radiology and Pathology of the participating centers. We thank the NKI trial lab for handling incoming blood samples. We are grateful to Annegien Broeks and the Core Facility of Molecular Pathology and Biobanking for the storage and handling of human tumor material and to the Genomics Core Facility for DNA and RNA sequencing. We acknowledge the supporting staff of the clinical trials of the Departments of Medical Oncology and the Triallab. We thank Chris Klaver and Maxime Duijst for blood sample experiments and the Flow Cytometry Facility the AKL for support in these experiments. We thank Bauke Stegenga from Bristol Myers Squibb for trial support and arranging supply of nivolumab and ipilimumab. R.S. is supported by the Breast Cancer Research Foundation (grant number 17-194). Research at the NKI is supported by institutional grants of the Dutch Cancer Society and of the Dutch Ministry of Health, Welfare and Sport. Research in the laboratory of M.K. is funded by the Netherlands Organization for Scientific Research (VIDI 09150172010043) and Victoria's Secret Global Fund for Women's Cancers Rising Innovator Research Grant, in Partnership with Pelotonia & AACR (23-30-73-KOK). Trial costs were supported by Bristol Myers Squibb. The funders had no role in study design, data collection or analysis, decision to publish or preparation of the manuscript.

Author Contributions

I.N. and O.I.I. contributed equally to this work as shared co-first authors. M.d.G., R.C.A.M.G. and N.A.M.B. contributed equally to this work as shared co-second authors. I.N. wrote the study protocol, coordinated trial procedures, performed wet lab experiments for single-cell RNA-Seq analyses, analyzed and interpreted clinical and translational data of the trial. O.I.I. designed, performed and interpreted computational analyses of the DNA, bulk and single-cell RNA sequencing data, analyzed and interpreted translational data. I.N., O.I.I., and M.K. wrote the paper. N.A.M.B., E.C. and H.G. were responsible for blood sample processing and analysis, supervised by K.E.d.V. and M.K., and H.G. designed the flow cytometry panel. M.d.G. performed the spatial analyses and helped with collection and analysis of clinical data. R.C.A.M.G. and A.L.R. coordinated trial procedures and collected clinical data for cohort C. B.B., J.G.H.T and M.C. performed bioinformatics analyses and contributed to their design. I.A.M.M. was the clinical projects manager. M.d.M. processed FFPE for IHC and isolated DNA and RNA from tissue biopsies. T.v.B. performed wet lab experiments for single-cell RNA-Seq analyses. M.L.-Y. performed the statistical analysis of the trial data. J.G.v.d.B., N.K.., H.M.H., K.v.d.V. and R.S. performed the TILs and histological scoring of the pathology slides. I.H. developed and performed double CD8-PD1 staining. R.M.M. and C.E.L. revised MRI scans and, together with colleagues, were involved in taking biopsies. Ek.K. organized the ctDNA experiments. Em.K., F.H.v.D., V.S., S.L., C.A.D., M.G.J.v.D., G.S.S., S.C.L. and M.K. were the main treating physicians. I.N., I.A.M.M, G.S.S., T.N.S., C.U.B., S.C.L. and M.K. wrote the trial protocol. H.M.H supervised the computational pathology analyses. L.F.A.W. and D.L. supervised computational analyses. M.K. was the principal investigator of the trial, supervised all the analyses presented in the paper and acquired funding. All authors edited and approved the paper.

Competing interests

I.N., O.I.I., M.d.G, R.C.A.M.G., N.A.M.B., A.L.R., H.G., B.B., J.G.H.T., I.A.M.M., M.d.M, T.v.B., M.C., E.C., M.L.-Y., K.v.d.V., J.G.v.d.B., I.H., N.K., C.E.L., F.H.v.D., V.S., S.L., Em.K., C.A.D., M.G.J.v.D., H.M.H. and D.L. have no competing interests to declare. R.M.M. reports research grants from Siemens Healhtineers, Bayer Healthcare, Screenpoint Medical, Beckton & Dickinson, PA Imaging, Lunit and Koning, and is an advisory board member for Screenpoint, Bayer, Siemens and Guerbet, all outside the scope of this work. Ek.K. is an employee of Natera, Inc. G.S.S. reports research funding to the institute from Merck, Agendia, AstraZeneca, Roche and Novartis and a consulting role for Novartis, Seattle Genetics and Biovica, outside the submitted work. S.C.L. reports research funding to the institute from Roche/Genentech, AstraZeneca, BMS, Tesaro, Merck, Immunomedics, Eurocept Pharmaceuticals, Agendia and Novartis and a consulting role and travel grant from Daiichi Sankyo, outside this work. C.U.B. has received research grants from Novartis, BMS and NanoString, is a paid advisory board member for BMS, MSD, Roche, Novartis, GlaxoSmithKline, AstraZeneca, Pfizer, Lilly, GenMab and Pierre Fabre and holds ownership interest in Uniti Card, Neon Therapeutics and Forty Seven, all outside this submitted work. K.E.d.V. reports research funding from Roche and is a consultant for Macomics, outside the scope of this work. R.S. reports non-financial support from Merck and Bristol Myers Squibb (BMS), research support from Merck, Puma Biotechnology and Roche and personal fees from Roche, BMS and Exact Sciences for advisory boards, all outside the scope of this paper. L.F.A.W. reports funding to the institute from Genmab BV. V.C.G.T.-H. reports research funding to the institute from Roche, Eisai, Pfizer, Novartis, Lilly, Daiichi Sankyo/AstraZeneca and Gilead Sciences, a consulting role from Pfizer, Lilly, Accord Healthcare and Novartis and honoraria from Novartis, Roche, Lilly and AstraZeneca, all outside this submitted work. T.N.S. is advisor for Allogene Therapeutics, Asher Bio, Merus, Neogene Therapeutics, and Scenic Biotech; is a stockholder in Allogene Therapeutics, Asher Bio, Cell Control, Celsius, Merus, and Scenic Biotech; and is venture partner at Third Rock Ventures, all outside of the current work. M.K. reports research funding to the institute from BMS, Roche and AstraZeneca/MedImmune and an advisory role/speakers' fee (all compensated to the institute) for Alderaan, BMS, Domain Therapeutics, Medscape, Roche, MSD and Daiichi Sankyo, outside the submitted work. Natera provided non-financial support to this study.

Supplementary Material

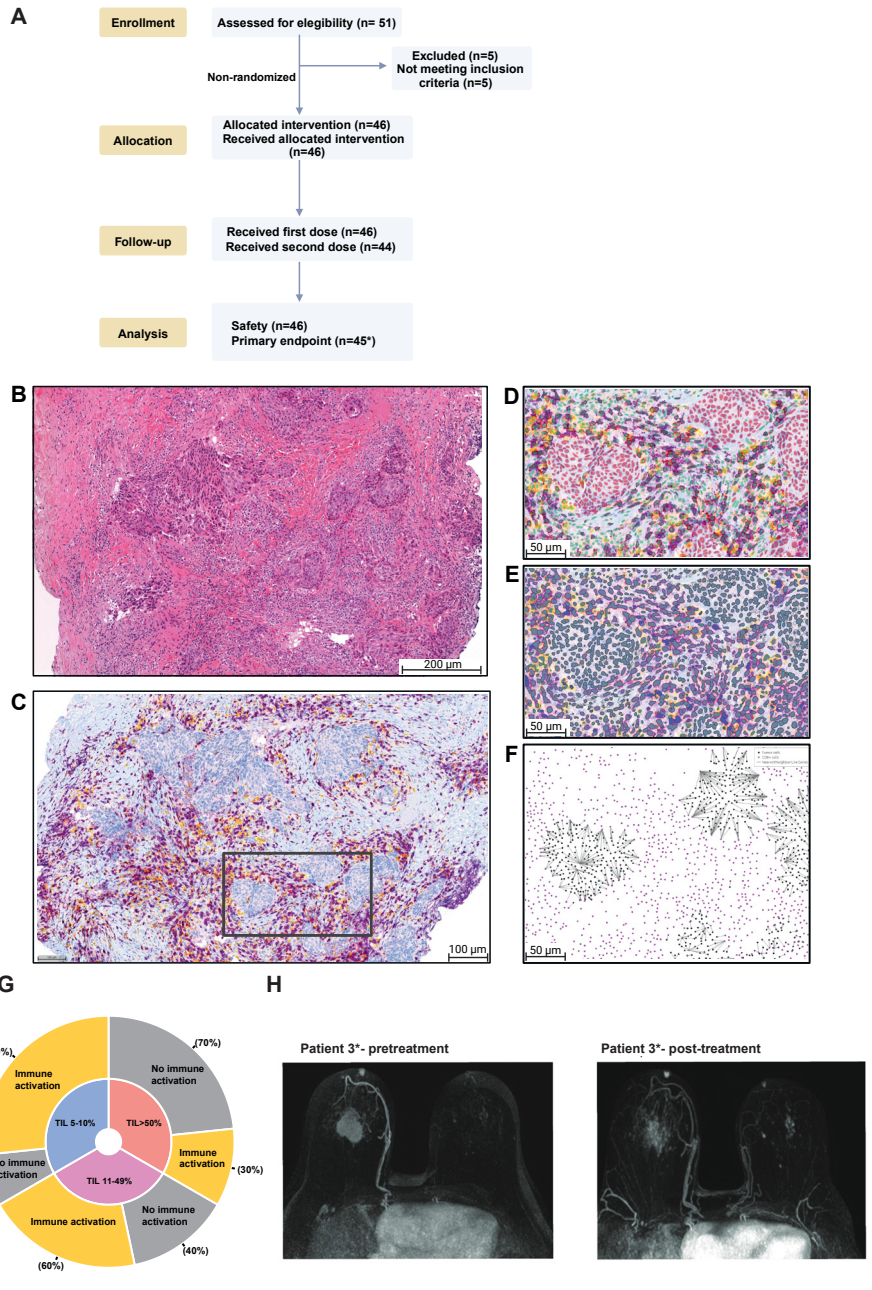

◀◀◀ ***Extended Data Fig. 1 IHC CD8 + T cell analysis. A.*** *CONSORT Flow Diagram. Consort diagram of patients eligible, recruited, numbers followed up and included in analysis. *max 15 patients per cohort analyzed for primary end point.* ***B.*** *H&E-stained image, corresponding to CD8/PD-1 stained tissue under* ***C. C.*** *Representative example of a CD8/PD-1 double-stained tissue (haematoxylin = blue, PD-1 = yellow, CD8 = purple).* ***D.*** *Representative example of the performance of the AI-based tumor cell classifier Tumor classification (red) and nontumor cells (green).* ***E.*** *Example of cell segmentation and tumor phenotype assignment. Cell with purple border = CD8+ cell, yellow border = PD-1+ cell, orange border = PD-1 + CD8+ cell.* ***F.*** *Corresponding distance analysis in the same tissue area as under* ***D*** *and* ***E.*** *The grey lines represent the shortest distance from a tumor cell to its nearest CD8 + T cell.* ***G.*** *Proportions of patients reaching immune activation stratified according to TIL levels at inclusion in cohorts A and B. 10 patients had 5–10% TILs, 10 patients 11–49% TILs and 10 patients had 50% or more TILs.* ***H.*** *Pretreatment and post-treatment MRI images of patient #3 with a pathological complete response (pCR) at surgery after ICI only (cT2N0, ypT0N0). Figure* ***A*** *was created with BioRender.com. In* ***A-B****, one biopsy was analyzed per patient.*

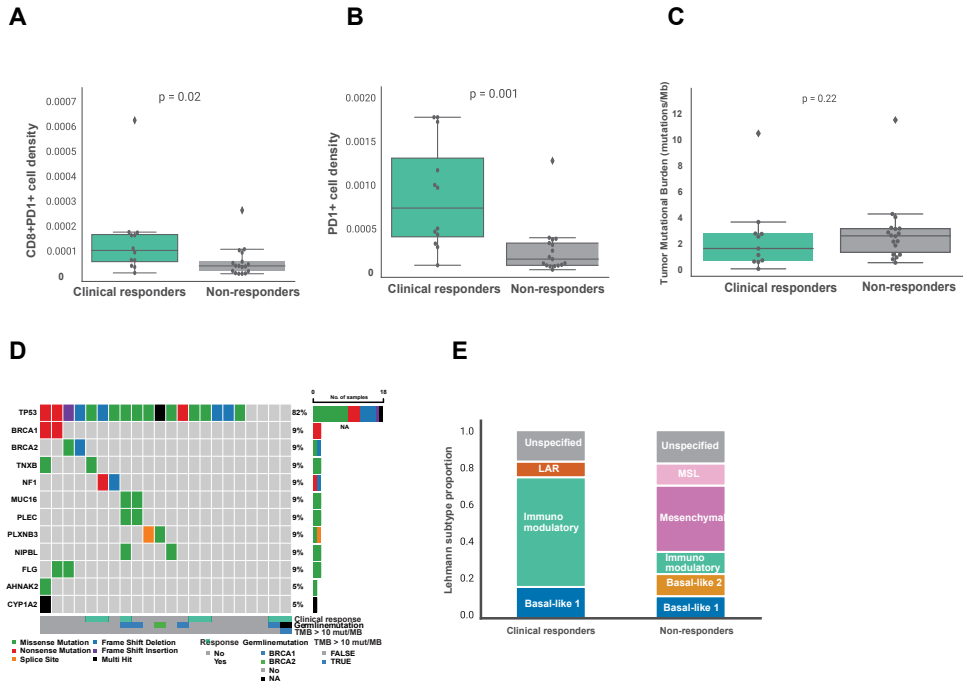

Extended Data Fig. 2 Baseline tumor microenvironment features and genomic profile of cohorts A and B. A. *PD-1 + CD8 + T cell density in pretreatment biopsies of patients with and without who did and did not experience clinical response in cohorts A and B. n = 31 patients.* ***B.*** *PD-1+ cell density in pretreatment biopsies of patients with and without who did and did not experience clinical response in cohorts A and B. n = 31 patients.* ***C.*** *Tumor mutational burden (TMB) in pretreatment biopsies of patients with and without clinical response in cohorts A and B. n = 30 patients. Boxplots display a minimum (Q0), a maximum (Q4), a median (Q2) and the interquartile range. Data were analyzed by a two-sided Mann–Whitney test.* ***D.*** *Oncoplot of TMB (mutations per megabase (Mb)) and top mutated genes in cohorts A and B.* ***E.*** *Proportions of Lehmann et al. subtypes33 in patients with and without clinical response in cohorts A and B. MSL, mesenchymal stem-like; LAR, luminal androgen receptor.*

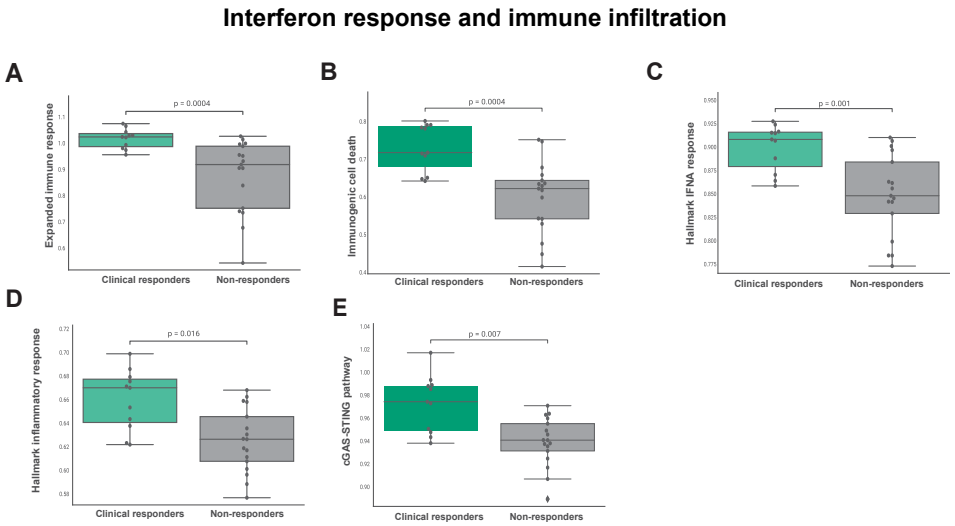

◀◀◀ ***Extended Data Fig. 3 Gene signatures in pretreatment biopsies associated with clinical response in cohorts A and B. A–L****. Gene set expression scores in pretreatment biopsies of patients with and without clinical response in cohorts A and B. n = 28 patients.* ***A.*** *Expanded immune signature from Ayers et al.56* ***B.*** *Immunogenic cell death signature57.* ***C.*** *Hallmark IFNA response gene set.* ***D.*** *Hallmark inflammatory response gene set.* ***E.*** *cGAS-STING pathway gene set58.* ***F.*** *Effector CD8 + T cell gene set59.* ***G.*** *Exhausted T cell gene set59.* ***H.*** *Checkpoint molecules gene set59.* ***I.*** *Naive T cell gene set60.* ***J.*** *Tertiary lymphoid structures gene set61.* ***K.*** *Hallmark TGF-beta signaling gene set.* ***L.*** *Hallmark Notch signaling. In* ***A–L****, boxplots display a minimum (Q0), a maximum (Q4), a median (Q2) and the interquartile range. P values were derived using a two-sided Mann–Whitney test. Reported p values were significant after Benjamini–Hochberg (FDR) correction at 10% significance level.*

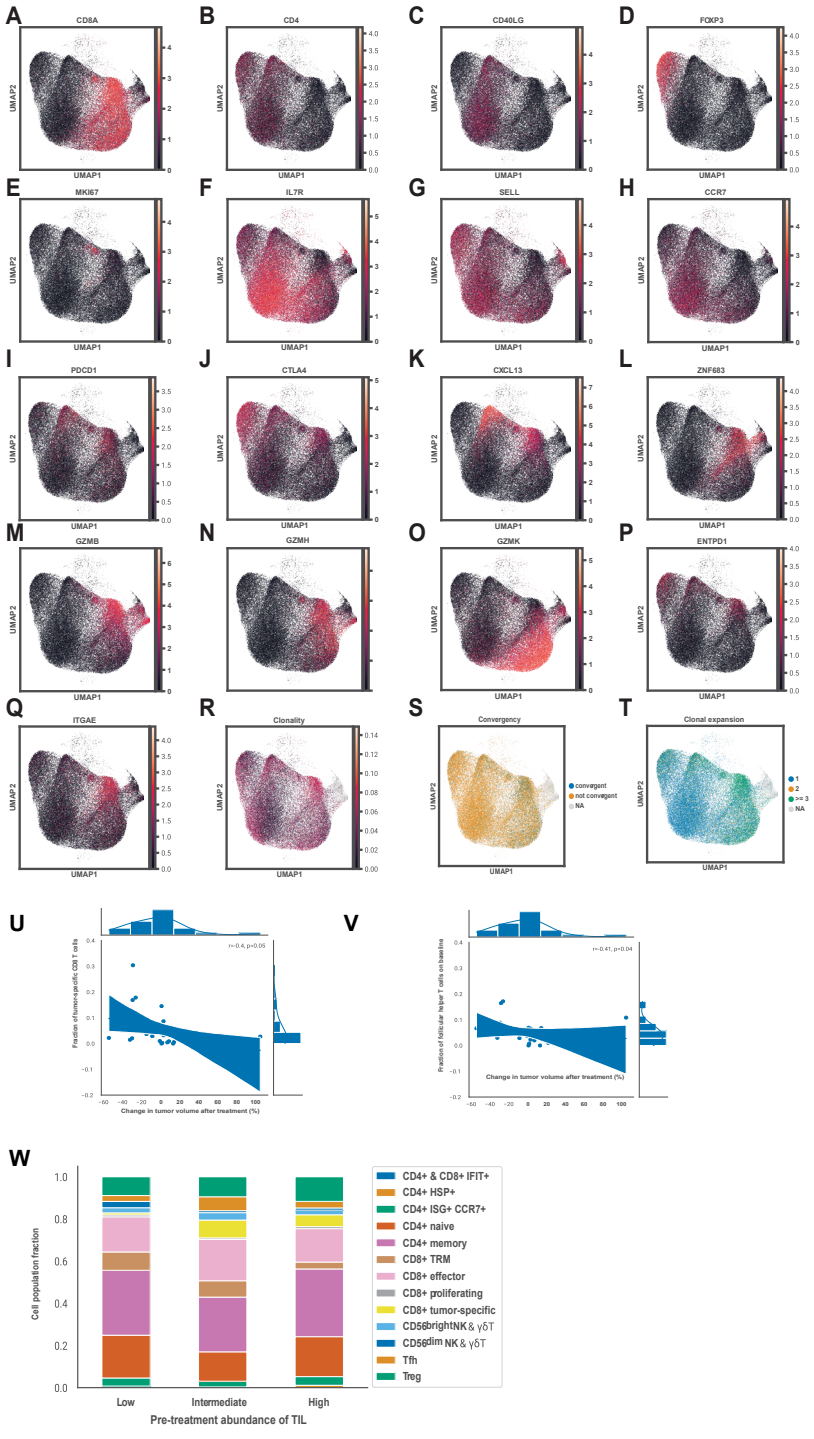

◀◀◀ ***Extended Data Fig. 4 Single-cell RNA-Seq pretreatment tumor microenvironment profile of the cohorts A and B. A-Q****. UMAP representations of the marker gene expression in the dataset.* ***A.*** *CD8A.* ***B.*** *CD4.* ***C.*** *CD40LG* ***D.*** *FOXP3* ***E.*** *MKI67* ***F.*** *IL7R.* ***G.*** *SELL.* ***H.*** *CCR7.* ***I.*** *PDCD1.* ***J.*** *CTLA4.* ***K.*** *CXCL13.* ***L.*** *ZNF683.* ***M.*** *GZMB.* ***N.*** *GZMH.* ***O.*** *GZMK.* ***P.*** *ENTPD1.* ***Q.*** *ITGAE.* ***R.*** *UMAP representation of the T cell clonality in the dataset.* ***S.*** *UMAP representation of the T cell clone convergence in the dataset.* ***T.*** *UMAP representation of the T cell clonal expansion in the dataset.* ***U.*** *Fractions of tumor-reactive CD8 + T cells relative to all T cells in pretreatment biopsies of patients based on single-cell RNA-Seq data in relation to the change in tumor volume after treatment based on RECIST 1.1 in cohorts A and B.* ***V.*** *Fractions of Tfh cells relative to all T cells in pretreatment biopsies of patients based on single-cell RNA-Seq data in relation to the change in tumor volume after treatment based on RECIST 1.1 in cohorts A and B.* ***W.*** *Fractions of different T cell clusters relative to all T cells based on single-cell RNA-Seq data in pretreatment biopsies of patients who had low (5–10%), intermediate (11–49%) and high (>=50%) presence of tumor-infiltrating lymphocytes before treatment in cohorts A and B. In* ***U-V****, correlation was estimated with Spearman's rank correlation coefficient, two-sided, with 95% confidence interval for the regression estimate.*

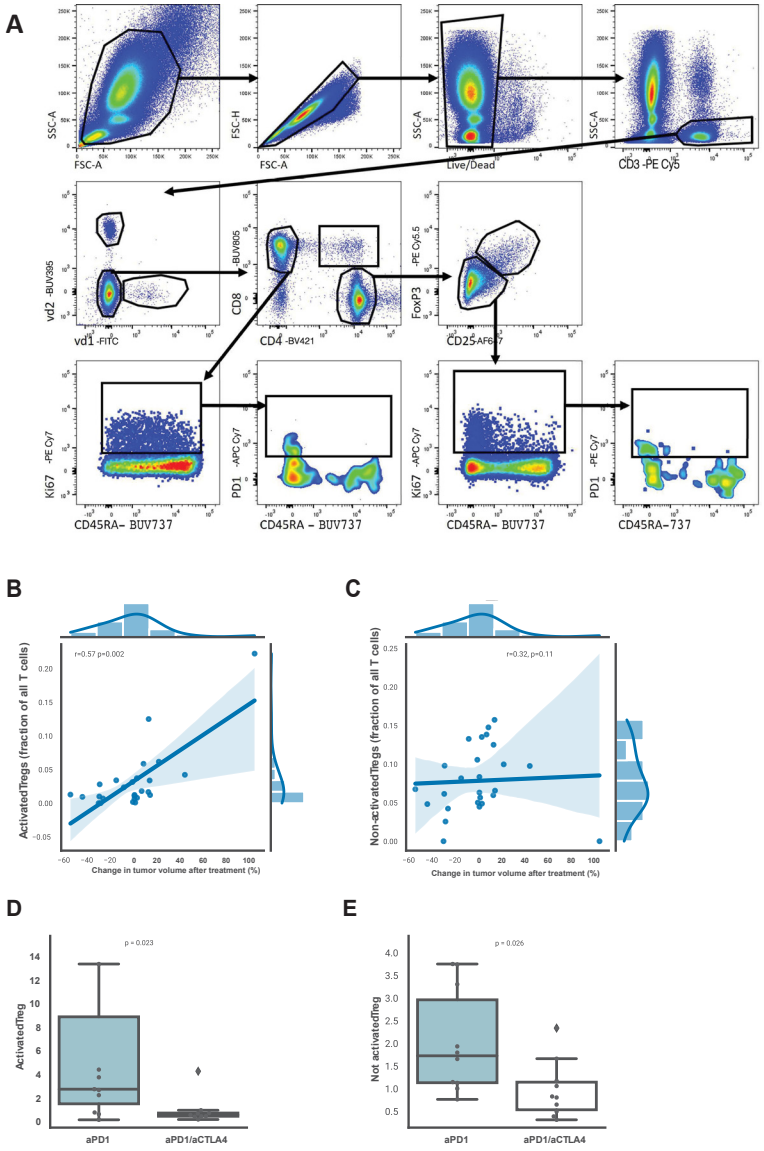

Extended Data Fig. 5 Gating strategy used for the flow cytometry data analysis and activated and non-activated Tregs in cohorts A and B. A. *Gating strategy used for the flow cytometry data analysis.* ***B.*** *Spearman correlation between fraction of activated Tregs and the change in tumor size on MRI (%).* ***C.*** *Spearman correlation between fraction of non-activated Tregs and the change in tumor size on MRI (%). Activated Tregs were defined as activated by the expression of CD137.* ***D–E.*** *Fold change in activated (**D**) and non-activated (**E**) Tregs after anti-PD-1 or anti-PD-1/anti-CTLA4 therapy. n = 22 patients. In **B-C**, correlation was estimated with Spearman's rank correlation coefficient, two-sided, with 95% confidence interval for the regression estimate. In **D–E**, boxplots display a minimum (Q0), a maximum (Q4), a median (Q2) and the interquartile range. P values were derived using a two-sided Mann–Whitney test.*

***Extended Data Table 1. Full lis**t of adverse events.*

	A: Nivolumab (N=16)			B: Nivo+Ipi 4 wks (N=15)			Nivo+Ipi 6 wks (N=15)		
Adverse event	Grade 1-2	Grade 3	Grade 4	Grade 1-2	Grade 3	Grade 4	Grade 1-2	Grade 3	Grade 4
Worst grade adverse event per patient	12 (75%)	1 (6%)	0 (0%)	13 (86.6%)	1 (7%)	1 (7%)	9 (60%)	5 (33%)	1 (7%)
Endocrine disorders									
Thyroid dysfunction	7 (44%)	1 (6%)[a]	0 (0%)	9 (60%)	0 (0%)	0 (0%)	9 (60%)	0 (0%)	0 (0%)
Hypothyroidism	6 (38%)	0 (0%)	0 (0%)	7 (47%)	0 (0%)	0 (0%)	6 (40%)	0 (0%)	0 (0%)
Hyperthyroidism	4 (25%)	1 (6%)	0 (0%)	8 (53%)	0 (0%)	0 (0%)	9 (60%)	0 (0%)	0 (0%)
Adrenal insufficiency*	1 (6%)	0 (0%)	0 (0%)	1 (7%)	1 (7%)[b]	0 (0%)	2 (13%)	1 (7%)[f]	0 (0%)
Diabetes Mellitus (Immune mediated)	0 (0%)	0 (0%)	0 (0%)	0 (0%)	0 (0%)	1 (7%)[b]	0 (0%)	0 (0%)	0 (0%)
Gastro-intestinal									
Abdominal pain	0 (0%)	0 (0%)	0 (0%)	1 (7%)	0 (0%)	0 (0%)	0 (0%)	0 (0%)	0 (0%)
Diarrhea	0 (0%)	0 (0%)	0 (0%)	1 (7%)	0 (0%)	0 (0%)	1 (7%)	0 (0%)	0 (0%)
Nausea	1 (6%)	0 (0%)	0 (0%)	0 (0%)	0 (0%)	0 (0%)	2 (13%)	0 (0%)	0 (0%)
Colitis	0 (0%)	0 (0%)	0 (0%)	0 (0%)	0 (0%)	0 (0%)	0 (0%)	1 (7%)[g]	0 (0%)
Rectal Ulcer	0 (0%)	0 (0%)	0 (0%)	1 (7%)	0 (0%)	0 (0%)	0 (0%)	0 (0%)	0 (0%)
Laboratory test									
Elevated liver function tests	0 (0%)	0 (0%)	0 (0%)	1 (7%)	0 (0%)	0 (0%)	7 (47%)	0 (0%)	0 (0%)
Hyperphosphatemia	0 (0%)	0 (0%)	0 (0%)	0 (0%)	0 (0%)	0 (0%)	1 (7%)	0 (0%)	0 (0%)
Hypophosphatemia	0 (0%)	0 (0%)	0 (0%)	0 (0%)	0 (0%)	0 (0%)	1 (7%)	0 (0%)	0 (0%)
Lymphocyte count decreased	0 (0%)	0 (0%)	0 (0%)	0 (0%)	0 (0%)	0 (0%)	1 (7%)	0 (0%)	0 (0%)
Troponine T increased	0 (0%)	0 (0%)	0 (0%)	0 (0%)	0 (0%)	0 (0%)	1 (7%)	0 (0%)	0 (0%)
Immune related hepatitis	0 (0%)	0 (0%)	0 (0%)	2 (13%)	0 (0%)	0 (0%)	0 (0%)	2(13%)[c,d]	1 (7%)[h]
Musculo-skeletal									
Arthralgia	3 (19%)	0 (0%)	0 (0%)	0 (0%)	0 (0%)	0 (0%)	0 (0%)	0 (0%)	0 (0%)
Myalgia	2 (12%)	0 (0%)	0 (0%)	0 (0%)	0 (0%)	0 (0%)	0 (0%)	0 (0%)	0 (0%)
Back pain	1 (6%)	0 (0%)	0 (0%)	0 (0%)	0 (0%)	0 (0%)	0 (0%)	0 (0%)	0 (0%)
Immune mediated polymyalgia rheumatica	0 (0%)	0 (0%)	0 (0%)	0 (0%)	0 (0%)	0 (0%)	1 (7%)	0 (0%)	0 (0%)
Cardiopulmonal									
Chest-pain	0 (0%)	0 (0%)	1 (6%)[a]	0 (0%)	0 (0%)	0 (0%)	0 (0%)	0 (0%)	0 (0%)
Ejection fraction decreased #	1 (6%)	0 (0%)	0 (0%)	0 (0%)	0 (0%)	0 (0%)	0 (0%)	0 (0%)	0 (0%)
Pneumonitis	0 (0%)	0 (0%)	0 (0%)	0 (0%)	0 (0%)	0 (0%)	1 (7%)	1 (7%)[e]	0 (0%)
Upper respiratory infection	0 (0%)	0 (0%)	0 (0%)	1 (7%)	0 (0%)	0 (0%)	0 (0%)	0 (0%)	0 (0%)
Cough	0 (0%)	0 (0%)	0 (0%)	1 (7%)	0 (0%)	0 (0%)	0 (0%)	0 (0%)	0 (0%)
Other									
Allergic reaction	1 (6%)	0 (0%)	0 (0%)	0 (0%)	0 (0%)	0 (0%)	0 (0%)	0 (0%)	0 (0%)
Anemia	0 (0%)	0 (0%)	0 (0%)	0 (0%)	0 (0%)	0 (0%)	3 (20%)	0 (0%)	0 (0%)
Dry eye	1 (6%)	0 (0%)	0 (0%)	0 (0%)	0 (0%)	0 (0%)	1 (7%)	0 (0%)	0 (0%)
Dry mouth	2 (12%)	0 (0%)	0 (0%)	0 (0%)	0 (0%)	0 (0%)	4 (27%)	0 (0%)	0 (0%)
Dry skin	1 (6%)	0 (0%)	0 (0%)	2 (13%)	0 (0%)	0 (0%)	1 (7%)	0 (0%)	0 (0%)
Fatigue	1 (6%)	0 (0%)	0 (0%)	1 (7%)	0 (0%)	0 (0%)	1 (7%)	0 (0%)	0 (0%)
Flu like symptoms	2 (12%)	0 (0%)	0 (0%)	0 (0%)	0 (0%)	0 (0%)	1 (7%)	0 (0%)	0 (0%)
Headache	2 (12%)	0 (0%)	0 (0%)	1 (7%)	0 (0%)	0 (0%)	0 (0%)	0 (0%)	0 (0%)
Infusion related reaction	2 (12%)	0 (0%)	0 (0%)	1 (7%)	0 (0%)	0 (0%)	1 (7%)	0 (0%)	0 (0%)
Skin rash	2 (12%)	0 (0%)	0 (0%)	1 (7%)	0 (0%)	0 (0%)	4 (27%)	0 (0%)	0 (0%)
Photosensitivity	1 (6%)	0 (0%)	0 (0%)	0 (0%)	0 (0%)	0 (0%)	0 (0%)	0 (0%)	0 (0%)
Itching	0 (0%)	0 (0%)	0 (0%)	1 (7%)	0 (0%)	0 (0%)	1 (7%)	0 (0%)	0 (0%)
Cervical lymphadenopathy	0 (0%)	0 (0%)	0 (0%)	0 (0%)	0 (0%)	0 (0%)	1 (7%)	0 (0%)	0 (0%)

Extended Data Table 2. Antibody overview

Human flow cytometry antibodies					
Antigen	**Fluorochrome**	**Clone**	**Dilution**	**Company**	**Catalogue number**
CD3	PE Cy5	UCHT1	1:200	BD Bioscience	555334
CD4	BV421	RPA-T4	1:100	BD Bioscience	562424
CD8	BUV805	SK1	1:200	BD Bioscience	612754
Pan γδ TCR	PE	11F2	1:100	BD Bioscience	555717
vδ1	FITC	TS8.2	1:100	Thermofisher	TCR2730
vδ2	BUV395	B6	1:100	BD Bioscience	748582
FoxP3	PE Cy5.5	FJK-16s	1:50	Thermofisher	35-5773-82
CCR7	APC R700	150503	1:50	BD Bioscience	565868
CD45RA	BUV737	HI100	1:400	BD Bioscience	612846
CD25	AF647	BC96	1:100	BioLegend	302618
PD-1	APC Cy7	EH12.2H7	1:100	BioLegend	329922
CTLA-4	PE CF594	BNI3	1:200	BD Bioscience	562742
IL-17	PerCP Cy5.5	N49-653	1:50	BD Bioscience	560799
IFNγ	BV785	4S.B3	1:200	BioLegend	502542
TNFα	PE Cy7	Mab11	1:400	BioLegend	502930
CD27	BV786	L128	1:100	BD Bioscience	563327
TIGIT	PerCP Cy5.5	A151536	1:100	BioLegend	372718
Ki-67	PE Cy7	B56	1:50	BD Bioscience	561283
CTLA-4	PE CF594	PE/Dazzle594	1:200	BioLegend	369616

References

1. Schmid, P. *et al.* Event-free Survival with Pembrolizumab in Early Triple-Negative Breast Cancer. *N. Engl. J. Med.* **386**, 556–567 (2022).
2. Loibl, S. *et al.* A randomised phase II study investigating durvalumab in addition to an anthracycline taxane-based neoadjuvant therapy in early triple-negative breast cancer: clinical results and biomarker analysis of GeparNuevo study. *Ann. Oncol.* **30**, 1279–1288 (2019).
3. Mittendorf, E. A. *et al.* Neoadjuvant atezolizumab in combination with sequential nab-paclitaxel and anthracycline-based chemotherapy versus placebo and chemotherapy in patients with early-stage triple-negative breast cancer (IMpassion031): a randomised, double-blind, phase 3 trial. *Lancet* **396**, 1090–1100 (2020).
4. Schmid, P. *et al.* Pembrolizumab for Early Triple-Negative Breast Cancer. *N. Engl. J. Med.* **382**, 810–821 (2020).
5. Gustafson, C. E. *et al.* Immune cell repertoires in breast cancer patients after adjuvant chemotherapy. *JCI Insight* **5**, (2020).
6. Mariniello, A. *et al.* Platinum-based chemotherapy attenuates the effector response of CD8 T cells to concomitant PD-1 blockade. *Clin. Cancer Res.* (2023) doi:10.1158/1078-0432.CCR-23-1316.
7. Blank, C. U. *et al.* Neoadjuvant versus adjuvant ipilimumab plus nivolumab in macroscopic stage III melanoma. *Nat. Med.* **24**, 1655–1661 (2018).
8. Cascone, T. *et al.* Neoadjuvant nivolumab or nivolumab plus ipilimumab in operable non-small cell lung cancer: the phase 2 randomized NEOSTAR trial. *Nat. Med.* **27**, 504–514 (2021).
9. Vos, J. L. *et al.* Neoadjuvant immunotherapy with nivolumab and ipilimumab induces major pathological responses in patients with head and neck squamous cell carcinoma. *Nat. Commun.* **12**, 7348 (2021).
10. van Dijk, N. *et al.* Preoperative ipilimumab plus nivolumab in locoregionally advanced urothelial cancer: the NABUCCO trial. *Nat. Med.* **26**, 1839–1844 (2020).
11. Chalabi, M. *et al.* Neoadjuvant immunotherapy in locally advanced mismatch repair-deficient colon cancer. *N. Engl. J. Med.* **390**, 1949–1958 (2024).
12. Bianchini, G., De Angelis, C., Licata, L. & Gianni, L. Treatment landscape of triple-negative breast cancer - expanded options, evolving needs. *Nat. Rev. Clin. Oncol.* **19**, 91–113 (2022).
13. Gianni, L., Huang, C., Egle, D. & Bermejo, B. … or without atezolizumab followed by an adjuvant anthracycline regimen in high-risk triple negative breast cancer (TNBC): NeoTRIP Michelangelo randomized study. *Annals of* (2023).
14. Rozeman, E. A. *et al.* Identification of the optimal combination dosing schedule of neoadjuvant ipilimumab plus nivolumab in macroscopic stage III melanoma (OpACIN-neo): a multicentre, phase 2, randomised, controlled trial. *Lancet Oncol.* **20**, 948–960 (2019).
15. Robert, C. *et al.* Ipilimumab plus dacarbazine for previously untreated metastatic melanoma. *N. Engl. J. Med.* **364**, 2517–2526 (2011).
16. Hodi, F. S. *et al.* Improved survival with ipilimumab in patients with metastatic melanoma. *N. Engl. J. Med.* **363**, 711–723 (2010).
17. Chalabi, M. *et al.* Neoadjuvant immunotherapy leads to pathological responses in MMR-proficient and MMR-deficient early-stage colon cancers. *Nat. Med.* **26**, 566–576 (2020).
18. Adams, S. *et al.* A Multicenter Phase II Trial of Ipilimumab and Nivolumab in Unresectable or Metastatic Metaplastic Breast Cancer: Cohort 36 of Dual Anti-CTLA-4 and Anti-PD-1 Blockade in Rare Tumors (DART, SWOG S1609). *Clin. Cancer Res.* **28**, 271–278 (2022).
19. de Jong, V. M. T. *et al.* Prognostic Value of Stromal Tumor-Infiltrating Lymphocytes in Young, Node-Negative, Triple-Negative Breast Cancer Patients Who Did Not Receive (neo)Adjuvant Systemic Therapy. *J. Clin. Oncol.* **40**, 2361–2374 (2022).
20. Loi, S. *et al.* Tumor-Infiltrating Lymphocytes and Prognosis: A Pooled Individual Patient Analysis of Early-Stage Triple-Negative Breast Cancers. *J. Clin. Oncol.* **37**, 559–569 (2019).
21. Denkert, C. *et al.* Tumour-infiltrating lymphocytes and prognosis in different subtypes of breast cancer: a pooled analysis of 3771 patients treated with neoadjuvant therapy. *Lancet Oncol.* **19**, 40–50 (2018).
22. Salgado, R. *et al.* The evaluation of tumor-infiltrating lymphocytes (TILs) in breast cancer: recommendations by an International TILs Working Group 2014. *Ann. Oncol.* **26**, 259–271 (2015).

23. Park, J. H. *et al.* Prognostic value of tumor-infiltrating lymphocytes in patients with early-stage triple-negative breast cancers (TNBC) who did not receive adjuvant chemotherapy. *Ann. Oncol.* **30**, 1941–1949 (2019).
24. Loi, S. *et al.* Association Between Biomarkers and Clinical Outcomes of Pembrolizumab Monotherapy in Patients With Metastatic Triple-Negative Breast Cancer: KEYNOTE-086 Exploratory Analysis. *JCO Precis Oncol* **7**, e2200317 (2023).
25. Voorwerk, L. *et al.* Publisher Correction: Immune induction strategies in metastatic triple-negative breast cancer to enhance the sensitivity to PD-1 blockade: the TONIC trial. *Nat. Med.* **25**, 1175 (2019).
26. Blank, C. U. *et al.* Neoadjuvant Nivolumab and Ipilimumab in Resectable Stage III Melanoma. *N. Engl. J. Med.* (2024) doi:10.1056/NEJMoa2402604.
27. Simon, R. Optimal two-stage designs for phase II clinical trials. *Control. Clin. Trials* **10**, 1–10 (1989).
28. Tumeh, P. C. *et al.* PD-1 blockade induces responses by inhibiting adaptive immune resistance. *Nature* **515**, 568–571 (2014).
29. Higgs, B. W. *et al.* Interferon Gamma Messenger RNA Signature in Tumor Biopsies Predicts Outcomes in Patients with Non-Small Cell Lung Carcinoma or Urothelial Cancer Treated with Durvalumab. *Clin. Cancer Res.* **24**, 3857–3866 (2018).
30. Eisenhauer, E. A. *et al.* New response evaluation criteria in solid tumours: revised RECIST guideline (version 1.1). *Eur. J. Cancer* **45**, 228–247 (2009).
31. Menzies, A. M. *et al.* Pathological response and survival with neoadjuvant therapy in melanoma: a pooled analysis from the International Neoadjuvant Melanoma Consortium (INMC). *Nat. Med.* **27**, 301–309 (2021).
32. Verschoor, Y. L. *et al.* Neoadjuvant atezolizumab plus chemotherapy in gastric and gastroesophageal junction adenocarcinoma: the phase 2 PANDA trial. *Nat. Med.* (2024) doi:10.1038/s41591-023-02758-x.
33. Lehmann, B. D. *et al.* Refinement of Triple-Negative Breast Cancer Molecular Subtypes: Implications for Neoadjuvant Chemotherapy Selection. *PLoS One* **11**, e0157368 (2016).
34. Oliveira, G. *et al.* Phenotype, specificity and avidity of antitumour CD8 T cells in melanoma. *Nature* **596**, 119–125 (2021).
35. Lowery, F. J. *et al.* Molecular signatures of antitumor neoantigen-reactive T cells from metastatic human cancers. *Science* **375**, 877–884 (2022).
36. van Gulijk, M. *et al.* PD-L1 checkpoint blockade promotes regulatory T cell activity that underlies therapy resistance. *Sci Immunol* **8**, eabn6173 (2023).
37. Geurts, V. C. M. *et al.* Tumor-Infiltrating Lymphocytes in Patients With Stage I Triple-Negative Breast Cancer Untreated With Chemotherapy. *JAMA Oncol* (2024) doi:10.1001/jamaoncol.2024.1917.
38. Unger, J. M. *et al.* Sex Differences in Risk of Severe Adverse Events in Patients Receiving Immunotherapy, Targeted Therapy, or Chemotherapy in Cancer Clinical Trials. *J. Clin. Oncol.* **40**, 1474–1486 (2022).
39. Nguyen, V. P. *et al.* A pilot study of neoadjuvant nivolumab, ipilimumab and intralesional oncolytic virotherapy for HER2-negative breast cancer. *Cancer Res. Commun.* (2023) doi:10.1158/2767-9764.crc-23-0145.
40. Maher, V. E. *et al.* Analysis of the Association Between Adverse Events and Outcome in Patients Receiving a Programmed Death Protein 1 or Programmed Death Ligand 1 Antibody. *J. Clin. Oncol.* **37**, 2730–2737 (2019).
41. Eggermont, A. M. M. *et al.* Association Between Immune-Related Adverse Events and Recurrence-Free Survival Among Patients With Stage III Melanoma Randomized to Receive Pembrolizumab or Placebo: A Secondary Analysis of a Randomized Clinical Trial. *JAMA Oncol* **6**, 519–527 (2020).
42. Beaufils, M. *et al.* Dysthyroidism during immune checkpoint inhibitors is associated with improved overall survival in adult cancers: data mining of 1385 electronic patient records. *J Immunother Cancer* **11**, (2023).
43. Street, S. *et al.* The positive effect of immune checkpoint inhibitor-induced thyroiditis on overall survival accounting for immortal time bias: a retrospective cohort study of 6596 patients. *Ann. Oncol.* **32**, 1050–1051 (2021).
44. Groha, S. *et al.* Germline variants associated with toxicity to immune checkpoint blockade. *Nat. Med.* **28**, 2584–2591 (2022).
45. Reijers, I. L. M. *et al.* IFN-γ signature enables selection of neoadjuvant treatment in patients with stage III melanoma. *J. Exp. Med.* **220**, (2023).

46. Bullock, A. J. *et al.* Botensilimab plus balstilimab in relapsed/refractory microsatellite stable metastatic colorectal cancer: a phase 1 trial. *Nat. Med.* (2024) doi:10.1038/s41591-024-03083-7.
47. Blomberg, O. S. *et al.* Neoadjuvant immune checkpoint blockade triggers persistent and systemic T activation which blunts therapeutic efficacy against metastatic spread of breast tumors. *Oncoimmunology* **12**, 2201147 (2023).
48. Simpson, T. R. *et al.* Fc-dependent depletion of tumor-infiltrating regulatory T cells co-defines the efficacy of anti-CTLA-4 therapy against melanoma. *J. Exp. Med.* **210**, 1695–1710 (2013).
49. Sharma, A. *et al.* Anti-CTLA-4 Immunotherapy Does Not Deplete FOXP3+ Regulatory T Cells (Tregs) in Human Cancers. *Clin. Cancer Res.* **25**, 1233–1238 (2019).
50. van der Leun, A. M. *et al.* Dual immune checkpoint blockade induces analogous alterations in the dysfunctional CD8+ T cell and activated Treg compartment. *Cancer Discov.* (2023) doi:10.1158/2159-8290.CD-22-0851.
51. Loibl, S. *et al.* Neoadjuvant durvalumab improves survival in early triple-negative breast cancer independent of pathological complete response. *Ann. Oncol.* **33**, 1149–1158 (2022).
52. Pathologic complete response (pCR) to neoadjuvant treatment with or without atezolizumab in triple-negative, early high-risk and locally advanced breast cancer: NeoTRIP Michelangelo randomized study. *Ann. Oncol.* **33**, 534–543 (2022).
53. Chalabi, M., Verschoor, Y. L. & Van den Berg, J. LBA7 Neoadjuvant immune checkpoint inhibition in locally advanced MMR-deficient colon cancer: The NICHE-2 study. *Annals of* (2022).
54. Rozeman, E. A. *et al.* Survival and biomarker analyses from the OpACIN-neo and OpACIN neoadjuvant immunotherapy trials in stage III melanoma. *Nat. Med.* **27**, 256–263 (2021).
55. Pusztai, L. *et al.* Event-free survival by residual cancer burden with pembrolizumab in early-stage TNBC: exploratory analysis from KEYNOTE-522. *Ann. Oncol.* **35**, 429–436 (2024).
56. Magbanua, M. J. M. *et al.* Circulating tumor DNA in neoadjuvant-treated breast cancer reflects response and survival. *Ann. Oncol.* **32**, 229–239 (2021).
57. Ayers, M. *et al.* IFN-γ-related mRNA profile predicts clinical response to PD-1 blockade. *J. Clin. Invest.* **127**, 2930–2940 (2017).
58. Garg, A. D., De Ruysscher, D. & Agostinis, P. Immunological metagene signatures derived from immunogenic cancer cell death associate with improved survival of patients with lung, breast or ovarian malignancies: A large-scale meta-analysis. *Oncoimmunology* **5**, e1069938 (2016).
59. Hu, X. E. *et al.* Clinical and biological heterogeneities in triple-negative breast cancer reveals a non-negligible role of HER2-low. *Breast Cancer Res.* **25**, 34 (2023).
60. Bagaev, A. *et al.* Conserved pan-cancer microenvironment subtypes predict response to immunotherapy. *Cancer Cell* **39**, 845–865.e7 (2021).
61. Gangaev, A. *et al.* Identification and characterization of a SARS-CoV-2 specific CD8+ T cell response with immunodominant features. *Nat. Commun.* **12**, 1–14 (2021).
62. Cabrita, R. *et al.* Tertiary lymphoid structures improve immunotherapy and survival in melanoma. *Nature* **577**, 561–565 (2020).
63. Oken, M. M. *et al.* Toxicity and response criteria of the Eastern Cooperative Oncology Group. *Am. J. Clin. Oncol.* **5**, 649–655 (1982).
64. Litton, J. K. *et al.* Standardized Definitions for Efficacy End Points in Neoadjuvant Breast Cancer Clinical Trials: NeoSTEEP. *J. Clin. Oncol.* **41**, 4433–4442 (2023).
65. Blakely, C. M. & McCoach, C. E. Role of MPR as an Early Signal for Efficacy in Neoadjuvant Studies. *Clinical cancer research: an official journal of the American Association for Cancer Research* vol. 26 3499–3500 (2020).
66. Cascone, T. *et al.* A Phase I/II Study of Neoadjuvant Cisplatin, Docetaxel, and Nintedanib for Resectable Non-Small Cell Lung Cancer. *Clinical cancer research: an official journal of the American Association for Cancer Research* vol. 26 3525–3536 (2020).
67. [No title]. https://ctep.cancer.gov/protocoldevelopment/electronic_applications/docs/ctcae_v5_quick_reference_5x7.pdf.
68. Website. R Core Team. 2022. 'R: A Language and Environment for Statistical Computing.' Vienna, Austria: R Foundation for Statistical Computing. https://www.R-project.org/.
69. slidescore.com
70. Dobin, A. *et al.* STAR: ultrafast universal RNA-seq aligner. *Bioinformatics* **29**, 15–21 (2013).
71. Wang, L., Wang, S. & Li, W. RSeQC: quality control of RNA-seq experiments. *Bioinformatics* **28**, 2184–2185 (2012).

72. Babraham Bioinformatics - FastQC A Quality Control tool for High Throughput Sequence Data. https://www.bioinformatics.babraham.ac.uk/projects/fastqc/.
73. Wingett, S. W. & Andrews, S. FastQ Screen: A tool for multi-genome mapping and quality control. *F1000Res.* **7**, 1338 (2018).
74. Hunter, J. D. Matplotlib: A 2D Graphics Environment. *Comput. Sci. Eng.* **9**, 90–95 (2007).
75. Picard. https://broadinstitute.github.io/picard.
76. Chen, X. *et al.* TNBCtype: A Subtyping Tool for Triple-Negative Breast Cancer. *Cancer Inform.* **11**, 147–156 (2012).
77. Lehmann, B. D. *et al.* Identification of human triple-negative breast cancer subtypes and preclinical models for selection of targeted therapies. *J. Clin. Invest.* **121**, 2750–2767 (2011).
78. Fang, Z., Liu, X. & Peltz, G. GSEApy: a comprehensive package for performing gene set enrichment analysis in Python. *Bioinformatics* **39**, btac757 (2022).
79. van Rossum, G. *Python Reference Manual*. (1995).
80. pandas-dev/pandas: Pandas. (2023) doi:10.5281/zenodo.8239932.
81. McKinney, W. Data Structures for Statistical Computing in Python. in *Proceedings of the 9th Python in Science Conference* (SciPy, 2010). doi:10.25080/majora-92bf1922-00a.
82. Harris, C. R. *et al.* Array programming with NumPy. *Nature* **585**, 357–362 (2020).
83. Waskom, M. *et al. Mwaskom/seaborn: v0.8.1 (September 2017)*. (Zenodo, 2017). doi:10.5281/ZENODO.883859.
84. Charlier, F. *et al.* trevismd/statannotations: v0.5. (2022) doi:10.5281/zenodo.7213391.
85. Li, H. & Durbin, R. Fast and accurate short read alignment with Burrows-Wheeler transform. *Bioinformatics* **25**, 1754–1760 (2009).
86. van der Auwera, G. & O'Connor, B. D. *Genomics in the Cloud: Using Docker, GATK, and WDL in Terra*. (O'Reilly Media, Incorporated, 2020).
87. Mayakonda, A., Lin, D.-C., Assenov, Y., Plass, C. & Koeffler, H. P. Maftools: efficient and comprehensive analysis of somatic variants in cancer. *Genome Res.* **28**, 1747–1756 (2018).
88. R Core Team. R: A Language and Environment for Statistical Computing. Preprint at https://www.R-project.org/ (2022).
89. Wolf, F. A., Angerer, P. & Theis, F. J. SCANPY: large-scale single-cell gene expression data analysis. *Genome Biol.* **19**, 1–5 (2018).
90. Hao, Y. *et al.* Dictionary learning for integrative, multimodal and scalable single-cell analysis. *Nat. Biotechnol.* 1–12 (2023).
91. Fleming, S. J. *et al.* Unsupervised removal of systematic background noise from droplet-based single-cell experiments using CellBender. *Nat. Methods* 1–13 (2023).
92. Bassez, A. *et al.* A single-cell map of intratumoral changes during anti-PD1 treatment of patients with breast cancer. *Nat. Med.* **27**, 820–832 (2021).
93. Data-Driven Phenotypic Dissection of AML Reveals Progenitor-like Cells that Correlate with Prognosis. *Cell* **162**, 184–197 (2015).
94. Chen, E. Y. *et al.* Enrichr: interactive and collaborative HTML5 gene list enrichment analysis tool. *BMC Bioinformatics* **14**, 128 (2013).
95. Kuleshov, M. V. *et al.* Enrichr: a comprehensive gene set enrichment analysis web server 2016 update. *Nucleic Acids Res.* **44**, W90–7 (2016).
96. Sturm, G. *et al.* Scirpy: a Scanpy extension for analyzing single-cell T-cell receptor-sequencing data. *Bioinformatics* **36**, 4817–4818 (2020).
97. GitHub - schillerlab/sc-toolbox: A collection of project templates and useful functions for single-cell data analysis with Scanpy. *GitHub* https://github.com/schillerlab/sc-toolbox.
98. Blomberg, O. S. *et al.* IL-5-producing CD4 T cells and eosinophils cooperate to enhance response to immune checkpoint blockade in breast cancer. *Cancer Cell* **41**, 106–123.e10 (2023)

CHAPTER 7

IL-5-producing CD4⁺ T cells and eosinophils cooperate to enhance response to immune checkpoint blockade in breast cancer

Olga S. Blomberg[1,2,3,*], Lorenzo Spagnuolo[1,2,*], Hannah Garner[1,2,*], Leonie Voorwerk[1,*], Olga I. Isaeva[1,4,**], Ewald van Dyk[1,2,4,**], Noor Bakker[1,2,**], Myriam Chalabi[5,6,7], Chris Klaver[1], Maxime Duijst[1], Kelly Kersten[1,11], Marieke Brüggemann[1], Dorien Pastoors[1,2,12], Cheei-Sing Hau[1,2], Kim Vrijland[1,2], Elisabeth A.M. Raeven[1,2], Daphne Kaldenbach[1,2], Kevin Kos[1,2,3], Inna S. Afonina[8,9], Paulien Kaptein[5], Louisa Hoes[2,5,7], Willemijn S.M.E. Theelen[10], Paul Baas[10], Emile E. Voest[2,5,7], Rudi Beyaert[8,9], Daniela S. Thommen[5], Lodewyk F.A. Wessels[2,4], Karin E. de Visser[1,2,3,***,#], and Marleen Kok[1,7,***]

Cancer Cell. 2023 Jan 9;41(1):106-123.e10

1 Division of Tumor Biology & Immunology, The Netherlands Cancer Institute, Amsterdam, the Netherlands
2 Oncode Institute, Utrecht, the Netherlands
3 Department of Immunology, Leiden University Medical Centre, Leiden, the Netherlands
4 Division of Molecular Carcinogenesis, The Netherlands Cancer Institute
5 Division of Molecular Oncology & Immunology, The Netherlands Cancer Institute
6 Department of Gastrointestinal Oncology, The Netherlands Cancer Institute
7 Department of Medical Oncology, Netherlands Cancer Institute
8 VIB-UGent Center for Inflammation Research, Ghent University, Ghent, Belgium
9 Department of Biomedical Molecular Biology, Ghent University, Ghent, Belgium
10 Department of Thoracic Oncology, Netherlands Cancer Institute
11 Present address: Department of Pathology, University of California San Francisco, San Francisco, CA, USA
12 Present address: Department of Hematology, Erasmus University Medical Center, Rotterdam, the Netherlands

*These authors contributed equally
**These authors contributed equally
***These authors contributed equally, co-corresponding authors
#Lead contact

Summary

Immune checkpoint blockade (ICB) has heralded a new era in cancer therapy. Research into the mechanisms underlying response to ICB has predominantly focused on T cells, however effective immune responses require tightly regulated crosstalk between innate and adaptive immune cells. Here, we combine unbiased analysis of blood and tumors from metastatic breast cancer patients treated with ICB with mechanistic studies in mouse models of breast cancer. We observe an increase in systemic and intratumoral eosinophils in patients and mice responding to ICB treatment. Mechanistically, ICB increased IL-5 production by $CD4^+$ T cells, stimulating elevated eosinophil production from the bone marrow, leading to systemic eosinophil expansion. Additional induction of IL-33 by ICB-cisplatin combination or recombinant IL-33 promotes intratumoral eosinophil infiltration and eosinophil-dependent $CD8^+$ T cell activation to enhance ICB response. This work demonstrates the critical role of eosinophils in ICB response and provides proof-of-principle for eosinophil engagement to enhance ICB efficacy.

Keywords

Eosinophils, breast cancer, immune checkpoint blockade, myeloid cells, IL-5, $CD4^+$ T cells, IL-33

Graphical Abstract

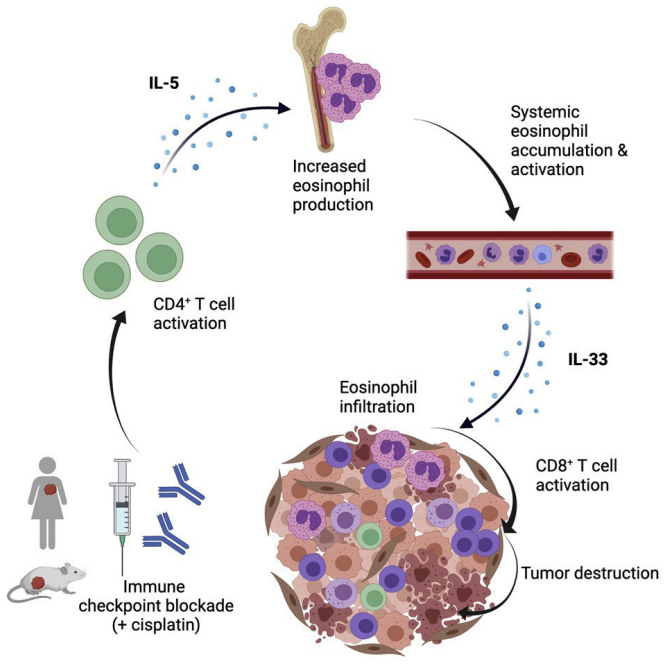

Introduction

Immune checkpoint blockade (ICB) has emerged in the last decade as an effective strategy for the treatment of multiple cancer types. However, in metastatic breast cancer, durable responses are only seen in approximately 5% of the patients and are mainly limited to triple-negative breast cancer (TNBC)[1,2]. Whilst response rates can be increased by selecting patients with PD-L1-positive tumors or by combining ICB with chemotherapy[3,4], most breast cancer patients do not benefit from ICB. A better understanding of the mechanisms that underlie response to ICB is crucial for the rational design of novel immunomodulatory strategies.

Research into the mechanisms of response to ICB has predominantly focused on T cells, however, an effective immune response requires tightly regulated crosstalk between adaptive and innate immune cells[5]. One innate immune cell type gaining increasing attention in the context of anti-tumor immunity is the eosinophil[6,7]. Eosinophils are bone marrow-derived granulocytes involved in tissue homeostasis and repair, parasite clearance and the pathophysiology of various diseases, including allergic asthma and autoimmunity[8]. In the context of cancer, opposing functions of eosinophils have been reported depending on cancer type and disease stage[9-18]. Recently, eosinophils have emerged as unexpected players in an effective response to ICB. Increased eosinophil levels during ICB treatment correlate with response to PD-1, PD-L1 or CTLA-4 targeting antibodies in patients with metastatic melanoma[19-21], non-small cell lung cancer (NSCLC)[22,23] and renal cell carcinoma (RCC)[24]. Whether eosinophils are associated with response to ICB in patients with less immunogenic cancer types, such as breast cancer, remains to be elucidated. Moreover, it is critical to assess whether eosinophils merely serve as a biomarker or are causally involved in ICB response. Preclinical studies point towards a functional involvement of eosinophils in anti-tumor immunity[11-14] and eosinophils were also recently reported to promote intratumoral vessel normalization and anti-tumor immunity upon CTLA-4 blockade[25]. Nonetheless, their role in ICB response remains poorly understood. Furthermore, the mechanisms leading to eosinophil accumulation and recruitment to the tumor upon ICB are still unknown.

In this study, we combined unbiased analyses of the systemic immune landscape upon ICB in patients with metastatic TNBC with in-depth mechanistic studies in spontaneous mouse models of primary and metastatic breast cancer (Figure 1A), which mimic the poorly immunogenic and highly immunosuppressive characteristics of human breast cancer[26,27]. We uncover a critical role for eosinophils during ICB response and elucidate the mechanisms that lead to systemic eosinophil expansion and tumor infiltration.

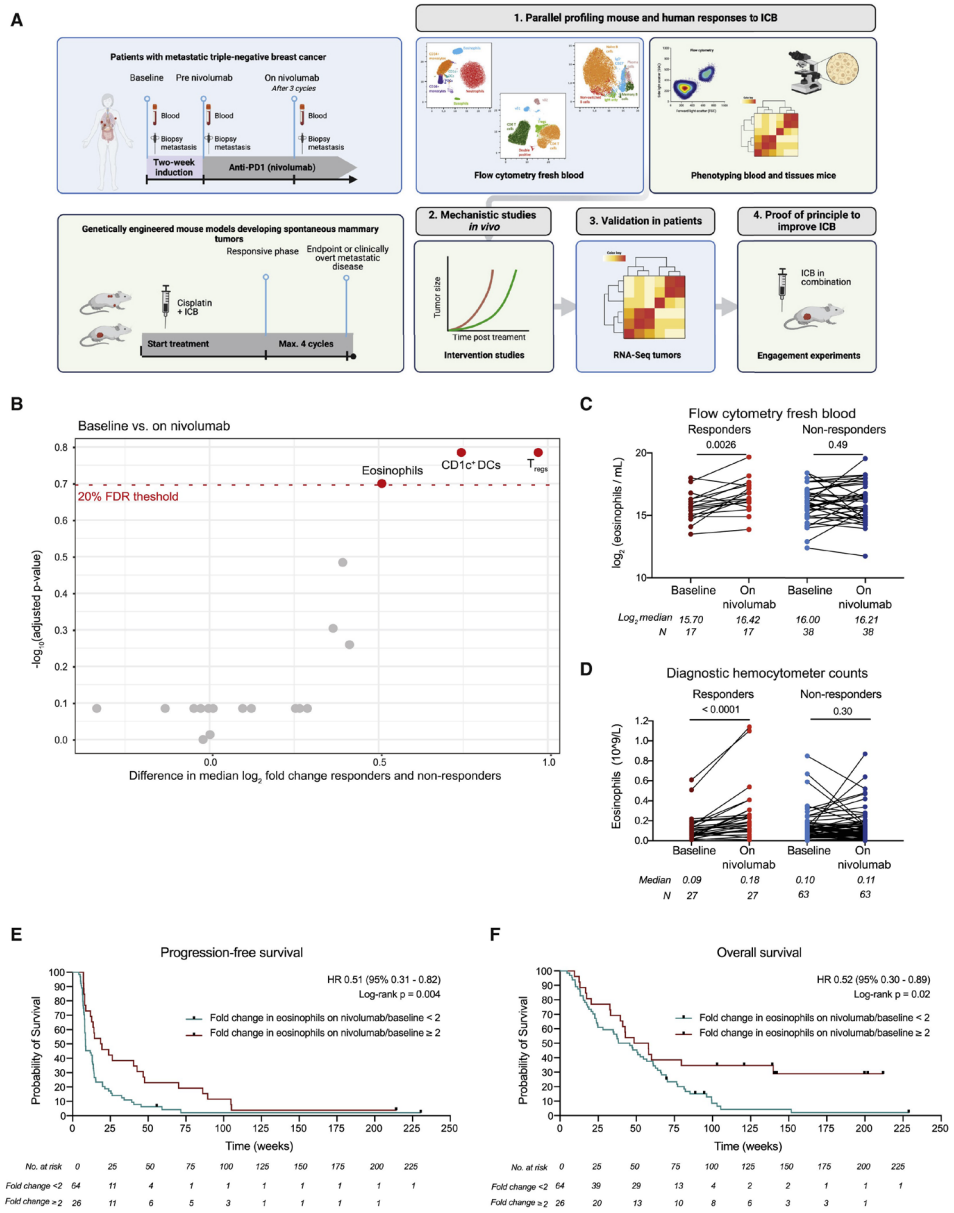

Figure 1. ICB response in metastatic TNBC patients is associated with systemic eosinophil expansion. *(A) Schematic overview of study design. Created with Biorender.com. (B) Volcano plot depicting the difference in median log_2 fold change from baseline to on-nivolumab between responding and non-responding patients with metastatic TNBC (TONIC-trial, NCT02499367) and adjusted p-values for systemic immune cell populations (cells/ml) analyzed by flow cytometry. (C-D) Paired analysis of circulating eosinophils at baseline versus on-nivolumab by flow cytometry (log_2 transformed cells/ml) (C) and by hemocytometer analysis (D). Wilcoxon Signed-Rank test. (E-F) Kaplan-Meier curve of progression-free survival (E) or overall survival (F) of patients according to the fold change in eosinophils (baseline to on-nivolumab) lower than 2 or equal to/higher than 2. Log-rank and univariate hazard ratios by Cox regression (fold change lower than 2 as reference category). See also Figures S1-S3 and Tables S1-S2.*

Results

Increase in circulating eosinophils in patients responding to ICB

To assess response-related changes in the systemic immune landscape of patients with metastatic breast cancer, we set up an immunomonitoring pipeline of fresh blood by high-dimensional flow cytometry (Figure 1A). We profiled patients with metastatic TNBC treated with anti-PD-1 (nivolumab) enrolled in a phase II clinical trial (TONIC-trial, n=111, Figure S1A-B; characteristics in Table S1-S2)[28]. Patients were treated with nivolumab alone or with nivolumab following a two-week induction period with either low dose chemotherapy, irradiation or a two-week waiting period (Figure S1A). Blood samples were analyzed by flow cytometry at baseline (before induction treatment), after induction treatment (pre-nivolumab) and after three cycles of nivolumab (on-nivolumab). Extensive analysis of individual timepoints did not reveal predictive immune cell populations that could distinguish responders from non-responders (Figure S1C-E). However, when analyzing the dynamics of immune cell populations upon ICB treatment by comparing baseline to on-nivolumab, we identified three differentially regulated immune cell populations associated with response: CD1c$^+$ dendritic cells (DCs), regulatory T cells (T_{regs}) and eosinophils (Figure 1B & S1F). We observed a decrease in CD1c$^+$ DCs in non-responding patients (Figure S2A). In contrast, eosinophils and T_{regs} were increased upon ICB specifically in responders (Figure 1C & S2B-C). The same three populations emerged when we compared the pre-nivolumab (post-induction) to on-nivolumab timepoints, indicating that the induction treatments did not significantly change the dynamics of these immune populations (Figure S2D-F). In light of recent reports of systemic eosinophil expansion correlating with ICB response in several tumor types[19-24], we further investigated the increase in eosinophils associated with response to ICB.

To validate our results in a technically independent manner we evaluated circulating eosinophil counts using routine hemocytometer analysis (Figure S1B for sample overlap with flow cytometry samples). We confirmed circulating eosinophils significantly increase in responders on-nivolumab, both compared to baseline and pre-nivolumab (Figure 1D & S2G-H). Importantly, patients with increased circulating eosinophils upon treatment had longer progression-free survival (Figure 1E & S2I) and overall survival (Figure 1F & S2J), underscoring the clinical relevance of an eosinophil increase in ICB response.

To evaluate whether increased eosinophils during ICB response extend beyond breast cancer, NSCLC[22,23], RCC[24] and melanoma[19-21], we investigated eosinophil counts in patients

treated with ICB in other phase II clinical trials at the Netherlands Cancer Institute. Comparing patients responding to ICB with non-responders, we observed a significantly higher fold change in circulating eosinophils in patients with advanced NSCLC (Figure S3A,B; PEMBRO-RT trial[29]) and in patients with early stage mismatch repair-proficient (pMMR) colon cancer (CC) (Figure S3C,D; NICHE-trial[30]). No statistically significant difference in paired eosinophil counts could be seen upon ICB in patients with mismatch repair-deficient (dMMR) cancers (Figure S3E,G; NICHE-trial and dMMR cohort DRUP-trial[30,31]), suggesting that an eosinophil increase might be less relevant in highly immunogenic tumors. In summary, we demonstrate that eosinophils accumulate systemically upon ICB response in three independent cohorts of patients with metastatic TNBC, metastatic NSCLC or early-stage pMMR CC, emphasizing that systemic eosinophil expansion is a common feature of ICB response across multiple cancer types.

Increase of intratumoral eosinophil-related gene expression correlates with response to ICB and increased CD8⁺ T cell signatures

To assess whether eosinophils accumulate intratumorally upon ICB, we evaluated the expression of *SIGLEC8* in paired metastases obtained at baseline and during nivolumab treatment of TNBC patients (TONIC-trial, NanoString IO360 panel, sample availability Figure S1B). SIGLEC8 is a marker expressed at high levels on human eosinophils and mast cells and to a lower degree on basophils[32]. We detected a statistically significant increase in *SIGLEC8* upon ICB in tumors from responders but not in non-responders (Figure 2A). To complement this analysis, we applied an eosinophil signature containing genes highly expressed by eosinophils to the RNA-sequencing dataset (Table S3). Intratumoral expression of these genes increased upon ICB in responders but not in non-responders (Figure 2B). Using this signature, we assessed whether elevation in intratumoral eosinophils is accompanied by an intratumoral increase in (activated) CD8⁺ T cells, as shown for metastatic melanoma[19]. We applied a widely used T cell inflamed gene signature[33], an IFNg signature[33] and a structural CD8⁺ T cell signature consisting of genes related to the CD8⁺ T cell receptor complex (Table S3*J*). We observed a significant correlation between increased expression upon ICB of eosinophil-related genes and all three T cell-related gene signatures in metastatic lesions of responders, and not in non-responders (Figure 2C-H). Together, our results indicate that response to ICB associates with an increase in circulating eosinophils and an increase of eosinophil-related genes in the tumor microenvironment. This increase in eosinophil-related genes correlates with increased CD8⁺ T cell related genes, suggesting a potential connection between eosinophils and CD8⁺ T cell activation during an effective ICB response.

ICB synergizes with cisplatin and induces eosinophil accumulation in spontaneous primary and metastatic breast cancer models

Our clinical observations raise the question whether eosinophil expansion is a bystander effect of ICB response, or whether eosinophils are functionally involved. To probe the causality between eosinophil dynamics and outcome after ICB in breast cancer, we used the *Keratin14-cre;Cdh1$^{F/F}$;Trp53$^{F/F}$* (KEP) mouse model for *de novo* mammary tumorigenesis[34] (Figure 3A) and the KEP-based mastectomy model for spontaneous multi-organ metastatic disease[35] (Figure 3B & S4A,B). KEP mice bearing established mammary tumors did not respond to blockade of PD-1 and CTLA-4 (referred to as ICB; Figure 3C). Similarly, metastasis-bearing mice did not respond to ICB alone (Figure 3D), recapitulating the poor response to ICB observed in metastatic breast cancer patients. Platinum-based drugs synergize with ICB in preclinical models[36,37] due to their beneficial immunomodulatory effects[38,39], in line with improved response rates when ICB is combined with chemotherapy in metastatic TNBC patients[3,4]. While combining cisplatin with either anti-PD-1 or anti-CTLA-4 was insufficient to improve the survival benefit provided by cisplatin (Figure S4C), the combination of cisplatin with anti-PD-1 and anti-CTLA-4 (CIS+ICB) resulted in extension of survival of KEP mice (Figure 3C) and led to durable responses in mice bearing established metastases (Figure 3D). The therapeutic synergy between CIS+ICB was characterized by a systemic increase in effector CD44⁺CD62L⁻ T cells and increased expression of activation markers and cytokines, such as IFNγ and TNFα by both CD4⁺ and CD8⁺ T cells (Figure S4D,E). Depletion of CD8⁺ T cells abrogated the synergistic effect observed upon CIS+ICB in mammary tumor-bearing KEP mice (Figure 3C), confirming a critical role of CD8⁺ T cells as effector cells in CIS+ICB therapy.

In addition to increased T cell activation, in-depth profiling of the immune landscape of primary tumors, metastases, and blood by flow cytometry of both models revealed that only eosinophils consistently increased in frequency upon CIS+ICB therapy (Figure 3E-H). Whilst ICB induced accumulation of circulating eosinophils (Figure 3E,F), increased eosinophil infiltration in primary tumors and metastatic lesions was only observed when ICB was combined with cisplatin (Figure G,H). Additionally, we observed an increase in eosinophils in the tumor-draining lymph node (TDLN) and spleen of KEP mice treated with CIS+ICB (Figure S4F). Immunohistochemical staining for Major Basic Protein (MBP), a granular protein specifically expressed by eosinophils, confirmed that the increase in eosinophils in primary KEP tumors was only achieved upon CIS+ICB (Figure S4G).

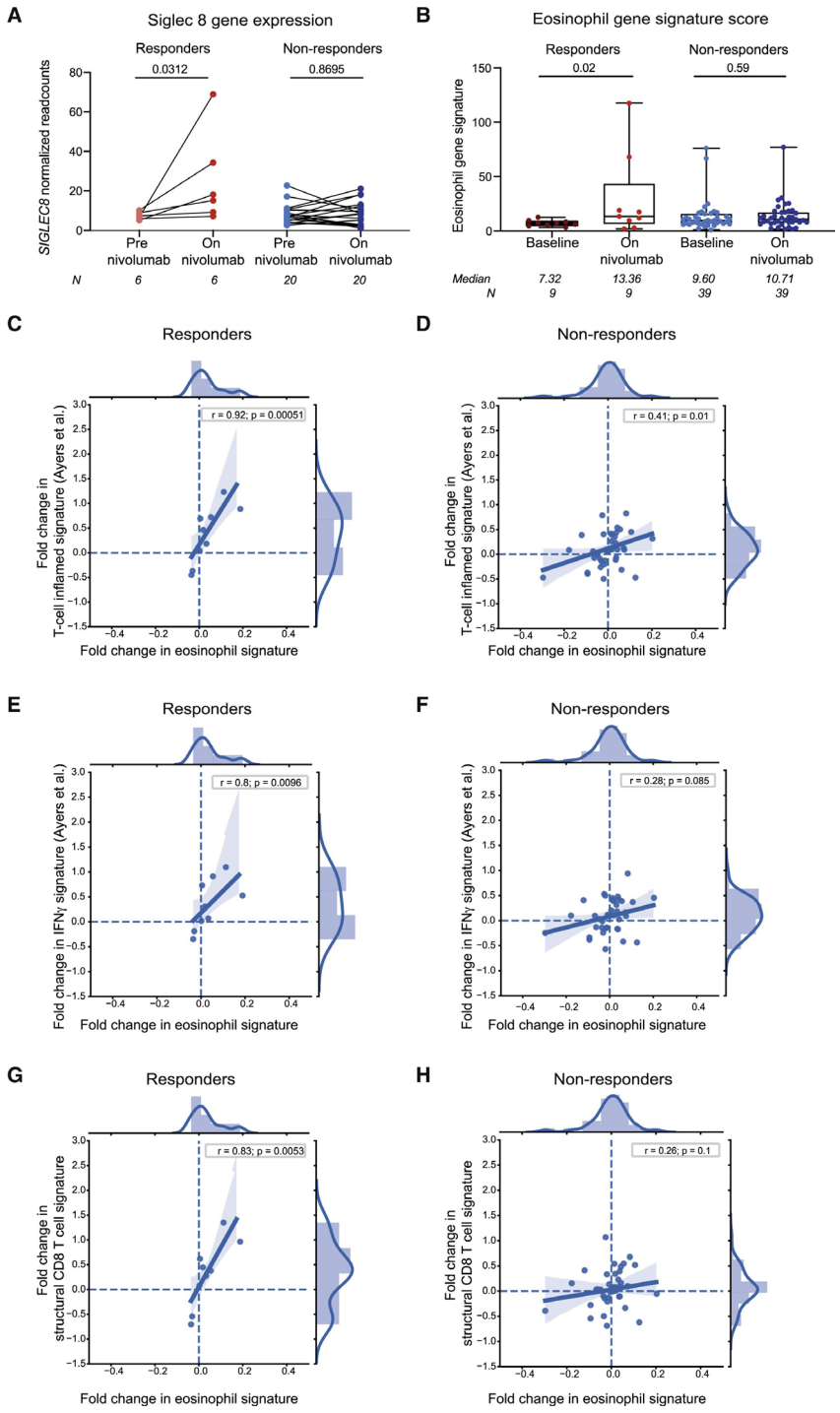

◀◀◀ ***Figure 2. ICB response in TNBC patients is associated with increased intratumoral eosinophil-related gene expression.*** *(A) Paired intratumoral SIGLEC8 normalized read counts from NanoString IO360 gene expression analysis from pre-nivolumab and on-nivolumab biopsies. Wilcoxon Signed-Rank test. (B) Mean of normalized expression values of eosinophil signature genes (Table S3) from paired biopsies of metastases as assessed by RNA-sequencing analysis. Boxplots display minimum and maximum values (whiskers), interquartile range (box) with median. Wilcoxon Signed-Rank test. (C-H) Correlation between the fold change (baseline to on-nivolumab) in an eosinophil gene signature (described in B) and the fold change (baseline to on-nivolumab) in a T cell inflamed gene signature (expanded immune gene signature of Ayers et al., 2017[33] (C,D), a structural CD8⁺ T cell gene signature (Table S3) (E,F), or an IFNg gene signature[33] (G,H) in responders (left) and non-responders (right). Lines with colored field represent the regression line with 95% confidence interval, including histogram and kernel density estimates. Spearman's correlation coefficient. See also Table S3.*

To evaluate whether treatment with CIS+ICB also influences the phenotype of eosinophils, we performed RNA-sequencing on eosinophils sorted from blood of metastasis-bearing mice during the responsive phase of therapy, namely 21 days after initiation of treatment. We observed 858 differentially expressed genes (fold change ≥1 and p-value ≤ 0.05) in eosinophils from CIS+ICB-treated mice compared to control antibody-treated mice (Figure S4H). Gene-set enrichment analysis identified IFNγ response as the top hit among the immune-related pathways enriched in eosinophils upon CIS+ICB (Figure S4I-J). Other immune-related pathways included TGFβ signaling, TNFα signaling via NF-κB, IL6-JAK-STAT3 signaling, and inflammatory response (Figure S4I). Moreover, we observed enrichment of oxidative phosphorylation pathway in eosinophils from control antibody-treated compared to combination-treated mice (Figure S4K). These observations indicate that, in CIS+ICB-treated mice, eosinophils are not only increased in number, but also phenotypically altered. Collectively, these data demonstrate that ICB synergizes with cisplatin resulting in improved survival and is associated with systemic and intratumoral expansion of eosinophils, in line with our clinical observations.

Eosinophil depletion abrogates CD8⁺ T cell activation and ICB response

To elucidate whether CIS+ICB-induced eosinophilia is critical for the observed therapeutic benefit, we depleted eosinophils with an antibody targeting SiglecF[11,12,25,40,41]. Anti-SiglecF treatment effectively depleted eosinophils without altering other immune cells including neutrophils (Figure S5A-C). In line with literature[42], we observed a subset of SiglecF⁺ neutrophils in our tumor models (5-20% of intratumoral neutrophils, data not shown). However, the expression levels of SiglecF on these neutrophils was lower than on eosinophils (Figure S5D). To exclude the possibility that anti-SiglecF treatment depletes SiglecF⁺ neutrophils, we quantified Ly6G⁺ (neutrophils) and MBP⁺ (eosinophils) cells by immunohistochemical staining. The total number of neutrophils was unaffected by anti-SiglecF treatment, whereas eosinophils were effectively depleted (Figure S5E,F). Importantly, eosinophils were also effectively depleted during anti-SiglecF treatment in combination with cisplatin+/-ICB (Figure 4A & S5G).

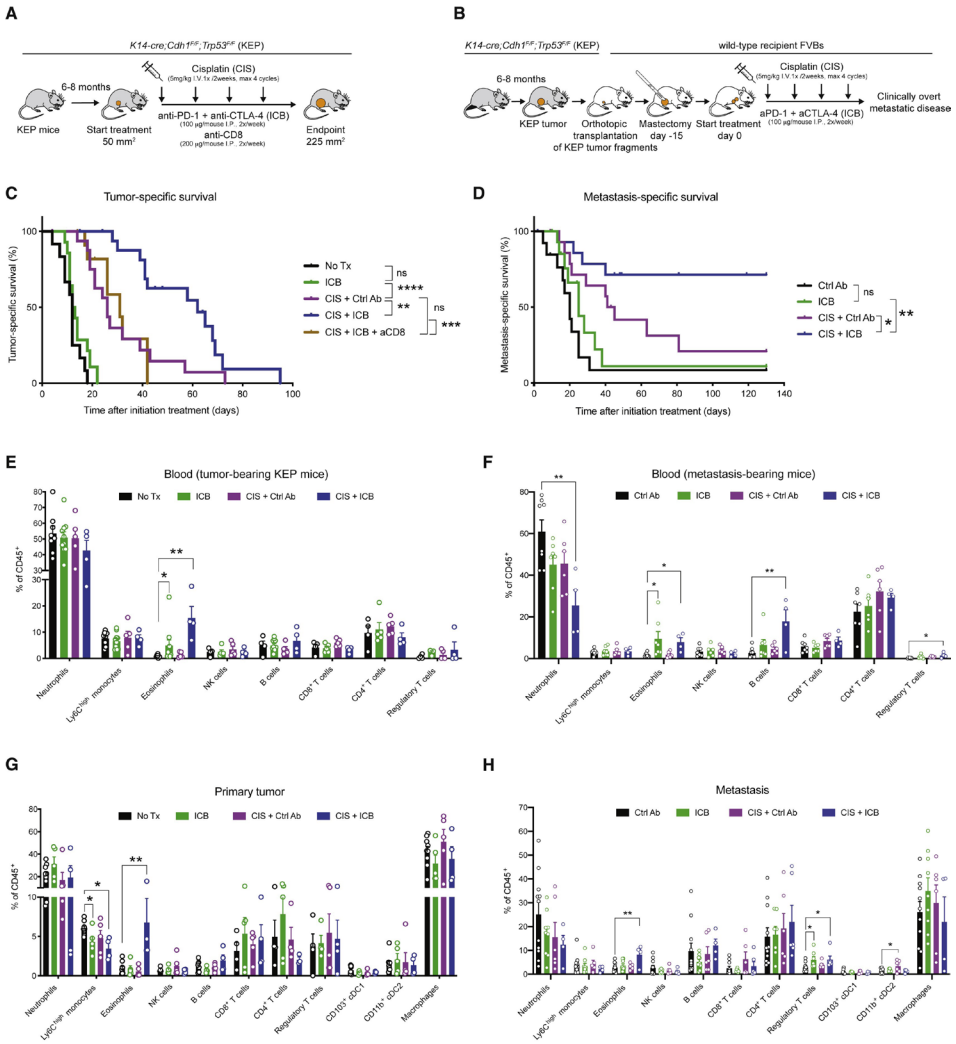

Figure 3. ICB synergizes with cisplatin and induces eosinophil expansion in mouse models. *(A-B) Experimental set-up of transgenic KEP model (A) and KEP-based metastasis model (B) including treatment schemes.(C) Kaplan-Meier survival curves of KEP mice treated as indicated (untreated, No Tx, n=12; ICB, n=14, 1 censored; CIS+Ctrl Ab, n=17, 2 censored; CIS+ICB, n=18, 5 censored; CIS+ICB+anti-CD8, n=12, 4 censored). Tumor-related endpoint was defined as cumulative tumor burden of 225 mm². (D) Kaplan-Meier survival curves of metastasis-bearing mice treated as indicated (control antibody, Ctrl Ab, n=13, 1 censored; ICB, n=15, 5 censored; CIS+Ctrl Ab, n=15, 3 censored; CIS+ICB, n=16, 7 censored). Metastasis-related endpoint was defined as mice displaying signs of respiratory distress caused by metastatic disease or when lymph node metastasis reached the size of 225mm². Censored events are mice sacrificed for weight loss (C&D) or local recurrence of the mastectomized tumor (D). Log-rank (Mantel Cox) test. (E-F) Frequency of immune cell populations in the blood of KEP mice at tumor-related endpoint (E) or metastasis-bearing mice at metastasis-related endpoint (F) as determined by flow cytometry. (G-H) Frequency of immune cell populations in the primary tumor of KEP mice at tumor-related endpoint (G) or metastatic lesions of mice at metastasis-related endpoint (H) as determined by flow cytometry. Eosinophils were defined CD11b⁺Ly6G^{low}SiglecF⁺SSC^{high} in blood and CD11b⁺Ly6G^{low}SiglecF⁺F4/80^{int} in tumor. Mean ±S.E.M.. 1-way ANOVA or Kruskal-Wallis followed by Dunnett's or Dunn's multiple comparisons test, comparing each group against control-treated mice. *p<0.05, **p<0.01, ***p<0.001, ****p<0.0001. See also Figure S4.*

The administration of anti-SiglecF alone did not affect KEP tumor growth (Figure S5H). Strikingly, depletion of eosinophils abrogated the synergistic effect observed between CIS+ICB, while depletion of eosinophils had no effect on therapeutic benefit of cisplatin alone (Figure 4B-D). Similarly, depletion of eosinophils completely abrogated the synergistic effect of CIS+ICB in metastasis-bearing mice but had no effect on the efficacy of cisplatin alone (Figure 4E). These findings reveal a causal role for eosinophils in the synergistic effect of CIS+ICB therapy, both in primary and metastatic breast cancer models.

Because the synergistic effect of CIS+ICB is dependent on both CD8⁺ T cells and eosinophils, we hypothesized that eosinophils play a role in inducing intratumoral CD8⁺ T cell infiltration or activation. It was previously shown that eosinophils can promote T cell activation and recruitment into tumors[11,13,18,25,40], and we observed an association between intratumoral eosinophils and CD8⁺ T cells in responding patients with advanced breast cancer (Fig 2C-H). To test this hypothesis, we analyzed the immune landscape of KEP tumors during the responsive phase of therapy. Intratumoral CD8 counts increased upon treatment with cisplatin compared to control antibody but did not further increase upon addition of ICB. Importantly, CD8 counts were not dependent on the presence of eosinophils (Figure 4F). Instead, eosinophil depletion completely reverted the increased activation of intratumoral CD8⁺ T cells induced by CIS+ICB, most notably in terms of CD44 expression and IFNγ production (Figure 4G,H). These data demonstrate that eosinophils are essential for increased intratumoral CD8⁺ T cell activation during CIS+ICB therapy.

Additionally, CD4 and FOXP3 cell counts increased upon cisplatin treatment compared to control, but did not change further upon CIS+ICB and was independent of eosinophil presence (Figure S5I,J). While CIS+ICB also increased the intratumoral frequency of effector CD44⁺ CD4⁺ T cells, this was independent of eosinophils (Figure S5K-N), demonstrating that eosinophils specifically affect intratumoral CD8⁺ T cell activation. Interestingly, we also observed a higher frequency of CD44⁺ and IFNγ⁺ CD8⁺ T cells in the TDLN upon CIS+ICB that was abrogated upon eosinophil depletion (Figure S5O). In contrast, the frequency of CD44⁺ CD4⁺ T cells or CD44⁺ T_{regs} in TDLN was not increased by combination treatment nor affected by eosinophil depletion (Figure S5P,Q). Collectively, these observations show that eosinophils are critical for the therapeutic action of CIS+ICB, by facilitating CD8⁺ T cell activation in the tumor and TDLN.

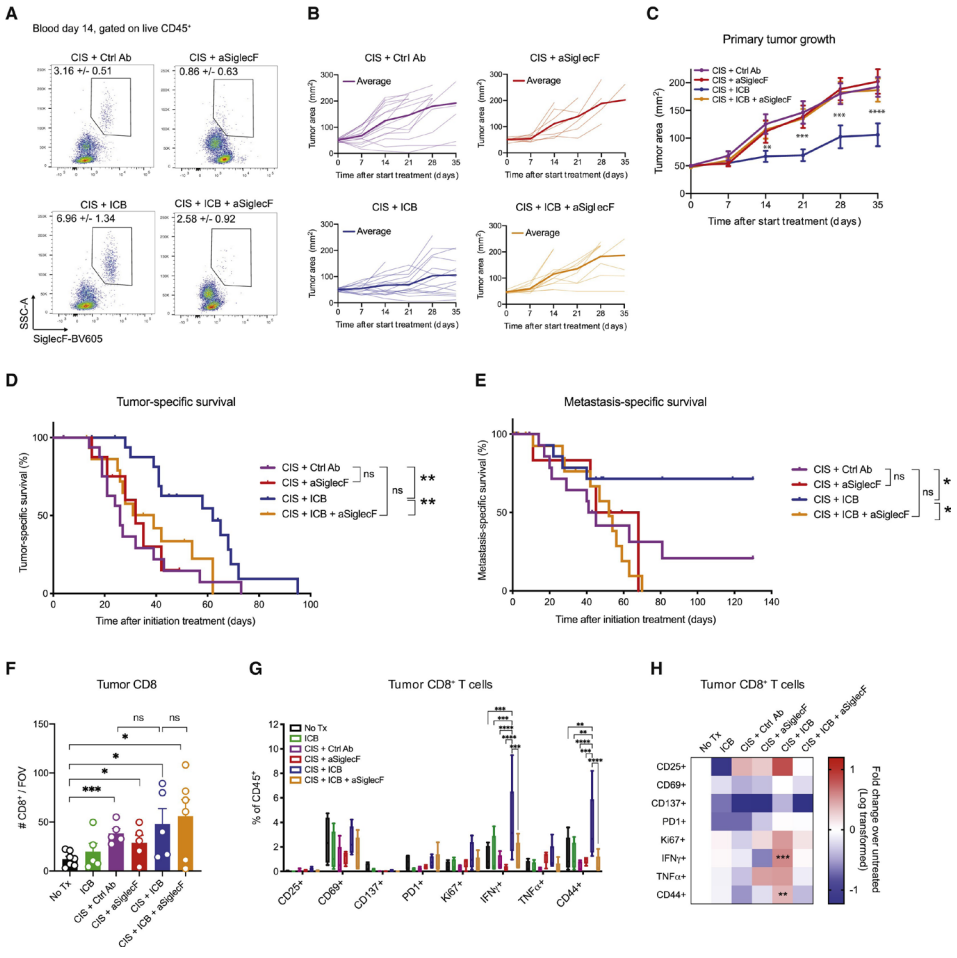

Figure 4. Eosinophils are critical for ICB-cisplatin response via CD8⁺ T cell activation. *(A) Representative dot plots showing eosinophil levels in blood of KEP mice 14 days after start of indicated treatments. Mean frequency of eosinophils as percentage of CD45⁺ cells ±S.E.M. is displayed. (B) Individual (light) and average (dark) tumor growth curves of KEP mice treated as indicated. (C) Average growth curve ±S.E.M. of the aforementioned treatment groups. 2-way ANOVA followed by Dunnett's multiple comparisons test. (D) Kaplan-Meier survival curves of KEP mice treated as indicated (CIS+Ctrl Ab, same curve as in Figure 3C); CIS+anti-SiglecF, n=8, 2 censored; CIS+ICB, same curve as in Figure 3C; CIS+ICB+anti-SiglecF, n=18, 5 censored). Log-rank (Mantel-Cox) test. (E) Kaplan-Meier survival curves showing metastasis-related survival of mice treated as indicated (CIS+Ctrl Ab, same curve as in Figure 3D; CIS+anti-SiglecF, n=6, 2 censored, CIS+ICB, same curve as in Figure 3D; CIS+ICB + anti-SiglecF, n=19, 7 censored). Log-rank (Mantel-Cox) test. (F) Number of tumor-infiltrating CD8⁺ T cells quantified by IHC (n=5-7 mice per group, average of 5-9 high power microscopic fields per mouse). KEP mice were treated as described in Figure 3A and analyzed 21 days after start of treatment or when tumors reached an area of 225 mm². Mean ±S.E.M. Student's t-test. (G) Frequency of indicated activation markers expressed on intratumoral CD8⁺ T cells upon different treatments, determined by flow cytometry (n=4-5). Boxes represent median and interquartile range; whiskers full range. 2-way ANOVA followed by Tukey's multiple comparison test. (H) Data of (G) was normalized to the frequency observed in control mice. Log transformed data is presented. ns, not significant, *p<0.05, **p<0.01, ***p<0.001, ****p<0.0001. See also Figure S5.*

IL-5 is required for ICB-induced eosinophil accumulation and therapeutic benefit

To investigate how ICB mediates the systemic eosinophil increase, we analyzed metastasis-bearing mice at different timepoints during the metastatic cascade and treatment. The eosinophil frequency in the blood increased after 7 days of ICB treatment and was maintained at high levels until at least 21 days (Figure S6A). Concomitantly, we observed an increase in eosinophils in the bone marrow (Figure 5A) and an increase of Lin⁻Sca1⁻CD34⁺cKit^{int}CD125⁺Gr1⁻ cells, which have been previously described as eosinophil progenitors (Figure 5B & S6B)[43]. Furthermore, both immature (cKit^{int}CCR3^{low}) and fully mature (cKit⁻CCR3⁺) eosinophils increased in the bone marrow upon ICB (Figure 5C-E), while all other hematopoietic progenitor and immune cell populations remained unaffected (Figure S6C). Altogether, these observations suggest that the systemic increase of eosinophils induced by ICB is caused by increased eosinophil production in the bone marrow.

To assess which systemic factors induced by ICB could promote eosinophil production in the bone marrow, followed by systemic eosinophil accumulation, we measured the expression of a panel of cytokines in the plasma of metastatic mice. Strikingly, the only significantly increased cytokine upon ICB was IL-5 (Figure 5F & S6D), which is a major eosinophil regulator[44]. To investigate whether ICB treatment in human tumors induces IL-5 upregulation, we made use of the patient-derived tumor fragment (PDTF) platform[45]. This platform allows interrogation of the early immunological response of human tumor tissues upon *ex vivo* ICB treatment (aPD1 and combined aPD1+aCTLA4). Importantly, the observed *ex vivo* response (defined as previously described[45,46]) correlates with the clinical response of the patient[45]. We assessed the protein levels of IL-5 upon *ex vivo* ICB stimulation in tumors of patients with different tumor types. We observed an increase in IL-5 expression specifically in tumors that showed an immunological response to *ex vivo* ICB (PDTF-R) as compared to non-responding tumors (PDTF-NR), both upon aPD1 alone and combined aPD1+aCTLA4 treatment (Figure 5G & Table S4), demonstrating that IL-5 can be induced in human tumors by ICB.

To assess whether IL-5 drives eosinophil expansion upon ICB in metastasis-bearing mice, we blocked IL-5 using a neutralizing antibody. Indeed, the number of eosinophils in bone marrow, blood, and (pre-)metastatic lungs was drastically reduced (Figure 5H-J). Importantly, ICB did not promote an eosinophil increase after IL-5 blockade in any of the organs analyzed, indicating that ICB-induced eosinophils are IL-5 dependent. In line with

our observations in metastasis-bearing mice, serum IL-5 levels were similarly increased in tumor-bearing KEP mice during the responsive phase of CIS+ICB therapy (Figure 5K). IL-5 blockade during CIS+ICB therapy in KEP mice reduced eosinophil levels both systemically and intratumorally (Figure 5L,M), without affecting other myeloid cells (Figure S6E,F). Importantly, anti-IL-5 treatment abolished the therapeutic benefit induced by CIS+ICB (Figure 5N), phenocopying the effect of anti-SiglecF-induced eosinophil depletion (Figure 4D). Collectively, these findings demonstrate that IL-5 is a key driver of eosinophil accumulation and therapeutic benefit of CIS+ICB therapy.

Figure 5. CD4⁺ T cell-derived IL-5 is required for ICB-induced eosinophil expansion and therapeutic benefit. *(A-E) KEP metastasis-bearing mice were treated as indicated (Ctrl Ab, n=10-13; ICB, n=10-13) and sacrificed 10 days after start of treatment. Frequency of total eosinophils (Live Lin⁻CD127⁻CD11b⁺CD115⁻SiglecF⁺) (A), Live Lin⁻Sca1⁻CD34⁺cKit^{int}CD125⁺Gr1⁻ eosinophil progenitors (B), representative dot plot (C) and quantification of cKit^{int}CCR3^{low} (D) and cKit⁻CCR3⁺ (E) eosinophils in bone marrow as determined by flow cytometry. (F) Relative expression of the indicated cytokines in the plasma of mice treated as described above (Ctrl Ab n=9, ICB n=10), determined by LEGENDplex, and normalized to Ctrl Ab-treated mice. (G) Fold change in IL-5 secretion by PDTF treated ex vivo with aPD-1+aCTLA-4 (left) or aPD-1 (right) compared to untreated condition, measured by LEGENDplex, comparing PDTF-R (responders) and PDTF-NR (non-responders), defined as described previously[45,46]. Tumor samples were collected from surgical material of patients with various tumor types (see STAR Methods and Table S4). (H-J) Metastasis-bearing mice were treated with IgG2a and IgG1 control antibodies (Ctrl Abs, n=14), ICB+IgG1 (n=14), IgG2a+anti-IL-5 (n=11) or ICB+anti-IL-5 (n=12) and analyzed 10 days after start of treatment. Number of eosinophils in bone marrow (H), blood (I) and lungs (J) determined by flow cytometry. Lung eosinophils were defined as CD45⁺CD11b⁺Ly6G⁻SiglecF⁺F4/80^{int}. (K) IL-5 levels in serum of tumor-bearing KEP mice analyzed 21 days after start of indicated treatments measured by ELISA. (L-M) Frequency of eosinophils in the blood (L) and tumor (M) of KEP mice treated as indicated and analyzed at tumor-related endpoint as determined by flow cytometry (n=4-5). Data from CIS+Ctrl Ab and CIS+ICB are the same mice as in Figure 3G. (N) Kaplan-Meier survival curves of KEP mice treated as indicated (CIS+Ctrl Ab, same curve as in Figure 3C; CIS+ICB, same curve as in Figure 3C; CIS+ICB+anti-IL-5, n=12, 3 censored). Log-rank (Mantel-Cox) test. (O) Number of eosinophils in blood of wild-type (wt) or Rag1 k.o. mice with KEP-derived orthotopic mammary tumors, treated as indicated (Ctrl Ab, wt n=10, Rag1 k.o. n=10; ICB, wt=10, Rag1 k.o. n=10), analyzed by flow cytometry when tumors reached an area of 144 mm². (P) IL5 gene expression in CD4⁺CD25⁻ T cells sorted from blood of metastasis-bearing mice treated indicated (Ctrl Ab n=4, ICB n=4), determined by RT-qPCR. Relative expression to Ctrl Ab-treated mice is shown. (Q-R) Metastasis-bearing mice were treated with isotype control antibodies (Ctrl Ab, n=13-25), ICB (n=13-21), Ctrl Ab+anti-CD4 (n=14) or ICB+anti-CD4 (n=13) and sacrificed 10 days after start of the treatment. (Q) Plasma IL-5 levels, measured by ELISA. (R) Number of eosinophils in the blood, as determined by flow cytometry. Pooled data of two independent experiments. (S) IL5 gene expression determined by RT-qPCR in CD4⁺ T cells sorted from PBMCs at baseline and after one cycle of nivolumab metastatic TNBC patients treated in the control arm of the TONIC trial (n=6). (T) Fold change in frequency of IL-5⁺ CD4⁺ T cells among total CD4⁺ T cells from TNBC patients (n=7) treated ex vivo with aPD1 compared to untreated condition, measured by intracellular flow cytometry. All data are mean ±S.E.M, statistical analysis by unpaired t-test or Mann-Whitney, unless differently indicated. ns, not significant, *p<0.05, **p<0.01, ***p<0.001, ****p<000.1. See also Figure S6 and Table S4.* ▶▶▶

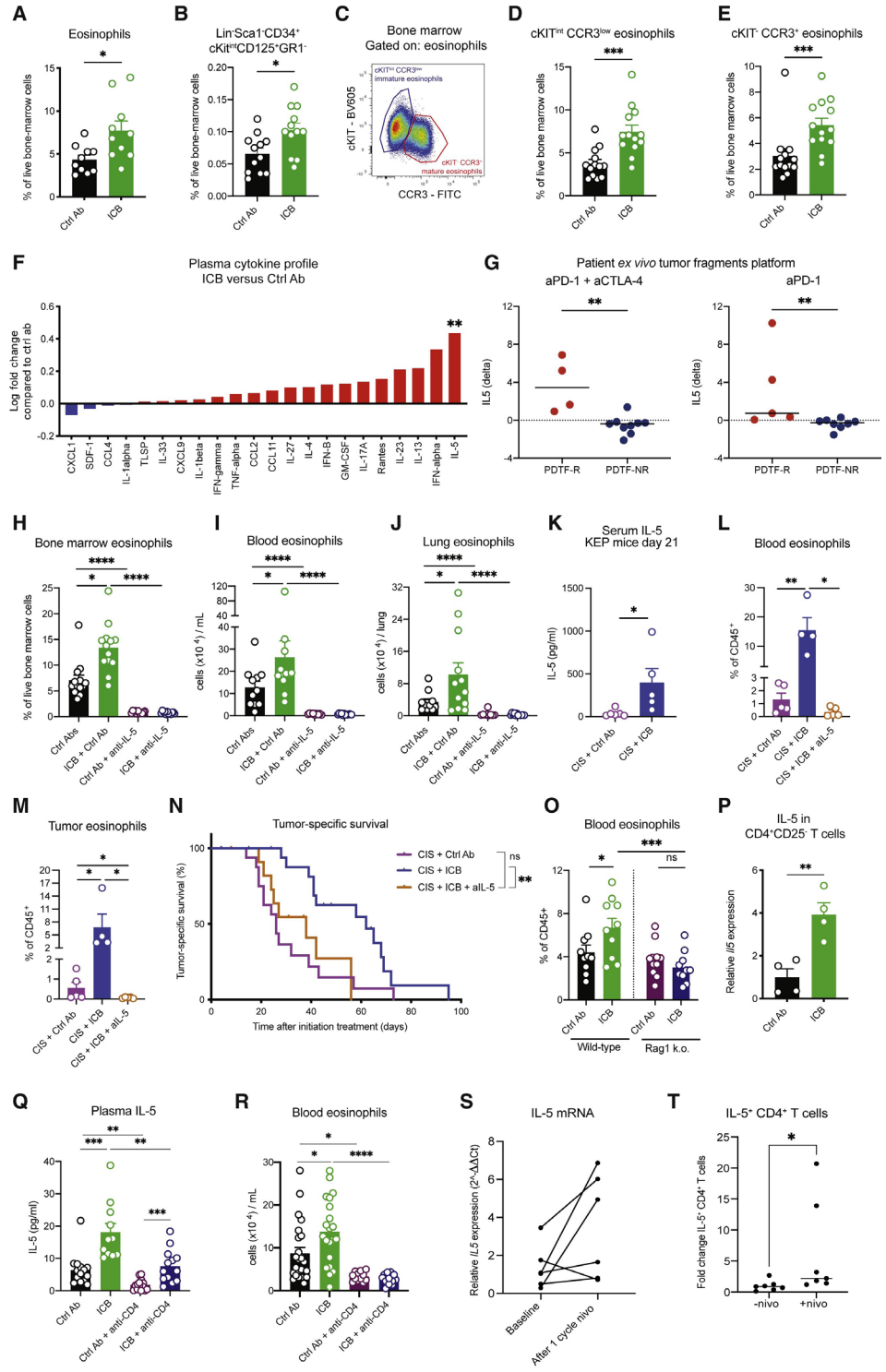

IL-5 producing CD4⁺ T cells drive eosinophil production and systemic expansion upon ICB

IL-5 can be produced by various cell types, principally CD4⁺ T cells, type 2 innate lymphoid cells (ILC2) and other innate immune cells, such as mast cells and eosinophils[44]. To evaluate whether adaptive or innate immune cells are needed to induce eosinophils upon ICB, we treated KEP tumor-bearing wild-type and *Rag-1*-deficient mice, which lack mature B and T cells but retain ILC2s and myeloid cells, with ICB or control antibody. Importantly, ICB failed to induce an increase in eosinophils in tumor-bearing *Rag*-1-deficient mice (Figure 5O), indicating that adaptive immune cells trigger eosinophil expansion upon ICB. Based on these findings, we hypothesized that CD4⁺ T cells are the main source of IL-5 upon ICB, and thus cause eosinophilia. Indeed, we observed increased expression of *IL-5* mRNA in circulating $CD4^+CD25^-$ T cells upon ICB in metastasis-bearing mice (Figure 5P). Depletion of CD4⁺ T cells reduced plasma IL-5 levels and the number of eosinophils in bone marrow and blood of metastasis-bearing mice (Figure 5Q,R & S6G), suggesting a role for CD4⁺ T cells in eosinophil homeostasis. Importantly, in the absence of CD4⁺ T cells, there was reduced induction of IL-5 by ICB (Figure 5Q). Notably, ICB treatment still induced a slight but significant increase of serum IL-5 in CD4⁺T cell-depleted mice compared to controls (Figure 5Q & S6G) suggesting other sources of IL-5, such as ILC2s, mast cells and eosinophils may produce the residual IL-5. Importantly, in line with the reduced induction of IL-5 upon ICB in the absence of CD4⁺ T cells, systemic eosinophil numbers did not increase upon ICB in CD4⁺ T cell-depleted mice (Figure 5R & S6H). In addition to mature bone marrow eosinophils, the frequency of $Lin^-Sca1^-CD34^+cKit^{Int}CD125^+Gr1^-$ eosinophil progenitors did not increase upon ICB after CD4⁺ T cell depletion (Figure S6I). These data demonstrate that CD4⁺ T cells are required for the ICB-induced increase in systemic IL-5 levels, eosinophil production in the bone marrow and systemic eosinophil accumulation. Importantly, CD4⁺ T cell depletion also reduced the number of circulating eosinophils in metastasis-bearing mice treated with CIS+ICB (Figure S6J), confirming that CD4⁺ T cells are required for eosinophil increase not only upon ICB treatment alone, but also during CIS+ICB. To exclude the potential contribution of T_{regs} in ICB-induced eosinophilia, we used KEP tumor-bearing *Foxp3*$^{DTR\text{-}GFP}$ mice allowing specific depletion of FOXP3 expressing T_{regs} (Figure S6K,L)[47]. Upon T_{reg} depletion, blood eosinophil numbers during ICB were further increased compared to T_{reg}-proficient mice (Figure S6M), indicating that T_{regs} do not facilitate ICB-induced eosinophil expansion, but hamper ICB-induced eosinophilia.

To address whether CD4⁺ T cells are a source of IL-5 in TNBC patients, we utilized peripheral blood mononuclear cells (PBMCs) isolated from patients of the TONIC trial treated with ICB without induction treatment at baseline and after one cycle of nivolumab and performed RT-qPCR for *IL-5* mRNA in sorted CD4⁺ T cells. 5 out of 6 patients had an increase in *IL-5* transcript in CD4⁺ T cells upon nivolumab treatment compared to baseline (Figure 5S). To further demonstrate that CD4⁺ T cells produce IL-5 protein in response to nivolumab, we stimulated PBMCs from TNBC patients with nivolumab for 48 hours and analyzed

intracellular IL-5 in CD4⁺ T cells by flow cytometry. These data show a statistically significant fold change in IL-5⁺ CD4⁺ T cells upon nivolumab stimulation (Figure 5T), demonstrating that aPD-1 induces IL-5 expression in circulating CD4⁺ T cells of TNBC patients. Collectively, our data demonstrate that IL-5 producing CD4⁺ T cells drive eosinophil expansion upon ICB.

IL-33 drives eosinophil recruitment to the TME and is required for the therapeutic benefit of CIS+ICB

Although ICB alone leads to systemic eosinophil accumulation, eosinophil recruitment to the tumor and their subsequent contribution to therapeutic benefit was only observed upon CIS+ICB combination therapy in our pre-clinical models (Figure 3). We therefore asked which eosinophil-recruiting or activating factors trigger the intratumoral accumulation of eosinophils upon CIS+ICB. Analysis of a broad panel of eosinophil-related cytokines and chemokines revealed that IL-33 was specifically increased upon CIS+ICB in the plasma of metastasis-bearing mice at the responsive phase of therapy (Figure 6A). Similarly, IL-33 levels were increased in tumor lysates and serum of KEP tumor-bearing mice treated with CIS+ICB (Figure 6B & S7A). Importantly, in patients with metastatic TNBC responding to ICB we observed a strong positive correlation between the eosinophil gene signature and *IL-33* expression in metastatic lesions which was not observed in non-responders, suggesting a link between *IL-33* expression and eosinophil infiltration in the TME (Figure 6C). Of note, in both patients and mice, cisplatin alone was not sufficient to induce a statistically significant increase in IL-33 levels (Figure 6B & S7A,B). IL-33 is an alarmin that amplifies immune responses during inflammation[48]. IL-33 directly promotes eosinophil activation, adhesion and survival[49 50], and IL-33 contributes to several eosinophilic disorders[51]. In the cancer context, IL-33 has been associated with both pro- and anti-tumor functions[14,52,53]. To assess the functional role of IL-33 in intratumoral eosinophil accumulation, we made use of the IL-33-TRAP fusion protein, a high-affinity IL-33 antagonist[54]. In line with our earlier observation that IL-5 is responsible for ICB-induced systemic eosinophilia (Figure 5), IL-33 neutralization did not affect systemic eosinophil accumulation during CIS+ICB (Figure 6D). However, intratumoral eosinophil infiltration was abrogated upon IL-33 blockade (Figure 6E), indicating that IL-33 is required, directly or indirectly, for eosinophil recruitment to the tumor. IL-33-TRAP also prevented the intratumoral CIS+ICB-induced CD8⁺ T cell activation without affecting other immune populations (Figure 6F & S7C,D), phenocopying the effect of eosinophil depletion (Figure 4). Importantly, IL-33-TRAP blocked the therapeutic benefit provided by CIS+ICB (Figure 6G). In summary, these data demonstrate that IL-33 is required for eosinophil infiltration in the tumor, CD8⁺ T cell activation, and therapeutic benefit observed upon ICS+ICB. These preclinical findings are supported by our clinical observation that increased intratumoral eosinophil infiltration is strongly correlated to IL-33 expression as well as to CD8⁺ T cells in the TME of TNBC patients responding to ICB (Figure 2C-H & 6C).

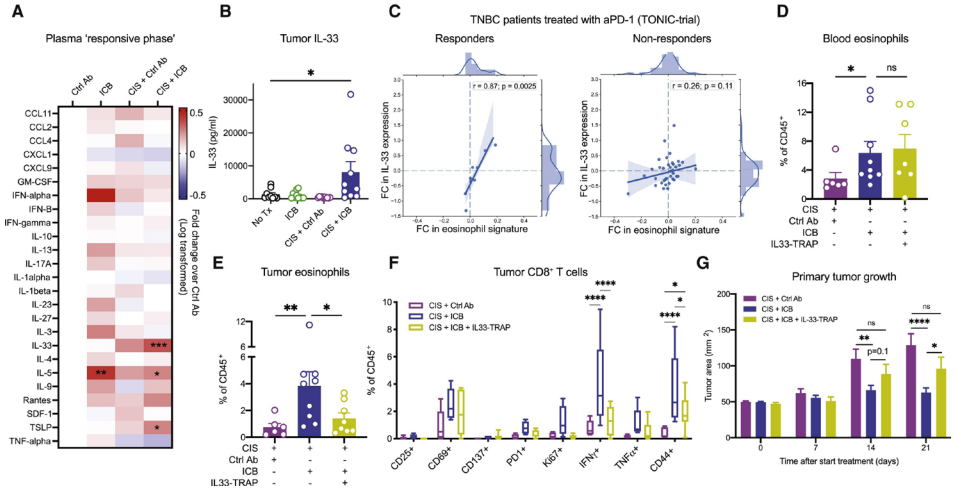

Figure 6. IL-33 drives intratumoral eosinophil infiltration and is required for the therapeutic benefit of CIS+ICB. *(A) Relative expression of the indicated cytokines in plasma of metastasis-bearing mice treated as described before (Ctrl Ab n=9 (same data as in Figure 5F), ICB n=10 (same data as in Figure 5F), CIS+Ctrl Ab n=9, CIS+ICB n=13), determined by LEGENDplex. Data is normalized to Ctrl Ab-treated mice. 1-way ANOVA or Kruskal-Wallis followed by Dunnett's or Dunn's multiple comparisons test, comparing each treatment against control-treated mice, for each cytokine. (B) IL-33 levels in tumor lysates of end-stage tumors as determined by LEGENDplex (n=9-10). 1-way ANOVA followed by Dunnett's multiple comparisons test, comparing each group against untreated. (C) Correlation between the fold change (baseline to on-nivolumab) in eosinophil gene signature (described in Figure 2B) and the fold change (baseline to on-nivolumab) in IL33 in RNA-seq analysis of paired biopsies from responding (left) and non-responding (right) patients with metastatic TNBC. Graph characteristics as in Figure 2. (D-E) Frequency of eosinophils in the circulation (D) and tumor (E) of KEP mice analyzed 21 days after start of treatment determined by flow cytometry (n=6-9). Mean ±S.E.M., Mann-Whitney. (F) Frequency of indicated activation markers expressed on intratumoral CD8⁺ T cells , determined by flow cytometry (n=5-9). Data from CIS+Ctrl Ab and CIS+ICB are same mice as Figure 4G. Boxes represent median and interquartile range; whiskers full range. 2-way ANOVA followed by Tukey's multiple comparison test. (G) Average tumor growth size ±S.E.M. of KEP mice treated as indicated (CIS+Ctrl Ab n = 23, CIS+ICB n=32), CIS+ICB+IL33-TRAP n = 12). Unpaired t-test. ns, not significant, *p<0.05, **p<0.01, ***p<0.001, ****p<000.1. See also Figure S7A-D.*

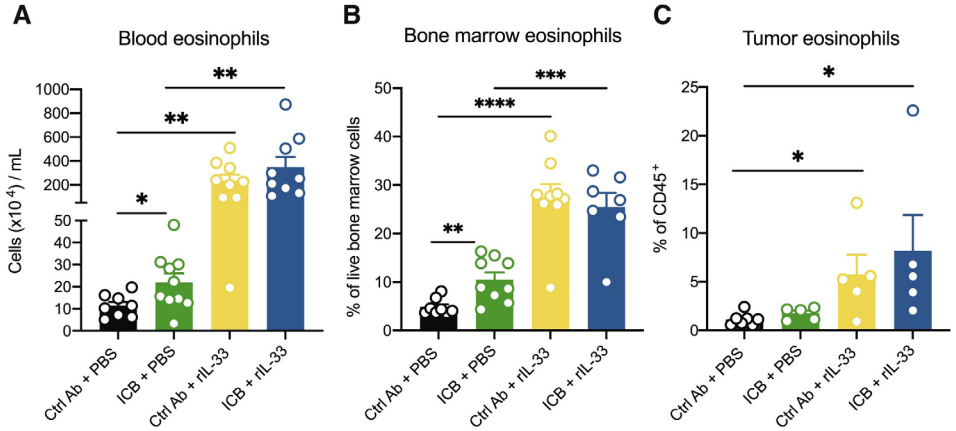

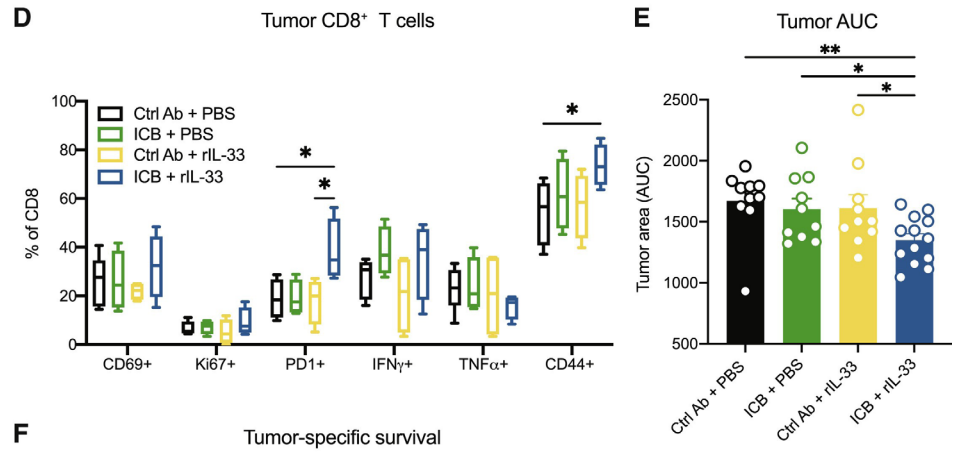

Figure 7. Recombinant IL-33 therapy engages eosinophils and enhances ICB response . *(A-C) Mice bearing orthotopically transplanted KEP tumors were treated as indicated (Ctrl Ab+PBS, n=10; ICB+PBS, n=15; Ctrl Ab+rIL-33, n=15; ICB+rIL-33, n=15). Frequency of eosinophils in the circulation (A), bone marrow (B), and tumor (C) were analyzed in the responsive phase of therapy, determined by flow cytometry. Mean ±S.E.M., t-test. (D) Frequency of indicated activation markers expressed on intratumoral CD8⁺ T cells in responsive phase of therapy, determined by flow cytometry (n=5-7). Boxes represent median and interquartile range; whiskers full range. 2-way ANOVA followed by Tukey's multiple comparison test. (E) Area under curve (AUC) of growth curves was determined up to day 14 after start of treatment. Mean ±S.E.M., 1-way ANOVA. (F) Kaplan-Meier survival curves showing tumor-related survival. Log-rank (Mantel-Cox) test. ns, not significant, *p<0.05, **p<0.01, ***p<0.001, ****p<0.0001. See also Figure S7E-F.* ▶▶▶

Recombinant IL-33 engages eosinophils and enhances response to ICB

In light of our finding that IL-33 drives eosinophil infiltration into the tumor, we hypothesized that deliberate induction of intratumoral accumulation of ICB-educated eosinophils by recombinant IL-33 (rIL-33) might represent a viable strategy to enhance the therapeutic benefit of ICB in breast cancer, in absence of chemotherapy. Treatment of mice bearing orthotopically transplanted KEP tumors with rIL-33 alone or in combination with ICB resulted in increased eosinophils in the blood and bone marrow, as well as increased intratumoral eosinophil infiltration (Figure 7A-C). However, only the combination of ICB and rIL-33 increased $CD8^+$ T cell activation, and most notably increased the frequency of effector $CD44^+$ and $PD\text{-}1^+$ $CD8^+$ T cells (Figure 7D), without altering other immune populations (Figure S7E-F). Importantly, IL-33-mediated engagement of eosinophils during ICB and the resulting $CD8^+$ T cell activation was accompanied by improved tumor control and extension of survival (Figure 7E-F). Collectively, these data provide proof-of-principle that rIL-33 can engage eosinophils and represents a viable strategy to enhance response to ICB in breast cancer.

Discussion

In this study, we take a translational approach by combining longitudinal analysis of fresh blood and tumor biopsy samples of a patient cohort with functional experiments in clinically relevant mouse models to identify the IL-5 and IL-33-eosinophil axis as crucial mediator of ICB response in breast cancer. The effect of ICB on myeloid cells and the influence of myeloid cells on ICB response is often overlooked. We here show that an ICB-induced increase in systemic IL-5, driven by $CD4^+$ T cells, pushes myelopoiesis towards increased eosinophil production resulting in systemic eosinophil accumulation. Here, parallels can be drawn with allergic conditions in which $CD4^+$ T cells and eosinophils have a pathogenic function. In patients with allergic asthma, $CD4^+$ T cells play a major role in the pathophysiology driving eosinophil expansion via IL-5 production[44,55]. How ICB triggers this mechanism in the cancer context is not fully elucidated, but we demonstrated that $CD4^+$ T cells of TNBC patients upregulate IL-5 *in vivo* and *in vitro* upon stimulation with nivolumab/aPD-1, indicating that ICB can directly stimulate $CD4^+$ T cells to secrete IL-5. A role for PD-1/PD-L1 signaling in controlling IL-5 secretion from $CD4^+$ T cells has previously been proposed in the context of allergy, where *in vitro* exposure of human allergen-specific $CD4^+$ T cells to PD-1 blockade stimulated their production of IL-5, among other cytokines[56]. Altogether, we demonstrate that ICB-activated $CD4^+$ T cells use a similar mechanism via IL-5 to drive eosinophil accumulation in cancer patients and preclinical models.

Although neutrophils and basophils also derive from common-myeloid progenitors (CMP), express IL5R and can respond to IL-5 in certain inflammatory conditions[57,58], IL-5 is the central cytokine specific to eosinophil development in the bone marrow[59]. IL-33 is also

implicated in eosinophil development, capable of inducing IL-5 and upregulating IL-5Rα on eosinophil progenitors[60]. Interestingly, we observe that ICB, in absence of chemotherapy, increases IL-5 expression but not IL-33, indicating that ICB-induced IL-5 is not dependent on IL-33. This is further supported by our observation that systemic eosinophil abundance was unchanged upon IL-33 blockade during CIS+ICB, confirming that IL-5 is the main driver of eosinophil production in the bone marrow and systemic eosinophil accumulation upon ICB.

We demonstrate that ICB can be sufficient to induce systemic eosinophil increase, but in the majority of patients and in our mouse models (which do not respond to ICB alone), this is not enough to achieve intratumoral eosinophil infiltration. We uncover that induction of IL-33 is needed to overcome this threshold and enable eosinophil infiltration into the tumor. IL-33 can either directly affect eosinophil activation and recruitment, as has been shown for eosinophils in inflammatory diseases[49,50], or indirectly by acting on other cells of the tumor microenvironment, for instance by promoting chemokine expression in tumor cells[16]. IL-33 can be passively released by epithelial cells upon cellular damage[61] or actively secreted by immune cells during infection[62] and tumor cells themselves[63]. Importantly, in our mouse models cisplatin alone was not sufficient to increase IL-33 expression, indicating that cell damage induced by chemotherapy is not the sole driver of increased IL-33. By combining CIS+ICB we were able overcome this threshold and kick start the IL-33 aspect of the cascade in our mouse models. Future research is warranted to understand which other therapeutic modalities besides cisplatin may induce intratumoral IL-33 and whether these depend on cancer cell-intrinsic features or context-dependent mechanisms remains to be elucidated. For example, in patients the net-biological effect of IL-33 is influenced by levels of soluble ST2 (also known as *IL1RL1*), which acts as a decoy receptor for IL-33, and for which different genetic variants exist in humans[64]. Thus, adding layers of complexity to the regulation of the identified immune axis.

Identifying the source of IL-33 and deciphering how its production is regulated during ICB would be important to further harness its full therapeutic potential to synergize with ICB.

The synergy between rIL-33 and ICB has been studied in highly immunogenic models[65,66], but not, to our knowledge, in poorly immunogenic breast cancer models. Our observation that IL-33 expression correlates with an eosinophil signature in metastases of breast cancer patients that respond to ICB and our preclinical proof-of-principle study demonstrating that rIL-33 mobilizes eosinophils to improve ICB response, indicate that IL-33 represents an attractive engager of eosinophils in breast cancer patients during ICB. However, IL-33 is reported to have pleiotropic functions[67]. The systemic administration of rIL-33, as performed in this study, induced an effective but modest anti-tumor response, especially in comparison with CIS+ICB, likely because of the direct anti-tumor effect and additional immunomodulatory properties of cisplatin[68,69]. Further studies are needed to evaluate whether IL-33 in

combination with ICB could be used to specifically engage eosinophils in patients, for instance by local IL-33 administration, although, in the context of multi-organ metastatic disease, local administration of rIL-33 would be challenging.

It has been suggested that ICB-induced eosinophils may exert direct tumoricidal effects or enhance anti-tumor immunity by changing the tumor vasculature or reshaping the immune landscape[6]. Eosinophils can facilitate recruitment of $CD8^+$ T cells by expression of T cell chemoattractants[11,25] or promote T cell activation in the tumor[13]. We demonstrate that eosinophils enhance $CD8^+$ T cell activation, rather than their recruitment, in mammary tumors responding to CIS+ICB. In line with our findings in mouse models, we observed that increased expression of an eosinophil gene signature correlated with increased $CD8^+$ T cell and IFNγ gene signatures in metastatic lesions of breast cancer patients responding to ICB. This suggests that in TNBC patients, eosinophils also contribute to ICB response via activation of $CD8^+$ T cells, as was previously proposed for melanoma patients[19]. It remains to be determined whether eosinophils exert this function directly, for example by producing T cell stimulating cytokines or chemokines, or indirectly via activation of for instance dendritic cells, as has been described during allergic inflammation[70-72].

In our study, the treatment of mice and patients differed. In our mouse models, cisplatin and dual ICB was needed to induce responses, while patients were treated with ICB alone or preluded by a brief induction treatment. Despite these differences in dosage regime and type of ICB therapy, we strikingly uncovered the same phenomena of increased eosinophils in response to ICB, indicating that the mechanism described in this study is a general feature of effective ICB response. This is supported by our observation that response to ICB leads to eosinophil accumulation in several cancer types and by a recent small series of 14 TNBC patients in which an eosinophil increase was observed upon response to anti-PD-L1 and paclitaxel[73]. Additionally, we validated in patients the different elements of the mechanism identified in our preclinical models. We observed that circulating $CD4^+$ T cells of TNBC patients upregulate IL-5 expression upon nivolumab treatment *in vivo* and *in vitro*. Moreover, our data demonstrating that IL-5 is secreted in tumors that show an immunological response upon *ex vivo* ICB stimulation with either aPD-1 or combined aPD-1+aCTLA-4, further strengthen our conclusion that IL-5 induction is a common mechanism across different tumor types and ICB regimens with or without chemotherapy.

Finally, it has been suggested that increased eosinophil counts upon ICB could be used as an early predictive biomarker for response[19-24]. Although we see expansion of these cells upon response to ICB in patients with metastatic TNBC, NSCLC and early-stage pMMR CC, on-treatment response biomarkers are rarely used in oncology due to widely available imaging methods for response assessment. Moreover, eosinophil expansion was not restricted to responders, but was also observed in a proportion of non-responders as previously reported, limiting its potential for clinical decision making[19-24]. Therefore, increased

eosinophils upon ICB response, combined with our preclinical proof of their causal role in ICB response, should be considered as an important lead for the development of novel immunomodulatory strategies to engage eosinophils rather than a biomarker.

In conclusion, this study highlights that combining translational research on clinical trials with mechanistic research in preclinical models is a powerful strategy to unravel novel mechanisms of ICB response. Our findings emphasize that successful anti-tumor immune responses are not only reliant on T cells, but that crosstalk with myeloid cells is critical for an effective response to ICB, providing new avenues for future research in immuno-oncology.

STAR Methods

RESOURCE AVAILABILITY

Lead contact

Requests for further information and resources of this study should be directed to Karin de Visser (k.d.visser@nki.nl)

Materials availability

This study did not generate new unique reagents.

Data and code availability

- RNA-sequencing data on mouse eosinophils generated in this study has been deposited at Gene Expression Omnibus (GEO) under accession number GSE210895 and are publicly available from the date of publication. RNA-sequencing data on tumor biopsies of TNBC patients treated in the TONIC-trial stage 1 are deposited at the European Genome-phenome Archive (EGA) under accession number EGAS0001003535 and will be made available from the corresponding author on reasonable request. NanoString data from TONIC-trial stage 1 and RNAseq data of TNBC patients treated in TONIC-trial stage 2 reported in the paper are not deposited in a public repository pending ongoing work but can be made available from the corresponding authors upon reasonable request. All human data requests will be reviewed by the Institutional Review Board (IRB) of the NKI and applying researchers have to sign a data transfer agreement after IRB approval before the data can be released.
- This paper does not report original code.
- Any additional information required to re-analyze the data reported in this paper is available from the lead contact upon request.

EXPERIMENTAL MODEL AND SUBJECT DETAILS

Preclinical models

The transgenic *Keratin14-cre;Cdh1$^{F/F}$;Trp53$^{F/F}$*(KEP) model for primary mammary tumorigenesis [34] (FVB/N genetic background), KEP-based orthotopic mammary tumor model and the KEP-based model for spontaneous breast cancer metastasis [35] were used as previously described [26,27]. Female KEP mice were monitored twice per week for spontaneous tumor formation by palpation starting at the age of 3.5 months. KEP mice develop palpable tumors between 6-8 months of age[34]. The perpendicular diameters of the tumors were measured using a caliper and tumor area was calculated accordingly. Female FVB/N mice of 8-12 weeks of age were obtained from Janvier Labs. *Rag1* k.o. in FVB/N genetic background were a gift from L. Coussens[74]. *Cdh1$^{F/F}$;Trp53$^{F/F}$;Foxp3$^{DTR-GFP}$* mice[75] in FVB background were generated by the Animal Modeling Facility (AMF) of the Netherlands Cancer Institute. All mice were kept in individually ventilated cages at the animal laboratory facility of the NKI. Food and water were provided ad libitum. All animal experiments were approved by the Animal Ethics Committee of the NKI and performed in compliance with the national and European guidelines for animal care and use.

Clinical trial procedures

Trial procedures were performed as described previously in the respective publications [28-31]. All patients included in stage 1 [28] and stage 2 of the TONIC-trial (NCT02499367) were included in the current analysis. In stage 1, 70 patients were included in the TONIC-trial, of which 67 patients received nivolumab and were available for efficacy and translational analysis, as previously described [28]. An additional 47 patients were included in stage 2 of the trial, of which 44 patients received nivolumab and were available for efficacy and translational analysis. From these 111 patients (Table S1), paired flow cytometry on fresh blood (baseline, after two-week induction period and after 3 cycles of nivolumab) was performed on 55 patients and paired routine eosinophil counts were available for 90 patients (sample availability in Table S2 and Figure S1b). Progression-free survival was measured as time between date of randomization and date of progression according to iRECIST or date of death. Overall survival was measured as time between first date of nivolumab and date of last follow-up or date of death. Data was cut-off at 1 March 2021.

Patients with metastatic NSCLC were treated in the PEMBRO-RT trial (NCT02492568)[29] at the NKI (paired data for n=40 from the total of 55 patients treated at the NKI and the total of 76 patients included in the trial), in which patients were randomized to pembrolizumab with or without upfront radiation [29]. To investigate eosinophil dynamics in patients with metastatic dMMR tumors, we made use of patients treated with nivolumab in the NKI within the dMMR cohort (paired data for n=9 of the total 11 patients treated at the NKI and the total of 30 patients included in the cohort) of the DRUP-trial (NCT02925234) [31]. Finally, patients with early-stage colon cancer (either dMMR (n=21) or pMMR (n=17)) were treated in the NICHE-trial, in which patients are treated with neo-adjuvant ipilimumab (1mg/kg) and nivolumab (3mg/kg), with or without additional celecoxib in pMMR patients (NCT03026140)[30]. In the patients with metastatic disease, response was defined as complete response (CR), partial response (PR) and stable disease (SD) of at least 24 weeks, defined according to RECIST1.1 [76]. Best overall response in the TONIC-trial was measured according to iRECIST[77]. Response in the NICHE-trial was defined as any pathological response (>10% tumor regression), assessed on surgical material after neo-adjuvant treatment. All clinical study protocols were approved by the medical-ethical committee of the NKI and conducted in accordance with the ICH Harmonized Tripartite Guideline for Good Clinical Practice and the principles of the Declaration of Helsinki. All patients provided written informed consent to participate in the clinical trial.

METHOD DETAILS

Preclinical intervention studies

In the spontaneous KEP model, all treatments started when tumor area reached 50mm^2. For the KEP-based orthotopic mammary tumor model, mammary tumor pieces of 1mm^2 size derived from KEP mice were orthotopically transplanted into the mammary glands of female FVB/N mice. In this model, treatments started when tumor area reached 25 mm^2. For the survival experiments and endpoint analysis mice were sacrificed when the cumulative tumor burden reached 225mm^2. KEP mice were sacrificed 21 days after initiation treatment to analyze the 'responsive phase' or at a tumor size of 150mm^2 for the KEP-based orthotopic mammary tumor model. Cisplatin (Accord Healthcare Limited) was injected intravenously once every two weeks at 5mg/kg, for a maximum of 4 cycles. Anti-mouse PD-1 (RMP1-14, BioXCell), anti-mouse CTLA-4 (9D9, BioXCell) or control (2A3, BioXCell) antibodies were each given intraperitoneally at 100µg per mouse, twice per week. Anti-CD8 (2.43, BioXCell) or anti-CD4 (GK1.5, BioXCell) antibody were given intraperitoneally at 200µg per mouse, twice per week. Anti-mouse SiglecF (238047, R&D systems) and control antibody (2A3, BioXCell) were administered intraperitoneally at 20µg per mouse, three times a week. Anti-IL-5 (TRFK5, BioXCell) and control antibody (HRPN, BioXCell) were given intraperitoneally at 500µg per mouse, twice per week. Recombinant mouse IL-33 (Biolegend) was given intraperitoneally at 0,4 µg per mouse, three times a week. IL-33-TRAP (provided by Rudi Beyaert laboratory, VIB, Belgium) was given intraperitoneally at 50µg per mouse daily. For the T_{reg} depletion in *Foxp3-GFP-DTR* mice, DT (Diptheria toxin from *Corynebacterium diphteriae*) was given intraperitoneally at 25µg/kg, at day 0 and day 4 after start of treatment. All antibody treatments continued until the experimental endpoint was reached.

For metastasis experiments, mammary tumor pieces of 1mm^2 size derived from KEP mice were orthotopically transplanted into the mammary glands. Mammary tumors were surgically removed when they reached the size of 100mm^2. In the metastasis experiments, all treatments started 15 days after mastectomy, when all mice have established metastasis in the lung and/or lymph node, and treatments continued until the experimental endpoint. All treatments were performed as described above. For survival experiments, mice were sacrificed when they developed signs of distress caused by metastatic disease (respiratory distress) or when lymph node metastasis reached the size of 225mm^2. For analysis of 'responsive phase', metastasis-bearing mice were sacrificed 10 days after start of treatment for Ctrl Ab and ICB groups and 21 days for CIS+Ctrl Ab and CIS+ICB groups.

Flow cytometry analysis

Tumors and organs from KEP mice and FVB/N mice with metastatic breast cancer were collected in ice-cold PBS. Blood was withdrawn by tail vein or heart puncture and collected in K_2EDTA-containing tubes (BD Microtainer Blood Collection Tubes). Tumor tissues and lungs were mechanically minced using the McIlwain tissue chopper (Mickle Laboratory

Engineering) and enzymatically digested at 37°C in DMEM medium containing 3mg/ml collagenase type A (Roche) plus 25µg/ml of DNase I (Sigma) for 45 min or in 100µg/mL Liberase TM (Roche) for 30 min, respectively. Half of the lymph nodes and spleen were enzymatically digested in RPMI medium containing 3mg/ml collagenase type IV (ThermoFisher Scientific), 2mM $CaCl_2$, 2% FCS and 25µg/mL DNase I for 30 min at 37°C and used to stain for myeloid cell populations. The other half was directly processed into single cell suspensions and used for lymphoid cell panels. All digestion reactions were stopped by adding cold DMEM medium containing 10% FCS. For the analysis of bone marrow, tibia and femurs were flushed with PBS and processed as the other organs. Single-cell suspensions were obtained by mashing through 70µm filter and resuspended in PBS containing 0.5% BSA (Roche) and 2mM EDTA (Lonza). Blood, spleen, lungs and bone marrow samples were treated for 5 min at room temperature with NH_4 lysis buffer to remove erythrocytes.

For flow cytometry analysis of patient sample preparations, peripheral blood was collected in an K_2EDTA vacutainer (BD) and processed and analyzed within 24 hours. Red blood cells were lysed (lysis buffer: dH_2O, NH_4Cl, $NaHCCO_3$, EDTA) and cells were resuspended in PBS containing 0.5% BSA and 2mM EDTA. To obtain absolute white blood cell counts per mL of human blood, the total post-lysis cell count was obtained using the NucleoCounter NC-200 (Chemometec) Automated cell counter was divided by the total volume (mL) of blood.

For intracellular cytokine staining, cells were stimulated *ex vivo* with 50ng/ml PMA, 1µM ionomycin and Golgi-Plug (1:1000; BD) for 3h at 37°C in IMDM medium supplemented with 8% FCS, 100 IU/ml Penicillin-Streptomycin (Roche) and 0.5% β-mercaptoethanol. For surface antigen staining, cells were first incubated with rat anti-mouse CD16/CD32 antibody (1:100; Mouse Fc Block, BD Bioscience) or human FcR Blocking Reagent (1:100 Miltenyi) for 15 min at 4°C and then incubated with fluorochrome-conjugated antibodies for 30 min at 4°C, in the dark. For intracellular antigen staining, cells were fixed with Fixation/Permeabilization solution 1X (Foxp3/Transcription Factor Staining Buffer Set, eBioscience) for 30 min at 4°C and stained with fluorochrome-conjugated antibodies in Permeabilization buffer 1X (eBioscience) for 30 min at room temperature. Viability was assessed by staining with either 7AAD staining solution (1:20; eBioscience), Zombie Red Fixable Viability Kit (1:800 BioLegend) or with Fixable Viability Dye APC-eFluor780 (1:1000; eBioscience). Data acquisition was performed on BD LSRII flow cytometer using Diva software (BD Biosciences) and data analysis was performed using FlowJo software version 10.6.2. All used flow cytometry antibodies can be found in Key Resources Table. Gating strategies are displayed in Figure S8 & 9.

Immunohistochemistry

KEP tumors were fixed for 24h in 10% neutral buffered formalin, embedded in paraffin and sectioned at 4µm. CD4, CD8, FOXP3 and Ly6G stainings were performed by the Experimental

Animal Pathology facility of the NKI. Antibodies are listed in Key Resources Table. For MBP staining, sections were deparaffinized in xylene for 20 min, rehydrated, and incubated with 3% H_2O_2 for 10 min at room temperature. Antigen retrieval was performed using Pepsin solution (ThermoFischer Scientific) for 10 min at room temperature. As blocking solution PBS with 2.5% BSA and 10% normal goat serum was used for 30 min at room temperature. Sections were incubated with rat anti-mouse MBP antibody (1:350, clone MT-14.7.3, Lee Laboratory, Mayo Clinic) diluted in 0.5X blocking solution, overnight at 4°C. Biotinylated goat anti-rat IgG antibody (1:300, Southern Biotech) was used as secondary antibody. Streptavidin-HRP and DAB solution (DAKO) were used following manufacturer's instructions. Sections were counterstained with hematoxylin solution. Slides were scanned using Aperio ScanScope and analyzed with Aperio ImageScope software version 12.4.3 (Aperio, Vista).

RNA-sequencing of mouse eosinophils

For the transcriptomic analysis, a minimum of 35000 eosinophils ($CD11b^+$ $Ly6G^{low}$ SSC^{high} $F4/80^+$) were sorted from the blood in RLT buffer containing 1% β-ME, using a BD FACSAria™ Fusion Cell Sorter. RNA was isolated following RNeasy Mini Kit (Qiagen) protocol, using 80% ethanol instead of RPE buffer. Smart-seq2 library preparation was performed as previously described[78], using 2100 Bioanalyzer System (Agilent) for quality control. Only samples with RIN ≥ 7 were used for RNA-sequencing analysis. The strand-specific reads (65bp single-end) were sequenced with the HiSeq 2500 System (Illumina). Demultiplexing of the reads was performed with Illumina's bcl2fastq software and demultiplexed reads were aligned against the mouse reference genome (build 38) using HISAT2. HISAT2 was supplied with known set of gene models (Ensembl version 87). Qlucore Omics Explorer (Qlucore AB, Lund, Sweden) software was used to calculate and visualize differentially expressed genes ($p<0,05$) and sample variation, after having discarded genes with fewer then 30 mapped reads in at least 9 samples and performed data normalization by TMM method. Gene set enrichment analysis (GSEA) was performed using the GSEA program version 4.0.3 (Broad Institute). Hallmarks gene sets from Molecular Signatures Database v7.2 were used. Mouse gene symbols were remapped to human orthologues using Mouse_Gene_Symbol_Remapping_Human_Orthologs_MSigDB.v7.2.chip annotation file.

Cytokine analysis

For the analysis of cytokines and chemokines expression in mouse plasma, serum or tumor lysate, custom-made Legend Plex bead-based immunoassay (Biolegend) was used, according to manufacturer instructions. 50 µg of total protein from lysed tissues was used for measurements. Data acquisition was performed on LSRFortessa (BD Biosciences) flow cytometer using Diva software (BD Biosciences) and analyzed using LEGENDplex™ Data Analysis Software Suite (Biolegend). In addition, mouse IL-5 ELISA detection kit (BioLegend) was used, according to manufacturer instructions.

Routine eosinophil counts in patient cohorts

Eosinophil counts were measured with a XN-2000 Hematology Analyzer of Sysmex at the diagnostic Clinical Chemistry Department. The variation coefficient was below 10%.

RNA extraction and NanoString gene expression analysis

RNA was isolated from freshly frozen sections of biopsies as previously described [28]. For each patient, sequential biopsies were taken from the same metastatic lesion, however per patient, the site of the metastatic lesion was different (predominantly, but not only, lymph nodes, recurrent lesion in breast, liver, skin). mRNA expression was measured with the nCounter technology provided by NanoString Technologies as previously described [28]. NanoString mRNA counts were available for patients included in stage 1 of the TONIC-trial (paired metastatic biopsies pre-nivolumab and on-nivolumab n = 26).

RNA-sequencing on patient tumor biopsies

The RNA-sequencing data was aligned to the reference genome GRCh38 with STAR (version 2.7.1a) [79] with two-pass mode option set to "Basic". For comparison between patients, a median of ratios normalization was performed with Deseq2 R package (version 1.24.0, [80]) and for within-patient comparisons TPM normalization was used. Data was analyzed using Python 3.7.6, with pandas (version 1.0.1,[81,82]) and NumPy (version 1.18.1,[83] packages. Plots were created using Matplotlib (version 3.1.3, [84]) and Seaborn (version 0.10.0,[85]), statistical annotation was added using statannot (version 0.2.2,[86]). All gene-signatures are listed in Table S3. Mean normalized expression values of individual genes were taken as a signature score. A fold change of the signature score baseline vs. on-nivolumab was taken for each signature. RNA-sequencing on paired metastatic lesions (baseline and on-nivolumab) was available for 48 patients, included in both stages of the trial.

RT-qPCR

Human $CD3^+$ $CD4^+$ T cells were sorted from TONIC patient PBMCs into RLT buffer containing 1% β-ME, using a BD FACSAria™ Fusion Cell Sorter. RNA was isolated following RNeasy Micro Kit (Qiagen) protocol. RNA was converted to cDNA with an AMV reverse transcriptase using Oligo(dT) primers (Invitrogen). For mouse $CD4^+CD25^-$ T cells, RNA was converted to cDNA using High-capacity cDNA reverse transcription kit (ThermoFisher Scientific), following kit instructions. cDNA (20 ng per well) was analyzed by SYBR green real-time PCR with 500 nM primers using a LightCycler 480 thermocycler (Roche). *Gapdh* was used as a reference gene. Primer sequences used for each gene are listed in the Key Resources Table. Fold change in expression was calculated using $2^{-(\Delta Ct.x - average(\Delta Ct.control))}$.

Human PBMC stimulation

PBMCs were isolated at baseline from patients with metastatic TNBC in the control arm of the TONIC trial. Patient PBMCs were seeded at a density of 500,000 cells per well in 96-well plates in DMEM (Sigma), 10% FBS (Sigma), 1 mM sodium pyruvate (Sigma), 1x MEM nonessential amino acids (Sigma), 1x Glutamax, 100 ng/ml penicillin/streptomycin, 50 nM 2-mercaptoethanol (Sigma). Cells were stimulated with a suboptimal concentration of 0.5µg/ml plate bound anti-CD3 (OKT3, BioLegend) and 2µg/ml anti-CD28 (28.2, eBioscience) for 48 hours. Anti-PD1 (Nivolumab,10µg/ml) was added where indicated. GolgiPlug was added to each well for the final 4 hours of stimulation and cells were analyzed by flow cytometry as described above.

PDTF culture and stimulation

PDTF cultures were performed as described previously[45,46]. Briefly, tumor samples were collected from surgical material of patients with renal cell carcinoma (anti-PD1+anti-CTLA-4 treated n=1 & anti-PD1 treated n=2), ovarian cancer (n=4 & n=1), melanoma (n=7 & n=5), non–small cell lung cancer (n=1 & n=3), and colorectal cancer (n=0 & n=1). Patient characteristics were described previously for samples stimulated with aPD-1 & aCTLA-4 [46] and listed in Supplementary Table 4 for samples stimulated with aPD-1. Definition of responder and non-responder PDTFs were described previously [45,46]. Samples were cut in fragments of 1-2 mm^3 and embedded in an artificial extracellular matrix in a 96-well plate. PDTF cultures were stimulated with medium supplemented with either anti-PD1 alone (nivolumab, Bristol-Myers Squibb) at 10 µg/ml or anti-PD-1 plus anti-CTLA4 (ipilimumab, Bristol-Myers Squibb) at 10 µg/ml where indicated. After 48 hours of culture at 37°C, supernatants were collected and IL-5 levels were measured using the LEGENDplex Human Th Cytokine (BioLegend), according to the manufacturer's protocol.

QUANTIFICATIONS AND STATISTICAL ANALYSIS

Statistical analysis was performed in GraphPad Prism (version 8.4.3) or SPSS Statistics (version 24). All statistical tests were two-sided. All p-values are uncorrected for multiple testing unless stated otherwise. For heatmaps of human flow cytometry data (Figure S1C-F), log_2 transformed cell count/mL or log_2 transformed fold change were depicted, centered around the median for each population (row) separately. Hierarchical clustering was performed on populations and patients based on 1 minus Pearson correlation and Euclidian distance respectively. Complete-linkage was used for both cell populations and patients. To assess dynamics in each cell population analyzed by flow cytometry between baseline and on-nivolumab, the median log_2 fold change from baseline to on-nivolumab (log_2(on-nivolumab) – log_2(pre-nivolumab) was plotted against Benjamini-Hochberg corrected p-values (Figure 1B). For dynamics in each cell population analyzed by flow cytometry between pre-nivolumab and on-nivolumab, linear modeling was performed (similar to a 2-way ANOVA) to predict log_2 fold changes between pre-nivolumab and on-nivolumab counts / mL based on response and induction treatment: Log_2-fold_change ~ response + induction_treatment. This model assumes that the response and induction treatment have an additive and independent effect on log fold changes. For each population responders were contrasted from non-responders. For Figure S2D, the regression coefficients associated with response for each population (x-axis) against the associated (Benjamini-Hochberg corrected) p-values (Wald-test) were plotted. The uncorrected (Wald-test) p-values associated with different induction treatments were estimated. For each population we performed a Shapiro-Wilk normality test on the regression residue to see if the normality assumption was violated.

ADDITIONAL RESOURCES

This paper included flow cytometry and hemocytometer data of blood samples and RNAseq data of tumor biopsies from patients with metastatic TNBC treated in the Netherlands Cancer Institute in the TONIC-trial **(**NCT02499367). This paper also included hemocytometer data on blood samples generated in the Netherlands Cancer Institute from patients with metastatic NSCLC treated in the PEMBRO-RT trial (NCT02492568), patients with metastatic dMMR tumors treated in the DRUP-trial (NCT02925234), and patients with early-stage colon cancer treated in the NICHE-trial (NCT03026140). Data were kindly provided by the principal investigators of the clinical trials. Further information on the clinical trial procedures and links to clinical publications can be found in the Methods section on clinical trial procedure and Key Resources Table.

KEY RESOURCES TABLE

The Key Resources Table is available in the online version of the paper.

Acknowledgements

We thank the patients and their families for participating in the clinical studies. We thank the Dutch Cancer Society (KWF10083, KWF13191) and Swiss National Science Foundation (P2FRP3_171794 and P400PM_18318/1 to L.S.) for funding the preclinical studies. We thank the BMS-International Immuno-Oncology Network (BMS/II-ON) and the Dutch Cancer Society (NKI2015-7710) for funding the TONIC study. The Dutch Cancer Society (10653ALPE) and A Sister's Hope contributed to the immunophenotyping of the TNBC patients. Research in the Kok group is funded by the Netherlands Organization for Scientific Research (NWO-VIDI 09150172010043) and the Hendrika Roet fund. Research in the De Visser laboratory is funded by the Dutch Cancer Society (KWF10623), Oncode Institute, KWF/Oncode grant 14339

and the Netherlands Organization for Scientific Research (NWO-VICI91819616). This research was further supported by an institutional grant to the NKI of the Dutch Cancer Society and the Dutch Ministry of Health, Welfare, and Sport. I.S.A. holds a fundamental mandate of the Foundation against Cancer. We acknowledge the supporting staff of the clinical trials of the departments of Medical Oncology, Biometrics, Clinical Chemistry and the Triallab. We acknowledge the Core Facility of Molecular Pathology & Biobanking and Michiel de Maaker for human RNA isolations and the Genomics Core Facility for RNA-sequencing support. We thank the Animal Laboratory Facility, Intervention Unit, Imaging Unit, Experimental Animal Pathology Facility and Flow Cytometry Facility for their support. Finally, we would like to thank everyone in the De Visser and Kok labs for inspiring discussions.

Author Contributions

O.S.B., H.G., L.S., L.V., K.E.d.V and M.K. designed and performed experiments, analyzed and interpreted the data and wrote the manuscript. O.S.B., and L.S. performed the preclinical experiments with contributions from K.Ke., H.G., D.P., C.-S.H., K.V., E.A.M.R., D.K., K.Ko., I.S.A. and R.B., supervised by K.E.d.V.. H.G. performed the blood phenotyping of the TONIC-trial together with N.B., C.K., M.D, M.B., and K.V., supervised by K.E.d.V, and M.K.. L.V. coordinated and analyzed the data of the TONIC-trial of which M.K. is the principal investigator. O.I.I. and E.v.D performed bioinformatic analysis on the RNA-sequencing and blood phenotyping data of the TONIC-trial, respectively. M.C., W.T. and L.H. coordinated trial procedures and collected clinical data of the NICHE-trial, PEMBRO-RT trial and DRUP-trial, respectively. P.B. and E.E.V. are the principal investigators of the PEMBRO-RT and the DRUP-trial, respectively. P.K. & D.S.T. developed and analyzed the data of the PDTF platform. L.F.A.W. supervised bioinformatic and statistical analysis and contributed to interpreting the results. All authors edited and approved the manuscript.

Declaration of interests

O.S.B., H.G., L.S., L.V., O.I.I., E.v.D., N.B., C.K., M.D., K.Ke., M.B., D.P., C.S.H., K.V., E.A.M.R., D.K., L.H., K.Ko., I.S.A., P.K., R.B., and D.S.T. have no competing interests to declare. M.C. reports funding to the institute from BMS and Roche/Genentech and an advisory role for BMS, outside the submitted work. W.T. reports receiving grants from MSD during the conduct of the PEMBRO-RT trial. P.B. reports receiving grants and medication delivery from MSD during the conduct of the PEMBRO-RT trial as well as grants and consultancy fees from BMS outside the submitted work. E.E.V. is legally responsible for all contracts with pharmaceutical companies at the NKI and reports research funding from BMS, outside the submitted work. L.F.A.W. reports funding to the institute from Genmab BV. K.E.d.V. reports research funding from Roche/Genentech and is consultant for Macomics, outside the scope of this work. M.K. reports funding to the institute from BMS, Roche/Genentech, AZ and an advisory role for BMS, Roche, MSD and Daiichi Sankyo, outside the submitted work.

Supplemental data

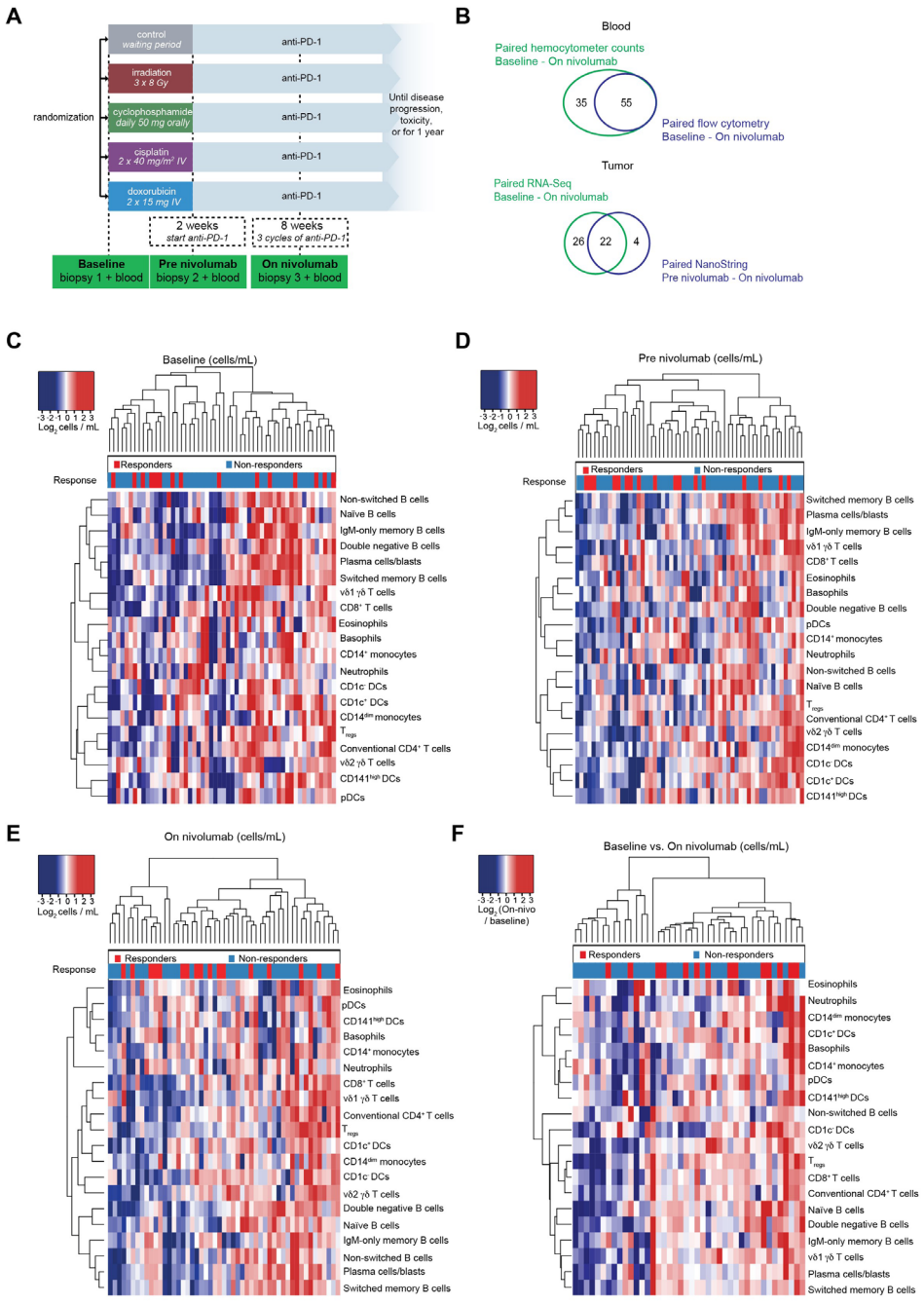

◀◀◀ ***Figure S1. Systemic immune cell landscape of patients treated in the TONIC trial at baseline, after induction therapy and on nivolumab, related to Figure 1.*** *(A) TONIC-trial design (NCT02499367). Patients with metastatic triple-negative breast cancer were randomized to 1 of 4 induction treatment arms (irradiation, cyclophosphamide, cisplatin or doxorubicin) or a two-week waiting period all followed by nivolumab (3mg per kg every 2 weeks) in stage 1 of the trial (19). In stage 2 of the trial, patients were randomized between doxorubicin induction for two weeks followed by nivolumab or immediate start of nivolumab treatment (no induction). 111 patients received at least one cycle of nivolumab (baseline characteristics in Table S1). Blood samples and biopsies were taken at baseline, after 2 weeks of induction treatment and after 3 cycles of nivolumab. Response was determined by iRECIST. (B) Venn diagrams showing the relation in TONIC-trial sample availability between the different analyses. The left panel demonstrates the overlap between availability of paired flow cytometry on fresh blood and paired hemocytometer eosinophil counts from baseline to on-nivo. For 3 patients pre-nivo flow cytometry or hemocytometer data were unavailable due to logistical reasons. The right panel demonstrates overlap between tumor samples available for gene expression analysis by NanoString (pre-nivo – on-nivo) and/or RNA-sequencing (baseline - on-nivo). NanoString analysis was performed on TONIC stage 1 samples, RNA-sequencing on TONIC stage 1 and stage 2. For 4 patients there was only pre-nivo RNA and no baseline RNA available. (C-E) Heatmaps depicting flow cytometry analysis of immune populations at baseline (C), pre-nivo (after induction) (D) and on-nivo (E). Colors in the heatmap correspond to* log_2 *transformed cells/mL and are centered to the median for each population (row) separately. (F) Heatmap representing the* log_2 *fold change of systemic immune cell populations (cells/ml) assessed by flow cytometry from baseline to on-nivo, centered around the median for each immune cell population (row) separately. For (C-F), hierarchical clustering was performed on cell populations and patients based on 1 minus Pearson correlation and Euclidian distance respectively. Complete-linkage was used for both cell populations and patients.*

Table S1: Baseline characteristics of all patients receiving at least one dose of nivolumab in the TONIC-trial (stage 1 and 2), related to Figure 1.

	Total population (n = 111)	
Median age, years (range)	52 (29-74)	
WHO performance status, n (%)		
0	70	63%
1	41	37%
gBRCA1/2, n (%)		
Mutation	6	5%
Wildtype	78	70%
Unknown	27	24%
Location of metastasis, n (%)		
Lymph node only	10	9%
Visceral metastasis	79	71%
Other metastasis	22	20%
No. of prior therapies for metastatic disease, n (%)		
0	29	26%
1	56	50%
2-3	26	23%
Previous neoadjuvant or adjuvant therapy, n (%)	96	86%
Previous chemotherapy exposure, n (%)		
Taxane	101	91%
Anthracycline	95	86%
Platinum	60	54%
Capecitabine	60	54%
LDH level, n (%)		
≤ ULN	70	63%
≤ 2x ULN	41	37%

ULN = upper limit of normal (= 250 U/L).

Table S2: Sample availability in the TONIC-trial (stage 1 and 2), related to Figure 1

	# of patients
All included patients	111
Routine eosinophil counts	
Paired baseline – on-nivo	90
Paired pre-nivo – on-nivo	87
Flow cytometry fresh blood	
Paired baseline – on-nivo	55
Paired pre-nivo – on-nivo	52
RNA-sequencing data	
Paired baseline – on-nivo	48
NanoString gene expression (TONIC stage 1 only)	
Paired pre-nivo – on-nivo	26

Table S3: List of gene signatures used for human RNA-seq analysis, related to Figure 2.

Gene signature	Genes
Eosinophil gene signature	*SIGLEC8*[87], *RNASE2*[88], *RNASE*[88], *IL5RA*[89], *CCR3*[90]
Expanded T cell signature[32]	CD3D, IDO1, CIITA, CD3E, CCL5, GZMK, CD2, HLA-DRA, CXCL13, IL2RG, NKG7, HLA-E, CXCR6, LAG3, TAGAP, CXCL10, STAT1, GZMB
Structural CD8⁺ T cell signature	*CD3D*[91], *CD3E*[91], *CD3G*[91], *CD8A*[92], *CD8B*[92], *TRA*[91], *TRBC1*[91], *TRBC2*[91], *CD247*[91]
IFNγ gene signature[33]	IDO1, CXCL9, CXCL10, HLA-DRA, STAT1, IFNG

Table S4. Patient characteristics of tumors included in PDTF analysis treated with aPD-1 alone. Related to Figure 5.

Patient ID	Tumor type	Tumor site	Ex vivo response to aPD-1
CRC003	Colorectal cancer	Primary	Yes
OV013-3	Ovarian cancer	Peritoneal metastasis	Yes
LU019	Non-small cell lung cancer	Primary	Yes
AKB803	Melanoma	Lymph node metastasis	Yes
MEL021	Melanoma	Lung metastasis	Yes
MEL025-1	Melanoma	Lymph node metastasis	No
LU027-2	Non-small cell lung cancer	Primary	No
MEL032	Melanoma	Metastasis muscle	No
RE015	Renal cell carcinoma	Primary	No
RE028	Renal cell carcinoma	Primary	No
MEL072	Melanoma	Lymph node metastasis	No
LU032	Non-small cell lung cancer	Primary	No
MEL077	Melanoma	Abdominal metastasis	No
LU028	Non-small cell lung cancer	Primary	No

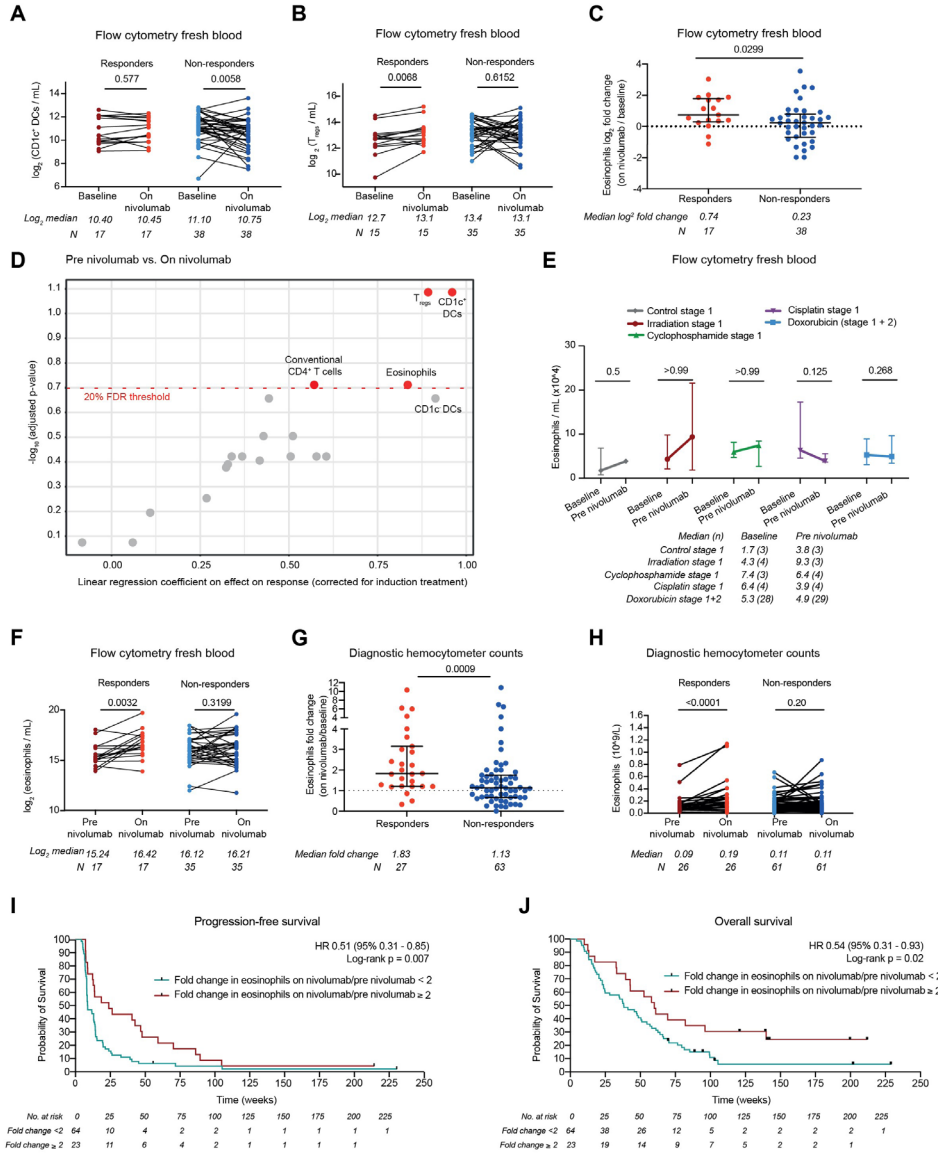

Figure S2. Systemic reduction of CD1c⁺ dendritic cells and expansion of T_{regs} and eosinophils during immune checkpoint blockade response is independent of induction treatment in TONIC trial, related to Figure 1. *(A-B) Paired flow cytometry analysis of systemic CD1c⁺ DCs (log2 transformed cells/ml) (A) and T_{regs} (log2 transformed cells/ml) (B) comparing baseline to on-nivo in responders and non-responders, treated in the TONIC-trial. Paired data are available for 55 patients (A) and (B). Statistics by Wilcoxon Signed-Rank. (C) Fold change in systemic eosinophils (log2 transformed cells/ml by flow cytometry) from baseline to on-nivo in responders and non-responders, treated in the TONIC-trial. Paired data is available for 55 patients. Statistics by Mann-Whitney, median with interquartile range (IQR). (D) Volcano plot depicting the linear regression coefficient on the effect of response by changes in immune populations analyzed by flow cytometry (pre-nivo to on-nivo; x-axis) and Benjamini-Hochberg corrected p-values (y-axis), while respecting additive influence of induction treatment (linear modeling). The regression coefficients associated with response for each population (x-axis) against the associated (Benjamini-Hochberg corrected) p-values (Wald-test) were plotted. (E) Induction treatment effect on eosinophil dynamics as determined by flow cytometry shown as median count and interquartile range, statistical analysis was performed using Wilcoxon Signed-Rank test comparing baseline to on-nivo in responders and non-responders. (F) Paired flow cytometry analysis of eosinophils (log2 transformed cells/ml) comparing pre-nivo to on-nivo in responders and non-responders, treated in the TONIC-trial. Paired data was available for 52 patients. Statistics by Wilcoxon Signed-Rank. (G) Fold change in systemic eosinophils assessed by hemocytometer from baseline to on-nivo in responders and non-responders. Paired data is available for 90 patients. Statistics by Mann-Whitney, median with interquartile range (IQR). (H) Paired hemocytometer analysis of systemic eosinophils comparing pre-nivo to on-nivo in responders and non-responders. Paired data is available for 87 patients. Statistics by Wilcoxon Signed-Rank. (I-J) Kaplan-Meier curve of progression-free survival (I) or overall survival (J) of patients divided between a fold change in eosinophils (pre-nivo to on nivo) lower than 2 or equal to/higher than 2. Statistics with log-rank and univariate hazard ratios by Cox regression (fold change lower than 2 as reference category). Data was cut-off at 1 March 2021.*

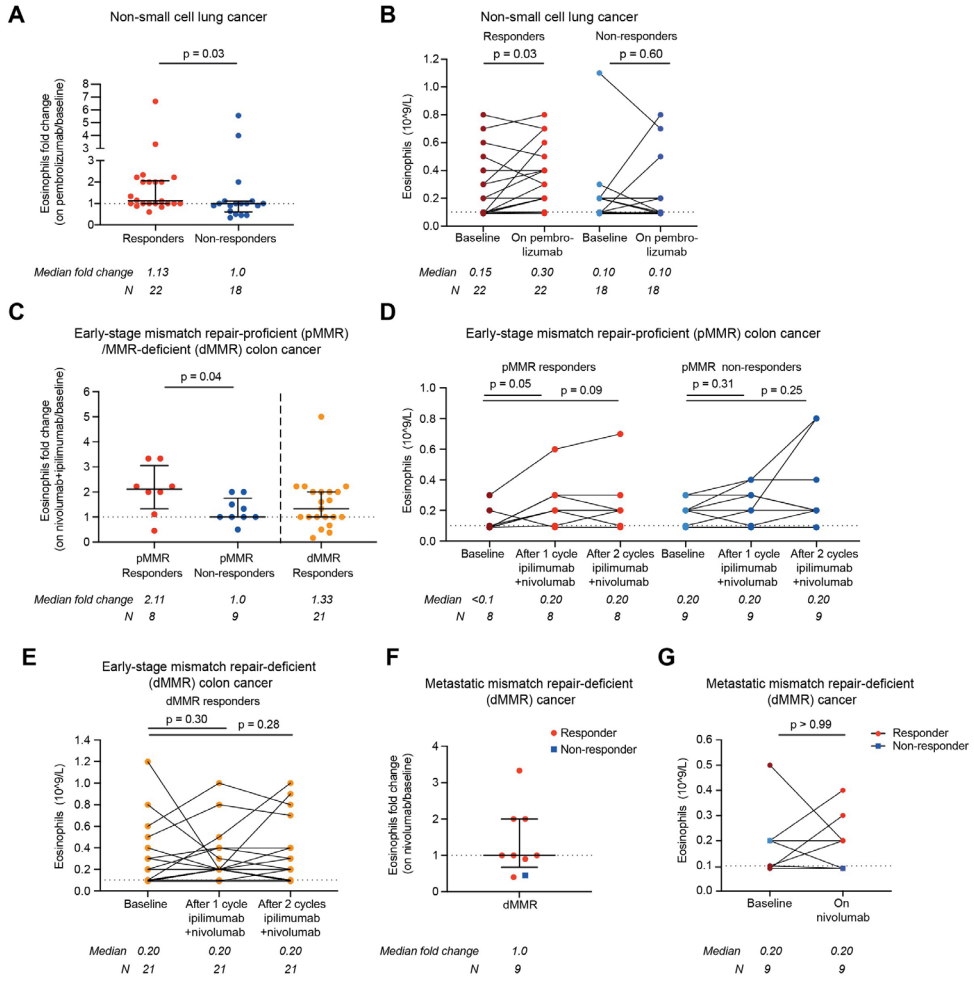

Figure S3. Systemic eosinophil accumulation after ICB and association with therapy response in different cancer types, related to Figure 1. *(A) Fold change of eosinophil counts after two cycles of pembrolizumab in patients with metastatic non-small lung cancer (NSCLC) treated with pembrolizumab (200 mg, q3w) with or without upfront radiation (NCT02492568)[29]. Paired data was available for 40 patients. (B) Paired analysis of absolute eosinophil counts in blood between baseline and two cycles of pembrolizumab in responding and non-responding patients with metastatic NSCLC. (C) Fold change of eosinophil counts after one cycle of ipilimumab/nivolumab treatment and baseline in patients with early-stage colon cancer, either mismatch repair-proficient (pMMR) or mismatch repair deficient (dMMR), treated with neo-adjuvant nivolumab (day 1 and day 15, 3 mg/kg) and ipilimumab (day 1, 1 mg/kg) in the NICHE-trial (NCT03026140)[30]. Response was defined as a pathological response (<90% tumor rest). Eosinophils were measured after 1 cycle of ipilimumab/nivolumab and after 1 additional cycle of nivo. All patients with early-stage dMMR colon cancer had a pathological response. Paired data was available for 21 patients. (D-E) Paired analysis of absolute eosinophil counts in blood between baseline and on treatment in responding and non-responding patients with mismatch repair-proficient (pMMR) (D) and mismatch repair deficient (dMMR) (E) early-stage colon cancer, treated with two cycles of neo-adjuvant nivolumab and ipilimumab in the NICHE-trial. (F) Fold change of eosinophil counts after two or three cycles of nivolumab treatment in patients with metastatic dMMR tumors, treated with nivolumab (240 mg, q2w) in the dMMR cohort of the Drug Rediscovery Protocol (NCT02925234)[31]. 7 patients with colorectal cancer (6 patients with paired data), 1 patient with urothelial cell cancer (no paired data), 1 patient with cervical cancer, 1 patient with breast cancer and 1 patient with endometrial cancer were included in this cohort. (G) Paired analysis of absolute eosinophil counts between baseline and two or three cycles of nivolumab in responding and non-responding patients with metastatic dMMR tumors, treated with nivolumab in the dMMR cohort of the Drug Rediscovery Protocol. Response was defined as complete response (CR), partial response (PR) or stable disease (SD) for 24 weeks or longer according to RECIST1.1 for (A-B and F-G). For (A,C,F), median and interquartile ranges are displayed; statistics by Mann-Whitney. For (B-E & G), statistics by Wilcoxon-signed-rank. Dashed lines indicate the threshold (0.1 x10^9 cells/L) of the hemocytometer counts reported in the patient records, counts below this threshold were replaced with a value of 0.09 x10^9 cells/L.*

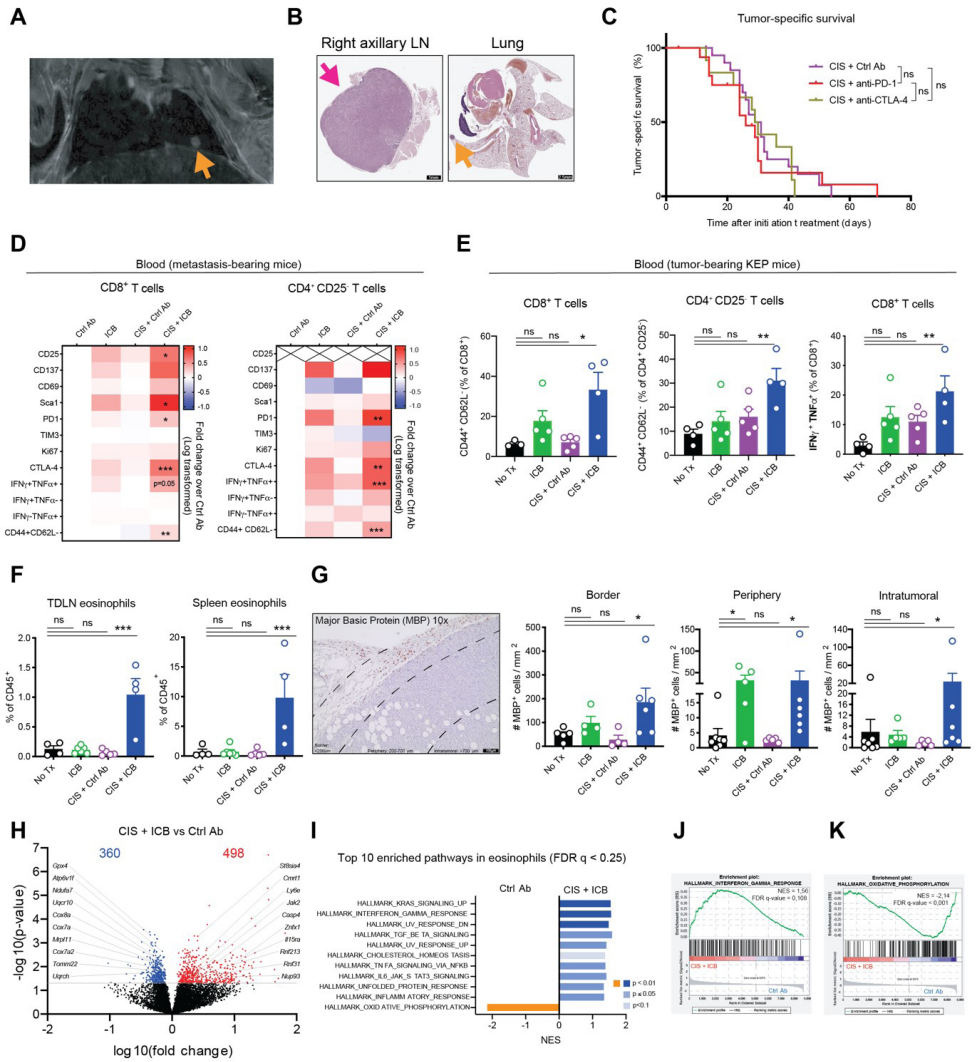

Figure S4. ICB and cisplatin induces systemic T-cell activation and eosinophil expansion in pre-clinical models of mammary tumorigenesis and advanced metastatic breast cancer, related to Figure 3. *(A-B) MRI images displaying the lung and axillary lymph nodes (A) and H&E staining of right axillary lymph node (= primary tumor draining lymph node) and lungs (B) of mice bearing KEP-derived metastases 15 days after mastectomy. Scale bars represent 1mm (left) and 2.5mm (right). Orange arrows indicate lung metastatic nodules and pink arrows indicate a lymph node affected by metastatic disease. (C) Kaplan-Meier survival curves of KEP mice treated as indicated (CIS + Ctrl Ab, n=22, 3 censored, CIS + anti-CTLA-4, n=12, 1 censored, or CIS + anti-PD-1, n=17, 3 censored). Log-rank (Mantel-Cox) test. (D) Fold change compared to Ctrl Ab-treated mice of CD8⁺ (left) and CD4⁺ CD25⁻ (right) T cells expressing the indicated activation markers expressed in blood at metastasis-related endpoint (n=4-7), determined by flow cytometry. Log transformed data are presented. Mean ±S.E.M., 1-way ANOVA followed by Dunnett's multiple comparisons test. (E) Frequency of effector CD8⁺ (left), effector CD4⁺ CD25⁻ (middle) T cells and IFNg⁺ and TNFa⁺ double positive CD8⁺ T cells (right) in blood of KEP mice at tumor-related endpoint (n=4-5), determined by flow cytometry. Mean ±S.E.M., 1-way ANOVA followed by Dunnett's multiple comparisons test. (F) Frequency of eosinophils (defined as: CD11b⁺ Ly6G^{low} F4/80^{int} SiglecF⁺) in the TDLN (left) and spleen (right) of KEP mice at tumor-related endpoint as determined by flow cytometry (n=4-6). Mean ±S.E.M., 1-way ANOVA followed by Dunnett's multiple comparisons test. (G) Representative image and quantification of immunohistochemical staining for major basic protein (MBP) of KEP tumors at tumor-related endpoint demonstrating eosinophil distribution in intratumoral, periphery and border regions. Intratumoral areas were defined as more than 700µm distant from the border of the tumor tissue; tumor periphery was defined as areas between 200µm and 700µm from the border of tumor tissue; border areas were defined as areas spanning from 200µm inside the tumor tissue to 300µm into the surrounding non-tumoral tissue. Scale bar represents 100µm. Each dot represents the average of 4-5 different tumor areas of 0.5mm² per mouse. Mean ±S.E.M., Kruskal-Wallis test. (H) Volcano plot demonstrating differentially expressed genes between eosinophils sorted from the blood of mice treated with Ctrl Ab or CIS + ICB in responsive phase of therapy. Genes contributing to the "Hallmark_Interferon_gamma_response" and "Hallmark_oxidative_phosphorylation" gene-sets are highlighted. (I) Gene sets derived from the Molecular Signatures Database Hallmark Gene Set Collection enriched in mice treated with CIS + ICB (blue) or Ctrl Ab (orange) (FDR q < 0,25). The Normalized Enrichment Scores (NES) of the top 10 enriched gene sets are shown, ordered based on ascending q-value. (J) Enrichment plot for the gene-set "Hallmark_Interferon_gamma_response" upregulated in eosinophils treated with CIS + ICB. (K) Enrichment plot for the gene-set "Hallmark_oxidative_phosphorylation" upregulated in eosinophils treated with Ctrl Ab. ns, not significant *p<0.05, **p<0.01, ***p<0.001, ****p<0.0001.*

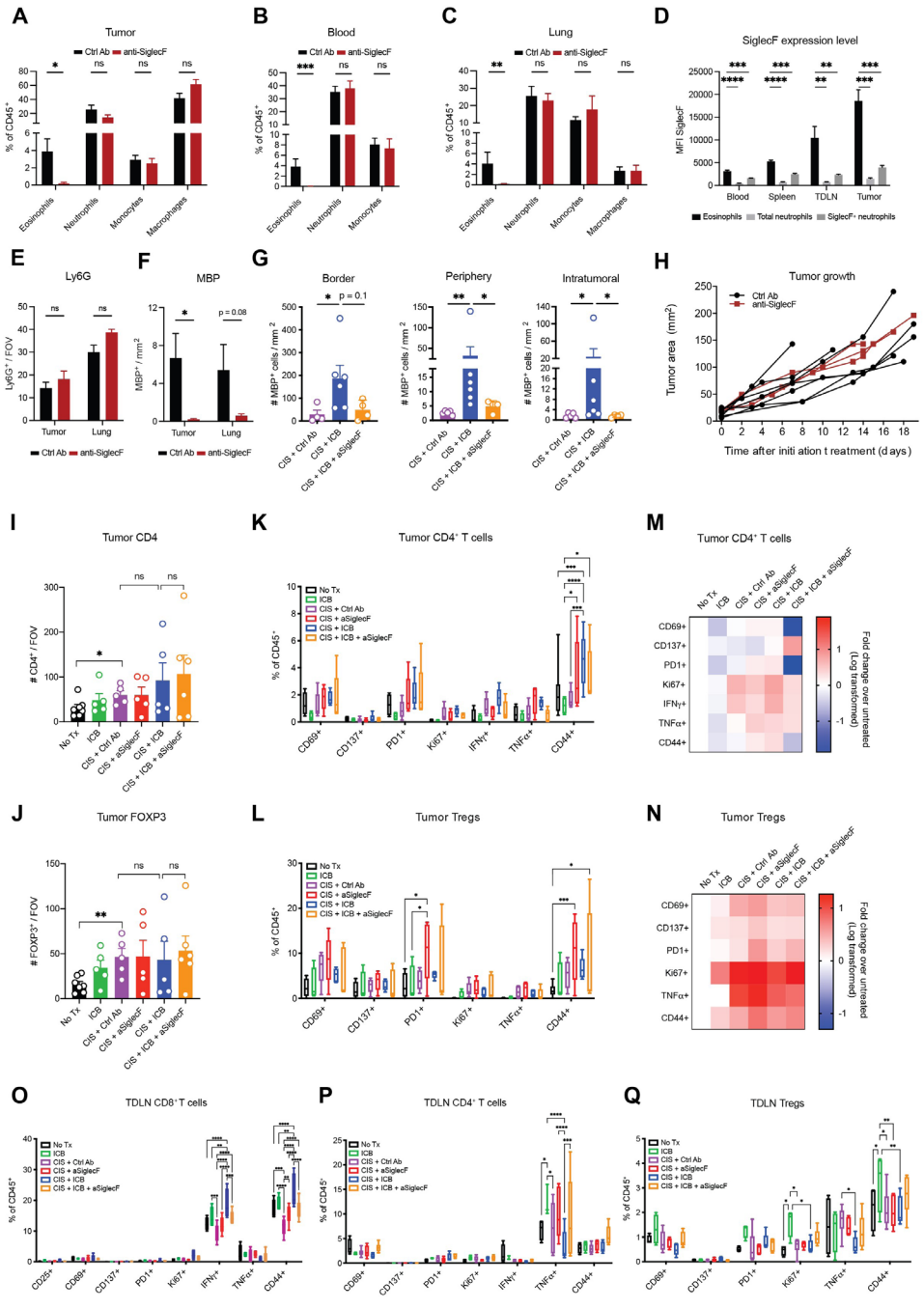

◀◀◀ ***Figure S5. Depletion of eosinophils using anti-SiglecF antibody does not promote CD4⁺ T cell or T_{reg} activation in the tumor and tumor-draining lymph node during combined ICB and cisplatin treatment, related to Figure 4.*** *(A-C) Frequency of indicated immune cells in the tumor (A), blood (B), and lungs (C) of treated KEP mice at tumor-related endpoint as determined by flow cytometry (n=4-10). Mean ±S.E.M., Mann-Whitney. (D) Mean Fluorescence Intensity (MFI) of SiglecF expression on eosinophils, total neutrophils or SiglecF⁺ neutrophils of KEP mice at tumor-related endpoint (n=4), measured by flow cytometry in indicated tissues. Mean ±S.E.M., Multiple unpaired t-tests followed by Holm-Sidak for multiple comparison. (E) Quantification of IHC staining for Ly6G⁺ cells per FOV in the tumor and lung of treated KEP mice at tumor-related endpoint (n=6-10 mice, the average of 5 FOVs per mouse). (F) Quantification of IHC staining for MBP⁺ cells per mm² in the tumor and lung of treated KEP mice at tumor-related endpoint (n=4-5 mice). (G) Quantification of IHC staining for MBP of KEP tumors at tumor-related endpoint demonstrating eosinophil distribution in intratumoral (left), periphery (middle) and border regions (right), defined and analyzed as described in Figure S4G. Data of CIS + Ctrl Ab and CIS + ICB groups are the same as displayed in Figure S4G. Mean ±S.E.M., Mann-Whitney. (H) Growth curve of mammary tumors in KEP mice treated with control antibody (n=7) or anti-SiglecF (n=3). (I-Q) KEP mice were sacrificed 21 days after start of treatment (responsive phase). Untreated KEP mice were analyzed 21 days after they reached a tumor area of 50 mm², or when the tumors reached an area of 225 mm². (I-J) Number of tumor-infiltrating CD4⁺ (I) and FOXP3⁺ (J) cells in 'responsive phase' of treatment, quantified by IHC (n=5-7 mice per group. For each mouse, the average of 5-9 FOVs ±S.E.M is displayed). Student's t-test. (K-L) Frequency of tumor-infiltrating CD4⁺CD25⁻ T cells (K) and regulatory T cells (L) expressing the indicated activation markers as determined by flow cytometry, measured 21 days after initiation of indicated treatments (n=5). (M-N) Data of (K-L) was normalized to the frequency observed in control mice. Log transformed data is presented. (O-Q) Frequency of CD8⁺ T cells (O), CD4⁺CD25⁻ T cells (P) and regulatory T cells (Q) expressing the indicated activation markers as determined by flow cytometry in the TDLN, measured 21 days after initiation of indicated treatments (n=5). Boxes represent median and interquartile range; whiskers represent full range. 2-way ANOVA followed by Tukey's multiple comparison test. *p<0.05, **p<0.01, ***p<0.001, ****p<0.0001.*

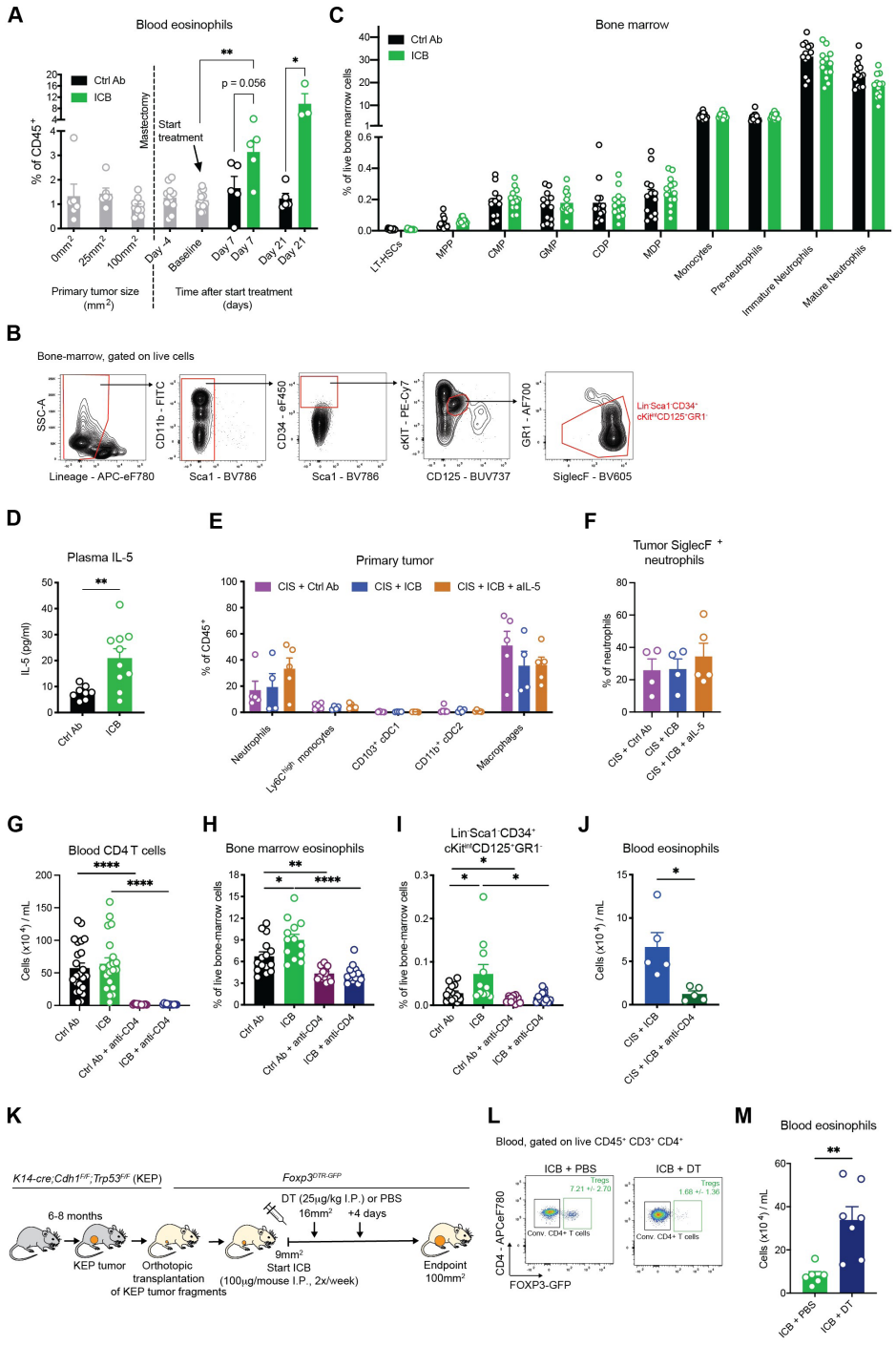

◀◀◀ ***Figure S6. Dynamics and properties of ICB-induced eosinophils in mice with KEP-derived metastatic disease or mammary tumors, related to Figure 5.*** *(A) Frequency of eosinophils in blood of mice with KEP-derived metastatic disease treated as described in Figure 3E, as determined by flow cytometry at the indicated time-points (Ctrl Ab n=3-11, ICB n=3-11). (B) Gating strategy for the identification of Lin$^-$Sca1$^-$CD34$^+$cKit^{Int}CD125$^+$Gr1$^-$ eosinophil progenitors in the bone marrow. (C) Frequency of indicated cell types in the bone marrow of mice with KEP-derived metastatic disease treated as indicated, as determined by flow cytometry (Ctrl Ab n=13, ICB n=13). LT-HSC, long-term hematopoietic stem cell; MPP, multipotent progenitor; CMP, common myeloid progenitor; GMP, granulocyte-monocyte progenitor; CDP, common dendritic cell progenitor; MDP, macrophage-dendritic cell progenitors. Multiple unpaired t-tests followed by Holm-Sidak for multiple comparison. (D) Absolute quantification of IL-5 levels in plasma of mice with KEP-derived metastatic disease treated as indicated (Ctrl Ab n=9, ICB n=10) as measured by Legend Plex. The mice shown here are the same used for the analysis of Figure 5F. (E) Frequency of indicated immune cell populations in tumors of treated KEP mice at tumor-related endpoint, as determined by flow cytometry (n=4-5). The mice shown here are the same used for the analysis of Figure 5K-N. 1-way ANOVA. (F) Frequency of SiglecF+ neutrophils in primary tumor of treated KEP mice at tumor-related endpoint, as determined by flow cytometry (n=4-5). (G) Number of CD4 T cells (gated as: CD3$^+$CD8$^-$CD25$^-$ cells) in the blood of mice with KEP-derived metastatic disease treated as described in Figure 5R, as determined by flow cytometry. Pooled data of two independent experiments. (H-I) Frequency of total eosinophils (H) and Lin$^-$Sca1$^-$CD34$^+$cKit^{Int}CD125$^+$Gr1$^-$ eosinophil progenitors (I) in the bone marrow of mice with KEP-derived metastatic disease treated as described in Figure 5R, as determined by flow cytometry (n=13-14). (J) Number of eosinophils in the blood of KEP-metastasis-bearing mice treated with CIS+ICB (n=5) or CIS+ICB+anti-CD4 (n=5) and analyzed on day 10 after start of treatment. (K) Experimental set-up and treatment scheme for the depletion of T_{regs} in mice with KEP-derived orthotopic mammary tumors. (L) Representative dot plots showing T_{reg} levels in the blood of mice at the experimental endpoint. Average frequency of T_{regs} as percentage of CD4$^+$ cells ±S.E.M. are displayed. DT, diphtheria toxin. (M) Number of eosinophils in blood of mice treated as described in (H) (ICB + PBS, n=6, ICB + DT n=7), as determined by flow cytometry. All data are mean ±S.E.M, unpaired t-test, unless indicated otherwise. ns, not significant, *p<0.05, **p<0.01, ****p<000.1.*

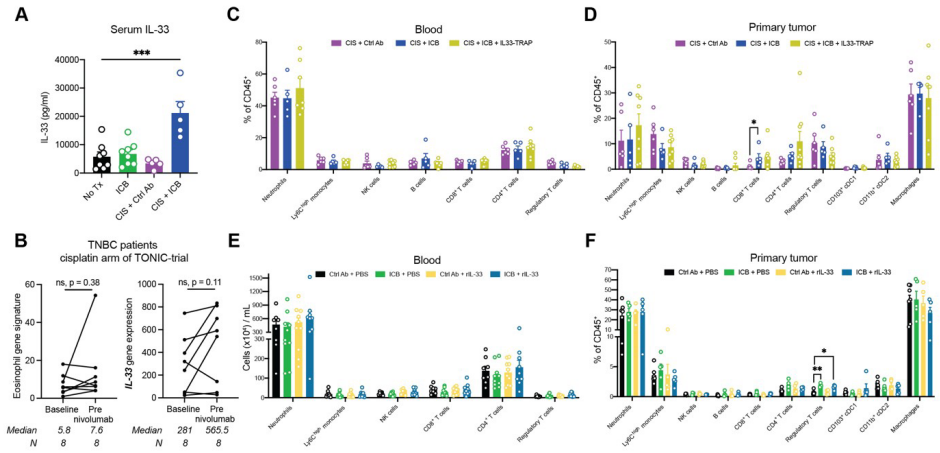

Figure S7. ICB and rIL-33 specifically promote the expansion and activation of eosinophils in mice with mammary tumors, related to Figure 6 and 7. (A) *IL-33 levels in serum determined by Legend Plex of KEP mice at tumor-related endpoint treated as indicated (n=5-8).* ***(B)*** *Eosinophil gene signature (left) and IL33 gene expression (right) from RNA-seq analysis of metastatic lesions of TNBC patients treated in the cisplatin arm of the TONIC trial.* ***(C-D)*** *Frequency of indicated immune cell populations in the blood* ***(C)*** *and primary tumor* ***(D)*** *as determined by flow cytometry of KEP mice treated as described in Figure 6D-F (n=5-8).* ***(E-F)*** *Frequency of indicated immune cell populations in the blood (n=8-10)* ***(E)*** *and primary tumor (n=5-7)* ***(F)*** *determined by flow cytometry of mice bearing orthotopically transplanted KEP tumors in responsive phase of therapy (i.e. tumor area of 150mm²) and treated as described in Figure 7. Statistical analysis performed by 1-way ANOVA or Kruskal-Wallis followed by Dunnett's or Dunn's multiple comparisons test, comparing each group against control mice, for each immune population. All data are mean ±S.E.M., *p<0.05, **p<0.01, ***p<0.001.*

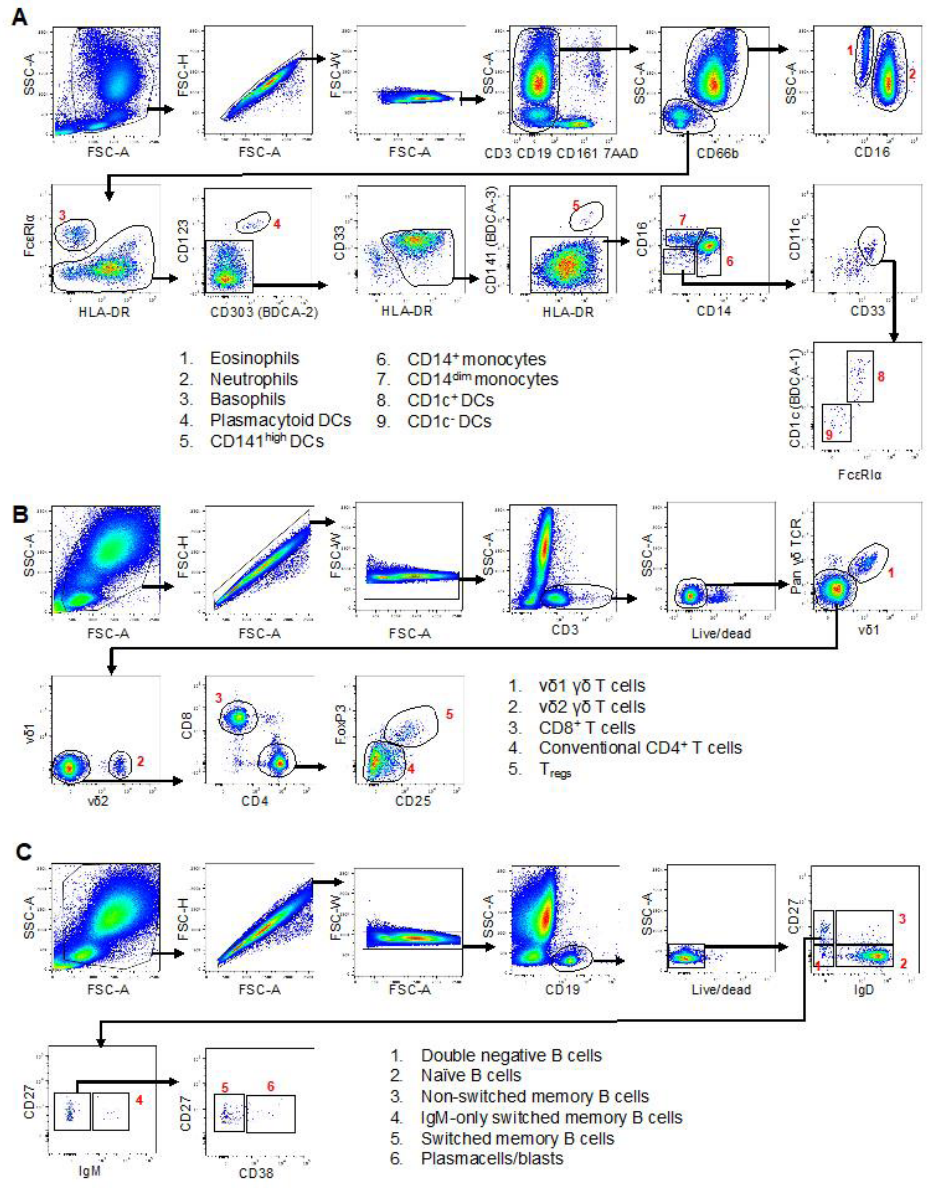

Figure S8. Gating strategy for flow cytometry analysis of human peripheral blood immune populations, related to STAR Methods. (A) *Myeloid panel gating strategy identifying eosinophils (lineage-, high side scatter, CD66b+, CD16-), neutrophils (lineage-, high side scatter, CD66b+, CD16+), basophils (lineage-, low side scatter, CD66b-, HLA-DR-, FceRIa+), plasmacytoid DCs (lineage-, low side scatter, CD66b-, HLA-DR+, CD303+, CD123+), CD141high DCs (lineage-, low side scatter, CD66b-, HLA-DR+, CD33+, CD141+), CD14+ monocytes (lineage-, CD66b-, HLA-DR+, CD33+, CD14+), CD14dim monocytes (lineage-, CD66b-, HLA-DR+, CD33+, CD14dim, CD16+), CD1c+ DCs (lineage-, CD66b-, HLA-DR+, CD33+, CD14- , CD16-, CD1c+, FceRIa+) and CD1c- DCs (lineage-, CD66b-, HLA-DR+, CD33+, CD14- , CD16-, CD1c-, FceRIa-).* ***(B)*** *T cell panel gating strategy to identify vd1 gd T cells (CD3+, vd1+, pan gd TCR+), vd2 gd T cells (CD3+, vd2+), CD8 T cells (CD3+, vd1-, pan gd TCR-, vd2-, CD8+, CD4-), conventional CD4 T cells (CD3+, vd1-, pan gd TCR-, vd2-, CD8-, CD4+, FoxP3-) and Tregs (CD3+, vd1-, pan gd TCR-, vd2-, CD8-, CD4+, FoxP3+, CD25high).* ***(C)*** *Gating strategy to identify B cell subsets identifying double negative B cells (CD19+, CD27-, IgD-), naïve B cells (CD19+, CD27-, IgD+), non-switched memory B cells (CD19+, CD27+, IgD+), IgM-only memory B cells (CD19+, CD27+, IgD-, IgM+), switched memory B cells (CD19+, CD27+, IgD-, IgM-, CD38-/+), and plasmacells/blasts (CD19+, CD27+, IgD-, IgM-, CD38high).* ▶▶▶

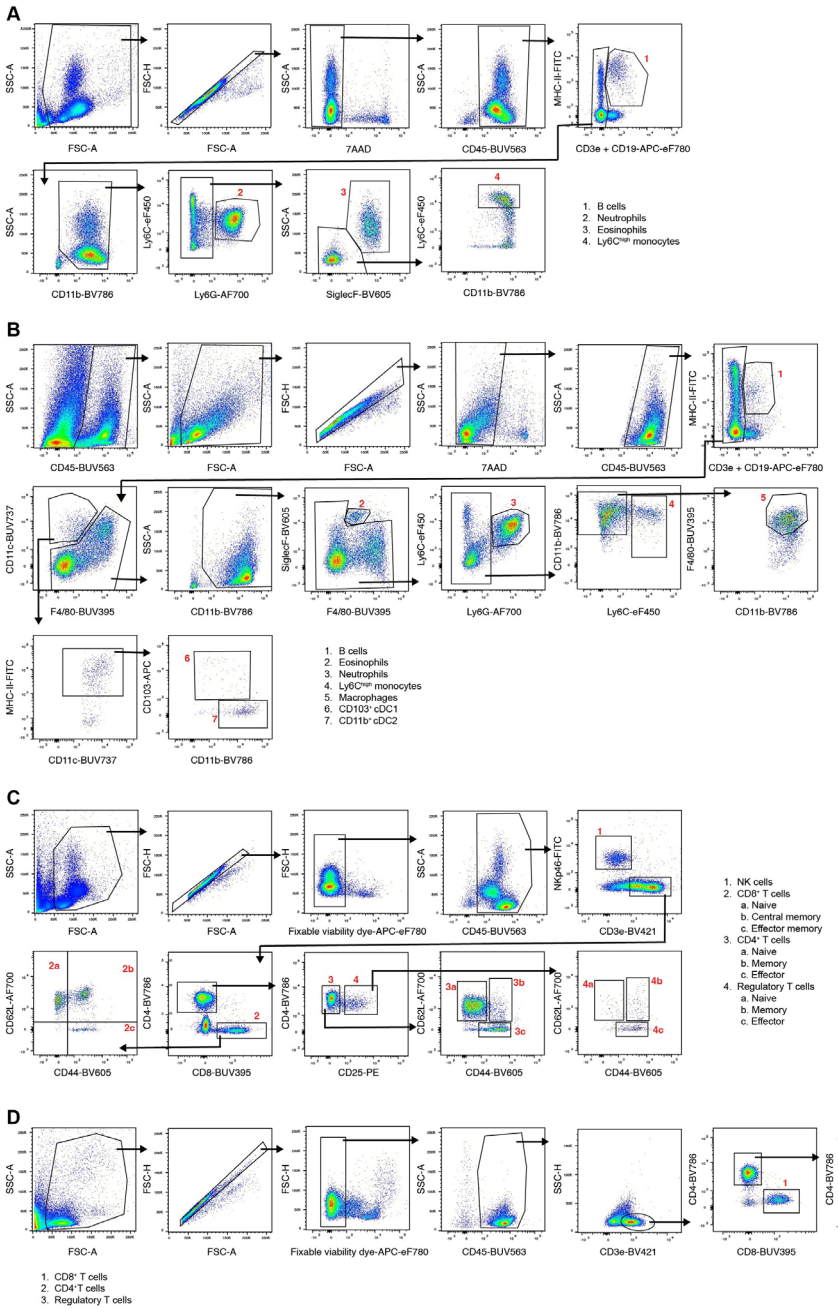

◀◀◀ ***Figure S9. Gating strategy for flow cytometry to identify immune cell populations in mouse blood and tumor, related to STAR Methods.*** *(A-B) Myeloid panel gating strategy for blood (A) and tumor (B) samples identifying B cells (CD45+, CD19+, MHC-II+), neutrophils (CD45+, CD3-, CD19-, CD11b+, Ly6g+), eosinophils (in blood: CD45+, CD3-, CD19-, Ly6g-, CD11b+, SSC-Ahigh, SiglecF+; in tumor: CD45+, CD3-, CD19-, CD11b+, SiglecF+, F4/80int), Ly6chigh monocytes (CD45+, CD3-, CD19-, Ly6g-, SiglecF-, CD11b+, Ly6chigh), macrophages (in tumor:, CD45+, CD3-, CD19-, SiglecF-, Ly6g-, Ly6c-, CD11b+, F4/80high), CD103+ cDC1 (in tumor: CD45+, CD3-, CD19-, F4/80-, CD11c+, MHC-II+ CD11blow, CD103+) and CD11b+ cDC2 (in tumor: CD45+, CD3-, CD19-, F4/80-, CD11c+, MHC-II+, CD103-, CD11b+).*
(C-D) Lymphoid panel gating strategy in blood analyzed unfixed (C) and fixed (D) identifying NK cells (unfixed: CD45+, CD3-, NKp46+), naïve CD8+ T cells (unfixed: CD45+, NKp46-, CD4-, CD3+, CD8+; CD44-, CD62L+), central memory CD8+ T cells (unfixed: CD45+, NKp46-, CD4-, CD3+, CD8+, CD44+, CD62L+), effector memory CD8+ T cells (unfixed: CD45+, NKp46-, CD4-, CD3+, CD8+, CD44+, CD62L-), total CD8+ T cells (fixed: CD45+, CD4-, CD3+, CD8+), naïve CD4+ T cells (unfixed: CD45+, NKp46-, CD8-, CD25-, CD3 +, CD4+, CD44-, CD62L+), memory CD4+ T cells (unfixed: CD45+, NKp46-, CD8-, CD25-, CD3+, CD4+, CD44+, CD62L+), effector CD4+ T cells (unfixed: CD45+, NKp46-, CD8-, CD25-, CD3+, CD4+, CD44+, CD62L-), total CD4+ T cells (fixed: CD45+, CD8-, FOXP3-, CD3+, CD4+), naïve Tregs (unfixed: CD45+, NKp46-, CD8-, CD25+, CD3+, CD4+, CD44-, CD62L+), memory Tregs (unfixed: CD45+, NKp46-, CD8-, CD25+, CD3+, CD4+, CD44+, CD62L+), effector Tregs (unfixed: CD45+, NKp46-, CD8-, CD25+, CD3+, CD4+, CD44+, CD62L-) and total Tregs (fixed: CD45+, CD8-, FOXP3+, CD3+, CD4+).

References

1. Adams, S., Schmid, P., Rugo, H.S., Winer, E.P., Loirat, D., Awada, A., Cescon, D.W., Iwata, H., Campone, M., Nanda, R., et al. (2019). Pembrolizumab monotherapy for previously treated metastatic triple-negative breast cancer: cohort A of the phase II KEYNOTE-086 study. Annals of Oncology *30*, 397-404. 10.1093/annonc/mdy517.
2. Winer, E.P., Lipatov, O., Im, S.A., Goncalves, A., Muñoz-Couselo, E., Lee, K.S., Schmid, P., Tamura, K., Testa, L., Witzel, I., et al. (2021). Pembrolizumab versus investigator-choice chemotherapy for metastatic triple-negative breast cancer (KEYNOTE-119): a randomised, open-label, phase 3 trial. Lancet Oncol *22*, 499-511. 10.1016/s1470-2045(20)30754-3.
3. Schmid, P., Rugo, H.S., Adams, S., Schneeweiss, A., Barrios, C.H., Iwata, H., Diéras, V., Henschel, V., Molinero, L., Chui, S.Y., et al. (2020). Atezolizumab plus nab-paclitaxel as first-line treatment for unresectable, locally advanced or metastatic triple-negative breast cancer (IMpassion130): updated efficacy results from a randomised, double-blind, placebo-controlled, phase 3 trial. The Lancet. Oncology *21*, 44-59. 10.1016/S1470-2045(19)30689-8.
4. Cortes, J., Cescon, D.W., Rugo, H.S., Nowecki, Z., Im, S.A., Yusof, M.M., Gallardo, C., Lipatov, O., Barrios, C.H., Holgado, E., et al. (2020). Pembrolizumab plus chemotherapy versus placebo plus chemotherapy for previously untreated locally recurrent inoperable or metastatic triple-negative breast cancer (KEYNOTE-355): a randomised, placebo-controlled, double-blind, phase 3 clinical trial. Lancet *396*, 1817-1828. 10.1016/s0140-6736(20)32531-9.
5. Demaria, O., Cornen, S., Daëron, M., Morel, Y., Medzhitov, R., and Vivier, E. (2019). Harnessing innate immunity in cancer therapy. Nature *574*, 45-56. 10.1038/s41586-019-1593-5.
6. Grisaru-Tal, S., Itan, M., Klion, A.D., and Munitz, A. (2020). A new dawn for eosinophils in the tumour microenvironment. Nat Rev Cancer *20*, 594-607. 10.1038/s41568-020-0283-9.
7. Grisaru-Tal, S., Rothenberg, M.E., and Munitz, A. (2022). Eosinophil-lymphocyte interactions in the tumor microenvironment and cancer immunotherapy. Nat Immunol *23*, 1309-1316. 10.1038/s41590-022-01291-2.
8. Rosenberg, H.F., Dyer, K.D., and Foster, P.S. (2013). Eosinophils: changing perspectives in health and disease. Nat Rev Immunol *13*, 9-22. 10.1038/nri3341.
9. Kratochvill, F., Neale, G., Haverkamp, J.M., Van de Velde, L.A., Smith, A.M., Kawauchi, D., McEvoy, J., Roussel, M.F., Dyer, M.A., Qualls, J.E., and Murray, P.J. (2015). TNF Counterbalances the Emergence of M2 Tumor Macrophages. Cell Rep *12*, 1902-1914. 10.1016/j.celrep.2015.08.033.
10. Zaynagetdinov, R., Sherrill, T.P., Gleaves, L.A., McLoed, A.G., Saxon, J.A., Habermann, A.C., Connelly, L., Dulek, D., Peebles, R.S., Jr., Fingleton, B., et al. (2015). Interleukin-5 facilitates lung metastasis by modulating the immune microenvironment. Cancer Res *75*, 1624-1634. 10.1158/0008-5472.can-14-2379.
11. Carretero, R., Sektioglu, I.M., Garbi, N., Salgado, O.C., Beckhove, P., and Hammerling, G.J. (2015). Eosinophils orchestrate cancer rejection by normalizing tumor vessels and enhancing infiltration of CD8(+) T cells. Nature immunology *16*, 609-617. 10.1038/ni.3159.
12. Jia, S., Li, W., Liu, P., and Xu, L.X. (2019). A role of eosinophils in mediating the anti-tumour effect of cryo-thermal treatment. Sci Rep *9*, 13214. 10.1038/s41598-019-49734-5.
13. Arnold, I.C., Artola-Boran, M., Gurtner, A., Bertram, K., Bauer, M., Frangez, Z., Becher, B., Kopf, M., Yousefi, S., Simon, H.U., et al. (2020). The GM-CSF-IRF5 signaling axis in eosinophils promotes antitumor immunity through activation of type 1 T cell responses. J Exp Med *217*, e20190706. 10.1084/jem.20190706.
14. Hollande, C., Boussier, J., Ziai, J., Nozawa, T., Bondet, V., Phung, W., Lu, B., Duffy, D., Paradis, V., Mallet, V., et al. (2019). Inhibition of the dipeptidyl peptidase DPP4 (CD26) reveals IL-33-dependent eosinophil-mediated control of tumor growth. Nature immunology *20*, 257-264. 10.1038/s41590-019-0321-5.
15. Reichman, H., Itan, M., Rozenberg, P., Yarmolovski, T., Brazowski, E., Varol, C., Gluck, N., Shapira, S., Arber, N., Qimron, U., et al. (2019). Activated Eosinophils Exert Antitumorigenic Activities in Colorectal Cancer. Cancer Immunol Res *7*, 388-400. 10.1158/2326-6066.CIR-18-0494.
16. Andreone, S., Spadaro, F., Buccione, C., Mancini, J., Tinari, A., Sestili, P., Gambardella, A.R., Lucarini, V., Ziccheddu, G., Parolini, I., et al. (2019). IL-33 Promotes CD11b/CD18-Mediated Adhesion of Eosinophils to Cancer Cells and Synapse-Polarized Degranulation Leading to Tumor Cell Killing. Cancers (Basel) *11*, 1664. 10.3390/cancers11111664.
17. Varricchi, G., Galdiero, M.R., Loffredo, S., Lucarini, V., Marone, G., Mattei, F., and Schiavoni, G. (2018). Eosinophils: The unsung heroes in cancer? Oncoimmunology *7*, e1393134. 10.1080/2162402x.2017.1393134.
18. Grisaru-Tal, S., Dulberg, S., Beck, L., Zhang, C., Itan, M., Hediyeh-Zadeh, S., Caldwell, J., Rozenberg, P., Dolitzky, A., Avlas, S., et al. (2021). Metastasis-Entrained Eosinophils Enhance Lymphocyte-Mediated Antitumor Immunity. Cancer Res *81*, 5555-5571. 10.1158/0008-5472.can-21-0839.
19. Simon, S.C.S., Hu, X., Panten, J., Grees, M., Renders, S., Thomas, D., Weber, R., Schulze, T.J., Utikal, J., and Umansky, V. (2020). Eosinophil accumulation predicts response to melanoma treatment with immune checkpoint inhibitors. Oncoimmunology *9*, 1727116. 10.1080/2162402X.2020.1727116.
20. Delyon, J., Mateus, C., Lefeuvre, D., Lanoy, E., Zitvogel, L., Chaput, N., Roy, S., Eggermont, A.M., Routier, E., and Robert, C. (2013). Experience in daily practice with ipilimumab for the treatment of patients with metastatic melanoma: an early increase in lymphocyte and eosinophil counts is associated with improved survival. Ann Oncol *24*, 1697-1703. 10.1093/annonc/mdt027.
21. Gebhardt, C., Sevko, A., Jiang, H., Lichtenberger, R., Reith, M., Tarnanidis, K., Holland-Letz, T., Umansky, L., Beckhove, P., Sucker, A., et al. (2015). Myeloid Cells and Related Chronic Inflammatory Factors as Novel Predictive Markers in Melanoma Treatment with Ipilimumab. Clinical Cancer Research *21*, 5453-5459. 10.1158/1078-0432.Ccr-15-0676.
22. Alves, A., Dias, M., Campainha, S., and Barroso, A. (2021). Peripheral blood eosinophilia may be a prognostic biomarker in non-small cell lung cancer patients treated with immunotherapy. J Thorac Dis *13*, 2716-2727. 10.21037/jtd-20-3525.
23. Okauchi, S., Shiozawa, T., Miyazaki, K., Nishino, K., Sasatani, Y., Ohara, G., Kagohashi, K., Sato, S., Kodama, T., Satoh, H., and Hizawa, N. (2021). Association between peripheral eosinophils and clinical outcomes in patients with non-small cell lung cancer treated with immune checkpoint inhibitors. Pol Arch Intern Med *131*, 152-160. 10.20452/pamw.15776.
24. Verhaart, S.L., Abu-Ghanem, Y., Mulder, S.F., Oosting, S., Van Der Veldt, A., Osanto, S., Aarts, M.J.B., Houtsma, D., Peters, F.P.J., Groenewegen, G., et al. (2020). Real-world Data of Nivolumab for Patients With Advanced Renal Cell Carcinoma in the Netherlands: An Analysis of Toxicity, Efficacy, and Predictive Markers. Clin Genitourin Cancer. 10.1016/j.clgc.2020.10.003.
25. Zheng, X., Zhang, N., Qian, L., Wang, X., Fan, P., Kuai, J., Lin, S., Liu, C., Jiang, W., Qin, S., et al. (2020). CTLA4 blockade promotes vessel normalization in breast tumors via the accumulation of eosinophils. Int J Cancer *146*, 1730-1740. 10.1002/ijc.32829.
26. Coffelt, S.B., Kersten, K., Doornebal, C.W., Weiden, J., Vrijland, K., Hau, C.S., Verstegen, N.J.M., Ciampricotti, M., Hawinkels, L., Jonkers, J., and de Visser, K.E. (2015). IL-17-producing γδ T cells and neutrophils conspire to promote breast cancer metastasis. Nature *522*, 345-348. 10.1038/nature14282.
27. Salvagno, C., Ciampricotti, M., Tuit, S., Hau, C.S., van Weverwijk, A., Coffelt, S.B., Kersten, K., Vrijland, K., Kos, K., Ulas, T., et al. (2019). Therapeutic targeting of macrophages enhances chemotherapy efficacy by unleashing type I interferon response. Nature cell biology *21*, 511-521. 10.1038/s41556-019-0298-1.
28. Voorwerk, L., Slagter, M., Horlings, H.M., Sikorska, K., van de Vijver, K.K., de Maaker, M., Nederlof, I., Kluin, R.J.C., Warren, S., Ong, S., et al. (2019). Immune induction strategies in metastatic triple-negative breast cancer to enhance the sensitivity to PD-1 blockade: the TONIC trial. Nat Med *25*, 920-928. 10.1038/s41591-019-0432-4.
29. Theelen, W., Peulen, H.M.U., Lalezari, F., van der Noort, V., de Vries, J.F., Aerts, J., Dumoulin, D.W., Bahce, I., Niemeijer, A.N., de Langen, A.J., et al. (2019). Effect of Pembrolizumab After Stereotactic Body Radiotherapy vs Pembrolizumab Alone on Tumor Response in Patients With Advanced Non-Small Cell Lung Cancer: Results of the PEMBRO-RT Phase 2 Randomized Clinical Trial. JAMA Oncol *5*, 1276-1282. 10.1001/jamaoncol.2019.1478.
30. Chalabi, M., Fanchi, L.F., Dijkstra, K.K., den Berg, J.G., Aalbers, A.G., Sikorska, K., Lopez-Yurda, M., Grootscholten, C., Beets, G.L., Snaebjornsson, P., et al. (2020). Neoadjuvant immunotherapy leads to pathological responses in MMR-proficient and MMR-deficient early-stage colon cancers. Nature Medicine *26*, 566-576. 10.1038/s41591-020-0805-8.
31. van der Velden, D.L., Hoes, L.R., van der Wijngaart, H., van Henegouwen, B.J.M., van Werkhoven, E., Roepman, P., Schilsky, R.L., de Leng, W.W.J., Huitema, A.D.R., Nuijen, B., et al. (2019). The Drug Rediscovery protocol facilitates the expanded use of existing anticancer drugs. Nature *574*, 127-131. 10.1038/s41586-019-1600-x.
32. Kikly, K.K., Bochner, B.S., Freeman, S.D., Tan, K.B., Gallagher, K.T., D'Alessio K, J., Holmes, S.D., Abra-

hamson, J.A., Erickson-Miller, C.L., Murdock, P.R., et al. (2000). Identification of SAF-2, a novel siglec expressed on eosinophils, mast cells, and basophils. J Allergy Clin Immunol *105*, 1093-1100. 10.1067/mai.2000.107127.
33. Ayers, M., Lunceford, J., Nebozhyn, M., Murphy, E., Loboda, A., Kaufman, D.R., Albright, A., Cheng, J.D., Kang, S.P., Shankaran, V., et al. (2017). IFN-gamma-related mRNA profile predicts clinical response to PD-1 blockade. The Journal of clinical investigation *127*, 2930-2940. 10.1172/jci91190.
34. Derksen, P.W., Liu, X., Saridin, F., van der Gulden, H., Zevenhoven, J., Evers, B., van Beijnum, J.R., Griffioen, A.W., Vink, J., Krimpenfort, P., et al. (2006). Somatic inactivation of E-cadherin and p53 in mice leads to metastatic lobular mammary carcinoma through induction of anoikis resistance and angiogenesis. Cancer cell *10*, 437-449. 10.1016/j.ccr.2006.09.013.
35. Doornebal, C.W., Klarenbeek, S., Braumuller, T.M., Klijn, C.N., Ciampricotti, M., Hau, C.S., Hollmann, M.W., Jonkers, J., and de Visser, K.E. (2013). A preclinical mouse model of invasive lobular breast cancer metastasis. Cancer research *73*, 353-363. 10.1158/0008-5472.Can-11-4208.
36. Beyranvand Nejad, E., van der Sluis, T.C., van Duikeren, S., Yagita, H., Janssen, G.M., van Veelen, P.A., Melief, C.J., van der Burg, S.H., and Arens, R. (2016). Tumor Eradication by Cisplatin Is Sustained by CD80/86-Mediated Costimulation of CD8+ T Cells. Cancer Res *76*, 6017-6029. 10.1158/0008-5472.CAN-16-0881.
37. Nolan, E., Savas, P., Policheni, A.N., Darcy, P.K., Vaillant, F., Mintoff, C.P., Dushyanthen, S., Mansour, M., Pang, J.B., Fox, S.B., et al. (2017). Combined immune checkpoint blockade as a therapeutic strategy for BRCA1-mutated breast cancer. Sci Transl Med *9*, eaal4922. 10.1126/scitranslmed.aal4922.
38. Grimaldi, A., Cammarata, I., Martire, C., Focaccetti, C., Piconese, S., Buccilli, M., Mancone, C., Buzzacchino, F., Berrios, J.R.G., D'Alessandris, N., et al. (2020). Combination of chemotherapy and PD-1 blockade induces T cell responses to tumor non-mutated neoantigens. Commun Biol *3*, 85. 10.1038/s42003-020-0811-x.
39. Wan, S., Pestka, S., Jubin, R.G., Lyu, Y.L., Tsai, Y.C., and Liu, L.F. (2012). Chemotherapeutics and radiation stimulate MHC class I expression through elevated interferon-beta signaling in breast cancer cells. PLoS One *7*, e32542. 10.1371/journal.pone.0032542.
40. Cheng, J.N., Luo, W., Sun, C., Jin, Z., Zeng, X., Alexander, P.B., Gong, Z., Xia, X., Ding, X., Xu, S., et al. (2021). Radiation-induced eosinophils improve cytotoxic T lymphocyte recruitment and response to immunotherapy. Sci Adv *7*, eabc7609. 10.1126/sciadv.abc7609.
41. Zimmermann, N., McBride, M.L., Yamada, Y., Hudson, S.A., Jones, C., Cromie, K.D., Crocker, P.R., Rothenberg, M.E., and Bochner, B.S. (2008). Siglec-F antibody administration to mice selectively reduces blood and tissue eosinophils. Allergy *63*, 1156-1163. 10.1111/j.1398-9995.2008.01709.x.
42. Pfirschke, C., Engblom, C., Gungabeesoon, J., Lin, Y., Rickelt, S., Zilionis, R., Messemaker, M., Siwicki, M., Gerhard, G.M., Kohl, A., et al. (2020). Tumor-Promoting Ly-6G(+) SiglecF(high) Cells Are Mature and Long-Lived Neutrophils. Cell Rep *32*, 108164. 10.1016/j.celrep.2020.108164.
43. Iwasaki, H., Mizuno, S., Mayfield, R., Shigematsu, H., Arinobu, Y., Seed, B., Gurish, M.F., Takatsu, K., and Akashi, K. (2005). Identification of eosinophil lineage-committed progenitors in the murine bone marrow. J Exp Med *201*, 1891-1897. 10.1084/jem.20050548.
44. Pelaia, C., Paoletti, G., Puggioni, F., Racca, F., Pelaia, G., Canonica, G.W., and Heffler, E. (2019). Interleukin-5 in the Pathophysiology of Severe Asthma. Front Physiol *10*, 1514. 10.3389/fphys.2019.01514.
45. Voabil, P., de Bruijn, M., Roelofsen, L.M., Hendriks, S.H., Brokamp, S., van den Braber, M., Broeks, A., Sanders, J., Herzig, P., Zippelius, A., et al. (2021). An ex vivo tumor fragment platform to dissect response to PD-1 blockade in cancer. Nat Med *27*, 1250-1261. 10.1038/s41591-021-01398-3.
46. Kaptein, P., Jacoberger-Foissac, C., Dimitriadis, P., Voabil, P., de Bruijn, M., Brokamp, S., Reijers, I., Versluis, J., Nallan, G., Triscott, H., et al. (2022). Addition of interleukin-2 overcomes resistance to neoadjuvant CTLA4 and PD1 blockade in ex vivo patient tumors. Sci Transl Med *14*, eabj9779. 10.1126/scitranslmed.abj9779.
47. Kos, K., Aslam, M.A., van de Ven, R., Wellenstein, M.D., Pieters, W., van Weverwijk, A., Duits, D.E.M., van Pul, K., Hau, C.S., Vrijland, K., et al. (2022). Tumor-educated T(regs) drive organ-specific metastasis in breast cancer by impairing NK cells in the lymph node niche. Cell Rep *38*, 110447. 10.1016/j.celrep.2022.110447.
48. Chan, B.C.L., Lam, C.W.K., Tam, L.S., and Wong, C.K. (2019). IL33: Roles in Allergic Inflammation and Therapeutic Perspectives. Front Immunol *10*, 364. 10.3389/fimmu.2019.00364.
49. Cherry, W.B., Yoon, J., Bartemes, K.R., Iijima, K., and Kita, H. (2008). A novel IL-1 family cytokine, IL-33, potently activates human eosinophils. J Allergy Clin Immunol *121*, 1484-1490. 10.1016/j.jaci.2008.04.005.
50. Suzukawa, M., Koketsu, R., Iikura, M., Nakae, S., Matsumoto, K., Nagase, H., Saito, H., Matsushima, K., Ohta, K., Yamamoto, K., and Yamaguchi, M. (2008). Interleukin-33 enhances adhesion, CD11b expression and survival in human eosinophils. Lab Invest *88*, 1245-1253. 10.1038/labinvest.2008.82.
51. Johnston, L.K., and Bryce, P.J. (2017). Understanding Interleukin 33 and Its Roles in Eosinophil Development. Front Med (Lausanne) *4*, 51. 10.3389/fmed.2017.00051.
52. Shani, O., Vorobyov, T., Monteran, L., Lavie, D., Cohen, N., Raz, Y., Tsarfaty, G., Avivi, C., Barshack, I., and Erez, N. (2020). Fibroblast-Derived IL33 Facilitates Breast Cancer Metastasis by Modifying the Immune Microenvironment and Driving Type 2 Immunity. Cancer Res *80*, 5317-5329. 10.1158/0008-5472.can-20-2116.
53. Lucarini, V., Zicchedda, G., Macchia, I., La Sorsa, V., Peschiaroli, F., Buccione, C., Sistigu, A., Sanchez, M., Andreone, S., D'Urso, M.T., et al. (2017). IL-33 restricts tumor growth and inhibits pulmonary metastasis in melanoma-bearing mice through eosinophils. Oncoimmunology *6*, e1317420. 10.1080/2162402X.2017.1317420.
54. Holgado, A., Braun, H., Van Nuffel, E., Detry, S., Schuijs, M.J., Deswarte, K., Vergote, K., Haegman, M., Baudelet, G., Haustraete, J., et al. (2019). IL-33trap is a novel IL-33-neutralizing biologic that inhibits allergic airway inflammation. J Allergy Clin Immunol *144*, 204-215. 10.1016/j.jaci.2019.02.028.
55. Ling, M.F., and Luster, A.D. (2016). Allergen-Specific CD4(+) T Cells in Human Asthma. Ann Am Thorac Soc *13 Suppl 1*, S25-30. 10.1513/AnnalsATS.201507-431MG.
56. Rosskopf, S., Jahn-Schmid, B., Schmetterer, K.G., Zlabinger, G.J., and Steinberger, P. (2018). PD-1 has a unique capacity to inhibit allergen-specific human CD4(+) T cell responses. Sci Rep *8*, 13543. 10.1038/s41598-018-31757-z.
57. Gorski, S.A., Lawrence, M.G., Hinkelman, A., Spano, M.M., Steinke, J.W., Borish, L., Teague, W.G., and Braciale, T.J. (2019). Expression of IL-5 receptor alpha by murine and human lung neutrophils. PLoS One *14*, e0221113. 10.1371/journal.pone.0221113.
58. Kolbeck, R., Kozhich, A., Koike, M., Peng, L., Andersson, C.K., Damschroder, M.M., Reed, J.L., Woods, R., Dall'acqua, W.W., Stephens, G.L., et al. (2010). MEDI-563, a humanized anti-IL-5 receptor alpha mAb with enhanced antibody-dependent cell-mediated cytotoxicity function. J Allergy Clin Immunol *125*, 1344-1353.e1342. 10.1016/j.jaci.2010.04.004.
59. Dent, L.A., Strath, M., Mellor, A.L., and Sanderson, C.J. (1990). Eosinophilia in transgenic mice expressing interleukin 5. J Exp Med *172*, 1425-1431. 10.1084/jem.172.5.1425.
60. Johnston, L.K., Hsu, C.L., Krier-Burris, R.A., Chhiba, K.D., Chien, K.B., McKenzie, A., Berdnikovs, S., and Bryce, P.J. (2016). IL-33 Precedes IL-5 in Regulating Eosinophil Commitment and Is Required for Eosinophil Homeostasis. J Immunol *197*, 3445-3453. 10.4049/jimmunol.1600611.
61. Pichery, M., Mirey, E., Mercier, P., Lefrancais, E., Dujardin, A., Ortega, N., and Girard, J.P. (2012). Endogenous IL-33 is highly expressed in mouse epithelial barrier tissues, lymphoid organs, brain, embryos, and inflamed tissues: in situ analysis using a novel Il-33-LacZ gene trap reporter strain. J Immunol *188*, 3488-3495. 10.4049/jimmunol.1101977.
62. Hung, L.Y., Tanaka, Y., Herbine, K., Pastore, C., Singh, B., Ferguson, A., Vora, N., Douglas, B., Zullo, K., Behrens, E.M., et al. (2020). Cellular context of IL-33 expression dictates impact on anti-helminth immunity. Sci Immunol *5*. 10.1126/sciimmunol.abc6259.
63. Taniguchi, S., Elhance, A., Duzer, A.V., Kumar, S., Leitenberger, J.J., and Oshimori, N. (2020). Tumor-initiating cells establish an IL-33-TGF--niche signaling loop to promote cancer progression. Science *369*, eaay1813. doi:10.1126/science.aay1813.
64. Saikumar Jayalatha, A.K., Hesse, L., Ketelaar, M.E., Koppelman, G.H., and Nawijn, M.C. (2021). The central role of IL-33/IL-1RL1 pathway in asthma: From pathogenesis to intervention. Pharmacol Ther *225*, 107847. 10.1016/j.pharmthera.2021.107847.
65. Jacquelot, N., Seillet, C., Wang, M., Pizzolla, A., Liao, Y., Hediyeh-Zadeh, S., Grisaru-Tal, S., Louis, C., Huang, Q., Schreuder, J., et al. (2021). Blockade of the co-inhibitory molecule PD-1 unleashes ILC2-dependent antitumor immunity in melanoma. Nat Immunol *22*, 851-864. 10.1038/s41590-021-00943-z.
66. Chen, L., Sun, R., Xu, J., Zhai, W., Zhang, D., Yang, M., Yue, C., Chen, Y., Li, S., Turnquist, H., et al. (2020). Tumor-Derived IL33 Promotes Tissue-Resident CD8(+) T Cells and Is Required for Checkpoint Blockade Tumor Immunotherapy. Cancer Immunol Res *8*, 1381-1392. 10.1158/2326-6066.cir-19-1024.
67. Shen, J.X., Liu, J., and Zhang, G.J. (2018). Interleukin-33 in Malignancies: Friends or Foes? Front Immunol *9*,

3051. 10.3389/fimmu.2018.03051.
68. Dasari, S., and Tchounwou, P.B. (2014). Cisplatin in cancer therapy: molecular mechanisms of action. Eur J Pharmacol *740*, 364-378. 10.1016/j.ejphar.2014.07.025.
69. de Biasi, A.R., Villena-Vargas, J., and Adusumilli, P.S. (2014). Cisplatin-induced antitumor immunomodulation: a review of preclinical and clinical evidence. Clin Cancer Res *20*, 5384-5391. 10.1158/1078-0432.CCR-14-1298.
70. Jacobsen, E.A., Zellner, K.R., Colbert, D., Lee, N.A., and Lee, J.J. (2011). Eosinophils regulate dendritic cells and Th2 pulmonary immune responses following allergen provocation. J Immunol *187*, 6059-6068. 10.4049/jimmunol.1102299.
71. Kanda, A., Fleury, S., Kobayashi, Y., Tomoda, K., Julia, V., and Dombrowicz, D. (2015). Th2-activated eosinophils release Th1 cytokines that modulate allergic inflammation. Allergol Int *64 Suppl*, S71-73. 10.1016/j.alit.2015.03.006.
72. Jacobsen, E.A., Ochkur, S.I., Pero, R.S., Taranova, A.G., Protheroe, C.A., Colbert, D.C., Lee, N.A., and Lee, J.J. (2008). Allergic pulmonary inflammation in mice is dependent on eosinophil-induced recruitment of effector T cells. J Exp Med *205*, 699-710. 10.1084/jem.20071840.
73. Ghebeh, H., Elshenawy, M.A., AlSayed, A.D., and Al-Tweigeri, T. (2022). Peripheral blood eosinophil count is associated with response to chemoimmunotherapy in metastatic triple-negative breast cancer. Immunotherapy *14*, 189-199. 10.2217/imt-2021-0149.
74. de Visser, K.E., Korets, L.V., and Coussens, L.M. (2005). De novo carcinogenesis promoted by chronic inflammation is B lymphocyte dependent. Cancer Cell *7*, 411-423. 10.1016/j.ccr.2005.04.014.
75. Kim, J.M., Rasmussen, J.P., and Rudensky, A.Y. (2007). Regulatory T cells prevent catastrophic autoimmunity throughout the lifespan of mice. Nat Immunol *8*, 191-197. 10.1038/ni1428.
76. Eisenhauer, E.A., Therasse, P., Bogaerts, J., Schwartz, L.H., Sargent, D., Ford, R., Dancey, J., Arbuck, S., Gwyther, S., Mooney, M., et al. (2009). New response evaluation criteria in solid tumours: revised RECIST guideline (version 1.1). European journal of cancer (Oxford, England : 1990) *45*, 228-247. 10.1016/j.ejca.2008.10.026.
77. Seymour, L., Bogaerts, J., Perrone, A., Ford, R., Schwartz, L.H., Mandrekar, S., Lin, N.U., Litiere, S., Dancey, J., Chen, A., et al. (2017). iRECIST: guidelines for response criteria for use in trials testing immunotherapeutics. Lancet Oncol *18*, e143-e152. 10.1016/S1470-2045(17)30074-8.
78. Picelli, S., Faridani, O.R., Björklund, A.K., Winberg, G., Sagasser, S., and Sandberg, R. (2014). Full-length RNA-seq from single cells using Smart-seq2. Nat Protoc *9*, 171-181. 10.1038/nprot.2014.006.
79. Dobin, A., Davis, C.A., Schlesinger, F., Drenkow, J., Zaleski, C., Jha, S., Batut, P., Chaisson, M., and Gingeras, T.R. (2013). STAR: ultrafast universal RNA-seq aligner. Bioinformatics *29*, 15-21. 10.1093/bioinformatics/bts635.
80. Love, M.I., Huber, W., and Anders, S. (2014). Moderated estimation of fold change and dispersion for RNA-seq data with DESeq2. Genome Biology *15*, 550. 10.1186/s13059-014-0550-8.
81. pandas, D.t. (2020). pandas-dev/pandas: Pandas. Zenodo. h10.5281/zenodo.3509134.
82. McKinney, W. (2010). Data Structures for Statistical Computing in Python from Proceedings of the 9th Python in Science Conference, 56 - 61. 10.25080/Majora-92bf1922-00a.
83. Harris, C.R., Millman, K.J., van der Walt, S.J., Gommers, R., Virtanen, P., Cournapeau, D., Wieser, E., Taylor, J., Berg, S., Smith, N.J., et al. (2020). Array programming with NumPy. Nature *585*, 357-362. 10.1038/s41586-020-2649-2.
84. Hunter, J.D. (2007). Matplotlib: A 2D Graphics Environment. Computing in Science & Engineering *9*, 90-95. 10.1109/MCSE.2007.55.
85. Waskom, M., Botvinnik, O., O'Kane, D., P., H., Lukauskas, S., Gemperline, D.C., Augspurger, T., Halchenko, Y., Cole, J.B., Warmenhoven, J., et al. (2017). mwaskom/seaborn: v0.8.1 (September 2017). Zenodo. 10.5281/zenodo.883859
86. Weber, M. (2020). statannot 0.2.2.
87. Tateno, H., Crocker, P.R., and Paulson, J.C. (2005). Mouse Siglec-F and human Siglec-8 are functionally convergent paralogs that are selectively expressed on eosinophils and recognize 6′-sulfo-sialyl Lewis X as a preferred glycan ligand. Glycobiology *15*, 1125-1135. 10.1093/glycob/cwi097.
88. Abu-Ghazaleh, R.I., Dunnette, S.L., Loegering, D.A., Checkel, J.L., Kita, H., Thomas, L.L., and Gleich, G.J. (1992). Eosinophil granule proteins in peripheral blood granulocytes. J Leukoc Biol *52*, 611-618. 10.1002/jlb.52.6.611.

89. Mori, Y., Iwasaki, H., Kohno, K., Yoshimoto, G., Kikushige, Y., Okeda, A., Uike, N., Niiro, H., Takenaka, K., Nagafuji, K., et al. (2009). Identification of the human eosinophil lineage-committed progenitor: revision of phenotypic definition of the human common myeloid progenitor. J Exp Med *206*, 183-193. 10.1084/jem.20081756.
90. Hochstetter, R., Dobos, G., Kimmig, D., Dulkys, Y., Kapp, A., and Elsner, J. (2000). The CC chemokine receptor 3 CCR3 is functionally expressed on eosinophils but not on neutrophils. Eur J Immunol *30*, 2759-2764. 10.1002/1521-4141(200010)30:10<2759::AID-IMMU2759>3.0.CO;2-A.
91. Alcover, A., Alarcón, B., and Di Bartolo, V. (2018). Cell Biology of T Cell Receptor Expression and Regulation. Annu Rev Immunol *36*, 103-125. 10.1146/annurev-immunol-042617-053429.
92. Li, Y., Yin, Y., and Mariuzza, R.A. (2013). Structural and biophysical insights into the role of CD4 and CD8 in T cell activation. Frontiers in immunology *4*, 206. 10.3389/fimmu.2013.00206.

CHAPTER 8

a

Noor A.M. Bakker[1, 7, 8, #], Jossie Rotman[2, 4, #], Marc van Beurden[2], Henry J.M.A.A. Zijlmans[2], Maartje van Ruiten[2], Sanne Samuels[2, 4], Bastiaan Nuijen[5], Jos H. Beijnen[5], Karin E. de Visser[7, 8], John B.A.G. Haanen[1, 6], Ton N. Schumacher[1, 8], Tanja D. de Gruijl[3], Ekaterina S. Jordanova[4], Gemma G. Kenter[2, 4], Joost H. van den Berg[1, 5, #] and Nienke E. van Trommel[2, #, ¤]

The Journal for ImmunoTherapy of Cancer (JITC). 2021 Aug 2; 9(8):e002547.
DOI: 10.1136/jitc-2021-002547

1 Division of Molecular Oncology & Immunology, The Netherlands Cancer Institute, Amsterdam, The Netherlands.
2 Center for Gynecologic Oncology Amsterdam (CGOA), The Netherlands Cancer Institute, Antoni van Leeuwenhoek, Amsterdam, The Netherlands
3 Department of Medical Oncology—Cancer Center Amsterdam, Amsterdam UMC, Vrije Universiteit, Amsterdam, The Netherlands
4 Center for Gynecological Oncology Amsterdam (CGOA), Amsterdam UMC, Vrije Universiteit Amsterdam, The Netherlands
5 Department of Pharmacy and Pharmacology, Netherlands Cancer Institute, Amsterdam, The Netherlands
6 Department of Medical Oncology, The Netherlands Cancer Institute, Antoni van Leeuwenhoek, Amsterdam, The Netherlands
7 Division of Tumor Biology and Immunology, The Netherlands Cancer Institute, Amsterdam, The Netherlands.
8 Oncode Institute, The Netherlands

# Authors contributed equally
¤ Corresponding author

Abstract

Background

Usual vulvar intraepithelial neoplasia (uVIN) is a premalignancy caused by persistent infection with high-risk types of human papillomavirus (HPV), mainly type 16. Even though different treatment modalities are available (e.g., surgical excision, laser evaporation or topical application of imiquimod), these treatments can be mutilating, patients often have recurrences and 2-8% of patients develop vulvar carcinoma. Therefore, immunotherapeutic strategies targeting the pivotal oncogenic HPV proteins E6 and E7 are being explored to repress carcinogenesis.

Method

In this phase I/II clinical trial, 14 patients with HPV16+ uVIN were treated with a genetically enhanced DNA vaccine targeting E6 and E7. Safety, clinical responses and immunogenicity were assessed. Patients received four intradermal HPV-16 E6/E7 DNA tattoo vaccinations, with a 2-week interval, alternating between both upper legs. Biopsies of the uVIN lesions were taken at screening and +3 months after last vaccination. Digital photography of the vulva was performed at every check-up until 12 months of follow-up for measurement of the lesions. HPV16-specific T-cell responses were measured in blood over time in *ex vivo* reactivity assays.

Results

Vaccinations were well tolerated, although one grade 3 suspected unexpected serious adverse reaction (SUSAR) was observed. Clinical responses were observed in 6/14 (43%) patients, with 2 complete responses (CR) and 4 partial responses (PR). 5/14 patients showed HPV-specific T-cell responses in blood, measured in *ex vivo* reactivity assays. Notably, all 5 patients with HPV-specific T-cell responses had a clinical response.

Conclusions

Our results indicate that HPV-16 E6/E7 DNA tattoo vaccination is a biologically active and safe treatment strategy in patients with uVIN, and suggest that T-cell reactivity against the HPV oncogenes is associated with clinical benefit.

Trial registration number: NTR4607

Keywords

HPV-16, E6, E7, DNA tattoo vaccination, uVIN, phase I/II clinical trial, immune monitoring.

Abbreviations

AIN	Anal intraepithelial neoplasia
APC	Antigen presenting cell
CIN	Cervical intraepithelial neoplasia
CMV	Cytomegalovirus
CR	Complete response
CTCAE	Common Terminology Criteria for Adverse Events
GM-CSF	Granulocyte-macrophage colony-stimulating factor
GMP	Good manufacturing practice
HIV	Human immunodeficiency virus
HLA	Human leukocyte antigen
HPV	Human papillomavirus
IFNγ	Interferon gamma
IL-2	Interleukin-2
NEF	Negative Factor
NR	No response
PADRE	Pan HLA DR epitope
PD-1	Programmed cell death protein 1
PeIN	Penile intraepithelial neoplasia
PBMCs	Peripheral blood mononuclear cells
PR	Partial response
SLP	Synthetic long peptide
SUSAR	Suspected unexpected serious adverse reaction
TLR	Toll-like receptor
TNFα	Tumor necrosis factor alpha
TTFC	Tetanus toxin fragment C
uVIN	Usual vulvar intraepithelial neoplasia
vHSIL	Vulvar high-grade squamous intraepithelial lesion
VIN	Vulvar intraepithelial neoplasia
WBC	White blood cell count

Introduction

Usual vulvar intraepithelial neoplasia (uVIN), also known as vulvar high-grade squamous intraepithelial lesions (vHSIL), is a premalignant chronic skin disorder of the vulva and associated with a persistent infection with high risk types of HPV, mainly HPV type 16[1-3]. Spontaneous regression is rare, restricted to 1-2% of women, and progression to vulvar cancer is observed in 2-8% of cases[4-8]. Current treatment strategies are laser ablation, local excision or topical treatment with the toll-like receptor (TLR) 7-ligand imiquimod. Since patients frequently suffer from recurrent disease, different sequential therapies are often applied over the years[5, 7-9]. Multiple surgical treatments can however be mutilating, and induce psychosexual dysfunction[10, 11]. Also, topical treatment with imiquimod is associated with side effects such as pruritus and pain[12]. In order to avoid the need for debilitating treatments, and prevent relapses and potential malignant transformation, new therapeutic strategies should be explored with a final goal to eradicate transformed, oncoprotein E6 and E7 expressing epithelial cells.

Infection with high-risk genotypes of HPV leads to the expression of the oncogenic HPV proteins E6 and E7. Together, E6 and E7 drive cellular immortalization and maintain the transformed phenotype during tumor progression[13-15]. The E6 and E7 oncoproteins are continuously expressed in transformed cells, consequently enabling presentation of E6 and E7 epitopes by the transformed cells and creating the opportunity for T-cell recognition. Notably, patients with persistent uVIN often have dysfunctional HPV16-specific T-cell responses[16-18], suggesting that immune stimulating therapies that induce or enhance functional HPV16-specific T-cell responses may lead to clinical benefit.

In line with this notion, several HPV-vaccination studies targeting E6 and/or E7 have been performed with some promising immunological and clinical responses, confirming the suitability of the target proteins. Strategies that have been studied included genetic vaccines (DNA/RNA/virus/bacterial), protein-based, peptide-based or dendritic cell-based vaccines[19-22]. To date, these vaccines have not found their way to clinical practice because of little efficacy, high production costs, or cumbersome production processes like dendritic cell-based vaccines which requires a personalized cell product. Also upscaling the cell expansion protocol for adoptive transfer can be complicated and troublesome.

DNA vaccination forms an attractive approach for the induction of cellular immune responses, as these vaccines are easy to produce, very stable, relatively cheap and do not suffer from the drawback of pre-existing immunity or induction of anti-vector immunity, as is the case for most viral vectors[23, 24]. Since subcutaneous administration with adjuvant of peptide-based therapeutic HPV-vaccines can cause significant adverse events (such as local skin swelling)[21] we focused on improving the administration route and optimization of immunogenicity of the vaccine. Therefore, we developed a DNA vaccination strategy based on DNA tattoo vaccination, which demonstrated a 10-100 fold increase in vaccine specific

T-cell responses as compared to classical intramuscular DNA vaccination when tested in non-human primates[25].

Recently, we performed for the first time a phase I clinical trial using the E7 directed DNA vaccine Tetanus Toxin Fragment C (TTFC)-E7SH, which was delivered using the tattooing technique in patients with uVIN[26]. This DNA vaccine was well tolerated and the tattoo-induced skin damage was completely reversible. However, no induction of E7 directed $CD8^+$ responses nor clinical responses could be observed[26].

The aim of the current study is to improve the immunological response and monitor clinical outcome in patients with uVIN. Therefore we developed a novel DNA vaccine that can be administered by DNA tattoo vaccination[27]. Since targeting both E6 and E7 has been reported to have a synergistic effect on HPV infection control[26, 28], both oncogenes are targeted in this new format. With the combined novel DNA vaccines sig-HELP-E6SH-KDEL and sig-HELP-E7SH-KDEL (further referred to as HPV-16 E6/E7 DNA tattoo vaccine), we aim to increase the immunogenicity towards E6 and E7 by inducing $CD4^+$ helper T cells and including signals for enhanced endoplasmic reticulum targeting and retention. Here, we describe the results of a phase I/II clinical trial in which we evaluated the toxicity, clinical response and immunogenicity of this HPV-16 E6/E7 DNA tattoo vaccination in patients with uVIN.

Materials & Methods

Patients

Fourteen female patients with histology and PCR proven HPV16+ uVIN lesions were included between January 2017 and December 2019. Patients needed to have adequate bone marrow function, renal function and liver function. Exclusion criteria were pregnancy/lactation, active infectious disease, autoimmune disease or immunodeficiency. Other exclusion criteria were use of oral anticoagulant drugs or an indication of severe cardiac, respiratory or metabolic disease. Furthermore, patients could not participate if the uVIN was treated with another modality within 6 weeks prior to enrolment, if patients were treated before with therapeutic HPV vaccines, or if patients participated in a study with another investigational drug (for different indications than uVIN) within 30 days prior to enrolment. Patient characteristics are shown in table 1.

The study was approved by the Central Committee on Research Involving Human Subjects (In Dutch: Centrale Commissie Mensgebonden Onderzoek; CCMO) in The Hague, the Netherlands (Number NL46637.000.13) and registered at trialregister.nl (NTR4607). All study protocols were conducted in accordance with the ICH Harmonised Tripartite Guideline for Good Clinical Practice and the principles of the Declaration of Helsinki. All patients provided written informed consent before enrolment.

Table 1: *Baseline characteristics of the study population. uVIN, usual vulvar intraepithelial neoplasia; LE, local excision. All patients were diagnosed with HPV type 16, but patient #10 had a co-infection with HPV type 56 and patient #13 had a co-infection with HPV type 40.*

Patient no.	Age	Multi/ unifocal	Symptoms	Smoker	Previous treatment(s)	First diagnosis uVIN	Lesion size (cm²)
1	51	Uni	Pruritis	No	Laser, LE (2x), imiquimod	2012	1,4
2	64	Multi	Pruritis	Former smoker (stopped in 2016)	Laser, imiquimod	2015	1,3
3	55	Multi	Pruritis	Smoker	None	2017	0,6
4	37	Multi	None	Former smoker (stopped in 2017)	LE	2013	3,5
5	65	Uni	Pain	Former smoker (stopped in 1998)	None	2017	3,5
6	69	Uni	None	Former smoker	Laser (2x), imiquimod	1996	0,9
7	46	Multi	None	Smoker	LE (3x)	2010	3,7
8	45	Uni	None	Former smoker (stopped in 2018)	Imiquimod	2018	3,8
9	41	Multi	Pruritis	Smoker	Laser (3x), LE (3x), imiquimod (3x)	2005	36
10	50	Multi	Pruritis	Smoker	LE (3x), laser (6x), imiquimod	1993	6,8
11	46	Multi	None	Smoker	Laser (2x), imiquimod	2016	1,7
12	61	Multi	Pruritis, pain	Former smoker (stopped in 1995)	Laser, LE, imiquimod	2003	3,5
13	29	Multi	None	Smoker	Imiquimod	2019	0,7
14	36	Multi	Pruritis, pain	Smoker	Laser	2017	2,0

Vaccine composition

The HPV-16 E6/E7 DNA vaccine comprises of sig-HELP-E6SH-KDEL and sig-HELP-E7SH-KDEL, which are plasmid DNA constructs of 4814 and 5240 base pairs respectively (Figure 1a). In this plasmid, the Cytomegalovirus (CMV) promoter drives the continuous expression of E6SH and E7SH. To prevent toxicity and protect against the transforming properties of E6 and E7, coding sequences were rearranged ('shuffled'). To prevent loss of potential immunogenic epitopes, sequences flanking the positions where the coding sequence was cut, were added 3' from the coding regions (Figure 1b). The HPV-16 E6/E7 DNA vaccine includes three CD4 helper sequences: antigenic epitopes of the Negative Factor (NEF) protein from Human immunodeficiency virus (HIV) (39bp)[29], the P30 epitope derived from Tetanus Toxin (63bp)[30] and the universal synthetic, non-natural pan HLA DR epitope PADRE (39bp)[31].

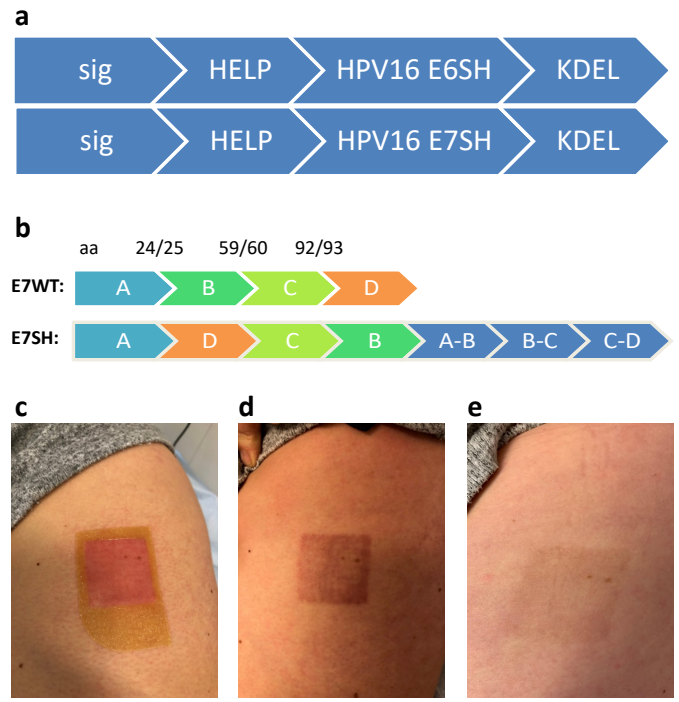

Figure 1: pUMC3 sig-HELP-E6SH-KDEL and pUMVC3 sig-HELP-E7SH-KDEL plasmids used in this trial and administered by tattoo vaccination. a) *schematic representation of the therapeutic region of the plasmid, including 3 helper sequences: Synthetic epitope PADRE (39bp), NEF from HIV (39bp) and P30 from Tetanus Toxin (63bp) for CD4 help. Sig and KDEL for improved ER targeting and retention, resulting in better antigen uptake by DCs, enhanced processing and presentation.* ***b)*** *To prevent toxicity, E6 and E7 coding sequences were shuffled. Splice sites are added at the back of the construct so no potential immunogenic epitopes are lost.* ***c)*** *Picture of the patients' skin immediately after vaccination with HPV-16 E6/E7 tattoo vaccination.* ***d)*** *Picture of the skin two weeks after vaccination.* ***e)*** *Picture of the skin 6 months after last vaccination, demonstrating hardly any visible tissue scar remains.*

By only inserting the relevant CD4 epitopes, and not the full protein domains, the risk of antigenic competition and skewing of the $CD8^+$ T cell response towards the helper epitopes was minimized. The C-terminal KDEL amino acid sequence was included to achieve endoplasmic reticulum targeting and retention, resulting in higher immunogenicity[24, 32].

For the manufacturing of both vaccines, a standard Good Manufacturing Practice (GMP) production process was followed as described earlier[33]. Resulting DNA vaccines were formulated as a lyophilized powder for solution for intradermal injection, using sucrose as stabilizer[33]. Just before administration, 1 mg of sig-HELP-E6SH-KDEL was reconstituted with 0.4 ml Water for Injection and mixed with 1 mg reconstituted sig-HELP-E7SH-KDEL to obtain

2 mg of the combined HPV-16 E6/E7 DNA tattoo vaccine at a concentration of 5mg/ml. For each of the four subsequent vaccinations, 2 mg of the combined HPV-16 E6/E7 DNA tattoo vaccine was used.

Study design

This was a single center, non-randomized phase I/II study, consisting of two cohorts. In the first cohort, 5 patients were treated, followed by an interim analysis that assessed vaccine immunogenicity. Since the criteria for continuation after interim analysis were met (a 2-fold increase in the T cell response compared to baseline in ≥2 out of 5 patients), an additional 9 patients were enrolled. Patients in both cohorts were treated identically. The primary objective of this trial was to study the systemic HPV-specific immune response of patients with HPV16+ uVIN that received the HPV-16 E6/E7 DNA tattoo vaccine. Secondary objectives were the safety and clinical responses. However, to improve the readability of the paper, we will first discuss our clinical findings, followed by the immunogenicity data.

The HPV-16 E6/E7 DNA tattoo vaccine was applied topically on the skin of the upper legs (close to a regional lymph node area) on days 0, 14, 28 and 42 and administered into the skin using a permanent make-up tattoo device (Derm.MT GmbH, Berlin, Germany). Patients received 2 mg of vaccine injected over a skin surface of 16 cm^2. Prior to tattoo vaccination the skin area was treated with an epilating cream (Veet; Reckitt Benckiser Healthcare B.V., Hoofddorp, The Netherlands). Vaccination at day 28 was administered to the same area as vaccination at day 0, and vaccination at day 42 was administered to the same area as vaccination at day 14. Patients were observed during one hour after tattooing. Peripheral blood mononuclear cell (PBMC) isolation was performed at day 0 and day 28 before vaccine administration, and at follow-up on day 56 and day 84. A biopsy of the uVIN was taken before treatment and 3 months after the last vaccination. Patients were seen for follow-up after 3, 6, 9 and 12 months after last vaccination with evaluation of the vulvar lesions including photography and measurement of the size of the lesion(s).

Safety & toxicity

The Common Terminology Criteria for Adverse Events (CTCAE) version 4.03 was used for the assessment of adverse events. All patients that received at least one vaccine dose were included in the evaluation of safety. Vital signs were measured at baseline and at all visiting days. Hematology and biochemistry tests were performed before inclusion, and at day 0, day 28, day 56 and day 84. Unacceptable toxicity was defined as an adverse event of the following types for which the relation to the study treatment was likely or not assessable: non-hematological toxicity of grade 3 or higher, hematological toxicity grade 4, neutropenia grade 3 plus fever, or non-reversible neurotoxicity of grade >2. In case unacceptable toxicity occurred in more than 30% of patients, the study would be discontinued. Local toxicity was scored as CTCAE 'injection site reaction'.

Clinical responses

Lesions were examined and the size was measured bi-dimensionally by an experienced gynecologist and another member of the study team. Drawings were made on a vulvoscopy form in the medical record. Furthermore, the lesions were monitored by digital photography. The total area (in mm^2) of the lesions was determined using ImageJ. A complete response (CR) was defined as a complete disappearance of the lesion(s) and a partial response (PR) defined as at least 50% regression of the lesion. A patient was classified as a Non Responder (NR) if lesion size was reduced by less than 50% compared to the original lesion size, or in case of progressive disease.

Immune monitoring

To assess systemic induction of HPV E6 and E7 specific T cells, PBMCs were collected at baseline (day 0) and at day 28, 56, and 84 after the first HPV-16 E6/E7 DNA tattoo vaccination. PBMCs were isolated from fresh heparinized blood samples by Ficoll density-gradient centrifugation and cryopreserved until further use.

Presence and magnitude of HPV E6 and E7 specific T-cell responses was determined by co-culture of T cells with autologous antigen presenting cells (APCs) loaded with long overlapping peptides for 6 hours (adapted protocol based on method described by Samuels *et al.*[26]). To obtain peptide loaded APCs, PBMCs were thawed and plated in 24 well plates at a concentration of 0.3-1.5 *10^6 cells/mL in T cell mixed media (20% Roswell Park Memorial Institute (RPMI)/ 80% AIM- V medium) without serum. Monocytes were separated by plate adherence, and the non-adherent cells were harvested to be used as T cell input in the co-culture. Monocytes were peptide loaded in T cell mixed media with 800 U/ml GM-CSF (Invitrogen/Thermo Fisher Scientific, California, USA) with 5 different peptide pools. Long overlapping peptides covering the entire E6 protein were split over pool 1 and 2, long overlapping peptides covering the entire E7 protein were combined in pool 3. Pool 4 consisted of all epitopes that arose as a consequence of shuffling E6 and E7 proteins. The full amino acid sequences of the long overlapping peptides from these 4 pools are listed in Supplementary Table 1. Pool 5 consisted of a set of 32 viral epitopes covering multiple HLA-alleles, and served as a positive control to assess immune competence (ICE peptide pool, U-CyTech biosciences, Utrecht, The Netherlands). Because these were short peptides that could be directly presented without processing, the ICE peptide pool was loaded onto the APCs for only 1.5 hrs prior to the start of co-cultures. An unloaded APC condition was taken along in order to determine the background reactivity. Five hours after peptide loading, monocytes were cultured overnight in the presence of 25 µg/ml poly(I:C) (InvivoGen, California, USA), to generate monocyte-derived APCs. The previously harvested non-adherent T cells were rested overnight in T cell mixed media without serum or cytokines. After

overnight incubation, peptide loaded APCs were washed and T cells were added, alongside the CD107a antibody. After 1 hour, 0.7 µl/ml Golgistop and 1 µl/ml Golgiplug was added to each well (BD Biosciences, USA), and cultures were continued for an additional 5 hours. Subsequently, T cells were harvested and stained for surface markers and intracellular cytokines and analyzed by multiparametric flow cytometry (antibody panel listed in Supplementary Table 2). Acquisition of cells was performed using an LSR II flowcytometer (BD Biosciences). FCS files were analyzed using FlowJo software (FlowJo_v10.6.1).

Immunological responses were assessed by measuring intracellular cytokine production (interferon gamma (IFNγ), tumor necrosis factor alpha (TNFα) and interleukin 2 (IL-2)) and the degranulation marker CD107a (LAMP-1). Gates were placed based on the negative population with the highest MFI and consistent for stimulated and unstimulated conditions. Patients were considered an immunological responder when the frequency of positive cells for one or more readout molecules exceeded that of the unloaded APC control by at least a factor two at any time point. In addition, the magnitude of the response should be greater than 0.1% from respectively the $CD4^+$- or $CD8^+$ T-cell parent population. A T-cell response was considered vaccine induced, when the response was not yet present at baseline.

Blood counts by hemocytometer

Routine blood counts were measured with a hemocytometer at the Clinical Chemistry Department at the Netherlands Cancer Institute. Blood was analyzed on the Xn2000 system (Sysmex). Lymphocyte, neutrophil, eosinophil and monocyte counts were extracted and analyzed from the patient records by the involved study team.

Statistical analysis

For sample size calculation, an optimal Simons two-stage design was implemented, aimed to exclude an immunological response rate of 30% and targeting a response rate of 60%. With alpha = 0.1 and power = 80%, five patients had to be enrolled in the first stage and the vaccine-induced immune response had to be observed in at least two patients to continue to the next stage (second cohort of n=9).

Patients were included in the evaluation of HPV-specific immune responses if they had received at least two doses of the vaccine, and if blood samples were drawn at baseline and at least two during therapy. Fishers exact test was used to test whether responding patients had significantly more immunological responses *ex vivo* compared to non-responding patients.

Blood counts were compared between responders (CR and PR) and non-responders using the non-parametric two-tailed Mann-Whitney U test. Paired analysis of the same patient over two time points was performed using the Wilcoxon signed rank test. *P*-value < 0.05 is * and *p*-value < 0.01 is **.

***Table 2**: Overview of treatment-related adverse events. Grades according to the Common Terminology Criteria for Adverse Events (CTCAE) v4.03.*

Toxicity	Grade	Related	No. of patients
Steven Johnsons Syndrome	3	Unlikely	1
Pruritus	1	Definitely	5
Injection site reaction	1	Definitely	3
Fatigue	1	Possibly	3
Flu like symptoms	1	Possibly	3
Dizziness	1	Possibly	2
Dysgeusia	1	Possibly	2
Local infection after skin biopsy	1	Definitely	1
Hot flushes	1	Possibly	1
Pain of skin	1	Possibly	1

Results

Safety and toxicity

13 patients received all four vaccinations and 1 patient received only two vaccinations due to adverse reactions. All adverse events are listed in table 2. The patient (patient #12) who had to discontinue vaccination was diagnosed (by biopsy of a skin eruption) with a Stevens-Johnson syndrome grade 3, two weeks after the second vaccination. Although she presented with similar symptoms earlier that year during imiquimod treatment and before she received the first vaccination, an effect of the vaccination could not be excluded, and this event was therefore reported as a suspected unexpected serious adverse reaction (SUSAR). This patient fully recovered from the SUSAR, within 4 months after last vaccination all skin lesions had disappeared. Other patients did not have treatment-related adverse events higher than grade 1 (table 2). Pruritus at the injection site after vaccination was the most commonly observed adverse event (36%). A picture of the injected skin immediately after vaccination, 2 weeks after vaccination and 6 months after vaccination is shown in Figure 1 c-e.

Observation of clinical responses after HPV-vaccination in patients with uVIN lesions

In the first cohort we included 5 patients. In this cohort a complete response was observed in 2 patients and a partial response was seen in 1 patient (Figure 2). Both complete responses were seen after 6 months of follow-up and the partial responses after 3 months. The uVIN lesions did not recur after a complete response had been observed for the duration of follow-up (12 months after the last vaccination). Patient #3 showed no clinical response and was treated with laser evaporation 2 years after vaccination. Patient #5 showed no response and started with imiquimod treatment 3 months after the last vaccination. Clinical responses

after the start of new treatments were not taken into account in this study. In the second cohort, 9 patients were included. In this second cohort 3 patients showed a durable partial response during follow-up. An example of a patient showing a partial response is shown in Figure 2a-b. The biopsies of the vulva at 3 months follow-up showed uVIN in all of the vaccinated patients. This correlates with the clinical observation that complete responses were first seen at 6 months after vaccination. Six patients showed no clinical response. One patient (patient #11) was diagnosed with micro-invasive vulvar cancer after 6 months of follow-up for which a local excision was performed. Patient #10 underwent laser treatment. Patient #12 underwent laser excision after 84 days of follow-up. Patient #14 showed no response. An overview of all clinical responses is given in Figure 2c-d. In Figure 2e the pre-treatment size of the lesions per group (NR, PR, CR) is illustrated. The patients with the biggest lesion size (#9 and #10), were both non-responders. These two patients also had received most previous treatments before inclusion in this study, as shown in Table 1.

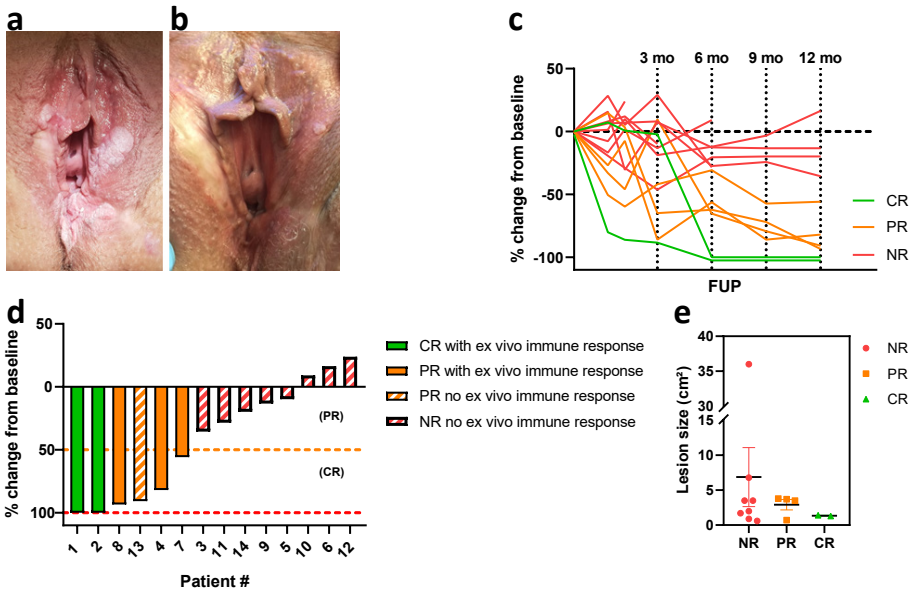

Figure 2: clinical response data of cohort 1 and 2 a) *uVIN lesions visible at screening visit.* ***b)*** *Partial response of uVIN lesions visible at follow-up +12 months after vaccination with HPV-16 E6/E7 tattoo vaccination.* ***c)*** *Overview of uVIN lesion size changes (as percentage change compared with baseline) during follow-up.* ***d)*** *Waterfall plot showing percentage change of uVIN lesion at last follow-up compared with baseline lesion size (= lesion size at screening).* ***e)*** *Lesion size before therapy per response category. Complete responders are depicted in green, partial responders in orange and non-responders in red.*

Phenotypic characterization of systemic T cells

Patient PBMCs from baseline samples, as well as from ~day 28, ~ 56, and ~ 84 after primary vaccination were subjected to basic phenotypic characterization, as determined by multiparameter flow cytometry (see Supplementary Figure 1 for gating strategy). Programmed cell death protein 1 (PD-1) expression on systemic T cells was overall low (<0,4%) and did not show any directionality in terms of response prediction or evaluation (see Supplementary Figure 2a). We also did not uncover an increase in PD-1 expression in $CD4^+$ and $CD8^+$ T cells upon vaccination. The absence of PD-1 expression on circulating T cells does not necessarily reflect expression levels of PD-1 on T cells infiltrating the uVIN lesions. No differences between responders and non-responders could be found in the differentiation state of T cells based on the surface marker expression of CD45RA and CCR7 (see Supplementary Figure 2b).

Systemic HPV-16 specific T-cell responses

The same PBMCs used for phenotypic characterization of T cells were also used to monitor systemic immune responses against the HPV16 E6 and E7 oncoproteins. A patient was considered an immunological responder if the percentage of positive $CD4^+$ and/or $CD8^+$ T cells for one or more of the measured molecules (IFNγ, TNFα, IL-2 and CD107a) was greater than 0.1% and at least two times higher than the background. Furthermore, a response was considered vaccine induced when it was not yet present at baseline. To illustrate an *ex vivo* immune response, expression of IFNγ in $CD4^+$ and $CD8^+$ T cells in the presence or absence of stimulation with peptide-loaded APCs from an immunological responder (patient #8) are displayed in Figure 3a. T-cell responses against E6-1, E6-2 and E7 peptide pool compared to unloaded APCs of all immunological responders are presented in Figure 3b. Table 3 provides an overview of the $CD4^+$ and $CD8^+$ T-cell responses against E6-1, E6-2 and E7 peptide pools from all patients, depicted as the fold change over the unloaded APC background.

The peak of the immunological response in blood was mostly detected at day 56; two weeks after the boost vaccination. From the 14 patients treated in this study, five showed an *ex vivo* immunological response (36% immunological response rate). Four of these immunological responses were not detected at baseline, and one response showed a substantial increase after vaccination (Figure 3b, patient #7 IFNγ). Furthermore, 4 out of 5 of these responses could still be detected at day 84, over a month after the last vaccination that was given at day 42 (namely in patient #1, #2, #7 and #8).

The effector molecule measured in the response varied between patients, but IFNγ was the dominant effector molecule (4/5). Interestingly, both $CD4^+$ and $CD8^+$ T-cell reactivity against all peptide pools was observed (Figure 3b). In all immunological responders (5/5) the response could be detected in both the $CD4^+$ and $CD8^+$ T cell compartments. A Boolean gating strategy was applied to distinguish single, double and triple producing T cells

(combinations of IFNγ, TNFα and IL2), with or without co-expression of degranulation marker CD107a in responding patients. T cells predominantly produced one cytokine (Supplementary Figure 3), indicating suboptimal functionality of the T cells[34, 35]. Time course graphs showing the IFNγ, TNFα, IL-2 and CD107a responses against E6-1, E6-2 and E7 peptide pool of all patients (including the non-responders), can be found in Supplementary Figure 4.

As described in the method section, E6 and E7 coding sequences needed to be shuffled for safety reasons. To assess the immunogenicity of the junction sites of the shuffled proteins, all possible epitopes covering those regions were taken along in a separate pool during the *ex vivo* immune reactivity assays. In Supplementary Figure 5, reactivity from $CD4^+$ and $CD8^+$ T cells against the shuffle points is depicted at day 0 and day 56. $CD8^+$ T cells from patient #1 and patient #8 (both responders) produced IFNγ upon stimulation with the shuffle point peptide pool. For patient #8, shuffle point reactivity seemed vaccine induced and for patient #1 the reactivity was also found in the baseline samples, possibly indicating cross reactivity towards another epitope. The magnitude of the response against the shuffle points was occasionally higher than the magnitude of the response against E6 and E7 epitopes. We do not know the exact reason for this, although we could speculate that this is due to differences in antigen processing and/or presentation between patients. In general, we do not see common reactivity against the shuffle point epitopes and it is important to note that no “on target, of lesion” toxicity was observed in any of the patients.

Reactivity against the ICE peptide pool consisting of 32 viral epitopes covering multiple HLA-alleles was tested to assess differences in immune competence between responding and non-responding patients (see Supplementary Figure 6). In total, $CD8^+$ T cells from baseline samples of 9/14 patients produced cytokines upon culturing with ICE peptide loaded APCs and no CD4 reactivity was measured against the ICE peptide pool (see Supplementary Figure 6). As a positive control we took along 4 healthy donors, which were all responsive towards the ICE peptide pool (see Supplementary Figure 6). Also, all patient samples produced high amounts of cytokines after PMA/ionomycin stimulation (data not shown).

Correlation between T-cell reactivity against the HPV oncogenes and clinical benefit

Notably, all patients who showed *ex vivo* HPV E6 or E7 specific T-cell responses also experienced clinical benefit from the vaccine (Figure 3c). In contrast, such HPV E6 or E7 specific T-cell responses were completely absent in clinical non-responders (0/8). For 1 out of 6 patients that showed a clinical response, no *ex vivo* immune reactivity could be determined (Table 3 and Supplementary Figure 4, patient #13). Collectively, these findings demonstrate that there is a strong correlation between the induction of immune reactivity and clinical response (Fischer’s exact test, p=0.003).

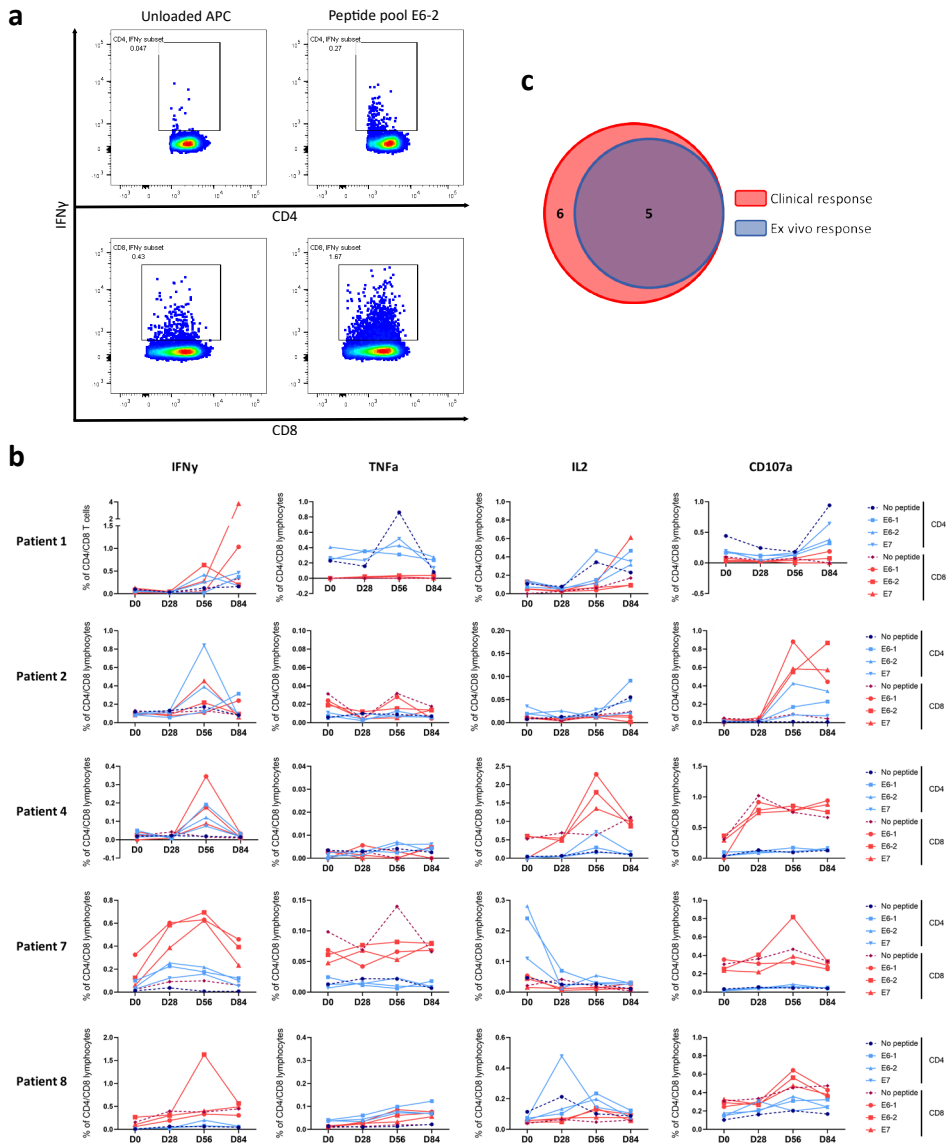

Figure 3: ex vivo reactivity data. a) *Example of an immunological responder (patient #8) at day 56, in which you can appreciate a cloud of IFNγ producing CD4 and CD8 cells, that also meets the fold increase over background requirement.* ***b)*** *Time course of all immunological responders. T cell responses against E6-1, E6-2 and E7 peptide pool are depicted. The dashed line represents the ‘no peptide’ control to visualize background reactivity. Time courses of IFNγ, TNFα, IL-2 and CD107a production for all patients are displayed in Supplementary Figure 4.* ***c)*** *Venn diagram visualizing the overlap between clinical responders (6/14) and immunological responders (5/14) (Fishers exact test, p=0.003).*

Table 3: *overview of immunological responses against E6 and E7 peptide pools.*

Patient	Ex vivo response	Clinical response			E6-1 IFNy	E6-1 TNFa	E6-1 IL2	E6-1 CD107a	E6-2 IFNy	E6-2 TNFa	E6-2 IL2	E6-2 CD107a	E7 IFNy	E7 TNFa	E7 IL2	E7 CD107a
1	Yes	CR	CD4	D0	<0,1%	1,1	<0,1%	0,4	<0,1%	1,8	1,3	0,4	<0,1%	1,2	1,2	0,4
				D56	<0,1%	0,4	0,4	0,7	3,4	0,5	0,3	0,9	2,0	0,6	1,4	0,7
			CD8	D0	<0,1%	n.d.	n.d	<0,1%	<0,1%	n.d.	n.d.	<0,1%	1,5	n.d.	n.d.	<0,1%
				D56	<0,1%	n.d.	<0,1%	<0,1%	8,7	n.d.	<0,1%	<0,1%	3,8	n.d.	2,0	0,0
2	Yes	CR	CD4	D0	<0,1%	<0,1%	<0,1%	<0,1%	<0,1%	<0,1%	<0,1%	<0,1%	0,8	<0,1%	<0,1%	<0,1%
				D56	0,7	<0,1%	<0,1%	15,9	2,3	<0,1%	<0,1%	39,9	4,9	<0,1%	<0,1%	<0,1%
			CD8	D0	0,9	<0,1%	<0,1%	<0,1%	<0,1%	<0,1%	<0,1%	<0,1%	<0,1%	<0,1%	<0,1%	0,2
				D56	0,8	<0,1%	<0,1%	9,5	1,7	<0,1%	<0,1%	5,9	3,4	<0,1%	<0,1%	6,3
3	No	NR	CD4	D0	<0,1%	<0,1%	<0,1%	<0,1%	<0,1%	<0,1%	1,1	<0,1%	<0,1%	<0,1%	1,0	<0,1%
				D56	<0,1%	<0,1%	1,0	<0,1%	<0,1%	<0,1%	0,9	<0,1%	<0,1%	<0,1%	1,0	<0,1%
			CD8	D0	1,2	<0,1%	0,6	0,8	0,9	<0,1%	1,0	1,2	0,7	<0,1%	1,0	0,8
				D56	<0,1%	<0,1%	1,0	1,7	<0,1%	<0,1%	1,0	1,0	<0,1%	<0,1%	1,0	0,9
4	Yes	PR	CD4	D0	<0,1%	<0,1%	<0,1%	<0,1%	<0,1%	<0,1%	<0,1%	<0,1%	<0,1%	<0,1%	<0,1%	<0,1%
				D56	10,1	<0,1%	1,6	1,8	6,4	<0,1%	0,9	1,2	<0,1%	<0,1%	4,0	<0,1%
			CD8	D0	<0,1%	<0,1%	<0,1%	<0,1%	<0,1%	<0,1%	1,2	1,2	<0,1%	<0,1%	1,1	0,9
				D56	24,2	<0,1%	3,6	1,0	12,4	n.d.	2,8	1,1	<0,1%	<0,1%	2,1	1,0
5	No	NR	CD4	D0	<0,1%	<0,1%	<0,1%	0,9	<0,1%	<0,1%	<0,1%	0,9	<0,1%	<0,1%	<0,1%	<0,1%
				D56	<0,1%	<0,1%	<0,1%	1,2	<0,1%	<0,1%	<0,1%	0,9	<0,1%	<0,1%	<0,1%	0,7
			CD8	D0	<0,1%	<0,1%	<0,1%	<0,1%	<0,1%	<0,1%	<0,1%	<0,1%	<0,1%	<0,1%	<0,1%	<0,1%
				D56	<0,1%	<0,1%	<0,1%	<0,1%	<0,1%	<0,1%	<0,1%	<0,1%	<0,1%	<0,1%	<0,1%	<0,1%
6	No	NR	CD4	D0	<0,1%	<0,1%	<0,1%	<0,1%	<0,1%	<0,1%	<0,1%	<0,1%	<0,1%	<0,1%	<0,1%	<0,1%
				D56	<0,1%	<0,1%	<0,1%	<0,1%	<0,1%	<0,1%	<0,1%	<0,1%	<0,1%	<0,1%	<0,1%	<0,1%
			CD8	D0	<0,1%	<0,1%	<0,1%	<0,1%	<0,1%	<0,1%	<0,1%	<0,1%	<0,1%	<0,1%	<0,1%	<0,1%
				D56	<0,1%	<0,1%	<0,1%	<0,1%	<0,1%	<0,1%	<0,1%	<0,1%	<0,1%	<0,1%	<0,1%	<0,1%
7	Yes, Vaccine enhanced, not induced	PR	CD4	D0	<0,1%	<0,1%	5,2	<0,1%	<0,1%	<0,1%	6,0	<0,1%	<0,1%	<0,1%	2,4	<0,1%
				D56	22,1	<0,1%	<0,1%	<0,1%	27,3	<0,1%	<0,1%	<0,1%	19,8	<0,1%	<0,1%	<0,1%
			CD8	D0	13,8	<0,1%	<0,1%	1,2	5,3	<0,1%	<0,1%	0,8	<0,1%	<0,1%	<0,1%	0,8
				D56	6,4	<0,1%	<0,1%	0,7	7,0	<0,1%	<0,1%	1,7	6,3	<0,1%	<0,1%	0,8
8	Yes	PR	CD4	D0	<0,1%	<0,1%	<0,1%	1,4	<0,1%	<0,1%	<0,1%	1,7	<0,1%	<0,1%	<0,1%	1,4
				D56	<0,1%	<0,1%	2,3	1,5	3,2	<0,1%	1,9	1,8	<0,1%	<0,1%	1,4	1,0
			CD8	D0	<0,1%	<0,1%	<0,1%	0,8	1,7	<0,1%	<0,1%	0,9	0,7	<0,1%	<0,1%	1,1
				D56	0,9	<0,1%	2,6	1,4	4,3	<0,1%	2,9	1,2	1,1	<0,1%	<0,1%	1,0
9	No	NR	CD4	D0	<0,1%	<0,1%	<0,1%	<0,1%	<0,1%	<0,1%	<0,1%	<0,1%	<0,1%	<0,1%	<0,1%	<0,1%
				D56	<0,1%	<0,1%	<0,1%	1,0	<0,1%	<0,1%	<0,1%	<0,1%	<0,1%	<0,1%	<0,1%	<0,1%
			CD8	D0	<0,1%	<0,1%	<0,1%	<0,1%	<0,1%	<0,1%	<0,1%	<0,1%	<0,1%	<0,1%	<0,1%	<0,1%
				D56	<0,1%	<0,1%	<0,1%	<0,1%	<0,1%	<0,1%	<0,1%	0,9	<0,1%	<0,1%	<0,1%	<0,1%
10	No	NR	CD4	D0	<0,1%	<0,1%	<0,1%	0,6	<0,1%	1,1	<0,1%	1,1	<0,1%	<0,1%	<0,1%	0,7
				D56	<0,1%	<0,1%	<0,1%	<0,1%	<0,1%	<0,1%	<0,1%	1,2	<0,1%	<0,1%	<0,1%	<0,1%
			CD8	D0	<0,1%	<0,1%	<0,1%	0,7	<0,1%	<0,1%	<0,1%	1,2	<0,1%	<0,1%	<0,1%	0,8
				D56	<0,1%	<0,1%	<0,1%	1,2	<0,1%	<0,1%	<0,1%	0,9	<0,1%	<0,1%	<0,1%	1,1
11	No	NR	CD4	D0	<0,1%	<0,1%	1,7	<0,1%	<0,1%	<0,1%	0,7	<0,1%	<0,1%	<0,1%	1,0	1,8
				D56	<0,1%	<0,1%	<0,1%	1,0	<0,1%	<0,1%	0,9	1,0	<0,1%	<0,1%	0,6	0,9
			CD8	D0	<0,1%	<0,1%	<0,1%	0,9	1,1	<0,1%	<0,1%	1,0	1,1	<0,1%	<0,1%	1,1
				D56	1,1	<0,1%	<0,1%	0,9	1,2	<0,1%	<0,1%	0,9	1,1	<0,1%	<0,1%	1,0
12	No	NR	CD4	D0	<0,1%	<0,1%	<0,1%	0,9	<0,1%	<0,1%	1,0	0,9	<0,1%	<0,1%	1,7	0,7
				D56	<0,1%	<0,1%	<0,1%	1,2	<0,1%	<0,1%	1,4	1,6	<0,1%	<0,1%	1,0	1,3
			CD8	D0	<0,1%	<0,1%	<0,1%	1,0	<0,1%	<0,1%	<0,1%	1,1	<0,1%	<0,1%	<0,1%	<0,1%
				D56	0,7	<0,1%	<0,1%	0,9	0,7	<0,1%	1,8	0,9	0,5	<0,1%	<0,1%	0,9
13	No	PR	CD4	D0	<0,1%	<0,1%	<0,1%	1,8	<0,1%	<0,1%	<0,1%	1,8	<0,1%	<0,1%	<0,1%	<0,1%
				D56	<0,1%	<0,1%	<0,1%	1,9	<0,1%	<0,1%	<0,1%	1,7	<0,1%	<0,1%	<0,1%	<0,1%
			CD8	D0	<0,1%	<0,1%	<0,1%	0,7	<0,1%	1,0	<0,1%	1,0	<0,1%	<0,1%	<0,1%	<0,1%
				D56	<0,1%	0,8	<0,1%	0,7	<0,1%	0,6	<0,1%	0,9	<0,1%	<0,1%	<0,1%	1,2
14	No	NR	CD4	D0	<0,1%	<0,1%	<0,1%	<0,1%	<0,1%	<0,1%	<0,1%	<0,1%	<0,1%	<0,1%	<0,1%	<0,1%
				D56	<0,1%	<0,1%	<0,1%	1,9	<0,1%	<0,1%	<0,1%	1,2	<0,1%	<0,1%	<0,1%	<0,1%
			CD8	D0	<0,1%	<0,1%	0,6	0,8	<0,1%	<0,1%	1,0	0,7	<0,1%	<0,1%	<0,1%	<0,1%
				D56	<0,1%	<0,1%	<0,1%	0,8	<0,1%	<0,1%	<0,1%	0,9	<0,1%	<0,1%	1,1	0,6

Numbers represent the fold change over background (unloaded APCs). n.d.: no positive cells detected. Fold changes greater than two are highlighted in green. <0.1% indicates that the fraction of positive cells was less than 0.1% from its parent ($CD4^+$ or $CD8^+$ T cells). CR = complete response, PR = partial response and NR = no response.

Lymphocyte counts in relation to clinical response

Regular blood cell counts were established at matching time points with the PBMC isolation for *ex vivo* reactivity assays. At baseline, no statistically significant differences in number of circulating lymphocytes, neutrophils, monocytes and eosinophils could be found between responding and non-responding patients (shown in Figure 4). During the vaccinations at day 28, as well as at the peak of the response at day 56, lymphocyte counts were significantly higher in responding patients than in non-responding patients (Figure 4a). Systemic neutrophil to lymphocyte ratio was decreased at the peak of the response compared to baseline in responding patients. No significant change in neutrophil to lymphocyte ratio over time was found in non-responding patients (Figure 4c). The number of circulating neutrophils, monocytes and eosinophils remained similar for responders and non-responders and unaltered compared to baseline levels (Figure 4 b, d, e).

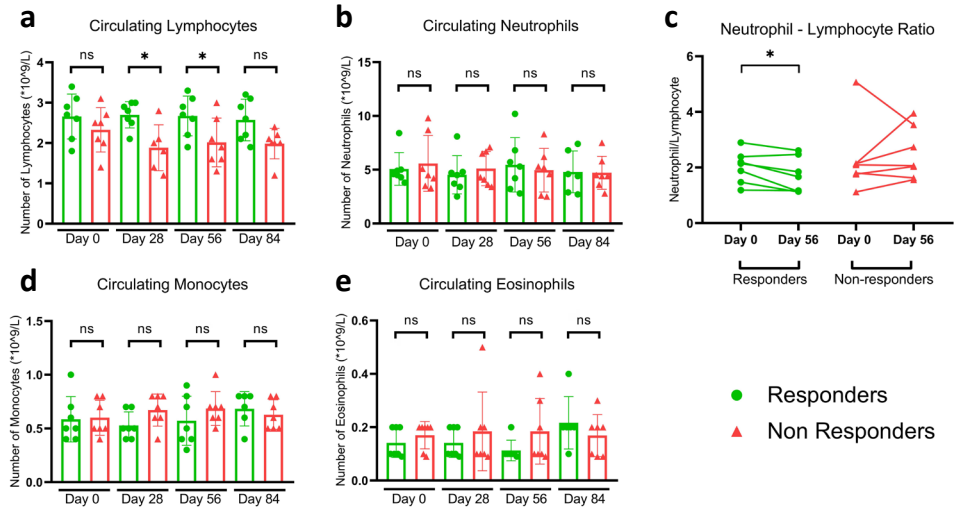

Figure 4: Systemic blood counts reveal differences between responders and non-responders during- and post vaccination a) *Significantly reduced number of circulating lymphocytes in non-responding patients, compared to responding patients. Two tailed Mann-Whitney test D28 p=0,015, D56 p=0,048.* ***b)*** *No statistically significant differences detected between responding and non-responding patients at any time point in neutrophils.* ***c)*** *Responding patients show a decreased Neutrophil to Lymphocyte ratio at the peak the immune response compared to baseline. No significant changes in Neutrophil to Lymphocyte ratio in non-responding patients. Wilcoxon matched-pairs signed rank test p=0,0469. No statistically significant differences detected between responding and non-responding patients at any time point in circulating* ***d)*** *monocytes and* ***e)*** *eosinophils.*

Discussion and Conclusion

Despite a variety of treatment modalities for patients suffering from uVIN, these patients are often confronted with recurrent disease and are at risk to progress to invasive disease. In this study, we have used a therapeutic HPV-16 E6/E7 DNA tattoo vaccine comprising of sig-HELP-E6SH-KDEL and sig-HELP-E7SH-KDEL. In mice, this DNA vaccine has shown to be much more immunogenic than the variants with other helper cassettes (such as TTFC) that were previously used in the clinic[24, 32]. This is the first clinical trial using this optimized DNA vaccine targeting the HPV oncoproteins E6 and E7 in patients with uVIN.

Several HPV-vaccination studies targeting E6 and/or E7 have been performed with varying results. Intramuscular TA-CIN (fusion protein HPV16 E6E7L2) administration preceded by local imiquimod application has been studied, with a clinical response rate of 63% in patients with uVIN, but all patients in this study displayed moderate (n=5, 26%), or severe (n=14, 74%) side effects[22]. TA-HPV, a recombinant vaccinia virus, encoding modified HPV 16 and 18 E6 and E7, has also been successfully applied in uVIN and vaginal intraepithelial neoplasia patients. This was resulting in both a potent clinical responses (8/18 and 5/12 respectively) and immunological responses (13/18 and 6/10 respectively)[16, 36]. However, the use of live vaccinia virus limits the broad application of this therapy. In trials investigating subcutaneously administered HPV16 E6 and E7 synthetic long peptides (SLP), clinical responses were observed after 12 months in 52-79% of women with uVIN[21, 37]. However, grade 1 and grade 2 side effects were reported at very high frequencies and were probably linked to the use of the Montanide ISA51. In our trial, no adverse events higher than grade 1 were reported, (apart from one patient with a grade 3 SUSAR that was probably unrelated as symptoms had occurred before the first vaccination) and at much lower frequencies, suggesting that HPV-16 E6/E7 DNA tattoo vaccination is safe to use. This difference in toxicity and tolerability can likely be explained by the fact that we used the tattoo technique, and no adjuvant or other initial treatment modality such as imiquimod was used in our trial. Since subcutaneous administration of a therapeutic HPV peptide vaccine with adjuvant can cause significant adverse events (such as local skin swelling), we focused on improving the administration route and optimization of immunogenicity of the vaccine.

Our data indicate a 43% clinical response rate. A clinically durable and ongoing complete response was seen in 14% of the patients. Partial responses were observed in 29% of patients and were ongoing at the time of most recent follow-up. Importantly, unlike other treatment modalities (e.g., laser ablation, surgical excision or imiquimod application) in which up to one-third of patients show a recurrence[9, 38], none of the responders in our study had recurrences or increasing lesion size over time. A likely explanation for this difference is that our vaccination strategy targets the cause of the disease, *i.e.* HPV16 E6 and E7 expressing cells, and this is underlined by the fact that 83% of the responding patients showed a clear E6/E7 specific T-cell response in their blood. However, recurrences often

occur over one year after treatment in this patient group and follow-up period in this study was only 12 months. Future studies have to point out whether the recurrence of uVIN is maintained more than a year after therapeutic HPV-vaccination. Furthermore, no HPV-testing at the end of follow-up was performed, which would be interesting to incorporate in follow-up studies to confirm the successful clearance of the virus at the uVIN lesions after vaccination.

Although responses were durable in our study, complete response rates were still low (2/14). Therefore we would like to advocate the combination of our vaccine with for instance immune checkpoint inhibitors such as (locally administrated) anti PD-(L)1 or TLR_agonists, such as poly (I:C) (TLR3 agonist) or Imiquimod (TLR7 agonist). Besides this, it might be beneficial for patients with large uVIN lesions to first decrease lesion size (e.g. by laser or topical therapy), before administering our vaccine, because patients with largest uVIN lesion size at baseline did not show any response to vaccination in this trial. However, since the sample size in this study was quite small, future studies have to reveal whether this effect will still be observed. Interestingly though, Kenter *et al.* also reported that lesions were smaller in the CR group after E6 and E7 synthetic long-peptide vaccination in uVIN patients[21].

Systemic immunological HPV-specific T-cell responses were found in both the $CD4^+$ as well as the $CD8^+$ compartment. These responses were either vaccine induced (4/5) or vaccine enhanced (1/5). Interestingly, 5 out of 6 patients with complete or partial responses showed systemic HPV-specific T-cell responses in *ex vivo* assays. Likewise, patients *without* a clinical response, did *not* show an HPV-specific T-cell response *ex vivo*. Previous HPV targeting vaccines, in the same patient group, observed a similar relationship. Both Kenter *et al.* and Van Poelgeest *et al.* reported a correlation between (the magnitude of) the *ex vivo* response and the clinical outcome of the patients after vaccination with HPV16 E6 and E7 synthetic long peptides[21, 37] However, in a study evaluating the effect of a TA-HPV vaccine against E6 and E7, *ex vivo* responsiveness to the vaccine vector was confirmed in all patients, there was no relation with clinical benefit[20]. The differences between clinical and immunological responses between our study and previous studies could be explained by a different study design, different vaccine, different patient group and a different technique used to identify *ex vivo* immune responses.

At baseline, the number of circulating lymphocytes, neutrophils, monocytes and eosinophils did not differ statistically significant between responders and non-responders. Upon treatment, non-responders had statistically significant fewer circulating lymphocytes than responders, which could potentially be a reflection of a less competent immune system.

Future experiments will tell whether responders will have relatively higher numbers of VIN lesion infiltrating lymphocytes compared to non-responders, and what potential immunosuppressive mechanisms in the lesions might have hampered a T-cell response in the non-responding patients.

Follow-up studies should be performed to determine the effects of this vaccination strategy in a larger cohort of patients with uVIN, as well as patients with other intraepithelial neoplasia caused by HPV 16, such as anal intraepithelial neoplasia (AIN), penile intraepithelial neoplasia (PeIN) and cervical intraepithelial neoplasia (CIN). HPV-16 and HPV-18 CIN2/3 patients have already shown to respond to other types of DNA vaccination targeting E6 and E7 proteins[39].

In conclusion, we found in this phase I/II clinical trial that HPV-16 E6/E7 DNA tattoo vaccination for the treatment of HPV16 positive uVIN is a safe and immunologically effective strategy. Interestingly, in 5 out of 6 clinically responding patients, E6/E7 specific $CD4^+$ and $CD8^+$ T cell reactivity could be detected in blood samples. Such responses were not observed in patients without a clinical response. Therefore, HPV-16 E6/E7 DNA tattoo could possibly be a clinically meaningful treatment strategy in patients with uVIN.

Competing interests

N.A.M.B., J.R., M.v.B., H.J.M.A.A.Z., M.R., S.S., **B.N., E.S.J., G.G.K.** and **N.E.v.T** have no competing interest to declare.

J.H.B. is (part time) employee of Modra Pharmaceuticals and stockholder in Modra Pharmaceuticals. (not related to the manuscript).

T.N.S. is advisor for Adaptive Biotechnologies, Allogene Therapeutics, Merus, Neogene Therapeutics, and Scenic Biotech; is a recipient of research support from Merck KgaA; is a stockholder in Allogene Therapeutics, Merus, Neogene Therapeutics and Scenic Biotech; and is venture partner at Third Rock Ventures, all not related to the current work.

J.B.A.G.H. is advisor to Achilles Therapeutics, Bristol-Myers Squibb, BioNTech USA, Ipsen, Gadeta, Immunocore, MSD, Merck Serono, Molecular Partners, Neogene Therapeutics, Novartis, Pfizer, Roche/Genentech, Sanofi, Seattle Genetics, Third Rock Ventures, is stock holder in Neogene Therapeutics, and is a recipient of grant or research support from Bristol-Myers Squibb, MSD, Novartis and BioNTech USA.

K.E.d.V. reports research funding from Roche and is consultant for Third Rock Ventures, all outside the scope of this work.

T.D.d.G. has served as advisor to TILT Biotherapeutics, LAVA Therapeutics, Macrophage Pharma and DCPrime, is a recipient of a grant from Idera Pharmaceuticals, and is co-founder and shareholder of LAVA Therapeutics.

J.H.v.d.B is a recipient of grant or research support from BioNTech USA and Astra Zeneca, and is currently employed at CellPoint B.V.

Authors' contributions

N.A.M.B. constructed the plasmids and produced DNA vaccines, designed and performed immune monitoring experiments, interpreted data and co-wrote the manuscript.

J.R. vaccinated patients, collected and interpreted clinical data and co-wrote the manuscript.

M.v.B. involved in patient care

H.J.M.A.A.Z. involved in patient care

S.S. involved in writing the study protocol

M.R. vaccinated patients and collected clinical data

B.N. and **J.H.B.** supervised DNA production

T.N.S. conceived the project, designed plasmids and interpreted data and reviewed the manuscript

J.B.A.G.H. conceived the project, designed plasmids and interpreted data

K.E.d.V. interpreted data and reviewed the manuscript

T.D.d.G. interpreted data

E.S.J. interpreted data

G.G.K. conceived the project, interpreted data

J.H.v.d.B conceived the project, interpreted data, designed plasmids, supervised DNA production and co-wrote the manuscript

N.E.v.T. conceived the project, interpreted clinical data and co-wrote the manuscript

Acknowledgements

The authors would like to thank Thomas Lanigan from the University of Michigan for kindly supplying us with the pUMVC3 backbone. The authors would also like to thank Renate de Boer, Maaike van Zon and Edith Vermeij for their help in manufacturing of DNA vaccines, and the QC and QA department of the Pharmacy of The Netherlands Cancer Institute- Antoni van Leeuwenhoek for the generous support.

We thank the Rational molecular Assessment Innovative Drug selection (RAIDs) consortium (http://www.raids-fp7.eu). This trial is part of the RAIDs project and received funding from the European Union's Seventh Program for Research, Technological Development, and Demonstration (Grant No. 304810). Additional funding was obtained through the Louise Vehmeijer Foundation, The Netherlands. Part of the salary costs were provided by Oncode Institute, The Netherlands.

References

1. De Vuyst H, Clifford GM, Nascimento MC, Madeleine MM, Franceschi S. Prevalence and type distribution of human papillomavirus in carcinoma and intraepithelial neoplasia of the vulva, vagina and anus: a meta-analysis. *Int J Cancer*. Apr 1 2009;124(7):1626-36. doi:10.1002/ijc.24116
2. Serrano B, de Sanjose S, Tous S, et al. Human papillomavirus genotype attribution for HPVs 6, 11, 16, 18, 31, 33, 45, 52 and 58 in female anogenital lesions. *Eur J Cancer*. Sep 2015;51(13):1732-41. doi:10.1016/j.ejca.2015.06.001
3. Srodon M, Stoler MH, Baber GB, Kurman RJ. The distribution of low and high-risk HPV types in vulvar and vaginal intraepithelial neoplasia (VIN and VaIN). *Am J Surg Pathol*. Dec 2006;30(12):1513-8. doi:10.1097/01.pas.0000213291.96401.48
4. Fehr MK, Baumann M, Mueller M, et al. Disease progression and recurrence in women treated for vulvovaginal intraepithelial neoplasia. *J Gynecol Oncol*. Jul 2013;24(3):236-41. doi:10.3802/jgo.2013.24.3.236
5. Jones RW, Rowan DM, Stewart AW. Vulvar intraepithelial neoplasia: aspects of the natural history and outcome in 405 women. *Obstet Gynecol*. Dec 2005;106(6):1319-26. doi:10.1097/01.AOG.0000187301.76283.7f
6. McNally OM, Mulvany NJ, Pagano R, Quinn MA, Rome RM. VIN 3: a clinicopathologic review. *Int J Gynecol Cancer*. Sep-Oct 2002;12(5):490-5. doi:10.1046/j.1525-1438.2002.01140.x
7. Satmary W, Holschneider CH, Brunette LL, Natarajan S. Vulvar intraepithelial neoplasia: Risk factors for recurrence. *Gynecol Oncol*. Jan 2018;148(1):126-131. doi:10.1016/j.ygyno.2017.10.029
8. van Seters M, van Beurden M, de Craen AJ. Is the assumed natural history of vulvar intraepithelial neoplasia III based on enough evidence? A systematic review of 3322 published patients. *Gynecol Oncol*. May 2005;97(2):645-51. doi:10.1016/j.ygyno.2005.02.012
9. Wallbillich JJ, Rhodes HE, Milbourne AM, et al. Vulvar intraepithelial neoplasia (VIN 2/3): comparing clinical outcomes and evaluating risk factors for recurrence. *Gynecol Oncol*. Nov 2012;127(2):312-5. doi:10.1016/j.ygyno.2012.07.118
10. Likes WM, Stegbauer C, Tillmanns T, Pruett J. Correlates of sexual function following vulvar excision. *Gynecol Oncol*. Jun 2007;105(3):600-3. doi:10.1016/j.ygyno.2007.01.027
11. Thuesen B, Andreasson B, Bock JE. Sexual function and somatopsychic reactions after local excision of vulvar intra-epithelial neoplasia. *Acta Obstet Gynecol Scand*. Feb 1992;71(2):126-8. doi:10.3109/00016349209007969
12. van Seters M, van Beurden M, ten Kate FJ, et al. Treatment of vulvar intraepithelial neoplasia with topical imiquimod. *N Engl J Med*. Apr 3 2008;358(14):1465-73. doi:10.1056/NEJMoa072685
13. Sher YP, Lee C, Liu SY, et al. A therapeutic vaccine targeting HPV E6/E7 with intrinsic Toll-like receptor 2 agonist activity induces antitumor immunity. *Am J Cancer Res*. 2018;8(12):2528-2537.
14. Tan S, de Vries EG, van der Zee AG, de Jong S. Anticancer drugs aimed at E6 and E7 activity in HPV-positive cervical cancer. *Curr Cancer Drug Targets*. Feb 2012;12(2):170-84. doi:10.2174/156800912799095135
15. Moody CA, Laimins LA. Human papillomavirus oncoproteins: pathways to transformation. *Nat Rev Cancer*. Aug 2010;10(8):550-60. doi:10.1038/nrc2886
16. Davidson EJ, Boswell CM, Sehr P, et al. Immunological and clinical responses in women with vulval intraepithelial neoplasia vaccinated with a vaccinia virus encoding human papillomavirus 16/18 oncoproteins. *Cancer Res*. Sep 15 2003;63(18):6032-41.
17. de Vos van Steenwijk PJ, Piersma SJ, Welters MJ, et al. Surgery followed by persistence of high-grade squamous intraepithelial lesions is associated with the induction of a dysfunctional HPV16-specific T-cell response. *Clin Cancer Res*. Nov 15 2008;14(22):7188-95. doi:10.1158/1078-0432.CCR-08-0994
18. van Poelgeest MI, van Seters M, van Beurden M, et al. Detection of human papillomavirus (HPV) 16-specific CD4+ T-cell immunity in patients with persistent HPV16-induced vulvar intraepithelial neoplasia in relation to clinical impact of imiquimod treatment. *Clin Cancer Res*. Jul 15 2005;11(14):5273-80. doi:10.1158/1078-0432.CCR-05-0616
19. Chabeda A, Yanez RJR, Lamprecht R, Meyers AE, Rybicki EP, Hitzeroth, II. Therapeutic vaccines for high-risk HPV-associated diseases. *Papillomavirus Res*. Jun 2018;5:46-58. doi:10.1016/j.pvr.2017.12.006
20. Davidson EJ, Faulkner RL, Sehr P, et al. Effect of TA-CIN (HPV 16 L2E6E7) booster immunisation in vulval intraepithelial neoplasia patients previously vaccinated with TA-HPV (vaccinia virus encoding HPV 16/18 E6E7). *Vaccine*. Jul 29 2004;22(21-22):2722-9. doi:10.1016/j.vaccine.2004.01.049
21. Kenter GG, Welters MJ, Valentijn AR, et al. Vaccination against HPV-16 oncoproteins for vulvar intraepithelial neoplasia. *N Engl J Med*. Nov 5 2009;361(19):1838-47. doi:10.1056/NEJMoa0810097
22. Daayana S, Elkord E, Winters U, et al. Phase II trial of imiquimod and HPV therapeutic vaccination in patients with vulval intraepithelial neoplasia. *Br J Cancer*. Mar 30 2010;102(7):1129-36. doi:10.1038/sj.bjc.6605611
23. Kutzler MA, Weiner DB. DNA vaccines: ready for prime time? *Nat Rev Genet*. Oct 2008;9(10):776-88. doi:10.1038/nrg2432
24. Oosterhuis K, van den Berg JH, Schumacher TN, Haanen JB. DNA vaccines and intradermal vaccination by DNA tattooing. *Curr Top Microbiol Immunol*. 2012;351:221-50. doi:10.1007/82_2010_117
25. Verstrepen BE, Bins AD, Rollier CS, et al. Improved HIV-1 specific T-cell responses by short-interval DNA tattooing as compared to intramuscular immunization in non-human primates. *Vaccine*. Jun 19 2008;26(26):3346-51. doi:10.1016/j.vaccine.2008.03.091
26. Samuels S, Marijne Heeren A, Zijlmans H, et al. HPV16 E7 DNA tattooing: safety, immunogenicity, and clinical response in patients with HPV-positive vulvar intraepithelial neoplasia. *Cancer Immunol Immunother*. Sep 2017;66(9):1163-1173. doi:10.1007/s00262-017-2006-y
27. Oosterhuis K, Aleyd E, Vrijland K, Schumacher TN, Haanen JB. Rational design of DNA vaccines for the induction of human papillomavirus type 16 E6- and E7-specific cytotoxic T-cell responses. *Hum Gene Ther*. Dec 2012;23(12):1301-12. doi:10.1089/hum.2012.101
28. Peng S, Tomson TT, Trimble C, He L, Hung CF, Wu TC. A combination of DNA vaccines targeting human papillomavirus type 16 E6 and E7 generates potent antitumor effects. *Gene Ther*. Feb 2006;13(3):257-65. doi:10.1038/sj.gt.3302646
29. Pancre V, Georges B, Angyalosi G, et al. Novel promiscuous HLA-DQ HIV Nef peptide that induces IFN-gamma-producing memory CD4+ T cells. *Clin Exp Immunol*. Sep 2002;129(3):429-37. doi:10.1046/j.1365-2249.2002.01934.x
30. Panina-Bordignon P, Tan A, Termijtelen A, Demotz S, Corradin G, Lanzavecchia A. Universally immunogenic T cell epitopes: promiscuous binding to human MHC class II and promiscuous recognition by T cells. *Eur J Immunol*. Dec 1989;19(12):2237-42. doi:10.1002/eji.1830191209
31. Alexander J, Sidney J, Southwood S, et al. Development of high potency universal DR-restricted helper epitopes by modification of high affinity DR-blocking peptides. *Immunity*. Dec 1994;1(9):751-61. doi:10.1016/s1074-7613(94)80017-0
32. Ahrends T, Spanjaard A, Pilzecker B, et al. CD4(+) T Cell Help Confers a Cytotoxic T Cell Effector Program Including Coinhibitory Receptor Downregulation and Increased Tissue Invasiveness. *Immunity*. Nov 21 2017;47(5):848-861 e5. doi:10.1016/j.immuni.2017.10.009
33. Quaak SG, van den Berg JH, Toebes M, et al. GMP production of pDERMATT for vaccination against melanoma in a phase I clinical trial. *Eur J Pharm Biopharm*. Oct 2008;70(2):429-38. doi:10.1016/j.ejpb.2008.05.002
34. Kannanganat S, Ibegbu C, Chennareddi L, Robinson HL, Amara RR. Multiple-cytokine-producing antiviral CD4 T cells are functionally superior to single-cytokine-producing cells. *J Virol*. Aug 2007;81(16):8468-76. doi:10.1128/JVI.00228-07
35. Almeida JR, Price DA, Papagno L, et al. Superior control of HIV-1 replication by CD8+ T cells is reflected by their avidity, polyfunctionality, and clonal turnover. *J Exp Med*. Oct 1 2007;204(10):2473-85. doi:10.1084/jem.20070784
36. Baldwin PJ, van der Burg SH, Boswell CM, et al. Vaccinia-expressed human papillomavirus 16 and 18 e6 and e7 as a therapeutic vaccination for vulval and vaginal intraepithelial neoplasia. *Clin Cancer Res*. Nov 1 2003;9(14):5205-13.
37. van Poelgeest MI, Welters MJ, Vermeij R, et al. Vaccination against Oncoproteins of HPV16 for Noninvasive Vulvar/Vaginal Lesions: Lesion Clearance Is Related to the Strength of the T-Cell Response. *Clin Cancer Res*. May 15 2016;22(10):2342-50. doi:10.1158/1078-0432.CCR-15-2594
38. Mahto M, Nathan M, O'Mahony C. More than a decade on: review of the use of imiquimod in lower anogenital intraepithelial neoplasia. *Int J STD AIDS*. Jan 2010;21(1):8-16. doi:10.1258/ijsa.2009.009309
39. Trimble CL, Morrow MP, Kraynyak KA, et al. Safety, efficacy, and immunogenicity of VGX-3100, a therapeutic synthetic DNA vaccine targeting human papillomavirus 16 and 18 E6 and E7 proteins for cervical intraepithelial neoplasia 2/3: a randomised, double-blind, placebo-controlled phase 2b trial. *Lancet*. Nov 21 2015;386(10008):2078-2088. doi:10.1016/S0140-6736(15)00239-1

Supplementary Material

***Supplementary table 1**: Overview of peptide pools used in the ex vivo reactivity screens, and the amino acid sequence of each peptide.*

Peptide Pool	Peptide Number	Amino Acid Sequence
Pool 1: E6-1	1	MHQKRTAMFQDPQERPRKLPQL
	2	DPQERPRKLPQLCTELQTTIHD
	3	QLCTELQTTIHDIILECVYCKQ
	4	HDIILECVYCKQQLLRREVYDF
	5	KQQLLRREVYDFAFRDLCIVYR
	6	DFAFRDLCIVYRDGNPYAVCDK
	7	YRDGNPYAVCDKCLKFYSKISE
	8	DKCLKFYSKISEYRHYCYSLYG
Pool 2: E6-2	9	SEYRHYCYSLYGTTLEQQYNKP
	10	YGTTLEQQYNKPLCDLLIRCIN
	11	KPLCDLLIRCINCQKPLCPEEK
	12	INCQKPLCPEEKQRHLDKKQRF
	13	EKQRHLDKKQRFHNIRGRWTGR
	14	RFHNIRGRWTGRCMSCCRSSRT
	15	GRWTGRCMSCCRSSRTRRETQL
Pool 3: E7	16	MHGDTPTLHEYMLDLQPETTDL
	17	YMLDLQPETTDLYCYEQLNDSS
	18	DLYCYEQLNDSSEEEDEIDGPA
	19	SSEEEDEIDGPAGQAEPDRAHY
	20	PAGQAEPDRAHYNIVTFCCKCD
	21	HYNIVTFCCKCDSTLRLCVQST
	22	CDSTLRLCVQSTHVDIRTLEDL
	23	STHVDIRTLEDLLMGTLGIVCP
	24	RTLEDLLMGTLGIVCPICSQKP
Pool 4: Potential epitopes that may have arisen as a consequence of shuffling the protein domains.	25	TDLYCICSQKPKCDSTLRL
	26	GTLGIVCPYEQLNDSS
	27	YNIVTFCCQPETTDLY
	28	HDIILECVNCQKPLCP
	29	GRWTGRCMKCLKFYSK
	30	CDLLIRCIYCKQQLLR
	31	GNPYAVCDSCCRSSRT
	32	RTRRETQLQLCTELQT

Supplementary table 2: *Antibody panel used for ex vivo reactivity screens.*

Target + Fluorochrome	Clone	Details	Vendor
CD3-APC-H7	Clone SK7	Mouse IgG1	BD Biosciences
CD14-Pacific Blue	Clone TùK4	Mouse IgG2a	Invitrogen
CD16-Pacific Blue	Clone 3G8	Mouse IgG1	Invitrogen
CD19-Pacific Blue	Clone SJ25-C1	Mouse IgG1	Invitrogen
CD4-PE	Clone S3.5	Mouse IgG2a	Invitrogen
CD8-PerCP-Cy5.5	Clone SK1	Mouse IgG1	BioLegend
CCR7-PE-CF594	Clone 150503	Mouse IgG2a	BD Biosciences
CD45RA-PE-Cy5.5	Clone MEM-56	Mouse IgG2b	Invitrogen
PD-1-eVolve 655	Clone J105	Mouse IgG1	eBiosciences
IFNγ-FITC	Clone B27	Mouse IgG1	BD Biosciences
IL-2-APC	Clone MQ1-17H12	Rat IgG2a	BD Biosciences
TNFα-PE-Cy7	Clone MAb11	Mouse IgG1	BD Biosciences
CD107a-Alexa Fluor 700	Clone H4A3	Mouse IgG1	BD Biosciences
Fixable Violet Dead Cell Stain Kit, 405 nm	Fluorescent reactive dye + DMSO		Invitrogen

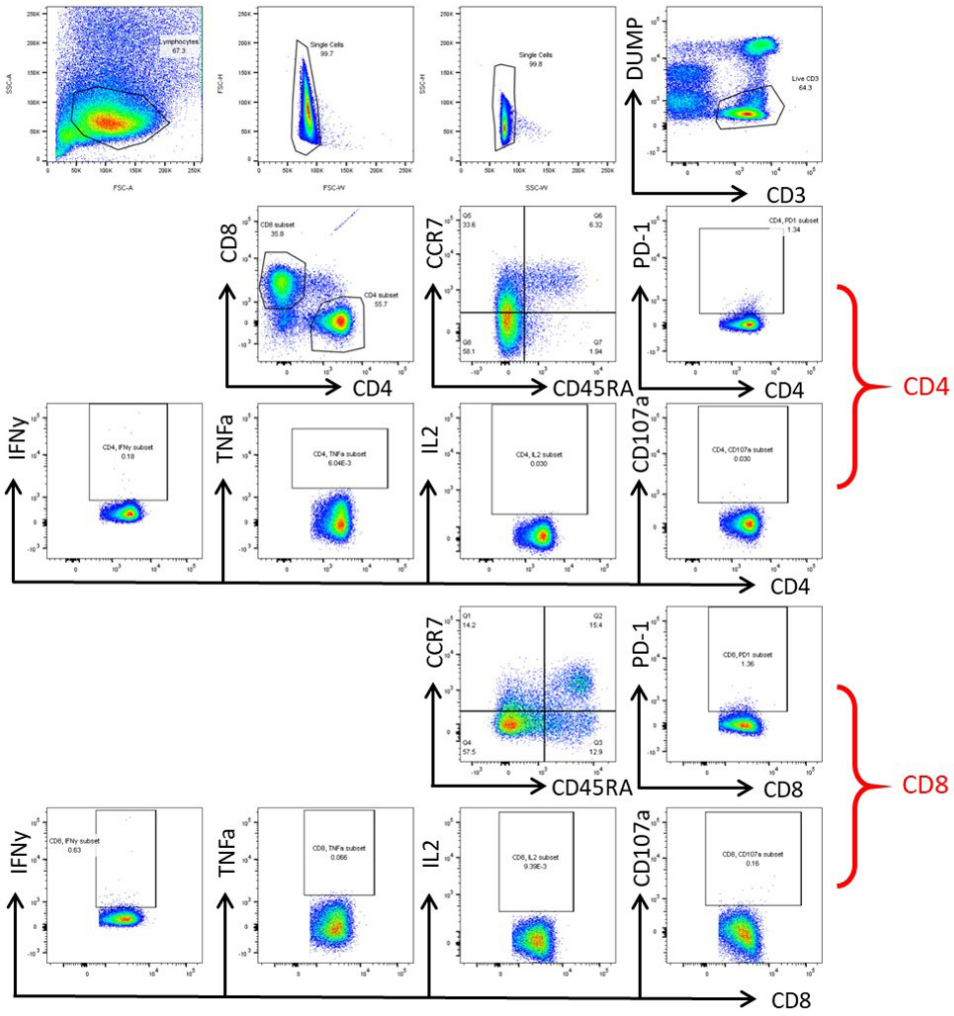

Supplementary figure 1: *Gating strategy example of phenotypic characterization and cytokine production of CD4 and CD8 T cells.*

Supplementary figure 2: *Phenotypic characterization of circulating T cells.* ***a)*** *Frequency of PD-1 positive CD4 and CD8 T cells over time.* ***b)*** *Differentiation state of CD4 and CD8 T cells defined by CD45RA and CCR7 surface marker expression. CD45RA+ CCR7+: naïve T cells, CD45RA- CCR7+: central memory T cells, CD45RA- CCR7-: effector memory T cells and CD45RA+ CCR7-: effector T cells. Responding patients are colored red and non-responding patients are colored blue.* ▶▶▶

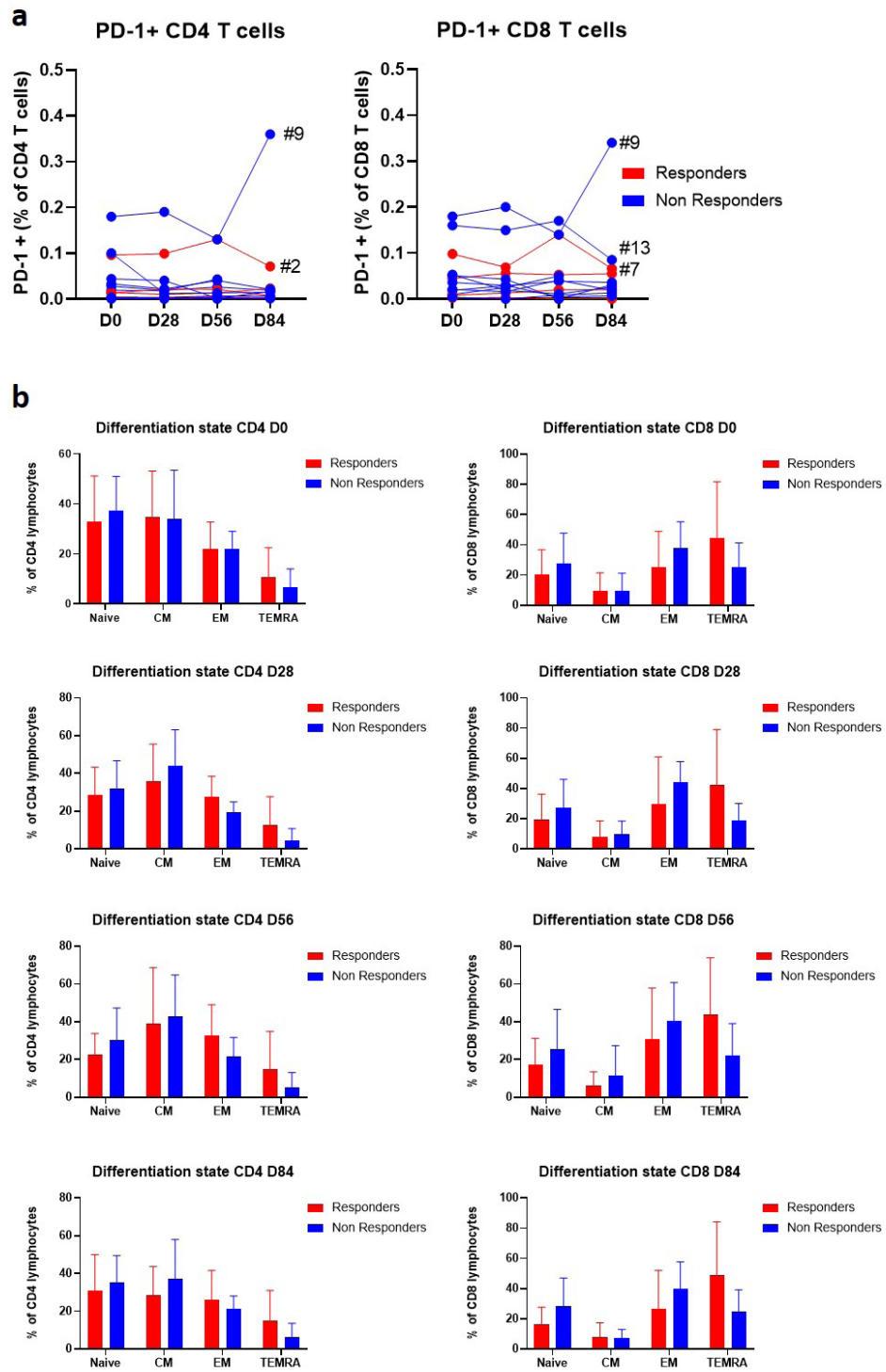

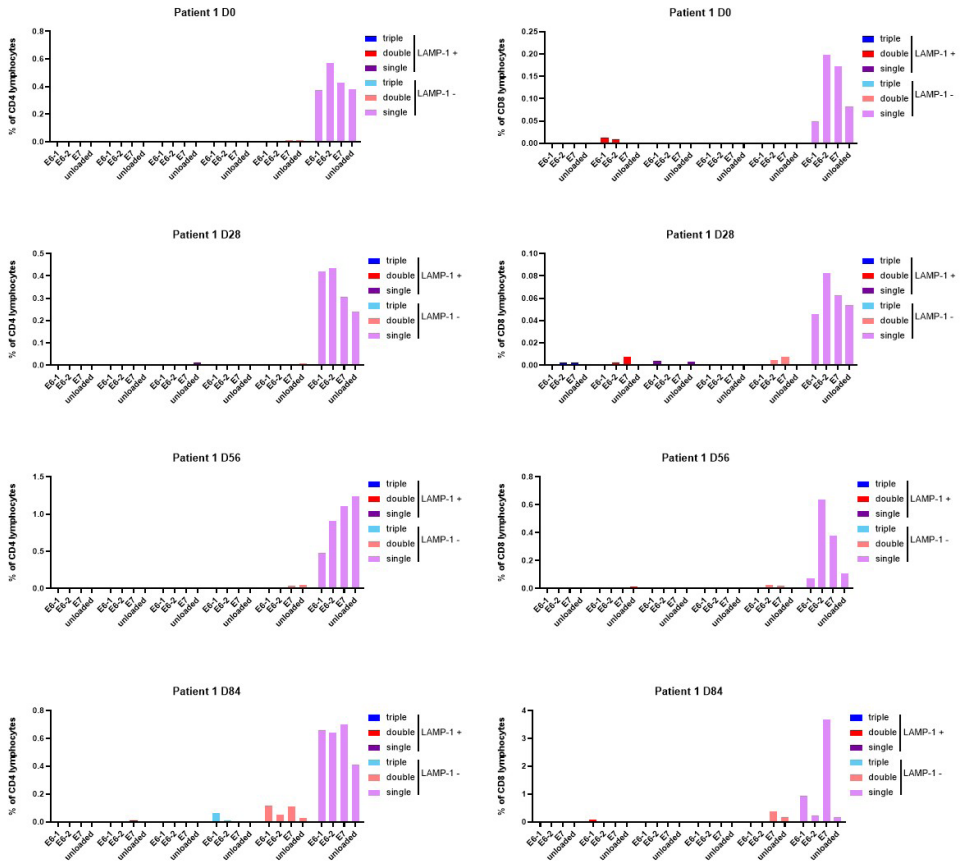

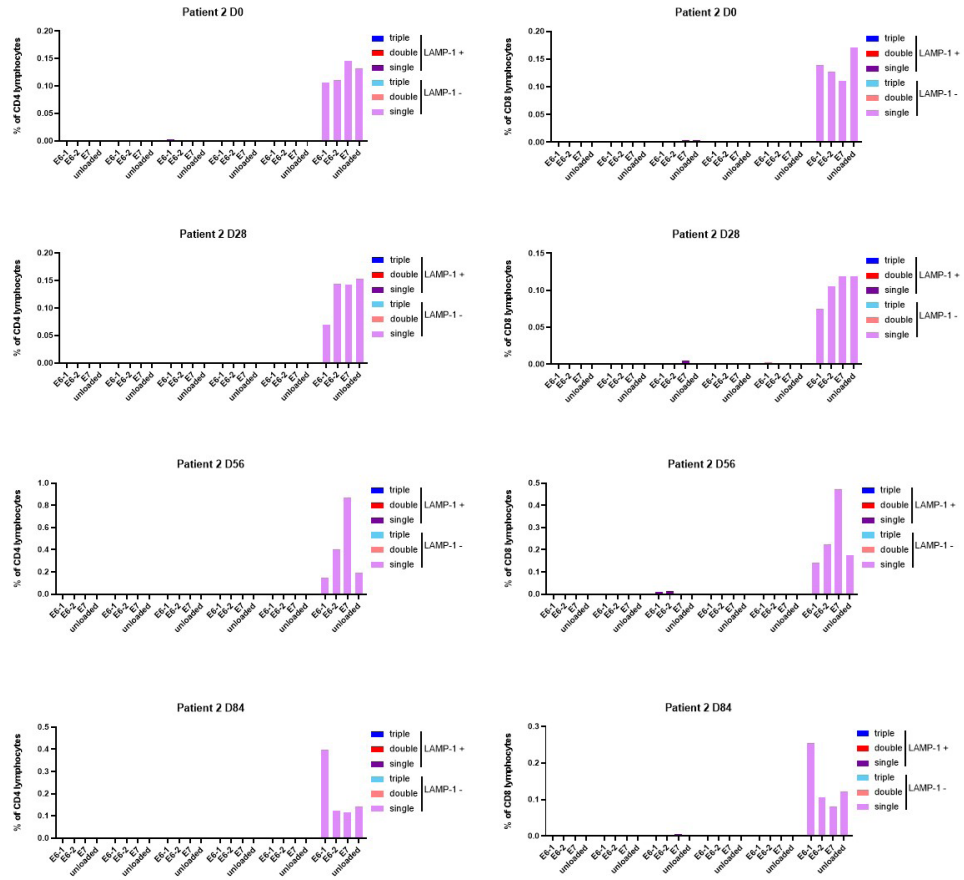

***Supplementary figure 3**: Depicted are the frequencies of single, double and triple cytokine producing CD4 and CD8 T cells, with and without co-expression of degranulation marker CD107a (LAMP-1), determined using Boolean gating. Depicted are immunologically responding patients **a** patient 1, **b** patient 2, **c** patient 4, **d** patient 7 and **e** patient 8.*

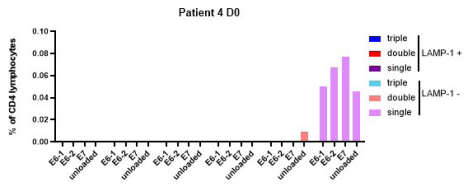
Patient 4 D0
% of CD4 lymphocytes
triple
double
single
LAMP-1 +
LAMP-1 -

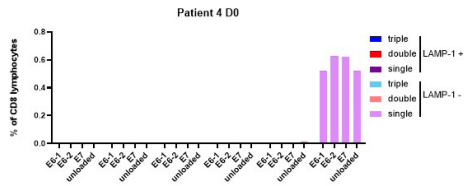
Patient 4 D0
% of CD8 lymphocytes
triple
double
single
LAMP-1 +
LAMP-1 -

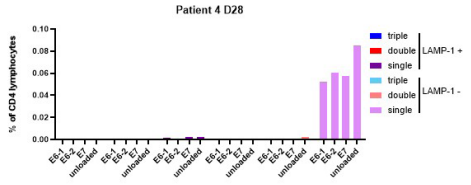
Patient 4 D28
% of CD4 lymphocytes
triple
double
single
LAMP-1 +
LAMP-1 -

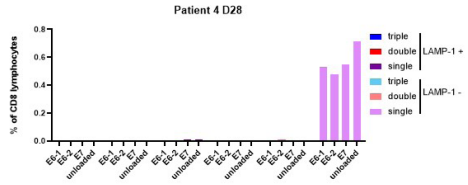
Patient 4 D28
% of CD8 lymphocytes
triple
double
single
LAMP-1 +
LAMP-1 -

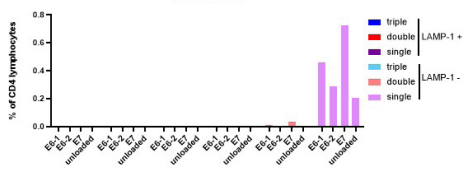
Patient 4 D56
% of CD4 lymphocytes
triple
double
single
LAMP-1 +
LAMP-1 -

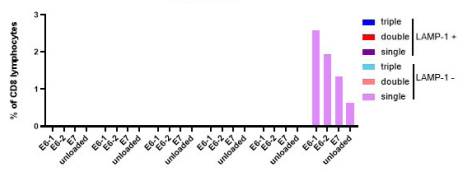
Patient 4 D56
% of CD8 lymphocytes
triple
double
single
LAMP-1 +
LAMP-1 -

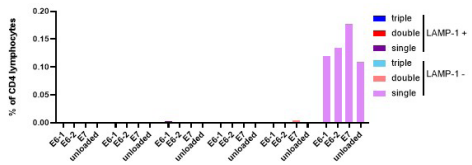
Patient 4 D84
% of CD4 lymphocytes
triple
double
single
LAMP-1 +
LAMP-1 -

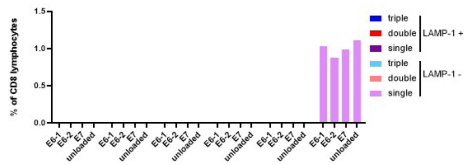
Patient 4 D84
% of CD8 lymphocytes
triple
double
single
LAMP-1 +
LAMP-1 -

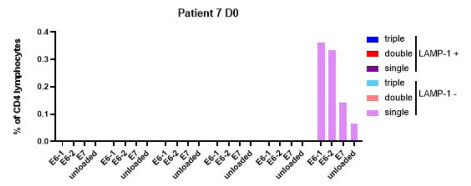
Patient 7 D0
% of CD4 lymphocytes
triple
double
single
LAMP-1 +
LAMP-1 -

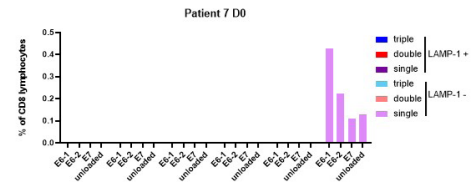
Patient 7 D0
% of CD8 lymphocytes
triple
double
single
LAMP-1 +
LAMP-1 -

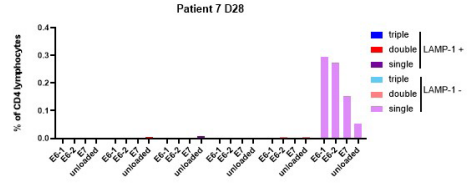
Patient 7 D28
% of CD4 lymphocytes
triple
double
single
LAMP-1 +
LAMP-1 -

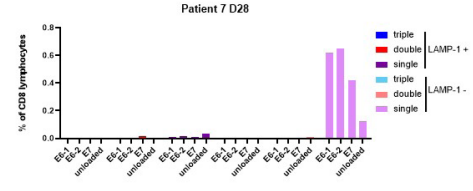
Patient 7 D28
% of CD8 lymphocytes
triple
double
single
LAMP-1 +
LAMP-1 -

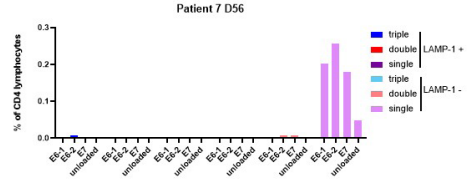
Patient 7 D56
% of CD4 lymphocytes
triple
double
single
LAMP-1 +
LAMP-1 -

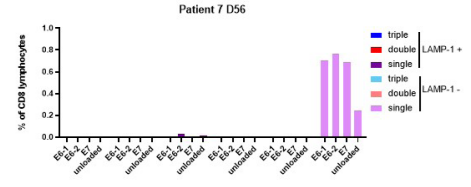
Patient 7 D56
% of CD8 lymphocytes
triple
double
single
LAMP-1 +
LAMP-1 -

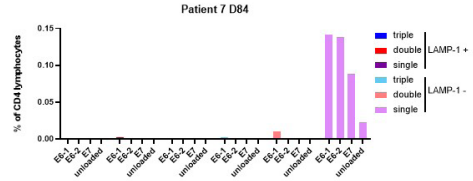
Patient 7 D84
% of CD4 lymphocytes
triple
double
single
LAMP-1 +
LAMP-1 -

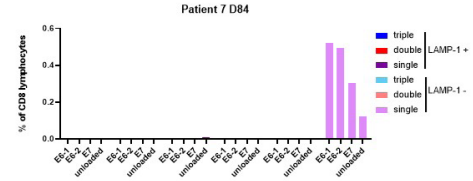
Patient 7 D84
% of CD8 lymphocytes
triple
double
single
LAMP-1 +
LAMP-1 -

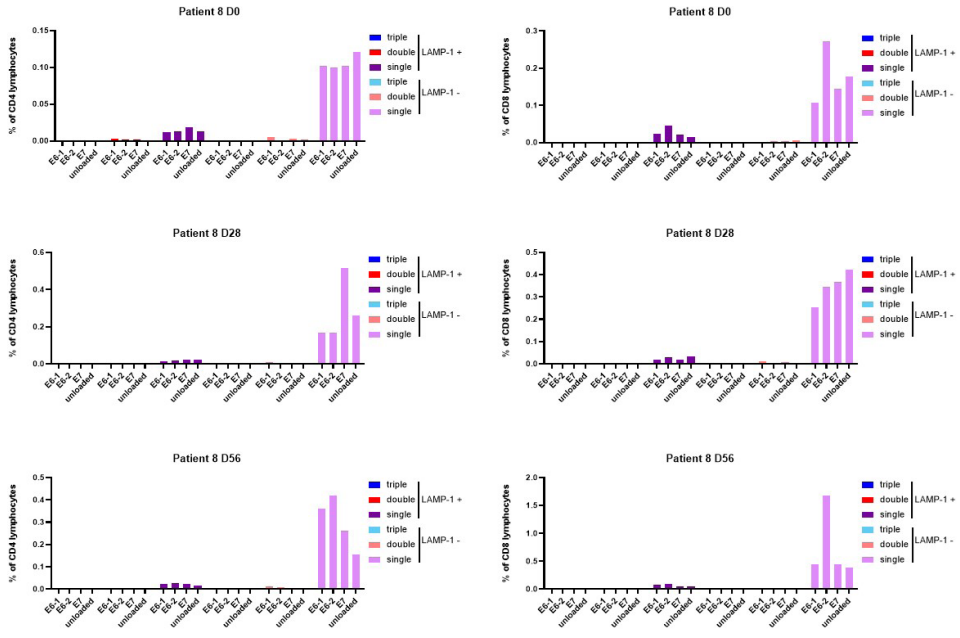

Supplementary figure 4: *Time course graphs showing the IFNy, TNFa, IL-2 and CD107a responses against E6-1, E6-2 and E7 peptide pool for each patient. No peptides indicate that T cells were co-cultured with unloaded APCs to access background or aspecific reactivity. The green boxes highlight the patients with an immunological response.* ▶▶▶

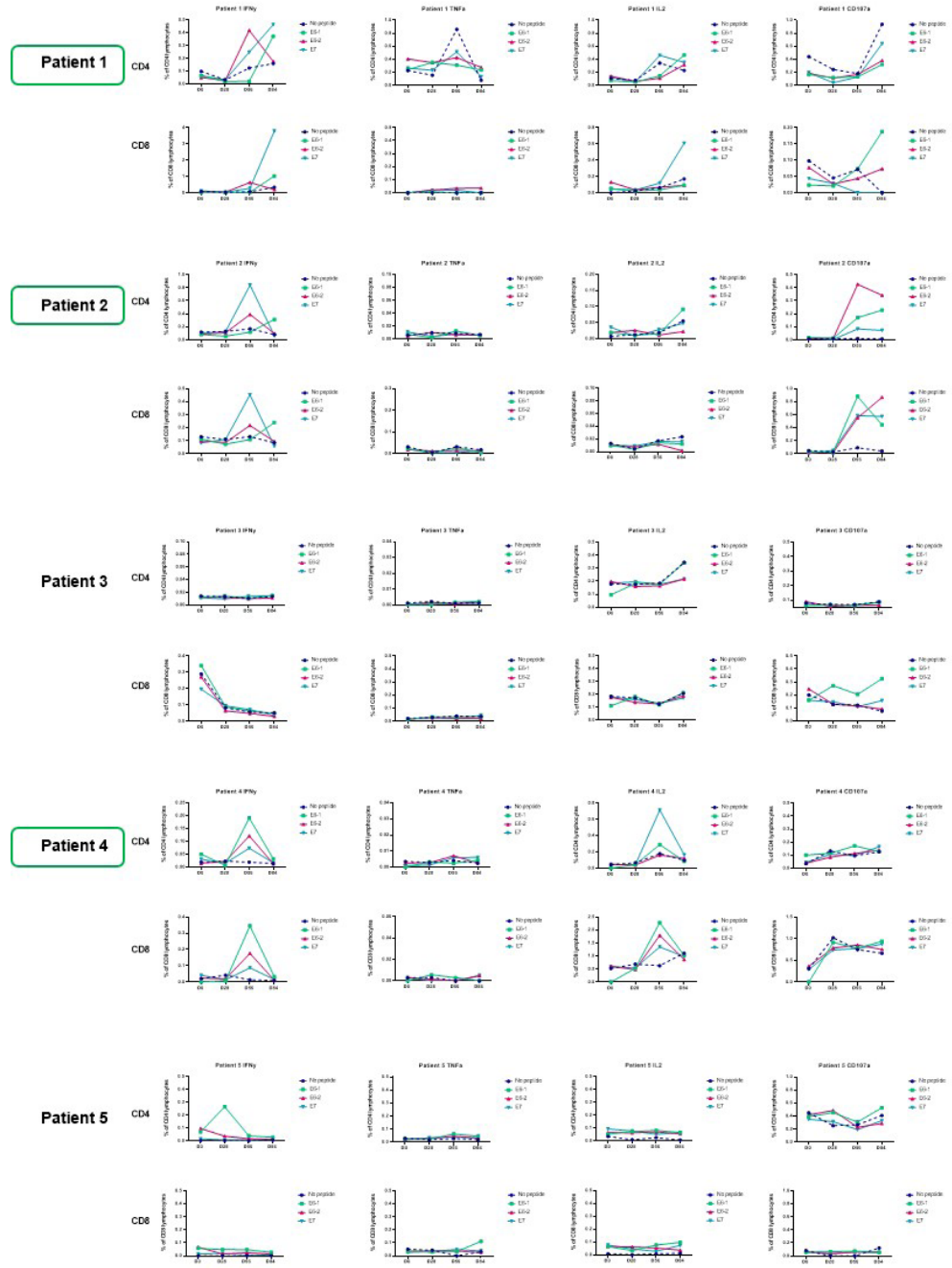

Patient 6

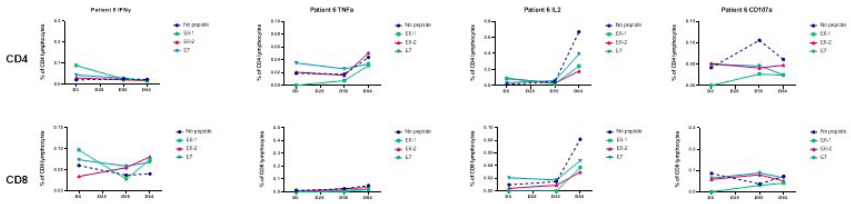

Patient 7

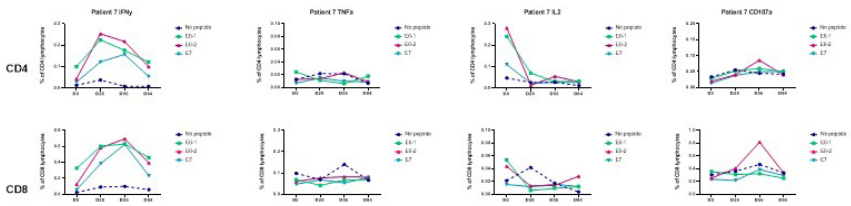

Patient 8

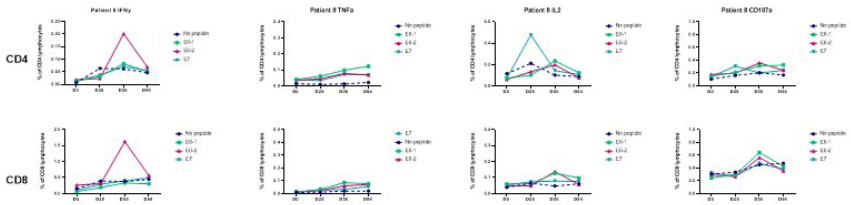

Patient 9

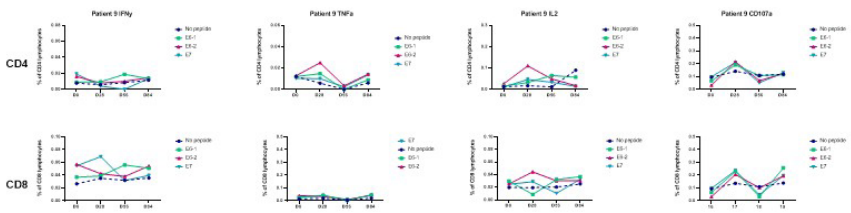

Patient 10

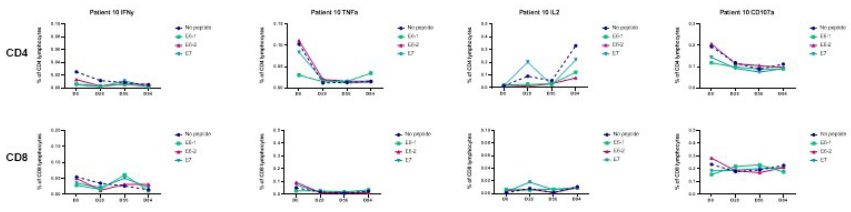

Patient 11

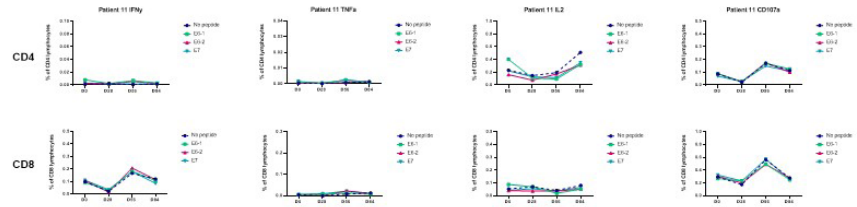

Patient 12

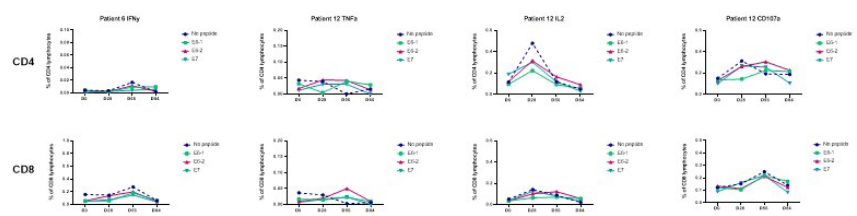

Patient 13

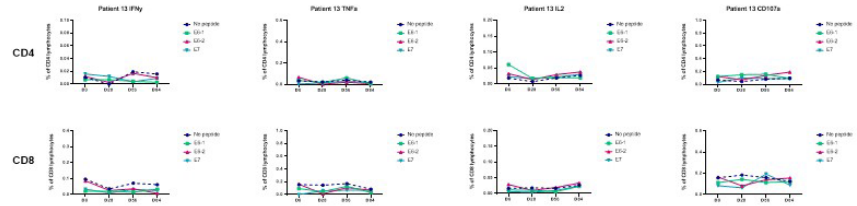

Patient 14

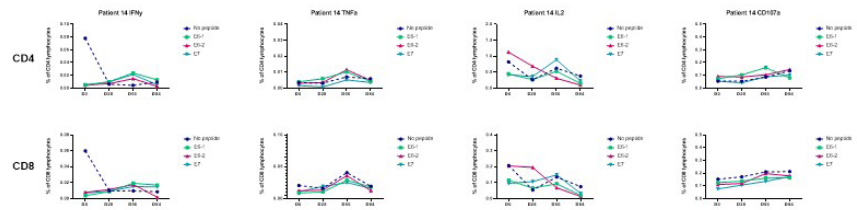

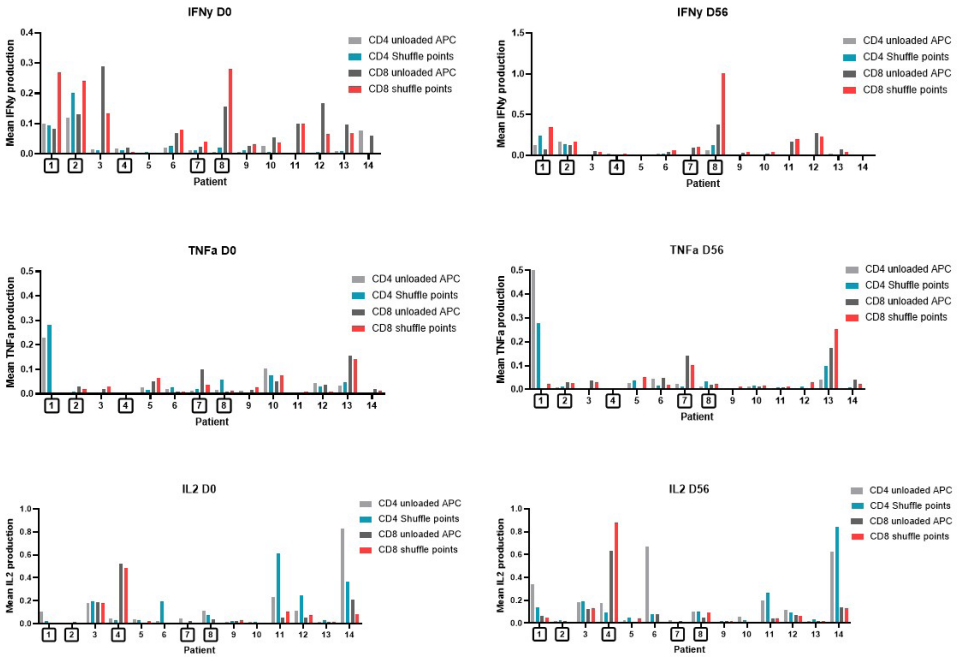

Supplementary figure 5: *Reactivity against the peptides that arose as a consequence of shuffling the E6 and E7 coding sequences. Boxes highlight responding patients.*

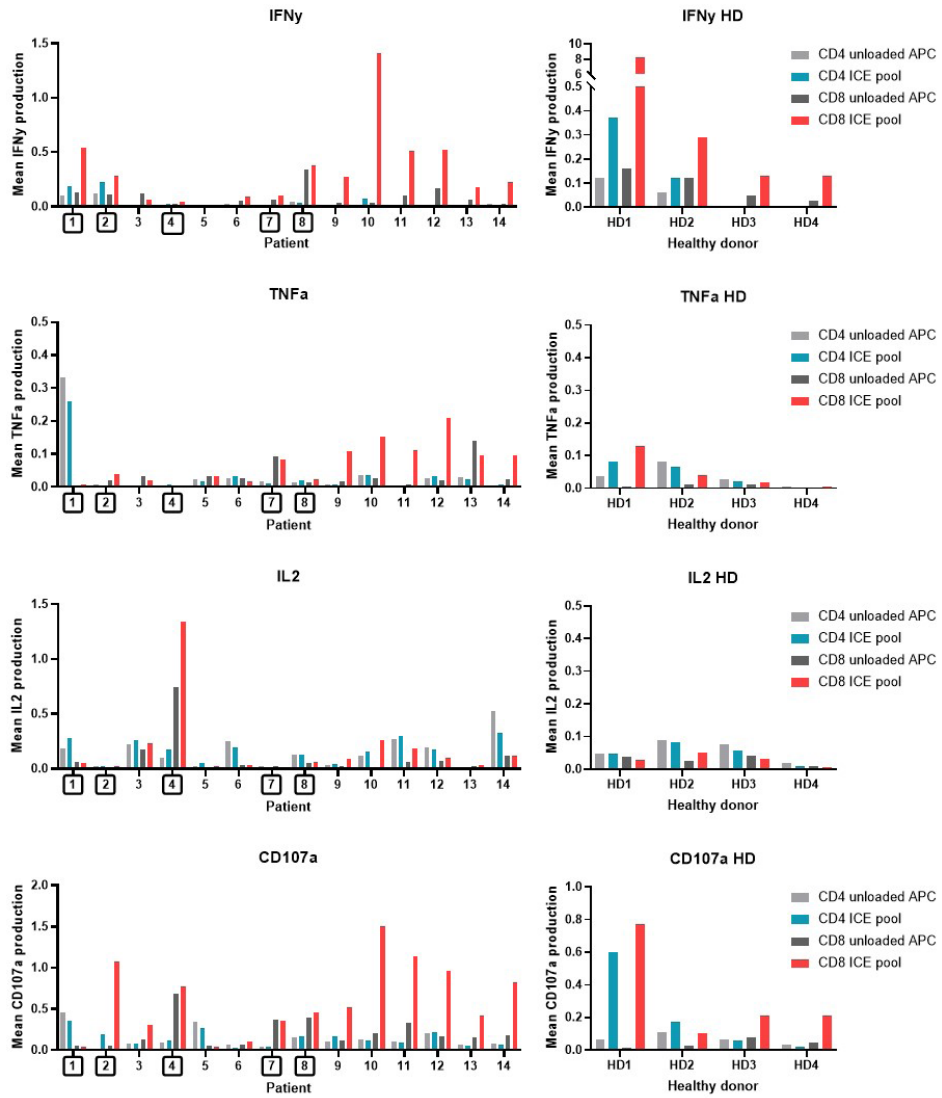

Supplementary figure 6*: Reactivity against ICE peptide pool at day 0. On the left, patient responses are depicted and on the right four healthy controls are depicted for the matched cytokines or LAMP-1. The black boxes on the x-axis highlight responding patients.*

CHAPTER 9

Discussion

Translational Research: Bridging the Gap Between the Lab and Clinic

In the modern landscape of biomedical science, a significant gap often exists between clinical practice and fundamental research. Clinical trials are pivotal for validating new interventions, ensuring their safety and efficacy. However, these trials often provide limited mechanistic insight, leaving many unanswered questions about how and why certain treatments work or do not work. Translational research—the crucial link between basic science and clinical application—plays a vital role in bridging this gap. It is particularly important in the context of immuno-oncology, where understanding the complex interplay between the immune system and cancer can lead to extremely durable remissions.

Clinical trials assess treatment efficacy through outcomes like safety, toxicity, tumor volume, and survival but often fail to reveal the biological mechanisms behind their success or failure. For example, immunotherapy has revolutionized cancer treatment, yet responses vary dramatically among patients. Some exhibit long-term remission, while others experience primary resistance or relapse. Without deeper mechanistic insight into immune cell behavior, tumor microenvironment dynamics, and genetic mutations, it remains challenging to predict which patients will benefit most. This limited understanding can impede the development of personalized treatment strategies. While a therapy may demonstrate clinical efficacy, understanding the specific immune pathways it targets is essential for refining its application, reducing side effects, and enhancing patient outcomes. Here, the importance of fundamental and translational research becomes clear.

Moreover, translational research takes discoveries from the lab—such as insights into immune cell signaling or tumor-immune interactions—and applies them to develop new treatment strategies. For instance, experiments using genetically engineered mouse models have revealed key details about the mechanisms of immune cell activation and suppression in the tumor microenvironment[1-3]. These findings can inspire new clinical trials. In immuno-oncology, fundamental and translational research has been instrumental in advancing therapies such as immune checkpoint inhibitors. By understanding the mechanisms of immune evasion employed by tumors, researchers have identified novel targets for intervention, leading to next-generation immunotherapies that can potentially overcome resistance. This coupling of mechanistic insights with clinical observations allows for a more personalized treatment approach, helping explain the varied responses seen in patients and identifying new avenues for therapeutic development. An example of this "from bench to bedside and back again" principle is described in this thesis in **Chapter 7**, where fundamental research both informs and is informed by clinical trial outcomes[4].

Mechanistic research clarifies how and why treatments work, enabling the development of targeted, effective therapies with fewer side effects. In the context of cancer immunotherapy, this might involve tailoring treatments based on an individual's unique immune landscape, tumor genetics, or environmental factors. By unraveling the mechanisms

and regulation of neutrophil migration in cancer for example, researchers can identify potential therapeutic targets. Modulating neutrophil migration may offer new strategies to manipulate the tumor microenvironment, enhance anti-tumor immune responses, and ultimately impact cancer progression and treatment outcomes.

To fully unlock the potential of translational research, strong collaborations between clinical and fundamental researchers are essential. Interdisciplinary teams combining clinical insight with deep mechanistic expertise can accelerate the development of novel treatment strategies. Furthermore, feedback loops between the clinic and the lab are crucial—clinical observations must inform fundamental research, and laboratory discoveries must be rapidly integrated into clinical trials. Fostering strong collaborations between clinical and fundamental scientists, has proven to be essential to keep advancing cancer immunotherapy. This thesis was shaped in such a collaborative work environment, serving as a testament to how strong partnerships can drive significant advancements in both scientific progress and the patient care of the future.

The influence of breast cancer subtype and disease stage on the circulating immune landscape

Cancer dysregulates intratumoral innate-adaptive immune cell crosstalk[5,6], but how the systemic immune landscape is altered during breast cancer progression remains largely unknown. Understanding these systemic immune modifications is crucial for uncovering mechanisms driving tumor growth, metastasis formation, and treatment resistance. A deeper insight into circulating immune alterations is essential for developing more precise and effective immunotherapeutic strategies. In **Chapters 3** and **4**, we investigated the circulating immune compartment in breast cancer patients compared to healthy donors (HDs) to determine how different stages of disease progression shape systemic immunity. We found that more advanced disease stages were associated with greater immune dysregulation, particularly characterized by immunosuppressive shifts. For example, we observed increases in neutrophils and (non-)classical monocytes, both described to be linked to poor prognosis and known to inhibit anti-tumor immune responses[7-13]. Transcriptional and proteomic analysis, alongside *ex vivo* functionality assays, of freshly isolated peripheral neutrophils revealed increased migratory capacity, higher abundance of granule proteins, and elevated ROS production in patients with mTNBC compared to HDs. The increased migratory capacity of neutrophils was already evident in patients with stage I-III TNBC. This means that neutrophils in patients with TNBC are not only more abundant, but are also phenotypically and functionally aberrant. Furthermore, we reported a reduction in CD8+ and CD4+ T cells and differentiated B cells. These changes could be partly driven by prior treatment, which we described for the triple negative subtype in **Chapter 4**. These findings align with previous reports that the immune system becomes progressively compromised

as the tumor grows and metastasizes, allowing the cancer to evade immune surveillance[5,14-17].

In addition, we explored the relationship between breast cancer subtypes and the circulating immune compartment. We hypothesized that distinct immune profiles would correlate with specific tumor subtypes, potentially providing insights into prognosis and therapeutic opportunities. Although we identified some subtype-specific immune changes, the influence of tumor subtype on the circulating immune compartment was less pronounced than expected. This may be partly due to the heterogeneity within subtypes, as some ER+ tumors exhibit basal-like transcriptional profiles and share characteristics with TNBC. In addition, also tumor-extrinsic factors may contribute to shaping the systemic immune landscape. This was well illustrated by the natural variation in immune profiles among HDs, which could be influenced by factors such as germline genetics, lifestyle, pathogenic infections, microbiome composition, and hormonal fluctuations. The relatively modest subtype-specific differences in circulating immune profiles suggest that disease stage may play a more pivotal role in systemic immune alterations than the tumor's molecular characteristics. While the systemic immune profiles provide valuable insights, it seems to be less related to breast cancer subtype than anticipated. This raises an important question for future research: should the focus shift toward tumor-intrinsic factors, such as mutations and gene expression profiles instead of focusing on the molecular tumor subtype?

The Role of Tumor Genetics in Shaping Immune Responses and Therapeutic Outcomes

Cancer cell intrinsic features, like the genetic makeup of the tumor, are increasingly recognized as a critical determinant of its behavior, immunogenicity, and therapeutic response[18-20]. Genomic and molecular studies have identified tumor-specific alterations, including mutations, copy number variations, and epigenetic modifications, that drive cancer progression and influence tumor-immune interactions. Mutations in TP53, KRAS, or PIK3CA can affect antigen presentation and immune cell recruitment to the tumor microenvironment (TME)[21-23]. Similarly, epigenetic changes, such as DNA methylation and histone modifications, modulate the expression of immune checkpoint molecules and cytokines, shaping immune evasion strategies[24-26]. Systemic immune changes, including T cell dysfunction and dysregulated cytokine levels, are integral to cancer progression, but understanding tumor-intrinsic factors enhances insights into the immune contexture of the TME. After all, the presence of tumor-specific neoantigens, arising from somatic mutations, can strongly dictate the tumor's immunogenic potential. Tumors with a high mutational burden or mismatch repair deficiencies often exhibit robust T cell infiltration and improved responses to checkpoint inhibitors[27-30]. Conversely, tumors with low immunogenicity, such as those with PTEN loss or Wnt/β-catenin pathway activation, are linked to immune exclusion and therapy resistance[31-34]. By focusing on the genetic landscape of tumors, researchers and clinicians may be able to identify actionable biomarkers and therapeutic targets. Genomic profiling

facilitates the development of precision medicine strategies, such as the use of PARP inhibitors in *BRCA*-mutant cancers or immune checkpoint inhibitors in tumors with high microsatellite instability. This tailored approach enables more precise treatment by exploiting tumor-intrinsic vulnerabilities.

In essence, integrating systemic immune modulation with tumor-specific genetic and molecular analyses offers a comprehensive understanding of cancer immunobiology. Systemic immune changes play essential roles in cancer progression, while tumor-intrinsic features, including mutations and gene expression profiles, shape the tumor microenvironment and guide therapeutic strategies. Our data show that in breast cancer, tumor molecular subtypes only have a modest impact on the circulating immune compartment compared to disease stage. However, the tumor's genetic landscape remains critical for advancing personalized therapies that integrate systemic and localized approaches to improve clinical outcomes.

Exploring Immune Cell States in mTNBC: Methodological Insights

Chapter 5 highlights the challenges and insights associated with analyzing systemic immune dysregulation in mTNBC using single-cell RNA-sequencing and matched TCR/BCR sequencing. Despite extensive analysis, no significant transcriptional differences or unique cell states were identified between patients with mTNBC and HDs, likely due to limited sample size and substantial inter-individual variability. Even though not disease-specific, the identification of eight distinct neutrophil states highlights the potential for further exploration of neutrophil diversity in cancer. This is particularly relevant given the clear differences observed in our bulk RNA sequencing data between neutrophils isolated from patients with mTNBC and HDs.

Key methodological insights derived from the experiments described in this chapter, include the benefits of leveraging barcoded antibodies to minimize batch effects, accurately retain low-RNA content cells like neutrophils, and enhance doublet removal. These approaches provide a framework for improving data quality and capturing underrepresented cell populations in future studies. To address the limitations encountered, future research should prioritize increased sample sizes and improved sequencing depth for neutrophils by targeted pre-processing of immune cell populations. Purifying neutrophils and integrating transcriptomic data with functional studies could yield critical insights into the role of neutrophil states in mTNBC. These refinements hold promise for uncovering immune dysregulation in cancer and advancing strategies for immune modulation in oncology.

Targeting Neutrophils: Harnessing Plasticity in Cancer Immunotherapy

Despite the growing attention directed toward neutrophils in recent years, their role in modulating cancer progression and immunotherapy responses remains a topic of considerable debate[35,36]. This ongoing controversy is largely attributable to the remarkable

heterogeneity and plasticity of neutrophils, which exhibit diverse phenotypes and functions depending on factors such as tumor subtype, disease stage, and the type of therapy employed[37-39]. The dynamic and context-dependent nature of neutrophils complicates efforts to define their exact role in either promoting or hindering therapeutic efficacy. Moreover, our understanding of their contribution to cancer progression and immunotherapy response is further hampered by the scarcity of robust tools for selectively and effectively targeting neutrophils in preclinical mouse models[40-42]. Although the studies are not always entirely unambiguous, accumulating data suggests that neutrophils in (breast) cancer predominantly exhibit a pro-tumorigenic functionality[43]. Previous research from our lab and others demonstrated that tumor-induced neutrophils promote mammary tumor progression and metastatic spread in mice[20,44-46]. In line with this, patients with TNBC with increased neutrophil-to-lymphocyte ratio (NLR) have a worse clinical prognosis[12]. Our data of **Chapter 4** demonstrate that neutrophils were the most profoundly and significantly increased immune cell type in the circulation of patients with mTNBC compared to HDs. This triggers the question whether it is possible to target neutrophils in cancer patients.

Reducing Neutrophil Migration

Since neutrophils are an indispensable part of the body's first line of defense against pathogenic infections, simply depleting a substantial proportion of the neutrophils in circulation is not a viable option. Therefore, one particular line of research is directed towards interfering with neutrophil recruitment to the TME: neutrophil migration. Data presented in **Chapter 4** further support that targeting neutrophil migration might be an interesting approach, because we showed that neutrophils from patients with mTNBC exhibit increased migratory capacity compared to those from healthy donors[47]. Given the central role of CXCR2 in guiding neutrophil migration to sites of inflammation and the TME, it has emerged as a promising therapeutic target. CXCR2 antagonists aim to reduce neutrophil migration, without compromising their systemic availability and functionality[48,49]. Preclinical studies in mouse models have shown that CXCR2 inhibition reduces neutrophil infiltration into tumors, decreasing their pro-tumorigenic activities, such as promoting angiogenesis and facilitating metastasis. For instance, Steele *et al.* demonstrated that pharmacological inhibition of CXCR2 in murine pancreatic cancer reduced tumor growth and metastasis by limiting neutrophil infiltration and enhancing T cell responses[50]. Similarly, in breast cancer models, inhibiting CXCR2 limited neutrophil recruitment and improved the efficacy of immune checkpoint inhibitors[51]. In human studies, CXCR1/2 antagonists, such as reparixin, have shown promise in early-phase trials. Reparixin, investigated in HER2-negative metastatic breast cancer, demonstrated safety, tolerability, and a 30% overall response rate with durable responses lasting over 12 months[52]. The CXCR2 antagonist navarixin, combined with pembrolizumab, failed to show efficacy in advanced cancers like prostate, colorectal, or lung cancer[53]. Another trial with the CXCR2 inhibitor AZD5069 and enzalutamide in metastatic castration-resistant prostate cancer (CRPC) was well tolerated and reduced neutrophil and myeloid cell infiltration, with some patients experiencing durable benefits[54]. These findings support targeting myeloid chemotaxis in metastatic CRPC and other cancers, but varied trial results highlight the need for further clinical evaluation to identify optimal patient populations.

Reducing Pro-Tumorigenic Inflammation

Beyond inhibition of neutrophil migration, targeting inflammatory mediators that mobilize neutrophils from the bone marrow has emerged as another promising approach to modulate neutrophil biology in cancer. IL-1β and other tumor-derived pro-inflammatory mediators (G-CSF, IL-6) signal to the bone marrow, altering hematopoiesis and increasing myeloid cells, especially neutrophils[5,20,44,55,56]. In the CANTOS trial (NCT01327846)[57], a monoclonal antibody targeting IL-1β called canakinumab was investigated in over 10,000 participants, primarily for cardiovascular outcomes. Unexpectedly, IL-1β inhibition reduced lung cancer incidence and mortality, prompting further trials[58]. However, initial adjuvant trials failed to meet efficacy goals[59-61]. Since systemic inflammation and neutrophilia are more pronounced in metastatic disease, IL-1β targeting may be more effective in advanced cancer. Another IL-1α/β inhibitor called anakinra has until now only been studied in clinical trials for patients with non-cancer inflammatory diseases like rheumatoid arthritis, hidradenitis suppurativa and COVID-19 with a favorable safety profile[62-65]. Its safety in cancer-related contexts requires additional clinical studies to fully evaluate and confirm potential long-term risks and benefits. In a mouse model of lung adenocarcinoma, blocking IL-1β slowed tumor progression, and targeting both IL-1α and IL-1β using anakinra prevented tumor initiation. The study suggests that targeting IL-1α and IL-1β with anakinra could help disrupt tumor growth and progression[66]. Further research is needed to confirm the benefits of targeting IL-1α and/or IL-1β in larger clinical cohorts and to determine the optimal timing for treatment, including its potential use as a preventative strategy in high-risk patient groups.

Harnessing Neutrophil Plasticity: From Tumor Promotion to Suppression

Another, potentially even more challenging yet promising line of research focusses on the phenotype conversion of neutrophils, turning them from a pro-tumorigenic into an anti-tumorigenic cell type[67,68]. Neutrophils have the potential to eliminate target cells through phagocytosis and directly kill cancer cells through the release of granules and via a process called antibody-dependent cellular cytotoxicity (ADCC)[69]. Neutrophil biology is influenced by a variety of factors such as cytokine signals like TGF-β and IFN-β. Studies suggest that TGF-β inhibition promotes anti-tumorigenic properties of neutrophils, enhancing anti-tumor

immunity and IFN-β supplementation can repolarize pro-tumoral neutrophils into a more anti-tumor state[68,70,71]. However, this classification of pro- and anti-tumorigenic neutrophils may oversimplify neutrophil diversity, as phenotypic plasticity exists within both mature and immature neutrophils. Recent studies also show that neutrophils can be influenced by immunotherapies, such as checkpoint inhibitors or tyrosine kinase inhibitors, which may alter their tumor-promoting or tumor-suppressing functions[72,73]. The exact origin of the phenotypic changes observed in neutrophils—whether occurring in fully matured cells or during the differentiation of progenitors—remains under investigation[69]. The growing understanding of neutrophil plasticity highlights their potential as therapeutic targets, with manipulation of their polarization offering promising strategies to enhance anti-tumor immunity.

Immune Profiling in Clinical Trials: Advancing Immunotherapy Treatment

Over the past decade, immunotherapy has revolutionized cancer treatment by targeting the immune system. While much research has focused on local immune responses within the TME, effective antitumor immunity requires ongoing coordination with the peripheral immune system[74]. In **Chapters 6**, the potential of short-term immune checkpoint blockade (ICB) was explored, to induce immune activation in patients with early-stage TNBC (BELLINI trial). The aim was to explore the potential of treating non-metastatic TNBC patients with neoadjuvant ICB in the absence of chemotherapy. The translational research project described in **chapter 7** aims to identify factors associated with the response to PD-1 blockade in patients with mTNBC (TONIC trial). I focused on the role of the circulating immune compartment in relation to ICB treatment in breast cancer. My primary objective was to identify baseline immune profiles that could serve as predictive biomarkers for treatment response. Specifically, we sought to determine whether particular (combinations of) immune cell populations in the blood could predict the efficacy of ICB therapy. However, after extensive analysis, we were unable to identify any reliable predictive biomarkers in blood that could be associated with treatment outcomes. This negative finding highlights the complexity of the immune response to ICB and suggests that predictive markers may reside in other compartments, such as the tumor microenvironment (TME) and/or lymph nodes, or be more dependent on dynamic changes during treatment.

Eosinophils in Cancer Immunotherapy: Enhancing ICB Response

In addition to baseline profiling, we examined the effects of ICB on the broader immune landscape during treatment. Notably, we observed a significant increase in circulating eosinophils upon ICB treatment in patients with TNBC who responded to ICB, a phenomenon absent in non-responders (**Chapter 7**). This discovery prompted further investigation into the role of eosinophils in the context of anti-tumor immunity. Mechanistic studies using

genetically engineered mouse models that develop spontaneous mammary tumors provided critical insights. We demonstrated that CD4+ T cell-derived IL-5 drives systemic eosinophil expansion, enabling their infiltration into the TME upon interleukin 33 (IL-33) induction. Within the TME, eosinophils actively contribute to an anti-tumor immune response by supporting CD8+ T cell-mediated tumor control (**Chapter 7**). This demonstrates that eosinophils are not merely passive bystanders but are actively involved in the anti-tumor immune response, contributing to the success of ICB in a subset of patients. Also in other cancer types like melanoma , eosinophil accumulation has been shown to positively correlate to ICB treatment outcomes[75].

The identification of eosinophils as key players in the immune response to tumors opens up new avenues for improving the efficacy of ICB. The fact that an increase in eosinophils upon ICB treatment is associated with response suggests that strategies aimed at modulating eosinophil activity in the TME could further enhance therapeutic outcomes. Future research efforts are therefore directed toward elucidating the precise mechanisms by which eosinophils contribute to the therapeutic benefits of ICB. A deeper understanding of how eosinophils interact with other immune cells, such as T helper cells, and how they influence the tumor milieu will be critical for developing new therapeutic approaches.

One of the key questions for future research is whether non-responders to ICB can be converted into responders by actively engaging eosinophils. This will require innovative strategies to recruit and activate eosinophils within the tumor. One potential approach is the use of intra-tumoral delivery of cytokines such as IL-33, which is known to attract and activate eosinophils. By enhancing eosinophil recruitment and activation in the TME, we may be able to convert immunologically “cold” tumors into “hot” tumors, thus improving the response to ICB. In summary, while circulating biomarkers for ICB response remain elusive, the role of eosinophils within the TME offers a promising new direction for improving cancer immunotherapy outcomes.

Exploring Chemotherapy-Free Immunotherapy in TNBC

To better understand how ICB can be leveraged in the treatment of early-stage TNBC, novel approaches are being explored. The aim was to explore the potential of treating early-stage TNBC patients with neoadjuvant ICB in the absence of chemotherapy. **Chapter 6** of this thesis discusses the BELLINI trial (trial registration number NCT03815890)[76], which explored the prospects of short-term ICB to induce immune activation in patients with early-stage TNBC. Three cohorts are described in this trial. In cohort A, patients received 4 weeks of anti-PD-1 therapy, while cohort B involved 4 weeks of anti-PD-1 combined with anti-CTLA4. In these two window-of-opportunity cohorts, patients could continue their treatment with standard of care neoadjuvant chemotherapy followed by surgery. High baseline levels of tumor-infiltrating lymphocytes (TILs) were found to correlate with treatment response. This

finding prompted the opening of cohort C, which enrolled patients with high TIL levels (≥50%). These patients received 6 weeks of neoadjuvant anti-PD-1 + anti-CTLA4, followed by surgery. The primary endpoint for cohorts A and B was immune activation, defined as a twofold increase of intra-tumoral CD8+ T cells or interferon-gamma gene expression. However, achieving this endpoint was more challenging in patients with an already high baseline TIL-score. After all, it is easier to go from 2% to 4% TIL than from 45% to 90%, and moreover, some patients already had a TIL score of 90% at the start of treatment, making further doubling impossible. Consequently, the primary endpoint for cohort C was adjusted to pathological complete response (pCR). Immune activation was observed in 53% (8/15) of patients in cohort A and 60% (9/15) in cohort B. In cohort C, 53% (8/15) of patients exhibited a major pathological response (<10% viable tumor at resection), with 33% (5/15) achieving a pCR. These results suggest that short-term ICB can induce immune activation and contribute to meaningful pathological responses even without chemotherapy in a substantial subset of patients with early-stage TNBC.

To gain a deeper understanding of immunotherapy response in early-stage TNBC, we performed spatial analyses and conducted in-depth comparisons between clinical responders and non-responders. These analyses included bulk RNA sequencing across all cohorts, as well as single-cell RNA-sequencing and TCR-sequencing in cohorts A and B, both pre- and post-treatment. Spatial analysis revealed that responders had shorter distances between tumor cells and the nearest CD8+ T cells, along with a higher density of double-positive CD8+PD-1+ cells and PD-1+ cells. Unsupervised sub-clustering of T cells from our single-cell RNA-sequencing dataset revealed multiple subpopulations, including a distinct CD8 T cell cluster with multiple previously described features of tumor-specific T cells. This cluster exhibited the highest clonality among all subclusters and showed the strongest enrichment of previously reported anti-tumor CD8 T cell signatures derived from functional tumor recognition experiments[77,78]. Single-cell RNA-sequencing revealed that higher pre-treatment levels of tumor-reactive CD8+ T cells and follicular helper T cells, correlated with treatment response, while elevated post-treatment regulatory T cells were linked to non-response. Flow cytometry of fresh blood samples showed an increase in Ki-67+ cells within the PD-1+ conventional CD4+ T cell population in responders compared to non-responders, with a similar trend observed for CD8+ T cells. This proliferative activity of PD-1+CD4+ T cells in the blood was also traced to the tumor, where responders had higher levels of Ki-67+ TFH cells—the CD4+ T cell cluster with the highest PDCD1 expression in tumor single-cell RNA-sequencing data. Notably, PD-1+ proliferating CD8+ T cells did not differ significantly between responders and non-responders, suggesting a special role for proliferating CD4+ T cells both systemically and within the tumor microenvironment. The observed proliferation of PD-1+ CD4+ T cells in responders, could suggest a potential role for the CD4-B cell axis in shaping the anti-tumor immune response. Given that Tfh cells are essential for B cell

activation and germinal center formation[79,80], they may contribute to the development of tertiary lymphoid structures (TLS), which have been strongly correlated with clinical benefit in multiple cancer types[80-82]. However, while this association is compelling, direct evidence linking the proliferation of PD-1+ CD4+ T cells to TLS formation and improved treatment outcomes remains to be established.

Our findings described in **Chapter 6** suggest that neoadjuvant immunotherapy, without chemotherapy, shows promising efficacy and could be a viable approach for patients with early-stage TNBC, particularly those with high levels of stromal TILs. Reducing the reliance on chemotherapy in a subset of patients is an important goal given the commonly experienced side-effects like gastrointestinal and neurological side effects, dermatologic and hair changes, fatigue, and the detrimental effect that chemotherapy has on the host immune system, but a careful evaluation of the potential benefits and risks of administering ICB in the neoadjuvant setting is essential. Long-term immune-related adverse events, such as adrenal gland insufficiencies or diabetes, could outweigh the anticipated benefits in early-stage disease. Therefore, it must be established whether the toxicities associated with ICB are indeed less severe than those induced by chemotherapy. If so, stromal TIL scores could serve as a promising biomarker to identify patients who may benefit from less aggressive treatment while maintaining excellent outcomes, paving the way for more personalized and less toxic therapeutic strategies.

Immunomonitoring HPV-specific T cell responses in blood

Breast cancer arises from genetic mutations that drive uncontrolled cell growth. However, some cancers are caused by viral infections, which in turn also introduce changes into the host DNA. One of the most well-known oncogenic viruses is human papillomavirus (HPV). HPV produces the oncoproteins E6 and E7, which inactivate the tumor-suppressor proteins p53 and RB, respectively. This disruption allows cells to evade apoptosis and bypass cell cycle regulation, leading to malignant transformation. HPV is linked to several cancers, including cervical and vulvar cancer. Vulvar intraepithelial neoplasia (VIN), the pre-malignant stage of vulvar cancer, is often associated with HPV. Despite being detectable due to viral epitopes, spontaneous regression of HPV-induced VIN is rare and progression to vulvar cancer is observed in 2-8% of cases[83-88]. Current treatments for VIN, including surgery and topical therapies, can have uncomfortable side effects and high recurrence rates, severely impacting women's quality of life. Therefore, immunotherapeutic strategies targeting the crucial oncogenic HPV proteins E6 and E7 are being explored as a potential approach to eliminate VIN lesions.

In **Chapter 8**, the clinical and translational results of the N16SIG trial were presented (trial registration number: NTR4607)[89], focusing on the efficacy of an HPV E6/E7 vaccine for patients with HPV-induced VIN lesions. Clinical responses were observed in 6 out of 14

patients (43%), with 2 complete responses and 4 partial responses. Interestingly, 5 of these 14 patients exhibited HPV-specific T-cell responses in the blood, as measured by *ex vivo* reactivity assays. Notably, all five patients with detectable HPV-specific T-cell responses had a corresponding clinical response, suggesting a strong correlation between immunological activity and clinical benefit.

To further investigate the reasons behind the lack of clinical benefit in the non-responders, tumor-infiltrating lymphocytes (TILs) were analyzed in both baseline and post-vaccination (day 56) tissue samples of the VIN lesions. The goal was to understand whether the presence or absence of TILs could explain the differential response to the vaccine. However, there was no statistically significant difference in TIL scores between responders and non-responders, either at baseline or after treatment (Figure 1a). This finding suggested that TIL levels alone might not be sufficient to predict clinical outcomes in patients receiving the HPV E6/E7 vaccine. Surprisingly, a statistically significant increase in TILs was observed between baseline and post-treatment samples in non-responders (Figure 1b). This increase was absent in the responding patients (Figure 1b). This observation raised several questions, particularly about the nature of the infiltrating immune cells. Since the increase in TILs did not correspond with clinical benefit, it is possible that the immune cells were not predominantly cytotoxic T cells, which would be expected to contribute to tumor control. Instead, the infiltrating cells might have included regulatory T cells or other immunosuppressive cell types that could dampen the anti-tumor immune response. In addition to quantifying stromal TILs, neutrophils and eosinophils were also assessed based on their morphology in the HE slide. No statistically significant differences were found in neutrophil and eosinophil counts between responders and non-responders, either at baseline or post-vaccination (Figure 1 c, e). Furthermore, we did not observe a statistically significant increase or decrease in neutrophils or eosinophils in VIN lesions during treatment (Figure 1 d, f).

Unfortunately, due to limitations in biopsy material, we were unable to conduct additional analyses, such as immunohistochemistry (IHC), high-dimensional imaging mass cytometry, or spatial transcriptomics. These techniques would have been valuable for identifying the specific immune cell populations present in the tumor microenvironment and determining whether immunosuppressive mechanisms were at play in the non-responding patients. Such insights could have provided guidance for future combination therapies aimed at increasing the response rate, potentially by adding immune checkpoint inhibitors or other agents that could counteract immunosuppression.

The results of the N16SIG trial highlight the complexity of immune responses in cancer patients and the need for deeper biological understanding to inform therapeutic strategies. While the HPV E6/E7 vaccine showed promising clinical activity in a subset of patients, it is clear that not all patients respond, and understanding the reasons behind this variability is

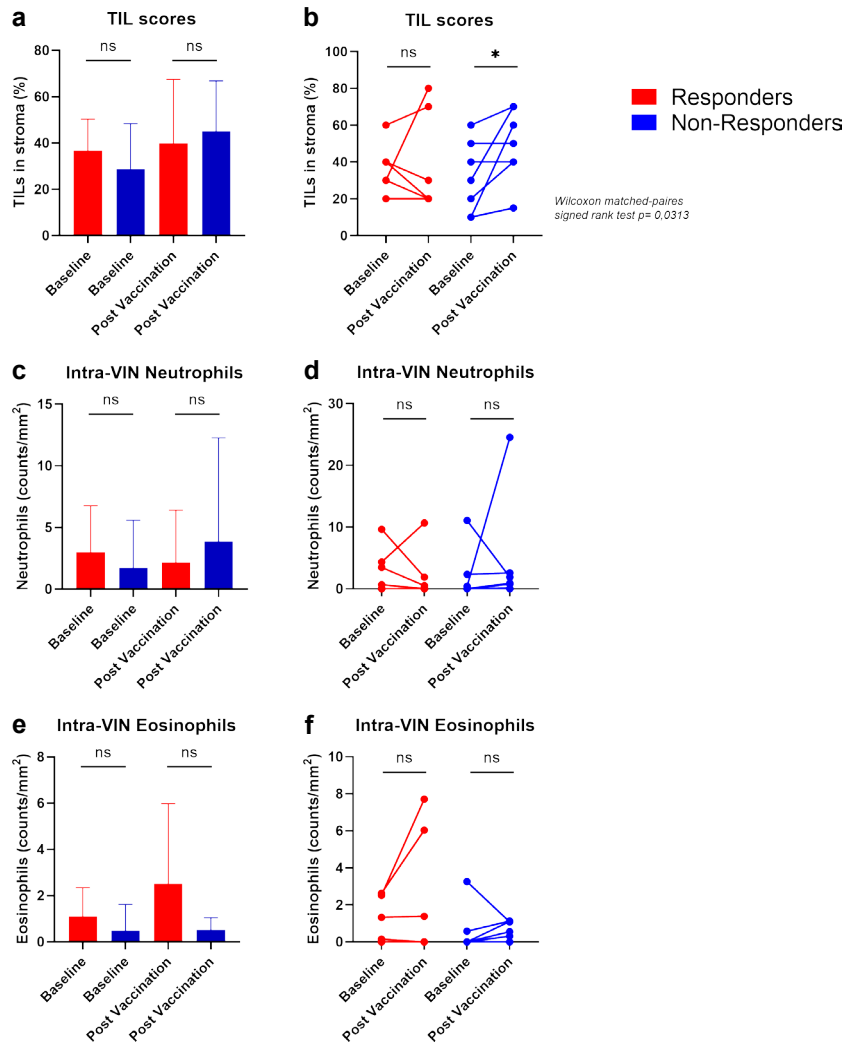

***Figure 1**: **(a-b)** Percentage of lymphocytes infiltrating the stroma of the VIN lesions, comparing **(a)** responders and non-responders at baseline and post treatment and **(b)** dynamic changes over time in responders and non-responders. **(c-d)** Neutrophil counts/mm² in VIN lesions, comparing **(c)** responders and non-responders at baseline and post treatment and **(d)** dynamic changes over time in responders and non-responders. **(e-f)** Eosinophil counts/mm² in VIN lesions, comparing **(e)** responders and non-responders at baseline and post treatment and **(f)** dynamic changes over time in responders and non-responders.*

crucial. In this context, the importance of obtaining and storing sufficient patient material for translational research cannot be overstated. By ensuring adequate tissue and blood samples are available, future studies can perform comprehensive analyses to uncover the mechanisms underlying both response and resistance.

Looking forward, therapeutic cancer vaccines targeting HPV epitopes hold significant potential. If these new treatment options prove to be long-term successful in HPV-related pre-malignancies such as vulvar intraepithelial neoplasia (VIN), they could potentially be extended to other HPV-induced conditions, including penile intraepithelial neoplasia (PIN) and anal intraepithelial neoplasia (AIN). Furthermore, their use might extend beyond pre-malignancies to encompass localized and advanced HPV-induced cancers, representing a significant breakthrough in the management of HPV-associated diseases. This progress could translate into improved outcomes and quality of life for patients globally. Additionally, combining these vaccines with other immune-modulating therapies, such as checkpoint inhibitors, may further enhance clinical outcomes by overcoming immunosuppressive mechanisms, particularly in non-responders.

Integrating vaccines with other immune-modulatory drugs may provide more durable responses for a broader range of patients[90]. This potential is becoming increasingly evident in various HPV-induced malignancies, where vaccines can counteract immune suppression and bolster anti-tumor immune responses. For instance, the phase II study NCT02426892 demonstrated encouraging results with the ISA101 synthetic long peptide vaccine combined with nivolumab, an anti-PD-1 checkpoint inhibitor. This combination achieved a 33% response rate (8 out of 24 patients) and a median survival of 17.5 months in individuals with incurable HPV-16-positive cancers, including oropharyngeal, cervical, and anal malignancies[91]. These findings highlight the promise of therapeutic vaccines to synergize with checkpoint blockade therapies, effectively targeting the immune-evasive mechanisms of HPV-driven tumors. Ongoing investigations continue to explore these synergies. Basket trials such as NCT04432597, NCT03439085, and NCT04287868 are currently evaluating therapeutic HPV vaccines in combination with diverse immunotherapy agents, targeting patients with locally advanced or metastatic HPV-positive cancers. These studies hold the potential to refine combination strategies and enhance the clinical efficacy of HPV vaccines. Moving forward, identifying optimal combinations, treatment sequences, and patient selection criteria will be crucial in translating these approaches into routine clinical practice. With continued research and innovation, the integration of therapeutic HPV vaccines into multimodal regimens may reshape the treatment landscape for HPV-related cancers.

Future Directions and Considerations for Improvement

There remain several promising avenues for advancing our research, particularly in enhancing our understanding of the interplay between the circulatory immune system and

the tumor microenvironment (TME). One critical next step would be to establish a direct link between systemic immune profiles and the TME, utilizing paired tumor and blood samples from the same patient. This would allow for a more comprehensive understanding of how systemic immune dynamics reflect or influence the local tumor environment or *vice versa*. While this approach was initially explored in my study on mTNBC, practical challenges impeded its full implementation. In The Netherlands, the majority of mTNBC patients undergo neoadjuvant chemotherapy, and as a result, the tumor samples I received post-treatment were not suitable for assessing intra-tumoral immune profiles. To effectively correlate the TME with systemic immune profiles, it is crucial to use pre-chemotherapy biopsies. Fortunately, the required approvals from the Medical Ethics Committee (METC) have recently been achieved, simplifying the process for subsequent researchers to carry out such studies. Analyzing matched blood and tumor samples can reveal important immunological shifts. For example, previous studies on a limited set of paired samples have demonstrated that a decline in memory B cells in the blood corresponds with an accumulation of class-switched memory B cells in the tumor[92]. This approach would provide valuable insights into how immune characteristics within the blood mirror those within the TME, uncovering a wealth of scientific knowledge and potentially offering novel biomarkers for treatment response.

Another important research focus is the long-term impact of various chemotherapy regimens on the peripheral immune composition in cancer patients. Recent findings show sustained lymphocyte depletion up to a year after chemotherapy for early breast cancer, similar to what we found in **Chapter 4**, highlighting potential long-term immune suppression[93]. While immediate immune effects post-treatment are well-documented, the prolonged influence of various chemotherapeutic regimens on both innate and adaptive immune compartments remains insufficiently explored. This line of research would involve the collection and analysis of fresh blood samples, which would enable the creation of comprehensive immune profiles that capture both adaptive and innate immune responses. By categorizing patients according to the types of chemotherapy received—such as taxanes, anthracyclines, and platinum-based agents—we could determine the specific immune alterations induced by each class of drugs. I recommend complementing these immune profiling efforts with functional assays to assess the key functional aspects of immune cells, such as cytotoxicity, antigen presentation, cytokine production, and several functional assays on neutrophils described in **Chapters 2** and **4**. Such a holistic approach would provide a deeper understanding of how different chemotherapy regimens influence immune competence, offering valuable insights into the interplay between chemotherapy and potential immune responses. This knowledge could be instrumental in guiding more tailored decision-making regarding chemotherapy and immunotherapy treatment strategies. Moreover, these insights would be crucial not only for refining current treatment protocols

to optimize patient outcomes but also for identifying specific patient populations that may derive the greatest benefit from combination therapies involving both chemotherapy and immunotherapy.

Concluding Remarks

Scientific progress is both purposeful and beautiful, driven by humanity's deep-seated curiosity to explore and understand the world. It reflects our innate desire to ask questions, seek answers, and expand the boundaries of knowledge. This pursuit is valuable in its own right, as each discovery adds to the intricate mosaic of human understanding and inspires future exploration. Beyond its intrinsic worth, scientific progress has a profound impact on our lives, especially in medicine. In breast cancer research, the quest to understand the disease's complexities has led to groundbreaking advancements that directly benefit patients. Insights into cancer subtypes, molecular mechanisms, and immune interactions have paved the way for innovative treatments such as immunotherapies and targeted therapies. These developments not only improve survival but also offer patients renewed hope and a better quality of life. It is my hope, that science may continue to serve a dual purpose: satisfying human curiosity while creating tools that can change lives. It is through this harmony of exploration and application that science achieves its fullest potential.

References

1 Blomberg, O. S. *et al.* Neoadjuvant immune checkpoint blockade triggers persistent and systemic T(reg) activation which blunts therapeutic efficacy against metastatic spread of breast tumors. *Oncoimmunology* **12**, 2201147 (2023). https://doi.org/10.1080/2162402X.2023.2201147

2 Kloosterman, D. J. *et al.* Macrophage-mediated myelin recycling fuels brain cancer malignancy. *Cell* **187**, 5336-5356 e5330 (2024). https://doi.org/10.1016/j.cell.2024.07.030

3 Kersten, K., de Visser, K. E., van Miltenburg, M. H. & Jonkers, J. Genetically engineered mouse models in oncology research and cancer medicine. *EMBO Mol Med* **9**, 137-153 (2017). https://doi.org/10.15252/emmm.201606857

4 Blomberg, O. S. *et al.* IL-5-producing CD4(+) T cells and eosinophils cooperate to enhance response to immune checkpoint blockade in breast cancer. *Cancer Cell* **41**, 106-123 e110 (2023). https://doi.org/10.1016/j.ccell.2022.11.014

5 Garner, H. & de Visser, K. E. Immune crosstalk in cancer progression and metastatic spread: a complex conversation. *Nat Rev Immunol* **20**, 483-497 (2020). https://doi.org/10.1038/s41577-019-0271-z

6 Chang, R. B. & Beatty, G. L. The interplay between innate and adaptive immunity in cancer shapes the productivity of cancer immunosurveillance. *J Leukoc Biol* **108**, 363-376 (2020). https://doi.org/10.1002/JLB.3MIR0320-475R

7 Cassetta, L. *et al.* Human Tumor-Associated Macrophage and Monocyte Transcriptional Landscapes Reveal Cancer-Specific Reprogramming, Biomarkers, and Therapeutic Targets. *Cancer Cell* **35**, 588-602 e510 (2019). https://doi.org/10.1016/j.ccell.2019.02.009

8 Kiss, M., Caro, A. A., Raes, G. & Laoui, D. Systemic Reprogramming of Monocytes in Cancer. *Front Oncol* **10**, 1399 (2020). https://doi.org/10.3389/fonc.2020.01399

9 Trovato, R. *et al.* Immunosuppression by monocytic myeloid-derived suppressor cells in patients with pancreatic ductal carcinoma is orchestrated by STAT3. *J Immunother Cancer* **7**, 255 (2019). https://doi.org/10.1186/s40425-019-0734-6

10 Ethier, J. L., Desautels, D., Templeton, A., Shah, P. S. & Amir, E. Prognostic role of neutrophil-to-lymphocyte ratio in breast cancer: a systematic review and meta-analysis. *Breast Cancer Res* **19**, 2 (2017). https://doi.org/10.1186/s13058-016-0794-1

11 Guo, W. *et al.* Prognostic value of neutrophil-to-lymphocyte ratio and platelet-to-lymphocyte ratio for breast cancer patients: An updated meta-analysis of 17079 individuals. *Cancer Med* **8**, 4135-4148 (2019). https://doi.org/10.1002/cam4.2281

12 Liu, Y., He, M., Wang, C., Zhang, X. & Cai, S. Prognostic value of neutrophil-to-lymphocyte ratio for patients with triple-negative breast cancer: A meta-analysis. *Medicine (Baltimore)* **101**, e29887 (2022). https://doi.org/10.1097/MD.0000000000029887

13 Templeton, A. J. *et al.* Prognostic role of neutrophil-to-lymphocyte ratio in solid tumors: a systematic review and meta-analysis. *J Natl Cancer Inst* **106**, dju124 (2014). https://doi.org/10.1093/jnci/dju124

14 Blomberg, O. S., Spagnuolo, L. & de Visser, K. E. Immune regulation of metastasis: mechanistic insights and therapeutic opportunities. *Dis Model Mech* **11** (2018). https://doi.org/10.1242/dmm.036236

15 Kersten, K. *et al.* Mammary tumor-derived CCL2 enhances pro-metastatic systemic inflammation through upregulation of IL1beta in tumor-associated macrophages. *Oncoimmunology* **6**, e1334744 (2017). https://doi.org/10.1080/2162402X.2017.1334744

16 Hao, X. *et al.* Solid tumour-induced systemic immunosuppression involves dichotomous myeloid-B cell interactions. *Nat Cell Biol* **26**, 1971-1983 (2024). https://doi.org/10.1038/s41556-024-01508-6

17 McAllister, S. S. & Weinberg, R. A. The tumour-induced systemic environment as a critical regulator of cancer progression and metastasis. *Nat Cell Biol* **16**, 717-727 (2014). https://doi.org/10.1038/ncb3015

18 Charoentong, P. *et al.* Pan-cancer Immunogenomic Analyses Reveal Genotype-Immunophenotype Relationships and Predictors of Response to Checkpoint Blockade. *Cell Rep* **18**, 248-262 (2017). https://doi.org/10.1016/j.celrep.2016.12.019

19 Jiang, P. *et al.* Signatures of T cell dysfunction and exclusion predict cancer immunotherapy response. *Nat Med* **24**, 1550-1558 (2018). https://doi.org/10.1038/s41591-018-0136-1

20 Wellenstein, M. D. *et al.* Loss of p53 triggers WNT-dependent systemic inflammation to drive breast cancer metastasis. *Nature* **572**, 538-542 (2019). https://doi.org/10.1038/s41586-019-1450-6

21 Li, B. *et al.* Comprehensive analyses of tumor immunity: implications for cancer immunotherapy. *Genome Biol* **17**, 174 (2016). https://doi.org/10.1186/s13059-016-1028-7

22 Rooney, M. S., Shukla, S. A., Wu, C. J., Getz, G. & Hacohen, N. Molecular and genetic properties of tumors associated with local immune cytolytic activity. *Cell* **160**, 48-61 (2015). https://doi.org/10.1016/j.cell.2014.12.033

23 Spranger, S., Bao, R. & Gajewski, T. F. Melanoma-intrinsic beta-catenin signalling prevents anti-tumour immunity. *Nature* **523**, 231-235 (2015). https://doi.org/10.1038/nature14404

24 Chiappinelli, K. B., Zahnow, C. A., Ahuja, N. & Baylin, S. B. Combining Epigenetic and Immunotherapy to Combat Cancer. *Cancer Res* **76**, 1683-1689 (2016). https://doi.org/10.1158/0008-5472.CAN-15-2125

25 Jones, P. A., Issa, J. P. & Baylin, S. Targeting the cancer epigenome for therapy. *Nat Rev Genet* **17**, 630-641 (2016). https://doi.org/10.1038/nrg.2016.93

26 Sharma, P., Hu-Lieskovan, S., Wargo, J. A. & Ribas, A. Primary, Adaptive, and Acquired Resistance to Cancer Immunotherapy. *Cell* **168**, 707-723 (2017). https://doi.org/10.1016/j.cell.2017.01.017

27 Le, D. T. *et al.* Mismatch repair deficiency predicts response of solid tumors to PD-1 blockade. *Science* **357**, 409-413 (2017). https://doi.org/10.1126/science.aan6733

28 Rizvi, N. A. *et al.* Cancer immunology. Mutational landscape determines sensitivity to PD-1 blockade in non-small cell lung cancer. *Science* **348**, 124-128 (2015). https://doi.org/10.1126/science.aaa1348

29 Schumacher, T. N. & Schreiber, R. D. Neoantigens in cancer immunotherapy. *Science* **348**, 69-74 (2015). https://doi.org/10.1126/science.aaa4971

30 Yarchoan, M., Hopkins, A. & Jaffee, E. M. Tumor Mutational Burden and Response Rate to PD-1 Inhibition. *N Engl J Med* **377**, 2500-2501 (2017). https://doi.org/10.1056/NEJMc1713444

31 Luke, J. J., Bao, R., Sweis, R. F., Spranger, S. & Gajewski, T. F. WNT/beta-catenin Pathway Activation Correlates with Immune Exclusion across Human Cancers. *Clin Cancer Res* **25**, 3074-3083 (2019). https://doi.org/10.1158/1078-0432.CCR-18-1942

32 Peng, W. *et al.* Loss of PTEN Promotes Resistance to T Cell-Mediated Immunotherapy. *Cancer Discov* **6**, 202-216 (2016). https://doi.org/10.1158/2159-8290.CD-15-0283

33 Spranger, S. *et al.* Up-regulation of PD-L1, IDO, and T(regs) in the melanoma tumor microenvironment is driven by CD8(+) T cells. *Sci Transl Med* **5**, 200ra116 (2013). https://doi.org/10.1126/scitranslmed.3006504

34 Duits, D. E. M. & de Visser, K. E. Impact of cancer cell-intrinsic features on neutrophil behavior. *Semin Immunol* **57**, 101546 (2021). https://doi.org/10.1016/j.smim.2021.101546

35 Huang, X. *et al.* Neutrophils in Cancer immunotherapy: friends or foes? *Mol Cancer* **23**, 107 (2024). https://doi.org/10.1186/s12943-024-02004-z

36 Wu, G. *et al.* Neutrophils' dual role in cancer: from tumor progression to immunotherapeutic potential. *Int Immunopharmacol* **140**, 112788 (2024). https://doi.org/10.1016/j.intimp.2024.112788

37 Hedrick, C. C. & Malanchi, I. Neutrophils in cancer: heterogeneous and multifaceted. *Nat Rev Immunol* **22**, 173-187 (2022). https://doi.org/10.1038/s41577-021-00571-6

38 Ng, L. G., Ostuni, R. & Hidalgo, A. Heterogeneity of neutrophils. *Nat Rev Immunol* **19**, 255-265 (2019). https://doi.org/10.1038/s41577-019-0141-8

39 Jaillon, S. *et al.* Neutrophil diversity and plasticity in tumour progression and therapy. *Nat Rev Cancer* **20**, 485-503 (2020). https://doi.org/10.1038/s41568-020-0281-y

40 Boivin, G. *et al.* Durable and controlled depletion of neutrophils in mice. *Nat Commun* **11**, 2762 (2020). https://doi.org/10.1038/s41467-020-16596-9

41 Duits, D. E. M. *et al.* hMRP8-ATTAC Mice: A New Model for Conditional and Reversible Neutrophil Ablation. *Cells* **11** (2022). https://doi.org/10.3390/cells11152346

42 Olofsen, P. A. *et al.* Effective, Long-Term, Neutrophil Depletion Using a Murinized Anti-Ly-6G 1A8 Antibody. *Cells* **11** (2022). https://doi.org/10.3390/cells11213406

43 Hwang, M. *et al.* Peripheral blood immune cell dynamics reflect antitumor immune responses and predict clinical response to immunotherapy. *J Immunother Cancer* **10** (2022). https://doi.org/10.1136/jitc-2022-004688

44 Coffelt, S. B. *et al.* IL-17-producing gammadelta T cells and neutrophils conspire to promote breast cancer metastasis. *Nature* **522**, 345-348 (2015). https://doi.org/10.1038/nature14282

45 Park, J. *et al.* Cancer cells induce metastasis-supporting neutrophil extracellular DNA traps. *Sci Transl Med* **8**, 361ra138 (2016). https://doi.org/10.1126/scitranslmed.aag1711

46 Wculek, S. K. & Malanchi, I. Neutrophils support lung colonization of metastasis-initiating breast cancer cells. *Nature* **528**, 413-417 (2015). https://doi.org/10.1038/nature16140

47 Bakker, N. A. M. *et al.* Triple-negative breast cancer modifies the systemic immune landscape and alters neutrophil functionality. *NPJ Breast Cancer* **11**, 5 (2025). https://doi.org/10.1038/s41523-025-00721-2

48 Kohli, K., Pillarisetty, V. G. & Kim, T. S. Key chemokines direct migration of immune cells in solid tumors. *Cancer Gene Ther* **29**, 10-21 (2022). https://doi.org/10.1038/s41417-021-00303-x

49 Jurcevic, S. *et al.* The effect of a selective CXCR2 antagonist (AZD5069) on human blood neutrophil count and innate immune functions. *Br J Clin Pharmacol* **80**, 1324-1336 (2015). https://doi.org/10.1111/bcp.12724

50 Steele, C. W. *et al.* CXCR2 Inhibition Profoundly Suppresses Metastases and Augments Immunotherapy in Pancreatic Ductal Adenocarcinoma. *Cancer Cell* **29**, 832-845 (2016). https://doi.org/10.1016/j.ccell.2016.04.014

51 Highfill, S. L. *et al.* Disruption of CXCR2-mediated MDSC tumor trafficking enhances anti-PD1 efficacy. *Sci Transl Med* **6**, 237ra267 (2014). https://doi.org/10.1126/scitranslmed.3007974

52 Schott, A. F. *et al.* Phase Ib Pilot Study to Evaluate Reparixin in Combination with Weekly Paclitaxel in Patients with HER-2-Negative Metastatic Breast Cancer. *Clin Cancer Res* **23**, 5358-5365 (2017). https://doi.org/10.1158/1078-0432.CCR-16-2748

53 Armstrong, A. J. *et al.* CXCR2 antagonist navarixin in combination with pembrolizumab in select advanced solid tumors: a phase 2 randomized trial. *Invest New Drugs* **42**, 145-159 (2024). https://doi.org/10.1007/s10637-023-01410-2

54 Guo, C. *et al.* Targeting myeloid chemotaxis to reverse prostate cancer therapy resistance. *Nature* **623**, 1053-1061 (2023). https://doi.org/10.1038/s41586-023-06696-z

55 Voronov, E. *et al.* Unique Versus Redundant Functions of IL-1alpha and IL-1beta in the Tumor Microenvironment. *Front Immunol* **4**, 177 (2013). https://doi.org/10.3389/fimmu.2013.00177

56 Casbon, A. J. *et al.* Invasive breast cancer reprograms early myeloid differentiation in the bone marrow to generate immunosuppressive neutrophils. *Proc Natl Acad Sci U S A* **112**, E566-575 (2015). https://doi.org/10.1073/pnas.1424927112

57 Ridker, P. M. *et al.* Antiinflammatory Therapy with Canakinumab for Atherosclerotic Disease. *N Engl J Med* **377**, 1119-1131 (2017). https://doi.org/10.1056/NEJMoa1707914

58 Ridker, P. M. *et al.* Effect of interleukin-1beta inhibition with canakinumab on incident lung cancer in patients with atherosclerosis: exploratory results from a randomised, double-blind, placebo-controlled trial. *Lancet* **390**, 1833-1842 (2017). https://doi.org/10.1016/S0140-6736(17)32247-X

59 Paz-Ares, L. *et al.* Canakinumab in combination with docetaxel compared with docetaxel alone for the treatment of advanced non-small cell lung cancer following platinum-based doublet chemotherapy and immunotherapy (CANOPY-2): A multicenter, randomized, double-blind, phase 3 trial. *Lung Cancer* **189**, 107451 (2024). https://doi.org/10.1016/j.lungcan.2023.107451

60 Tan, D. S. W. *et al.* Canakinumab Versus Placebo in Combination With First-Line Pembrolizumab Plus Chemotherapy for Advanced Non-Small-Cell Lung Cancer: Results From the CANOPY-1 Trial. *J Clin Oncol* **42**, 192-204 (2024). https://doi.org/10.1200/JCO.23.00980

61 Lythgoe, M. P. & Prasad, V. Repositioning canakinumab for non-small cell lung cancer-important lessons for drug repurposing in oncology. *Br J Cancer* **127**, 785-787 (2022). https://doi.org/10.1038/s41416-022-01893-5

62 Ramirez, J. & Canete, J. D. Anakinra for the treatment of rheumatoid arthritis: a safety evaluation. *Expert Opin Drug Saf* **17**, 727-732 (2018). https://doi.org/10.1080/14740338.2018.1486819

63 Cavalli, G. & Dinarello, C. A. Anakinra Therapy for Non-cancer Inflammatory Diseases. *Front Pharmacol* **9**, 1157 (2018). https://doi.org/10.3389/fphar.2018.01157

64 Tzanetakou, V. *et al.* Safety and Efficacy of Anakinra in Severe Hidradenitis Suppurativa: A Randomized Clinical Trial. *JAMA Dermatol* **152**, 52-59 (2016). https://doi.org/10.1001/jamadermatol.2015.3903

65 King, A. *et al.* Anakinra in COVID-19: important considerations for clinical trials. *Lancet Rheumatol* **2**, e379-e381 (2020). https://doi.org/10.1016/S2665-9913(20)30160-0

66 Park, M. D. *et al.* Hematopoietic aging promotes cancer by fueling IL-1α-driven emergency myelopoiesis. *Science* **386**, eadn0327 (2024). https://doi.org/10.1126/science.adn0327

67 Mantovani, A., Allavena, P., Sica, A. & Balkwill, F. Cancer-related inflammation. *Nature* **454**, 436-444 (2008). https://doi.org/10.1038/nature07205

68 Fridlender, Z. G. *et al.* Polarization of tumor-associated neutrophil phenotype by TGF-beta: "N1" versus

"N2" TAN. *Cancer Cell* **16**, 183-194 (2009). https://doi.org/10.1016/j.ccr.2009.06.017
69 Siwicki, M. & Pittet, M. J. Versatile neutrophil functions in cancer. *Semin Immunol* **57**, 101538 (2021). https://doi.org/10.1016/j.smim.2021.101538
70 Jablonska, J., Leschner, S., Westphal, K., Lienenklaus, S. & Weiss, S. Neutrophils responsive to endogenous IFN-beta regulate tumor angiogenesis and growth in a mouse tumor model. *J Clin Invest* **120**, 1151-1164 (2010). https://doi.org/10.1172/JCI37223
71 Wu, C. F. *et al.* The lack of type I interferon induces neutrophil-mediated pre-metastatic niche formation in the mouse lung. *Int J Cancer* **137**, 837-847 (2015). https://doi.org/10.1002/ijc.29444
72 Glodde, N. *et al.* Reactive Neutrophil Responses Dependent on the Receptor Tyrosine Kinase c-MET Limit Cancer Immunotherapy. *Immunity* **47**, 789-802 e789 (2017). https://doi.org/10.1016/j.immuni.2017.09.012
73 Nielsen, S. R. *et al.* Suppression of tumor-associated neutrophils by lorlatinib attenuates pancreatic cancer growth and improves treatment with immune checkpoint blockade. *Nat Commun* **12**, 3414 (2021). https://doi.org/10.1038/s41467-021-23731-7
74 Spitzer, M. H. *et al.* Systemic Immunity Is Required for Effective Cancer Immunotherapy. *Cell* **168**, 487-502 e415 (2017). https://doi.org/10.1016/j.cell.2016.12.022
75 Simon, S. C. S. *et al.* Eosinophil accumulation predicts response to melanoma treatment with immune checkpoint inhibitors. *Oncoimmunology* **9**, 1727116 (2020). https://doi.org/10.1080/2162402X.2020.1727116
76 Nederlof, I. *et al.* Neoadjuvant nivolumab or nivolumab plus ipilimumab in early-stage triple-negative breast cancer: a phase 2 adaptive trial. *Nat Med* (2024). https://doi.org/10.1038/s41591-024-03249-3
77 Lowery, F. J. *et al.* Molecular signatures of antitumor neoantigen-reactive T cells from metastatic human cancers. *Science* **375**, 877-884 (2022). https://doi.org/10.1126/science.abl5447
78 Oliveira, G. *et al.* Phenotype, specificity and avidity of antitumour CD8(+) T cells in melanoma. *Nature* **596**, 119-125 (2021). https://doi.org/10.1038/s41586-021-03704-y
79 Crotty, S. T Follicular Helper Cell Biology: A Decade of Discovery and Diseases. *Immunity* **50**, 1132-1148 (2019). https://doi.org/10.1016/j.immuni.2019.04.011
80 Schumacher, T. N. & Thommen, D. S. Tertiary lymphoid structures in cancer. *Science* **375**, eabf9419 (2022). https://doi.org/10.1126/science.abf9419
81 Cabrita, R. *et al.* Tertiary lymphoid structures improve immunotherapy and survival in melanoma. *Nature* **577**, 561-565 (2020). https://doi.org/10.1038/s41586-019-1914-8
82 Sautes-Fridman, C., Petitprez, F., Calderaro, J. & Fridman, W. H. Tertiary lymphoid structures in the era of cancer immunotherapy. *Nat Rev Cancer* **19**, 307-325 (2019). https://doi.org/10.1038/s41568-019-0144-6
83 Fehr, M. K. *et al.* Disease progression and recurrence in women treated for vulvovaginal intraepithelial neoplasia. *J Gynecol Oncol* **24**, 236-241 (2013). https://doi.org/10.3802/jgo.2013.24.3.236
84 Hilton, J., Perkins, N., Tabrizi, S. N. & Jones, R. W. A case series of young women with spontaneous regression of vulval intraepithelial neoplasia: Demographics and associated HPV genotypes. *Aust N Z J Obstet Gynaecol* **56**, 312-314 (2016). https://doi.org/10.1111/ajo.12455
85 Jones, R. W., Rowan, D. M. & Stewart, A. W. Vulvar intraepithelial neoplasia: aspects of the natural history and outcome in 405 women. *Obstet Gynecol* **106**, 1319-1326 (2005). https://doi.org/10.1097/01.AOG.0000187301.76283.7f
86 McNally, O. M., Mulvany, N. J., Pagano, R., Quinn, M. A. & Rome, R. M. VIN 3: a clinicopathologic review. *Int J Gynecol Cancer* **12**, 490-495 (2002). https://doi.org/10.1046/j.1525-1438.2002.01140.x
87 Satmary, W., Holschneider, C. H., Brunette, L. L. & Natarajan, S. Vulvar intraepithelial neoplasia: Risk factors for recurrence. *Gynecol Oncol* **148**, 126-131 (2018). https://doi.org/10.1016/j.ygyno.2017.10.029
88 van Seters, M., van Beurden, M. & de Craen, A. J. Is the assumed natural history of vulvar intraepithelial neoplasia III based on enough evidence? A systematic review of 3322 published patients. *Gynecol Oncol* **97**, 645-651 (2005). https://doi.org/10.1016/j.ygyno.2005.02.012
89 Bakker, N. A. M. *et al.* HPV-16 E6/E7 DNA tattoo vaccination using genetically optimized vaccines elicit clinical and immunological responses in patients with usual vulvar intraepithelial neoplasia (uVIN): a phase I/II clinical trial. *J Immunother Cancer* **9** (2021). https://doi.org/10.1136/jitc-2021-002547
90 Rafael, T. S. *et al.* Immunotherapeutic Approaches for the Treatment of HPV-Associated (Pre-)Cancer of the Cervix, Vulva and Penis. *J Clin Med* **11** (2022). https://doi.org/10.3390/jcm11041101
91 Massarelli, E. *et al.* Combining Immune Checkpoint Blockade and Tumor-Specific Vaccine for Patients With Incurable Human Papillomavirus 16-Related Cancer: A Phase 2 Clinical Trial. *JAMA Oncol* **5**, 67-73 (2019). https://doi.org/10.1001/jamaoncol.2018.4051
92 Harris, R. J. *et al.* Tumor-Infiltrating B Lymphocyte Profiling Identifies IgG-Biased, Clonally Expanded Prognostic Phenotypes in Triple-Negative Breast Cancer. *Cancer Res* **81**, 4290-4304 (2021). https://doi.org/10.1158/0008-5472.CAN-20-3773
93 Dixon-Douglas, J. *et al.* Sustained lymphocyte decreases after treatment for early breast cancer. *NPJ Breast Cancer* **10**, 94 (2024). https://doi.org/10.1038/s41523-024-00698-4

Appendices

English summary

Cancer presents a major global health burden, with a lifetime risk of approximately one in five individuals and mortality affecting about one in nine men and one in twelve women. In the Netherlands, the incidence is even higher, with one in two individuals expected to develop cancer. Among all cancer types, breast cancer is the most common malignancy in women worldwide and the leading cause of cancer-related death in women, underscoring the urgent need to deepen our understanding of breast cancer biology and to develop more effective therapeutic strategies.

Over the past decades, immunotherapy has emerged as a transformative approach in cancer treatment. Immune checkpoint inhibitors targeting CTLA-4 and PD-(L)1 have shown remarkable efficacy in melanoma, lung cancer, and renal cell carcinoma. Historically, breast cancer was considered relatively unresponsive to immunotherapy due to its low mutational burden and limited immune infiltration. However, it has become increasingly evident that breast cancer is immunologically heterogeneous, with tumor microenvironments ranging from immune-desert to immune-infiltrated phenotypes based on the presence of tumor-infiltrating lymphocytes (TILs). This diversity opens new opportunities for immunotherapy, particularly for specific subtypes and disease stages.

Neutrophils play a pivotal role in orchestrating tumor-induced systemic inflammation and are increasingly recognized for their involvement in both the initiation and progression of cancer. A key feature of neutrophil biology is their migratory capacity, which enables them to extravasate and infiltrate tumors and other tissues, where they execute essential effector functions. Unraveling the mechanisms of neutrophil motility and migration is crucial for understanding immune responses and inflammatory processes and highlights their contribution to cancer progression. In **chapter 2**, a comprehensive protocol was described to assess the direct *ex vivo* motility and migration of freshly isolated human neutrophils, offering valuable insights into their behavior.

To study the effect of molecular subtype and disease stage on the systemic immune landscape in breast cancer, a comprehensive immune profiling study was conducted using multiparameter flow cytometry on freshly collected blood samples from a large cohort of breast cancer patients across various subtypes and disease stages, compared to healthy donors (HDs). The use of fresh samples allowed the inclusion of short-lived granulocyte populations, such as neutrophils and eosinophils, which are typically lost in cryopreserved material. The data described in **chapter 3** revealed that patients with early-stage breast cancer exhibited elevated levels of neutrophils, classical monocytes, and CD1c− dendritic cells (DCs) compared to HDs. In metastatic disease, neutrophils and classical monocytes remained elevated, and non-classical monocytes were also increased. In contrast, memory B cells, plasmablast-like cells, conventional CD4+ T cells, and Tregs were reduced in patients

with metastatic disease, suggesting that systemic immune dysregulation becomes more pronounced with disease progression. Further stratification by molecular subtype showed that these immune alterations were also subtype-specific. In early-stage HR+ breast cancer, neutrophils, classical monocytes, and CD1c− DCs were increased, whereas HER2+ early-stage tumors showed no significant deviations from HDs. TNBC patients in early-stage disease exhibited increased levels of non-classical monocytes and Vδ2 γδ T cells. In the metastatic setting, HR+ disease was associated with elevated neutrophils and non-classical monocytes and decreased Tregs. HER2+ disease showed reductions in plasmablast-like cells, conventional CD4+ T cells, and Tregs. The most pronounced immune alterations were observed in metastatic TNBC, characterized by increased neutrophils and classical monocytes and decreased levels of multiple adaptive immune subsets.

In **chapter 4**, we investigated the immune alterations found in patients with TNBC in more detail. It turned out that neutrophils were not only more abundant in mTNBC compared to HDs, but also altered on a transcriptional and functional level. Transcriptional, proteomic, and functional analyses revealed that neutrophils from patients with mTNBC exhibited enhanced migratory capacity, elevated granule protein content, and increased ROS production. The data described in **chapters 3 and 4** demonstrated that immune dysregulation in breast cancer is influenced by both disease stage and subtype, with the most extensive changes occurring in TNBC. Together, these results point to an opportunity to mitigate systemic immune dysregulation in breast cancer through new immune-based therapies and underscore the importance of considering both disease stage and subtype in therapeutic strategies.

In **chapter 5**, we explore the transcriptional differences in the systemic immune landscape of patients with mTNBC and HDs using single-cell RNA-sequencing of fresh whole blood, complemented by matched TCR- and BCR-sequencing to assess lymphocyte clonality and diversity. We identified multiple transcriptional states within neutrophils, suggesting greater heterogeneity within this cell type than traditionally recognized. However, given the high interindividual variability among the five HDs and five mTNBC patients, the limited group sizes likely hindered the identification of clear discriminating differences between the two groups.

The second part of the thesis, described in **chapters 6, 7, and 8**, focused on translational research and immunomonitoring embedded in clinical trials. These studies assessed treatment-induced changes in the immune system and the dynamics of immune responses during immunotherapy, with the goal of identifying biomarkers and mechanisms of response or resistance.

Chapter 6 described the BELLINI trial, a window-of-opportunity phase II study that evaluated short-term immune checkpoint inhibition (ICI; anti-PD-1 ± anti-CTLA-4) in patients with non-metastatic TNBC. The primary aim was to assess whether immune activation could

be achieved in the absence of chemotherapy. In the first two cohorts (n=15 each), patients received standard chemotherapy and surgery immediately after short-term ICI. We investigated whether this brief immunotherapy exposure could stimulate immune activation within the tumor. Our analyses showed that patients with a high percentage of TILs responded particularly well. These findings led to a third cohort enrolling patients with ≥50% TILs to assess the potential of ICI (anti-PD-1 + anti-CTLA-4) as a stand-alone treatment. In this cohort, patients underwent surgery directly after six weeks of immunotherapy, without chemotherapy. A major pathological response (≥90% tumor cell eradication) was observed in 53% of patients, with a pathological complete response (pCR) achieved in 33%. Immune monitoring by flow cytometry revealed increased frequencies of proliferating (Ki-67$^+$) PD-1$^+$ conventional CD4$^+$ T cells in responders, with similar trends in CD8$^+$ T cells. These results demonstrated that ICI alone can induce robust immune activation in early-stage TNBC and support further exploration of chemotherapy-free immunotherapeutic strategies. In summary, short-course anti-PD-1 ± anti-CTLA-4 before surgery can induce immune activation in ~60% of early TNBC cases, and among highly infiltrated tumors (TIL ≥ 50%) yields a pCR rate of ~33%—offering a potential chemotherapy-sparing approach worth exploring further.

Chapter 7 focused on identifying mechanisms of response to PD-1 blockade in patients with metastatic TNBC. While most studies have emphasized the role of T cells in ICI response, effective antitumor immunity relies on coordinated crosstalk between innate and adaptive immune cells. Using immune profiling of paired blood samples and tumor biopsies, we observed that responders exhibited increased eosinophils both systemically and within the tumor microenvironment—an effect absent in non-responders. These findings were supported by mechanistic studies in mouse models of primary and metastatic breast cancer, which confirmed a functional role for eosinophils in mediating ICI responses. Mechanistically, ICI enhanced IL-5 production by CD4$^+$ T cells, driving eosinophil expansion from the bone marrow. Additionally, the combination of ICI with cisplatin, or administration of recombinant IL-33, promoted IL-33 induction, leading to increased intratumoral eosinophil infiltration and eosinophil-dependent activation of CD8$^+$ T cells. These results revealed a novel mechanism by which eosinophils contribute to effective antitumor immunity and demonstrated that their therapeutic engagement may enhance ICI efficacy in breast cancer. Together, this work underscores the importance of innate–adaptive immune interactions in shaping ICI responses and provides proof-of-principle for eosinophil-targeting strategies in mTNBC.

Chapter 8 described a phase I/II clinical trial in which a genetically enhanced HPV-16 E6/E7 DNA tattoo vaccine was evaluated in 14 patients with HPV16-positive usual vulvar intraepithelial neoplasia (uVIN), a premalignant condition with a risk of progression to vulvar carcinoma. The study aimed to assess safety, immunogenicity, and clinical efficacy. Patients received four intradermal vaccinations at two-week intervals using a tattoo device,

alternating between both upper legs. Clinical responses were evaluated through lesion measurements by digital photography up to 12 months post-treatment, and immune responses were assessed via *ex vivo* T-cell reactivity assays using peripheral blood samples. The vaccine was generally well tolerated; one patient experienced a grade 3 suspected unexpected serious adverse reaction. Clinical responses were observed in 6 of 14 patients (43%), including 2 complete and 4 partial responses. HPV-specific T-cell responses were detected in 5 of 14 patients (36%), all of whom showed clinical benefit. This correlation suggests a potential link between systemic T-cell reactivity and lesion regression. This study demonstrated that HPV-16 E6/E7 DNA tattoo vaccination is biologically active and safe in patients with uVIN. The findings support the potential of therapeutic vaccination as a non-invasive immunotherapeutic approach for virus-induced premalignant disease and provide a rationale for further clinical investigation.

In conclusion, this thesis provided a comprehensive analysis of how breast cancer subtype and disease stage influence systemic immunity. It also presented translational insights from clinical trials that aimed to modulate and monitor immune responses during immunotherapy. The findings underscore the potential of immunotherapy in breast cancer, particularly TNBC, and highlight the importance of integrating immune profiling into clinical strategies to enhance patient selection and monitor treatment effects, with the ultimate goal of developing more effective therapeutic approaches.

Nederlandse samenvatting

Kanker vormt wereldwijd een groot probleem voor de volksgezondheid, met een levenslange kans van ongeveer één op de vijf mensen om de ziekte te ontwikkelen. In Nederland ligt de incidentie zelfs hoger: één op de twee mensen krijgt ooit kanker. Ongeveer één op de negen mannen, en één op de twaalf vrouwen overlijdt aan kanker. Van alle kankersoorten komt borstkanker het meest voor bij vrouwen wereldwijd en in Nederland. Borstkanker is ook de belangrijkste oorzaak van kanker gerelateerde sterfte onder vrouwen. Dit benadrukt de noodzaak om ons begrip van de biologie van borstkanker te verdiepen en effectievere behandelingsstrategieën te ontwikkelen.

In de afgelopen decennia is gebleken dat immuuntherapie een baanbrekende behandelmethode kan zijn. Immuuncheckpointremmers gericht tegen CTLA-4 en PD-(L)1 hebben indrukwekkende resultaten laten zien bij onder andere melanoom, longkanker en niercelcarcinoom. Borstkanker werd traditioneel beschouwd als weinig gevoelig voor immuuntherapie vanwege het lage aantal mutaties en de beperkte infiltratie van immuuncellen in de tumor. Inmiddels is duidelijk geworden dat borstkanker immunologisch heterogeen is en dat het aantal tumor infiltrerende lymfocyten (TILs) erg kan verschillen tussen mensen. Deze diversiteit opent nieuwe mogelijkheden voor immuuntherapie, in het bijzonder bij bepaalde subtypes en stadia van de ziekte.

Eén bepaalde immuuncel, de neutrofiel, speelt een centrale rol in door tumoren geïnduceerde systemische ontsteking. Neutrofielen worden steeds meer erkend als belangrijke actoren in zowel het ontstaan, als de progressie van kanker. Een essentiële eigenschap van neutrofielen is hun migratievermogen, waarmee zij vanuit de bloedbaan weefsels, waaronder tumoren, kunnen binnendringen om daar effectorfuncties uit te voeren. In **hoofdstuk 2** wordt een uitgebreid protocol beschreven om *ex vivo* migratie van vers geïsoleerde humane neutrofielen te meten, wat waardevolle inzichten biedt in hun gedrag.

Om het effect van het stadium en het subtype van borst kanker op het systemische immuunlandschap te bestuderen, werd een uitgebreide immuunprofilering uitgevoerd met multiparameter flowcytometrie op vers verzamelde bloedmonsters van een grote groep patiënten met verschillende subtypes en ziektestadia, en vergeleken met het immuunprofiel van gezonde donoren (HDs). Het gebruik van verse monsters maakte analyse van kortlevende granulocyten, zoals neutrofielen en eosinofielen mogelijk; cellen die vrijwel geheel verloren gaan in ingevroren materiaal. De resultaten beschreven in **hoofdstuk 3** laten zien dat patiënten met vroeg-stadium borstkanker verhoogde niveaus van neutrofielen, klassieke monocyten en CD1c− dendritische cellen (DCs) vertonen ten opzichte van HDs. Bij gemetastaseerde ziekte bleven neutrofielen en klassieke monocyten verhoogd, en waren ook niet-klassieke monocyten toegenomen. Tegelijkertijd waren geheugen B-cellen,

plasmablasten, conventionele CD4+ T-cellen en Tregs verlaagd bij deze patiënten, wat wijst op toenemende immuundisregulatie naarmate de ziekte vordert. Verdere uitsplitsing per borstkanker subtype toonde subtype-specifieke verschillen aan: bij vroeg-stadium HR+ borstkanker waren neutrofielen, klassieke monocyten en CD1c− DCs verhoogd terwijl HER2+ tumoren geen significante afwijkingen ten opzichte van HDs vertoonde. Het systemische immuun profiel van patiënten met niet-gemetastaseerde TNBC werd gekenmerkt door verhoogde niet-klassieke monocyten en Vδ2 γδ T-cellen. In de gemetastaseerde setting was HR+ ziekte geassocieerd met verhoogde neutrofielen en niet-klassieke monocyten en verlaagde Tregs. HER2+ ziekte toonde verlaging van plasmablasten, conventionele CD4+ T-cellen en Tregs. De meest uitgesproken afwijkingen werden gezien bij gemetastaseerd TNBC, met verhoogde neutrofielen en klassieke monocyten en verlaagde niveaus van diverse adaptieve immuuncellen.

In **hoofdstuk 4** werd dieper ingegaan op TNBC. Het bleek dat patiënten met mTNBC niet alleen meer neutrofielen hadden dan HDs, maar dat deze neutrofielen ook functioneel en transcriptioneel anders waren. Experimenten die het transcriptoom, het proteoom en de functionaliteit in kaart brachten, toonden aan dat neutrofielen van patiënten met mTNBC een verhoogd migratievermogen, hogere expressie van granulaire eiwitten en verhoogde productie van reactieve zuurstofsoorten (ROS) vertoonden. De gegevens uit **hoofdstukken 3 en 4** tonen aan dat immuun disregulatie bij borstkanker wordt beïnvloed door zowel subtype als ziektestadium, met de meest uitgesproken veranderingen bij TNBC. Deze bevindingen bieden aanknopingspunten voor het ontwikkelen van therapieën die de systemische verstoringen van het immuun systeem als gevolg van de kanker tegengaan, en onderstrepen het belang van subtype- en stadiumspecifieke benaderingen.

In **hoofdstuk 5** onderzochten we de verschillen in transcriptionele activiteit van circulerende immuun cellen van patiënten met mTNBC en HDs met behulp van single-cell RNA-sequencing van vers volbloed, aangevuld met matchende TCR- en BCR-sequencing om de klonaliteit en diversiteit van lymfocyten te beoordelen. We hebben meerdere transcriptiestaten binnen neutrofielen geïdentificeerd, wat wijst op een grotere heterogeniteit binnen dit celtype dan traditioneel wordt aangenomen. Gezien de grote interindividuele variabiliteit tussen de vijf HDs en vijf patiënten met mTNBC, heeft de beperkte groepsomvang waarschijnlijk het identificeren van duidelijke onderscheidende verschillen tussen de twee groepen verhinderd.

Het tweede deel van dit proefschrift, beschreven in **hoofdstukken 6, 7 en 8**, richtte zich op translationeel onderzoek en immunomonitoring binnen klinische studies. Deze onderzoeken evalueerden veranderingen in het immuunsysteem tijdens behandeling en de dynamiek van immuunresponsen bij immuuntherapie, met als doel het identificeren van biomarkers en mechanismen van respons of immunosuppressie.

Hoofdstuk 6 beschrijft de BELLINI-studie, een fase II klinische studie waarin kortdurende

immuuntherapie (anti-PD-1 ± anti-CTLA-4) werd onderzocht bij patiënten met niet-gemetastaseerd TNBC. In de eerste twee cohorten (n=15 elk) kregen patiënten kortdurende immuuntherapie gevolgd door standaard behandeling (chemotherapie en chirurgie). Onze analyses toonden aan dat patiënten met een hoog percentage TILs bijzonder goed reageerden. Deze bevindingen leidden tot de opening van een derde cohort waarin alleen patiënten zaten met ≥50% TILs. In dit derde cohort (ook n=15) werden de patiënten direct geopereerd na de immuuntherapie, zonder chemotherapie. Een majeure pathologische respons (≥90% tumorcel-eradicatie) werd gezien bij 53% van de patiënten, en een pathologisch complete respons (pCR) bij 33%. Flowcytometrie analyses op verse bloedsamples van de patiënten voor en tijdens hun behandeling, liet zien dat responderende patiënten verhoogde niveaus van delende (Ki-67$^+$) PD-1$^+$ conventionele CD4$^+$ T-cellen hadden, met een vergelijkbare trend bij CD8$^+$ T-cellen. Deze resultaten tonen aan dat immuuntherapie op zichzelf robuuste immuunactivatie kan induceren bij vroeg-stadium TNBC. Samengevat kan een korte kuur met nivolumab ± ipilimumab vóór chirurgie immuunactivatie induceren in ~60% van de vroege TNBC-gevallen, en bij sterk geïnfiltreerde tumoren (TIL ≥ 50%) een pCR opleveren in ~33%, wat een potentieel chemotherapiesparend behandelschema vertegenwoordigt.

In **hoofdstuk 7** werd onderzocht welke immuunkenmerken geassocieerd zijn met respons op PD-1-blokkade bij patiënten met mTNBC. Hoewel eerder onderzoek vooral gericht was op T-cellen, blijkt effectieve anti-tumorimmuniteit afhankelijk van interactie tussen het aangeboren en adaptieve immuunsysteem. Immuunprofilering van gekoppelde bloedmonsters en tumorbiopten liet zien dat responders een toename vertoonden van eosinofielen, zowel systemisch als in de tumor; een effect dat bij non-responders ontbrak. Diversen proeven in relevante muismodellen bevestigden de functionele rol van eosinofielen in de respons op immunotherapie. Immuuntherapie bleek de IL-5-productie door CD4$^+$ T-cellen te verhogen, wat eosinofielenexpansie vanuit het beenmerg stimuleerde. Toevoeging van cisplatine of recombinant IL-33 verhoogde bovendien de IL-33-spiegels, wat leidde tot verhoogde intratumorale eosinofieleninfiltratie en eosinofiel-afhankelijke activatie van CD8$^+$ T-cellen. Deze resultaten onthullen een nieuw mechanisme waarbij eosinofielen bijdragen aan de effectiviteit van immuuntherapie en onderbouwen het potentieel van eosinofiel gerichte therapieën bij borstkanker.

In **hoofdstuk 8** werd een fase I/II-studie beschreven waarin een genetisch geoptimaliseerd HPV-16 E6/E7 DNA-tatoeagevaccin werd getest bij 14 patiënten met HPV16-positieve usual vulvaire intra-epitheliale neoplasie (uVIN), een premaligne aandoening met risico op progressie naar carcinoom. Patiënten ontvingen vier intradermale vaccinaties met twee weken tussenpozen, afwisselend in beide bovenbenen, toegediend via een tatoeageapparaat. Klinische respons werd geëvalueerd aan de hand van digitale fotografie tot 12 maanden na behandeling. T-celresponsen werden bepaald in *ex vivo* assays op

perifere bloedmonsters. De vaccinatie werd goed verdragen; één patiënt kreeg een ernstige onverwachte bijwerking (graad 3). In totaal vertoonden 6 van de 14 patiënten (43%) een klinische respons (2 compleet, 4 partieel). HPV-specifieke T-celresponsen werden gemeten bij 5 patiënten (36%), allemaal met klinisch voordeel. Deze studie toont aan dat HPV-16 E6/E7 DNA-vaccinatie biologisch actief en veilig is bij uVIN en ondersteunt het potentieel van therapeutische vaccinatie als niet-invasieve immuuntherapie voor virus-geïnduceerde premaligne aandoeningen.

Concluderend biedt dit proefschrift een uitgebreid overzicht van hoe borstkankersubtype en ziektefase het immuunsysteem beïnvloeden. Daarnaast worden translationele inzichten gepresenteerd uit klinische studies die gericht waren op het moduleren en monitoren van immuunreacties tijdens immuuntherapie. De bevindingen benadrukken het potentieel van immuuntherapie bij borstkanker, vooral bij TNBC, en onderstrepen het belang van geïntegreerde immuunprofilering voor betere patiëntselectie en effectmeting, met als uiteindelijk doel effectievere behandelingen te ontwikkelen.

Curriculum Vitae

Eleonora Alida Maria Bakker, known as Noor, was born on September 27, 1988, in Heemstede, the Netherlands. She obtained her VWO diploma from Vrije School De Berkel in Zutphen in 2007. She then pursued a BSc in Biology at the Vrije Universiteit Amsterdam, graduating in 2010. Building on this foundation, she completed an MSc in Biomolecular Sciences with a specialization in Cell Biology in 2013.

After her master's, Noor worked as a research technician in the group of Prof. Dr. Peter J. Peters at the Netherlands Cancer Institute (NKI), where she focused on structural biology using (cryo) electron microscopy. She then spent five years as a technician in the GMP therapeutic production facility at NKI, where she was involved in the production of clinical-grade TILs, TCR-transduced T cells, and multiple vaccines. She also played a key role in the immunomonitoring of clinical trials and contributed to translational research projects in collaboration with the groups of Prof. Dr. Ton N. Schumacher and Prof. Dr. John B. A. G. Haanen. Her work contributed to the development of a novel method to induce neoantigen-specific T cells using peptide-loaded DCs, a technique that was patented and is now being tested in clinical studies.

After this productive period, Noor decided to further her scientific career by pursuing a PhD. In 2018, she joined the lab of Prof. Dr. Karin E. de Visser at the Netherlands Cancer Institute, working closely with her co-promotor Dr. Marleen Kok. Her research focused on the influence of tumor subtype and stage on the systemic immune landscape of breast cancer patients, with a particular interest in neutrophil biology. She was involved in the translational research of multiple clinical studies led by Dr. Marleen Kok and served as a bridge between the Kok and De Visser labs. Additionally, she studied systemic responses and immunotherapy effects in patients with breast cancer and uVIN lesions. The findings of this work are presented in this thesis.

List of Publications

Comprehensive analysis of the systemic immune landscape across breast cancer subtypes and disease stages
Noor A.M. Bakker, H. Garner*, V.C.M. Geurts*, E. Champanhet, C. Klaver, M. Duijst, I. Nederlof, R.C.A.M. Gielen, M. de Graaf, R. Voorthuis, M.C. Liefaard, E.H. Lips, H.M. Oosterkamp, M. Kok , K.E. de Visser
Immuno-Oncology and Technology. 2025 July 23; 27. https://doi.org/10.1016/j.iotech.2025.101065

Understanding and reversing mammary tumor-driven reprogramming of myelopoiesis to reduce metastatic spread
Hannah Garner , Moreno Martinovic, Ning Qing Liu, Noor A.M. Bakker, Irene Querol Velilla, Cheei-Sing Hau, Kim Vrijland, Daphne Kaldenbach, Marleen Kok, Elzo de Wit and Karin E. de Visser
Cancer Cell. 2025 July 14; 43, (1-17). doi.org/10.1016/j.ccell.2025.04.007

Triple-negative breast cancer modifies the systemic immune landscape and alters neutrophil functionality
Noor A. M. Bakker, Hannah Garner*, Ewald van Dyk*, Elisa Champanhet, Chris Klaver, Maxime Duijst, Leonie Voorwerk, Iris Nederlof, Rosie Voorthuis, Marte C. Liefaard, Marja Nieuwland, Iris de Rink, Onno B. Bleijerveld, Hendrika M. Oosterkamp, Lodewyk F. A. Wessels, Marleen Kok & Karin E. de Visser
NPJ Breast Cancer. 2025 January 23; 11-1(5). doi.org/10.1038/s41523-025-00721-2

***Ex vivo* assessment of human neutrophil motility and migration**
Noor A. M. Bakker, Claudia Burrello, Karin E. de Visser
Methods in Cell Biology. 2024 November 19; 2025-191(115-133). doi: 10.1016/bs.mcb.2024.10.008

Neoadjuvant nivolumab or nivolumab plusipilimumab in early-stage triple-negativebreast cancer: a phase 2 adaptive trial
Iris Nederlof* Olga I. Isaeva*, Manon de Graaf#, Robbert C. A. M. Gielen#, Noor A. M. Bakker#, Adrianne L. Rolfes, Hannah Garner, Bram Boeckx, Joleen J. H. Traets, Ingrid A. M. Mandjes, Michiel de Maaker, Thomas van Brussel, Maksim Chelushkin, Elisa Champanhet, Marta Lopez-Yurda, Koen van de Vijver, José G. van den Berg, Ingrid Hofland, Natasja Klioueva, Ritse M. Mann, Claudette E. Loo, Frederieke H. van Duijnhoven, Victoria Skinner, Sylvia Luykx, Emile Kerver, Ekaterina Kalashnikova, Marloes G. J. van Dongen, Gabe S. Sonke, Sabine C. Linn, Christian U. Blank, Karin E. de Visser, Roberto Salgado, Lodewyk F. A. Wessels, Caroline A. Drukker, Ton N. Schumacher, Hugo M. Horlings, Diether Lambrechts, Marleen Kok
Nature Medicine. 2024 September 16; 30 (3223–3235). doi: 10.1038/s41591-024-03249-3

Neoadjuvant immune checkpoint blockade triggers persistent and systemic T_{reg} activation which blunts therapeutic efficacy against metastatic spread of breast tumors
Olga S. Blomberg, Kevin Kos, Lorenzo Spagnuolo, Olga I. Isaeva, Hannah Garner, Max D. Wellenstein, Noor Bakker, Danique E. M. Duits, Kelly Kersten, Sjoerd Klarenbeek, Cheei-Sing Hau, Daphne Kaldenbach, Elisabeth A. M. Raeven, Kim Vrijland, Marleen Kok, Karin E. de Visser
Oncoimmunology. 2023 April 13; 12-1(2201147). doi: 10.1080/2162402X.2023.2201147

PD-L1 blockade in combination with carboplatin as immune induction in metastatic lobular breast cancer: the GELATO trial
Leonie Voorwerk, Olga I. Isaeva, Hugo M. Horlings, Sara Balduzzi, Maksim Chelushkin, Noor A. M. Bakker, Elisa Champanhet, Hannah Garner, Karolina Sikorska, Claudette E. Loo, Inge Kemper, Ingrid A. M. Mandjes, Michiel de Maaker, Jasper J. L. van Geel, Jorianne Boers, Maaike de Boer, Roberto Salgado, Marloes G. J. van Dongen, Gabe S. Sonke, Karin E. de Visser, Ton N. Schumacher, Christian U. Blank, Lodewyk F. A. Wessels, Agnes Jager, Vivianne C. G. Tjan-Heijnen, Carolien P. Schröder, Sabine C. Linn, Marleen Kok
Nature Cancer. 2023 April 10; 4(535–549). doi: 10.1038/s43018-023-00542-x

IL-5-producing CD4+ T cells and eosinophils cooperate to enhance response to immune checkpoint blockade in breast cancer
Olga S. Blomberg*, Lorenzo Spagnuolo*, Hannah Garner*, Leonie Voorwerk*, Olga I. Isaeva#, Ewald van Dyk#, Noor Bakker#, Myriam Chalabi, Chris Klaver, Maxime Duijst, Kelly Kersten, Marieke Brüggemann, Dorien Pastoors, Cheei-Sing Hau, Kim Vrijland, Elisabeth A.M. Raeven, Daphne Kaldenbach, Kevin Kos, Inna S. Afonina, Paulien Kaptein, Louisa Hoes, Willemijn S.M.E. Theelen, Paul Baas, Emile E. Voest, Rudi Beyaert, Daniela S. Thommen, Lodewyk F.A. Wessels, Karin E. de Visser , Marleen Kok
Cancer Cell. 2023 January 9; 41-1(106-123.e10). doi: 10.1016/j.ccell.2022.11.014

MART-1 TCR gene modified peripheral blood T cells for the treatment of metastatic melanoma: a phase Ib/IIa clinical trial
M. W. Rohaan*, R. Gomez-Eerland*, J. H. van den Berg, M. H. Geukes Foppen, M. van Zon, B. Raud, I. Jedema, S. Scheij, R. de Boer, Noor A. M. Bakker, D. van den Broek, L. M. Pronk,

L. G. Grijpink-Ongering, A. Sari, R. Kessels, M. van den Haak, H. A. Mallo, M. Karger, B. A. van de Wiel, C. L. Zuur, C. W. Duinkerken, F. Lalezari, J. V. van Thienen, S. Wilgenhof, C. U. Blank, J. H. Beijnen, B. Nuijen, T. N. Schumacher, J. B. A. G. Haanen
Immuno-Oncology and Technology. 2022 June 18; 15(100089). doi: 10.1016/j.iotech.2022.100089

HPV-16 E6/E7 DNA tattoo vaccination using genetically optimized vaccines elicit clinical and immunological responses in patients with usual vulvar intraepithelial neoplasia (uVIN): a phase I/II clinical trial
Noor A. M. Bakker*, Jossie Rotman*, Marc van Beurden, Henry J. Zijlmans, Maartje van Ruiten, Sanne Samuels, Bastiaan Nuijen, Jos Beijnen, Karin E. de Visser, John Haanen, Ton Schumacher, Tanja D. de Gruijl, Ekaterina S. Jordanova, Gemma G. Kenter, Joost H. van den Berg#, Nienke E. van Trommel#
The Journal for ImmunoTherapy of Cancer. 2021 August 2; 9-8(e002547). doi: 10.1136/jitc-2021-002547

Tumor infiltrating lymphocytes (TIL) therapy in metastatic melanoma: boosting of neoantigen-specific T cell reactivity and long-term follow-up
Joost H. van den Berg, Bianca Heemskerk, Nienke van Rooij, Raquel Gomez-Eerland, Samira Michels, Maaike van Zon, Renate de Boer, Noor A. M. Bakker, Annelies Jorritsma-Smit, Marit M. van Buuren, Pia Kvistborg, Hergen Spits, Remko Schotte, Henk Mallo, Matthias Karger, Joris A. van der Hage, Michel W. J. M. Wouters, Loes M. Pronk, Marnix H. Geukes Foppen, Christian U. Blank, Jos H. Beijnen, Bastiaan Nuijen, Ton N. Schumacher, John B. A. G. Haanen
The Journal for ImmunoTherapy of Cancer. 2020 August 4; 8-2(e000848). doi: 10.1136/jitc-2020-000848

Immune induction strategies in metastatic triple-negative breast cancer to enhance the sensitivity to PD-1 blockade: the TONIC trial
Leonie Voorwerk*, Maarten Slagter*, Hugo M. Horlings, Karolina Sikorska, Koen K. van de Vijver, Michiel de Maaker, Iris Nederlof, Roelof J. C. Kluin, Sarah Warren, SuFey Ong, Terry G. Wiersma, Nicola S. Russell, Ferry Lalezari, Philip C. Schouten, Noor A. M. Bakker, Steven L. C. Ketelaars, Dennis Peters, Charlotte A. H. Lange, Erik van Werkhoven, Harm van Tinteren, Ingrid A. M. Mandjes, Inge Kemper, Suzanne Onderwater, Myriam Chalabi, Sofie Wilgenhof, John B. A. G. Haanen, Roberto Salgado, Karin E. de Visser, Gabe S. Sonke, Lodewyk F. A. Wessels, Sabine C. Linn, Ton N. Schumacher, Christian U. Blank, Marleen Kok
Nature Medicine. 2019 June 17; 25(920–928). doi: 10.1038/s41591-019-0432-4

Small-scale GMP production of plasmid DNA using a simplified and fully disposable production method
Noor A. M. Bakker, Renate de Boer, Corinne Marie, Daniel Scherman, John B. A. G. Haanen, Jos H. Beijnen, Bastiaan Nuijen, Joost H. van den Berg
Journal of Biotechnology. 2019 May 11; 306S(100007). doi: 10.1016/j.btecx.2019.100007

Glutaminyl cyclase is an enzymatic modifier of the CD47- SIRPα axis and a target for cancer immunotherapy
Meike E. W. Logtenberg, J. H. Marco Jansen, Matthijs Raaben, Mireille Toebes, Katka Franke, Arianne M. Brandsma, Hanke L. Matlung, Astrid Fauster, Raquel Gomez-Eerland, Noor A. M. Bakker, Simone van der Schot, Koen A. Marijt, Martijn Verdoes, John B. A. G. Haanen, Joost H. van den Berg, Jacques Neefjes, Timo K. van den Berg, Thijn R. Brummelkamp, Jeanette H. W. Leusen, Ferenc A. Scheeren, Ton N. Schumacher
Nature Medicine. 2019 March 4; 25(612–619). doi: 10.1038/s41591-019-0356-z

* and # Equal contribution; corresponding author(s)

Dankwoord

Allereerst mijn grote dank aan de patiënten die deelgenomen hebben aan de studies beschreven in dit proefschrift, en aan de gezonde donoren die als controlegroep wilden dienen. Zonder hen waren deze wetenschappelijke inzichten er niet geweest.

Karin, jij bent voor mij een groot voorbeeld: leiderschap en excellentie in de wetenschap combineer jij moeiteloos met eerlijkheid, compassie en integriteit, en jouw enthousiasme en passie voor wetenschap zijn inspirerend. Dank voor het vertrouwen, de waardevolle feedback, en de vrijheid en kansen die je mij gaf; ik ben trots dat jij mijn promotor bent.

Marleen, vanaf het begin van mijn PhD heb je mij opgenomen in jouw team en vertrouwd gemaakt met het klinische perspectief. Ik bewonder hoe jij wetenschappelijke nieuwsgierigheid combineert met toewijding aan je patiënten; ik ben trots dat jij mijn co-promotor bent.

All former and present KdV colleagues: thank you Hannah and Ewald for our brainstorms and feedback. Traveling to Canada with you, Hannah, for the keystone meeting on myeloid cells was a highlight. Thank you Claudia for your constant encouragement. Antoinette, jij stond altijd voor mij klaar met mentale steun en waardevolle feedback. Extra speciaal dat jij mijn paranimf wilt zijn; bedankt! Thank you Lorenzo, Quinte, Elham, Jelle, Kim, Tisee, Daphne, Lisanne, Anne and Margherita. Thanks also to my fellow PhD students Danique, Olga, Max, Kevin, Annemieke, Daniil, Jinne, Tom and Irene: together we made lunches, K-fish meetings, and brainstorms both content-rich and enjoyable.

All former and present Kokkies: mijn extra dank gaat naar de fantastische technicians Chris, Maxime en Elisa, essentieel voor het werk in het lab en de gezellige sfeer. Dank aan mijn MD PhD collega's Leonie, Iris, Veerle, Manon, Rianne en Robbert-Jan voor jullie hulp bij patiënten en het medisch perspectief. En natuurlijk dank aan Marieke, Nicole, Olga, Maksim, Mi, Aaron, Kat, Michiel en Sara; samen vormden wij een diverse en sterke groep.

Dank aan alle mensen van B3 en B6 voor gedeelde meetings, kennisuitwisseling en de gezellige events. Dank aan Jossie Rotman, Nienke van Trommel, Joost van den Berg en Katja Jordanova voor de samenwerking aan de N16SIG vaccinatiestudie. Ook de flow-, sequencing-, proteomics- en microscopie faciliteiten van het NKI waren cruciaal.

Dank aan mijn vrienden! Jolien, Jacobien en de andere NYXies en Skøllies: bijzonder dat onze vriendschappen zijn geëvolueerd van samen sporten en uitgaan naar de hechte band van nu. Elsje, Myrthe, Wiesje en Florinde: ruim 34 jaar vriendschap. Mooie tijden en moeilijke tijden, open en eerlijk: wij zijn er voor elkaar. Ook Evelien hoort daar voor mij nog steeds bij; in gedachte nog altijd aan mijn zijde, net als vroeger. En aan al mijn Haarlemse vrienden: dank voor jullie aanhoudende interesse, aanmoediging en gezelligheid.

Ria, dank voor alle steun en eindeloze oppasmiddagen, ook na het overlijden van Cees. Harm, Lieke en Jesper: dank voor de gezelligheid en interesse door de jaren heen. @Jesper: jij bent de volgende.

Jet, Roos en Thijs: mijn lieve, krachtige zussen en broer. Wat zijn wij vieren verschillende kanten op gegaan, en wat mooi om te zien hoe ieder op zijn manier bijdraagt (heel relativerend ook). Zo fijn om altijd dat vangnet onder me te voelen. Ik hoop op nog heel veel volbloed-etentjes en gezellige activiteiten met Judith en Jacques in de toekomst.

Papa en Mama: dank voor mijn fijne, stabiele jeugd, jullie aanmoedigingen mijn hart te volgen en voor jullie oppas en steun. Jullie hebben mij geleerd trouw te blijven aan mezelf.

Dan mijn vier prachtige kinderen: ik ben oneindig trots op jullie! Jullie hebben absoluut bijgedragen aan het succesvol afronden van mijn PhD avontuur. Filian; jij maakte ons warme gezin compleet. Suze; jouw komst zette onze wereld even stil. Jouw vechtlust, relaxte ontspannenheid en doorzettingsvermogen zijn eigenschappen die ik ook goed kon gebruiken tijdens het afmaken van dit boekje. Freya; ik voelde mij gesterkt in mijn ambities als ik jou hoorde zeggen dat jij ook "beterschapper" wilt worden als je later groot bent (al is die ambitie inmiddels verdwenen). Jonna; dankjewel dat je altijd mij altijd zo begripvol mijn werktijd hebt gegund, ook al betekende dat soms dat ik je 's morgens al welterusten moest kussen. Jij klaagde nooit en wenste mij altijd vrolijk een fijne dag en succes toe.

Als laatste gaat mijn allergrootste dank uit naar mijn leuke vriendje Stijn! Jij maakt het mogelijk voor mij om de vrouw te zijn die ik wil zijn, en dus ben. Je bent een absolute kanjer Stijn. Zonder jouw mentale en praktische steun had ik dit nooit kunnen doen. Ik ben blij en trots dat ik jou nog altijd aan mijn zijde vind; steunend, stimulerend, liefhebbend. Wij zijn een top-team, door dik en dun en ik kijk met plezier en vertrouwen een toekomst met jou tegemoet.